Synthetic and Structural Studies on Auraboranes.

by Andrew J. Wynd

Thesis Presented for the Degree of
Doctor of Philosophy
University of Edinburgh
1988

EDINA! Scotia's darling seat!
All hail thy palaces and towers,
Where once beneath a Monarch's feet,
Sat Legislation's sovereign powers!
From marking wildly-scatter'd flowers,
As on the banks of Ayr I stray'd
And singing lone, the lingering hours,
I shelter in thy honour'd shade.

Here wealth still swells the golden tide,
As busy Trade his labours plies,
There Architecture's noble pride,
Bids elegance and splendour rise;
Here Justice from her native skies,
High wields her balance and her rod;
There Learning, with his eagle eyes,
Seeks Science in her coy abode.

- *Robert Burns* (from his "Address to Edinburgh")

Dedicated to my parents for their love and understanding.

Acknowledgements.

This work could not have been done without the help and encouragement of my supervisor, Dr. Alan Welch. Thanks also to John Millar, Lawrence Bell, Heather Grant and especially Dr. David Reed for obtaining n.m.r. spectra. Elaine MacDougall did the microanalyses, and Elizabeth Stevenson, the mass spectrum.

Thanks are also due to Prof. J. Fornies and his group for the help and friendliness I found at the Universidad de Zaragoza in Spain. Then there were the people, too numerous to mention, from whom I obtained advice, encouragement or chemicals. The University computers, affectionately known as EMAS, EMAS-A or EMAS-C were invaluable in the crystallography, and EMAS-C was used, in conjunction with the document-processing program SCRIBE and the laser-printer, to produce this thesis. Finally financial assistance came from the S.E.R.C. and N.A.T.O. provided a travel grant. Intergold lent gold salts.

Abstract.

In *Chapter 1* is an outline of Polyhedral Skeletal Electron Pair Theory and its Molecular Orbital Theory background. A review of the chemistry of decaborane and a survey of known gold-borane complexes follows. Techniques for chemical characterisation and structural analysis are discussed, then there is an outline of Extended Huckel Molecular Orbital (EHMO) calculations and their uses.

Chapter 2 reports the complexes : 5,6-μ-(R_3PAu)-*nido*-$B_{10}H_{13}$. After discussing probable mechanisms of formation, there are the structural studies on the cage architecture. Distortions in the cage geometry are accounted for by a weak gold-μ-H interaction which was modelled by EHMO calculations. The ^{11}B-$\{^1H\}$ n.m.r. spectrum was assigned using an ^{11}B(COSY), and the spectroscopic studies were discussed in terms of the solid state structure. Finally there is a Section on the chemistry of these complexes.

Chapter 3 starts with the structure of $[B_{10}H_{13}]^-$. Following this is the chemical characterisation of $[NHEt_3]^+$ $[Cy_3PAuB_{10}H_{12}]^-$, and the analysis of its structure. Mössbauer spectroscopy and EHMO calculations on models were used to decide that this anion was a $\{Cy_3PAu^I\}$ fragment μ_4-bridging a decaboranyl cage. The n.m.r. spectra, reprotonation, and rearrangement of this anion are then discussed. Next is $(Cy_3PAu)_2B_8H_{10}$ whose synthesis and structure are reported. Using EHMO calculations, observed differences in structure between this complex and $(\{dtc\}Au)_2B_8H_{10}$ (dtc = diethyldithiocarbamate) are due to steric crowding and that $(Cy_3PAu)_2B_8H_{10}$ is best described as two $\{Cy_3PAu^I\}$ fragments η^3-ligated to a $\{B_8H_{10}\}^{2-}$ cage.

Chapter 4 reports the auraborane 'sandwich' complexes. In the first, $[(B_{10}H_{12})Au(B_{10}H_{13})]^{2-}$, the gold is η^4-ligated to one $\{B_{10}H_{12}\}$ cage and

η^3-ligated to a $\{B_{10}H_{13}\}$ one. In view of the disorder in the crystal structure, the n.m.r. spectra are used to justify this structure. The second species, the $[(B_{10}H_{12})_2Au]^-$ anion, was structurally characterised by two different crystal structures and these are discussed, followed by the EHMO calculations which probed the electronic structure.

Chapter 5 discusses the multiple clusters of gold and boranes. The structure and spectra of the *triple cluster* $(B_{10}H_{12}Au)_2(AuPPh_3)_4$ are first discussed, and the opening-out of the Au_6 cluster is assigned as steric in origin, but in $(B_{10}H_{12}Au)_2(AuPCy_3)_4$, in which only the Au_6 core could be located, this is absent. Then there are Sections on the spectroscopic characterisation and reactions of these species. The final new complex reported herein is the *double cluster*, $(B_{10}H_{12}Au)(AuPCy_3)_3$. After considering the structure of both halves of the molecule, there is a Section on its spectroscopic properties.

Chapter 6. The first half of this Chapter details the experimental procedures used to synthesise all of the complexes. This is followed by an account of the crystallographic procedures and computer programs used.

Conclusions reached about the work in the whole of this thesis are followed by the *references* cited. In *Appendix 1* is the (required) list of postgraduate lecture courses, or equivalents, attended. *Appendix 2* comprises all the crystallographic data for the structures, divided into sections on the experimental details, followed by the tables of derived parameters. *Appendix 3* comprises the fractional coordinates of the models used in the EHMO calculations, and *Appendix 4* gives details of all the published work.

Table of Contents.

Appendices.

Abbreviations.

ABMO	anti-bonding molecular orbital
AO	atomic orbital
BMO	bonding molecular orbital
COSY	correlated spectroscopy
Cp	η^5-cyclopentadienyl
Cp^*	η^5-pentamethylcyclopentadienyl
Cy	cyclohexyl
dtc	N,N-diethyldithiocarbamate
EHMO	extended Huckel molecular orbital
EI	electron impact
e.s.d.	estimated standard deviation
Et	ethyl
FMO	fragment molecular orbital
FMO-EHMO	fragment molecular orbital - extended Huckel molecular orbital
HOMO	highest occupied molecular orbital
IR	infra-red
IS	isomer shift
IUPAC	International Union of Pure and Applied Chemistry
LCAO	linear combination of atomic orbitals
LUMO	lowest unoccupied molecular orbital
Me	methyl
MO	molecular orbital
n.m.r.	nuclear magnetic resonance
OMO	occupied molecular orbital
ORTEP	Oak Ridge thermal ellipsoid plotting (program)
o-tolyl	C_6H_4Me-2
Ph	phenyl
PSEPT	polyhedral skeletal electron pair theory
QS	quadrupolar splitting
RCME	reduced charge matrix element
SEP	skeletal electron pair
thf	tetrahydrofuran

tol	C_6H_4Me-2
UMIST	University of Manchester Institute of Science and Technology
UMO	unoccupied molecular orbital
UV	ultraviolet
vis	visible

The following list consists of the abbreviations used for compounds:

(1)	$Ph_3PAuC_2B_{10}H_{10}R$
(2)	$Ph_3PAuC_2B_4H_7$
(3)	μ-$(AuPPh_3)$-$(CpNi)$-$C_2B_8H_{10}$
(4)	$[(C_2B_9H_{11})_2Au]^-$
(4a)	$[NMe_4]^+$ **(4)**
(4b)	$[(Et_2NCS_2)_2Au]^+$ **(4)**
(5)	$Et_2NCS_2AuC_2B_9H_{11}$
(6)	$Ph_3PAuC_2B_8H_{11}$
(7)	$B_{10}H_{14}$
(8)	5,6-μ-$(AuPR_3)$-*nido*-$B_{10}H_{13}$
(8a)	R = Cy
(8b)	R = *o*-tolyl
(8c)	R = H
(9)	$[B_{10}H_{13}]^-$
(9b)	$[B_{10}H_{13}]^-$ (model)
(10)	$[B_{10}H_{14}]^{2-}$
(11)	$[B_{11}H_{13}]^{2-}$
(12)	$[\{Cp\}CoMe_2C_2B_3H_4]HgCl$
(12a)	$\{Cp\}$ = Cp
(12b)	$\{Cp\}$ = Cp^*
(13)	$[\{Cp\}CoMe_2C_2B_3H_4]_2Hg$
(13a)	$\{Cp\}$ = Cp
(13b)	$\{Cp\}$ = Cp^*
(14)	$[H_3PAuB_{10}H_{12}]^-$
(15)	$[Cy_3PAuB_{10}H_{12}]^-$
(15b)	$[H_3PAuB_{10}H_{12}]^-$

(16) $[B_{10}H_{12}]^{2-}$

(17) $[AuPH_3]^+$

(17a) **(17)** excluding P 3d orbitals

(17b) **(17)** including P 3d orbitals

(18) $(LAu)_2B_8H_{10}$

(18a) L = Cy

(18b) L = dtc

(18c) $[H_3PAuB_8H_{10}]^-$

(18d) L = H

(19) $[(B_{10}H_{12})Au(B_{10}H_{13})]^{2-}$

(19a) $\{AuB_{10}H_{12}\}$ fragment of **(19)**

(19b) $\{AuB_{10}H_{13}\}$ fragment of **(19)**

(20) $[(B_{10}H_{12})_2Au]^-$

(20b) $(H_3P)_2PtB_{10}H_{12}$

(20c) $[(B_{10}H_{12})_2Au]^-$ (model)

(21) $(B_{10}H_{12}Au)_2(AuPEt_3)_4$

(22) $(B_{10}H_{12}Au)_2(AuPPh_3)_4$

(23) $(B_{10}H_{12}Au)_2(AuPCy_3)_4$

(24) $(B_{10}H_{12}Au)(AuPCy_3)_3$

(25) $Au_4(\mu\text{-}I)_2(PPh_3)_4$

(26) $Au_4(I)(\mu_3\text{-}I)(dppm)_3$

(27) $Au_4(dppm)_3Au(dppm\text{-}H)$

(28) $[Au_4(PPh_3)_4N]^+$

Figures.

In the Figures herein, unless otherwise stated, all of the boron atoms are bonded to a terminal H atom, which has been omitted for clarity. If any μ-H atoms are present in the complex, their position (whether known or postulated) is shown by a shaded connectivity.

Chapter 1 :

Background and Techniques.

"All statements about the hydrides of boron earlier than 1912, when Stock began to work on them, are untrue" [1]

1.1 Introduction.

This Chapter introduces the work in the rest of this thesis, and, in the process, provides a general introduction to metallaborane chemistry. It has been broken down into five parts. The first part, Section 1.2, consists of an outline of the theoretical principles underlying cluster chemistry. These are then derived and rationalised in molecular orbital terms. The breakdown of these rules, when applied to metallaboranes, is then discussed, and the reasons for this breakdown are explored.

Section 1.3 then explores the chemistry of decaborane ($B_{10}H_{14}$). The main routes to other boron hydrides are outlined, and this leads into a discussion of the main inorganic derivatives and their syntheses (Section 1.4). The reactions of metal alkyls with decaborane are then reviewed, and following on from this is a more detailed discussion of the known chemistry of auracarboranes and auraboranes (Section 1.5). This is then used, along with some related work, to explain why the synthetic routes were chosen.

In the penultimate Section (1.6) the techniques used to characterise these complexes are outlined, and the more unusual ones are discussed in greater depth. Two computational techniques were used to analyse these molecules in terms of their bonding and structure. A derivation of the parameters of Extended

Huckel Molecular Orbital (EHMO) Theory is outlined, and what they mean is discussed. The second computational method is an analysis of the geometries of these clusters, and the method for calculating the derived parameters is explained. The relevance of these parameters to boron hydrides is then justified with examples. Finally in Section 1.7, the work discussed in this Chapter is summarised and some conclusions are drawn.

Using the geometry analysis technique, certain of the geometries discovered during this work were compared against the geometries obtained for other metallaboranes. The coordinates of these were extracted from the Cambridge Crystallographic Database. Whilst IUPAC conventions have been used throughout this thesis, when different molecules are being compared, all the structures are renumbered into a common numbering scheme, because in general, changing the size of the cluster changes the number of any particular vertex. This has been done for ease of discussion. However, to avoid any confusion, when this has been done, a diagram on the facing page shows the correct numbering and the chosen renumbering.

1.2 The Boron Hydrides and their Electron-Counting Principles.

From 1912 onwards, Alfred Stock and co-workers, in a classic series of experiments [2], isolated and characterised a series of polyhedral boron hydrides (boranes), of general formula B_nH_{n+m}. Rationalising the structures of these species was an equally difficult task, requiring non-classical bonding ideas, involving the concept of multicentre, two-electron bonds.

It was Lipscomb *et al* [3] who first successfully rationalised these structures using a topological approach. This is quite useful for discussing the bonding within a cluster, but its predictive powers are very limited, and it also breaks

down when applied to very symmetrical (usually *closo*) boranes. Hence, a second approach was preferred. This is derived from molecular orbital theory [4,5], and is generally known as Polyhedral Skeletal Electron Pair Theory (PSEPT).

While the trends in the structures of these species had been pointed out[6], it was Wade [7] who showed that there was a simple relationship between structure and the total number of skeletal electrons. Let n equal the number of atoms which are cluster vertices, then the relationship between n and the cluster electron count, expressed as the number of skeletal electron pairs (SEP's) is :-

no. of SEP's	no. of vacant vertices	terminology
n+1	0	*closo*
n+2	1	*nido*
n+3	2	*arachno*
n+4	3	*hypho*

This is explainable in the following manner [8]. Consider a *closo* polyhedron which has been broken down into its constituent parts of {B-H} fragments and additional H atoms. Each of these additional H atoms has one orbital and one electron. Each B atom has three valence electrons and four valence atomic orbitals (AO's). It uses one of each in *exo*-polyhedral σ-bonding to the terminal H atom, and so a {B-H} fragment is a two electron, three orbital donor to cluster bonding. The three AO's look like:

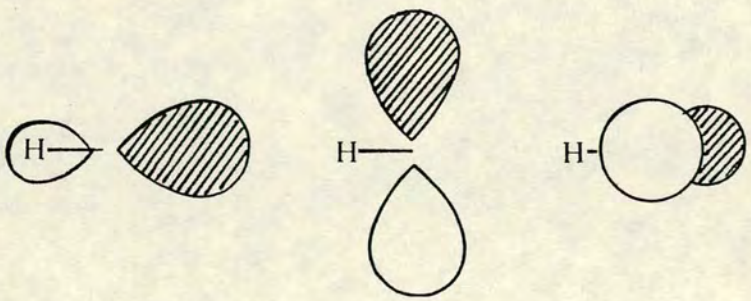

(1) **(2)**

All the n **(1)**-type orbitals interact to produce one MO which is strongly bonding

and n - 1 either weakly bonding or strongly antibonding MO's This type of bonding is referred to as *radial* bonding because each lobe of the bonding MO points down the radius towards the centre and is very important in transition metal clusters. The orbitals of type **(2)** interact at a tangent to the cluster surface, and so this is known as *tangential* bonding. These overlap to generate n bonding molecular orbitals (BMO's) and n anti-bonding MO's (ABMO's). In all, there are n + 1 BMO's, and hence a n + 1 SEP count for maximum thermodynamic stability. If this cluster had n + 2 SEP's, then one ABMO would be occupied. However cluster expansion to n' vertices (n' = n + 1) would require the cluster to have n' + 1 (= n + 2) BMO's which is as expected from the rules above. Similar arguments can be extended to the *arachno* and higher families of boranes.

To illustrate these rules, consider decaborane

10 B-H fragments : 10 x 2 = 20 electrons
4 μ-H 's : 4 x 1 = 4 "

TOTAL = 24 "

Therefore no. of SEP's = 12.

Now n = 10, since there are ten boron atoms, and so this is a n + 2 case, i.e. *nido*. Because the number of SEP's is calculable from first principles, this is a more useful theory than the topological approach, both for rationalising known structures, and for predicting the shapes of unknown boranes.

With the discovery [9] of the metallacarboranes, it was realised [4,10] that the boranes and carboranes were not chemical curiosities, since many other elements could behave in a similar manner. In particular, the metallaboranes acted as a link between the boranes and the other inorganic cluster compounds: low-valent transition metal cluster compounds, and even metal-hydrocarbon π-complexes could be rationalised in terms of PSEPT [4,10,11].

Now that the boron hydrides are regarded as structural archetypes, underpinning large areas of chemistry, it is important to explore PSEPT to see where its deficiencies lie, and perhaps to develop a more general theory. PSEPT's major breakdown occurs in metallaborane chemistry. This arises primarily where the metal does not act as a three orbital donor, when deviations from predicted structures may occur. One well-known [12-14] example is the series of derivatives which contain the bis(trialkylphosphine)platinum(II) fragment. Metallaboranes with this unit tend to have an electron-count which is two lower than expected (eg $[(PMe_2Ph)_2PtB_{10}H_{12}]$ [15] has 11 vertices and 12 SEP's, although it has a *nido* geometry). There are different views about the internal bonding in these systems, and so there are several explanations for this deviation. This is discussed in more depth in Chapter 4.

Another common type of deviation occurs in those metallaboranes where the geometry of the cage is not one of the polyhedra seen in boron hydride structures. In particular, there are the *isocloso* [16-18] metallaboranes. In these, a *closo* geometry is obtained by capping *with one vertex,* an *arachno* borane fragment. A pictorial representation of this is shown in Figure 1.1 (page 6). This probably arises for two reasons. The first is the metal-boron internuclear distance, which is longer than the typical boron-boron connectivity. This longer 'reach' enables the cluster to adopt a geometry which is inaccessible to a purely boron cluster. The second reason is the ability of metals to occupy very highly connected sites within the cluster: positions that boron rarely adopts. An example of this is the complex $[1,1\text{-}(PMe_2Ph)_2\text{-}2,5\text{-}(OMe)_2\text{-}1,2\text{-}\mu\text{-}(H)\text{-}$ *isocloso*$\text{-}1\text{-}RhB_{10}H_8]$ where the rhodium atom is bound to six boron atoms.

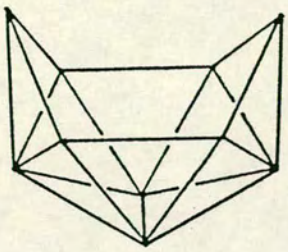

(a)

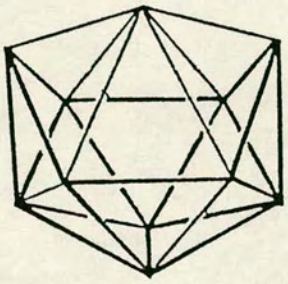

(b)

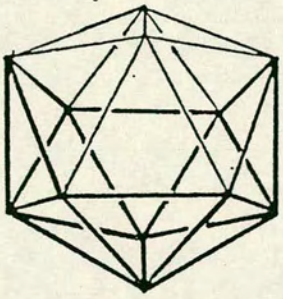

(c)

Figure 1.1. The relationship between fragments which are: (a) *arachno* 10 vertex, (b) *isocloso* 11 vertex (c) *closo* 12 vertex.

1.3 The Chemistry of Decaborane and its Derivatives.

One major group amongst the large number of known boron hydrides consists of decaborane and its derivatives. Since decaborane is commercially available, is reasonably air-stable and consequently relatively easily handled, it was chosen as the starting-point for this project. Another advantage is the large number of boron hydride derivatives which are readily synthesised (see below) from decaborane. The chemistry of decaborane has been extensively investigated[19,20]. It has been divided into three parts. First there are the other boron hydrides which are most readily synthesised from decaborane. Secondly, there are the inorganic derivatives, and finally there are the metallaboranes which can be synthesised from decaborane or its derivatives.

The major routes [21-27] to the derivatives of decaborane are outlined in Scheme 1 (page 8). As can be seen from this, decaborane is a very versatile reagent. Even when reacted with the same reagent, under different conditions, different products are obtained. The best illustration of this is the plethora [22-24] of reactions involving triethylamine.

$$B_{10}H_{14} + NEt_3 \longrightarrow [NHEt_3]^+ [B_{10}H_{13}]^-$$
$$\text{or} \quad B_{10}H_{12}(NEt_3)_2$$
$$\text{or} \quad [NHEt_3]^+_2 [B_{10}H_{10}]^{2-}$$

$$B_{10}H_{14} + BH_3NEt_3 \longrightarrow [NHEt_3]^+_2 [B_{12}H_{12}]^{2-}$$

There are two other main classes of derivatives. There are those derivatives where a substituent is outwith the main polyhedral surface (either σ- or μ-bonded) and there are the heteroboranes where the substituent is a vertex. Of the first type, there are two general types which are divided into whether the substituent is a two electron donor (L) or a one electron donor (X). Since a

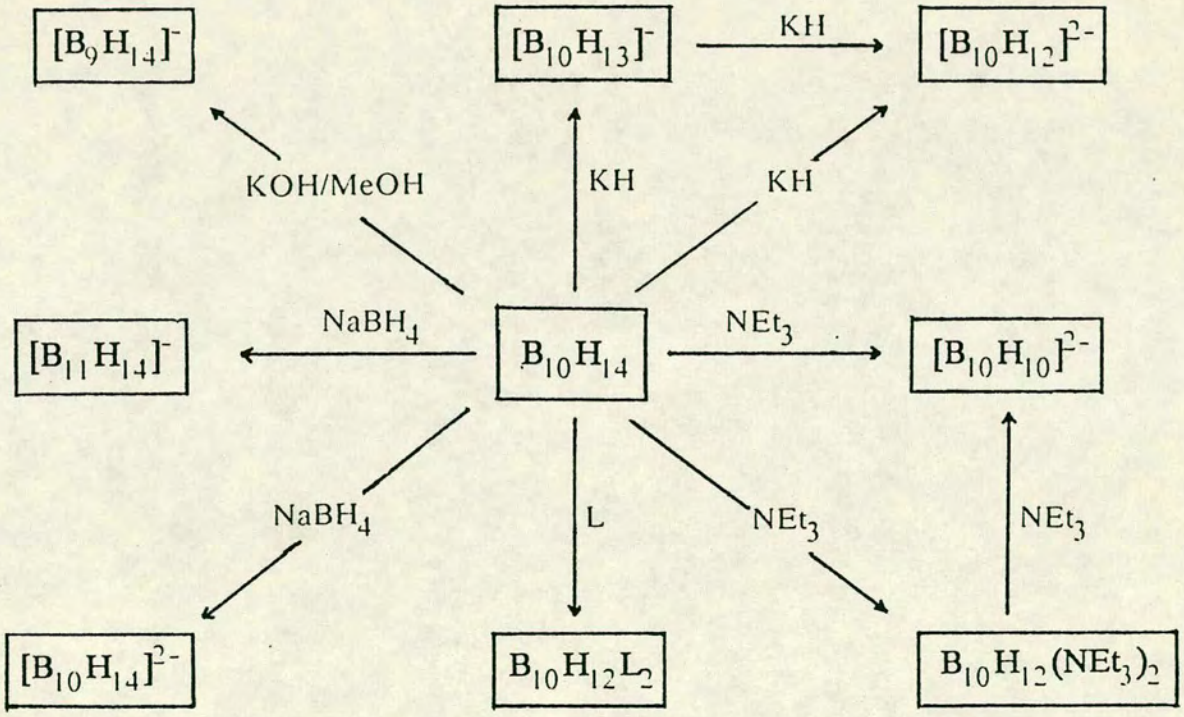

Scheme 1. The Synthesis of the Derivatives of Decaborane.

hydrogen atom is a one-electron donor, substitution by L will cause polyhedral expansion. The general reaction [24] is

$$B_{10}H_{14} + 2L \longrightarrow B_{10}H_{12}L_2 + H_2$$

A series of experiments has been carried out [28] to establish the order of stability of these adducts. This concluded that the order was

$$SMe_2 < MeCN < NEt_3 \simeq PPh_3$$

Increasing stability $\longrightarrow$

The crystal structures of the complexes with L = MeCN [29], NEt_3 [30], and SMe_2 [31] have been determined, and all have the basic geometry shown in Figure 1.2(a) (page 10). Since the cluster has lost two hydrogen atoms (1-e^- donors) and gained two L, the cluster has gained one SEP and so is an *arachno*-fragment of a an icosahedron where two adjacent vertices have been lost, as illustrated in Figure 1.2(b).

These are of theoretical interest, as the electron-pair used in *endo*-polyhedral bonding to the *endo*-hydrogen atoms on B(6) and B(9) is formally included in the skeletal electron count. This is justified by the bond in question being located on the polyhedral surface.

These compounds are of synthetic utility because they react principally with the loss of one or both of L. This means the cluster closes to *nido* or *closo*, but the temporary opening-up of the open face enables reagents to attack the cage. For example, this is the principal means of synthesising carboranes [32], although the intermediate is rarely isolated. Some of the reactions undergone by these compounds are [23,33-35] shown on page 11.

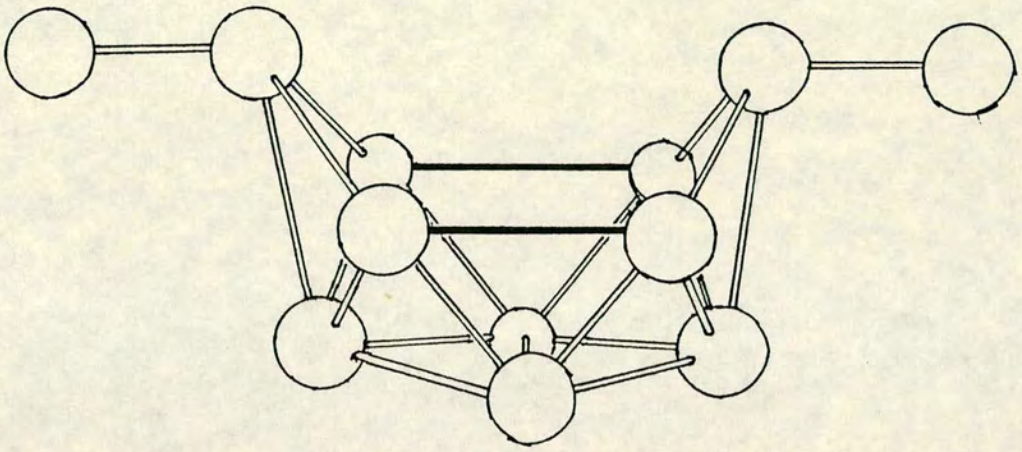

(a)

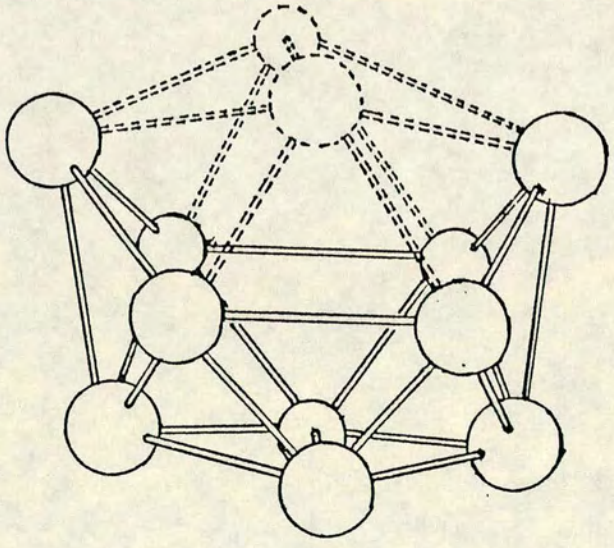

(b)

Figure 1.2. The structures of (a) $B_{10}H_{12}L_2$ and (b) the icosahedron from which the *arachno* 10 vertex fragment is derived by removal of two adjacent vertices (shown by dashed connectivities).

$$B_{10}H_{12}L_2 \longrightarrow B_{10}H_{12}L$$
$$B_{10}H_{12}(NEt_3)_2 \longrightarrow [NHEt_3]^+_2\,[B_{10}H_{10}]^{2-}$$

$$B_{10}H_{12}(SMe_2)_2 + H\text{-}X \longrightarrow 6\text{-}X\text{-}B_{10}H_{13}$$
$$+ H_2SO_4 \longrightarrow (B_{10}H_{13})_2O$$
$$+ R\text{-}C{\equiv}C\text{-}R \longrightarrow R_2C_2B_{10}H_{12}$$

The majority of derivatives where the substituent is outwith the polyhedral surface have the 6-(X)-*nido*-$B_{10}H_{13}$ structure. These are made from several decaborane-based reagents, and the main reaction [34-39] types are :-

$$B_{10}H_{14} + MeLi \longrightarrow B_{10}H_{13}Me$$
$$+ I_2 \longrightarrow B_{10}H_{13}I$$
$$[B_{10}H_{13}]^- + R\text{-}I \longrightarrow B_{10}H_{13}R$$
$$+ Ph_2PCl \longrightarrow B_{10}H_{13}PPh_2$$
$$B_{10}H_{12}(SMe_2)_2 + H\text{-}Cl \longrightarrow B_{10}H_{13}Cl$$
$$+ H_2SO_4 \longrightarrow (B_{10}H_{13})_2O$$

The second type of derivative of boranes is the heteroboranes where the heteroatom is a polyhedral vertex[40]. Typical of these are the azaboranes whose syntheses are as follows[41-43].

$$B_{10}H_{14} + NaNO_2 \longrightarrow Na^+[B_{10}H_{12}NO_2]^- \longrightarrow \textit{arachno}\text{-}B_8H_{12}NH$$
$$\downarrow H_2SO_4$$
$$\textit{nido}\text{-}B_9H_{11}NH \longrightarrow \textit{closo}\text{-}B_9H_9NH$$

The routes to thiaboranes are very similar[44-46]. These reactions have two main features of interest. There is the loss of at least one boron atom in the reaction, and secondly, there is the mechanism of formation, which is thought to go via an initial adduct, which then inserts into the cage[41,45]. However in arsenaborane chemistry, as demonstrated overleaf, this first feature is not always[47] observed, although the mechanism proposed was similar.

$$[B_{10}H_{13}]^- + AsCl_3 \longrightarrow [B_{10}H_{13}(AsCl_2)] + NEt_3 \longrightarrow B_{10}H_{12}AsCl$$

$$\downarrow Zn$$

$$[B_{10}H_{12}As]^-$$

1.4 Metallaborane Chemistry.

This area has recently been comprehensively reviewed[20,48,49]. Some general points should, however, be mentioned. In general, when a metal substrate is reacted to become a polyhedral vertex, it will ligate to three or more boron atoms which will therefore occupy two or more coordination sites. It therefore follows that one of two things must happen. Either the metal must expand its coordination sphere to include the extra atoms, as happens, for example[50,51] in:

$$[B_{10}H_{13}]^- + HgCl_2 \longrightarrow [(B_{10}H_{12})_2Hg]^{2-}$$

$$B_{10}H_{14} + Pt(PR_3)_3 \longrightarrow (PR_3)_2PtB_{10}H_{12}$$

In the first reaction above, the mercury formally goes from linear to tetrahedral and in the second, the platinum goes from trigonal to square planar.

The other alternative is that the metal must lose one or more of the ligands that it is already bonded to. These can be of two sorts : neutral molecules such as phosphines or carbonyls; or anionic species such as halides. The two reactions above show this behaviour, although other examples[15,52] include:

$$[B_{10}H_{13}]^- + (PMe_2Ph)_2PtCl_2 \longrightarrow (Me_2PhP)_2PtB_{10}H_{12}$$

$$[B_9H_{14}]^- + (CO)_5MnBr \longrightarrow [(CO)_3MnB_9H_{13}]^-$$

The second pertinent point is that in most reactions, the borane loses at least one of its hydrogen atoms. Principal means of their elimination are:

(a) dihydrogen elimination: e.g. the synthesis of $B_{10}H_{12}L_2$.

(b) elimination as HX, X = anionic ligand on the metal e.g. halide,alkyl.

(c) removal as a proton by base present in the reaction.

(d) transfer to the metal to become one of its ligands.

Option (d) also allows for a "half-way" point when the hydrogen bridges a metal-boron connectivity. The best example of this is the series of cupraboranes: $(PPh_3)_2CuB_3H_8$[53], $(PPh_3)_4Cu_2B_{10}H_{10}$[54], and $Cu_2B_{10}H_{10}$[55] all have established structures with hydrogen-bridged copper-boron connectivities.

The problems associated with each route, when applied to auraborane synthesis, are discussed in the next Section. It was concluded that the species, methyltrialkylphosphinegold(I), was the best starting-point. As far as the points raised above are concerned, this complex meets the requirements for a useful precursor. It is coordinatively unsaturated and so insertion into a cage can occur without ligand loss, it has both a neutral ligand which can be eliminated, and a species, X, which can abstract a proton as HX.

An interesting point is to examine the known reactions of metal alkyls and boranes. These have been examined only for main group metals, and include[56-59]:

$$B_{10}H_{14} + CdEt_2 \longrightarrow [(OEt_2)_2CdB_{10}H_{12}]_2$$

$$[(OEt_2)_2Cd(B_{10}H_{12})]_2 + H_2O \longrightarrow Cd^{2+}[(B_{10}H_{12})_2Cd]^{2-} + OEt_2$$

$$B_{10}H_{14} + ZnMe_2 \longrightarrow [(B_{10}H_{12})_2Zn]^{2-}$$

$$+ TlMe_3 \longrightarrow [TlMe_2]^+[Me_2TlB_{10}H_{12}]^-$$

As can be seen from this, formation of the *nido*-7-metallaundecaborane geometry is the dominant product. For the zinc triad, in particular, the final product consists of two *nido*-7-metallaundecaborane clusters fused about a common metal vertex.

1.5 Previous Gold-Borane and Related Work.

Despite the large amount of work that has gone into developing metallaborane chemistry, little has been done with the group 1b elements : copper, silver and gold. The work which has been carried out with gold substrates is now detailed.

1.5.1 Auracarborane Chemistry.

There are only a handful of auracarboranes known, but despite this, they exhibit a wide variety of bonding modes between the gold and the rest of the cage.

Auracarboranes with the Gold outwith the Polyhedral Surface.

The gold can bond to the cage in one of two ways: it can form a gold-(cage) σ-bond to either a boron or carbon atom; or else it can edge-bridge a connectivity. There are examples of both modes known[60-62]:

$$Li[C_2B_{10}H_{10}R] \quad (R = H, Me, Ph) \quad + Ph_3PAuCl \longrightarrow Ph_3PAuC_2B_{10}H_{10}R \qquad (1)$$

$$Na[C_2B_4H_7] + Ph_3PAuCl \longrightarrow Ph_3PAuC_2B_4H_7 \qquad (2)$$

$$(Cp)NiC_2B_8H_{11} + Ph_3PAuMe \longrightarrow \mu\text{-}(AuPPh_3)\text{-}(CpNi)\text{-}C_2B_8H_{10} \qquad (3)$$

In **(1)**, it has been suggested[63] that the gold atom is σ-bonded to one of the cage carbon atoms. It was subsequently found that this Au-C bond was very inert, and this was assigned to the electron-withdrawing properties of the cage. Thus, for example, the reaction with dibromine leads to oxidative addition at the gold atom, and not gold-carbon bond cleavage

$$Ph_3PAuC_2B_{10}H_{10}R + Br_2 \longrightarrow (Ph_3P)Au(Br)_2(C_2B_{10}H_{10}R)$$

The proposed[61] structure of **(2)** was based on its n.m.r. spectra, and it consisted of a $\{AuPPh_3\}$ bridge on one of the connectivities. However, **(3)** was structurally characterised[62], and its structure is shown in Figure 1.3(c), on page 16. The $\{Au\text{-}PPh_3\}$ bridges the B(10)-B(11) connectivity and there is no nickel-gold interaction- the gold bridge is tilted away from the nickel. This is also the first example of a gold-methyl complex being reacted with the bridging hydride on a boron cage to synthesise a gold-boron bond.

Auracarboranes with a Gold Vertex.

There are three auracarboranes which have been reported in the literature which have, or are thought to have, at least one gold vertex. The reactions to synthesise these compounds all involve attack of carborane anions to displace halide ligand(s) on the gold[64-66]:

$$[C_2B_9H_{11}]^{2-} + AuCl_3 \longrightarrow \underset{\textbf{(4a)}}{[(C_2B_9H_{11})_2Au]^-}$$

$$Tl[TlC_2B_9H_{11}] + Et_2NCS_2AuBr_2 \longrightarrow \underset{\textbf{(4b)}}{[(Et_2NCS_2)_2Au]^+}\,[(C_2B_9H_{11})_2Au]^- + \underset{\textbf{(5)}}{[(Et_2NCS_2)Au(C_2B_9H_{11})]}$$

$$Na[C_2B_8H_{11}] + Ph_3PAuCl \longrightarrow \underset{\textbf{(6)}}{Ph_3PAuC_2B_8H_{11}}$$

The structures of **(4b)**[65] and **(5)**[67] have been determined crystallographically, and are shown in Figures 1.3(b) and 1.3(a) respectively (page 16). **(4)** is a 'sandwich' compound, and has been described as the inorganic analogue of 'auracene' $[Cp_2Au]$.

The series of molecules of general formula $[(C_2B_9H_{11})_2M]^{n-}$ (M = Fe, Co, Ni, Cu, Au, Hg) has been examined theoretically[68]. The main interest lay in rationalising why, as the d-configuration increased, the metal 'slipped' away from

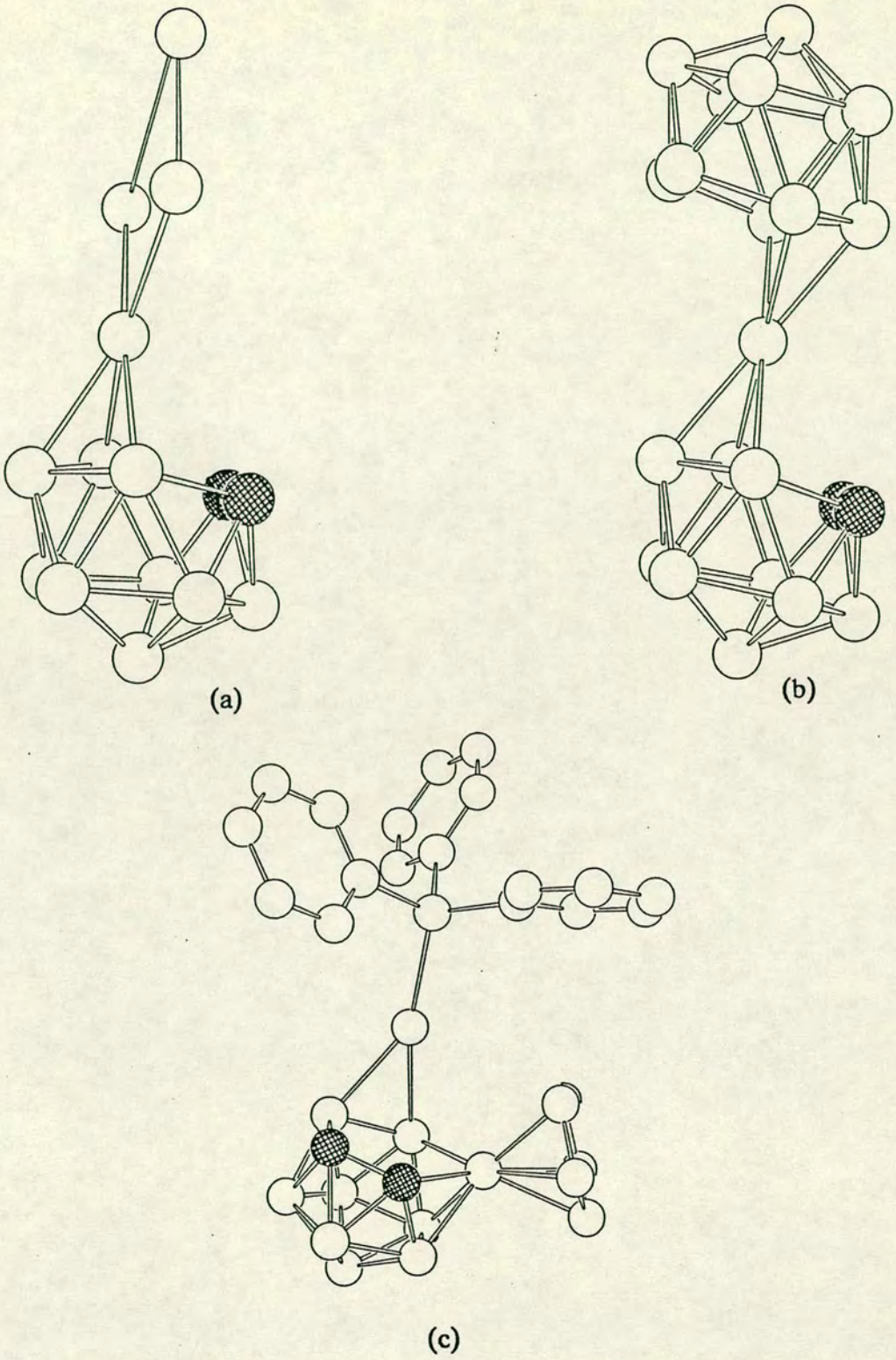

Figure 1.3. The structures which have been determined for auracarboranes.

(a) $[(Et_2NCS_2)Au(C_2B_9H_{11})]$ with the NEt_2 group omitted.

(b) the $[(C_2B_9H_{11})_2Au]^-$ anion.

(c) 9-Cp-10,11-μ-($AuPPh_3$)-*nido*-9-Ni-7,8-$C_2B_8H_{10}$.

the pseudo-fivefold axis which passed through the two cages. The direction of this slip was away from the two carbon atoms (see Figure 1.3(b)).

This was rationalised simply as due to increasing the d-orbital configuration beyond eighteen, and so the metal slipped across to reduce this electron density. A more thorough treatment showed that it was quite a complex effect, which was related to π-back-bonding from the cage to the metal. As the metal d-configuration increased, there were fewer empty d-orbitals on the metal, and so the back-bonding was reduced, so that for M = Au there were two orbitals which could bond effectively to only three boron atoms, hence the slip.

The structure of **(5)** is very similar[65], consisting of a square-planar gold atom which is slipped and bonded to the three boron atoms which were on the open face.

(6) is unusual in that its synthesis is very similar to that of **(1)** except that the carborane cage was *nido* instead of *closo*. The crystal structure of the analogous silver complex has been determined[66] and it is thought that the gold complex is isostructural. In this silver complex, the metal has partially inserted into the open face so the structure was interpreted as an 11 vertex *arachno* fragment of a 13-vertex docosahedron. An alternative interpretation is that the presence of the μ-H atom, along with the previously-discussed tendency of these metals to *slip* away from the carbon atoms, means that this is a distorted-open *closo* structure. Examples like this emphasise the need to consider the structure very carefully, and the need for more work to be done on the bonding in these systems.

1.5.2 Auraborane Chemistry.

Auraborane chemistry was not as well-developed as auracarborane chemistry. Several research groups had tried to synthesise auraboranes, and concluded [69-71]

that they were too unstable to be isolated. This is typified by the following reactions of the octahydrotriborate anion ($[B_3H_8]^-$) [70] :-

$$Cs^+[B_3H_8]^- + CuSO_4 + PPh_3 \longrightarrow (Ph_3P)_2CuB_3H_8$$
$$+ AgNO_3 + PPh_3 \longrightarrow "(Ph_3P)_2AgB_3H_8"$$
$$+ NaAuCl_4 + PPh_3 \longrightarrow \text{no identified products.}$$

The cupraborane was fully characterised by a single crystal X-ray diffraction study[54]; the argentaborane was identified by microanalysis, although it was reported as being very light-sensitive which precluded obtaining any spectroscopic parameters; but no auraboranes could be identified. The reaction reported [70] was reduction of the complex, with production of the metal. In this respect, gold has two disadvantages over the other group 1b metals. Firstly it is the most readily reduced [72] of the three, and secondly it has the highest metal-metal bond energy [73], and so reduction to form gold clusters is more thermodynamically favoured. An example of this is the reported [74] reaction :-

$$B_2H_6 + AuCl(PPh_3) \longrightarrow Au_{55}(PPh_3)_{12}Cl_6$$

Another major problem in these syntheses was the presence of free trialkylphosphine, which was added to stabilise the complex formed. However, this tended to encourage the formation of bis-, tris-, or tetrakis-trialkylphosphine-gold cations, and so no direct Au-B bonds were formed. One example of this was the reaction[70]:

$$Na^+[B_{10}H_{13}]^- + Na^+[AuCl_4]^- + PPh_3 \longrightarrow [(Ph_3P)_3Au]^+[B_{10}H_{13}]^-$$

However, it was concluded [75] that use of gold complexes with one phosphine ligand already attached prior to reaction might prove more fruitful.

Despite these difficulties, in 1984, Greenwood and co-workers reported [76] the reaction overleaf.

$Au(Br)_2(Et_2NCS_2) + [B_9H_{14}]^- \longrightarrow$ *arachno*-$(Et_2NCS_2)AuB_8H_{12}$

+ *arachno*-$(\{Et_2NCS_2\}Au)_2B_8H_{10}$

which were the first two structurally characterised *auraboranes*, although the reported yields were only 1 % and 5 % respectively.

1.5.3 Other Developments

It was in 1975 that Hoffmann and co-workers proposed [77] the isolobal analogy. This stated that two molecular fragments were *isolobal* if their frontier molecular orbitals had similar energies, extents in space, and symmetries. One of the best-known [78] examples of this is hydrogen $\leftrightarrow$ Au-PR_3, where the symbol $\leftrightarrow$ indicates 'isolobal with' and the Au is in its +1 oxidation state and **must be** linear. Based on this concept, several research groups have developed [73,79,80] syntheses of mixed-metal clusters by the isolobal substitution of bridging hydrides by gold-phosphine fragments. There are two routes to this substitution :-

(cluster)-μ-H + $R_3PAuCH_3 \longrightarrow$ (cluster)-μ-$(AuPR_3)$ -Route 1

$(cluster)^-$ + $R_3PAuQ \longrightarrow$ (cluster)-μ-$(AuPR_3)$ + Q^- -Route 2

Route 2 was extended to the metallaboranes when Wallbridge *et al* reported[81] the reaction :-

$Li^+[B_5H_8]^- + Ph_3PAu^+NO_3^- \longrightarrow Ph_3PAuB_5H_8$ (see Fig. 1.4, next page)

where the gold-phosphine moiety bridges a basal boron-boron connectivity.

The final development came when Robins and Welch carried out some EHMO calculations which suggested [82] that replacing a bridging hydride on decaborane(14) by a bridging gold-phosphine stabilised the cage to some extent. Based on this, and in view of the difficulties mentioned earlier, when using the metal halides and anionic boron hydrides, route 1 was tried in preference to route 2, only to yield a novel species, the *triple cluster*[83] (Figure 1.5, over).

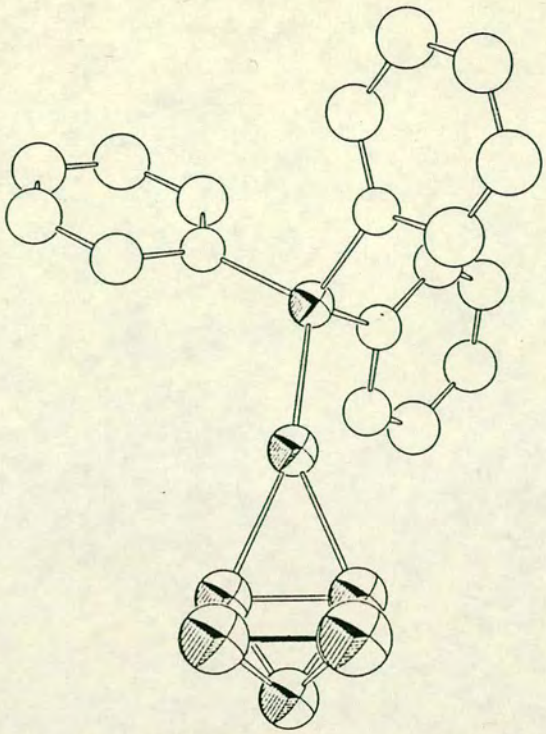

Figure 1.4. The molecular structure of $Ph_3PAuB_5H_8$ showing the gold-phosphine unit bridging the B(2)-B(3) connectivity. The three μ-H atoms bridge the three connectivities on the open face.

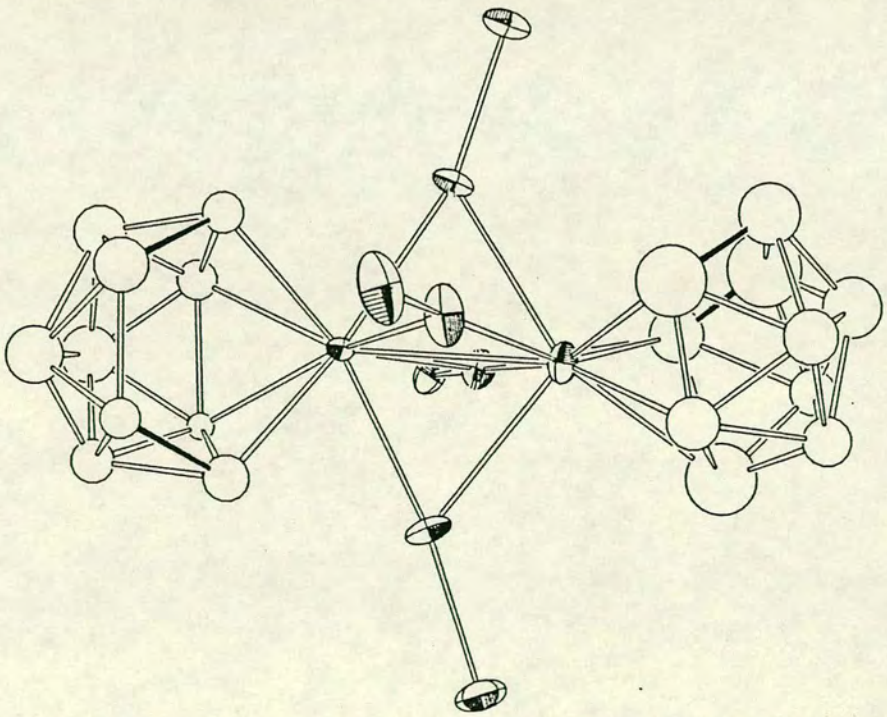

Figure 1.5. The molecular structure of $(B_{10}H_{12}Au)_2(AuPEt_3)_4$ showing the three clusters fused about common vertices. The μ-H atom positions are shown by the shaded connectivities and the ethyl groups have been omitted for clarity.

$$B_{10}H_{14} + 3Et_3PAuCH_3 \longrightarrow (B_{10}H_{12}Au)(AuPEt_3)_4(AuB_{10}H_{12})$$

In this species, two *nido*-icosahedral {7-$AuB_{10}H_{12}$} fragments are linked by a direct gold-gold bond, which is bridged by four {Au-PEt_3} fragments in a regular, but asymmetric manner. The four gold atoms, plus the two golds ligated by the boranes, form a central hexanuclear gold cluster whose geometry is a radially-compressed octahedron. It is worthy of note that theoretical studies[84] on the model species, $[Au_6(PH_3)_6]^{2+}$, have suggested that the octahedral geometry for hexanuclear gold clusters is less stable than distorted geometries, and that to date, five other geometries for Au_6 clusters have been structurally characterised:

Formula	Structure	Reference
$[Au_6\{P(C_6H_4Me\text{-}2)_3\}_6]^{2+}$:	distorted octahedron	85
$[Au_6(PPh_3)_6]^{2+}$:	edge-sharing bitetrahedron	86
$[Au_6(S_2CC_6H_4Me\text{-}2)_6]$:	planar *raft*	87
$[Au_6(dppp)_4]^{2+}$:	tetrahedron with two gold-phosphine bridges	88
$[Au_6(\mu\text{-}O)_2(PCy_2Ph)_6]^{2+}$:	open chair conformation	89

The *aufbau agglomeration* [90] which produced the triple cluster was unprecedented, but opened up some very interesting possibilities, particularly the *template synthesis* of hexanuclear gold clusters, if the boron cages could be specifically cleaved off. Since then, the area of *multiple clusters* has grown, with examples of a ruthenaborane double cluster[90,91], and a cupracarborane quadruple cluster[92,†]. Subsequently, I investigated[93] the effect of increasing the cone angle [94] of the phosphine ligand to see if different products were obtained when very sterically-demanding phosphines were used. One successful[93]

† Although the $Cu_3(\mu\text{-}H)_3(C_2B_9H_9NC_5H_4CO_2CH_3)_3$ complex reported in reference 92 was not described as such, it can be regarded as a quadruple cluster where a central Cu_3 cluster is vertex-sharing with three cupracarborane clusters.

when very sterically-demanding phosphines were used. One successful[93] reaction was :-

$$Cy_3PAuCH_3 + B_{10}H_{14} \longrightarrow 5,6\text{-}\mu\text{-}(Cy_3PAu)\text{-}\textit{nido}\text{-}B_{10}H_{13}$$
(see Figure 2.1, page 37)

where one μ-H on decaborane has been isolobally substituted. Addition of Et_3PAuCH_3 to this complex led to the formation of the triple cluster, and the PCy_3 was detected as $OPCy_3$ by $^{31}P\text{-}\{^1H\}$ n.m.r. spectroscopy.

Since both of these reactions go in high yield, the opportunity arose to investigate the chemistry of these complexes. The 5,6-μ-(Cy_3PAu)-*nido*-$B_{10}H_{13}$ complex is of interest because it is a decaborane framework with an unusual substituent. As discussed previously, decaborane has a rich chemistry, so one aspect of particular interest was to see how this $\{AuPCy_3\}$ bridge influenced the behaviour of the B_{10} cage compared to that of decaborane. The main difference that is evident, between a hydrogen bridge and a gold-phosphine one, is that the gold atom can insert into the cage to become a vertex, and in the process, be formally oxidised to gold(III).

1.6 Experimental Techniques.

1.6.1 Characterisation of these Complexes.

The structures of new complexes described in this thesis are primarily determined by single crystal X-ray diffraction studies. This is the only technique which will precisely determine the geometry around the metal and the degree of ligation of a boron hydride to a metal, although the cage symmetry may be determined by $^{11}B\text{-}\{^1H\}$ n.m.r. spectroscopy. Another feature of auraborane chemistry, that was subsequently discovered, was that there were subtle distortions in these cages which profoundly influenced our ideas of the structures of these

complexes. In order to maximise the information obtained by these experiments, most of the later crystal structures were done at 185±1 K. This minimised the errors in the positions of the atoms by reducing thermal vibrations, and also inhibited solvent loss, which prevented several structures from being determined at room temperature due to crystal decay.

These studies were supplemented by ^{1}H-{^{11}B, selective} [95] and ^{11}B-{^{1}H} n.m.r. studies, particularly to obtain information on the position and number of cage hydrogens, which were not always located in the X-ray study. We also used ^{11}B(COSY) n.m.r. spectroscopy [96,97] to characterise several complexes. This is especially useful for asymmetric cages when the majority of boron atoms have individual resonances which can be assigned by this technique. However, when the cage has symmetry, and single resonances arise from several polyhedral boron atoms, less information is obtained. The cluster shape can be assigned by building up a connectivity map of the cluster, from which the number of vacant vertices can be determined. Its major disadvantage is that no information is directly gained on the metal-boron interaction which is especially problematic for nuclei such as ^{197}Au which are n.m.r.-silent. A straightforward explanation of this spin sequence, and how it works is available in the literature [98,99]. The use of U.V./visible spectroscopy to determine the nuclearity of a gold cluster is well documented[73], and was therefore used on the double and triple clusters.

The final technique used to obtain information on the oxidation state and geometry of the gold atom in the auraboranes was Mössbauer spectroscopy, and since this is a fairly uncommon technique, a brief explanation[100] of it and its uses could be useful.

The basic principle is as follows :- If an atom emits a quantum of radiation of energy E_{ν}, then by the conservation of momentum, the atom must recoil with

velocity v_R and energy E_R. For γ-radiation ($E_v = E_\gamma$), if the nuclear transition energy is E_t, then:

$$E_\gamma = E_t - E_R$$

For absorption, by the same arguments,

$$E_\gamma = E_t + E_R.$$

Since this is a resonant process, then an emitter cannot reabsorb, since the quanta are different. Since nuclear processes are not tuneable, the energy emitted by a standard sample is varied by the Doppler Effect, and so the energy differences are quoted in mms^{-1}, which is the relative velocity of the emitter and absorber. This technique is useful because E_t is very slightly influenced by the electronic environment of the nucleus. This is normally expressed as a (chemical) *isomer shift* (IS). In many respects, this is similar to the chemical shift concept in n.m.r. spectroscopy. Since ^{197}Au has a nuclear spin of 3/2, it normally has a quadrupolar splitting (QS) if the gold has an electric field gradient at the nucleus. This is produced in an anisotropic environment, and so gives information on the coordination around the gold atom. These two parameters, in tandem, can give information on the oxidation state of the gold, and it is this that we were particularly interested in, because this information is **crucial** in electron-counting arguments[101], but is very rarely independently determined. The actual spectroscopy was carried out by Dr. R.V. Parrish in Manchester, who also interpreted the spectra. Further information on this technique is readily available from the literature [102-104].

1.6.2 Analysis of the Structures.

EHMO Calculations

In order to try and understand why these particular cluster geometries were preferred, the electronic structures of key complexes were probed by the use of EHMO calculations [105,106]. In this theory, molecular orbitals (MO's) are derived by the linear combination of atomic orbitals (LCAO) approach. i.e. if Ψ is the mathematical function for an MO, and ψ_1, ψ_2 are the corresponding AO's then:

$$\Psi = c_i\psi_i + c_j\psi_j$$

where c_i and c_j are the coefficients. There are two useful parameters which can be obtained from an EHMO calculation. Firstly there is the bond overlap population between two atoms, r and s, defined by:-

$$P_{rs} = \sum_{i}\sum_{n}(Nc_{in}c_{jn}S_{ij})$$

where there are *n* MO's; c_{in} is the coefficient of ψ_i in the n^{th} MO, S_{ij} is the overlap integral, given by $S_{ij} = \int\psi_i\psi_j$ and N is the number of electrons in the orbital (N = 0,1,2 only).

P_{rs} is a measure of the bond strength between atoms r and s. For various reasons, this value is not normally integral; for example a C-H single bond has a P_{CH} of about 0.7.

The net atomic charge on each atom is then calculated using the formula:

$$q(i) = \sum_{i}\sum_{n}(Nc_{in}^{2} + Nc_{in}c_{jn}S_{ij})$$

where q(i) is the atomic charge contribution from the i^{th} orbital. The atomic charge, q, is then given by:

$$q = \sum_{i} q(i)$$

If the atom has atomic number, z, then the net atomic charge is given simply by q - z.

As its name implies, the n.a.c. is a measure of the ionic character resident on an atom. Unfortunately, the electronegativities of hydrogen and boron are very similar (2.0 and 2.1 respectively). The effect of this is that the program calculates the hydrogen atoms to have a negative charge, ie hydridic, whereas chemically they are normally regarded as protonic.

However the main interest in these figures normally lies in the relative charges on atoms of the element, for example in determining which hydrogen atom is the most acidic. In these cases, the fact that the values are negative instead of positive does not matter, because the interest is solely in their relative values.

Interpretation of the Experimentally-Determined Structures

All of the structures reported in this thesis have been characterised crystallographically, and so a set of atomic coordinates has been calculated. This enables the calculation of many molecular parameters such as bond lengths and angles. However Edinburgh software (the computer program *CALC*[107]) has additional features of a more sophisticated nature. These include the ability to calculate how far from a specified plane any atom is : a feature used extensively in Chapter 3.

Another feature is the calculation of a *r.m.s. misfit* (in pm) for two fragments with the same numbering scheme. This maps every pair of atoms (B[1] with B[1'], etc.) and then, as its name implies, calculates the square root of the mean of the squares of the difference in the positions of the two atoms in each pair.

This technique has tremendous potential as a means of analysing borane and metallaborane geometries. Its main advantage is that it considers the geometry of

the whole, or a large part of, the cluster. This is very useful when such very delocalised systems are considered.

Whilst a change in skeletal geometry is probably the major influence in the variation in atomic positions, there are other factors which should be considered as well. The first of these is the experimental error in the atomic positions. This is more serious in early determinations which were less precise than is possible with modern instrumentation. Comparison of complexes which have cages which are unambiguously of the same skeletal type should enable the setting of a 'baseline' of insignificance for these values (see later).

A second important influence is the well-known effect[108] of H-bridges on connectivity lengths. This will obviously cause variation in atomic positions and will thus alter the misfit value. This can be overcome by using model complexes which have H-bridges in the same positions as they are in the complex being investigated. This is however not always possible but should be taken into consideration.

A final consideration is that in the determination of the structures of some of the metallaborane derivatives of the third row transition metals, the cage H atoms were not located or refined. This means that the determined B atom position is actually that of the {B-H} fragment, and so the position of the boron atom will be displaced slightly away from the cluster centroid. This is potentially a serious source of error as these deviations are in a consistent direction because the first action of the computer program is to superimpose the cluster centroids, and so the misfit value will be greater than expected.

Comparison of $\{B_{10}\}$ Cages

Figure 1.6, overleaf, shows the parent *nido* and *arachno* ten-vertex fragments. As can be seen, they appear very similar in geometry and so make a good test of

(a) (b)

Figure 1.6. The structures of (a) *nido* and (b) *arachno* 10 vertex fragments.

Table 1.1. The Misfit Values for the Comparisons, and the Individual Misfits Between Atoms.

Compar^n	misfit	B(1)	B(2)	B(3)	B(4)	B(5)	B(6)	B(7)	B(8)	B(9)	B(10)
(7)/(8)	6.4	3.9	4.3	3.1	3.3	7.4	6.2	4.8	7.6	12.0	6.4
(7)/(9)	7.7	4.5	4.4	1.3	4.6	14.7	4.2	4.7	3.1	15.8	4.2
(7)/(10)	12.0	11.5	11.0	10.8	14.4	9.3	16.4	8.4	9.0	16.2	9.3
(7)/(11)	17.2	14.2	7.3	12.2	12.3	8.9	33.3	6.3	9.5	31.2	13.2
(8)/(9)	6.7	3.5	2.9	5.6	5.3	3.9	2.9	1.2	6.1	11.7	4.8
(8)/(10)	12.7	7.9	10.1	13.3	11.6	10.6	12.4	12.3	13.6	20.3	10.8
(8)/(11)	17.2	11.7	7.3	13.8	9.6	12.7	29.3	9.9	12.2	33.8	9.4
(9)/(10)	12.1	9.3	7.3	10.7	14.3	16.5	14.3	8.0	10.9	16.3	9.2
(9)/(11)	15.2	10.5	3.6	12.0	11.9	13.2	30.9	7.9	11.3	22.0	10.6
(10)/(11)	9.8	5.5	4.0	1.9	2.8	3.7	20.3	3.7	2.3	19.8	8.6

the sensitivity of this method. The parent species are $[B_{10}H_{14}]$, **(7)**, and $[B_{10}H_{14}]^{2-}$, **(10)**, both of whose structures have been determined[109,110]. The main differences found experimentally included the lengths of the B(5)-B(10) and B(7)-B(8) connectivities : in **(7)** they were both 197.3(4)pm and in **(10)** they were 188.2(12) and 189.2(12)pm respectively. In contrast to this contraction in the length of the open face, the mean B-B connectivity in **(7)** was 179.0 pm, whereas in **(10)** it has increased to 180.3 pm. Structurally, the other big difference is that **(7)** has 4 μ-H atoms and **(10)** has 2 μ-H atoms and two $\{BH_2\}$ fragments.

The following complexes were used in the comparisons which were undertaken to calibrate and test this method.

$B_{10}H_{14}$	**(7)**
5,6-μ-(Cy_3PAu)-*nido*-$B_{10}H_{13}$	**(8)**
$[B_{10}H_{13}]^-$	**(9)**
$[B_{10}H_{14}]^{2-}$	**(10)**
$[B_{11}H_{13}]^{2-}$	**(11)**

(7), **(8)**, and **(9)**[112] all have *nido*-$\{B_{10}\}$ cages albeit with minor structural distortions, and so comparison of their structures will reveal at what level the misfit is insignificant. Both **(10)** and **(11)**[111] have *arachno*-$\{B_{10}\}$ cages so this comparison has a similar function. Comparison between the two groups will show how significant the change in geometry is. The results are listed in Table 1.1. on page 28.

These results are interesting. Note how the values for the comparisons between two *nido*-$\{B_{10}\}$ cages vary from 6.4 - 7.7 pm, whilst the comparison between the two *arachno*-$\{B_{10}\}$ cages was slightly greater at 9.8 pm, although it should be remembered that the structure of $[B_{11}H_{13}]^{2-}$ was determined[111] in

1967, and so is probably not as accurate as modern determinations.

When the two different cage geometries are compared, the misfit value varies from 12.0 to 17.2 pm, values which are significantly greater.

These results suggest that using this 'idealisation' is useful, although the range of values for slightly different clusters is small, and so very careful interpretation of the results is required.

1.7 Conclusions.

In conclusion, this introduction has shown that, at the time of starting this work, there was a gap in metallaborane chemistry: that of the group 1b derivatives. The auracarborane chemistry which had been investigated to a greater extent, showed that there was a tremendous variety in the ways that gold could bond to borane clusters. In auraborane chemistry, however, the initial reactions had failed to synthesise any complexes with gold-boron bonds, although by the mid-1980's, several species had finally been characterised.

The development of the gold-methyl/neutral borane approach to the synthesis of auraboranes had yielded several novel species in high yield, thereby offering the opportunity to investigate their derivative chemistry.

The techniques for their characterisation of these complexes have been introduced and the less common ones briefly discussed. The use of Mössbauer spectroscopy to probe the electronic structure, together with EHMO calculations meant that the structure of these complexes could be examined very closely, and the effectiveness of applying Wade's Rules to metallaboranes be assessed.

Chapter 2:

Studies on 5,6-μ-(AuPR$_3$)-*nido*-B$_{10}$H$_{13}$.

2.1 Introduction.

This chapter reports work carried out on the complexes 5,6-μ-(Cy$_3$PAu)-*nido*-B$_{10}$H$_{13}$, **(8a)**, and 5,6-μ-(*o*-tolyl$_3$PAu)-*nido*-B$_{10}$H$_{13}$, **(8b)**. First synthetic routes to these complexes are reviewed, and then some experiments designed to probe the mechanism of their formation are discussed.

The structure of **(8a)** was determined by a single crystal X-ray diffraction study. This suggested that there was an unusual interaction present, and EHMO calculations on model complexes were used to probe this. The subsequent determination of the structure of **(8b)** confirmed that most, although not all of the distortions from the cage architecture of B$_{10}$H$_{14}$ that were shown by **(8a)** are also present here.

Next the results obtained from spectroscopic techniques (particularly n.m.r.) are discussed in terms of the solid state structure. The ^{11}B-{^{1}H} n.m.r. spectrum was assigned using a ^{11}B(COSY) n.m.r. spectrum, and this was also used to interpret some of the bonding within the cage. The Mössbauer spectrum was also acquired to establish what signal arose from a linear Au(I) species bonded to a {B$_{10}$} cage. In addition, the mass spectrum was recorded, to see if any useful information could be obtained by this technique.

The next section discusses the reactions of this complex with acids, bases, and electron-pair donors. As a consequence of identifying the products obtained in these reactions, the reactivity of this species is rationalised in terms of the internal electronic structure.

2.2 The Synthesis and Mechanism of Formation of this Complex.

2.2.1 Synthesis.

As discussed in chapter 1, **(8a)** has been synthesised (75% yield) by the direct reaction of decaborane(14) and methyltricyclohexylphosphinegold(I). A coworker, A.J. McLennan, has subsequently shown[113] that **(8a)** can also be synthesised (51% yield) by the reaction:-

$$[NHEt_3]^+ [B_{10}H_{13}]^- + AuCl(PCy_3) \longrightarrow Cy_3PAuB_{10}H_{13} + [NHEt_3]^+ Cl^-$$

However, if a phosphine with a smaller cone angle is used in either reaction, then other products are obtained (see Chapters 4 and 5).

2.2.2 Mechanistic Studies.

We were interested in the mechanism of formation of **(8a)**, partly because it could shed light on the formation of triple clusters, and partly because an intermediate could conceivably contain a direct gold-hydrogen bond, there being no known[114] examples of monometallic gold hydrides. We concentrated on the reaction of decaborane with the gold methyl complex. There were two main reasons for this. It was more likely to involve a gold hydride, because the borane has still to lose any of its μ-H's, and also the reaction is much cleaner with fewer byproducts.

Initially the reaction was followed by variable temperature $^{31}P-\{^1H\}$ n.m.r. spectroscopy. This failed to show any resonances apart from those assignable to either starting materials or products. A second experiment using $^1H-\{^{11}B\}$ n.m.r. spectroscopy also failed to detect an intermediate, and so alternative techniques were pursued.

One way of detecting the presence of a metal hydride is by utilising the reaction[115]:-

$$CCl_4 + L_nM\text{-}H \longrightarrow CHCl_3 + L_nM\text{-}Cl$$

where L_n is the rest of the ligand set around the metal centre.

Trichloromethane is readily identified by ^1H n.m.r. spectroscopy (δ^1H = 7.25 ppm). Although we have found that the reaction of $B_{10}H_{14}$ with $AuMe(PCy_3)$ in the presence of excess tetrachloromethane using CD_2Cl_2 as solvent affords trichloromethane, we cannot conclude that this implies a gold-hydride intermediate since it was also found that both $B_{10}H_{14}$ and **(8a)** react in CD_2Cl_2 solution with CCl_4 to produce trichloromethane.

Precise mechanistic information is therefore still lacking, although bench observations provide some evidence. When $AuMe(PR_3)$ is added to $B_{10}H_{14}$, the initially colourless solution goes yellow, followed by decolourisation with concomitant gaseous evolution. This implies that the initial stages of the reaction involve oxidation of the gold atom, followed by reductive elimination to produce **(8)**.

Two structures for the Au(III) intermediate that such a reaction could involve are outlined in Scheme 2, overleaf, . Route (a) involves insertion of $[AuMe(PR_3)]$ into the B(5)-H-B(6) bond of decaborane to afford the transient species 5,6-μ-$[Au^{III}(H)(Me)(PR_3)]$-*nido*-$B_{10}H_{13}$. This species would be unique in having a terminal Au-H bond.

Alternatively, route (b) involves the Au(III) atom as a polyhedral vertex in an 11-atom polyhedron with a Au-H-B bridging function. Whilst the precise cage geometry in such a system would depend on how many electrons the gold atom would utilise in cage bonding, a similar mode of bonding is found in the $[(B_{10}H_{12})Au(B_{10}H_{13})]^{2-}$ anion (see figure 4.2, page 117) where the gold atom is

Scheme 2. Possible Intermediates in the Reaction of $B_{10}H_{14}$ with $MeAu(PCy_3)$.

Au ◍ BH ◯ H ○

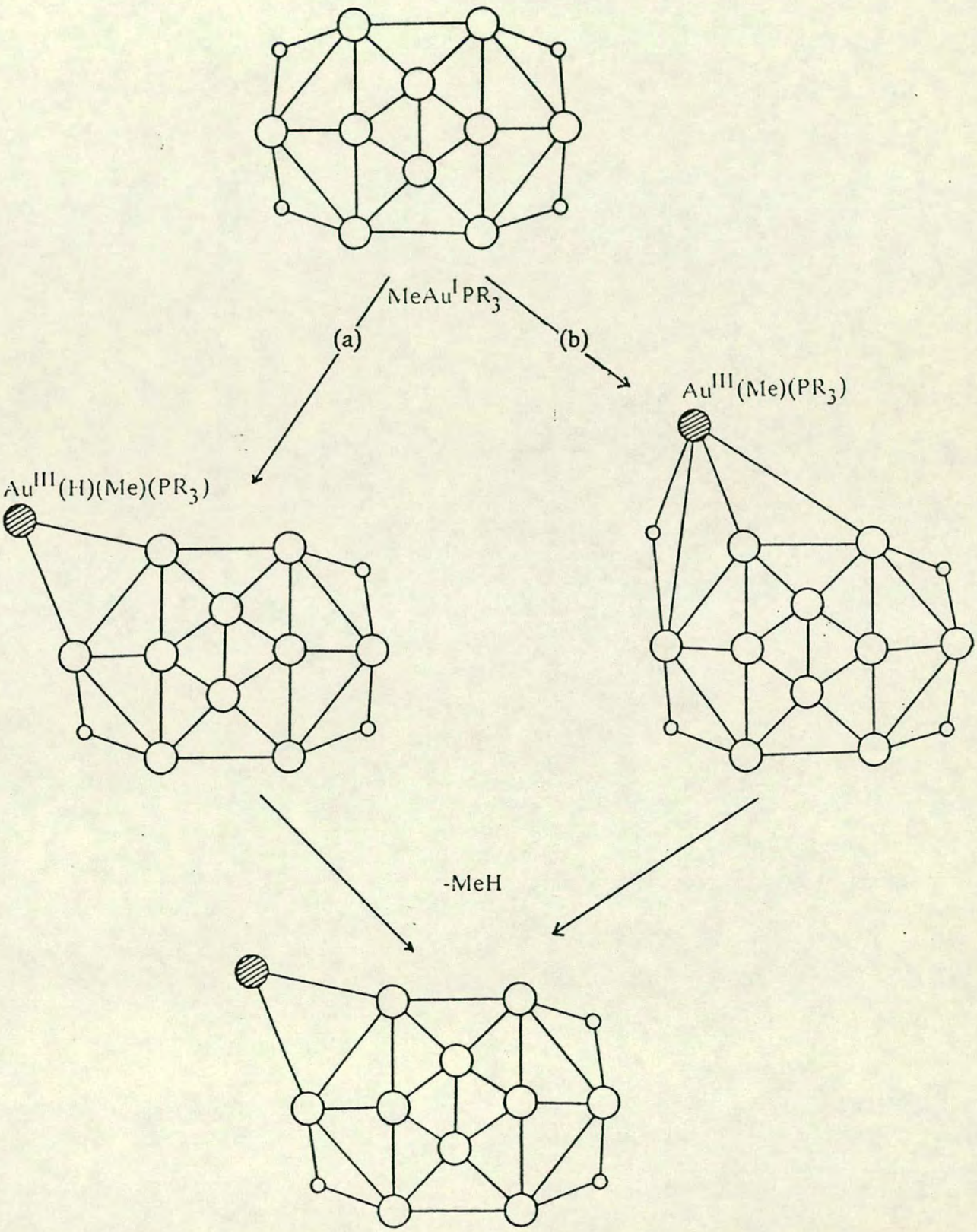

a 3-connected vertex in an *arachno*-docosahedron. Vertex to bridge 'reductive slipping' with concomitant loss of MeH would yield **(8)**. Another attraction of this route is that all proven gold-hydride species characterised to date involve heteronuclear Au-H-X fragments.

2.3 The Structure of (8a).

Initially, this was identified by a single crystal X-ray diffraction study, which had been done at room temperature, on a limited data set ($\Theta_{max} = 20^{o}$, Mo-K_{α} radiation) and measuring the intensities relatively quickly (scan speeds 1.27 to 5.49 $^{o}min^{-1}$). Consequently the errors on the boron-boron internuclear distances were quite high, and when the individual bond lengths were examined, to see if the presence of the $\{AuPCy_3\}$ bridge caused any distortions in the cage architecture relative to that of decaborane, it was found that, due to the large errors, variations in bond lengths were of dubious statistical significance. For present purposes statistical significance is defined as a variation greater than three times the estimated standard deviation (e.s.d.) of that variation. For the difference (Δ) in two quantities, x and y, where each has an associated e.s.d., σ_x and σ_y, then the e.s.d. of the difference, σ_Δ, is given by the formula:-

$$\sigma_\Delta = \surd(\sigma_x^2 + \sigma_y^2)$$

At this point, it is worth emphasising that the variation in bond lengths can be assigned to the presence of the $\{AuPCy_3\}$ bridge when the bonds are equivalent *except for and only for* the presence of the $\{AuPCy_3\}$ bridge.

It was therefore decided to repeat the single crystal X-ray diffraction study of **(8a)** at very low temperature and to collect the data to higher angle and more slowly (and hence more precisely). The experimental procedure used in this redetermination is outlined in Section 6.5, starting on page 187. The structure is

shown in Figure 2.1 (overleaf) and some of the important bond lengths and angles are listed in Table 2.1 (page 60). All the bond lengths and angles, as well as the rest of the crystallographic data appear as part of Appendix 2 (starting on page 204).

This molecule is derived from decaborane by the isolobal substitution of one μ-H atom by a $\{AuPCy_3\}$ fragment. Despite there being many examples of isolobal substitution of bridging hydrides in the smaller boranes (e.g. 2,3-μ-$(AuPPh_3)$-B_5H_8, ref. 81), 5,6-μ-(Cy_3PAu)-*nido*-$B_{10}H_{13}$, and a cadmaborane $[(OEt_2)_2CdB_{10}H_{12}]_2$, in which the cadmium atom is η^2-ligated to both of two cages[57] are the only two structurally characterised metallaboranes with $\{B_{10}\}$ cages which have such a function.

There are two features of interest about the shape of **(8a)**. First is the steric protection afforded to the open face by one cyclohexyl ring which 'overhangs' it. This may be one reason why this complex can be isolated, unlike analogues with smaller phosphines, which, despite numerous attempts, have still not been successfully synthesised. However this steric protection may make derivatisation of this complex difficult by protecting the open face against added reagents.

Secondly, this molecule is chiral. The two enantiomers are shown in Figure 2.2 (page 38). Since the space group ($P2_1/a$) is centrosymmetric, it must consist of a racemic mixture of the two enantiomers. There are few reports (see for example ref. 15) of chiral metallaboranes, and there are no reports of successful attempts to resolve the two enantiomers. Until more is known about their derivative chemistry, enabling reasonable chemical routes to this separation to be devised, the only way in which the enantiomers could be separated is by Pasteur's original method - separation of the two different crystal forms. Since the crystals of **(8a)** are racemic, this is not an option in this case, and no pure enantiomers

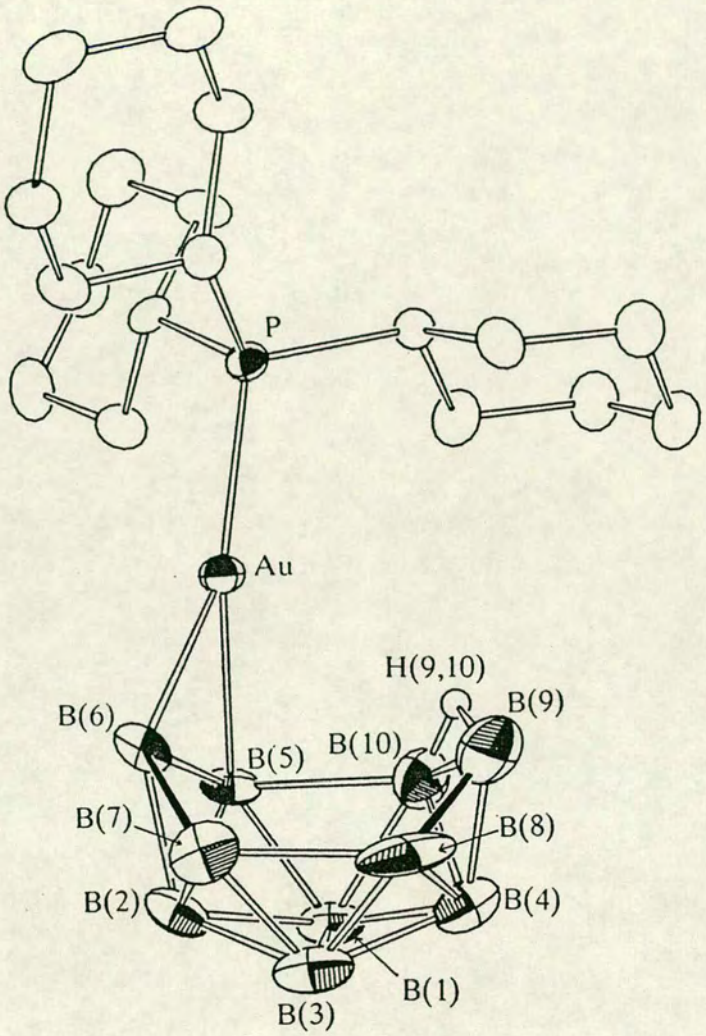

Figure 2.1. The molecular structure of 5,6-μ-(Cy_3PAu)-*nido*-$B_{10}H_{13}$ showing the μ-H which interacts with the gold.

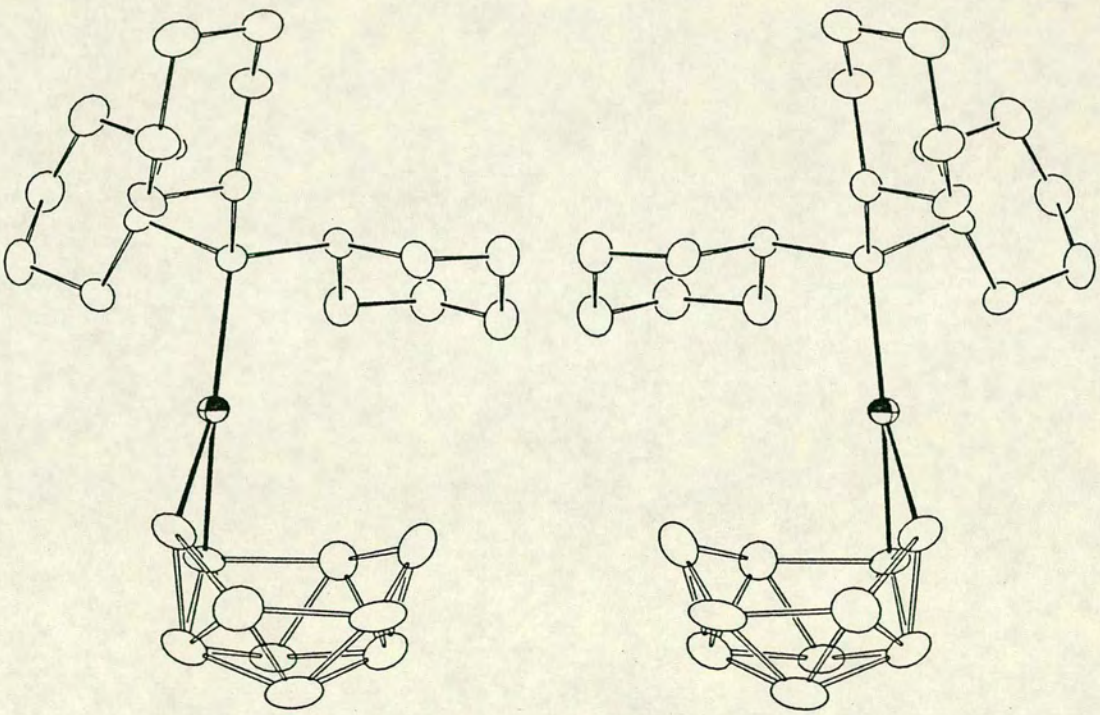

Figure 2.2. The two enantiomers of **(8a)**.

have been isolated.

Three suggestions for their resolution are:

(8a) to use a chiral phosphine on the gold. This would result in the synthesis of diastereomers, and hence their separation would be more straightforward.

(2) to reprotonate the deprotonated $[Cy_3PAuB_{10}H_{12}]^-$ anion with a chiral acid in the hope that this would favour formation of one enantiomer.

(3) to do the reaction in a chiral solvent, and hope that this will favour formation of one enantiomer.

The gold atom is a conventional[116] linear Au(I) species: the P-Au-midpoint(B5,B6) angle is 176.4(4)°.

The structure of several species with $\{AuPCy_3\}$ fragments have been determined crystallographically, and so comparison of the Au-P bond lengths may yield information on the cage-gold bonding. The structure of the $[(Cy_3P)_2Au]^+$ cation has been determined for its Cl^- [117] and SCN^- [118] salts, and the Au-P distances are 232.6(2),† 229.5(11) and 231.6(13) pm. In Cy_3PAuCl [117], it is 224.2(4) pm; and for the two clusters $(PCy_3Au)(PtPCy_3)_3L_3$, $L_3 = (CO)_3$ [119], and $(CO)_2(SO_2)$ [120], it is 227(3), and 224.3(7) pm respectively. Since the Au-P distance in **(8a)** (230.88(21) pm) is most similar to that in the $[(Cy_3P)_2Au]^+$ cation, this would suggest that the boron cage has a very similar trans influence to that of a trialkylphosphine.

The Au-B(5) and Au-B(6) connectivities are 224.6(10) and 227.1(10) pm long. This compares against the two Au-B distances in $Ph_3PAuB_5H_8$ [81] of 226.9(12)

† In the chloride salt, the Au atom is located on a crystallographic inversion centre and so there is only one independent Au-P distance.

and 228.1(8) pm, and those of 230.8(7) and 225.6(8) in $(Ph_3PAu)(CpNi)C_2B_8H_{10}$[62]. Hence the bond lengths are very similar, although the comparison is not strictly valid because of the different phosphines on the gold atoms.

As discussed in Chapter 1, the geometry of the B_{10} cage in $B_{10}H_{14}$ was compared against that in **(8a)**. The overall misfit of the two cages was only 6.4 pm, indicating that the two cages have the same basic shape.

Individual misfits are:

B(1) 3.9	B(3) 3.1	B(5) 7.4	B(7) 4.8	B(9) 12.0
B(2) 4.3	B(4) 3.3	B(6) 6.2	B(8) 7.6	B(10) 6.4

As can be seen from this, atoms B(5), B(6), B(8), B(9), and B(10) were the most badly fitted to the shape of the $B_{10}H_{14}$ cage.

Whilst this global shape is almost identical, there are some subtle differences in the individual internuclear distances. The most notable feature of the structure of decaborane itself is the very long B(5)-B(10) and B(7)-B(8) connectivities of 197.3(4) pm. These have lengthened to 200.1(16) pm and 201.2(18) pm, respectively, in **(8a)**. Whilst most of the boron-boron connectivities have unexceptional lengths, there are several interesting features about this structure. First, the B(8)-B(9) connectivity is unusually short (164.3(20) pm) for a H-bridged one. This effect is discussed later.

Secondly, the gold bridges the B(5)-B(6) connectivity in an asymmetric manner - it is bent slightly towards the B(9)-B(10) connectivity, as evidenced by the difference in the P-Au-B angles (Δ/σ = 10.25), and by the shorter Au-B(5) connectivity (Δ/σ = 1.79). Also the B(9)-B(10) connectivity is the longest of the four bridged connectivities (Δ/σ = 4.53, 4.17, 8.48, compared against the B(5)-B(6), B(6)-B(7), and B(8)-B(9) connectivities respectively).

Bond lengthening in these systems is normally associated[108.‡] with removal of electron density from that bond. This is shown, for example in the $B_{10}H_{14}$/ $[B_{10}H_{13}]^-$ system where the bond in decaborane which is deprotonated is shortened from 178.2 pm to 165.7(5) pm. This can explained, simply, as due to an increase in interatomic electron density caused by going from a localised 3-centre, 2-electron bond to a 2-centre, 2-electron one.

The H atom bridging the B(9)-B(10) connectivity (H[9,10]) is of special interest here. Iterative full-matrix, least-squares refinement and ΔF synthesis suggested that H[9,10] was in the following position.

Fractional Coordinates			Distance (/pm) from		
x	y	z	B(9)	B(10)	Au
0.364	0.234	0.733	116.9	108.4	314.3

Since this atom, like the rest of the cage H atoms, could not subsequently be satisfactorily refined, its position was included in the structure refinement, as fixed. In this (unrefined) position, the H atom is slightly tilted towards B(10), although this is of dubious significance, given the large uncertainty in the position of a H atom in the presence of gold (because H(9,10) was not refined, no e.s.d.'s were calculated for the B-H distances). It is also within bonding distance of the gold atom, although that does not necessarily mean that there is a bond between the two atoms.

Nevertheless, these observations, together with the asymmetric manner in which the gold bridges the B(5)-B(6) edge, are consistent with a bonding interaction between the gold atom and H[9,10]. There has been a report [121] of a similar sort of interaction (albeit Hg..H) in a mercuracobaltacarborane. In that case, the paper reported the reactions on the next page.

---

‡There are exceptions. Best known is the octahydrotriborate anion, see ref. 108.

$$[\{Cp\}CoMe_2C_2B_3H_4]^- + HgCl_2 \xrightarrow[\textbf{(12)}]{} [\{Cp\}CoMe_2C_2B_3H_4]HgCl$$

$$[\{Cp\}CoMe_2C_2B_3H_4]HgCl + [\{Cp\}CoMe_2C_2B_3H_4]^- \xrightarrow[\textbf{(13)}]{} [\{Cp\}CoMe_2C_2B_3H_4]_2Hg$$

where {Cp} was either Cp (**(12a)** or **(13a)**) or C_5Me_5 (**(12b)** or **(13b)**) respectively. **(12b)** and **(13a)** were both characterised crystallographically and spectroscopically, and some important results are:-

	(12b)	**(13a)**
Hg-μ-H distance/pm	279(9)	242(9)
tilt[a] from Co-B(5)-B(6) plane/°	9.5	-10.9
δ^1H/ppm[b]	-5.58	-6.37
$^2J_{Hg-H}$/Hz	67	113

Notes

(a) + signifies tilt towards the Hg atom, and - away from the Hg atom.

(b) **(12b)** in C_6D_6 and **(13a)** in $CDCl_3$.

This evidence is quite conclusive that there is a significant, although small interaction between the mercury and the bridging hydrogen. It may be related to the well-known [122] weak intermolecular Hg-Cl interactions found in many species, including **(12b)**. The n.m.r. evidence, particularly the deshielding of the δ^1H resonance, suggests moreover that in this interaction, electron-density is formally donated from the μ-H atom to the metal.

It is also similar to M-H agostic interactions[123] common in organometallic chemistry, but there are several differences.

First, the Au has a d^{10} configuration and is therefore relatively electron-rich. Some of the evidence suggests that the B(9)-B(10) connectivity has *lost* electron density, would imply that an electron-deficient centre is donating electron-density in bonding with an electron-rich centre. Secondly, it is a μ-H, and agostic interactions are with terminal hydrides.

In order to investigate this interaction further, EHMO calculations were performed on model complexes. All of the calculations discussed in this thesis were carried out using the same procedure. In order that the difference in bonding between auraboranes and their borane analogues could be analysed, the $\{B_{10}\}$ cage in the model was the same as that observed for $B_{10}H_{14}$, which is located[109] on a crystallographic two-fold axis. Onto this cage was superimposed the gold (and its ligand(s)) in the same manner as that observed experimentally for the particular product in question. Due to limitations in the computer program on the number of atoms permitted in the model, trialkylphosphine ligands were replaced by $\{PH_3\}$.

The coordinates of the atoms in the model are given in Appendix 3, starting on page 279. The program uses a locally-modified version of ICON8 [105], and orbital exponents and H_{ii}'s are also in Appendix 3. The calculations were charge-iterated at the METH1 level, and used the modified H_{ij} formula[106].

The two models discussed here were $[H_3PAuB_{10}H_{13}]$, **(8c)**, and the anion $[H_3PAuB_{10}H_{12}]^-$, **(14)**, with the same structure except that $[H(9,10)]^+$ has been omitted. Some useful parameters which were obtained from these calculations are listed in Table 2.2, on page 61. The most significant result is that there is a small, but positive Mulliken overlap population, between the gold and H(9,10) (0.010), and between the Au and B(10) (0.018).

In order to try and understand how H(9,10) interacts with the rest of the complex, the following approach was used. If the complex is deprotonated, then on reprotonation, the empty 1s AO of an incoming proton will interact with the HOMO of the anion. Thus performing an EHMO calculation on **(14)**, and examining its HOMO will show how the hydrogen atom interacts with the rest of the complex. A similar approach was used to interpret the structure of $[B_{10}H_{13}]^-$

(see Chapter 3 and ref. 112).

The calculation on **(14)** was used to analyse this Au..H(9,10) interaction. The HOMO (orbital 43, Figure 2.3, overleaf) has its major contribution from B(9) and B(10) as expected. However, there is also a significant contribution from Au(s/p_x) and B(6) ($p_x/p_y/p_z$). This contribution from Au and B(6) arises from a Au hybrid orbital which is hybridised in order to bond to B(6). There is a small lobe on the other side of the gold which points at the B(9)-B(10) connectivity, and it is this part of the orbital which interacts with the proton. Since the commonly directed contributions from Au, B(9), and B(10) are all in phase, there is a bonding interaction between the Au and H(9,10) upon protonation of **(14)**.

The calculations can be used to further rationalise the observed distortions in **(8a)**. When two AO's (one occupied, the other empty) interact, the character of the BMO formed is comprised of contributions from both orbitals, and so the previously occupied orbital is 'deoccupied' to an extent. In this case, this means that the B(6)-Au bonding is weakened on protonation (Mulliken overlap populations: in **(8c)**, B(5)-Au = 0.334, and B(6)-Au = 0.276; in **(14)** B(5)-Au is 0.336, and B(6)-Au is 0.281), and so the Au-B(6) connectivity is lengthened.

Similarly, the B(9)-B(10) connectivity is lengthened because the B-H-B BMO overlaps with the Au hybrid to become a B-H-Au-B 4-centre, 2-electron bond, thereby weakening the boron-boron bonding.

The final significant bond length difference between **(8a)** and $B_{10}H_{14}$ is the unusually short B(8)-B(9) connectivity in **(8a)**. The thermal ellipsoid describing B(8) (Figure 2.1, page 37) is very anisotropic, and its major axis is aligned in a similar direction to the B(8)-B(9) connectivity. This short bond may therefore be a crystallographic quirk. In the structure of **(8b)** discussed in the next section, the B(8)-B(9) connectivity is much longer, at 177.9(24)pm.

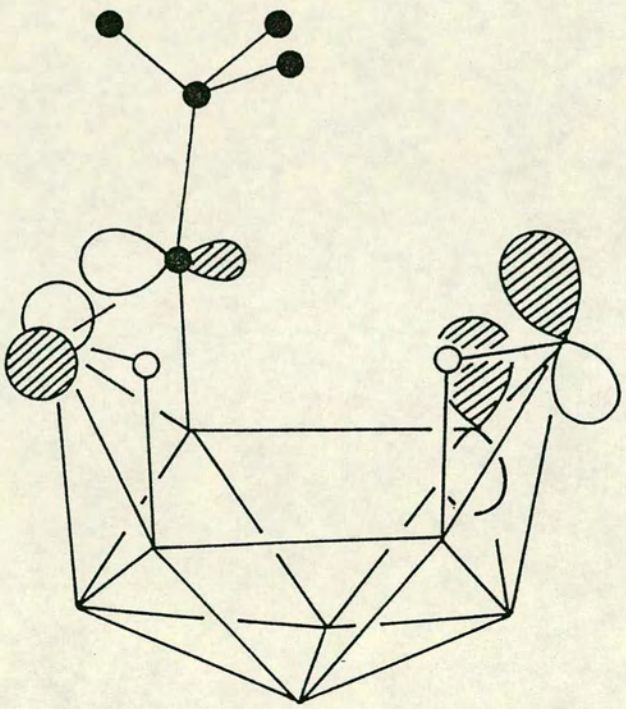

Figure 2.3. The bonding molecular orbital for the gold-(μ-H) interaction.

2.4 The Structure of (8b).

In order to fully characterise **(8)**, the $^{1}H-\{^{11}B\}$, ^{11}B, and $^{11}B-\{^{1}H\}$ n.m.r. spectra were recorded. However **(8a)** has one practical disadvantage - it is very insoluble in common solvents. It was therefore decided to try and synthesise analogous complexes with different phosphine ligands on the gold to try to improve solubility.

As discussed in the introduction, the use of $AuMe(PR_3)$ when the phosphine has a small cone angle leads to the formation of triple clusters, and so another sterically-demanding phosphine was used: tri(*o*-tolyl)phosphine. Accordingly, methyltri(*o*-tolyl)phosphinegold(I) was synthesised (see Chapter 6) and reacted with decaborane in 1:1 molar ratios. A colourless product was obtained and structurally characterised as 5,6-μ-(*o*-tolyl$_3$PAu)-*nido*-$B_{10}H_{13}$, **(8b)**.

An ORTEP plot of **(8b)** is shown in Figure 2.4, overleaf, some important bond lengths and angles are given in Table 2.3, on page 62, and the crystallographic details start on page 211. The structure of **(8b)** is very similar to that of **(8a)**. The misfit of the two $\{B_{10}\}$ cages is 5.1 pm, and when the gold (5.0) and then the phosphorus (5.3 pm) atoms are included, there is negligible difference. The principal bond length differences are that in **(8a)**, the Au-B(6) (227.0(10)/232.5(16); Δ/σ = 2.9), B(7)-B(8) (201.0(18)/208.6(23); Δ/σ = 2.6), and B(8)-B(9) (164.3(20)/177.9(24); Δ/σ = 4.25) connectivities are all shorter.

2.5 N.M.R. Studies.

Since **(8b)** is more soluble than its cyclohexyl counterpart, it allowed the acquisition of an ^{11}B(COSY) n.m.r. spectrum, because these take a considerable time to accumulate (usually at least overnight) and having more of the compound in solution mitigates this to an extent.

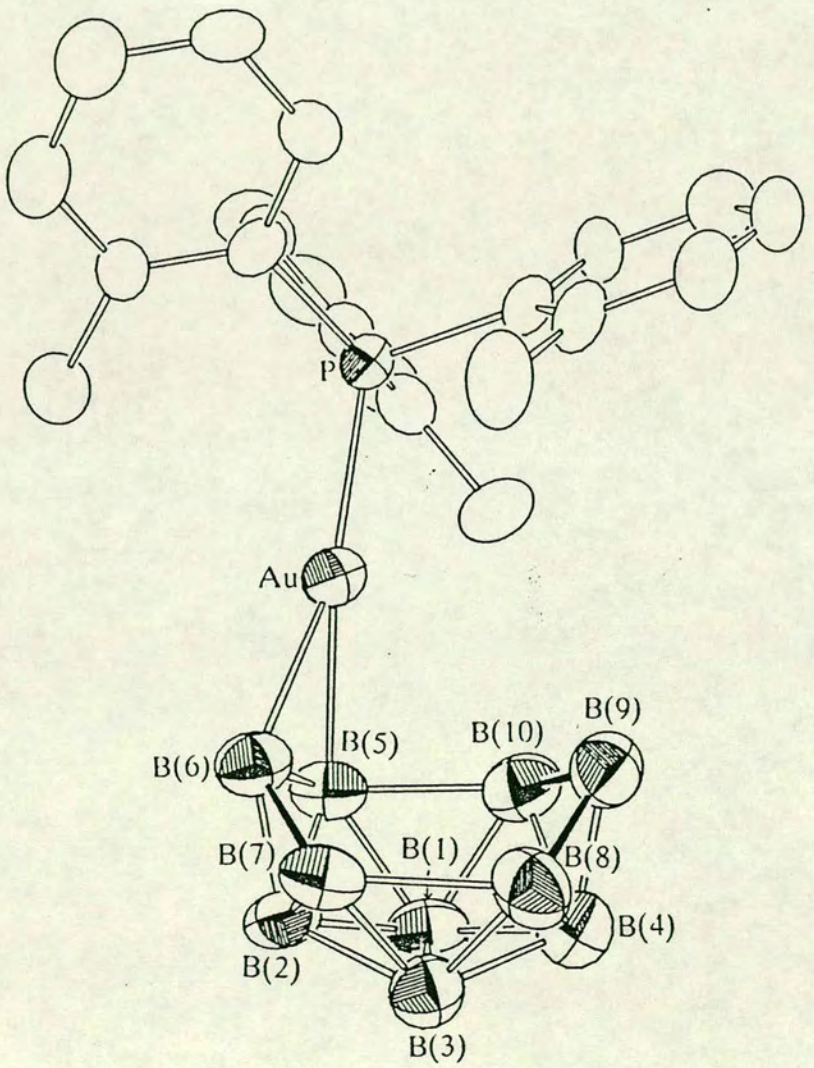

Figure 2.4. The molecular structure of 5,6-μ-(*o*-tolyl$_3$PAu)-*nido*-$B_{10}H_{13}$.

The ^{31}P-$\{^{1}H\}$ n.m.r. spectra of both **(8a)** and **(8b)** consist of one broad singlet, the width at half-height being of the order of *ca.* 90 Hz. This compares against the spectrum of, for example $[(Cy_3P)_2Au]^+$, which has a half-height width of *ca.* 10 Hz. This broadening has also been observed in phosphineplatinaboranes[15], where it was explained as due to 'thermal coupling'[124] to the boron atoms. The main disadvantage is the increased acquisition times necessary to obtain a reasonable peak *height*: noise ratio. Its main advantage is that it is also indicative of a phosphine bonded to a gold which is ligated to a boron cage, and so shows that reaction has occurred.

As expected, the ^{11}B-$\{^{1}H\}$ n.m.r. spectrum (Figure 2.5(a), overleaf) shows that the cage has no symmetry in solution, consistent with the crystal structure. However there is an accidental coincidence at $\delta^{11}B$ = -1.00 ppm, meaning that less information than possible was obtainable. Since there are so many individual resonances, they should be assignable by using an ^{11}B(COSY) n.m.r. spectrum. Not only would this increase the amount of information on this compound, but it would also give information on the different bonding capability of a bridging H atom and a μ-$\{AuPR_3\}$. from the different boron chemical shifts.

The ^{11}B(COSY) n.m.r. spectrum (Figure 2.5(b), next page) was acquired and interpreted by Dr. David Reed[113]. Its assignment was mostly based on its analogy with decaborane whose multinuclear n.m.r. spectra have been thoroughly investigated[125]. The proposed assignments, and the spectral details are given in Table 2.4, on page 63. The ^{11}B-$\{^{1}H\}$ n.m.r. spectrum shows that the $\{AuPR_3\}$ bridge is not exchanging at room temperature, otherwise, on the n.m.r. timescale, atoms B(5),B(7), B(8) and B(10), for example, would become equivalent, and this is evidently not so.

It has been observed[126] that H-bridged connectivities show no coupling

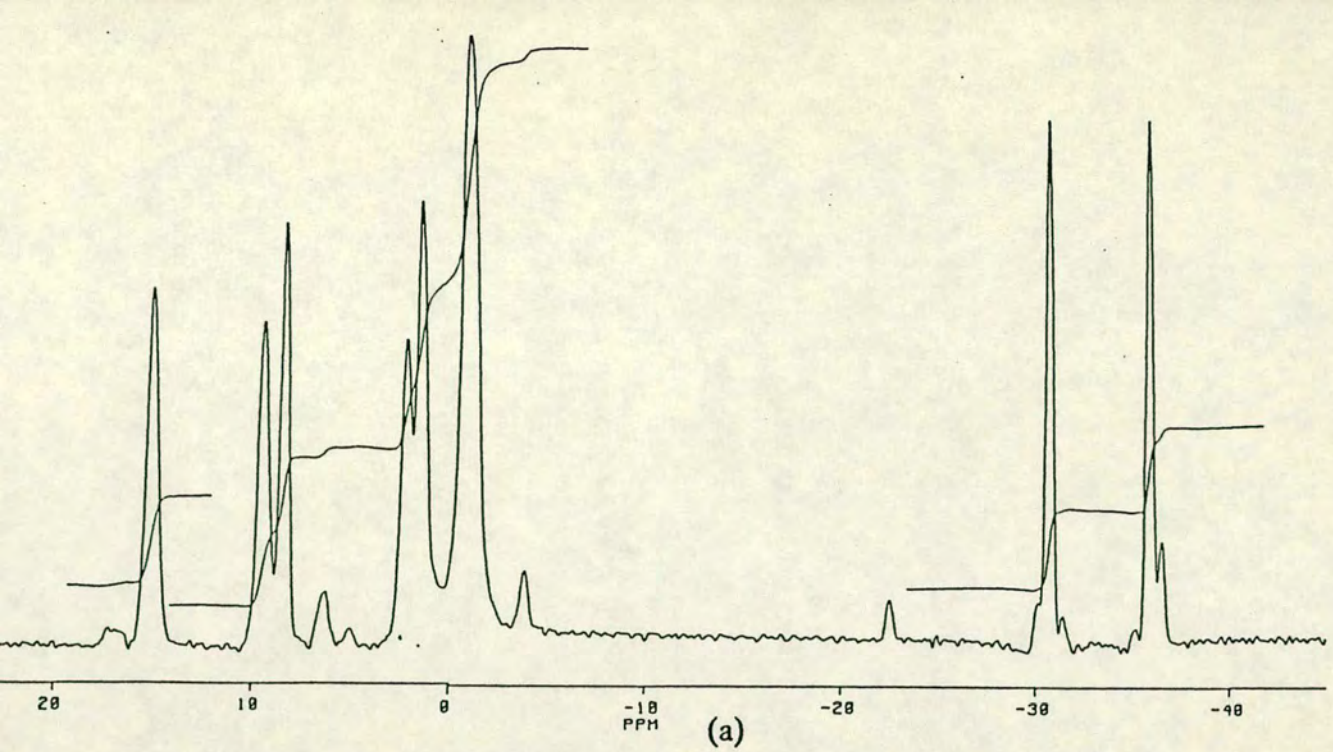

(a)

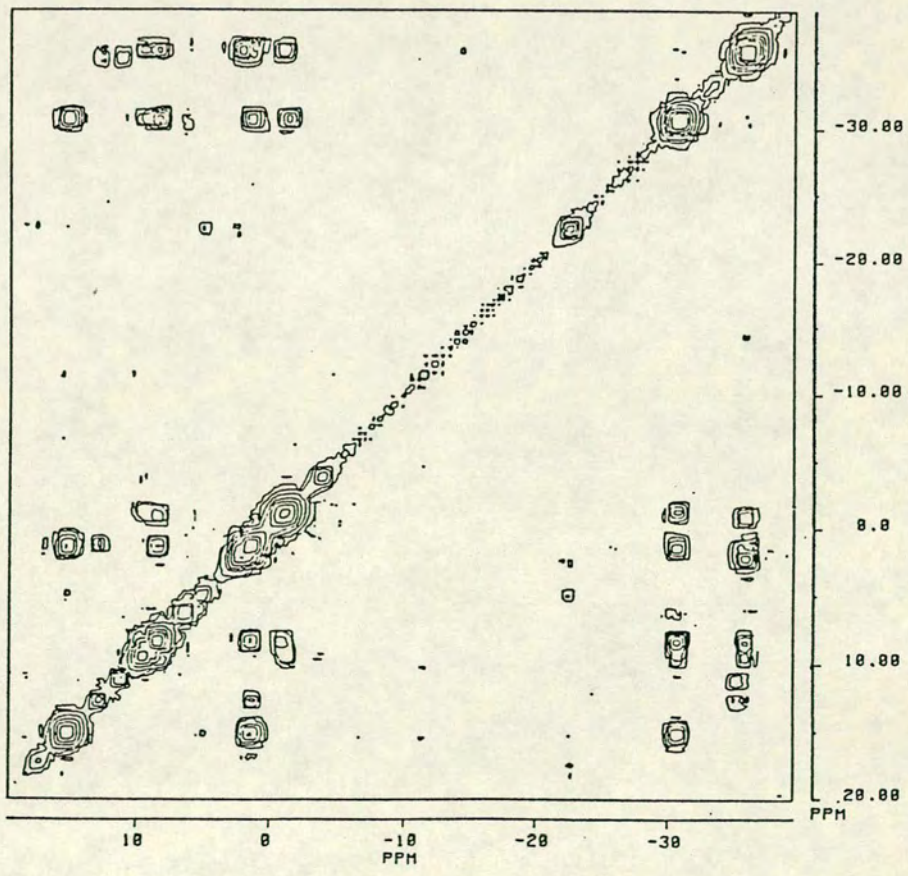

(b)

Figure 2.5. The n.m.r. spectra of **(8b)** : (a) ^{11}B-{^{1}H}
(b) the ^{11}B(COSY) n.m.r. spectrum

between the two relevant boron atoms in an ^{11}B(COSY) plot. This has been interpreted as showing that there is no direct B-B bonding in such systems i.e. all of the bonding electron density passes through the H atom. As can be seen from Figure 2.5(b), there is no off-resonance signal between B(5) and B(6), indicating that a {AuP *o*-tolyl$_3$} bridge is the same in this respect.

The other feature of interest is the extent of bonding along the B(5)-B(10) and B(7)-B(8) connectivities. These are exceptionally long, and this implies that the bonding is relatively weaker. Since these four atoms are all equivalent in decaborane, no couplings can be seen. In $tol_3PAuB_{10}H_{13}$ however, they are inequivalent, although the resonances are very close together. However no couplings can be seen, indicating that in this complex, at least, the bonding along these two connectivities appears to be very weak.

Once the ^{11}B resonances had been assigned, it was a simple matter to selectively decouple each boron resonance and observe which proton resonances were affected. This enabled the complete assignment of all the B-*H* resonances. However, as shown in Figure 2.6 (page 51), the B-*H*-B resonances were all decoupled by the same resonances (B(5), B(7), B(8) and/or B(10), and B(9)). B(6) decouples only the signal at δ^1H = -3.3 ppm and so this ^1H resonance is assigned as due to H(6,7). The EHMO calculations suggest that H(9,10) was more acidic (and therefore more deshielded) than the others, and this implies that H(9,10) resonates at δ^1H = -0.1 ppm. Unfortunately, due to the accidental coincidence of the resonances assigned to B(8) and B(10) at $\delta^{11}B$ = -1.00ppm, it is not possible to differentiate between the H(8,9) and H(9,10) resonances by selective decoupling experiments.

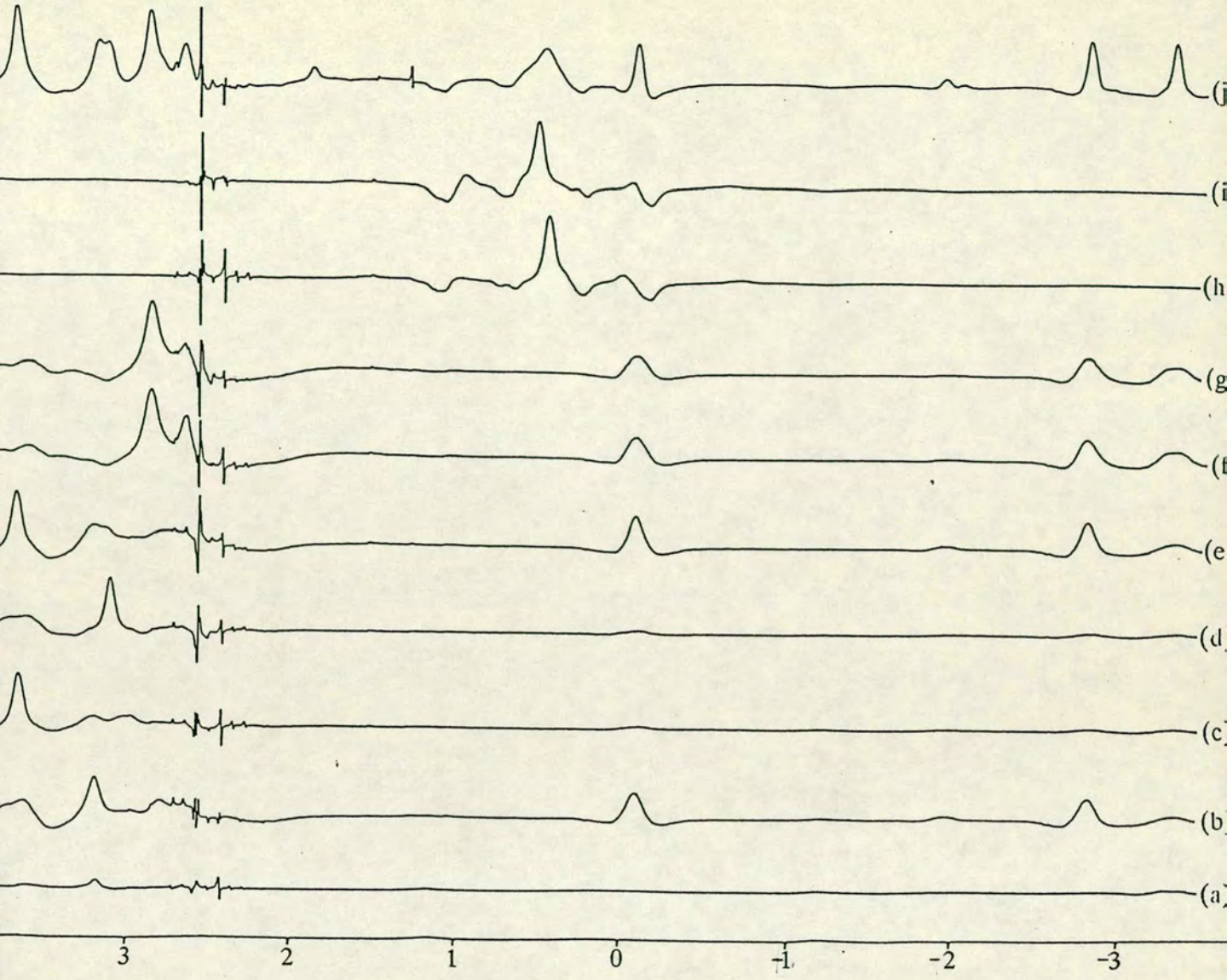

Figure 2.6. The ^{1}H-{^{11}B,selective) n.m.r. spectra showing the fluxionality of the μ-H atoms at room temperature.

Each trace is the difference spectrum obtained when an off-resonance decoupled spectrum is subtracted from the selectively-decoupled one. ν(^{11}B) corresponds to the following $\delta^{11}B$ resonance (with its assignment) : (a) 15.13 - B(6) (b) 9.41 - B(9) (c) 8.34 - B(3) (d) 2.15 - B(1) (e) 1.40 - B(7) (f) -1.00 (high ν component) - B(8),B(10) (g) -1.00 (low ν component) - B(5) (h) -30.73 - B(2) (i) -35.85 - B(4) (j) broad-band noise decoupling.

2.6 Further Structural Studies.

2.6.1 Mössbauer Spectroscopy.

As discussed in Chapter 1, we have begun to obtain the Mössbauer spectra of auraboranes, to help establish the oxidation state of the metal, Whilst **(8)** is undoubtedly a Au(I) species, the Mössbauer spectrum of **(8a)** was obtained to see what effect ligating a boron cage to the gold has on the spectrum. It would also serve as a very useful standard for future work.

The Mössbauer spectrum was acquired and interpreted by Dr. R.V.Parish at UMIST. The results were that the isomer shift (IS) was 4.51, and the quadrupolar splitting (QS) was 9.01 mms^{-1}. These results indicate that this is a linear Au(I) species, although the value for QS is very near the bottom of the expected range [127]. However the IS value is well above the range expected (*ca.* 2 - 3) for a three-coordinate gold.

2.6.2 Mass Spectrum.

The other principal means of identifying complexes is by mass spectrometry. Since boron has two isotopes (20% ^{10}B and 80% ^{11}B), metallaboranes have complex mass spectra. However it is possible to calculate (computer program *MSS*, ref. 128) what pattern arises from a given formula, and so this disadvantage can be overcome. To see how useful mass spectrometry could be when applied to unknown samples, the E.I. mass spectrum of **(8a)** was obtained. This is shown in Figure 2.7, page 53, and the observed and calculated intensities for the parent ion are given in Table 2.5 on the same page.

There is very little correlation between the observed parent ion spectrum and that calculated for $Cy_3PAuB_{10}H_{13}$. The highest peak in the observed spectrum occurs at a mass of 595, which is three a.m.u.'s less than predicted. This

Figure 2.7. The e.i. mass spectrum of 5,6-μ-(Cy_3PAu)-*nido*-$B_{10}H_{13}$.

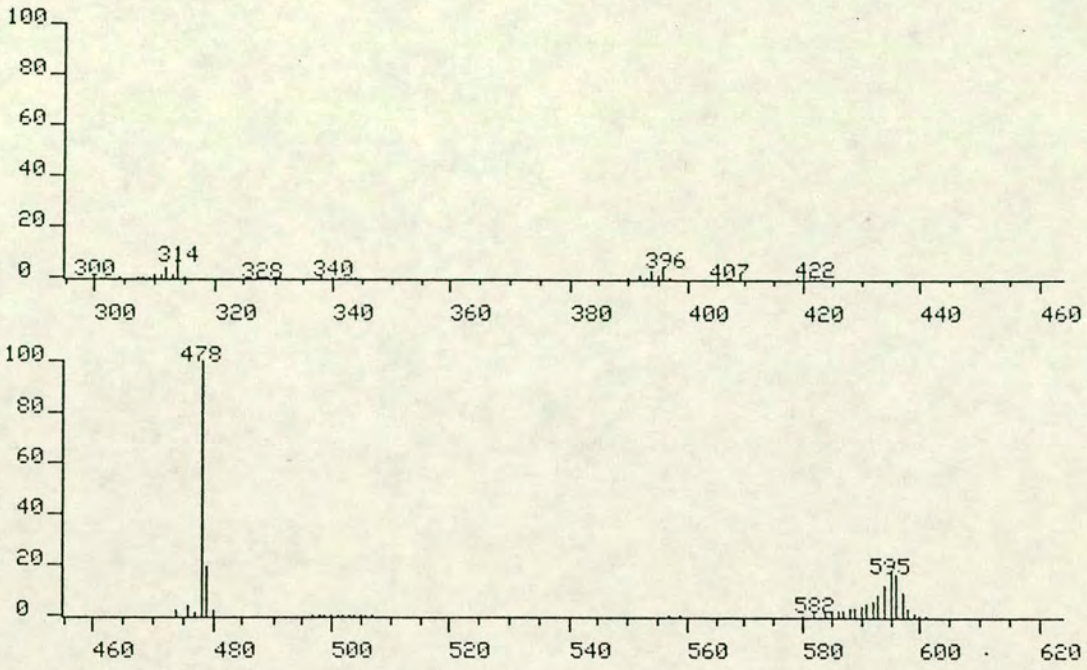

Table 2.5. The Observed and Calculated Intensities for the Mass Spectrum of 5,6-μ-(Cy_3PAu)-*nido*-$B_{10}H_{13}$. The values are %'s of that for the highest peak in each column; which was assigned a value of 100.

		Calculated for				Calculated for	
Mass	Observed	$[M]^+$	$[M-3]^+$	Mass	Observed	$[M]^+$	$[M-3]^+$
603	0.00	0.03	—	592	35.03	0.01	7.41
602	0.00	0.75	—	591	27.12	—	1.49
601	1.13	8.57	—	590	22.03	—	0.20
600	3.96	51.30	0.03	589	20.34	—	0.01
599	6.78	99.35	0.75	588	18.64	—	—
598	16.38	100	8.55	587	15.82	—	—
597	53.11	62.17	51.27	586	13.56	—	—
596	94.12	25.81	99.33	585	11.23	—	—
595	100.00	7.41	100.00	584	10.73	—	—
594	71.75	1.49	62.17	583	0	—	—
593	51.41	0.20	25.81	582	11.12	—	—

presumably means that the major peak is due to $[M-3]^+$ implying that the three μ-H atoms are lost. The spectrum calculated for $[Cy_3PAuB_{10}H_{10}]$ is also shown in Table 2.5, and as can be seen from this, there is very good agreement when the peaks of mass > 595 are considered. There is still, however, poor agreement for mass < 595, where there must be a significant contribution from peaks arising from partial fragmentation of the cage. As a means of determining the number of H atoms, for example, it is obviously of little use.

2.7 Reactions of this Complex.

2.7.1 Reaction with Hydrogen Chloride.

As discussed in Section 2.1, the intermediate in the reaction of methyltricyclohexylphosphinegold(I) and decaborane was too unstable to be detected by n.m.r. spectroscopy. In an attempt to synthesise a more stable analogue, the oxidative addition reaction:-

$$Cy_3PAuB_{10}H_{13} + H\text{-}Cl \longrightarrow Cy_3PAu(H)(Cl)(B_{10}H_{13})$$

was proposed. This is one well-known [115] route to metal hydrides and it was hoped that the chloride ligand would stabilise the gold centre better than a methyl group could. The reaction products were characterised spectroscopically, and the reaction was found to be:-

$$Cy_3PAuB_{10}H_{13} + H\text{-}Cl \longrightarrow AuCl(PCy_3) + B_{10}H_{14}$$

However, it was hoped that this reaction could ultimately prove to be of general use as a means of specifically cleaving only gold-boron bonds.

2.7.2 Reaction with Triethylamine.

It is well-known [129] that the bridging hydrides in boranes are acidic, and that decaborane is easily deprotonated by, for example [22] triethylamine:-

$$B_{10}H_{14} + NEt_3 \longrightarrow [NHEt_3]^+ [B_{10}H_{13}]^-$$

Accordingly, the reaction of triethylamine and **(8a)** was carried out, especially when, as argued in Section 2.2, one of the three remaining μ-H atoms was thought to be more acidic than the other two - this was one way to test the hypothesis.

It was found that the reaction was indeed deprotonation to form the $[Cy_3PAuB_{10}H_{12}]^-$ anion - this is discussed far more fully in Chapter 3, but for present purposes, H(9,10) is specifically the proton removed, although some structural rearrangement is found to accompany the deprotonation (see Figure 3.3 page 71).

2.7.3 Reaction with Alcoholic Potassium Hydroxide.

Decaborane is deboronated by methanolic potassium hydroxide :-

$$B_{10}H_{14} + KOH/MeOH \rightarrow K^+ [B_9H_{14}]^-$$

Hence **(8a)** was reacted under the same conditions with the same reagent, but the product was found to be, after cation metathesis, $[PhCH_2NMe_3]^+ [Cy_3PAuB_{10}H_{12}]^-$. Since this deprotonation accompanies a structural rearrangement, presumably this anion is then inert to any subsequent deboronation. One minor product of this reaction was the *double cluster*, $(B_{10}H_{12}Au)(AuPCy_3)_3$ which is described in Chapter 5 (see Figure 5.7, page 162). This was first synthesised as a rearrangement product of $[NHEt_3]^+$ $[Cy_3PAuB_{10}H_{12}]^-$.

2.7.4 Reaction with Electron-Pair Donors.

As mentioned in the introduction, one important reaction of decaborane is:

$$B_{10}H_{14} + 2L \longrightarrow B_{10}H_{12}(L)_2 + H_2$$

These complexes are important intermediates in the reactions of decaborane, as discussed in Chapter 1. Hence it was very important to see how **(8a)** reacts with electron-pair donors, because it could give an important insight into its chemistry. Another feature of interest is that in the above reaction, two μ-H functions are lost. This then begged the question of what would happen to a $\{AuPCy_3\}$ bridge. The first reaction attempted was to reflux **(8a)** in acetonitrile, in an analogous reaction to the synthesis of $B_{10}H_{12}(MeCN)_2$. The reaction however proceeded as follows:

$$Cy_3PAuB_{10}H_{13} + MeCN \longrightarrow [(Cy_3P)_2Au]^+ [(B_{10}H_{12})_2Au]^-$$

(see Fig.4.7, page 128)

This reaction is best described as an *oxidative disproportionation* because two Au(I) complexes disproportionate into a Au(I) and a Au(III) complex.

It has been shown that the bridging $\{AuPR_3\}$ fragment is stabilised by an interaction with a neighbouring μ-H atom. It will subsequently be shown that removal of this H atom with base leads to a product in which the gold atom has 'slipped' from η^2 to η^4-ligated. Hence one possible explanation for the reaction of **(8a)** with acetonitrile is that an adduct (e.g. μ-$(AuPCy_3)$-$B_{10}H_{13}(MeCN)$) was formed. This would open up the cage from *nido* to *arachno* and would probably disrupt the stabilising Au..μ-H interaction. This would destabilise the bridging position of the $\{AuPCy_3\}$ fragment, causing rearrangement to the observed product with the loss of dihydrogen.

A second experiment tried was to stir a solution of $Cy_3PAuB_{10}H_{13}$ in dimethylsulphide for twenty four hours. The product was the same : $[(Cy_3P)_2Au]^+ [(B_{10}H_{12})_2Au]^-$.

2.7.5 Reaction with $AuMe(PR_3)$.

In the introduction, it was mentioned that one reaction of $Cy_3PAuB_{10}H_{13}$ was reported to be :-

$$Cy_3PAuB_{10}H_{13} + AuMe(PEt_3) \longrightarrow (B_{10}H_{12}Au)_2(AuPEt_3)_4$$

Two other, analagous, reactions were therefore investigated. First was the reaction with methyltriphenylphosphinegold(I), to isolate and characterise the triple cluster formed - due to the greater steric bulk of the triphenylphosphine compared to triethylphosphine (Tolman cone angles[94] of 145° and 132° respectively), there was the possibility that fewer than four $\{Au\text{-}PPh_3\}$ fragments may bridge the gold-gold bond. Second methyltricyclohexylphosphinegold(I) was used, as a further extension of this principle.

However the products of both reactions were identified as hexagold triple clusters, $(B_{10}H_{12}Au)_2(AuPPh_3)_4$ and $(B_{10}H_{12}Au)_2(AuPCy_3)_4$ respectively. These complexes are discussed more fully in Chapter 5, including the effects of the steric demands of the phosphine ligands on the hexagold cluster geometry (see Figures 5.3 on page 153).

2.8 Conclusions

This chapter has investigated the structure and chemistry of 5,6-μ-$(AuPR_3)$-*nido*-$B_{10}H_{13}$. The molecular structure is that of a linear gold(I) species which has one tricyclohexylphosphine ligand and is η^2-ligated to a *nido*-decaboranyl cage. The observed structural distortions in the cage framework

are accounted for by a weak interaction between the gold and the hydrogen bridging the nearby B(9)-B(10) connectivity. The only other example of a metal..μ-H interaction is in a mercuracobaltacarborane, and such interactions presumably help to stabilise the bridging $\{ML_n\}$ function.

The $^{11}B-\{^1H\}$ n.m.r. spectrum was interpreted using an ^{11}B(COSY), and the $^1H-\{^{11}B\}$ n.m.r. spectrum was then partially interpreted. Due to an accidental coincidence in the $^{11}B-\{^1H\}$ n.m.r. spectrum, two of the μ-H resonances could not be unambiguously assigned, although these were distinguished on the basis of the Au-μ-H interaction.

Interpretation of the Mössbauer spectrum showed that **(8a)** is a linear Au(I) species, and that there are no significant difficulties caused by the presence of the boron cage. However, there is poor agreement between the observed and calculated mass spectra, and so no further complexes were examined by this technique.

The reactions of **(8a)** are summarised in Scheme 3, on page 59. The reactivity of this species is very different to that of decaborane. The biggest difference is the failure to synthesise analogues of the $B_{10}H_{12}L_2$ complexes which are intermediates in many of the reactions of decaborane.

In all of the derivatives of **(8a)** so far characterised, the gold atom has slipped from η^2 to η^4 ligated, implying that this is a more stable mode of bonding. This slipping is presumably due to disruption of the weak, but stabilising, gold..μ-H interaction. The complex is deprotonated by bases and the gold-boron bond is cleaved by H-Cl which demonstrates the amphoteric nature of this species.

Scheme 3: The reactions of 5,6-μ-(Cy_3PAu)-*nido*-$B_{10}H_{13}$.

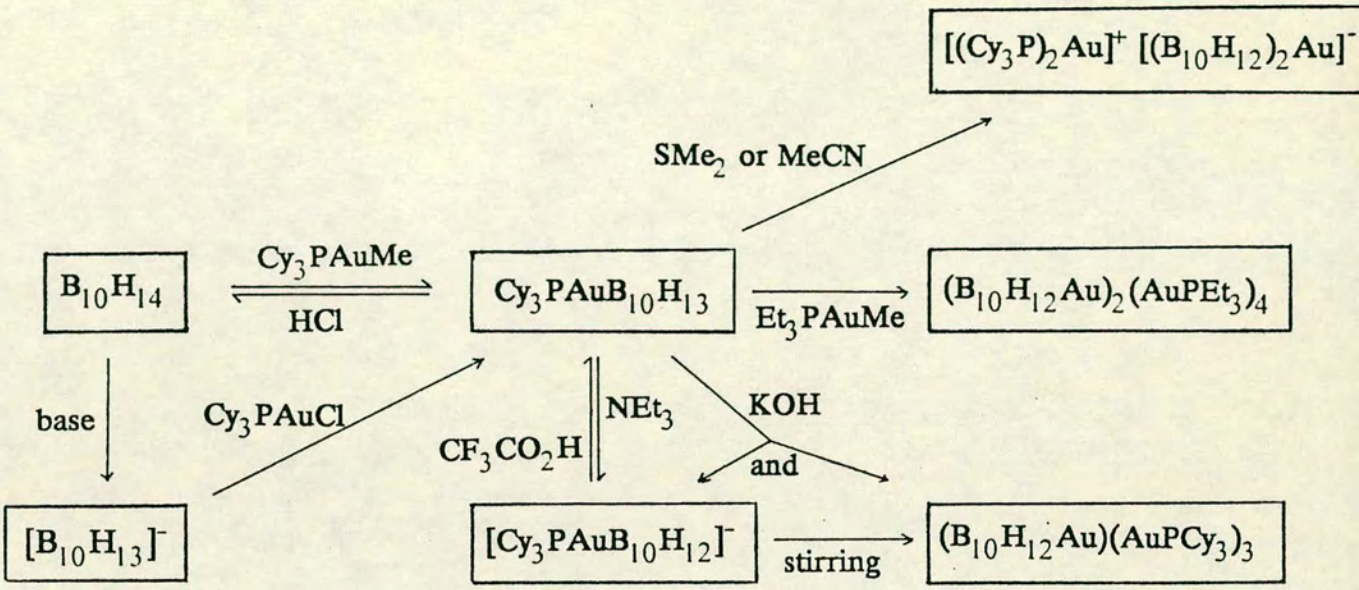

Table 2.1. Bond Lengths(pm) and Angles(^{o}) for the $\{B_{10}AuP\}$ Fragment in 5,6-μ-(Cy_3PAu)-*nido*-$B_{10}H_{13}$.

Au - P	230.91(21)	B(3) - B(4)	178.8(17)
Au - B(5)	224.5(10)	B(3) - B(7)	174.3(17)
Au - B(6)	227.0(10)	B(3) - B(8)	171.7(19)
B(1) - B(2)	180.7(15)	B(4) - B(8)	172.0(18)
B(1) - B(3)	182.8(17)	B(4) - B(9)	170.1(19)
B(1) - B(4)	180.6(15)	B(4) -B(10)	178.9(16)
B(1) - B(5)	178.5(14)	B(5) - B(6)	177.0(14)
B(1) -B(10)	177.0(16)	B(5) -B(10)	199.4(15)
B(2) - B(3)	177.7(17)	B(6) - B(7)	177.6(15)
B(2) - B(5)	180.3(14)	B(7) - B(8)	201.0(18)
B(2) - B(6)	175.1(15)	B(8) - B(9)	164.3(20)
B(2) - B(7)	174.0(16)	B(9) -B(10)	187.7(19)

P - Au - B(5)	158.8(3)	B(8) - B(4) - B(9)	57.4(8)
P - Au - B(6)	154.7(3)	B(9) - B(4) -B(10)	65.0(7)
B(5) - Au - B(6)	46.2(4)	Au - B(5) - B(6)	67.7(5)
B(2) - B(1) - B(3)	58.5(6)	B(1) - B(5) - B(2)	60.5(6)
B(2) - B(1) - B(5)	60.2(6)	B(1) - B(5) -B(10)	55.5(5)
B(3) - B(1) - B(4)	58.9(6)	B(2) - B(5) - B(6)	58.7(6)
B(4) - B(1) -B(10)	60.0(6)	Au - B(6) - B(5)	66.2(4)
B(5) - B(1) -B(10)	68.2(6)	B(2) - B(6) - B(5)	61.6(6)
B(1) - B(2) - B(3)	61.3(6)	B(2) - B(6) - B(7)	59.1(6)
B(1) - B(2) - B(5)	59.3(6)	B(2) - B(7) - B(3)	61.3(7)
B(3) - B(2) - B(7)	59.4(7)	B(2) - B(7) - B(6)	59.7(6)
B(5) - B(2) - B(6)	59.7(6)	B(3) - B(7) - B(8)	53.9(7)
B(6) - B(2) - B(7)	61.1(6)	B(3) - B(8) - B(4)	62.7(7)
B(1) - B(3) - B(2)	60.2(6)	B(3) - B(8) - B(7)	55.1(6)
B(1) - B(3) - B(4)	59.9(6)	B(4) - B(8) - B(9)	60.7(8)
B(2) - B(3) - B(7)	59.2(7)	B(4) - B(9) - B(8)	61.9(8)
B(4) - B(3) - B(8)	58.7(7)	B(4) - B(9) -B(10)	59.8(7)
B(7) - B(3) - B(8)	71.0(8)	B(1) -B(10) - B(4)	61.0(6)
B(1) - B(4) - B(3)	61.1(6)	B(1) -B(10) - B(5)	56.3(6)
B(1) - B(4) -B(10)	59.0(6)	B(4) -B(10) - B(9)	55.2(7)
B(3) - B(4) - B(8)	58.6(7)		

Table 2.2. Relevant Parameters Obtained from the EHMO Calculations on Model Complexes.

Mulliken Overlap Populations in (8c).

Au-P	0.793	B(5)-B(6)	0.606
Au-B(5)	0.334	B(6)-B(7)	0.390
Au-B(6)	0.276	B(8)-B(9)	0.400
Au-B(10)	0.175	B(9)-B(10)	0.397
Au-H(6,7)	-0.009	B(6)-H(9,10)	-0.009
Au-H(7,8)	-0.002	B(9)-H(9,10)	0.421
Au-H(9,10)	0.010	B(10)-H(9,10)	0.421

$[H_3PAuB_{10}H_{12}]^-$ Orbital 43 (HOMO) Terms(x 10^4).

	orbital			Orbitals		
Atom	s	Atom	s	p_x	p_y	p_z
H(1)	685	B(1)	-252	-829	-332	-769
H(2)	-365	B(2)	86	-525	185	858
H(3)	-501	B(3)	219	1920	540	-9
H(4)	1091	B(4)	-476	-641	-1503	-1705
H(5)	433	B(5)	-82	901	768	-732
H(6)	399	B(6)	-229	-1340	-1701	-1491
H(7)	-140	B(7)	-23	-951	497	436
H(8)	657	B(8)	-178	-470	-581	-954
H(9)	-363	B(9)	736	-2445	3050	2575
H(10)	-618	B(10)	806	-520	-945	4285
H(6,7)	-393	H(P1)	415			
H(8,9)	192	H(P2)	263			
		H(P3)	-596			

	s	p_x	p_y	p_z	$d_{x^2y^2}$	d_{z^2}	d_{xy}	d_{xz}	d_{yz}
Au	-1087	1166	567	81	-478	335	280	473	461
P	28	854	137	-546	-745	418	-768	-640	-659

Net Atomic Charges for the Atoms in (8c).

Atom	Charge	Atom	Charge	Atom	Charge	Atom	Charge
Au	0.0703	B(3)	0.1595	B(10)	0.2271	H(7)	-0.1991
P	0.0393	B(4)	0.1130	H(1)	-0.2154	H(8)	-0.1986
H(P1)	0.0888	B(5)	0.0922	H(2)	-0.2106	H(9)	-0.1782
H(P2)	0.0891	B(6)	0.1680	H(3)	-0.2124	H(10)	-0.1978
H(P3)	0.0879	B(7)	0.2109	H(4)	-0.2112	H(6,7)	-0.0390
B(1)	0.1424	B(8)	0.2240	H(5)	-0.2121	H(8,9)	-0.0256
B(2)	0.1097	B(9)	0.2920	H(6)	-0.1937		

Table 2.3. The Bond Lengths(pm) and Angles(°) for the Boron, Gold and Phosphorus Atoms in 5,6-μ-(*o*-tolyl$_3$PAu)-*nido*-$B_{10}H_{13}$.

Au - P	230.8(3)	B(3) - B(4)	178.7(22)
Au - B(5)	225.6(15)	B(3) - B(7)	179.0(22)
Au - B(6)	232.5(16)	B(3) - B(8)	176.5(23)
B(1) - B(2)	178.6(22)	B(4) - B(8)	178.3(23)
B(1) - B(3)	178.8(22)	B(4) - B(9)	173.8(23)
B(1) - B(4)	181.8(22)	B(4) -B(10)	183.8(23)
B(1) - B(5)	177.6(22)	B(5) - B(6)	174.5(22)
B(1) -B(10)	177.9(23)	B(5) -B(10)	201.3(22)
B(2) - B(3)	176.7(22)	B(6) - B(7)	173.5(22)
B(2) - B(5)	174.5(21)	B(7) - B(8)	208.6(23)
B(2) - B(6)	167.7(22)	B(8) - B(9)	177.9(24)
B(2) - B(7)	172.6(22)	B(9) -B(10)	183.0(23)

B(5)	- Au	- B(6)	44.8(5)	B(8) - B(4)	- B(9)	60.7(9)
B(5)	- Au	- P	157.4(4)	B(9) - B(4)	-B(10)	61.5(9)
B(6)	- Au	- P	157.3(4)	Au - B(5)	- B(6)	69.7(7)
B(2)	- B(1)	- B(3)	59.3(9)	B(1) - B(5)	- B(2)	61.0(9)
B(2)	- B(1)	- B(5)	58.6(9)	B(1) - B(5)	-B(10)	55.6(8)
B(3)	- B(1)	- B(4)	59.4(9)	B(2) - B(5)	- B(6)	57.5(9)
B(4)	- B(1)	-B(10)	61.4(9)	Au - B(6)	- B(5)	65.5(7)
B(5)	- B(1)	-B(10)	69.0(9)	B(2) - B(6)	- B(5)	61.3(9)
B(1)	- B(2)	- B(3)	60.4(9)	B(2) - B(6)	- B(7)	60.7(9)
B(1)	- B(2)	- B(5)	60.4(9)	B(2) - B(7)	- B(3)	60.3(9)
B(3)	- B(2)	- B(7)	61.7(9)	B(2) - B(7)	- B(6)	58.0(9)
B(5)	- B(2)	- B(6)	61.3(9)	B(3) - B(7)	- B(8)	53.5(8)
B(6)	- B(2)	- B(7)	61.3(9)	B(3) - B(8)	- B(4)	60.5(9)
B(1)	- B(3)	- B(2)	60.3(9)	B(3) - B(8)	- B(7)	54.6(8)
B(1)	- B(3)	- B(4)	61.1(9)	B(4) - B(8)	- B(9)	58.4(9)
B(2)	- B(3)	- B(7)	58.0(9)	B(4) - B(9)	- B(8)	60.9(9)
B(4)	- B(3)	- B(8)	60.3(9)	B(4) - B(9)	-B(10)	62.0(9)
B(7)	- B(3)	- B(8)	71.8(9)	B(1) -B(10)	- B(4)	60.3(9)
B(1)	- B(4)	- B(3)	59.5(9)	B(1) -B(10)	- B(5)	55.4(8)
B(1)	- B(4)	-B(10)	58.2(9)	B(4) -B(10)	- B(9)	56.6(9)
B(3)	- B(4)	- B(8)	59.3(9)			

Table 2.4. The Proposed Assignments for the ^{11}B-{^{1}H} and ^{1}H-{^{11}B} N.M.R. Spectra.

Proposed Assignment	$\delta^{11}B$[a]	$\delta^{1}H$[b]
6	15.13	5.27 (-3.3)
9	9.41	3.18 (-0.1, -2.8, -3.3)
3	8.34	3.66
1	2.15	3.10
7	1.40	3.67 (-0.1, -2.8, -3.3)
8,10	-1.00[c]	2.64, 2.85 (-0.1, -2.8, -3.3)
5	-1.00[d]	2.85 (-0.1, -2.8, -3.3)
2	30.73	0.45
4	35.85	0.51
H(6,7)	–	-3.3
H(8,9)	–	-2.8
H(9,10)	–	-0.1

Notes

(a) $\delta^{11}B$ relative to external $BF_3.OEt_2$.

(b) $\delta^{1}H$ relative to external $SiMe_4$ from ^{1}H-{^{11}B,selective} experiments. Chemical shifts of bridge protons enhanced by irradiation at ^{11}B frequencies shown in parentheses.

(c) and (d) high and low frequency components respectively of an asymmetric singlet.

Chapter 3:

Auraboranes with $\{AuPCy_3\}$ Groups -

The $[Cy_3PAuB_{10}H_{12}]^-$ Anion and $(Cy_3PAu)_2B_8H_{10}$.

3.1 Introduction.

This Chapter is divided into two parts, each of which considers a complex in which a $\{AuPCy_3\}$ fragment is ligated to a boron cage. The majority of the work is in the first part, which examines the consequences of the action of base on *nido*-$\{B_{10}\}$ cages.

In the first Section (3.2) is a brief description of the structure of the $[B_{10}H_{13}]^-$ anion, which was determined so that comparison of its structure with other boranes and metallaboranes could be made.

Then, in Section 3.3, there is an examination of the reaction of different bases with $Cy_3PAuB_{10}H_{13}$, and this leads into a full discussion on the synthesis and characterisation of the $[Cy_3PAuB_{10}H_{12}]^-$ anion. The structure of this was determined by a single crystal X-ray diffraction study, which showed that deprotonation was accompanied by a structural rearrangement.

In a following Section (3.6) is a detailed analysis of this compound. After comparing the structure of the $\{B_{10}\}$ cage in complexes with at least one η^4-ligated $\{B_{10}H_{12}\}$ fragment with borane analogues, the observed trends indicate that transition metal and main group metal complexes show distinct differences in bonding. When this trend was extended to auraboranes, it could be used to predict the oxidation state of the gold in the $[Cy_3PAuB_{10}H_{12}]^-$ anion. This, as well as the geometry of the gold, was also probed by Mössbauer spectroscopy.

The interaction of the gold with the $\{B_{10}H_{12}\}$ ligand was investigated by EHMO calculations in Section 3.7, then in Section 3.8, the ^{11}B(COSY) n.m.r. spectrum was acquired, and the multinuclear n.m.r. spectra were interpreted on the basis of the information that this provided. Finally in Section 3.9, two reactions of the $[Cy_3PAuB_{10}H_{12}]^-$ anion are discussed.

The second part of the Chapter considers the complex $(Cy_3PAu)_2B_8H_{10}$ which was synthesised by reacting $(B_{10}H_{12})(PPh_3)_2$ with $AuMe(PCy_3)$. The structure of this is examined next, followed by comparison with the very similar species $(\{dtc\}Au)_2B_8H_{10}$, (dtc = diethyldithiocarbamate). The electronic structure of $(Cy_3PAu)_2B_8H_{10}$ was examined by EHMO calculations, and then the spectroscopic details are reviewed. In the final Section (3.15) some conclusions are drawn.

3.2 The Structure of the $[B_{10}H_{13}]^-$ Anion.

This has been reported in the literature[130] as its $[NHEt_3]^+$ salt. However the paper was a communication and no atomic coordinates were published or deposited, nor is the structure in either the Inorganic (ICSD) or the Cambridge Crystallographic Database (CSSR). A letter was written to the authors directly, but no reply has been received.

For reasons which are discussed later, it became important that structural comparisons were made with the $[B_{10}H_{13}]^-$ anion, **(9)**, and so it was decided to redetermine the structure ourselves. When the structure of $[B_3H_8]^-$ was determined in this Department [108], the most suitable salt was found to be the $[PhCH_2NMe_3]^+$ one. In view of this, $[PhCH_2NMe_3]^+$ **(9)** was synthesised, suitable crystals were grown, and the structure determined.

One view of the ion-pair is shown in Figure 3.1, overleaf, and the

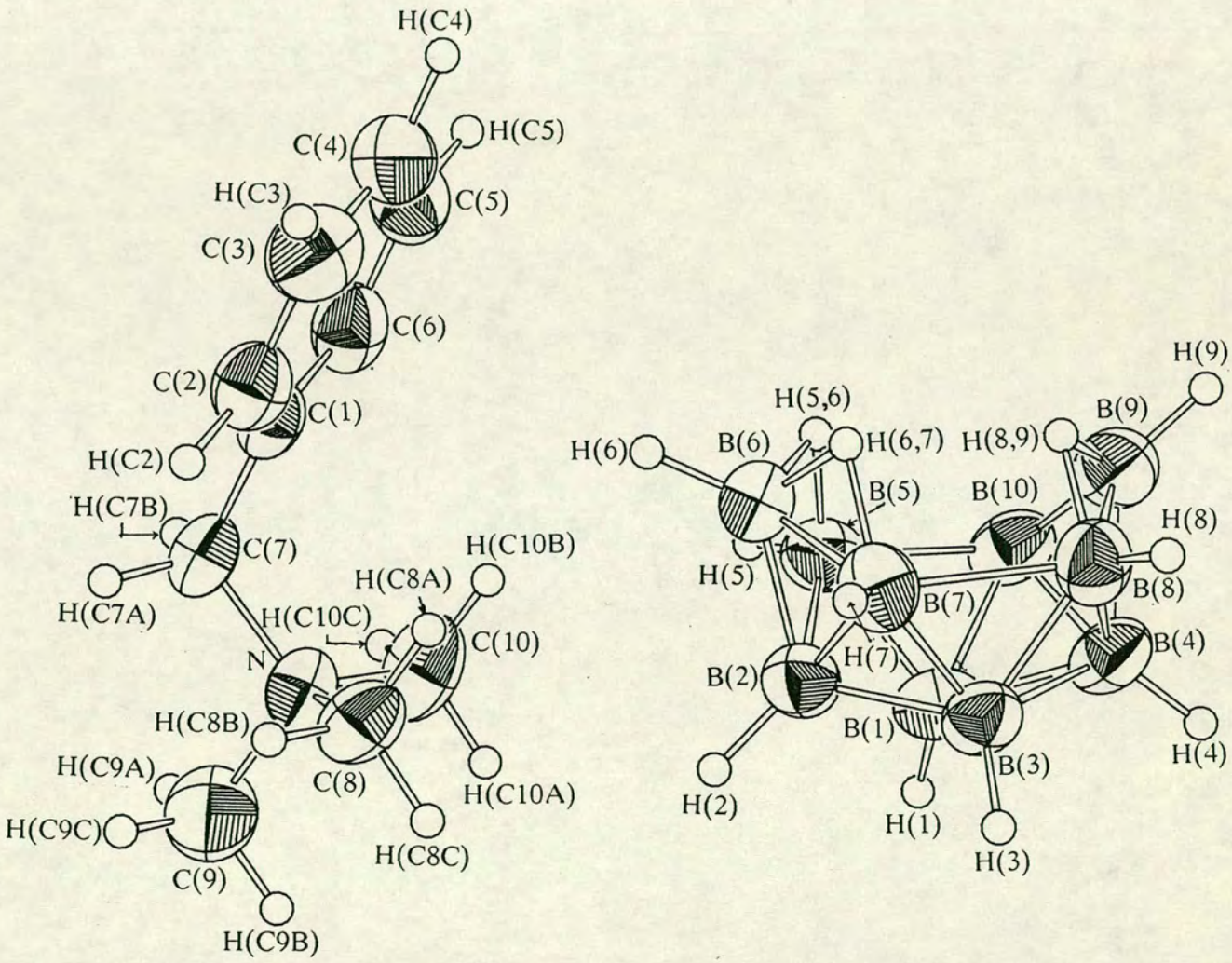

Figure 3.1. The structure of $[PhCH_2NMe_3]^+$ $[B_{10}H_{13}]^-$. H atoms have been given an artificial radius of 10pm.

boron-boron bond lengths and angles are listed in Table 3.1 on page 105. The structure determination details start on page 217.

When $B_{10}H_{14}$ is singly deprotonated, one μ-H, nominally H(9,10), is lost, but there is no accompanying rearrangement of the cage, nor is there any evidence that, in the crystal, the structure is disordered. The connectivity which is deprotonated is shortened from 178.8(4) pm (average) in decaborane to 165.7(5)pm. Similarly, B(5)-B(10) shortens from 198.7(3) to 184.8(5)pm. No other connectivities show significant deviations from their equivalents in $B_{10}H_{14}$, although the B(6)-B(7) connectivity is slightly shorter than the other two H-bridged ones. These results are consistent with the few details reported for the previous determination.

These changes in structure can be rationalised by an EHMO calculation on a model of **(9)**. This model, **(9b)** was constructed from the geometry of $B_{10}H_{14}$ with $[H(9,10)]^+$ removed. The coordinates are listed in Appendix 3, starting on page 281, and Figure 3.2, overleaf, is one view of the HOMO of this model.

As can be seen, the HOMO is primarily localised on, and bonding between, B(9) and B(10) (reduced charge matrix elements (RCME's) B(9) 0.6339, B(10) 0.7056). There is also a smaller contribution on B(5) which is in phase with that on B(10) (RCME : 0.0359). Protonation will partially deoccupy (see Chapter 2, page 44) the HOMO, thus weakening the bonding along the B(5)-B(10) and (especially) B(9)-B(10) connectivities, thus causing their observed lengthening.

3.3 Reactions of $Cy_3PAuB_{10}H_{13}$ with Bases.

As was described in the last Chapter, it has been found that **(8a)** reacts with bases. Its reaction with two bases has been investigated.

(1) Triethylamine. This reaction is discussed in more depth below.

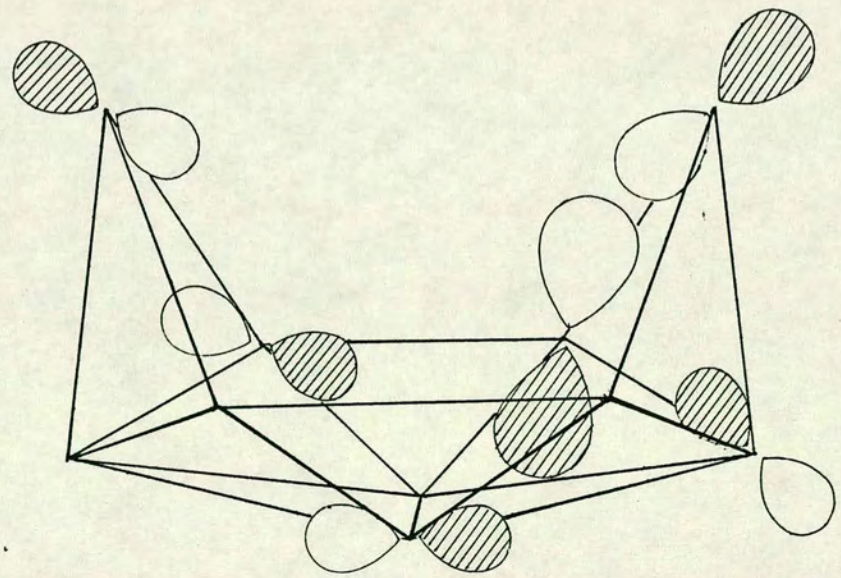

Figure 3.2. The HOMO of the $[B_{10}H_{13}]^-$ anion.

(2) Methanolic potassium hydroxide. This is the standard reagent [25] for deboronation reactions, but reaction with **(8a)**, followed by cation metathesis yielded only $[PhCH_2NMe_3]^+$ $[Cy_3PAuB_{10}H_{12}]^-$. However, one minor product which was characterised was the double cluster, whose structure is discussed in Chapter 5 (see Figure 5.7, page 162). This was first identified as a rearrangement product of $[NHEt_3]^+$ $[Cy_3PAuB_{10}H_{12}]^-$.

3.4 Spectroscopic Characterisation.

After reacting NEt_3 and **(8a)**, an orange powder was obtained, which yielded red crystals upon crystallisation from CH_2Cl_2/hexane. As explained in Chapter 1, triethylamine can either deprotonate or form a complex with a borane, and either could have happened here.

The microanalysis was consistent with the formulation $Cy_3PAuB_{10}H_{13} : NEt_3 = 1 : 1$. The i.r. spectrum showed peaks assignable to B-H, N-H, and Au-P stretches, indicating that deprotonation was more probable.

The ^1H-$\{^{11}B\}$ n.m.r. spectrum showed that there are ten terminal H atoms associated with the cage, signal ratios 2 : 2 : 2 : 2 : 1 : 1, and also two equivalent μ-H atoms. Since one μ-H atom has been lost from 5,6-μ-(Cy_3PAu)-*nido*-$B_{10}H_{13}$, it is reasonable to assume that deprotonation has occurred.

Furthermore, the ^{11}B-$\{^1H\}$ n.m.r. spectrum, which is discussed fully in Section 3.8, revealed that the $[Cy_3PAuB_{10}H_{12}]^-$ anion, **(15)**, had C_s symmetry in solution at least, indicating that it was possible that there had been a structural rearrangement and so a single crystal X-ray diffraction study was undertaken to determine the solid state structure.

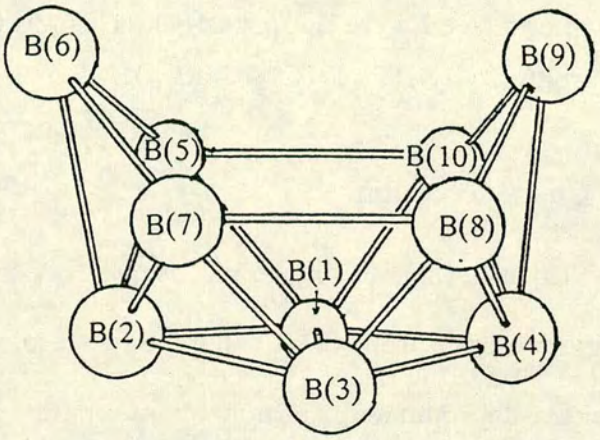

The renumbering for the discussion in the text.

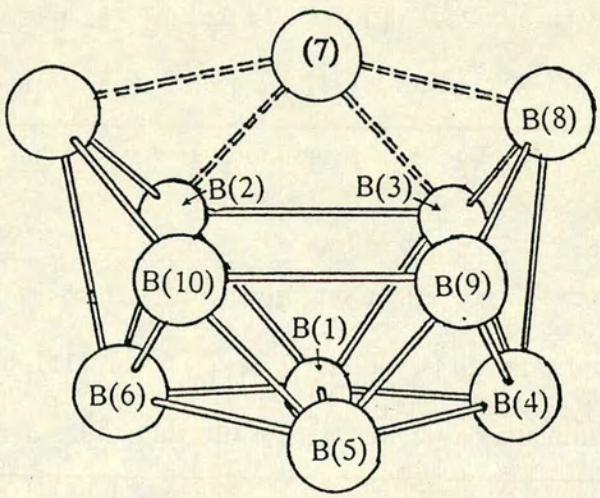

The correct numbering scheme for a *nido*-icosahedron with the heteroatom at the '7' position.

3.5 Crystallographic Characterisation.

This study conclusively showed that $[NHEt_3]^+$ **(15)** was indeed the product formed. Figure 3.3 (overleaf) shows two ORTEP plots of **(15)** ; important bond lengths and angles are in Table 3.2 (page 106), and the experimental details are given in Section A2.4 of Appendix 2 (starting on page 223).

For reasons which will be discussed later, this structure was numbered as a *nido*-B_{10} cage, and the gold has no numerical suffix. In this Chapter, many different boranes and metallaboranes and their structures are discussed. For clarity, and to avoid confusion, all of these complexes were renumbered into the same scheme : that of the $\{B_{10}\}$ cage in decaborane. If an eleventh atom/vertex is present it is unnumbered. The diagram opposite should make this clear.

As was suspected from the spectroscopic data, there has indeed been a structural change in which the $\{AuPCy_3\}$ fragment has 'slipped' across the open face and is now η^4-ligated. The molecule does not use any molecular symmetry crystallographically, but the bond lengths (except for the B(5)-B(6) and B(9)-B(10) ones) are consistent, within experimental error, with mirror symmetry.

In the last Chapter, it was shown that in **(8a)** there was a bonding interaction between the gold and H(9,10). Since in this deprotonation it is the H(9,10) atom which is lost, presumably this 4-centre, 2-electron Au-H-B-B bond becomes a 3-centre, 2 electron Au-B-B one. This specificity does reinforce the argument that this μ-H atom is the most acidic in **(8a)**. However it could be also be argued that the driving force for this product is the rearrangement, and that any of the μ-H atoms are removed. The anion which is formed then rearranges to the most stable one, which is the observed product.

The final point of interest is that, unlike every other auraborane structure

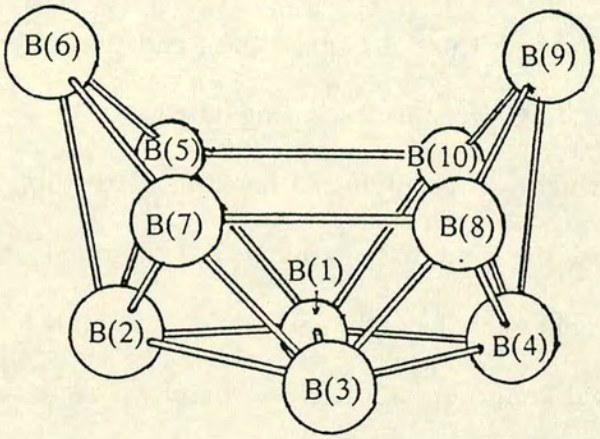

The renumbering for the discussion in the text.

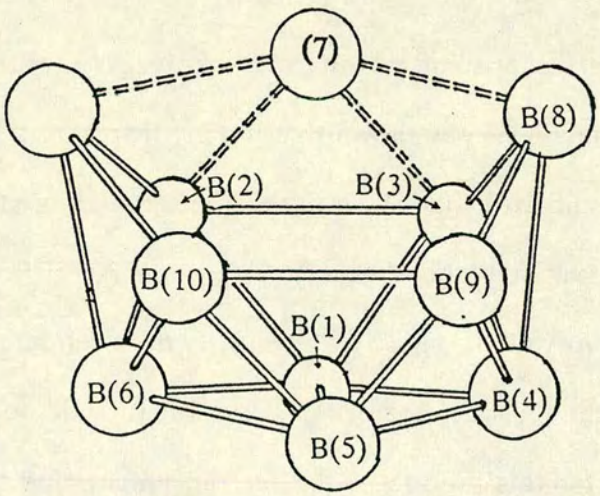

The correct numbering scheme for a *nido*-icosahedron with the heteroatom at the '7' position.

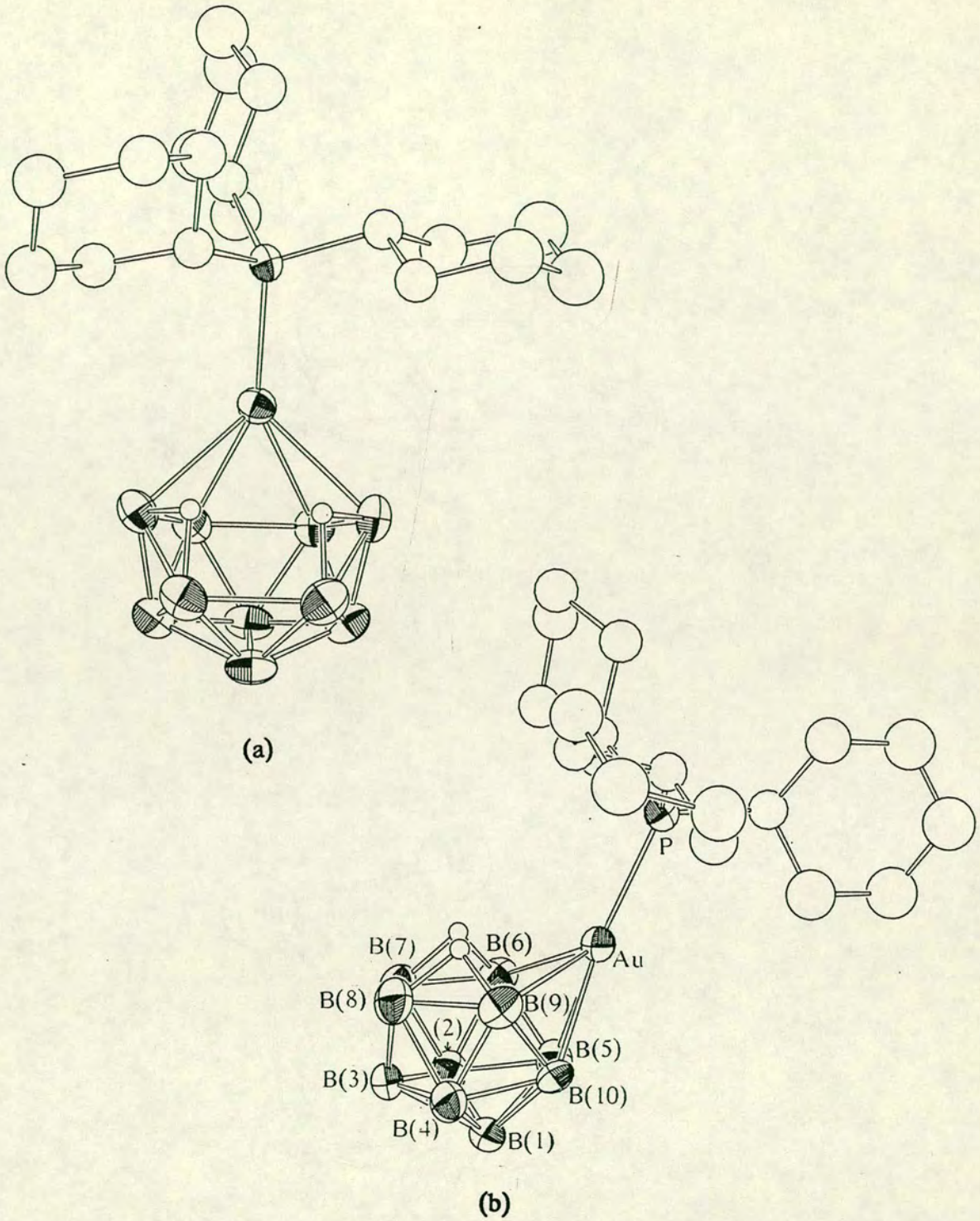

Figure 3.3. The ORTEP plots of the $[Cy_3PAuB_{10}H_{12}]^-$ anion.
(a) shows its relationship with $Cy_3PAuB_{10}H_{13}$, and
(b) shows the open face.

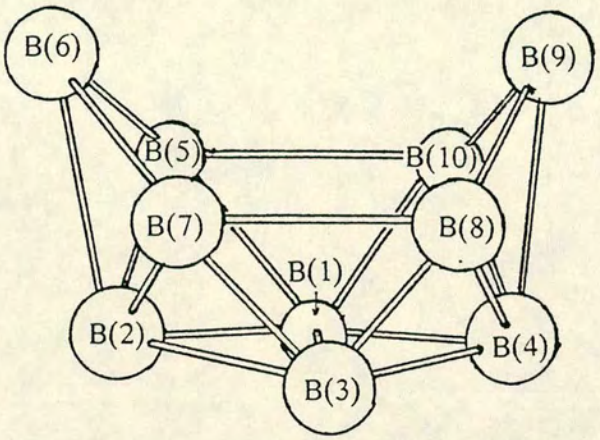

The renumbering for the discussion in the text.

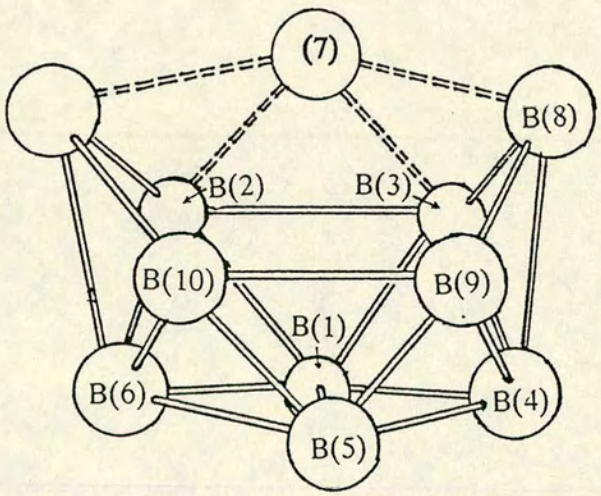

The correct numbering scheme for a *nido*-icosahedron with the heteroatom at the '7' position.

with a $\{AuPCy_3\}$ fragment present, there is poor steric protection of the open face in **(15)**. This is probably the reason why this complex undergoes the rearrangement discussed in Section 3.10.2.

3.6 Geometrical Analysis.

3.6.1 The Geometry of the Gold Atom.

Before examining the structure of the polyhedron in detail, first consider the geometry of the gold atom to see if this sheds any light on the bonding within the complex. The gold atom is still bonded to the tricyclohexylphosphine ligand and the Au-P distance of 229.52(20) pm is very similar to that found in **(8a)** and also in the $[(Cy_3P)_2Au]^+$ cation. This implies that the cages in **(8a)** and **(15)** have similar electronic influence on the bonding within the $\{AuPCy_3\}$ moiety. The $^{31}P-\{^1H\}$ n.m.r. chemical shifts are however different : 68.9 and 60.9 ppm for **(8a)** and **(15)** respectively, and this implies that the chemical environment of the gold has been modified.

However the geometry of the gold atom is not easily determined. For example, consider the following possibilities :

Geometry	Three Positions	Angle/^{o}
Linear	P-Au-mid[B(5),B(10)][a]	173.9(14)
Trigonal Planar	P-Au-mid[B(5),B(6)]	141.4(14)
	P-Au-mid[B(9),B(10)]	138.4(14)
	mid[B(5),B(6)]-Au-mid[B(9),B(10)]	75.5(20)

Notes

[a] mid(X,Y) is the midpoint of the X-Y connectivity.

For the trigonal planar geometry outlined above, the sum of the three angles is $355(3)^o$, indicating that the geometry is very close to planar. This is also shown by

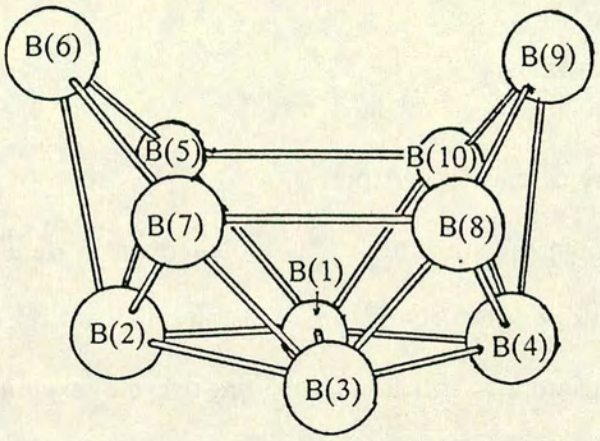

The renumbering for the discussion in the text.

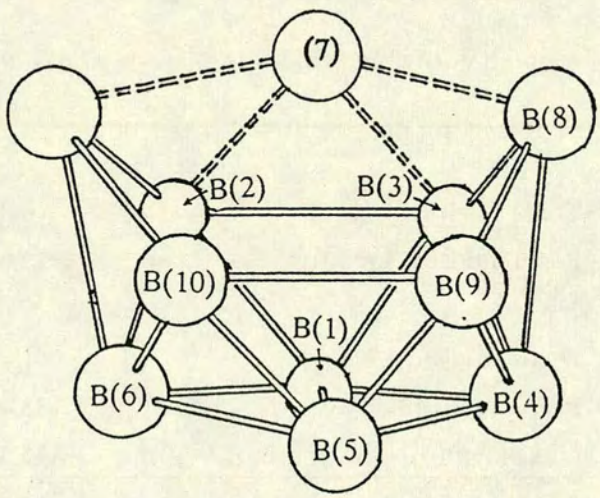

The correct numbering scheme for a *nido*-icosahedron with the heteroatom at the '7' position.

the gold atom being out of the P-mid[B(5),B(6)]-mid[B(9),B(10)] plane by only 23.6 pm. The difficulty arises because the formal geometry of the gold atom solely depends on how many orbitals the gold uses in bonding. One way of analysing the geometry of the gold is to use Mössbauer spectroscopy, and this is discussed below.

3.6.2 The Structure of the $\{B_{10}\}$ Cage.

Since complexes with a metal atom η^4-ligated to a $\{B_{10}H_{12}\}$ fragment (or its derivatives) are amongst the most common geometries known for metallaboranes, and there are some whose structures have been crystallographically determined, this offered an excellent opportunity to examine the structures using the *idealisation* technique discussed in Chapter 1.

3.6.3 Theoretical Considerations

It has been argued[131] that there are two distinct types of bonding in $\{MB_{10}H_{12}\}$ fragments. In the first type, there is only a two-orbital donation from the metal, the structure of the complex is analogous to that of decaborane, and so the bonding can be formally regarded as being between a M^{n+} centre and a *nido*-$[B_{10}H_{12}]^{2-}$ ligand. Formally the complex would have an electron count of 12 SEP's, and hence the B_{10} cage will have a lot of *nido*-undecaborane character. Chemically the M-B bonding is relatively weak, as shown by the cleavage reaction[59] using H-Cl:-

$$[Me_2TlB_{10}H_{12}]^- + H\text{-}Cl \longrightarrow Me_2TlCl + B_{10}H_{14} + Cl^-$$

In the second type however, it is argued that the metal uses three orbitals in bonding to the cage, and so the bonding in the compound is thought to be more complex and the structure is closer to that which comes from complexing a M^{n+} centre with an *arachno*-$[B_{10}H_{12}]^{4-}$ fragment. This cluster will have a 13 SEP

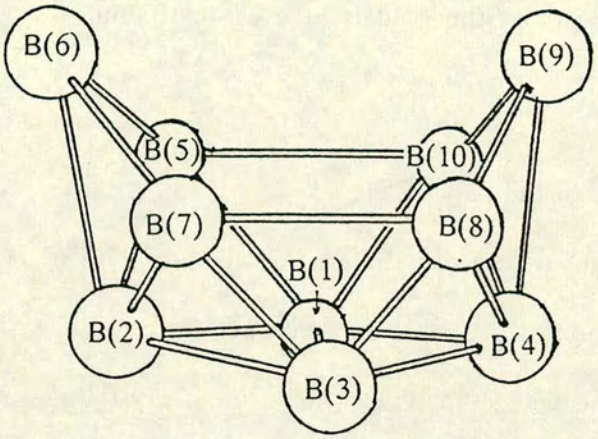

The renumbering for the discussion in the text.

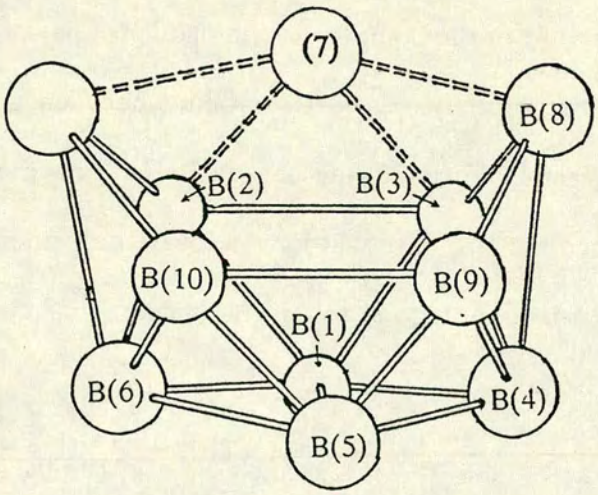

The correct numbering scheme for a *nido*-icosahedron with the heteroatom at the '7' position.

count, and therefore the geometry has much more *nido*-icosahedral character.

Initial evidence for the structure of **(15)** being anomalous came from an investigation into the planarity of the open face. In a perfect *nido*-icosahedron, the open face of the cage will be planar, and so the extent of icosahedral nature in a cluster can be gauged by measuring how far the fifth atom is from the best-fit plane defined by the atoms B(6), B(7), B(8), and B(9). For example, in $[B_{11}H_{13}]^{2-}$, the boron capping the B(6)-B(5)-B(10)-B(9) edge is 5.1 pm above this plane, and the equivalent figure for $[B_{12}H_{12}]^{2-}$ [132] is 3.2 pm. For $[(B_{10}H_{12})_2Au]^-$, the Au is out of this plane by 46.3pm. In other complexes with $\{AuB_{10}H_{12}\}$ fragments, this figure varies from 40.1 to 54.5 pm, except for **(15)** which is well above this, at 71.7 pm. The other transition metal metallaboranes listed below produce values ranging from 37.4 to 47.4 pm. The thallium atom is out by 88.3, and the zinc by 57.5 pm. In view of the anomalous structure of **(15)** when compared against the other $\{AuB_{10}H_{12}\}$ fragments, its geometry was further investigated by the misfit technique discussed earlier.

3.6.4 Idealisations

Based on these arguments, the $\{B_{10}\}$ fragments of a number of metallaboranes were compared against the similar parts of the structures of *nido*-$B_{10}H_{14}$, *arachno*-$[B_{10}H_{14}]^{2-}$, and *nido*-$[B_{11}H_{13}]^{2-}$. The results are listed overleaf.

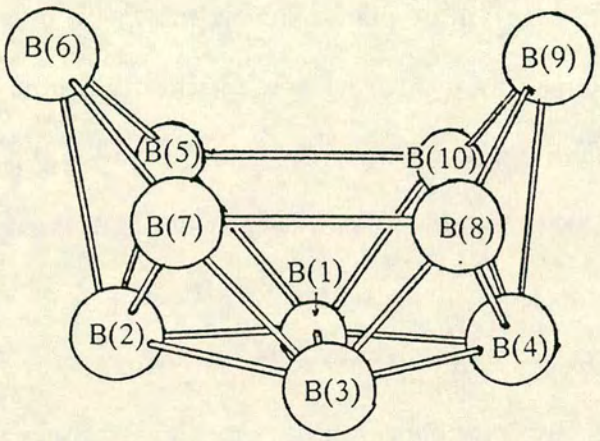

The renumbering for the discussion in the text.

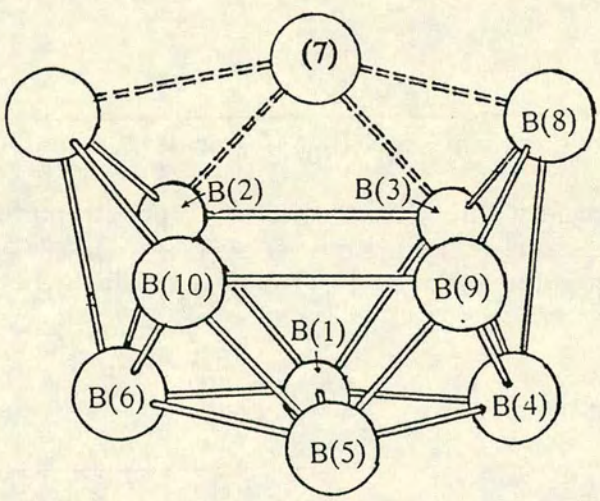

The correct numbering scheme for a *nido*-icosahedron with the heteroatom at the '7' position.

Compound	Reference	Comparison with $[B_{10}H_{14}]$	$[B_{10}H_{14}]^{2-}$	$[B_{11}H_{13}]^{2-}$
$\{(CO)(PPh_3)_2\}IrB_{10}H_{11}(PPh_3)$	133	15.8	8.9	7.6
$(Cp^*Rh)Cl(Me_2PhP)B_{10}H_{11}$	134	13.3	5.4	7.5
$[(B_{10}H_{12})_2Ni]^{2-}$	135	8.0	7.3	10.8
$(Me_2PhP)_2PtB_{10}H_{12}$	15	10.9	7.4	7.9
$(Me_2PhP)_2PtB_{10}H_{11}Cl$	136	11.4	6.6	7.3
(15)		4.8	12.1	16.3
$[(B_{10}H_{12})_2Au]^-$	137	10.6	6.5	9.0
$[(B_{10}H_{12})_2Zn]^{2-}$	138	4.9	11.4	15.2
$[Me_2TlB_{10}H_{12}]^-$	59	4.2	12.3	16.7

As can be seen from these results, there is a distinct pattern. If it is a complex of a main group metal, then the structure of the $\{B_{10}\}$ cage is based on that of $B_{10}H_{14}$. The transition metal derivatives, however, exhibit more variety in their comparisons. They can be subdivided into the derivatives of the typical transition metals (the Ir and Rh complexes) and the late transition metals (Ni and Pt). The former subset are characterised by a structure which compares more closely with that of $[B_{11}H_{13}]^{2-}$ than $[B_{10}H_{14}]^{2-}$ or $B_{10}H_{14}$. The latter category fit best with $[B_{10}H_{14}]^{2-}$, although the fit versus $[B_{11}H_{13}]^{2-}$ is not much worse (except for the Ni complex). The Ni complex is slightly ambiguous in that its fit with $B_{10}H_{14}$ is quite reasonable, although not as good as it is with $[B_{10}H_{14}]^{2-}$.

A generalised discussion of the structures of $\{MB_{10}H_{12}\}$ metallaborane derivatives, that includes critical use of the above misfits to quantify the "verticity" of the metal centre, appears in Section 4.10, starting on page 135.

Based on the above trends, consider the two Au structures. The $[(B_{10}H_{12})_2Au]^-$ anion has a square planar gold atom (see Chapter 4), and hence is likely to be Au(III) i.e. d^8 and so a late transition metal. On the other hand, **(15)** is clearly analogous to the main group complexes suggesting that the gold

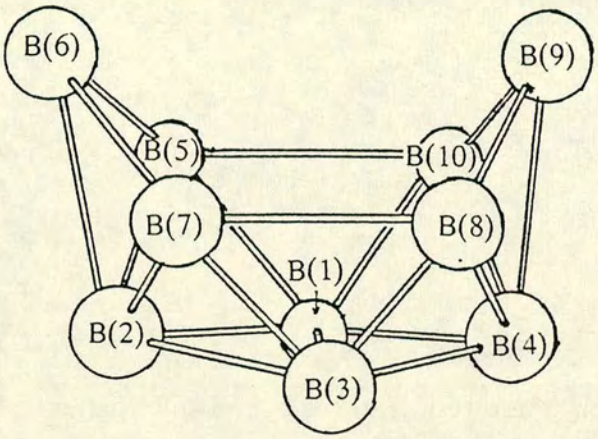

The renumbering for the discussion in the text.

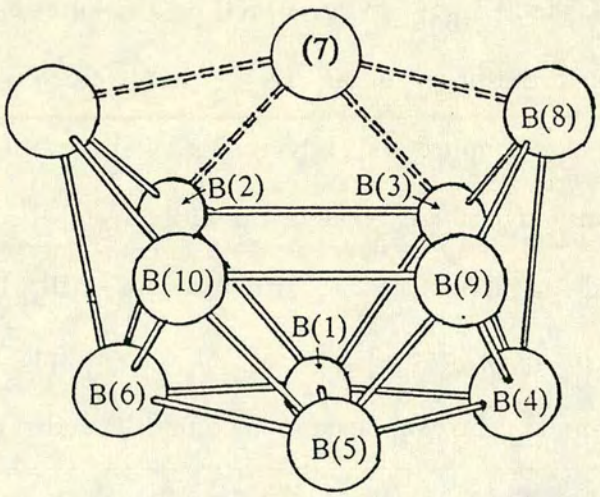

The correct numbering scheme for a *nido*-icosahedron with the heteroatom at the '7' position.

atom is therefore d^{10} and Au(I).

This is one way of assessing the usefulness of this technique : using it to make predictions and then devising other experiments to test them. As previously explained, one of the few ways in which the oxidation state of certain metals (including Au) can be determined is by Mössbauer spectroscopy. A sample of **(15)** was sent to UMIST where Dr. R.V.Parish acquired and interpreted its Mössbauer spectrum. The observed scattering and the calculated spectrum are shown in Figure 3.4, overleaf. The experimental results are that the IS was 3.68, and the QS was 8.13 mms^{-1}. These data are consistent[126] with this complex being a linear Au(I) species, although the values are not substantially different from those of a trigonal Au(I) species (IS < 3.23, QS > 9.09 mms^{-1}).

This suggests that **(15)** is analogous to **(9)**, and the differences, which are observed in the two structures when the B(9)-B(10) connectivity of **(8a)** or $B_{10}H_{14}$ is deprotonated, are due to the different bonding capabilities of the different groups bridging the B(5)-B(6) connectivity in **(8a)** or $B_{10}H_{14}$ - the formally isolobal $\{AuPCy_3\}$ fragment and the H atom respectively.

It was therefore very important to compare the structure of **(15)** with that of **(9)**. As was mentioned in Section 3.2, when **(9)** is compared against $B_{10}H_{14}$, the misfit is 7.7 pm,due almost entirely to variations in the positions of atoms B(5) (14.7 pm) and B(9) (15.8 pm). This is presumably due to the variation in the two bond lengths discussed above.

When **(9)** was compared against **(15)** the resulting misfit was 6.0pm, with the biggest deviation in the positions of B(6), B(9), and B(10). Whilst this misfit is greater than that of **(9)** versus $B_{10}H_{14}$, the difference is so small that it is probably statistically insignificant.

Since both **(8a)** and **(15)** both have structures similar to that of decaborane,

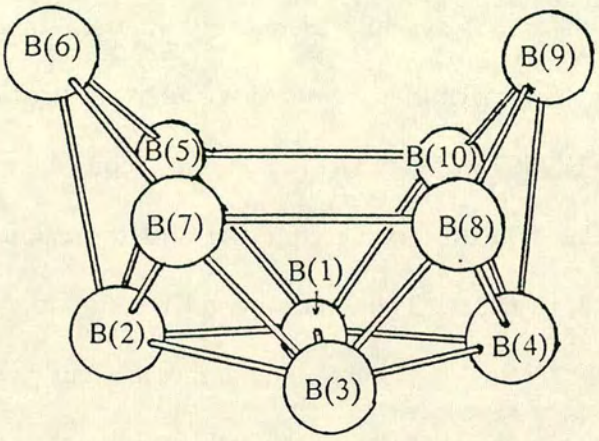

The renumbering for the discussion in the text.

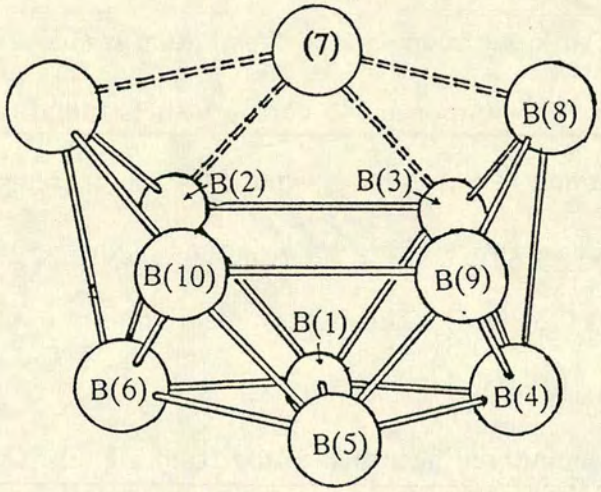

The correct numbering scheme for a *nido*-icosahedron with the heteroatom at the '7' position.

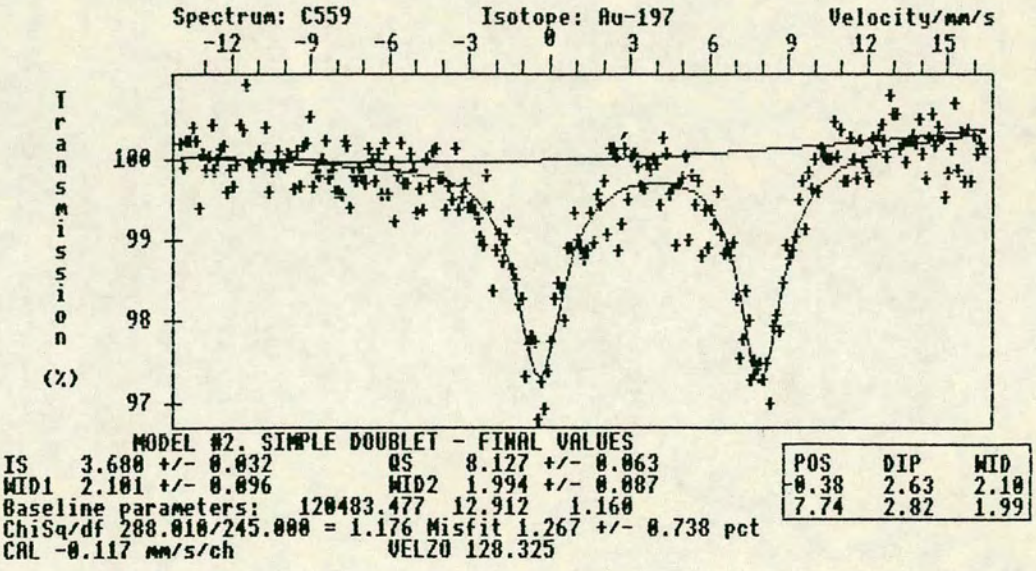

Figure 3.4. The Mossbauer spectrum of $[NHEt_3]^+$ **(15)** showing the observed intensities(x) and the calculated values(line).

the two were compared directly, to see what the 'global' and 'local' effects of the deprotonation are. The comparison yields a misfit of 7.5 pm, primarily due to large variations in the positions of B(6) (16.1 pm), B(10) (12.1 pm), and B(8) (8.0 pm). The variation in the positions of B(6) and B(10) is probably due to the shift in the position of the gold atom. The reason for the large variation in the position of B(8) is probably related to the increased B(8)-B(9) bond length upon deprotonation (from 164.3(20) to 181.3(15) pm). When the gold atom is included in the comparison, the misfit increases to 30.9 pm, and the principal variations are in the atomic positions of Au (84.8 pm) and B(9) (40.1 pm).

3.6.5 Comparison with Other Metallaboranes.

As previously discussed, **(15)** has a cage architecture similar to the main group metallaborane derivatives of $B_{10}H_{14}$, and so a detailed comparison of their structures was made in order to find out what differences there are in the cage geometries.

The relevant parameters are listed in Table 3.3, overleaf. First, note how the metal-B(6) and metal-B(9) connectivities are similar in length, but are much longer than the two inner metal-boron connectivities which are of similar size. The Au-B(5) and Au-B(10) distances are similar to the gold-boron connectivities in **(8a)**.

Secondly, the length of the B(5)-B(10) connectivity is shorter than the B(7)-B(8) one when there is a metal bonded to the cage. This also holds for the connectivities whose equivalents in $B_{10}H_{14}$ are H-bridged - when a metal replaces two H-bridges, the B(5)-B(6) and B(9)-B(10) connectivities shorten when compared against the B(8)-B(9) and B(6)-B(7) connectivities. These effects are rationalised in Section 3.7.4.

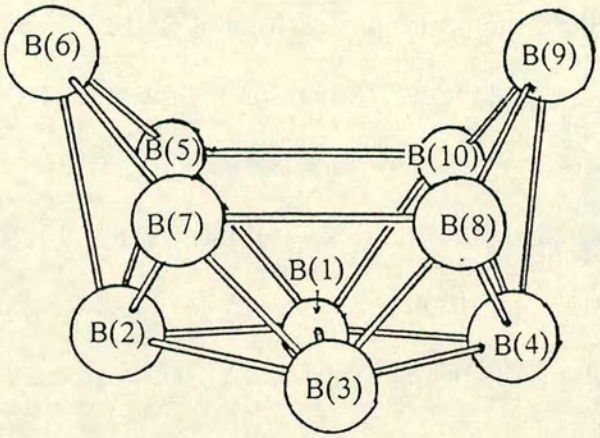

The renumbering for the discussion in the text.

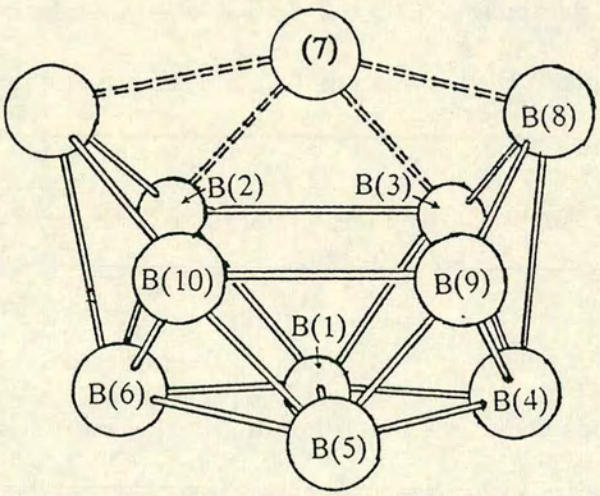

The correct numbering scheme for a *nido*-icosahedron with the heteroatom at the '7' position.

Table 3.3. A Comparison of Certain Connectivity Lengths(pm) For Relevant Boranes and Metallaboranes. Numbering is as in the text.

Bond[a]	$B_{10}H_{14}$	(8a)	(15)	$[Me_2TlB_{10}H_{12}]^-$	$[(B_{10}H_{12})_2Zn]^{2-}$[b]
M-B(5)	——	224.5(10)	229.4(10)	251(2)	220.7(14)
M-B(6)	——	227.0(10)	246.9(10)	276(2)	244.4(15)
M-B(9)	——	——	249.0(10)	277(2)	244.8(14)
M-B(10)	——	——	228.5(10)	261(2)	219.9(14)
B(5)-B(10)	198.7[c]	199.4(15)	190.3(13)	197(3)	192.6(15)
B(7)-B(8)	198.7[c]	201.0(18)	207.4(16)	206(3)	206.8(17)
B(5)-B(6)	178.2[d]	177.0(14)	175.4(15)	170(3)	167.6(16)
B(6)-B(7)	179.0[e]	177.6(15)	178.6(15)	177(3)	178.6(20)
B(8)-B(9)	178.2[d]	164.3(20)	181.3(15)	179(3)	180.5(18)
B(9)-B(10)	179.0[e]	187.7(19)	168.7(14)	174(3)	170.5(16)

Notes

a. *nido*-decaborane numbering.

b. Averaged for the two independent cages.

c.
d. } symmetry-related pairs.
e.

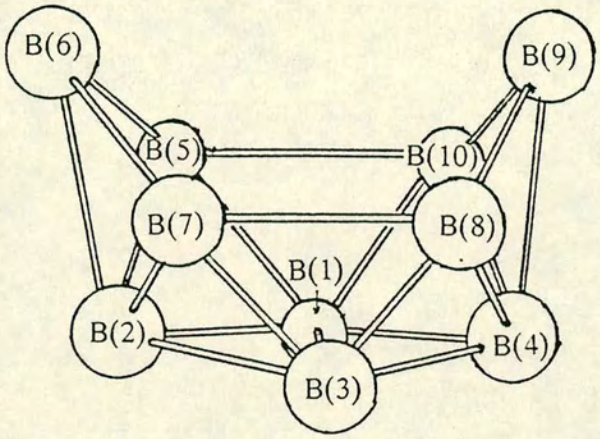

The renumbering for the discussion in the text.

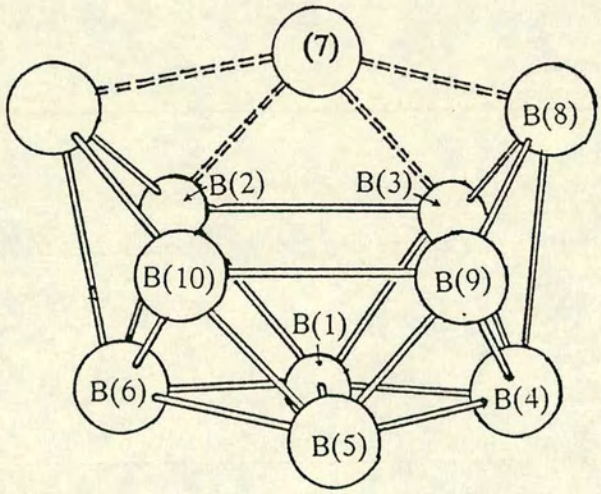

The correct numbering scheme for a *nido*-icosahedron with the heteroatom at the '7' position.

3.7 EHMO Calculations on the Structure of (15).

In an attempt to understand how the gold bonds to the cage in **(15)**, EHMO calculations were performed. The coordinates of these models are in Appendix 3, starting on page 281. Both the modelling and interpretation of the results was less straightforward than those discussed in Chapter 2.

3.7.1 The $[B_{10}H_{12}]^{2-}$ Ligand

The first model was of the $[B_{10}H_{12}]^{2-}$ ligand, **(16)**. The geometry of **(16)** is the same as that of $B_{10}H_{14}$ with $[H(5,6)]^{+}$ and $[H(9,10)]^{+}$ omitted. The frontier orbitals, (FO's), of **(16)** are shown in Figure 3.5 on page 81, and relevant parameters are listed in Table 3.4 on page 107. They bear a striking resemblance to the FO's of *cis*-butadiene[139], although there are differences in both the orientation and coefficients of the contributing AO's. Especially, note that the occupied *a'* orbital of *cis*-butadiene appears as two components : the 2nd and 3rd HOMO's. These differ in the contributions from atoms below the open face. Secondly, all of the atomic orbitals of **(16)** point slightly towards the centre of the B(6)-B(5)-B(10)-B(9) trapezoid, whereas those of *cis*-butadiene are all vertical with respect to the C_4 plane.

3.7.2 EHMO Calculations without P 3d Orbitals

The FO's of a $[AuPH_3]^{+}$ fragment, **(17a)**, have been investigated[140] by other authors. Their calculations emphasised the isolobal relationship between **(17a)** and the H atom in that the only fragment molecular orbital (FMO) of a suitable energy for effective bonding was the Au 6s/$6p_z$ hybrid of a_1 symmetry. The Au 5d orbitals were regarded as essentially 'core' orbitals, and the $6p_x$ and $6p_y$ *e* pair were of too high an energy to be efficient acceptor orbitals.

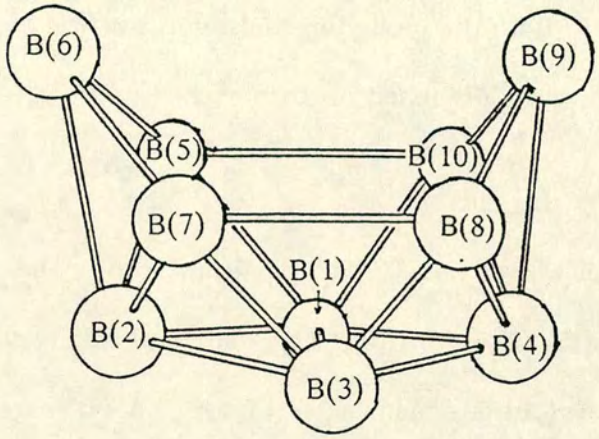

The renumbering for the discussion in the text.

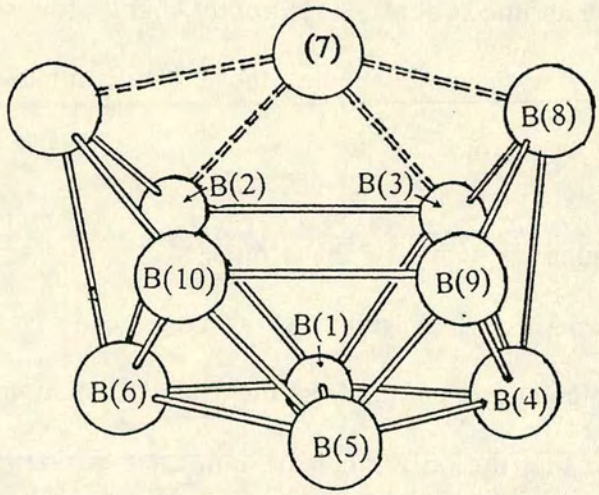

The correct numbering scheme for a *nido*-icosahedron with the heteroatom at the '7' position.

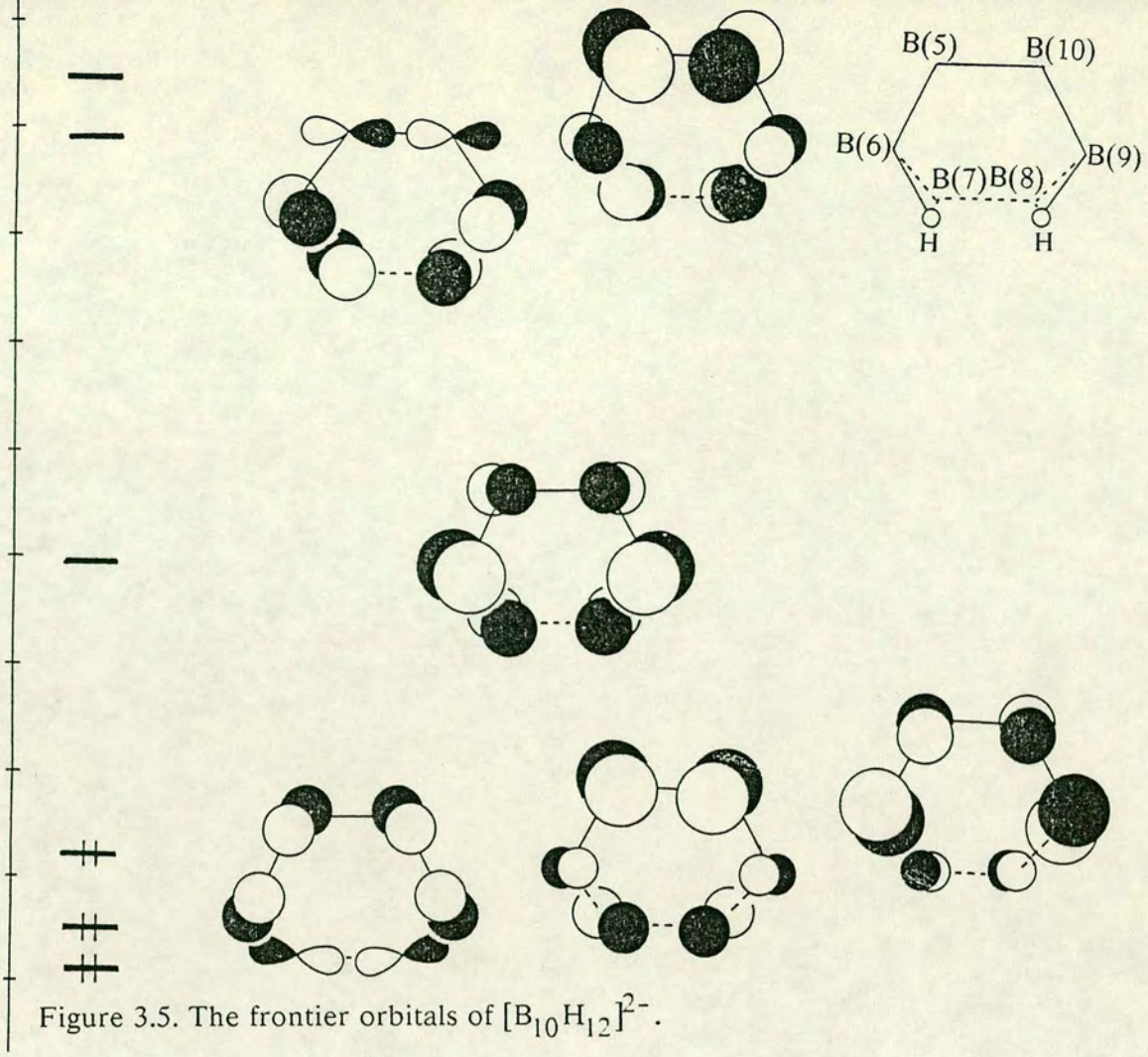

Figure 3.5. The frontier orbitals of $[B_{10}H_{12}]^{2-}$.

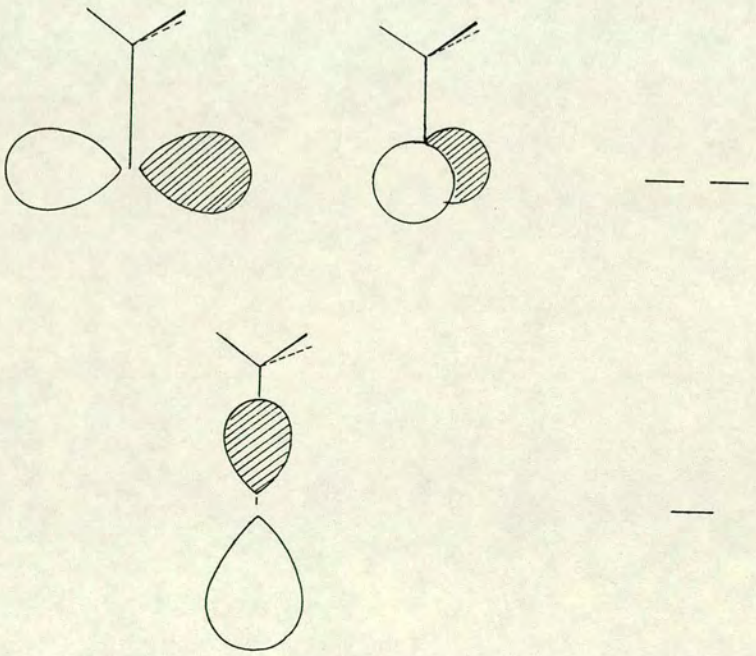

Figure 3.6. The frontier orbitals of $[AuPH_3]^+$ without including the P 3d orbitals in the basis set.

This orbital set explains the strong preference in gold chemistry for linear $[AuX(PR_3)]$ species such as **(8)**. However, the authors did not include the P d-orbitals in their basis set (the set of atomic orbitals from which the molecular orbitals are derived), and when these are included, the orbital set is more complex, but presumably more accurate as well. First, however, the simpler set will be considered. The FO's of **(17a)** are shown, schematically, in Figure 3.6 overleaf, and their composition is listed in Table 3.5 on page 108. All three orbitals are unfilled.

The final model, **(15b)**, is of **(15)** itself. This has the same $\{B_{10}\}$ cage geometry as $B_{10}H_{14}$ except that $[H(5,6)]^+$ and $[H(9,10)]^+$ have been removed. The $[AuPH_3]^+$ fragment is then superimposed orthogonal to the B(5)-B(6)-B(9)-B(10) plane, with bond lengths similar to those in **(15)**.

The overlap of **(16)** with **(17a)** in the z-direction is shown schematically in Figure 3.7 on page 83. As can be seen, there is clearly allowed overlap of:

(i) the second and third HOMO's of **(16)** with the Au $6s/6p_z$ orbital of **(17a)** (thus affording a' MO's).

(ii) the HOMO of **(16)** with the Au $6p_x/5d_{xz}$ orbital of **(17a)** (thus affording a'' MO's).

(iii) the LUMO of **(16)** with the Au $6p_y$ orbital of **(17a)**.

However interaction (iii) is between two empty orbitals, and so will not contribute to Au-borane bonding.

The formal geometry of the gold is determined by the extent to which the interaction (ii) takes place. If it is negligible, the gold is formally linear. The occupation of the Au AO's in **(15b)** are : Au $6p_x$ 0.1824 $6p_y$ 0.0152, and $6p_z$ 0.2763. These results suggest that interaction (ii) takes place to a significant extent, implying that the gold geometry is most accurately described as

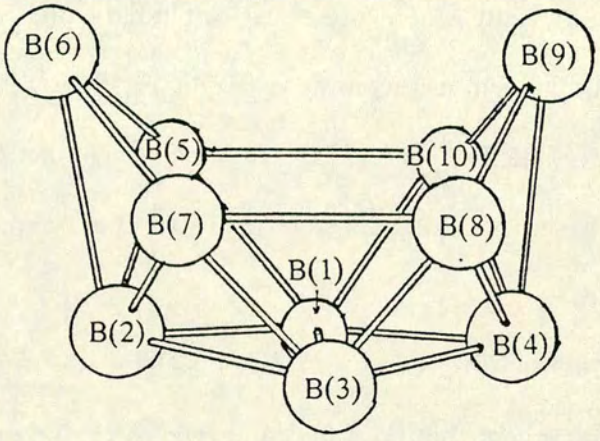

The renumbering for the discussion in the text.

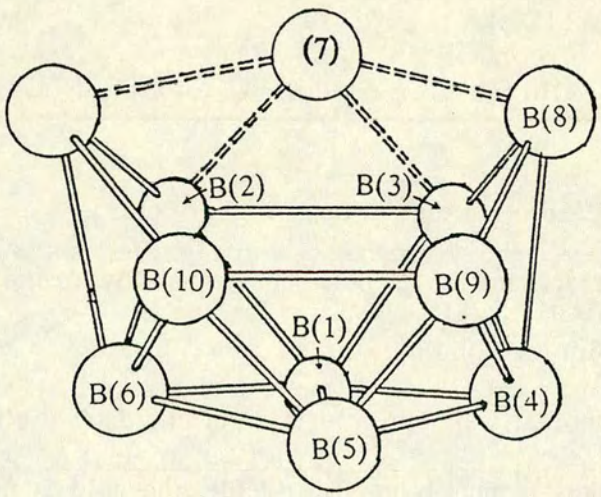

The correct numbering scheme for a *nido*-icosahedron with the heteroatom at the '7' position.

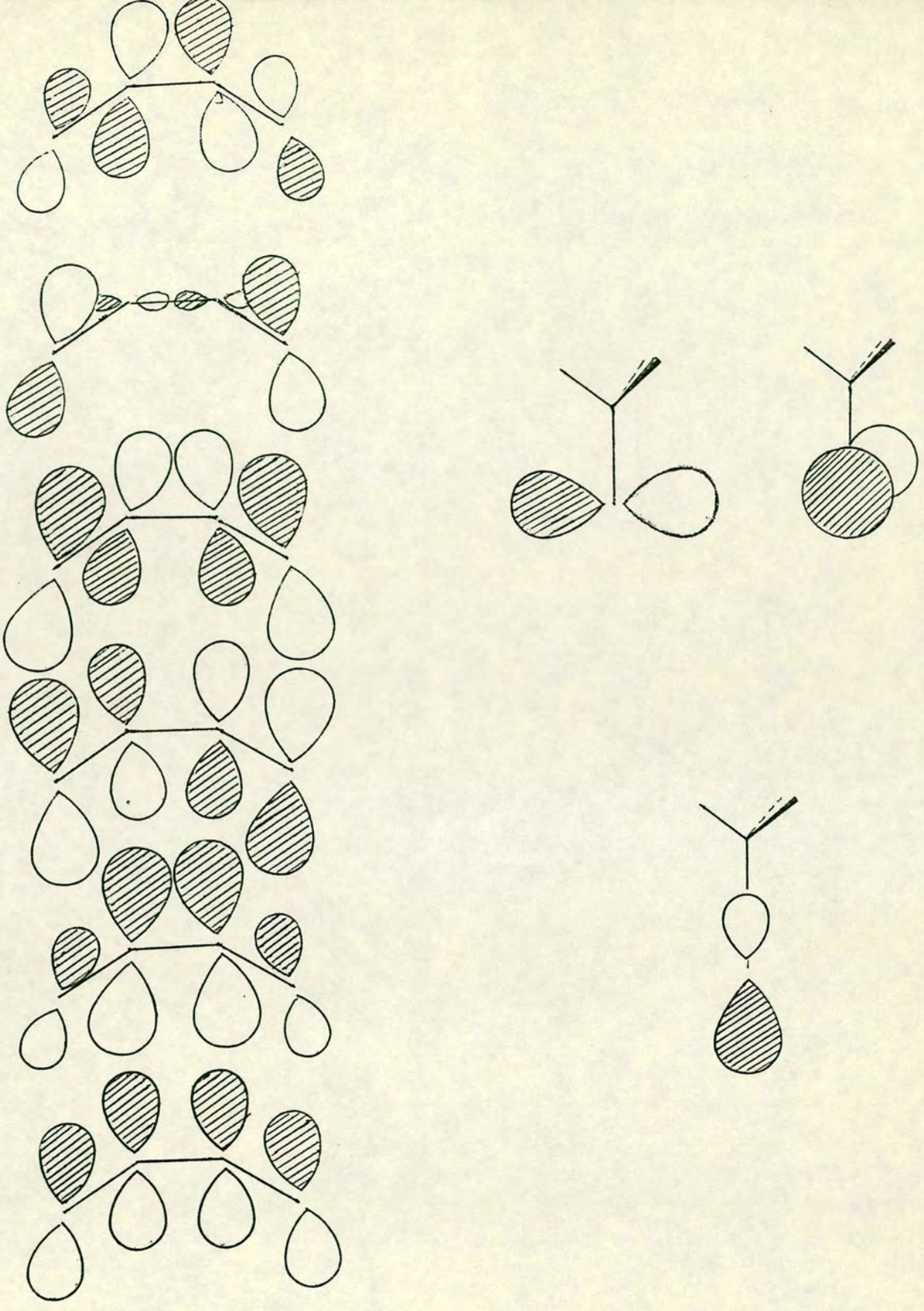

Figure 3.7. A schematic view of the molecular bonding in $[H_3PAuB_{10}H_{12}]^-$.

intermediate between linear and trigonal planar.

3.7.3 Calculations Including P 3d Orbitals

When the P 3d orbitals are included in the basis set, the major differences are as follows. The highest occupied MO's of $[AuPH_3]^+$, **(17b)**, are still primarily of Au 5d character, but now there are another five unoccupied orbitals between the HOMO and the Au $6s/6p_x$ hybrid. These are mainly of P 3d character, but there are significant amounts of Au-based orbitals mixed-in. These five orbitals are shown in Figure 3.8, overleaf, and relevant atomic orbital occupations are listed in Table 3.6 on page 109. The lower and upper *e* pairs differ in respect of the hybridisation at P. The a_1 orbital, whilst out-of-phase between Au and P, is of lower energy than the Au-based orbital because of its predominant P character.

The orbital scheme for **(16)** is, of course, unchanged. Since the orbital scheme of **(17b)** is more complex, a different approach to this problem was used - the fragment molecular orbital (FMO-EHMO) approach. Instead of analysing the MO's in terms of the contributing AO's, this approach emphasises the importance of the bonding capabilities of molecular fragments, and the advantage of his approach is that it enables the user to follow how the fragments bond together - which tends to simplify the interpretation of the problem.

The derived MO scheme is in Figure 3.9 on page 85. The effective result is that the combined deoccupation of the *a'* orbitals is 0.3443 and that of the *a''* is 0.3352, and the Au 5p orbital occupations are now p_x 0.2212 and p_z 0.2873. However since the interaction also involves the P 3d orbitals, the gold orbital occupations do not fully reflect the interaction, and so their values should be treated cautiously.

These parameters suggest that whilst the geometry of the gold is not fully

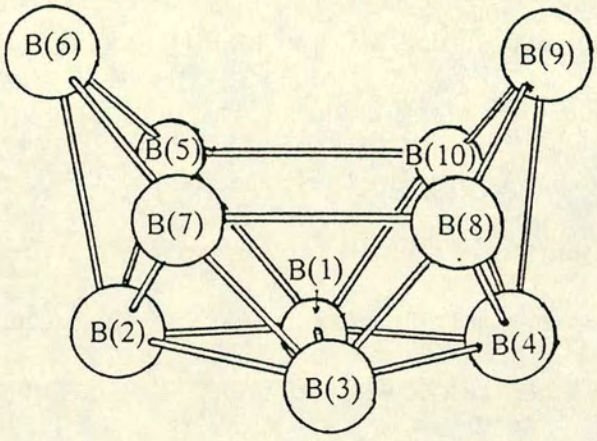

The renumbering for the discussion in the text.

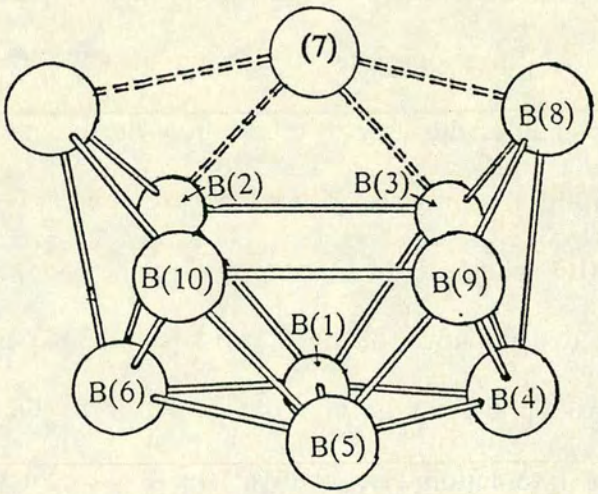

The correct numbering scheme for a *nido*-icosahedron with the heteroatom at the '7' position.

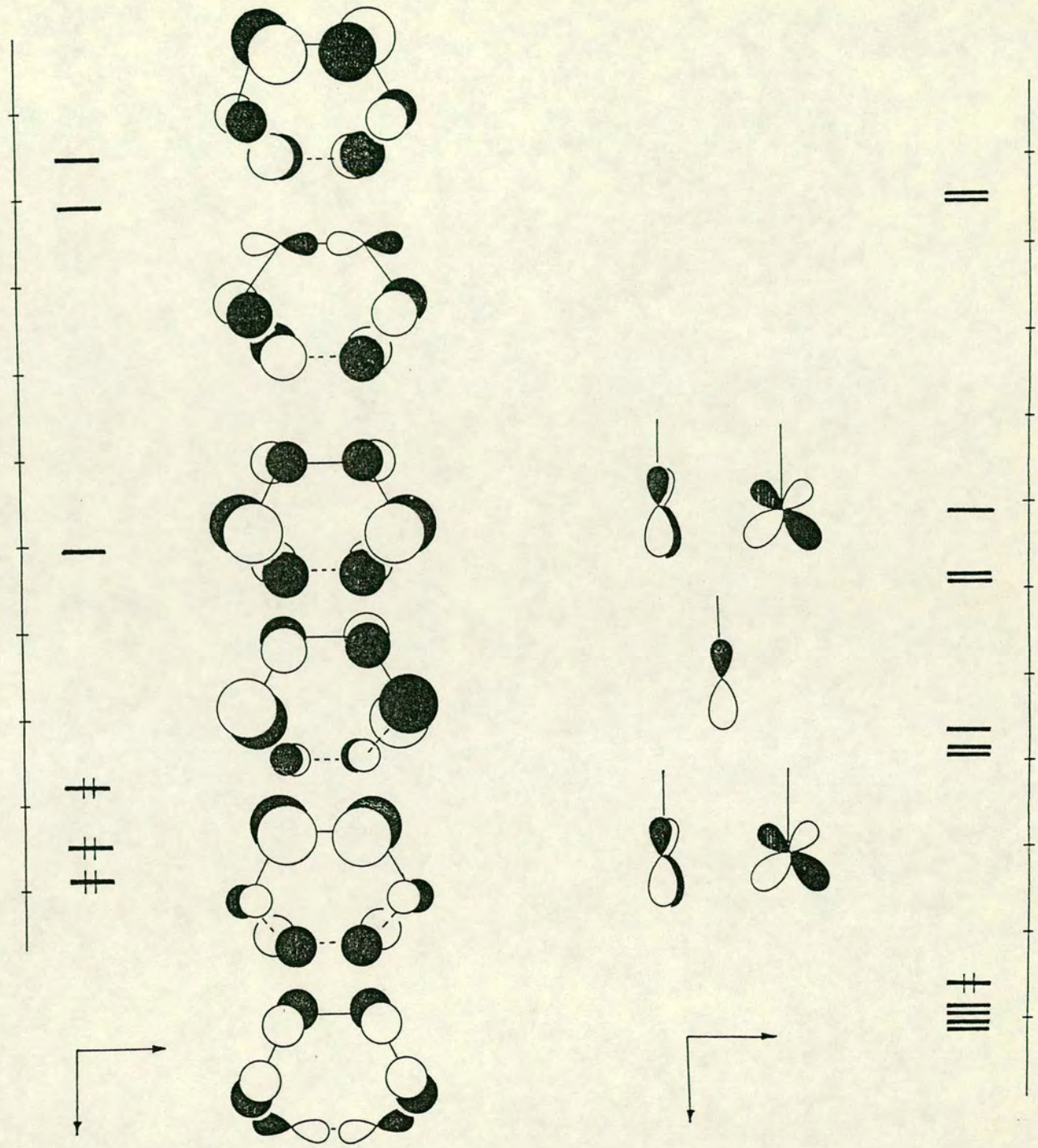

Figure 3.8. The lowest unoccupied molecular orbitals of $[H_3PAu]^+$ when the P 3d orbitals are included in the basis set.

Figure 3.9. The molecular orbital scheme for $[H_3PAuB_{10}H_{12}]^-$.

trigonal planar, it is more so than the earlier calculations suggested. The effect of including the P 3d orbitals is therefore to emphasise the tangential bonding component of the $\{AuPH_3\}$ fragment. Furthermore, the overall occupation of the gold 6p orbitals is increased, implying that the Au-borane bonding is stronger. Since the inclusion of these orbitals has caused a slight change in the interaction, in future calculations, these orbitals will be included in the basis set.

3.8 Rationalisation of Some Structural Parameters.

Earlier, it was observed that in the main group metal derivatives, the B(5)-B(10) is shorter than the B(7)-B(8), and that both the B(5)-B(6) and B(9)-B(10) connectivities are similarly shorter than the B(6)-B(7) and B(8)-B(9) ones.

The former shortening can be explained as follows. The difference in bond lengths is due to the different bonding capabilities of the metal+ligand(s) fragment on one side, and that of [H...H] on the other. When an FMO-EHMO calculation is performed on the interaction of $[B_{10}H_{12}]^{2-}$ with $[H..H]^{2+}$, the result is a combined deoccupation of the *a'* orbitals of 0.7958, and 0.8781 for the *a''* orbital. The equivalent figures for **(15)** are 0.3443 and 0.3352.

When the *a'* orbitals are deoccupied by bonding, the B(5)-B(10), and to a lesser extent, the B(5)-B(6) and B(9)-B(10) connectivities will all lengthen. When the *a''* orbital is deoccupied, the B(5)-B(10) will (slightly) shorten, and the B(5)-B(10) and B(6)-B(9) will both lengthen.

For the side of **(15)**, by analogy, which is bonded to [H..H], there is more deoccupation of the *a''* orbital than the *a'*. The effect of this is that all three bonds will lengthen. The side with the $[AuPH_3]$ fragment however, has much less deoccupation of these orbitals, and so the lengthening will be less, i.e. *they will be*

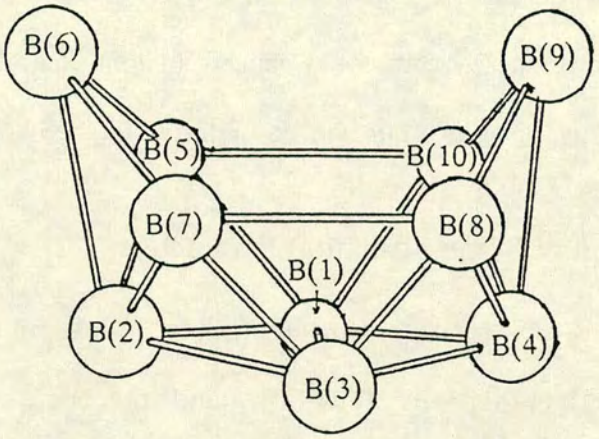

The renumbering for the discussion in the text.

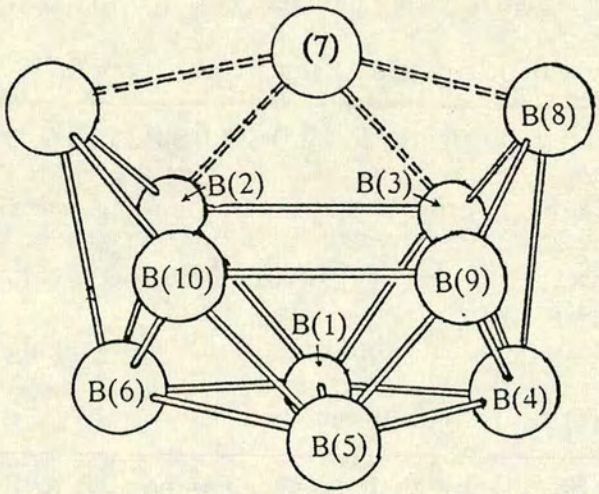

The correct numbering scheme for a *nido*-icosahedron with the heteroatom at the '7' position.

relatively shorter. This can be extended to consider the bonds in decaborane as well. These arguments predict that the B(5)-B(10) and B(7)-B(8) (both 198.7pm); the B(5)-B(6), B(6)-B(7), B(7)-B(8), and B(9)-B(10) (178.2, 179.0, 178.2 and 179.0pm) all will be longer than the equivalent distances which are bridged by the $\{AuPCy_3\}$ fragment in **(15)** (B(5)-B(10) 190.3(13), B(5)-B(6) 175.4(15), and B(9)-B(10) 168.7(14)pm).

It is thought that the reason why the $\{AuPCy_3\}$ fragment is not orthogonal to the cage, but has tilted 26^o towards the open face is related to a similar phenomenon in Ph_3PAuCp[141]. In this species, the gold-phosphine fragment makes an angle of 83^o with the best-fit C_5 plane, resulting in a coordination described as intermediate between η^1 and η^3. This structure has been rationalised [140,142] by the following explanation.

As stated earlier, the Au p_x and p_y orbitals are high-lying. This means that they cannot overlap effectively with the cyclopentadienyl π orbitals of e_1 symmetry, and therefore the e_1 (which are filled) interact with the (filled) Au $5d_{xz}$ and $5d_{yz}$ orbitals. Since both the bonding and antibonding combinations are occupied, the molecule is destabilised by this interaction. The destabilisation can be reduced by a sideways slip of the gold atom.

When **(17)** overlaps with **(16)**, there is potentially a similar destabilising interaction of the Au $5d_{xz}$ and the HOMO of **(16)**. However, by tilting towards the open face, this destabilisation is minimised, and additionally, the FO's on the gold point more directly at B(5) and B(10), which, as can be seen in Figure 3.5 on page 81, have greater coefficients on the second HOMO, and so the bonding will be strengthened.

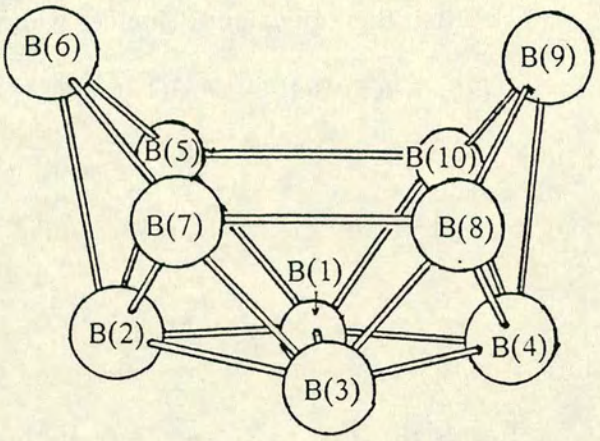

The renumbering for the discussion in the text.

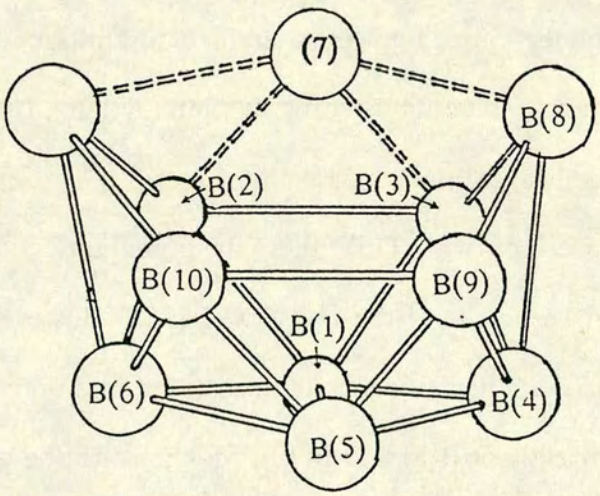

The correct numbering scheme for a *nido*-icosahedron with the heteroatom at the '7' position.

3.9 Multinuclear N.M.R. Spectroscopy.

The ^{31}P-{^{1}H} n.m.r. spectrum of **(15)** consists of one broad peak, very similar to that of $Cy_3PAuB_{10}H_{13}$. As already mentioned, the ^{11}B-{^{1}H} n.m.r. spectrum consists of six peaks (see Figure 3.10 (upper half), on page 89) with integrals in the ratio of 2 : 1 : 2 : 2 : 1 : 2, as expected for a $\{B_{10}\}$ cage with mirror symmetry. However when the ^{1}H-{^{11}B,selective} n.m.r. spectrum (Figure 3.11, page 90) was obtained, it proved difficult to interpret. Every resonance couples to the bridging hydrogen atoms, and when the ^{11}B(COSY) (Figure 3.10 (lower half)) spectrum was acquired, there were very few off-diagonal couplings.

It was shown previously that the $\{B_{10}\}$ cage in $[Cy_3PAuB_{10}H_{12}]^-$ is analogous to that of $B_{10}H_{14}$. In order to assign this spectrum, consider the spectra of related species which have previously been fully investigated. There are three in particular : $[B_{10}H_{14}]$ [125], $[B_{10}H_{13}]^-$ [129], and $[Me_2TlB_{10}H_{12}]^-$ [143]. The chemical shifts and assignments of all of these are listed in Table 3.7 on page 110. In all of these spectra, there are two consistent details : the peak at highest frequency has been assigned to B(1)‡ , B(3), B(6), or B(9) ; and the signal at lowest frequency to B(2) and B(4).

Now the two peaks in the spectrum of the $[Cy_3PAuB_{10}H_{12}]^-$ anion at $\delta^{11}B$ = -6.38 and -28.18 ppm (with relative integrals of 1) must be due to B(1) and B(3) on symmetry grounds, and so the signal at $\delta^{11}B$ = 3.74 ppm (2B), which is the one at highest frequency, must arise from B(6) and B(9). The signal at $\delta^{11}B$ = -31.07 ppm (2B), which is the one with lowest frequency, must be due to B(2) and B(4). The only other signal at very low frequency, at $\delta^{11}B$ = -28.18 ppm has

---

‡ *nido*-$\{B_{10}\}$ numbering

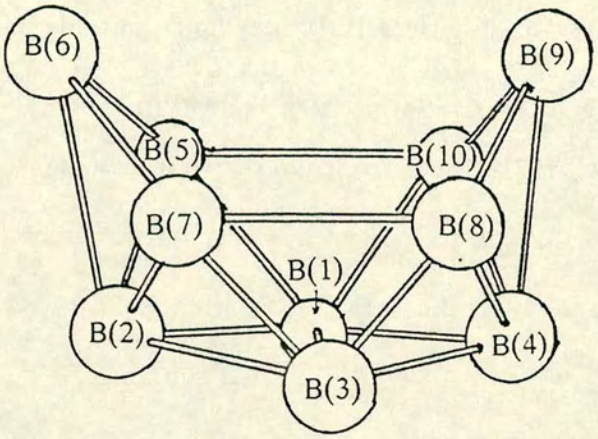

The renumbering for the discussion in the text.

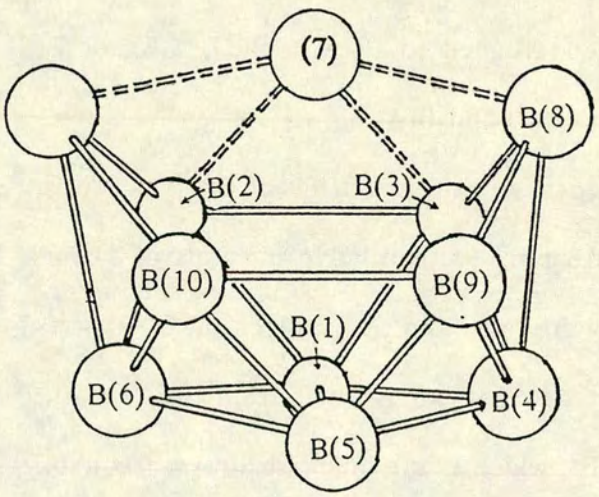

The correct numbering scheme for a *nido*-icosahedron with the heteroatom at the '7' position.

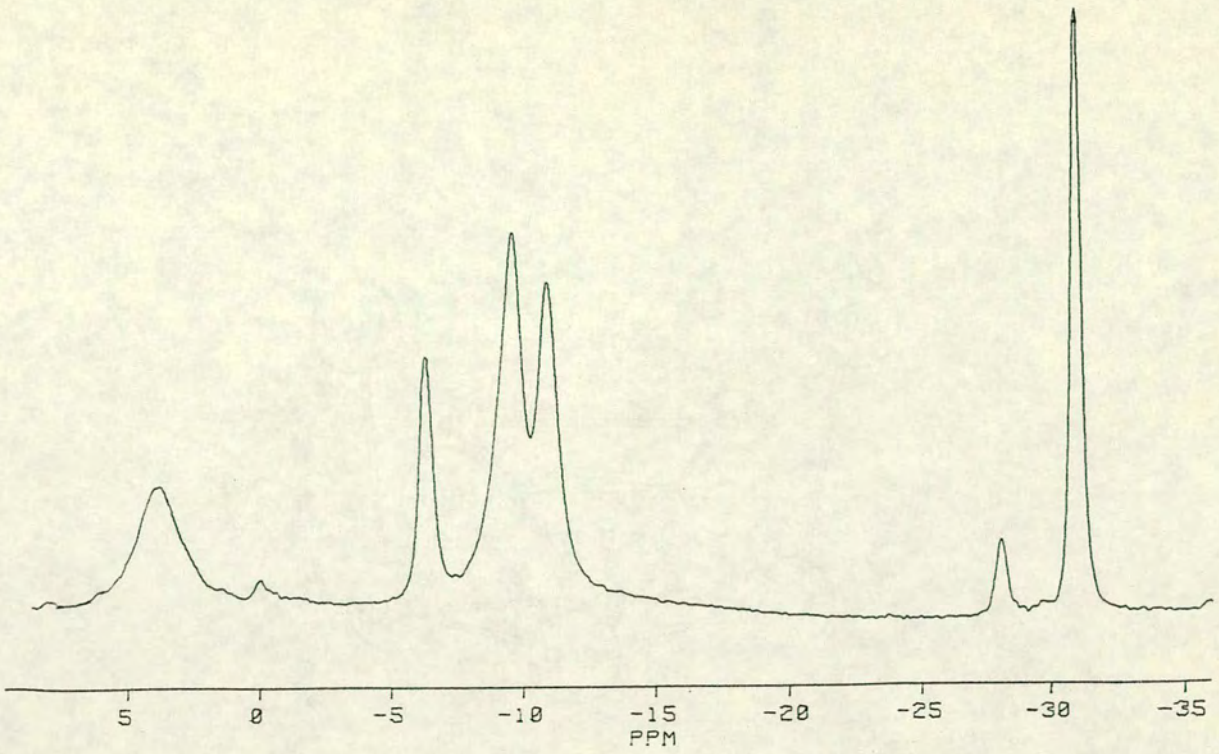

(a)

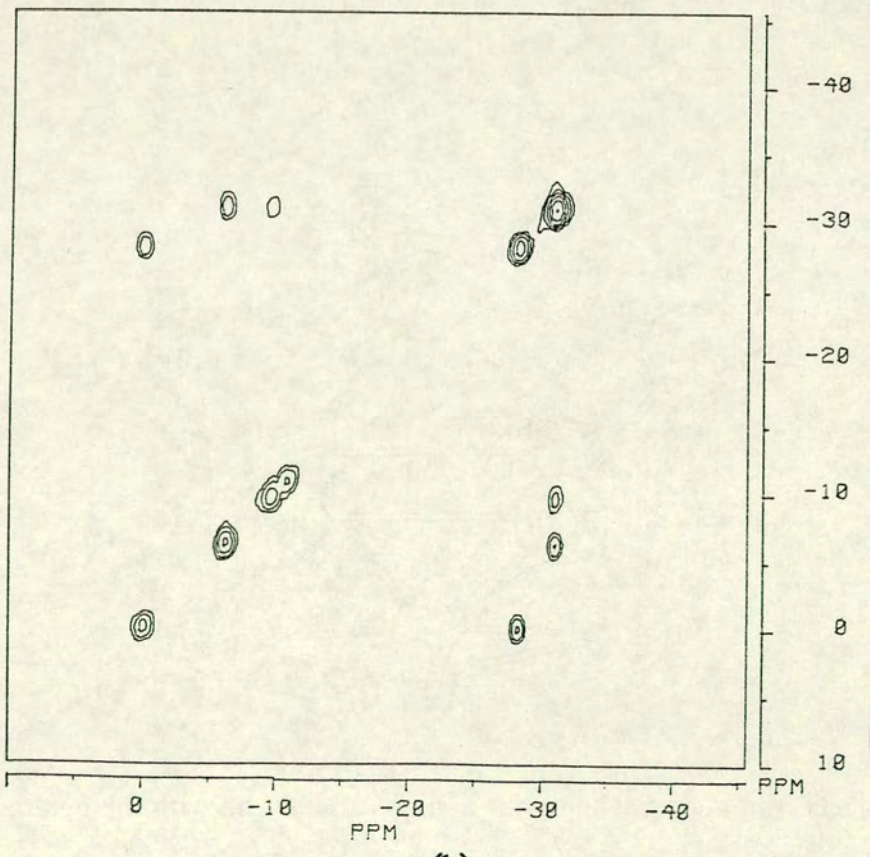

(b)

Figure 3.10. (a) the ^{11}B-{^{1}H} and (b) is the ^{11}B(COSY) n.m.r. spectrum of **(15)**.

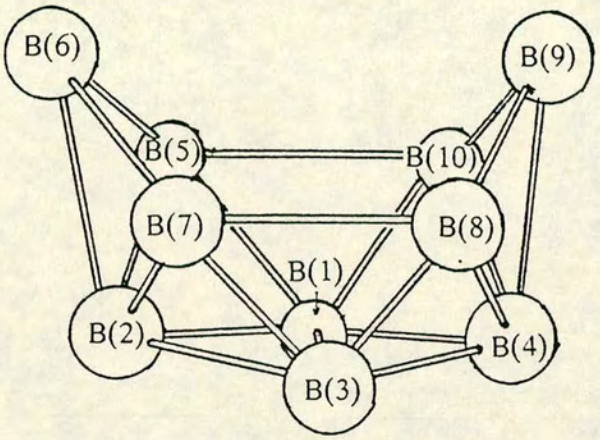

The renumbering for the discussion in the text.

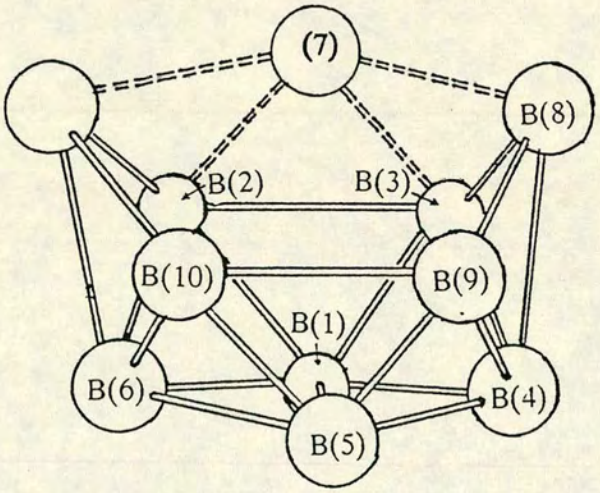

The correct numbering scheme for a *nido*-icosahedron with the heteroatom at the '7' position.

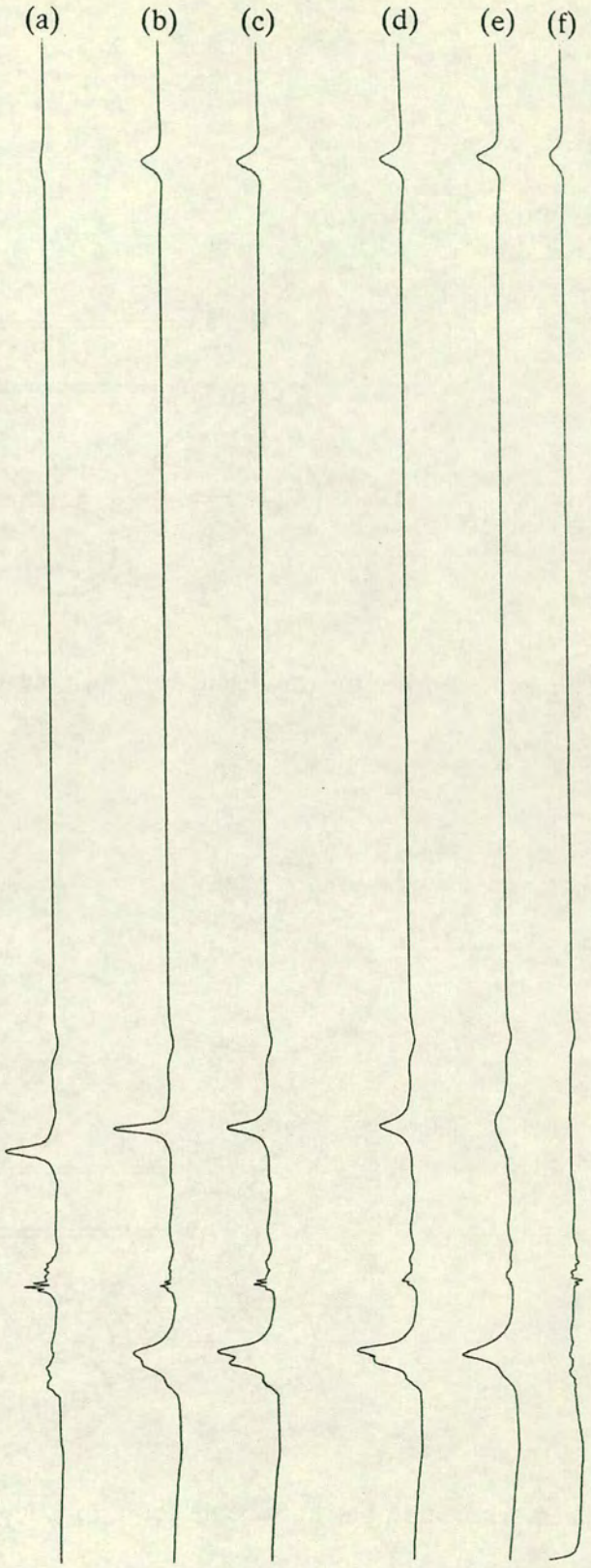

Figure 3.11. The ^{1}H-{^{11}B,selective} n.m.r. spectrum of **(15)**. Traces correspond to decoupling at $\delta^{11}B$ = (a) 3.740, (b) -6.383, (c) -9.689, (d) -10.988, (e) -28.180, (f) -31.068 ppm.

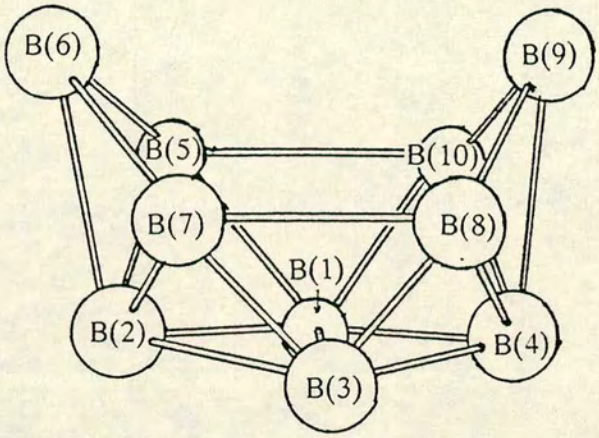

The renumbering for the discussion in the text.

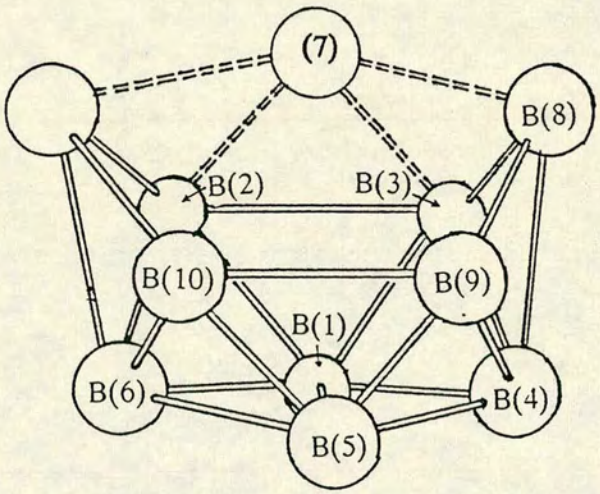

The correct numbering scheme for a *nido*-icosahedron with the heteroatom at the '7' position.

a relative integral of 1B, implying that it arises from B(1) or B(3). Note however that there are no off-diagonal resonances between these signals.

In the other spectra, the signal due to B(1) comes at a higher frequency than that due to B(3), although their chemical shifts are normally quite close. This would suggest that the signals at $\delta^{11}B$ = -6.38 (1B) and -28.18 (1B) ppm arise from B(1) and B(3) respectively, but since the chemical shifts are usually close together, this conclusion should be treated with caution. However it does not matter how these two peaks are assigned since there is yet another inconsistency - the signal at $\delta^{11}B$ = -28.18 ppm couples to that at $\delta^{11}B$ = 3.74 ppm which was assigned as arising from B(6) and B(9). Since neither B(1) nor B(3) is adjacent to either of B(6) or B(9), there should be no coupling but there evidently is.

The other two resonances, at $\delta^{11}B$ = -9.69 and -10.99 ppm cannot clearly be distinguished on the basis of their coupling patterns, especially since the signal at $\delta^{11}B$ = -10.99 ppm couples to no other signals. They are also too close together to be distinguished on chemical shift grounds, and so no assignments are suggested.

The proposed assignments are listed in Table 3.7 on page 110. This assignment is only partial, and there are a number of discrepancies in the coupling pattern. How can this be rationalised?

As was pointed out above, the μ-H atoms couple to all of the boron atoms. It is therefore possible that these H atoms are fluxional, and migrate over all or part of the cage. Since H-bridged connectivities do not give rise to off-resonance signals, this would explain the paucity of off-diagonal signals.

3.10 The Reactions of (15).

3.10.1 Reaction with CF_3CO_2H

Since the deprotonation of **(8a)** is accompanied by structural rearrangement, there arose the possibility that reprotonation of **(15)** could yield a structural isomer of **(8a)** with the gold atom η^4-ligated to a $\{B_{10}H_{13}\}$ cage. Such structural isomerism would be unprecedented. As discussed in Chapter 2, **(8a)** reacts with hydrogen chloride to cleave the gold-boron connectivities. In view of this, the acid used was trifluoroacetic acid. There were two reasons for this. First $[CF_3CO_2]^-$ is a poor ligand, therefore the acid was much less likely to attack the gold atom. Secondly, a solution of trifluoroacetic acid could be made with a known concentration and only one equivalent of acid added. This would (hopefully) prevent double protonation of the auraborane. However, when the experiment was carried out the red colour of the solution instantly disappeared and the ^{31}P-$\{^1H\}$ n.m.r. spectrum showed only one resonance, assignable to **(8a)**.

3.10.2 Synthesis of $(B_{10}H_{12}Au)(AuPCy_3)_3$.

It was observed that solid **(15)** slowly goes brown if left in air for several weeks. In an attempt to find out why this complex is unstable, **(15)** was left stirring in a dichloromethane solution under a nitrogen atmosphere for five days, and then the reaction products were worked up. Only one species was subsequently identified. This was the gold-boron *double cluster*, $(B_{10}H_{12}Au)(AuPCy_3)_3$, which is illustrated in Figure 5.7, on page 162. This complex is considered in detail in Chapter 5.

3.11 Reaction of $AuMe(PCy_3)$ with $B_{10}H_{12}(PPh_3)_2$

As was explained in Chapter 2, when the preparation of *arachno*-$\{B_{10}\}$ derivatives of **(8)** was attempted by reaction with acetonitrile or dimethylsulphide, rearrangement to $[(Cy_3P)_2Au]^+ [(B_{10}H_{12})_2Au]^-$ occurred.

In a second route to such derivatives, the *arachno*-$B_{10}H_{12}L_2$ species where L = MeCN, SMe_2, and PPh_3 were prepared and reacted with $AuX(PCy_3)$, where X = Cl or Me. Reaction of X = Cl and L = MeCN or SMe_2 led to formation of $[(Cy_3P)_2Au]^+ [(B_{10}H_{12})_2Au]^-$, and when L was changed to PPh_3, there was no reaction.

When X was changed to Me, however, the reaction was different. For L = MeCN or SMe_2 reaction led to formation of unidentified red-brown species which readily decomposed. When L was changed to PPh_3, however, the reaction went cleanly to one yellow product which was fully characterised as $(Cy_3PAu)_2B_8H_{10}$, **(18a)**.

This reaction is in contrast to two previous reactions. The first report[134] was that $(Me_2PhP)_2PtCl_2$ and $(B_{10}H_{12})(PPhMe_2)_2$ do not react, even when refluxed in toluene. The second was the reaction[144] :

$$\{Cp^*RhCl\}_2 + B_{10}H_{12}(PPhMe_2)_2 \longrightarrow (Cp^*Rh)B_{10}H_{11}Cl(PPhMe_2)$$

3.12 The Structure of (18a).

The starting borane was synthesised using non-dried ether, and this showed in the crystal structure when, despite all the other stages being carried out in pre-dried solvents, the product formula was $(Cy_3PAu)_2B_8H_{10}.2H_2O$!

The structure of this compound is shown in Figure 3.12, overleaf; Table 3.8 on page 111 gives the bond lengths and angles of the Au_2B_8 fragment; and all the crystallographic details start on page 230. **(18a)** is located on a crystallographic

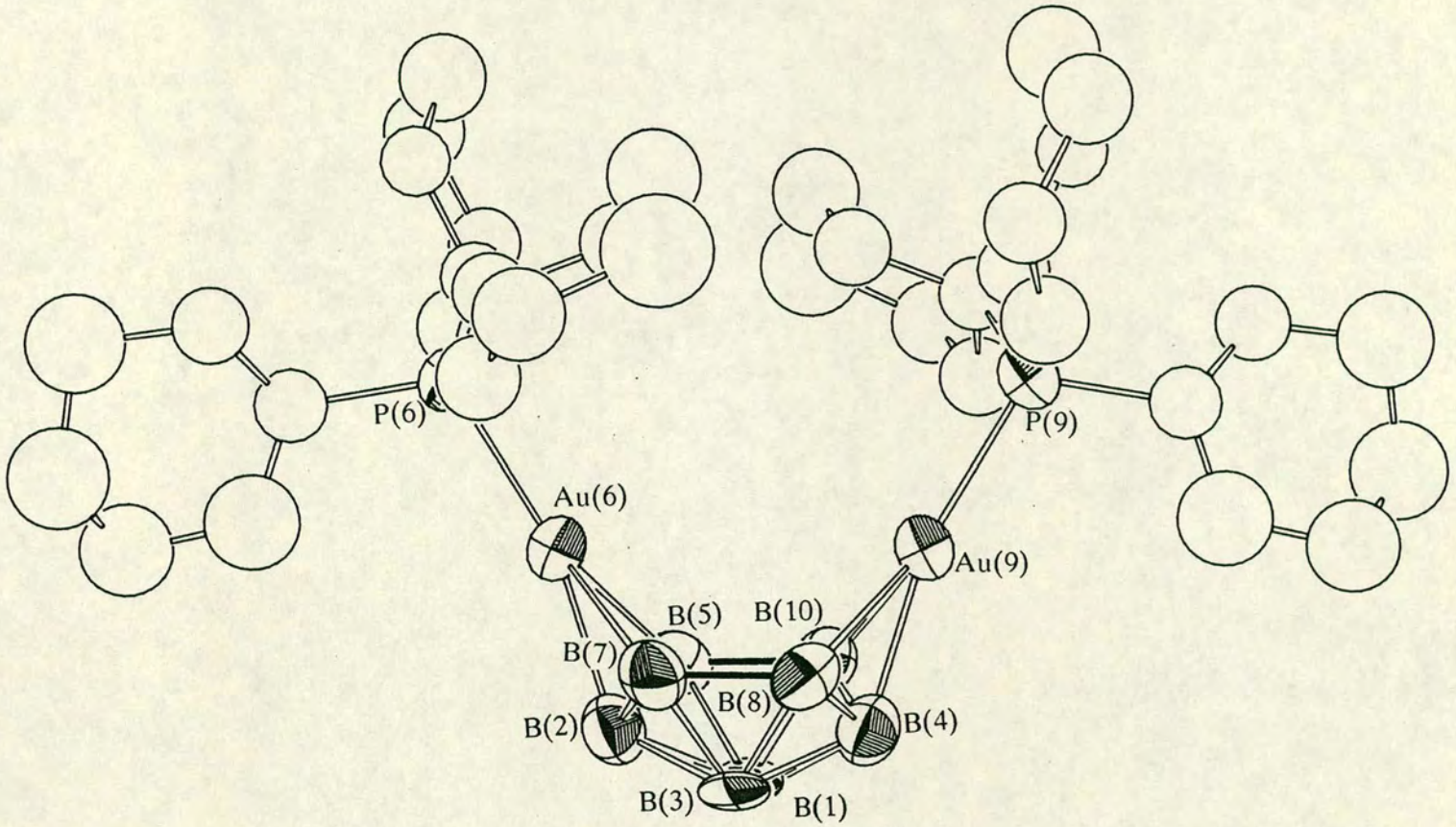

Figure 3.12. The ORTEP plot of $(Cy_3PAu)_2B_8H_{10}$.

two-fold axis, which passes through the centre of the cluster, but not through any atoms. This means that, crystallographically, B(3) is B(1'), B(4) is B(2'), B(8) is B(5'), Au(9) is Au(6'), and B(10) is B(7').

Of particular interest is the loss of two boron atoms, because this is the first reaction reported in this thesis in which degradation of the cage has occurred. The cluster which remains is simply generated by replacement of the two $\{BHPPh_3\}$ vertices by two $\{AuPCy_3\}$ fragments.

Again there is very good steric protection afforded to the open face by the tricyclohexylphosphine ligands. The Au-P distance of 230.7(3) pm is very similar to that observed in both 5,6-μ-(Cy_3PAu)-*nido*-$B_{10}H_{13}$ and the $[Cy_3PAuB_{10}H_{12}]^-$ anion. The $\{PCy_3\}$ ligand is to one side of the cage, as shown by the two angles : P-Au(6)-B(5) is 129.8(3)^o, whereas P-Au(6)-B(7) is significantly smaller, at 147.4(3)^o. Further evidence is that the P atoms are 35.6pm out of the best-fit plane through the atoms : B(2), Au(6), Au(9), and B(4). This distortion is probably due to steric repulsion of the two $\{PCy_3\}$ ligands. This tilt of the $\{PCy_3\}$ does not seem to affect the gold atom - the Au(6)-B(5) and Au(6)-B(7) connectivities are insignificantly different, as are the Au(6)-B(5)-B(10) and Au(6)-B(7)-B(8) angles.

3.13 Structural Comparisons with (18a).

One of the very few auraboranes which had been structurally-characterised[76] prior to this work was the complex $\{(dtc)Au\}_2B_8H_{10}$, **(18b)**, (dtc = N,N-diethyldithiocarbamate), shown in Figure 3.13, overleaf. This was described as an *arachno* 10-vertex species. The gold geometry in **(18b)** is square-planar, with the gold acting as a two-electron, two-orbital donor to cage bonding. The three Au-B bond lengths were all very similar, the average being 223 pm.

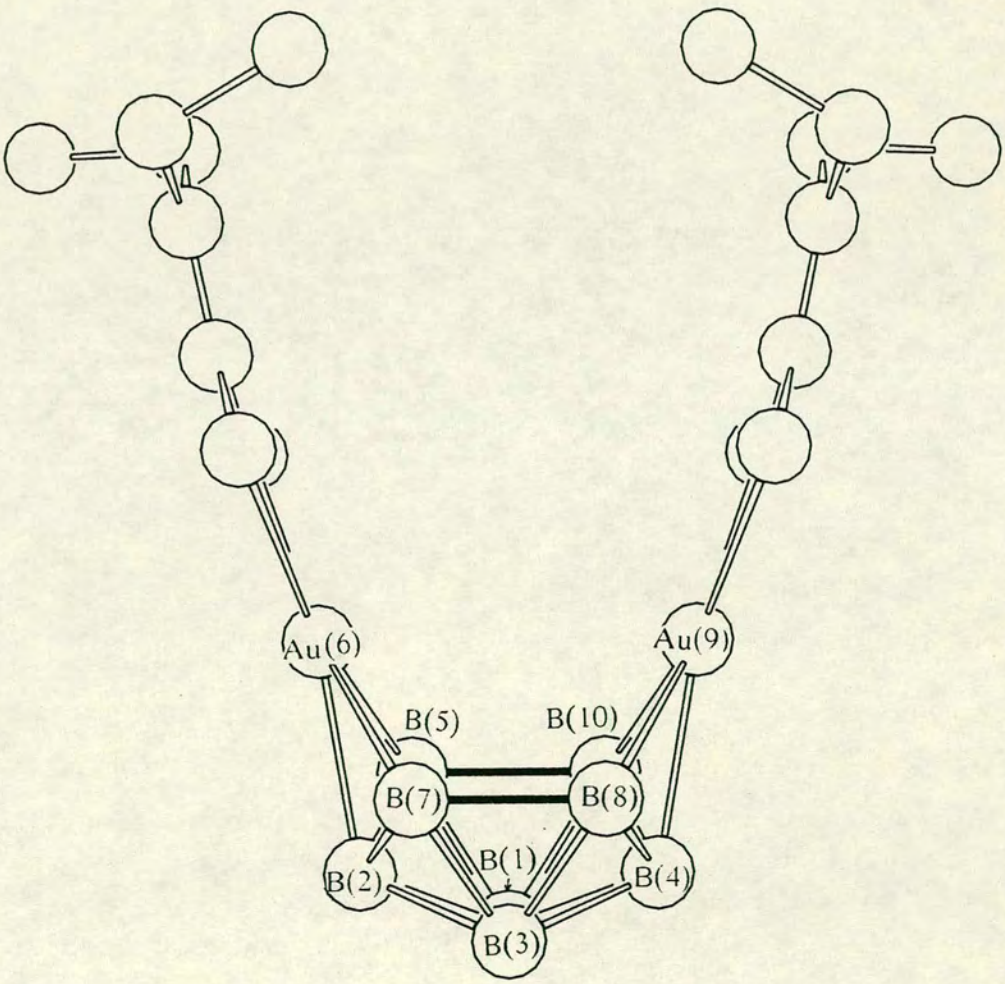

Figure 3.13. The molecular structure of $(dtcAu)_2B_8H_{10}$ drawn with all atomic radii set to 50pm.

When **(18a)** was compared against **(18b)**, the result was a misfit of 6.8 pm when the $\{B_8\}$ cages are compared, rising to 15.7 pm when the two gold atom positions are included in the comparison. The differences in the atom positions are:

B(1)	2.9	Au(6)	32.4
B(2)	6.5	B(7)	9.9
B(3)	5.7	B(8)	9.4
B(4)	6.6	Au(9)	32.4
B(5)	5.0	B(10)	5.6

The largest misfit in the comparison which only involved the boron atoms was 9.9 pm, and so it can be seen that the enormous increase in the misfit is solely due to the variation in the positions of the gold atoms.

In **(18a)**, the Au(6)-B(5) and Au(6)-B(7) connectivities are *ca.* 20 pm longer than they are in **(18b)**, whereas the Au(6)-B(2) connectivities are insignificantly different. Moreover the perpendicular distance from the gold to the B(5)-B(7)-B(8)-B(10) plane was calculated and found to be 137.8 pm for **(18a)**, and 135.8 pm for **(18b)**. This suggests that the variation in gold-borane distance is parallel to the B(5)-B(7)-B(8)-B(10) plane, i.e. that the two gold atoms repel each other. This is confirmed by the Au...Au distances which are 422.7(1) and 358.1(1)pm in **(18a)** and **(18b)** respectively.

This comparison (especially the misfit) suggests that the cage in **(18a)** can also be described as an *arachno* 10-vertex species. In order to further examine this, the following comparisons were made:

Comparison with	$[B_{10}H_{14}]$	$[B_{10}H_{13}]^-$	$[B_{10}H_{14}]^{2-}$	$[B_{11}H_{13}]^{2-}$
$(Cy_3PAu)_2B_8H_{10}$	18.8	18.9	11.0	12.3
$(\{dtc\}Au)_2B_8H_{10}$	13.7	14.1	6.4	7.9

As can be seen from this, whilst the $\{B_8\}$ cage in **(18b)** fits satisfactorily with the same B_8 fragment in the *arachno*-$\{B_{10}\}$ complexes, that of **(18a)** does not. Since it was shown earlier that in the $[Cy_3PAuB_{10}H_{12}]^-$ anion, the gold is not formally a

vertex, it was then thought that this could be a similar system, especially when, as was noted above, in the four species : $[(Cy_3P)_2Au]^+$, 5,6-μ-(Cy_3PAu)-*nido*-$B_{10}H_{13}$, $[Cy_3PAuB_{10}H_{12}]^-$, and **(18a)**, the Au-P bond length is *the same* within experimental error.

Unfortunately, reported octaboron chemistry is very sparse, but one of the few structurally-characterised species is B_8H_{12}[145]. This has an anomalous geometry in that its geometry is an *arachno* fragment of a ten-vertex polyhedron, whilst it has only a *nido* electron-count. This has been ascribed to excessive steric crowding of four bridging hydrogen atoms around the open face of a 8-vertex *nido* fragment.

Its structure is shown in Figure 3.14, overleaf, and this view emphasises the relationship to the ten-vertex polyhedron, and also shows the renumbered scheme for the comparison. When the structure of B_8H_{12} was compared against those of **(18a)** and **(18b)**, the resultant misfits were 3.9 and 7.7 pm, showing that the cages in B_8H_{12} and **(18a)** are virtually identical.

3.14 The Electronic Structure of (18a).

In order to examine this further, EHMO calculations were performed. For these calculations, several models were used. The first was the $[AuPH_3]^+$ cation, **(17a)**, discussed earlier. The P 3d orbitals were included in all of these calculations.

The second was a model of the $[B_8H_{10}(AuPH_3)]^-$, **(18c)**. This was built-up from the same $\{B_8H_{10}\}$ fragment in B_8H_{12} to which the $\{AuPH_3\}$ fragment was ligated in the same manner as that found experimentally. Finally, a similar model was constructed of **(18a)**- **(18d)**.

The coordinates of all of these models are listed in Appendix 3, starting on

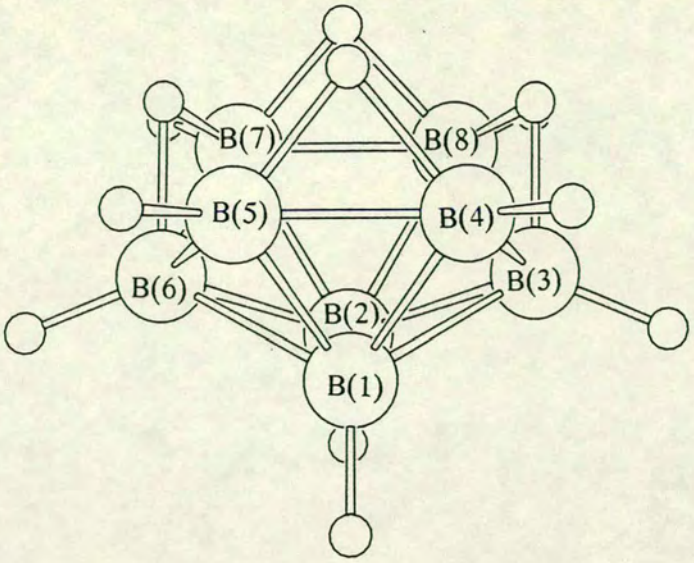

(a)

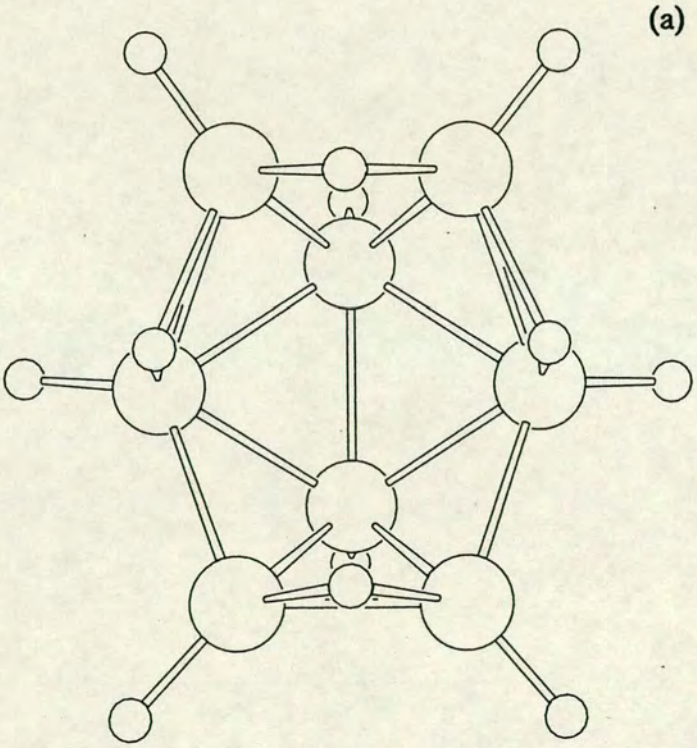

(b)

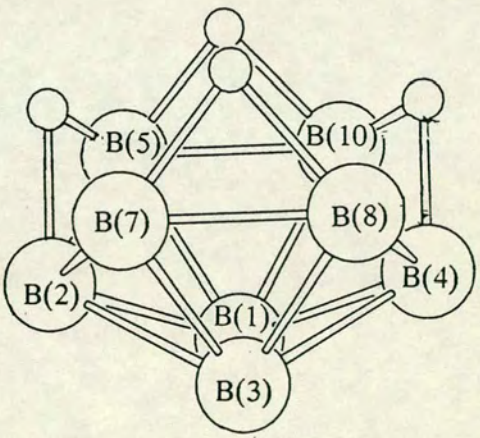

(c)

Figure 3.14. (a) the molecular structure of B_8H_{12} with B atom radii of 50pm, and H atom radii of 10 pm. This view emphasises the relationship to the ten-vertex species. (b) is a different view with the correct numbering scheme. (c) is the renumbering for the misfit calculations.

page 284. Relevant parameters are listed in Table 3.9 on page 111, and Figure 3.15, on page 101, is a schematic view of the FO's of **(18c)**.

(17b) bonds to **(18c)** in a straightforward manner. The Au 6p orbital occupations are $6p_x$ 0.0972, $6p_y$ 0.0450, and $6p_z$ 0.2884. Since the p_x occupation is half that found in **(15a)**, above, whilst that of the p_z is slightly greater, this suggests that in **(18c)**, the gold coordination is essentially linear, with only a very small tangential bonding component.

The different bonding is due to the placing of the node : in **(18c)**, the nodal plane runs through B(7), and so the tangential bonding is vastly reduced since there can only be overlap with the other two atoms which are quite some distance apart.

3.14.1 The Structure of (18b).

In **(18a)**, the description of the cluster is as an eight-vertex polyhedron to which two gold atoms are μ_3-ligated. The $\{AuPCy_3\}$ fragment is a 1-electron, 1-orbital donor to cage bonding.

In **(18b)**, however, the {dtcAu} fragments are 2-electron, 2-orbital donors, and the structure is consistent with a ten-vertex geometry. These differences are all part of the same problem which will be considered in more detail in Chapter 4 : what constitutes a polyhedral vertex?

3.15 Spectroscopic Details

The multinuclear n.m.r. parameters of **(18a)** were obtained in order to fully characterise this species. Firstly the ^{11}B-$\{^1H\}$ n.m.r. spectrum (Figure 3.16, page 102) consists of three peaks, showing that the complex has C_{2v} symmetry in solution, although the very broad nature of the peak due to B(5), B(7), B(8), and

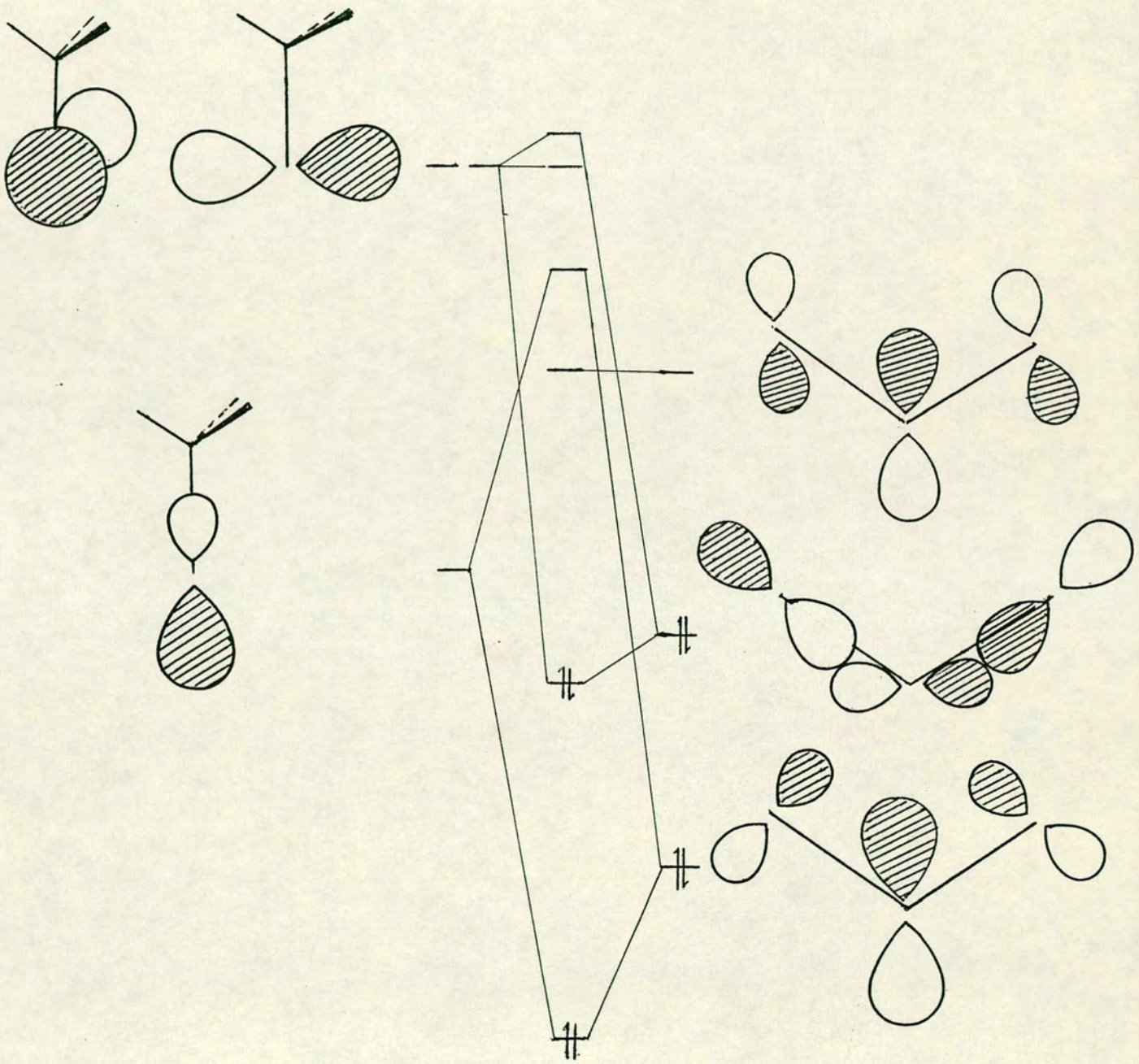

Figure 3.15. The interaction of $[AuPH_3]^+$ with $[H_3PAuB_8H_{10}]^-$.

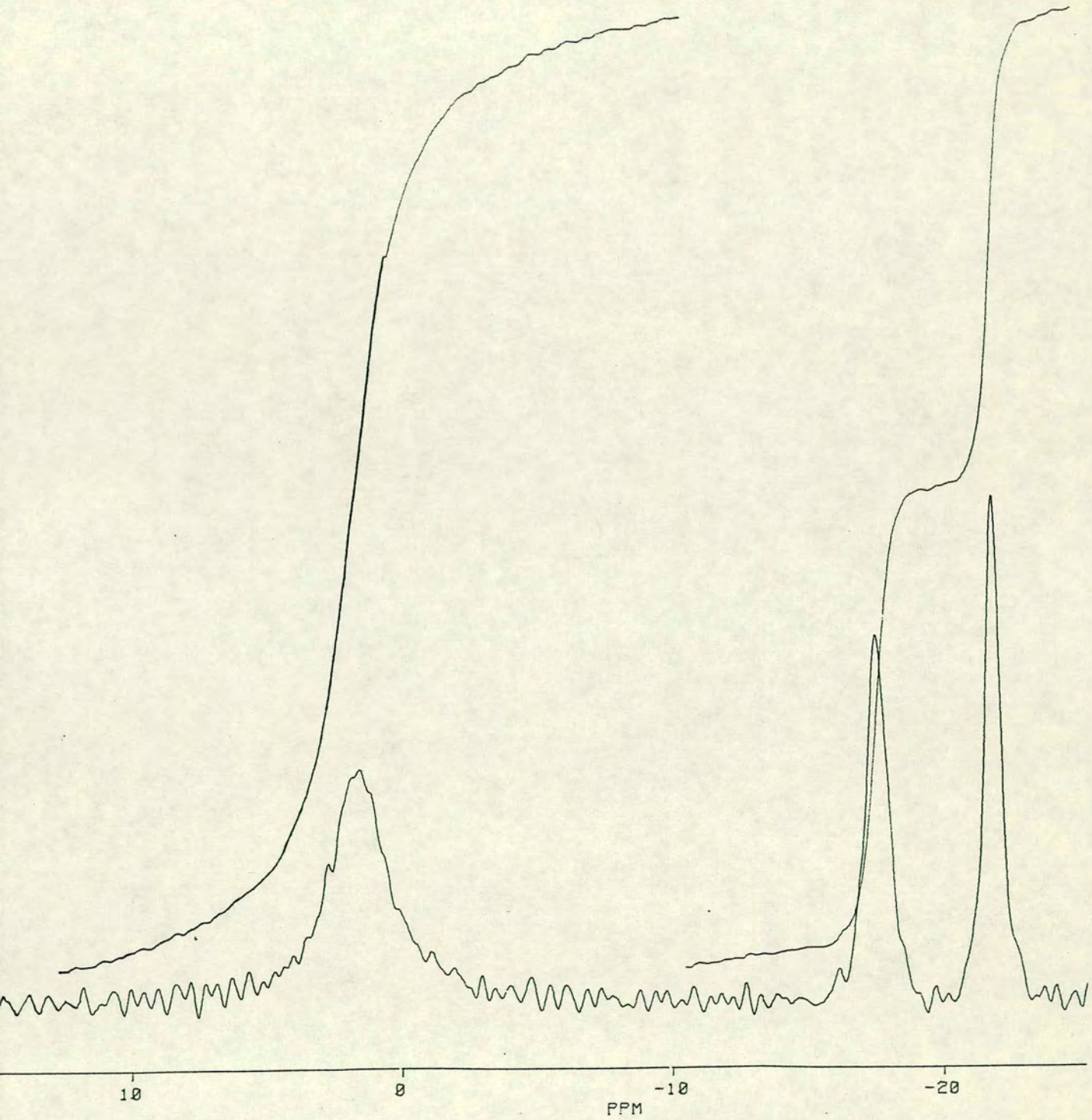

Figure 3.16. The ^{11}B-{^{1}H} n.m.r. spectrum of $(Cy_3PAu)_2B_8H_{10}$.

B(10) suggests that this is beginning to break down.

The ^{1}H-{^{11}B,selective} n.m.r. revealed that only the resonances due to B(5), B(7), B(8), and B(10) couple to the bridging H atoms, indicating that these bridges are located on the B(5)-B(10) and B(7)-B(8) connectivities. When the chemical shifts of the ^{11}B-{^{1}H} and ^{1}H-{^{11}B} n.m.r. spectra of **(18)** and **(19)** were compared, it was found that there was little correlation either in the magnitude or the relative ordering of these signals. In view of the different structures found for the two species, this is reasonable, and in fact is further evidence for this.

3.16 Conclusions.

Three complexes have been discussed in this Chapter. The first, the $[B_{10}H_{13}]^-$ anion, was found to have the structure of decaborane with one μ-H atom removed - no structural rearrangement was observed. The principal reason for determining this structure was to compare it with the $[Cy_3PAuB_{10}H_{12}]^-$ anion, which was found to be the principal product of base attack upon 5,6-μ-(Cy_3PAu)-*nido*-$B_{10}H_{13}$.

This anion was shown to be a Au(I) complex, and the geometry of the gold is best described as intermediate between linear and trigonal planar. The structure of the $\{B_{10}\}$ cage is the same as that of $B_{10}H_{14}$, and the deprotonation and accompanying 'slip' of the gold were both shown to be reversible under acidic conditions. The ^{11}B-{^{1}H} n.m.r. spectrum could only be partially assigned by using a ^{11}B(COSY) n.m.r. spectrum, owing to difficulties in the interpretation, which were accounted for by fluxional processes.

When AuMe(PCy_3) was reacted with $(B_{10}H_{12})(PPh_3)_2$, the reaction went cleanly to one product : $(Cy_3PAu)_2B_8H_{10}$. This was characterised crystallographically, and when the structure of the $\{B_8\}$ fragment was compared

against other relevant boranes, it emerged that this is a $[B_8H_{10}]^{2-}$ species, to which are bonded two $[AuPCy_3]^+$ fragments *via* a *pseudo*-face capping mode of bonding.

So far in this thesis, three different auraboranes containing $\{AuPCy_3\}$ fragments have been structurally characterised, respectively ligated to two, three, and four boron atoms, and *in none* can the gold be accurately described as a cluster vertex!

Table 3.1. Bond Lengths(pm) and Angles(^{o}) for the Refined Atoms in the $[B_{10}H_{13}]^{-}$ Anion.

B(1) - B(2)	178.3(5)	B(3) - B(8)	175.8(5)
B(1) - B(3)	178.0(5)	B(4) - B(8)	175.4(5)
B(1) - B(4)	174.5(5)	B(4) - B(9)	173.6(5)
B(1) - B(5)	178.0(5)	B(4) -B(10)	178.6(5)
B(1) -B(10)	173.1(5)	B(5) - B(6)	178.3(5)
B(2) - B(3)	176.5(5)	B(5) -B(10)	184.8(5)
B(2) - B(5)	179.8(5)	B(6) - B(7)	176.8(5)
B(2) - B(6)	170.7(5)	B(7) - B(8)	200.3(5)
B(2) - B(7)	176.7(5)	B(8) - B(9)	178.8(5)
B(3) - B(4)	175.6(5)	B(9) -B(10)	165.7(5)
B(3) - B(7)	173.4(5)		

B(2) - B(1) - B(3)	59.39(19)	B(8) - B(4) - B(9)	61.63(21)
B(2) - B(1) - B(5)	60.61(20)	B(9) - B(4) -B(10)	56.13(20)
B(3) - B(1) - B(4)	59.74(19)	B(1) - B(5) - B(2)	59.78(20)
B(4) - B(1) -B(10)	61.81(20)	B(1) - B(5) -B(10)	56.98(19)
B(5) - B(1) -B(10)	63.48(21)	B(2) - B(5) - B(6)	56.93(20)
B(1) - B(2) - B(3)	60.20(19)	B(2) - B(6) - B(5)	61.99(21)
B(1) - B(2) - B(5)	59.61(20)	B(2) - B(6) - B(7)	61.10(21)
B(3) - B(2) - B(7)	58.80(19)	B(2) - B(7) - B(3)	60.54(20)
B(5) - B(2) - B(6)	61.08(21)	B(2) - B(7) - B(6)	57.74(20)
B(6) - B(2) - B(7)	61.16(21)	B(3) - B(7) - B(8)	55.57(19)
B(1) - B(3) - B(2)	60.41(19)	B(3) - B(8) - B(4)	59.98(20)
B(1) - B(3) - B(4)	59.16(19)	B(3) - B(8) - B(7)	54.43(18)
B(2) - B(3) - B(7)	60.66(20)	B(4) - B(8) - B(9)	58.68(21)
B(4) - B(3) - B(8)	59.89(20)	B(4) - B(9) - B(8)	59.69(21)
B(7) - B(3) - B(8)	70.01(21)	B(4) - B(9) -B(10)	63.46(22)
B(1) - B(4) - B(3)	61.10(20)	B(1) -B(10) - B(4)	59.48(20)
B(1) - B(4) -B(10)	58.71(20)	B(1) -B(10) - B(5)	59.55(20)
B(3) - B(4) - B(8)	60.13(20)	B(4) -B(10) - B(9)	60.40(21)

Table 3.2. Bond Lengths(pm) and Angles(^{0}) for the $\{B_{10}Au\}$ Fragment in $[NHEt_3]^+ [Cy_3PAuB_{10}H_{12}]^-$.

Au - B(5)	229.4(10)	B(3) - B(4)	176.3(15)
Au - B(6)	246.9(10)	B(3) - B(7)	174.6(15)
Au - B(9)	249.0(10)	B(3) - B(8)	174.3(15)
Au -B(10)	228.5(10)	B(4) - B(8)	177.0(15)
B(1) - B(2)	178.4(15)	B(4) - B(9)	172.9(14)
B(1) - B(3)	180.4(15)	B(4) -B(10)	176.6(14)
B(1) - B(4)	176.5(15)	B(5) - B(6)	175.4(15)
B(1) - B(5)	176.7(15)	B(5) -B(10)	190.3(14)
B(1) -B(10)	178.3(14)	B(6) - B(7)	178.6(15)
B(2) - B(3)	178.5(15)	B(7) - B(8)	207.4(15)
B(2) - B(5)	180.4(15)	B(8) - B(9)	181.3(15)
B(2) - B(6)	172.9(14)	B(9) -B(10)	168.7(14)
B(2) - B(7)	174.0(15)		

B(5) - Au - B(6)	43.0(4)	Au - B(5) - B(6)	73.8(5)
B(5) - Au -B(10)	49.1(4)	Au - B(5) -B(10)	65.2(4)
B(9) - Au -B(10)	41.1(3)	B(1) - B(5) - B(2)	59.9(6)
B(2) - B(1) - B(3)	59.7(6)	B(1) - B(5) -B(10)	58.0(6)
B(2) - B(1) - B(5)	61.1(6)	B(2) - B(5) - B(6)	58.1(6)
B(3) - B(1) - B(4)	59.2(6)	Au - B(6) - B(5)	63.2(5)
B(4) - B(1) -B(10)	59.7(6)	B(2) - B(6) - B(5)	62.4(6)
B(5) - B(1) -B(10)	64.8(6)	B(2) - B(6) - B(7)	59.3(6)
B(1) - B(2) - B(3)	60.7(6)	B(2) - B(7) - B(3)	61.6(6)
B(1) - B(2) - B(5)	59.0(6)	B(2) - B(7) - B(6)	58.7(6)
B(3) - B(2) - B(7)	59.4(6)	B(3) - B(7) - B(8)	53.4(6)
B(5) - B(2) - B(6)	59.5(6)	B(3) - B(8) - B(4)	60.2(6)
B(6) - B(2) - B(7)	62.0(6)	B(3) - B(8) - B(7)	53.6(6)
B(1) - B(3) - B(2)	59.6(6)	B(4) - B(8) - B(9)	57.7(6)
B(1) - B(3) - B(4)	59.3(6)	Au - B(9) -B(10)	62.9(5)
B(2) - B(3) - B(7)	59.0(6)	B(4) - B(9) - B(8)	59.9(6)
B(4) - B(3) - B(8)	60.7(6)	B(4) - B(9) -B(10)	62.2(6)
B(7) - B(3) - B(8)	72.9(7)	Au -B(10) - B(5)	65.7(4)
B(1) - B(4) - B(3)	61.5(6)	Au -B(10) - B(9)	76.0(5)
B(1) - B(4) -B(10)	60.7(6)	B(1) -B(10) - B(4)	59.7(6)
B(3) - B(4) - B(8)	59.1(6)	B(1) -B(10) - B(5)	57.2(5)
B(8) - B(4) - B(9)	62.4(6)	B(4) -B(10) - B(9)	60.1(6)
B(9) - B(4) -B(10)	57.7(6)		

Table 3.4. Relevant Parameters from the EHMO Calculations on $[B_{10}H_{12}]^{2-}$.

$[H(5,6)]^+$ and $[H(9,10)]^+$ removed from decaborane. Hence the sequence of four boron atoms which have lost their μ-H atoms is B(6)-B(5)-B(10)-B(9). The molecule is orientated such that all four have z = 0; B(10) ⟶ B(5) is -x to +x; and B(6) ⟶ B(5) is -y to +y.

2^{nd}. LUMO. Energy = -3.0636 eV.

		Orbital Contribution(x 10^4)		
Atom	s	p_x	p_y	p_z
B(5)	526	-1916	-1071	-1512
B(6)	714	-3502	2542	3467
B(9)	-714	-3502	-2542	-3467
B(10)	-526	-1916	1071	1512

LUMO. Energy = -7.1394 eV.

		Orbital Contribution(x 10^4)		
Atom	s	p_x	p_y	p_z
B(5)	263	-2391	212	2327
B(6)	-413	2779	-1409	-3870
B(9)	-413	-2779	-1409	-3870
B(10)	263	2391	212	2327

HOMO. Energy = -9.7721 eV.

		Orbital Contribution(x 10^4)		
Atom	s	p_x	p_y	p_z
B(5)	-592	-377	-2366	-2228
B(6)	-640	2231	1490	-3495
B(9)	640	2231	-1490	3495
B(10)	592	-377	2366	2228

2^{nd}. HOMO. Energy = -10.4136 eV.

		Orbital Contribution(x 10^4)		
Atom	s	p_x	p_y	p_z
B(5)	-627	2315	-1373	-3288
B(6)	-420	1244	51	-1416
B(9)	-420	-1244	51	-1416
B(10)	-627	-2315	-1373	-3288

Net Charges.

B(5) -0.1370 B(6) -0.0181 B(9) -0.0181 B(10) -0.1370

Table 3.5. Gold and Phosphorus Atomic Orbital Contributions(x 10^4) in the Frontier Orbitals of $[H_3PAu]^+$.

	HOMO	LUMO	2nd. LUMO	3rd. LUMO
Orbital Energy/eV	-11.5759	-7.1359	-4.5664	-4.5664
P Orbitals				
3s	451	-810	0	0
$3p_x$	0	0	0	-2012
$3p_y$	0	0	-2012	0
$3p_z$	-1367	2605	0	0
Au Orbitals				
6s	2554	8001	0	0
$6p_x$	0	0	0	-9449
$6p_y$	0	0	-9449	0
$6p_z$	711	-5567	0	0
$5d_{x^2-y^2}$	0	0	-24	0
$5d_{z^2}$	-9541	1461	0	0
$5d_{xy}$	0	0	0	-24
$5d_{xz}$	0	0	0	290
$5d_{yz}$	0	0	290	0

Table 3.6. Calculations on $[AuPH_3]^+$ when the P 3d Orbitals are Included.

	LUMO	2nd. LUMO	3rd. LUMO	4th. LUMO	5th. LUMO
Orbital Energy/eV	-8.9068	-8.9068	-8.6726	-6.9160	-6.9160
P Orbitals					
3s	0	0	555	0	0
$3p_x$	5280	0	0	0	144
$3p_y$	0	-5280	1	-144	0
$3p_z$	0	1	3710	0	0
$3d_{x^2-y^2}$	0	6312	-1	5469	0
$3d_{z^2}$	0	1	6724	0	0
$3d_{xy}$	-6312	0	0	0	-5469
$3d_{xz}$	-3057	0	0	0	7349
$3d_{yz}$	0	3057	0	-7349	0
Au Orbitals					
6s	0	1	5197	0	0
$6p_x$	1656	0	0	0	-2445
$6p_y$	0	-1656	0	2445	0
$6p_z$	0	0	-2156	0	0
$5d_{x^2-y^2}$	0	-750	0	-456	0
$5d_{z^2}$	0	0	-3	0	0
$5d_{xy}$	750	0	0	0	456
$5d_{xz}$	-2970	0	0	0	2112
$5d_{yz}$	0	2970	0	-2112	0

Table 3.7. The Chemical Shifts(ppm) and Assignments of the ^{11}B-{^{1}H} N.M.R. Spectra of Relevant Compounds.

$B_{10}H_{14}$		$[B_{10}H_{13}]^-$	
Chemical Shift	Assignment	Chemical Shift	Assignment
11.3	B(1),B(3)	6.8	B(9),B(6)
9.7	B(9),B(6)	2.5	B(1)
0.7	B(5),B(10),B(8),B(7)	-5.0	B(5),B(10),B(3),B(8),B(7)
-35.8	B(4),B(2)	-35.2	B(4),B(2)

$[Me_2TlB_{10}H_{12}]^-$		$[Cy_3PAuB_{10}H_{12}]^-$	
Chemical Shift	Assignment	Chemical Shift	Proposed Assignment
8.2	B(9),B(6)	3.74	B(9),B(6)
3.0	B(1)	-6.38	B(1) or B(3)
-3.1	B(5),B(10)	-9.69	B(5),B(10) or B(8),B(7)
-2.8	B(3)	-10.99	B(8),B(7) or B(5),B(10)
-4.7	B(8),B(7)	-28.18	B(3) or B(1)
-31.7	B(4),B(2)	-31.07	B(4),B(2)

Notes

nido-decaborane numbering.

Table 3.8. Bond Lengths(pm) and Angles(°) for the Refined Atoms in $(Cy_3PAu)_2B_8H_{10}$.

Au(6) - P	230.7(3)	B(1) - B(5)	177.4(18)
Au(6) - B(2)	222.5(13)	B(1) -B(10)	176.1(18)
Au(6) - B(5)	244.2(14)	B(2) - B(3)	176.1(19)
Au(6) - B(7)	244.3(12)	B(2) - B(5)	182.0(19)
B(1) - B(2)	177.2(19)	B(2) - B(7)	182.9(18)
B(1) - B(3)	168.9(18)	B(5) -B(10)	170.3(18)

B(2) -Au(6) - P	164.2(4)	Au(6)- B(2) - B(5)	73.5(6)
B(5) -Au(6) - P	129.8(3)	Au(6)- B(2) - B(7)	73.4(6)
B(7) -Au(6) - P	147.4(3)	B(5) - B(2) - B(1)	59.2(7)
B(2) -Au(6) - B(5)	45.6(5)	B(7) - B(2) - B(3)	58.7(7)
B(2) -Au(6) - B(7)	45.9(4)	B(1) - B(2) - B(3)	57.1(7)
B(5) -Au(6) - B(7)	80.1(5)	Au(6)- B(5) - B(2)	60.9(6)
B(2) - B(1) - B(5)	61.8(7)	B(2) - B(5) - B(1)	59.1(7)
B(2) - B(1) - B(3)	61.1(8)	B(1) - B(5) -B(10)	60.8(5)
B(5) - B(1) -B(10)	57.6(7)	Au(6)- B(7) - B(2)	60.8(5)
B(4) - B(1) - B(3)	61.8(8)	B(2) - B(7) - B(3)	58.7(7)
B(4) - B(1) -B(10)	62.6(7)	B(10)- B(7) - B(3)	61.6(7)

Table 3.9. Some Relevant Parameters for the EHMO Calculations on $(Cy_3PAu)_2B_8H_{10}$.

Orbitals on the B_3 Face of $[H_3PAuB_8H_{10}]^-$.

Orbital	2nd. HOMO	HOMO	LUMO	2nd. LUMO
Energy/eV	-10.5166	-10.2067	-9.0398	-8.9668
B(2)				
2s	-753	-96	27	-8
$2p_x$	409	-2715	-81	-1135
$2p_y$	3344	454	-48	34
$2p_z$	3991	402	14	-12
B(5)				
2s	-637	-216	-42	-191
$2p_x$	2349	2466	98	1300
$2p_y$	261	-514	511	539
$2p_z$	1957	2724	267	1638
B(7)				
2s	-572	28	-26	146
$2p_x$	-2915	2042	80	1370
$2p_y$	-157	742	470	-474
$2p_z$	2170	-2009	49	-1526

Chapter 4:

Studies on Auraborane 'Sandwich' Complexes -

The $[(B_{10}H_{12})_2Au]^-$ and $[(B_{10}H_{12})Au(B_{10}H_{13})]^{2-}$ Anions.

4.1 Introduction.

This Chapter reports work carried out on complexes where a gold atom is 'sandwiched' between two borane cages.

Section 4.2 discusses the $[(B_{10}H_{12})Au(B_{10}H_{13})]^{2-}$ anion which has two B_{10} cages ligated to the gold in *different* manners. The synthesis is first discussed, and then the structure which was determined crystallographically is discussed in the subsequent Section. This is followed by geometrical analysis of the two different halves of the molecule. Finally the n.m.r. data on this complex are analysed.

The next Section describes work carried out on compounds containing the $[(B_{10}H_{12})_2Au]^-$ anion. First the synthetic routes to this anion are reviewed, and then the following Section discusses the structure of this anion, as determined crystallographically for both the $[(o\text{-tolyl}_3P)_2Au]^+$ and $[(Cy_3P)_2Au]^+$ salts. The next Section discusses the geometrical analysis of this anion, and this leads into studies, particularly EHMO calculations, which probed the electronic structure, and why it is different to that found in the $[Cy_3PAuB_{10}H_{12}]^-$ anion. Based on this work, and that in Chapter 3, the general pattern in the structures of the $\{MB_{10}H_{12}\}$ metallaboranes is discussed.

Finally there is the Section which draws conclusions from the work presented in this Chapter.

4.2 The Formation of $[(Cy_3P)_2Au]^+_2\ [(B_{10}H_{12})Au(B_{10}H_{13})]^{2-}$.

The dropwise addition of a solution of $B_{10}H_{14}$ into a solution of methyltricyclohexylphosphinegold(I) leads to formation of $Cy_3PAuB_{10}H_{13}$ in > 75% yield. However it is also a means of synthesising other species whose formation is very dependent on the precise reaction conditions such as rate of addition, exact amounts of reagents, and volume of solvent. Due to the low solubility of $Cy_3PAuB_{10}H_{13}$, it is readily separated by filtration, and the other products are readily purified by preparative t.l.c. (see Chapter 6) on the filtrate.

To date, $[(Cy_3P)_2Au]^+_2\ [(B_{10}H_{12})Au(B_{10}H_{13})]^{2-}$, $[(Cy_3P)_2Au]^+\ [(B_{10}H_{12})_2Au]^-$, and $(B_{10}H_{12}Au)_2(AuPCy_3)_4$ have all been synthesised in very low yield by this method.

4.2.1 Alternative Routes

As a synthesis of the $[(B_{10}H_{12})Au(B_{10}H_{13})]^{2-}$ anion, **(19)**, this route has two disadvantages : there is the very low yield, and also the unpredictability in product formation. Accordingly, other means of potentially synthesising this complex or analogues were sought to overcome these difficulties. One proved successful.

This was based on the stoichiometry of the reaction product: 4 PCy_3 : 3 Au : 2 B_{10} cages. Accordingly, reaction between three equivalents of $AuMe(PCy_3)$, one of PCy_3 and two of $B_{10}H_{14}$ was successfully tried. This route had the advantage that the additional PCy_3 could be used to convert the *nido*-$\{B_{10}\}$ cage to an *arachno*-$\{B_{10}\}$ one, as is observed in the final product.

Whilst some $[(Cy_3P)_2Au]^+_2$ **(19)** was synthesised, it was very difficult to separate from the other (unidentified) products.

It was therefore concluded that until a high yield route to this species is developed, there is no prospect of fully investigating the properties of this

complex which is the only characterised species with two different $\{B_{10}\}$ cages ligated to a central metal atom.

4.3 The Structure of the $[(Cy_3P)_2Au]^+_2$ $[(B_{10}H_{12})Au(B_{10}H_{13})]^{2-}$ Complex.

4.3.1 The Structure of the $[(Cy_3P)_2Au]^+$ Cation.

One view of this species is shown in Figure 4.1, overleaf. It is a conventional linear Au(I) species (P(1)-Au(2)-P(2) = 178.68(7)^o). As discussed in Chapter 2, the structure of this cation has previously been determined as its Cl^- and SCN^- salts. The Au-P distances of 231.05(19) and 231.32(18) pm in this determination are not only insignificantly different from each other; but they are close to the values obtained previously (232.6(2) [114], 229.5(11) and 231.6(13) pm [115]).

4.3.2 The Interpretation of the Disordered Structure of (19).

The cation is monopositive, and there are two cations to every anion, which is due to the anion being located on an inversion centre, whilst the cation is located in a general position†. It therefore follows that this must be a dianionic cluster. Since the crystallographic site of the gold is a centre of inversion, it follows that without any disorder, this should be a Au(II) complex. Such compounds are very rare indeed, and this suggests that disorder may be present. The structure of **(19)** is shown in Figure 4.2(a), on page 117, and the crystallographic details start on page 235.

Since the Au atom in **(19)** lies on a crystallographic inversion centre, one

---

† It is ironic that the cation has effective C_i point group symmetry which is not utilised in the crystal, whereas the anion is free of molecular symmetry, yet is disordered about a symmetry centre in the solid state. The root of this irony is, of course, that the anion is dianionic and the cation is monocationic, and there are always fewer special positions than general ones in a crystal lattice.

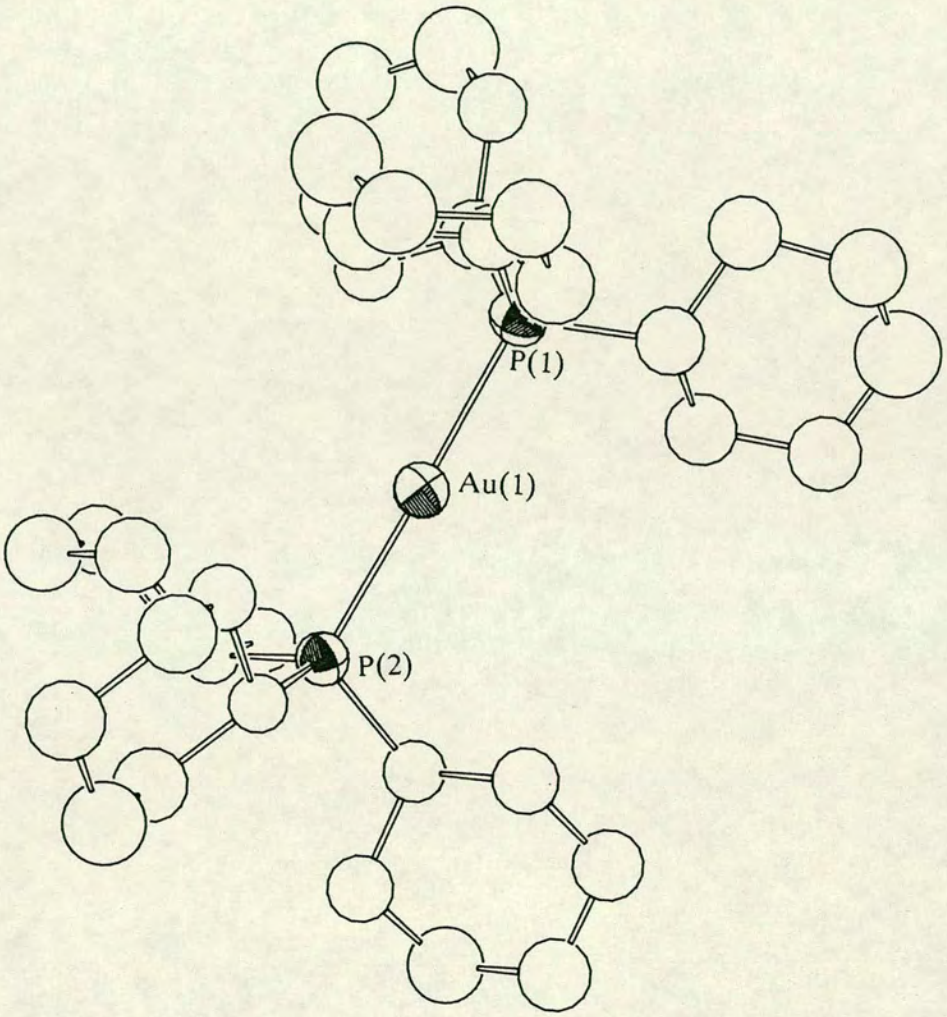

Figure 4.1. The Molecular Structure of the $[(Cy_3P)_2Au]^+$ Cation.

cage is generated, crystallographically, by the transformation of the other through this centre. As such, the two cages should be identical, but there is partial disorder in the structure. This occurs in the following manner. Nine boron atoms map acceptably well across the inversion centre, as shown by their refined anisotropic thermal parameters (although consider the shapes of B(10,8) and B(2,9)† in Figure 4.2(a)). However the tenth boron atom could only be satisfactorily refined, as evidenced by reasonable anisotropic thermal parameters, in two different locations, each with an occupancy factor of 0.5. It is this that distinguishes the two different polyhedra present in the anion. The following two Sections consider each half of the molecule separately, but it should be emphasised that this is a disordered structure, and thus the calculated misfits are probably slightly inaccurate as a consequence of the crystallographic superimposition of the two different fragments.

4.3.3 The Structure of the Upper Half of (19).

The top half of **(19)**, **(19a)**, (see Figures 4.2(a), and 4.2(b)) consists of a gold atom η^4-ligated to a $\{B_{10}H_{12}\}$ cage. The bond lengths and angles are listed in Table 4.1, on page 140, and Figure 4.2(b) shows the relationship of **(19a)** to decaborane. This is a similar cage bonding scheme to that discussed in the previous Chapter, and so, in order to examine its shape in detail, the $\{B_{10}\}$ cage was compared against those of $B_{10}H_{14}$ and $[B_{10}H_{14}]^{2-}$. This produced misfits of 12.1 and 8.8 pm respectively, indicating that **(19a)** has a similar cage architecture to that of $[B_{10}H_{14}]^{2-}$ and hence $[(B_{10}H_{12})_2Au]^-$, **(20)**. Comparison of **(19a)** and

---

† The crystallographic superimposition of the two different cages necessitates that the boron atoms are numbered B(i,j), where i refers to the correctly numbered (ref. 146) vertex in a *nido*-icosahedron, and j refers to the same in an *arachno*-docosahedron.

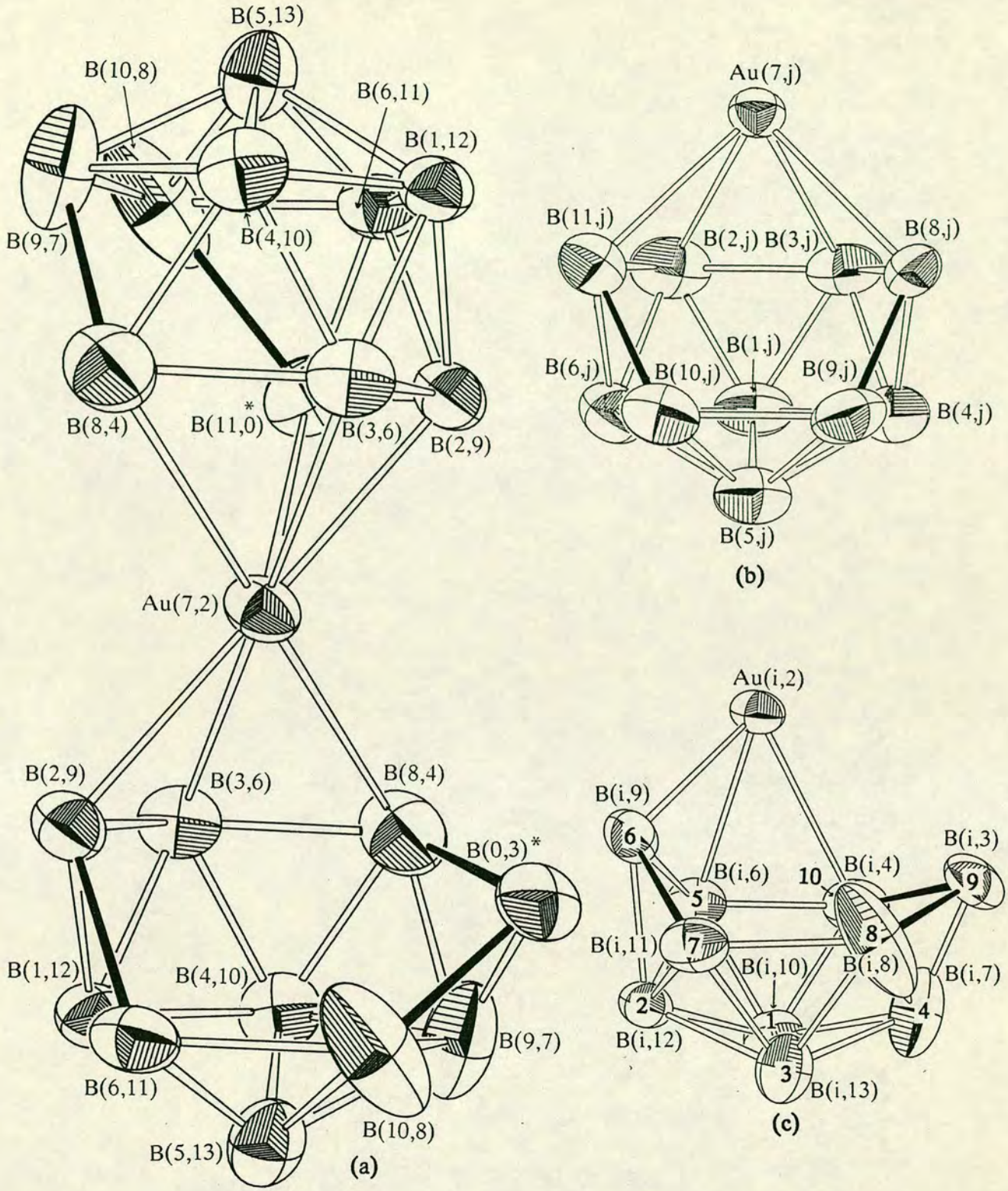

Figure 4.2. Three views of the $[(B_{10}H_{12})Au(B_{10}H_{13})]^{2-}$ anion. (a) shows the complete structure with the two disordered sites marked with a '*' (see text). (b) shows the relationship of the upper half to decaborane, and is numbered as found in the Tables. (c) shows the relationship of the lower half to decaborane, the B(i,j) numbering is as found in the Tables, and the bold numbers refer to the renumbering for the idealisations.

(20) yielded a misfit of 8.2 pm. These comparisons produce values which are a little high but this is probably due to the disorder in the structure of **(19)**. The structure and bonding in these $\{AuB_{10}H_{12}\}$ fragments of **(19a)** and **(20)** is discussed in detail in Sections 4.9 and 4.10 .

4.3.4 The Structure of the Lower Half of (19), (19b).

This is shown in Figure 4.2(a), and its relationship to decaborane is shown in Figure 4.2(c). Bond lengths and angles are given in Table 4.2 on page 141.

The structure is a new metallaborane cluster fragment : an *arachno*-docosahedral 2-$AuB_{10}H_{13}$. Although the H atoms could not be satisfactorily refined and remain absent, electron-counting arguments suggest that there are thirteen of them. This is supported by the ^{1}H-$\{^{11}B\}$ n.m.r. spectrum, as discussed in Section 4.3.5.

Whilst this geometry has previously been ascribed[68] to the complex $(Ph_3P)AgC_2B_8H_{11}$ (Figure 4.3, overleaf), close examination of its geometry suggests otherwise. First, the Ag-C(9) distance of 282.7pm, whilst greater than that of the Ag-boron connectivities (Ag-B(6) 242.0, Ag-B(7) 235.2, Ag-B(8) 252.2pm), is a short distance for a non-bonding contact.

Secondly, the B(6)-C(9) distance of 322.2pm is similar to those for the late transition metal $\{MB_{10}H_{12}\}$ fragments: $[(B_{10}H_{12})_2Au]^-$ 328.4, $(Me_2PhP)_2PtB_{10}H_{12}$ 324.0, $(Me_2PhP)_2PtB_{10}H_{11}Cl$ 323.4, $(Cp^*Rh)Cl(Me_2PhP)B_{10}H_{11}$ 327.1 pm. Furthermore, comparison of the $\{B_8\}$ fragment against the same atoms in other $\{B_{10}\}$ cages produces the misfits on page 120.

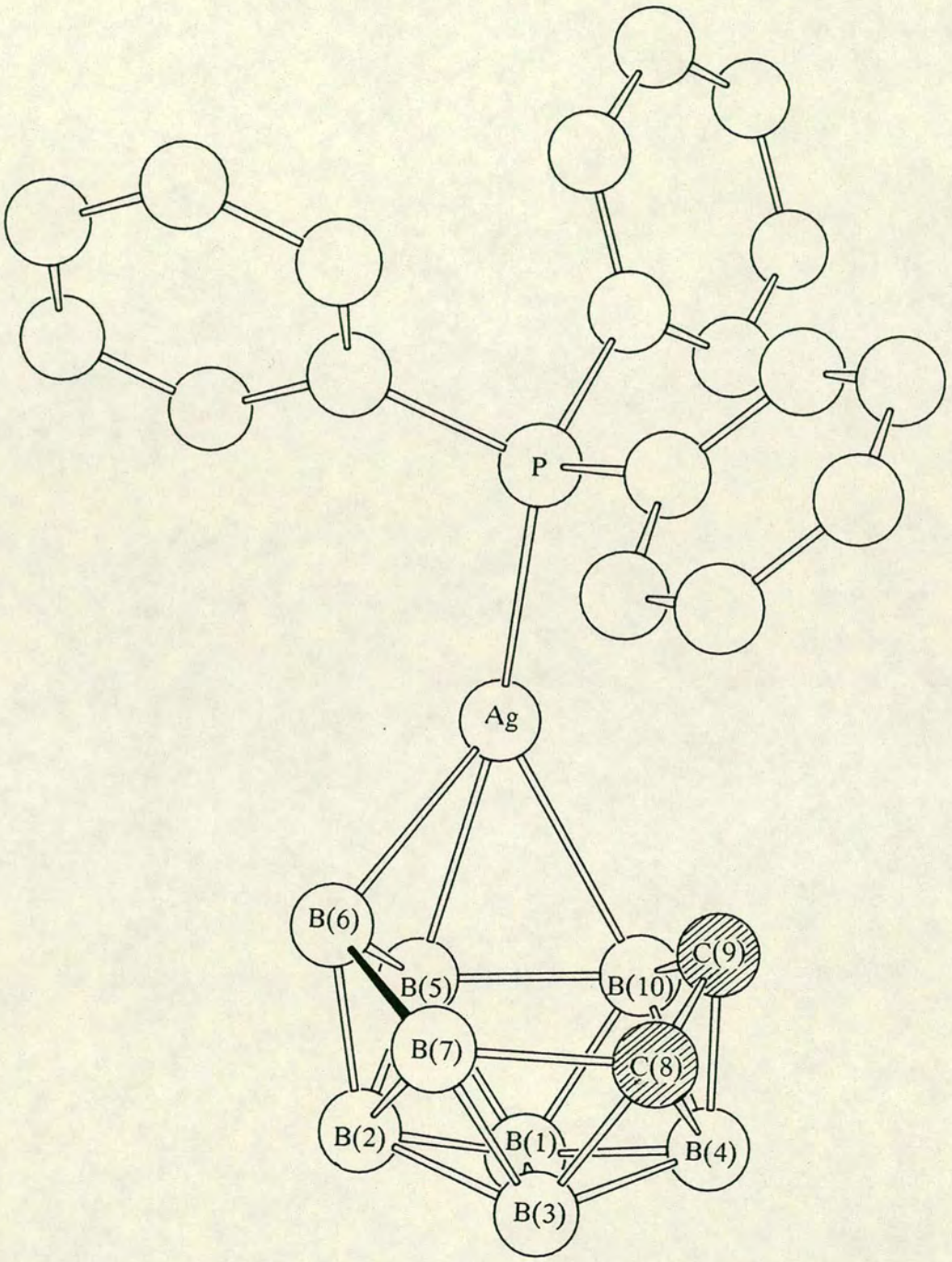

Figure 4.3. The molecular structure of $Ph_3PAgC_2B_8H_{11}$. The two carborane C atoms are shown shaded, all cage B and C atoms have a terminal H atom, and there is a μ-H atom between B(6) and B(7).

Complex	Misfit/pm	Complex	Misfit/pm
$B_{10}H_{14}$	9.1	$[B_{10}H_{14}]^{2-}$	14.2
$[B_{10}H_{13}]^-$	6.3	$[B_{11}H_{13}]^{2-}$	14.0
$[Cy_3PAuB_{10}H_{12}]^-$	7.9	$[(B_{10}H_{12})_2Au]^-$	11.9

As can be seen from this, the structure of the silver complex is probably best described as a 10-vertex $\{C_2B_8\}$ *nido*-fragment, with the $\{AgPPh_3\}$ formally bridging the B(7)-B(8)-B(9) unit in a manner similar to that observed in $(Cy_3PAu)_2B_8H_{10}$. It is, however, worth noting that this is a *carborane* cage and that the carbon atoms will perturb the cage architecture to an extent because of the difference in electronegativity between carbon and boron.

Finally the reason for the η^3 coordination as opposed to the metallaborane η^4 mode is probably due to the well-known 'slip' of metal atoms away from the carbon atoms in these systems (see Chapter 1, page 15).

After renumbering the $\{B_{10}\}$ cage in **(19b)** as shown in Figure 4.2(c), its structure was compared against those of the same six boranes used above. The results are:

Complex	Misfit/pm	Complex	Misfit/pm
$B_{10}H_{14}$	13.6	$[B_{10}H_{14}]^{2-}$	15.3
$[B_{10}H_{13}]^-$	16.8	$[B_{11}H_{13}]^{2-}$	20.4
$[Cy_3PAuB_{10}H_{12}]^-$	15.1	$[(B_{10}H_{12})_2Au]^-$	15.6

As can be seen from this, neither model is really accurate - the misfits are too high. Furthermore, unlike the example above, the cage is more open - the B(6)-B(9) internuclear distance is 365.7pm, and secondly the gold-B(9) distance of 312.5 pm is very long. It is therefore likely, in view of this evidence, that the cage geometry is most accurately described as an *arachno* 11-vertex fragment of a

docosahedron.

4.3.5 N.M.R. Studies.

Since this is a disordered crystal structure, the final, average, structure of the complex is open to interpretation. For example, the $[(B_{10}H_{12})Au(B_{10}H_{13})]^{2-}$ anion is one view of the complex; alternatively it could be argued that this is a cocrystallisation of salts of $[(B_{10}H_{12})_2Au]^-$ and $[(B_{10}H_{13})Au(B_{10}H_{13})]^{3-}$ anions. Whilst this is unlikely in view of the different charges on the ions (it would be very unlikely that they (and the $[(Cy_3P)_2Au]^+$ counterions) would pack in identical positions), it should be considered.

One way of resolving the situation is to consider the ^{11}B-$\{^1H\}$ n.m.r. spectrum. If the $[(B_{10}H_{12})_2Au]^-$ anion is present, it will show up at $\delta^{11}B$ = 17.16(3B), 15.13(2B), 4.96(1B), 2.50(2B), and -22.56(2B) ppm (see Section 4.4.6).

The ^{11}B-$\{^1H\}$ n.m.r. spectrum is shown in Figure 4.4, overleaf, and for example, there is clearly no resonance at $\delta^{11}B$ = -22.56 ppm, thereby disproving the above suggestion. Therefore the most likely explanation of the structure is that it is indeed a $[(B_{10}H_{12})Au(B_{10}H_{13})]^{2-}$ anion.

As discussed earlier, the only evidence for the number of hydrogen atoms present comes from electron-counting arguments, and so the ^1H-$\{^{11}B\}$ n.m.r. spectrum was acquired to conclusively prove this. Due to the large number of peaks in the ^{11}B-$\{^1H\}$ n.m.r. spectrum, as well as the small amount of the sample, it was not considered feasible to obtain the ^1H-$\{^{11}B$,selective$\}$ n.m.r. spectrum. However the ^1H-$\{^{11}B$,broad-band noise$\}$ n.m.r. spectrum was obtained, and this is shown in Figure 4.5, overleaf. This shows four main resonances with the ratio of their integrals being 1 : 1 : 2 : 1.

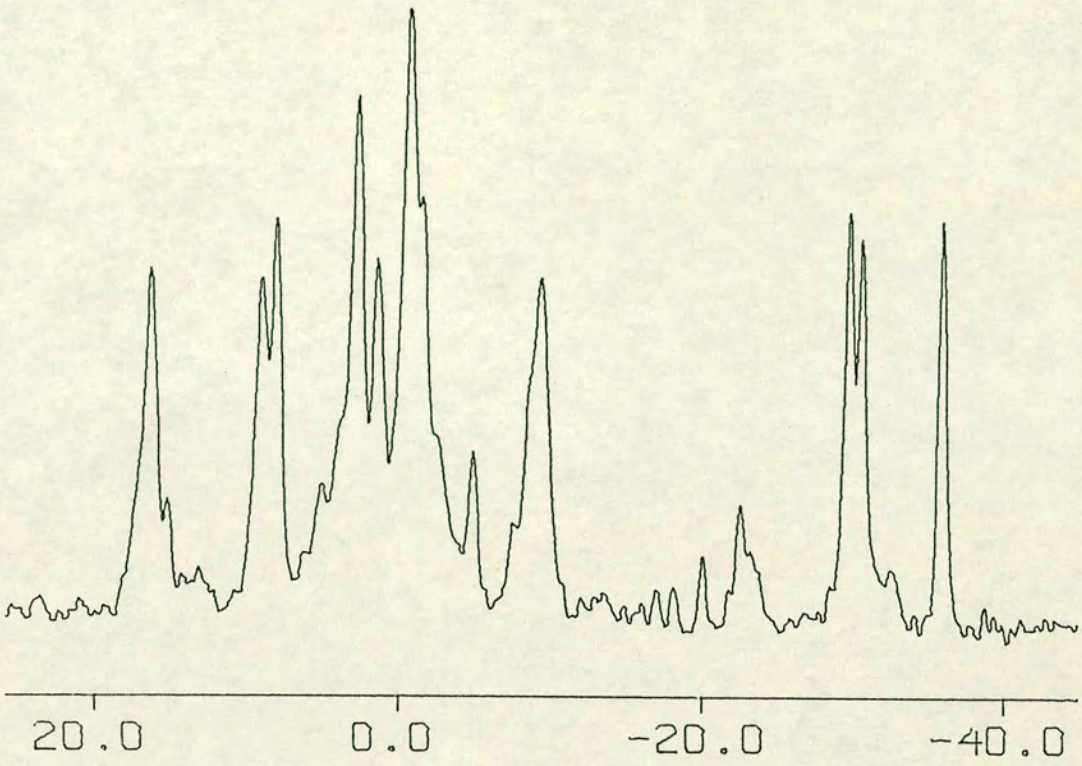

Figure 4.4. The ^{11}B-{^{1}H} n.m.r. spectrum of $[(Cy_3P)_2Au]^+_2$ $[(B_{10}H_{12})Au(B_{10}H_{13})]^{2-}$ (in CD_2Cl_2).

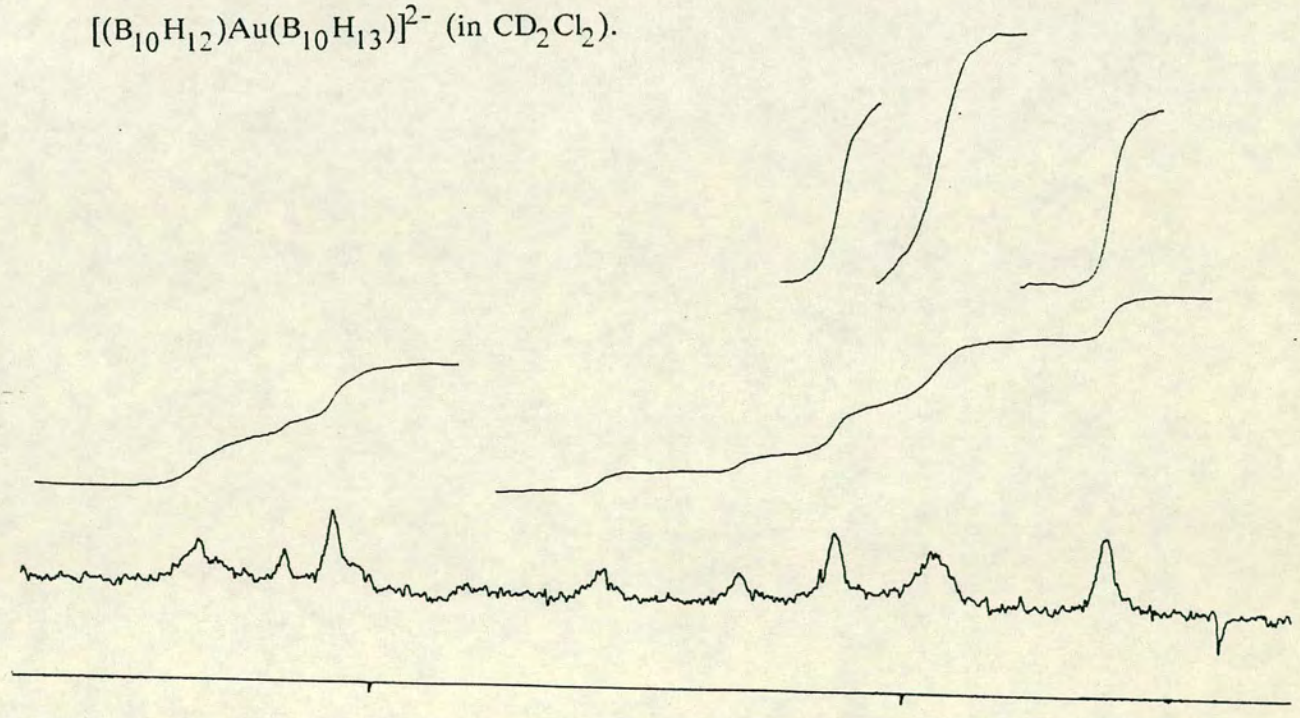

Figure 4.5. The ^{1}H-{^{11}B,broad-band noise} n.m.r. spectrum of **(19)**.

4.4 Reactions of this Complex.

Since so little of this compound was synthesised it was not possible to do any reactions with it. The one reaction which should be tried is to react it with $[Ph_3C]^+ BF_4^-$ to see if it will lose a hydride and form the $[(B_{10}H_{12})_2Au]^-$ anion.

4.5 The Synthesis of the $[(B_{10}H_{12})_2Au]^-$ Anion.

This anion, together with a $[(R_3P)_2Au]^+$ cation, appears to be one of the most readily synthesised auraboranes, having been identified as a product in a number of reactions:

Reaction	Yield
(1) $AuMe(PCy_3) + B_{10}H_{14}$	Very low,difficult to reproduce
(2) $Cy_3PAuB_{10}H_{13}$ refluxed in MeCN	60%, easily purified
(3) $Cy_3PAuB_{10}H_{13}$ stirred in SMe_2	decomposition evident
(4) $Cy_3PAuB_{10}H_{13} + [NHEt_3]^+ [B_{10}H_{13}]^-$	difficult to purify
(5) $AuCl(PPh_3) + [NHEt_3]^+ [B_{10}H_{13}]^-$	variable, purification not easy
(6) $AuCl(PCy_3) + B_{10}H_{12}(MeCN)_2$	identified spectroscopically
(7) $AuCl(PCy_3) + B_{10}H_{12}(SMe_2)_2$	poor yield

Routes (4) and (5) are probably related, as the first step in (5) is likely to be the synthesis of $Ph_3PAuB_{10}H_{13}$ which then undergoes reaction with more $[B_{10}H_{13}]^-$ to synthesise the $[(B_{10}H_{12})_2Au]^-$ anion.

4.6 The Structure of $[(o\text{-tolyl}_3P)_2Au]^+ [(B_{10}H_{12})_2Au]^-$.

The crystallographic details for this determination start on page 243, two views of the structure of the anion are shown in Figure 4.6 on page 125, and the bond lengths and angles for the anion are in Table 4.3, on page 142.

4.6.1 The Structure of the Cation

This is the *o*-tolyl version of the linear Au(I) species. Since the gold is located on a crystallographic inversion centre, the P(1)-Au-P(2) angle is 180°. The Au-P bond length of 230.37(19) is similar to those obtained for the $[(Cy_3P)_2Au]^+$ cation.

The only other example of a structurally-characterised $\{(o\text{-tolyl})_3PAu\}$ fragment is in the species 5,6-μ-(*o*-tolyl$_3$PAu)-*nido*-$B_{10}H_{13}$ discussed in Chapter 2. Its Au-P distance of 230.8(3)pm is not significantly different than that determined above - a feature also noted for the respective cyclohexyl derivatives.

4.6.2 The Geometry of the Gold Atom in the Anion.

There are two other crystallographically characterisd species of the general type $[(B_{10}H_{12})_2M]^{2-}$. The first, M = Zn, [136] has a pseudo-tetrahedral geometry, with the two cages rotated by 87.90°, as defined by the angle that the plane through the Zn and the mid-points of the B(5)-B(6) and B(9)-B(10) connectivities makes with the plane defined by the Zn and the other pair of mid-points. The mid(B[2],B[11])-Zn-mid(B[3],B[8]) angle is 77.3 °.

In the second, M = Ni [133], the anion is located on an inversion centre, and so the two cages are rotated by 180°. The mid(B[2],B[11])-Ni-mid(B[3],B[8]) angle is 82.7 °, and the nickel is formally square-planar (although see below). **(20)** is isostructural with this nickel complex, and it is interesting to note that this is the first *monoanionic* derivative.

(20) is shown in Figure 4.6, overleaf. The gold atom is located on a crystallographic inversion centre, and so one cage is generated by the other by transformation through this centre. The gold is (superficially at least) square-planar. The mid(B[3],B[8])-Au(7)-mid(B[2],B[11]) angle is 76.15°, and

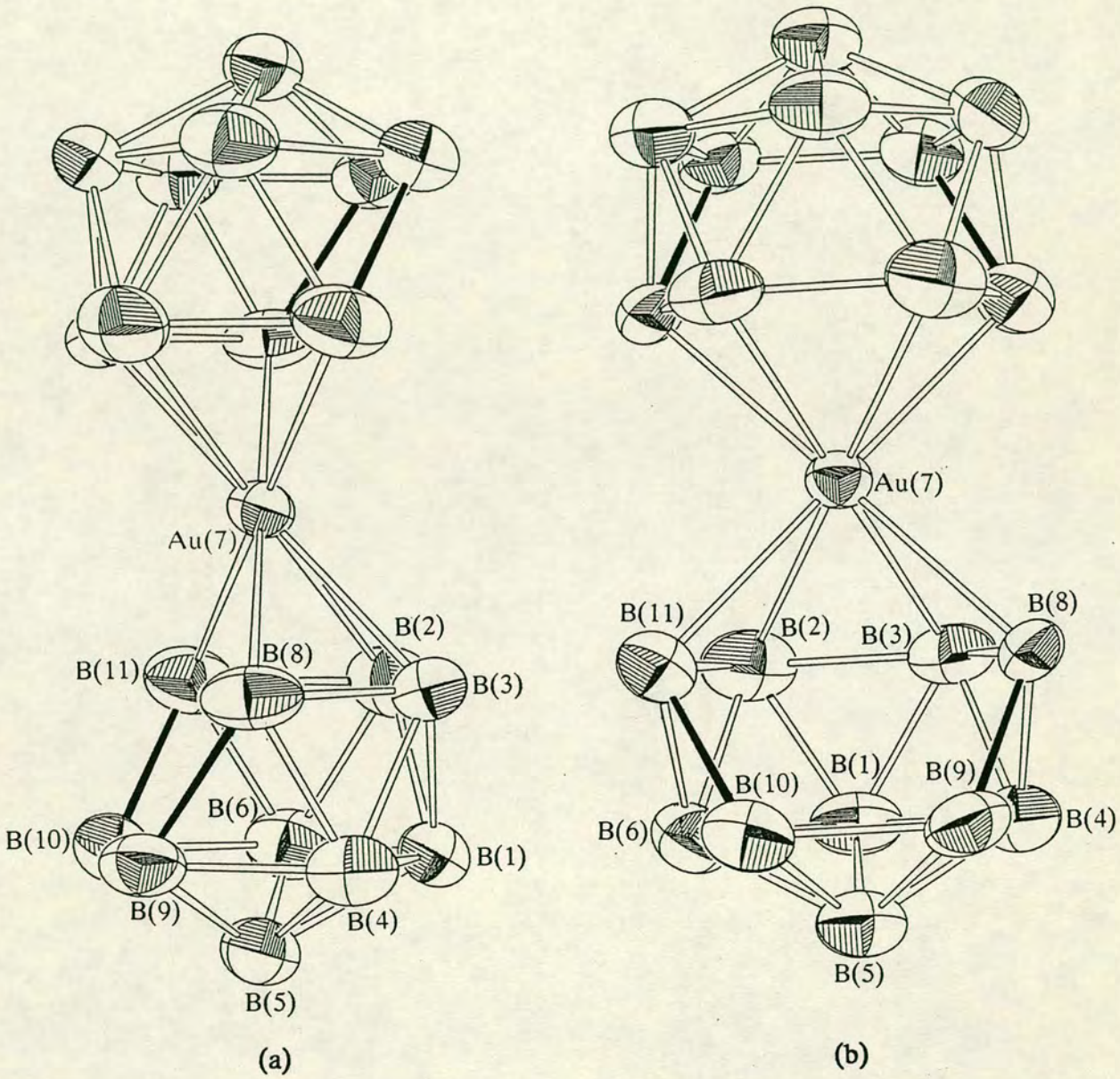

Figure 4.6. Two views of the $[(B_{10}H_{12})_2Au]^-$ anion: (a) shows the open face of the *nido*-icosahedron, and
(b) shows the relationship of the cages to $B_{10}H_{14}$.

since the two midpoints generate their equivalents in the other cage, the gold is perfectly planar (since there are only three independent points defining the plane). The gold-boron connectivities are all of similar length, and this contrasts with the situation in the $[Cy_3PAuB_{10}H_{12}]^-$ anion.

4.6.3 The Structure of the Cages in the Anion.

The crystal structure of this anion is also disordered. This is the well-known rotational disorder in *nido* 11-vertex heteroboranes where the vacant site has partial occupancy, and adjacent sites have occupancy factors of less than one. However this should not seriously affect the structure, and so the values obtained for comparisons are probably accurate.

This was the structure used in Chapter 3 as a comparison with the $[Cy_3PAuB_{10}H_{12}]^-$ anion, and it was shown to have a B_{10} cage very similar to that of $[B_{10}H_{14}]^{2-}$. It has been suggested[147] that in these transition metal derivatives, the metal centre formally contributes three orbitals to cage bonding, and contributions from higher oxidation states are invoked.

However, if this is a complex between a gold centre and two $[B_{10}H_{12}]^{4-}$ ligands, then the gold is formally in its +VII oxidation state. Furthermore, this explanation of the structure requires that the gold acts as a three-orbital donor to cluster bonding and so will use six orbitals in all i.e. it is octahedral. Since it was discussed as square planar, earlier, it was decided to perform an EHMO calculation to try and rationalise this. This is discussed in detail in Section 4.9.

4.7 The Structure of $[(Cy_3P)_2Au]^+$ $[(B_{10}H_{12})_2Au]^-$.

A second crystallographic determination was subsequently carried out - that of $[(Cy_3P)_2Au]^+$ **(20)**. This is interesting because the ions do not lie on

crystallographic inversion centres, and so there was the opportunity to investigate how the two cages pack : the previous determination showed the open faces of the two clusters to be 'trans'. However this phenomenon could have been crystallographically imposed, whereas in $[(Cy_3P)_2Au]^+$ **(20)** there is no such constraint.

A perspective view of one ion-pair is shown in Figure 4.7, overleaf. The crystallographic details about this structure start on page 250. The cation is the linear species discussed above and is insignificantly different in this structure determination.

4.7.1 The Structure of the $[(B_{10}H_{12})_2Au]^-$ Anion

The boron atoms in the two cages were independently refined, unlike the previous determination which provided the average of the two cages. For convenience, the two cages will be referred to as Cage 1 and Cage 2. The bond lengths and angles for Cage 1 are in Table 4.4 on page 143; those of Cage 2 are in Table 4.5 on page 144.

The two cages were compared against each other, and this yielded a misfit of 3.9 pm, which fell to 3.8 pm when the gold atom position was included. Furthermore, the B(9)-B(10) connectivities are both 200(4)pm long, suggesting that the $\{B_{10}\}$ fragments of these cages have less *arachno* 10-vertex character, and the gold atom is more out of the B(6)-B(7)-B(8)-B(9) plane : in Cage 1 by 53.9 pm, in Cage 2 by 53.3 pm, whereas in $[(o\text{-tolyl}_3P)_2Au]^+$ **(20)** it was only 46.3 pm.

4.7.2 Geometrical Analysis

In view of these differing data, the cage structures were compared against those of other $\{B_{10}\}$ cages in an attempt to unravel the differences.

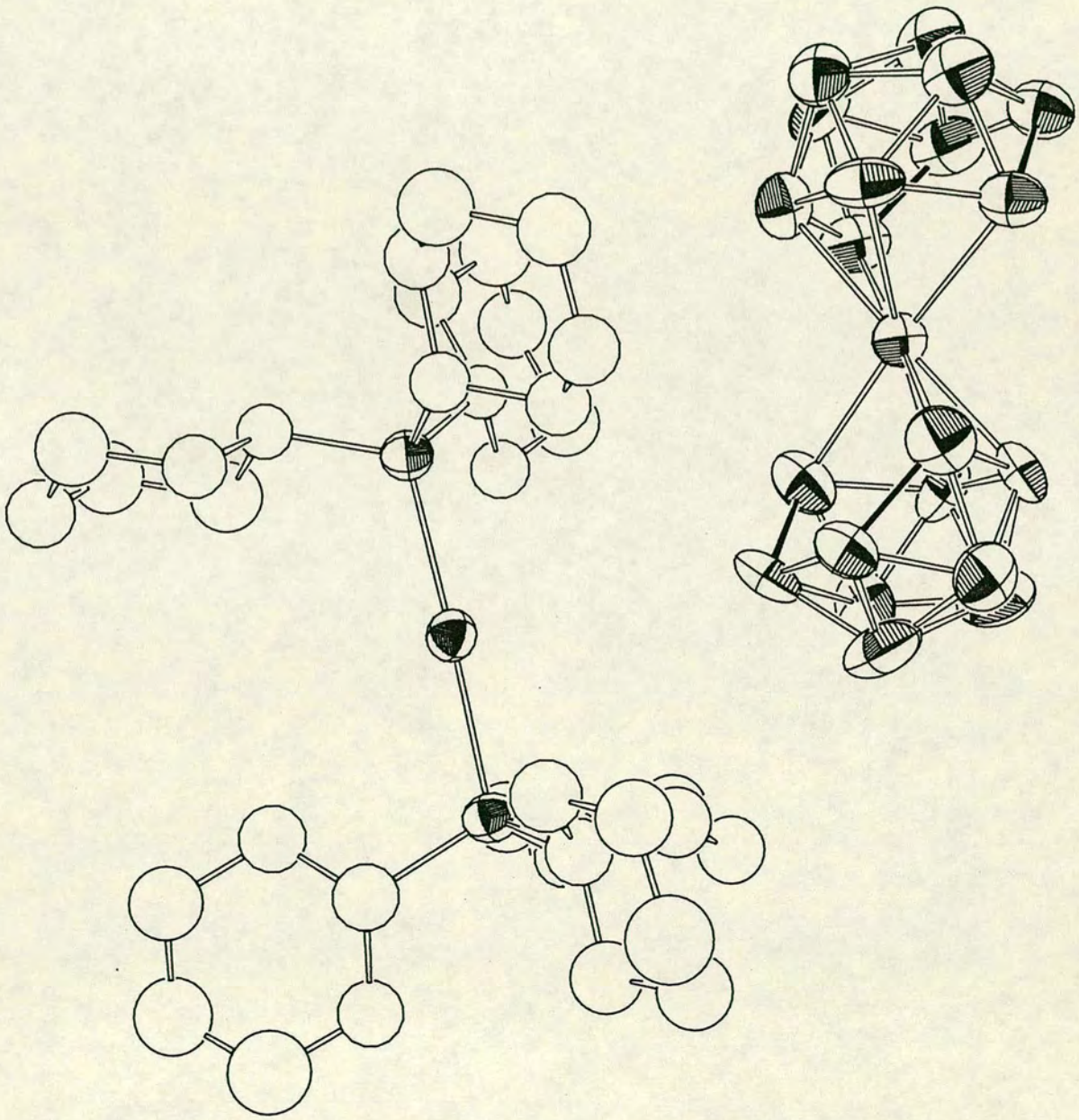

Figure 4.7. One ion-pair in $[(Cy_3P)_2Au]^+ [(B_{10}H_{12})_2Au]^-$.

Complex	(20a)	(20b)
$B_{10}H_{14}$	6.7	7.4
$[B_{10}H_{13}]^-$	7.0	7.5
$Cy_3PAuB_{10}H_{13}$	7.9	8.8
$[NHEt_3]^+ [Cy_3PAuB_{10}H_{12}]^-$	6.3(6.5)†	6.9(7.2)
$[Me_2TlB_{10}H_{12}]^-$	7.0	8.1
$[(B_{10}H_{12})_2Zn]^{2-}$	6.1	7.2
$[(B_{10}H_{12})_2Ni]^{2-}$	5.0	5.2
$[B_{10}H_{14}]^{2-}$	8.3	8.5
$[B_{11}H_{13}]^{2-}$	12.9	13.0
$(Cp^*Rh)Cl(Me_2PhP)B_{10}H_{11}$	9.8	9.6
$(Me_2PhP)_2PtB_{10}H_{12}$	7.0	7.0
$(Me_2PhP)_2PtB_{10}H_{11}Cl$	7.2	7.2
$[(B_{10}H_{12})_2Au]^-$	7.5(7.2)	6.9(6.7)

Notes

† Including gold atom position in misfit.

As can be seen from these results, the cages fit reasonably well with a lot of the other structures. The best fit is with the isostructural Ni complex, and, in general, the fit is as good with the *nido* 10-vertex compounds as it is with the metallaboranes with an *arachno* 10-vertex $\{B_{10}\}$ fragment. However, the fit with $[B_{11}H_{13}]^{2-}$ is not very good.

The only explanation for the different cage structures in the two salts of **(20)** is that the subtle effect of changing the cation or the space group, and its associated symmetry constraints, leads to slightly different cage geometries, and this difference is such that in the $[(Cy_3P)_2Au]^+$ salt, the $\{B_{10}\}$ fragment is more like a *nido*-$\{B_{10}\}$ cage than it is in the $[(o\text{-tolyl}_3P)_2Au]^+$ salt. Since the misfit values are very small, this leads to the observed results. This does illustrate

the need for caution in interpreting these values.

4.8 Spectroscopic Data.

It has been shown that the structure of the $\{B_{10}\}$ fragment can be slightly different to that of $B_{10}H_{14}$ in the solid state, depending on the cation present. In solution, the effects of the cation are averaged out, and so the n.m.r. spectra were recorded to see if the electronic environment of the $\{B_{10}\}$ cage caused variations in the chemical shifts of the boron atom resonances to be when compared against other metallaborane and borane systems.

The $^{11}B-\{^{1}H\}$ n.m.r. spectrum (Figure 4.8, overleaf) consists of six peaks in the ratio 2 : 1 : 2 : 1 : 2 : 2, although the first two resonances (Figure 4.8) overlap to an extent. A similar pattern (including this accidental coincidence) was observed for $(Me_2PhP)_2PtB_{10}H_{12}$, whose multinuclear n.m.r. spectra were thoroughly investigated[95].

Comparison of the two spectra shows that they are broadly similar :

$[(B_{10}H_{12})_2Au]^-$: 17.16(2B), 16.64(1B), 15.13(2B), 4.96(1B), 2.50(2B), and -22.56(2B) ppm.

$(Me_2PhP)_2PtB_{10}H_{12}$ ‡ : 16.1(B(5)), 15.1(B(2),B(3)), 9.3(B(8),B(11)), 2.3(B(1)), -3.1(B(10),B(9)), and -26.9(B(4),B(6)) ppm.

‡ *nido* 11-vertex numbering.

Whilst no firm conclusions can be drawn from this due to the lack of assignments for the spectrum of **(20)**, such evidence as the good agreement between the resonances for B(1) and B(5) in $(Me_2PhP)_2PtB_{10}H_{12}$, compared to the two resonances of integral 1 in the spectrum of **(20)**, which must arise, on symmetry grounds from the same two atoms, suggests that in these two complexes, the $\{B_{10}\}$ cages have similar electronic environments. Furthermore the bridging

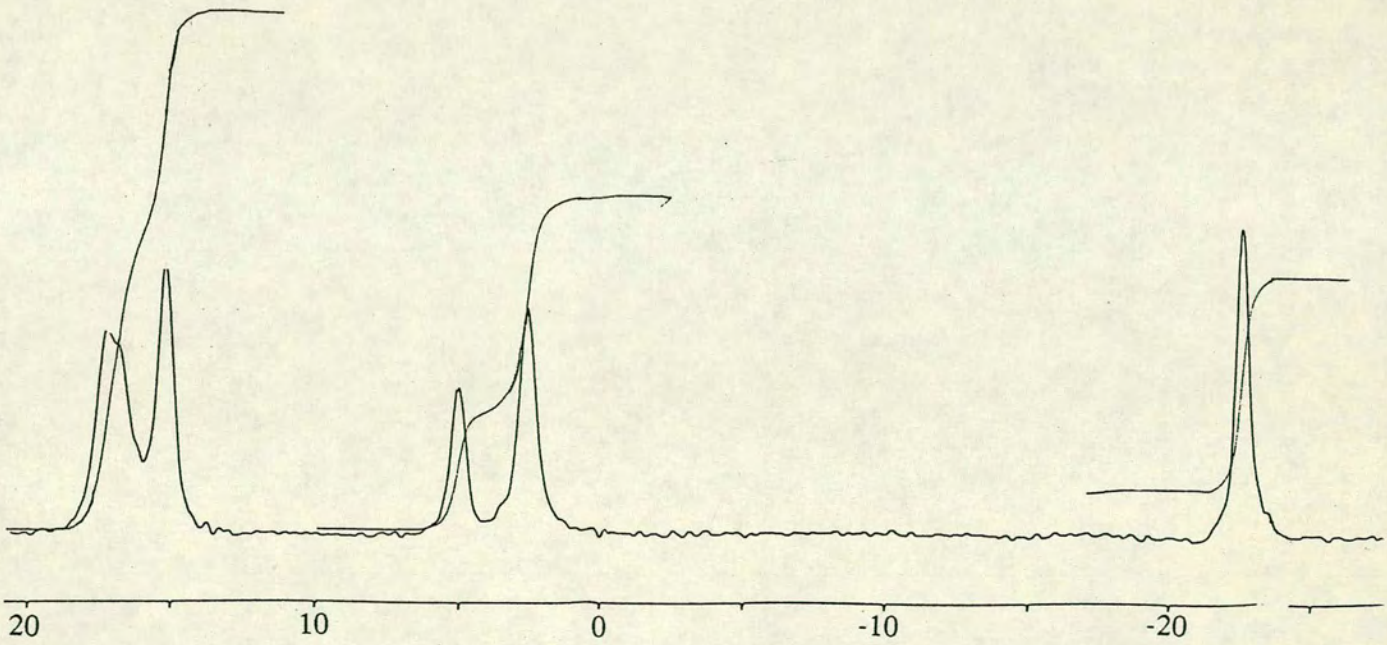

Figure 4.8. The ^{11}B-{^{1}H} n.m.r. spectrum of the $[(B_{10}H_{12})_2Au]^-$ anion.

hydrogen resonances are very close : -2.09 for $(Me_2PhP)_2PtB_{10}H_{12}$ versus -1.96ppm for **(20)**. In the $[Cy_3PAuB_{10}H_{12}]^-$ anion, for example they resonate at -4.80ppm. All of this does reinforce the suggestion that $(Me_2PhP)_2PtB_{10}H_{12}$ and **(20)** have isostructural cages.

4.9 Electronic Structure of the $[(B_{10}H_{12})_2Au]^-$ Anion.

There are two $\{B_{10}H_{12}\}$ fragments in the $[(B_{10}H_{12})_2Au]^-$ anion, and this complicates the interpretation of the results since all the orbitals of interest are duplicated. In view of this, it was decided to first examine the structure of the isostructural complex $(Me_2PhP)_2PtB_{10}H_{12}$. Accordingly, a model, **(20b)**, was constructed by replacing the dimethylphenylphosphine ligands by phosphine ones. The complex was then rotated such that the $\{B_4\}$ unit to which the Pt bonds is in the xy plane. The atomic coordinates of **(20b)** are in Appendix 3, starting on page 285. The model of $[B_{10}H_{12}]^{2-}$, **(16)**, is the same as that discussed in Chapter 3.

The frontier orbitals of the $[(H_3P)_2Pt]^{2+}$ fragment have previously been investigated[14] (albeit without P 3d orbitals), and they are shown in Figure 4.9, overleaf. Of especial interest are two UMO's. The LUMO is a $6p_x/5d_{xz}$ hybrid and the second LUMO is a $6s/6p_z$ hybrid. The interaction of the two fragments is also shown in Figure 4.9. Consider the occupation of the metal atomic orbitals. The 5d orbitals are deoccupied, varying from 1.7879 to 1.8422, except for the d_{xz} which has an occupation of 1.4949. This one is presumably much more deoccupied because it is part of the LUMO which clearly can have an in-phase overlap with the HOMO of **(16)**. The others presumably are involved in metal-cage back-bonding. For example, there is clearly allowed overlap of the LUMO of **(16)** with the platinum d_{yz}, and it has one of the highest deoccupations

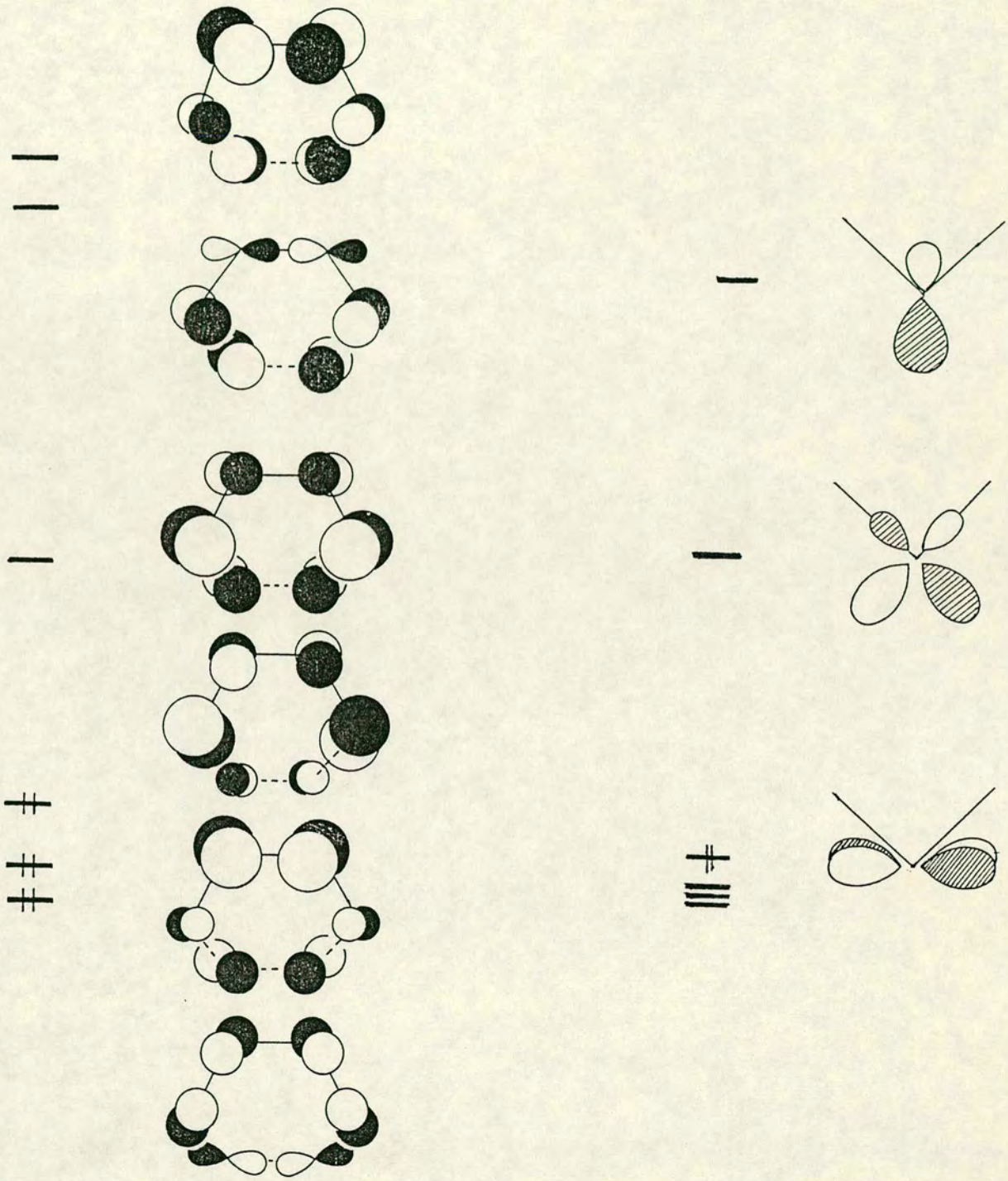

Figure 4.9. The frontier orbitals of the two fragments $[(H_3P)_2Pt]^{2+}$ and $[B_{10}H_{12}]^{2-}$.

of the four d orbitals being considered. In view of this involvement of the Pt 5d orbitals, it is probably more accurate to describe the Pt orbital contribution to cage bonding as greater than two. However such incipient back-bonding is much more characteristic of platinum(II) than gold(III). The Pt $6p_y$ is virtually unoccupied, but the $6p_x$ (0.3140) and $6p_z$ (0.2557) both have a substantial occupation.

The difference in bonding capability between the $\{AuPH_3\}$ and the $\{Pt(PH_3)_2\}$ fragments is that in the former, the fragment hybrid orbitals comprise a low-lying a_1 and a high-lying e, thus causing the dominant linear geometry, whereas in the latter case, there are two low-lying UMO's - the $6s/6p_x$ and the $6p_x/5d_{xz}$, and it is presumably this difference that causes the metallaboranes with these two metal-ligand fragments to have differing structures.

Following on from this, the structure of the $[(B_{10}H_{12})_2Au]^-$ anion was examined. The model, **(20c)**, used for these calculations was constructed from the experimental geometry, except that the terminal H atoms were set in idealised positions (B-H 120pm). The coordinates are given in Appendix 3, starting on page 286.

If the metal orbital occupations are again examined, the results are interesting. First, the four d-orbitals d_z2 (1.9533), $d_x2_{-y}2$ (1.9811), d_{xy} (1.9480), and d_{yz} (1.9131) are imperceptibly involved in the bonding, but the d_{xz} (1.7924) participates to a greater extent. As in **(20b)**, the p_y has negligible occupation, but the p_x (0.3032) and p_z (0.2143) dictate the bond strength.

When these two orbital occupations are compared against those in the $[Cy_3PAuB_{10}H_{12}]^-$ anion (0.2212 and 0.2873 respectively), there are two relevant points. Firstly the extent to which the orbitals are occupied with respect to one another has altered. As with **(20b)**, now the p_x is involved to a greater extent

than the p_z. Secondly, the sum of the two occupancies is greater for **(20c)** (0.5175 against 0.5085 for **(15)**), and it is presumably these two factors which decide on the final metallaborane geometry.

4.10 The Structures of the $\{MB_{10}\}$ Metallaboranes.

Based on all of this, it has become apparent that these structures are more complex than they appear. To summarise, the following two trends have emerged.

(1) As the atomic number of the metal increases across the third row metals, the amount by which the metal is out of the B(6)-B(7)-B(8)-B(9) plane increases. (Ir 21.9, Pt 40.1-47.0, Au 40.1-53.9(+III) or 71.7 pm(+I), Tl 88.3)

(2) Similarly, the misfit against first $[B_{11}H_{13}]^{2-}$, then $[B_{10}H_{14}]^{2-}$ becomes progressively worse, and that against $B_{10}H_{14}$ improves.

This is shown diagrammatically overleaf, in Figure 4.10. This graph was plotted in the following manner. First the misfit between $B_{10}H_{14}$ and $[B_{11}H_{13}]^{2-}$ (17.2pm) was calculated, and this defined the length of the x-axis (with appropriate scaling). Next the metallaboranes were plotted along the x-axis, such that the scaled distance between the left-hand end and the datum point is the misfit of the metallaborane versus $B_{10}H_{14}$, and the distance between the right-hand end and the datum point is the length equivalent to the metallaborane misfit versus $[B_{11}H_{13}]^{2-}$. This plot is therefore a measure of the 'extent of incorporation into the cage as a vertex' (verticity?).

Then the "% verticity" was calculated in an analogous manner, and the values of these are scaled such that $B_{10}H_{14}$ will produce a value of 0, and $[B_{11}H_{13}]^{2-}$ is 100%. The results are listed in Table 4.6, overleaf.

The explanation for these trends is quite straightforward, although not entirely satisfactory. The $\{(CO)(PPh_3)_2\}IrB_{10}H_{11}(PPh_3)$ complex has an

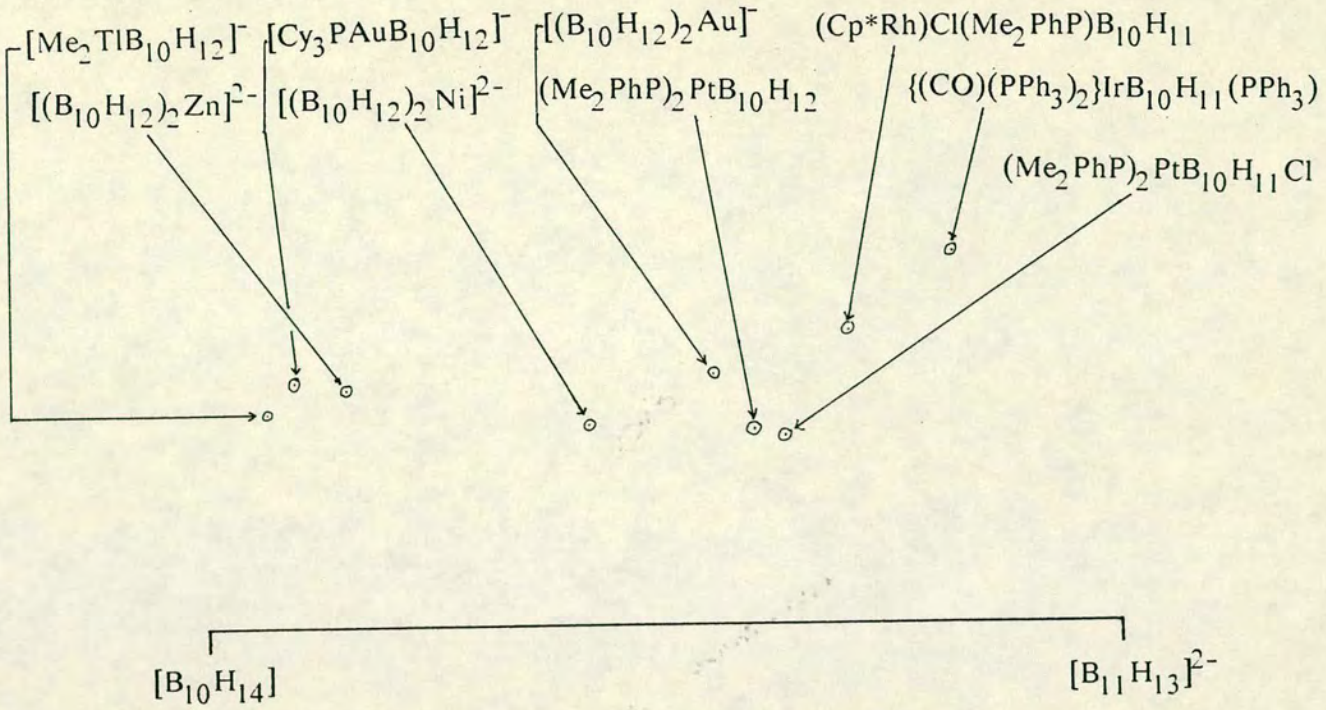

Figure 4.10. The plot showing how close to a *nido* 11-vertex fragment the $\{MB_{10}H_{12}\}$ fragments are.

Table 4.6. The "% Verticity" in the Metallaboranes (see text).

Method of Calculation of % verticity of X:

$$\frac{(\text{misfit of } B_{10}H_{14}/[B_{11}H_{13}]^{2-}) + (\text{misfit of } X/B_{10}H_{14}) - (\text{misfit of } X/[B_{11}H_{13}]^{2-})}{2 \times (\text{misfit of } B_{10}H_{14}/[B_{11}H_{13}]^{2-})} \times 100\ \%$$

Metallaborane	% Verticity
$\{(CO)(PPh_3)_2\}IrB_{10}H_{11}(PPh_3)$	73.8
$(Cp^*Rh)Cl(Me_2PhP)B_{10}H_{11}$	66.9
$(Me_2PhP)_2PtB_{10}H_{11}Cl$	61.9
$(Me_2PhP)_2PtB_{10}H_{12}$	58.7
$[(B_{10}H_{12})_2Au]^-$	54.6
$[(B_{10}H_{12})_2Ni]^{2-}$	41.9
$[(B_{10}H_{12})_2Zn]^{2-}$	20.0
$[Cy_3PAuB_{10}H_{12}]^-$	16.6
$[Me_2TlB_{10}H_{12}]^-$	13.7

octahedral geometry at the iridium, and so the iridium is a three orbital donor to cage-bonding. Hence the complex has the correct *orbital* count, as well as electron-count for this to be a *nido* 11-vertex polyhedron. The Rh complex probably has a similar electronic structure, although this has not been investigated.

The next subgroup are the Pt complexes; $(H_3P)_2PtB_{10}H_{12}$ was shown to have an orbital contribution > 2, due to metal-ligand back-bonding, and so while the fit against $[B_{11}H_{13}]^{2-}$ is as good as it is for the iridium compound, the fit against $B_{10}H_{14}$ is improved because the metal now better mimics a $[H..H]^{2+}$ group.

The gold and nickel complexes are next. In these, the in-phase mixing of the d_{xz} orbital causes the lowering in energy of a UMO, and it is this which improves the orbital overlaps, but this is still primarily a two-orbital interaction, and so the fit against $[B_{11}H_{13}]^{2-}$ is poorer than above, and the fit against $B_{10}H_{14}$ is better.

Finally there are the main group derivatives : $[Cy_3PAuB_{10}H_{12}]^-$, $[(B_{10}H_{12})_2Zn]^{2-}$, and $[Me_2TlB_{10}H_{12}]^-$. In these, the d orbitals are essentially core orbitals, so metal-borane is a two-orbital interaction, but the overlap is not as good due to the higher energies of at least one of the metal-based orbitals, hence the bonding closely mimics that of $B_{10}H_{14}$.

However, there are weaknesses in this explanation. First is the structure of $[B_{10}H_{14}]^{2-}$. Its correct orbital and electron count are obtained by including the two *endo* B-H bonds in the skeletal counts, and the justification for this is that these two bonds are located on the spherical surface, and as such are available for skeletal bonding. The arguments outlined above, imply that these bonds are not efficiently used for this purpose. The energetics should not be unfavourable because the boron AO's should be ideal for interacting with borane ones! However it should be noted that the structural comparison with this fragment is

not rigorously valid, because of structural differences such as the different locations of the bridging hydrogens (which, through their influence on bond lengths, can indirectly influence the misfit calculation).

The structure of $[B_{11}H_{14}]^-$ has recently been communicated[148] although the coordinates were not published, and we have yet to receive them direct from the authors. This is of interest here because it has a $\{BH_2\}$ group where the metal atom would be, so such factors as the extent to which this boron atom is out of the B(6)-B(7)-B(8)-B(9) plane, and its fit with $[B_{11}H_{13}]^{2-}$ or $[B_{10}H_{14}]^{2-}$ would help illuminate these problems.

The next point that arises from this is that if a boron atom can use an *endo* B-H bond in skeletal bonding, why doesn't the Tl atom in $[Me_2TlB_{10}H_{12}]^-$ use its *endo* Tl-C bond for the same purpose, and thus become more involved in the cage structure?

The final point concerns the two complexes discussed in Chapter 3, $(Cy_3PAu)_2B_8H_{10}$ and $(dtcAu)_2B_8H_{10}$. These were also shown to have different structures, and the arguments as to why are presumably similar, namely that in the second complex, the gold is square-planar (implying Au(III)) and so it is more efficiently bonded to the cage, thus slightly altering its geometry. In $(Cy_3PAu)_2B_8H_{10}$, it is presumably Au(I), thus the cage-gold bonding is weaker, and so the $\{B_8\}$ unit retains much *nido*-octaborane character.

However, these tentative conclusions do suggest that more work, especially crystallographic studies, should be carried out on $\{MB_{10}H_{12}\}$ species, particularly the early transition metal derivatives, of which none have been structurally characterised, and also main group derivatives.

4.11 Conclusions

The unique structure of the $[(B_{10}H_{12})Au(B_{10}H_{13})]^{2-}$ anion was shown to involve two $\{B_{10}\}$ cages ligated to the gold in different manners. One half of the molecule is a *nido*-7-$AuB_{10}H_{12}$ fragment, whilst the other is a *arachno*-2-$AuB_{10}H_{13}$. The multinuclear n.m.r. spectra are in good agreement with this structure.

The second complex is the $[(B_{10}H_{12})_2Au]^-$ anion which has been synthesised by a multitude of routes, although the easiest is to reflux 5,6-μ-(Cy_3PAu)-*nido*-$B_{10}H_{13}$ in acetonitrile. The structure of the anion as its $[(o\text{-tolyl}_3P)_2Au]^+$ salt was determined crystallographically, and using this geometry in EHMO calculations, it was shown that the differences in cage geometries of the $\{MB_{10}H_{12}\}$ derivatives were mostly due to the efficiency with which the bonding AO's overlap. This differs for transition metals because there is an empty d-orbital which hybridises with p_x, thus reducing its energy towards those of the borane orbitals, which improves the effectiveness of the overlap, and so significantly alters the cage architecture.

The structure of the $[(B_{10}H_{12})_2Au]^-$ anion was also determined as its $[(Cy_3P)_2Au]^+$ salt, however, the misfit values were more difficult to interpret because the cage geometries were found to be as consistent with the *nido*-$\{B_{10}\}$ structures as with the *arachno*-$\{B_{10}\}$ models. This is probably due to the metal acting as a two-orbital donor to cage bonding which means that all of these complexes are *pseudo-nido* icosahedra.

Finally, all of this work was used in an attempt to rationalise the structures of the $\{MB_{10}H_{12}\}$ fragments (or their derivatives). Then the same explanation is used for the two $\{Au_2B_8\}$ complexes discussed in Chapter 3.

Table 4.1. Bond Lengths(pm) and Angles(^{o}) for the *nido*-7-$AuB_{10}H_{12}$ Fragment in the $[(B_{10}H_{12})Au(B_{10}H_{13})]^{2-}$ Anion. For clarity, the *arachno* component in the numbering of B(i,j) has been replaced by j.

Au(7,j)-B(2,j)	226.2(10)	B(3,j)-B(8,j)	180.8(15)
Au(7,j)-B(3,j)	223.1(10)	B(4,j)-B(5,j)	175.8(14)
Au(7,j)-B(8,j)	244.7(12)	B(4,j)-B(8,j)	176.8(15)
Au(7,j)-B(11,j)	249.9(21)	B(4,j)-B(9,j)	176.7(16)
B(1,j)-B(2,j)	177.9(13)	B(5,j)-B(6,j)	176.3(14)
B(1,j)-B(3,j)	180.3(13)	B(5,j)-B(9,j)	175.3(17)
B(1,j)-B(4,j)	176.2(14)	B(5,j)-B(10,j)	179.7(17)
B(1,j)-B(5,j)	175.9(14)	B(6,j)-B(10,j)	180.6(17)
B(1,j)-B(6,j)	177.6(13)	B(6,j)-B(11,j)	167.8(23)
B(2,j)-B(3,j)	186.8(13)	B(8,j)-B(9,j)	183.5(17)
B(2,j)-B(6,j)	183.5(14)	B(9,j)-B(10,j)	195.2(19)
B(2,j)-B(11,j)	175.0(23)	B(10,j)-B(11,j)	200.0(25)
B(3,j)-B(4,j)	174.4(14)		

B(2,j)-Au(7,j)-B(3,j)	49.1(3)	B(1,j)-B(5,j)-B(4,j)	60.2(6)
B(2,j)-Au(7,j)-B(11,j)	42.8(5)	B(1,j)-B(5,j)-B(6,j)	60.6(6)
B(3,j)-Au(7,j)-B(8,j)	45.2(4)	B(4,j)-B(5,j)-B(9,j)	60.4(6)
B(2,j)-B(1,j)-B(3,j)	62.9(5)	B(6,j)-B(5,j)-B(10,j)	61.0(6)
B(2,j)-B(1,j)-B(6,j)	62.2(5)	B(9,j)-B(5,j)-B(10,j)	66.7(7)
B(3,j)-B(1,j)-B(4,j)	58.6(5)	B(1,j)-B(6,j)-B(2,j)	59.0(5)
B(4,j)-B(1,j)-B(5,j)	59.9(6)	B(1,j)-B(6,j)-B(5,j)	59.6(5)
B(5,j)-B(1,j)-B(6,j)	59.8(5)	B(2,j)-B(6,j)-B(11,j)	59.6(9)
Au(7,j)-B(2,j)-B(3,j)	64.6(4)	B(5,j)-B(6,j)-B(10,j)	60.4(6)
Au(7,j)-B(2,j)-B(11,j)	75.8(8)	B(10,j)-B(6,j)-B(11,j)	70.0(9)
B(1,j)-B(2,j)-B(3,j)	59.2(5)	Au(7,j)-B(8,j)-B(3,j)	61.1(4)
B(1,j)-B(2,j)-B(6,j)	58.8(5)	B(3,j)-B(8,j)-B(4,j)	58.4(6)
B(6,j)-B(2,j)-B(11,j)	55.7(8)	B(4,j)-B(8,j)-B(9,j)	58.7(6)
Au(7,j)-B(3,j)-B(2,j)	66.3(4)	B(4,j)-B(9,j)-B(5,j)	59.9(6)
Au(7,j)-B(3,j)-B(8,j)	73.8(5)	B(4,j)-B(9,j)-B(8,j)	58.8(6)
B(1,j)-B(3,j)-B(2,j)	58.0(5)	B(5,j)-B(9,j)-B(10,j)	57.7(7)
B(1,j)-B(3,j)-B(4,j)	59.6(5)	B(5,j)-B(10,j)-B(6,j)	58.6(6)
B(4,j)-B(3,j)-B(8,j)	59.7(6)	B(5,j)-B(10,j)-B(9,j)	55.6(6)
B(1,j)-B(4,j)-B(3,j)	61.9(5)	B(6,j)-B(10,j)-B(11,j)	52.0(8)
B(1,j)-B(4,j)-B(5,j)	60.0(6)	Au(7,j)-B(11,j)-B(2,j)	61.4(7)
B(3,j)-B(4,j)-B(8,j)	61.9(6)	B(2,j)-B(11,j)-B(6,j)	64.7(9)
B(5,j)-B(4,j)-B(9,j)	59.7(6)	B(6,j)-B(11,j)-B(10,j)	58.0(8)
B(8,j)-B(4,j)-B(9,j)	62.5(7)		

Table 4.2. Bond Lengths(pm) and Angles(°) for the *Arachno*-2-$AuB_{10}H_{13}$ Fragment of the $[(B_{10}H_{12})Au(B_{10}H_{13})]^{2-}$ Anion. For clarity, the *nido* numbering of the atoms B(i,j) has been replaced by i.

Au(i,2)-B(i,4)	244.7(12)	B(i,7) -B(i,10)	176.7(16)
Au(i,2)-B(i,6)	223.1(10)	B(i,7) -B(i,13)	175.3(17)
Au(i,2)-B(i,9)	226.2(10)	B(i,8) -B(i,11)	180.6(17)
B(i,3)-B(i,7)	152.8(24)	B(i,8) -B(i,13)	179.7(17)
B(i,3)-B(i,8)	191.3(24)	B(i,9) -B(i,11)	183.5(14)
B(i,4)-B(i,6)	180.8(15)	B(i,9) -B(i,12)	177.9(13)
B(i,4)-B(i,7)	183.5(17)	B(i,10)-B(i,12)	176.2(14)
B(i,4)-B(i,10)	176.8(15)	B(i,10)-B(i,13)	175.8(14)
B(i,6)-B(i,9)	186.8(13)	B(i,11)-B(i,12)	177.6(13)
B(i,6)-B(i,10)	174.4(14)	B(i,11)-B(i,13)	176.3(14)
B(i,6)-B(i,12)	180.3(13)	B(i,12)-B(i,13)	175.9(14)
B(i,7)-B(i,8)	195.2(19)		

B(i,4)-Au(i,2) -B(i,6)	45.2(4)	B(i,6) -B(i,9) -B(i,12)	59.2(5)
B(i,6)-Au(i,2) -B(i,9)	49.1(3)	B(i,11)-B(i,9) -B(i,12)	58.8(5)
B(i,7)-B(i,3) -B(i,8)	68.1(10)	B(i,4) -B(i,10) -B(i,6)	61.9(6)
Au(i,2)-B(i,4) -B(i,6)	61.1(4)	B(i,4) -B(i,10) -B(i,7)	62.5(7)
B(i,6)-B(i,4) -B(i,10)	58.4(6)	B(i,6) -B(i,10) -B(i,12)	61.9(5)
B(i,7)-B(i,4) -B(i,10)	58.7(6)	B(i,7) -B(i,10) -B(i,13)	59.7(6)
Au(i,2)-B(i,6) -B(i,4)	73.8(5)	B(i,12)-B(i,10) -B(i,13)	60.0(6)
Au(i,2)-B(i,6) -B(i,9)	66.3(4)	B(i,8) -B(i,11) -B(i,13)	60.4(6)
B(i,4)-B(i,6) -B(i,10)	59.7(6)	B(i,9) -B(i,11) -B(i,12)	59.0(5)
B(i,9)-B(i,6) -B(i,12)	58.0(5)	B(i,12)-B(i,11) -B(i,13)	59.6(5)
B(i,10)-B(i,6) -B(i,12)	59.6(5)	B(i,6) -B(i,12) -B(i,9)	62.9(5)
B(i,3)-B(i,7) -B(i,4)	72.5(10)	B(i,6) -B(i,12) -B(i,10)	58.6(5)
B(i,3)-B(i,7) -B(i,8)	65.4(10)	B(i,9) -B(i,12) -B(i,11)	62.2(5)
B(i,4)-B(i,7) -B(i,10)	58.8(6)	B(i,10)-B(i,12) -B(i,13)	59.9(6)
B(i,8)-B(i,7) -B(i,13)	57.7(7)	B(i,11)-B(i,12) -B(i,13)	59.8(5)
B(i,10)-B(i,7) -B(i,13)	59.9(6)	B(i,7) -B(i,13) -B(i,8)	66.7(7)
B(i,3)-B(i,8) -B(i,7)	46.5(8)	B(i,7) -B(i,13) -B(i,10)	60.4(6)
B(i,7)-B(i,8) -B(i,13)	55.6(6)	B(i,8) -B(i,13) -B(i,11)	61.0(6)
B(i,11)-B(i,8) -B(i,13)	58.6(6)	B(i,10)-B(i,13) -B(i,12)	60.2(6)
Au(i,2)-B(i,9) -B(i,6)	64.6(4)	B(i,11)-B(i,13) -B(i,12)	60.6(6)

Table 4.3. The Bond Lengths(pm) and Angles(^{o}) for the Non-Hydrogen Atoms in the $[(B_{10}H_{12})_2Au]^-$ Anion, Studied as its $[(o\text{-tolyl}_3P)_2Au]^+$ Salt.

Au(7) - B(2)	225.3(10)	B(4) - B(5)	177.5(15)
Au(7) - B(3)	227.5(11)	B(4) - B(8)	178.7(19)
Au(7) - B(8)	231.9(15)	B(4) - B(9)	183.3(16)
Au(7) -B(11)	229.6(14)	B(5) - B(6)	176.8(15)
Au(7) - B(x)	226(3)	B(5) - B(9)	174.2(15)
B(1) - B(2)	180.4(14)	B(5) -B(10)	174.9(14)
B(1) - B(3)	176.9(15)	B(6) -B(10)	179.9(15)
B(1) - B(4)	179.8(15)	B(6) -B(11)	172.6(17)
B(1) - B(5)	176.7(14)	B(8) - B(9)	185.0(18)
B(1) - B(6)	180.0(15)	B(9) -B(10)	187.0(15)
B(2) - B(3)	187.6(15)	B(10)-B(11)	179.3(17)
B(2) - B(6)	176.9(15)	B(8) - B(x)	218(3)
B(2) -B(11)	178.6(17)	B(9) - B(x)	184(3)
B(3) - B(4)	181.3(16)	B(10)- B(x)	172(3)
B(3) - B(8)	190.2(19)	B(11)- B(x)	195(3)

B(2)	-Au(7)	- B(3)	49.0(4)	B(2) - B(6)	-B(11) 61.4(7)
B(2)	-Au(7)	-B(11)	46.2(4)	B(5) - B(6)	-B(10) 58.7(6)
B(3)	-Au(7)	- B(8)	48.9(5)	B(10)- B(6)	-B(11) 61.1(7)
B(2)	- B(1)	- B(3)	63.4(6)	Au(7)- B(8)	- B(3) 64.3(6)
B(2)	- B(1)	- B(6)	58.8(6)	B(3) - B(8)	- B(4) 58.8(7)
B(3)	- B(1)	- B(4)	61.1(6)	B(4) - B(8)	- B(9) 60.5(7)
B(4)	- B(1)	- B(5)	59.7(6)	B(4) - B(9)	- B(5) 59.5(6)
B(5)	- B(1)	- B(6)	59.4(6)	B(4) - B(9)	- B(8) 58.0(7)
Au(7)	- B(2)	- B(3)	66.2(5)	B(5) - B(9)	-B(10) 57.8(6)
Au(7)	- B(2)	-B(11)	68.2(5)	B(5) -B(10)	- B(6) 59.7(6)
B(1)	- B(2)	- B(3)	57.4(6)	B(5) -B(10)	- B(9) 57.4(6)
B(1)	- B(2)	- B(6)	60.5(6)	B(6) -B(10)	-B(11) 57.4(6)
B(6)	- B(2)	-B(11)	58.1(6)	Au(7)-B(11)	- B(2) 65.6(5)
Au(7)	- B(3)	- B(2)	64.9(5)	B(2) -B(11)	- B(6) 60.5(7)
Au(7)	- B(3)	- B(8)	66.7(6)	B(6) -B(11)	-B(10) 61.5(7)
B(1)	- B(3)	- B(2)	59.2(6)	Au(7)- B(x)	- B(8) 62.9(9)
B(1)	- B(3)	- B(4)	60.3(6)	B(8) -Au(7)	- B(x) 56.8(8)
B(4)	- B(3)	- B(8)	57.5(7)	B(11)-Au(7)	- B(x) 50.6(8)
B(1)	- B(4)	- B(3)	58.6(6)	Au(7)- B(8)	- B(x) 60.3(9)
B(1)	- B(4)	- B(5)	59.3(6)	B(9) - B(8)	- B(x) 53.5(9)
B(3)	- B(4)	- B(8)	63.8(7)	B(8) - B(9)	- B(x) 72.4(11)
B(5)	- B(4)	- B(9)	57.7(6)	B(10)- B(9)	- B(x) 55.4(10)
B(8)	- B(4)	- B(9)	61.4(7)	B(9) -B(10)	- B(x) 61.4(11)
B(1)	- B(5)	- B(4)	61.0(6)	B(11)-B(10)	- B(x) 67.2(12)
B(1)	- B(5)	- B(6)	61.2(6)	Au(7)-B(11)	- B(x) 63.8(10)
B(4)	- B(5)	- B(9)	62.8(6)	B(10)-B(11)	- B(x) 54.7(10)
B(6)	- B(5)	-B(10)	61.5(6)	Au(7)- B(x)	-B(11) 65.6(10)
B(9)	- B(5)	-B(10)	64.8(6)	B(8) - B(x)	- B(9) 54.1(9)
B(1)	- B(6)	- B(2)	60.7(6)	B(9) - B(x)	-B(10) 63.2(11)
B(1)	- B(6)	- B(5)	59.4(6)	B(10)- B(x)	-B(11) 58.1(11)

Table 4.4. Bond Lengths(pm) and Angles(°) for Cage 1 in $[(Cy_3P)_2Au]^+$ $[(B_{10}H_{12})_2Au]^-$.

Au(7) -B(12)	225(3)	B(13) -B(18)	181(4)
Au(7) -B(13)	229.0(24)	B(14) -B(15)	172(4)
Au(7) -B(18)	238(3)	B(14) -B(18)	179(4)
Au(7) -B(111)	237(3)	B(14) -B(19)	178(4)
B(11) -B(12)	179(4)	B(15) -B(16)	179(4)
B(11) -B(13)	172(4)	B(15) -B(19)	179(4)
B(11) -B(14)	173(4)	B(15) -B(110)	175(4)
B(11) -B(15)	180(5)	B(16) -B(110)	177(4)
B(11) -B(16)	182(5)	B(16) -B(111)	174(4)
B(12) -B(13)	190(4)	B(18) -B(19)	175(4)
B(12) -B(16)	177(4)	B(19) -B(110)	200(4)
B(12) -B(111)	177(4)	B(110)-B(111)	180(4)
B(13) -B(14)	171(4)		

B(12) -Au(7)	-B(13)	49.4(9)	B(11) -B(15)	-B(14)	58.9(17)
B(12) -Au(7)	-B(111)	45.0(10)	B(11) -B(15)	-B(16)	60.8(18)
B(13) -Au(7)	-B(18)	45.6(9)	B(14) -B(15)	-B(19)	60.7(16)
B(12) -B(11)	-B(13)	65.6(17)	B(16) -B(15)	-B(110)	59.8(17)
B(12) -B(11)	-B(16)	58.8(17)	B(19) -B(15)	-B(110)	68.8(17)
B(13) -B(11)	-B(14)	59.7(17)	B(11) -B(16)	-B(12)	59.9(17)
B(14) -B(11)	-B(15)	58.4(17)	B(11) -B(16)	-B(15)	59.6(18)
B(15) -B(11)	-B(16)	59.6(18)	B(12) -B(16)	-B(111)	60.7(16)
Au(7) -B(12)	-B(13)	66.3(11)	B(15) -B(16)	-B(110)	58.9(17)
Au(7) -B(12)	-B(111)	71.0(13)	B(110)-B(16)	-B(111)	61.8(17)
B(11) -B(12)	-B(13)	55.3(15)	Au(7) -B(18)	-B(13)	64.7(11)
B(11) -B(12)	-B(16)	61.3(17)	B(13) -B(18)	-B(14)	56.9(14)
B(16) -B(12)	-B(111)	58.7(16)	B(14) -B(18)	-B(19)	60.2(15)
Au(7) -B(13)	-B(12)	64.3(10)	B(14) -B(19)	-B(15)	57.6(15)
Au(7) -B(13)	-B(18)	69.7(12)	B(14) -B(19)	-B(18)	61.0(15)
B(11) -B(13)	-B(12)	59.2(16)	B(15) -B(19)	-B(110)	54.6(15)
B(11) -B(13)	-B(14)	60.5(17)	B(15) -B(110)	-B(16)	61.2(17)
B(14) -B(13)	-B(18)	60.9(15)	B(15) -B(110)	-B(19)	56.5(15)
B(11) -B(14)	-B(13)	59.8(17)	B(16) -B(110)	-B(111)	58.3(16)
B(11) -B(14)	-B(15)	62.8(18)	Au(7) -B(111)	-B(12)	64.0(12)
B(13) -B(14)	-B(18)	62.2(15)	B(12) -B(111)	-B(16)	60.6(16)
B(15) -B(14)	-B(19)	61.7(16)	B(16) -B(111)	-B(110)	59.9(17)
B(18) -B(14)	-B(19)	58.8(15)			

Table 4.5. Bond Lengths(pm) and Angles(°) in Cage 2 of $[(Cy_3P)_2Au]^+$ $[(B_{10}H_{12})_2Au]^-$.

Au(7) -B(22)	226(3)	B(23) -B(28)	183(4)
Au(7) -B(23)	226(3)	B(24) -B(25)	177(4)
Au(7) -B(28)	236(3)	B(24) -B(28)	177(4)
Au(7) -B(211)	237(3)	B(24) -B(29)	179(4)
B(21) -B(22)	177(4)	B(25) -B(26)	182(4)
B(21) -B(23)	174(4)	B(25) -B(29)	177(4)
B(21) -B(24)	174(4)	B(25) -B(210)	168(4)
B(21) -B(25)	179(4)	B(26) -B(210)	176(4)
B(21) -B(26)	184(4)	B(26) -B(211)	171(4)
B(22) -B(23)	184(4)	B(28) -B(29)	174(4)
B(22) -B(26)	180(4)	B(29) -B(210)	200(4)
B(22) -B(211)	184(4)	B(210)-B(211)	185(4)
B(23) -B(24)	176(4)		

B(22) -Au(7)	-B(23)	47.8(9)	B(21) -B(25)	-B(24)	58.6(16)
B(22) -Au(7)	-B(211)	46.6(9)	B(21) -B(25)	-B(26)	61.2(16)
B(23) -Au(7)	-B(28)	46.5(10)	B(24) -B(25)	-B(29)	60.7(17)
B(22) -B(21)	-B(23)	63.0(16)	B(26) -B(25)	-B(210)	60.3(16)
B(22) -B(21)	-B(26)	59.9(16)	B(29) -B(25)	-B(210)	70.8(18)
B(23) -B(21)	-B(24)	60.6(16)	B(21) -B(26)	-B(22)	58.1(15)
B(24) -B(21)	-B(25)	60.1(16)	B(21) -B(26)	-B(25)	58.5(16)
B(25) -B(21)	-B(26)	60.3(16)	B(22) -B(26)	-B(211)	62.9(16)
Au(7) -B(22)	-B(23)	66.1(11)	B(25) -B(26)	-B(210)	55.7(16)
Au(7) -B(22)	-B(211)	69.7(12)	B(210)-B(26)	-B(211)	64.5(16)
B(21) -B(22)	-B(23)	57.8(15)	Au(7) -B(28)	-B(23)	64.1(12)
B(21) -B(22)	-B(26)	62.0(16)	B(23) -B(28)	-B(24)	58.5(15)
B(26) -B(22)	-B(211)	56.1(15)	B(24) -B(28)	-B(29)	61.2(17)
Au(7) -B(23)	-B(22)	66.1(11)	B(24) -B(29)	-B(25)	59.7(16)
Au(7) -B(23)	-B(28)	69.4(12)	B(24) -B(29)	-B(28)	60.4(17)
B(21) -B(23)	-B(22)	59.2(15)	B(25) -B(29)	-B(210)	52.5(15)
B(21) -B(23)	-B(24)	59.7(16)	B(25) -B(210)	-B(26)	64.0(17)
B(24) -B(23)	-B(28)	59.2(15)	B(25) -B(210)	-B(29)	56.7(16)
B(21) -B(24)	-B(23)	59.7(16)	B(26) -B(210)	-B(211)	56.4(15)
B(21) -B(24)	-B(25)	61.3(17)	Au(7) -B(211)	-B(22)	63.7(11)
B(23) -B(24)	-B(28)	62.3(16)	B(22) -B(211)	-B(26)	61.0(15)
B(25) -B(24)	-B(29)	59.6(16)	B(26) -B(211)	-B(210)	59.1(15)
B(28) -B(24)	-B(29)	58.4(16)			

Chapter 5:

Multiple Clustering in Auraboranes -

The Double and Triple Clusters.

5.1 Introduction.

This Chapter describes work carried out on complexes where at least one auraborane cage is linked by a common vertex to a homonuclear gold cluster. The first half of the Chapter is concerned with the first species of this type : the *triple clusters.* First there are Sections on the synthesis and characterisation of these species, and then the next Section (5.4) examines the structure of the original triple cluster : $(B_{10}H_{12}Au)_2(AuPEt_3)_4$. The structure was not well determined, but detailed analysis showed that it was more complex than originally thought.

Section 5.5 details work carried out on $(B_{10}H_{12}Au)_2(AuPPh_3)_4$. The structural analysis examines the auraborane fragment geometry and then compares the central Au_6 core with that of $(B_{10}H_{12}Au)_2(AuPEt_3)_4$. The third species, $(B_{10}H_{12}Au)_2(AuPCy_3)_4$, was not as well characterised, but what work there is, is reviewed. Finally there is a Section on the reactivity of these complexes.

The second half of the Chapter examines the *double cluster* synthesised as a byproduct of base attack on 5,6-μ-(Cy_3PAu)-*nido*-$B_{10}H_{13}$. Its structure was determined crystallographically and this is examined in the next Section. Comparison with the other structurally characterised Au_4 tetrahedra follows, and the unusual features of $(B_{10}H_{12}Au)(AuPCy_3)_3$ are examined. Next the

spectroscopic details are discussed, and finally conclusions about this work are drawn.

5.2 Synthesis of the Triple Clusters.

These are synthesised in one of two ways. These are:

$2B_{10}H_{14} + 6AuMe(PR_3) \longrightarrow (B_{10}H_{12}Au)_2(AuPR_3)_4 + 4MeH + C_2H_6 + 2PR_3$

$2Cy_3PAuB_{10}H_{13} + 4AuMe(PR_3) \longrightarrow (B_{10}H_{12}Au)_2(AuPR_3)_4 + 2PCy_3 + 2MeH + C_2H_6$

can be used. The reason why 5,6-μ-(Cy_3PAu)-*nido*-$B_{10}H_{13}$ can be isolated is probably a combination of its insolubility coupled with the slow reaction of **(8a)** with $AuMe(PCy_3)$, taking hours to show a distinct red colour if the reagents are left stirring at room temperature.

5.3 Characterisation of the Nuclearity of the Triple Clusters.

One feature of interest in these systems is the influence that the steric bulk of the phosphine has on the structure of the central gold cluster. It is conceivable that if the phosphine is made sufficiently sterically-demanding then fewer than four $\{AuPR_3\}$ moieties could form the centre of the triple cluster.

In order to determine the nuclearity of the three triple clusters that were successfully isolated, their UV/visible spectra were recorded. The positions of the peak maxima are shown below, together with data from the literature[86] on $[Au_6(PPh_3)_6]^{2+}$.

Compound	UV/vis. peak centres/nm			
$[Au_6(PPh_3)_6]^{2+}$	319	331	453	476
$(B_{10}H_{12}Au)_2(AuPEt_3)_4$	315	340(sh)	425	500
$(B_{10}H_{12}Au)_2(AuPPh_3)_4$	310	345(sh)	445	520
$(B_{10}H_{12}Au)_2(AuPCy_3)_4$	320(sh)	385(sh)	450	525

A general pattern of four peaks in similar positions can be observed for all of the

Au_6 clusters. Any difference in the positions of the bands is probably due to either variations caused by the different ligands on the gold atoms or to different cluster geometries between the literature gold cluster and the triple clusters (see page 21 for details). The structure of $(B_{10}H_{12}Au)_2(AuPEt_3)_4$ was discussed in Chapter 1, but more details are in the next Section. The structures of $(B_{10}H_{12}Au)_2(AuPPh_3)_4$ and $(B_{10}H_{12}Au)_2(AuPCy_3)_4$ are discussed in Sections 5.5 and 5.6 respectively.

5.4 The Structure of $(B_{10}H_{12}Au)_2(AuPEt_3)_4$, (21).

This was briefly described in Chapter 1, starting on page 20, and one view of its molecular structure is shown in Figure 5.1, overleaf. The single crystal X-ray diffraction study was undertaken by Welch and Robins[83], but the structure was not fully examined.

5.4.1 The Structure of the Auraborane Clusters.

The structures of the two $\{AuB_{10}H_{12}\}$ fragments was analysed by r.m.s. misfit comparisons with the following structures:

Comparison with	Cage 1.	Cage 2.
$B_{10}H_{14}$	10.0	20.4
$[B_{10}H_{13}]^-$	10.5	22.5
$[B_{10}H_{14}]^{2-}$	7.4	20.6
$[B_{11}H_{13}]^{2-}$	12.5	21.7
$Cy_3PAuB_{10}H_{13}$	11.5	18.5
$[Cy_3PAuB_{10}H_{12}]^-$	10.8(10.7)†	20.6(20.3)
$[(B_{10}H_{12})_2Au]^-$	7.4(7.3)	18.1(18.0)

Notes

† Including the gold atom position in the misfit calculation.

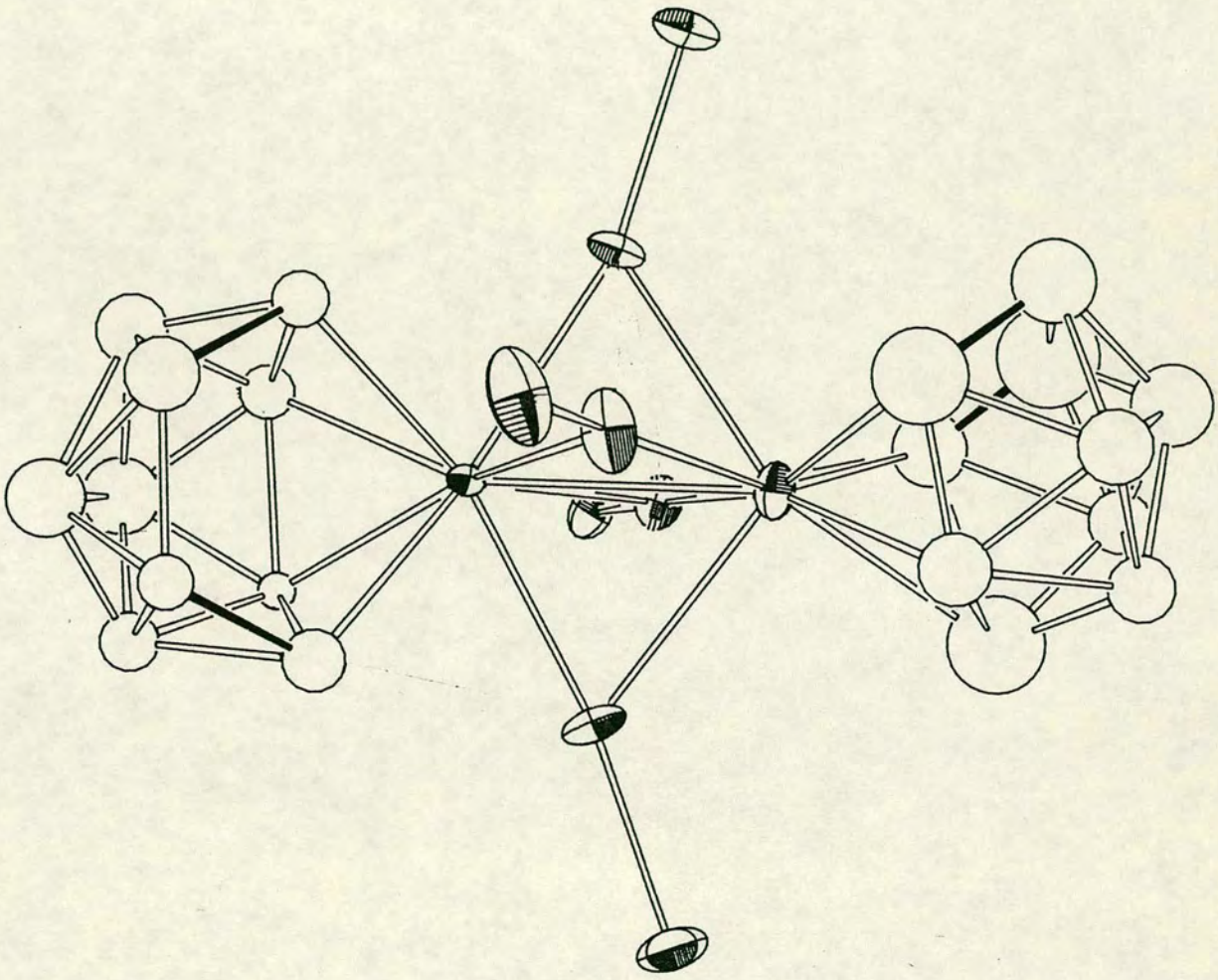

Figure 5.1. (a) the molecular structure of $(B_{10}H_{12}Au)_2(AuPEt_3)_4$.

As can be seen from these results, the structure of cage 2 does not fit well with either set of models, and this is reflected in the bond lengths which in some cases are unusual. For example, B(5)-B(10) (in Cage 2) is 209(9) pm, and B(9)-B(10) is 223(8). If it is assumed that the two cages are isostructural (since, for example, the ^{11}B-$\{^{1}H\}$ n.m.r. spectrum shows only one set of resonances) and that the structure of cage 1 is more accurately determined, then its best description is that of a $[B_{10}H_{12}]^{4-}$ ligand. As discussed in Chapter 3 (page 75) this suggests that the ligated gold atom is in its +III oxidation state.

5.4.2 The Structure of the Central Au_6 Core.

Figure 5.2, overleaf, shows different views of the Au_6 core along with the chosen numbering scheme. Table 5.1 on page 168 gives some relevant bond lengths and angles.

The two gold atoms, Au(1), and Au(6), which are bonded to boron cage 1, and boron cage 2, respectively, will be considered first. They both have approximately square-planar geometries because each gold atom has significantly shorter bond lengths to the two gold atoms which are in the same plane as the midpoints of the ligated B-B connectivities (i.e. Au(1) is closer to Au(2) and Au(4); Au(6) to Au(3) and Au(5)). However there is a significant deviation from planarity, Au(1) being 102pm out of the plane defined by Au(2), Au(4), and the midpoints of the B(2)-B(11) and B(3)-B(8) connectivities, and Au(6) is 36.6pm out of the equivalent plane. Whilst this approach is simplistic, it does provide an explanation as to why the two boron cages are rotated by *ca.* 90° with respect to one another whereas in the $[(B_{10}H_{12})_2Au]^-$ anion, for example, the rotation is 180°.

The gross structure of the Au_6 cluster is quite unusual. Since Au(1)-Au(6) is

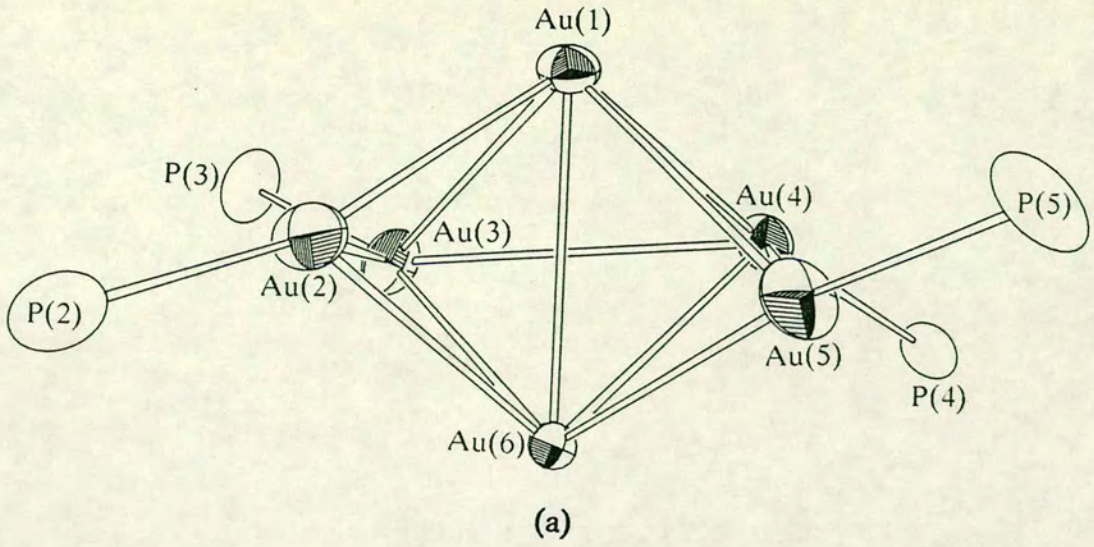

(a)

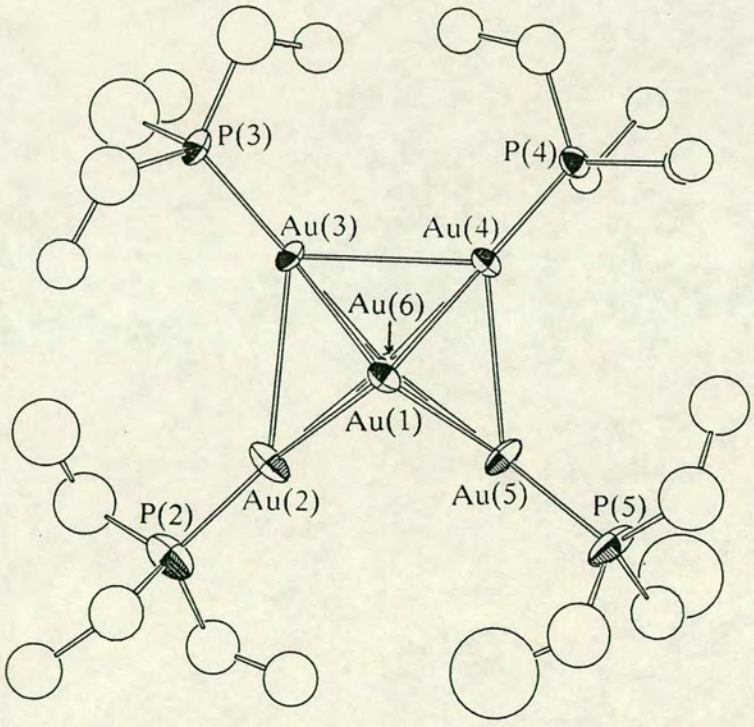

(b)

Figure 5.2. Two views of the $\{Au_6\}$ core. (a) shows the chosen numbering scheme, and the 'absent' Au(2)-Au(5) bond. The boron cages are bonded to Au(1) and Au(6). (b) is a second view including the $\{PEt_3\}$ ligands.

significantly shorter than the other two 'diagonals', this implies that the structure is distorted from octahedral. In addition, the Au_4 'belt' is also modulated, with Au(1)-Au(2), Au(1)-Au(4), Au(6)-Au(3), and Au(6)-Au(5) all being significantly shorter than Au(1)-Au(3), Au(1)-Au(5), Au(6)-Au(2), and Au(6)-Au(4). This modulation is extended by the phosphorus atoms - when the best-fit plane for Au(2), Au(3), Au(4), and Au(5) is calculated, the gold atoms are, on average, 14.9pm from this plane, whereas the P atoms are 55.1 pm (average) away. The tilting is such that, for both $\{AuB_{10}H_{12}\}$ cages, one P atom 'leans' over the open face, thus providing a degree of steric protection.

Furthermore, if the 'belt' bond lengths are considered, whilst Au(2)-Au(3) is insignificantly different from Au(3)-Au(4), Au(4)-Au(5) is longer, and Au(2)-Au(5) is so long it is probably non-bonding!

In view of these distortions, the structure of the central Au_6 core has been reinterpreted as being composed of *three face-fused tetrahedra.* The individual bond lengths and angles for these three sub-clusters are in Table 5.1, along with the equivalent distances for the "fourth" tetrahedron, for comparison. As can be seen, whilst the angles for the first three tetrahedra are all within 13^o of the tetrahedral angle, 60^o, those for "tetrahedron 4" are up to 26^o out. The variation in the bond lengths in this "tetrahedron" is also more marked. greater

Hence it is probably more accurate to describe this system as a *quintuple* rather than triple cluster, since there are (in order) a $\{B_{10}H_{12}Au\}$ cluster fused about a common vertex (Au(1)) with a gold tetrahedron (Au(1)-Au(2)-Au(3)-Au(6)) which is face-fused with a second Au_4 tetrahedron (Au(1)-Au(3)-Au(4)-Au(6)), joined to the third Au_4 tetrahedron (Au(1)-Au(4)-Au(5)-Au(6)) which bonds to the final $\{AuB_{10}H_{12}\}$ cluster by the common vertex, Au(6).

As well as the single crystal X-ray diffraction study, the multinuclear n.m.r. spectra of **(21)** were also obtained. The $^{1}H-\{^{11}B\}$ n.m.r. spectrum confirmed that there were twelve hydrogen atoms associated with each $\{B_{10}\}$ cage : ten terminal B-H units, and two bridges. The $^{11}B-\{^{1}H\}$ n.m.r. spectrum consists of four peaks at $\delta^{11}B$ = 11.93(4B), 0.70(2B), -4.93(2B), and -24.48(2B). This distribution of peaks is reminiscent of $B_{10}H_{14}$, although the chemical shifts, as well as the integrals, differ (for $B_{10}H_{14}$, $\delta^{11}B$ = 11.3(2B), 9.7(2B), 0.7(4B), and -35.5(2B) ppm). The spectrum of **(21)** does suggest that there is a degree of fluxionality in this system.

Unfortunately, the program ICON which performs the EHMO calculations, can only do so for a maximum of 50 atoms. Since the theoretical model $(B_{10}H_{12}Au)_2(AuPH_3)_4$ contains 70 atoms, it is not possible to perform EHMO calculations to probe the electronic structures of these complexes at the moment.

5.5 The Structure of $(B_{10}H_{12}Au)_2(AuPPh_3)_4$.

Whilst I have successfully isolated and spectroscopically characterised this species, it was a coworker, Dr. A.J.McLennan[149] who successfully grew crystals for the structural determination. The crystal of $(B_{10}H_{12}Au)_2(AuPPh_3)_4$, **(22)**, probably contained solvent (although none was found) as it decayed in the *X*-ray beam, and so this structural determination was carried out at 185K.

The determination is not as accurate as was hoped, presumably owing to the twin problems of crystal decay and absorption effects which are a feature of these systems. However the gold atom positions are located with a great deal of precision, so the central cluster geometry will be considered first, followed by an analysis of the geometry of the two $\{AuB_{10}H_{12}\}$ fragments. The molecular structure of **(22)** is shown in Figure 5.3, overleaf. Its structure is broadly similar

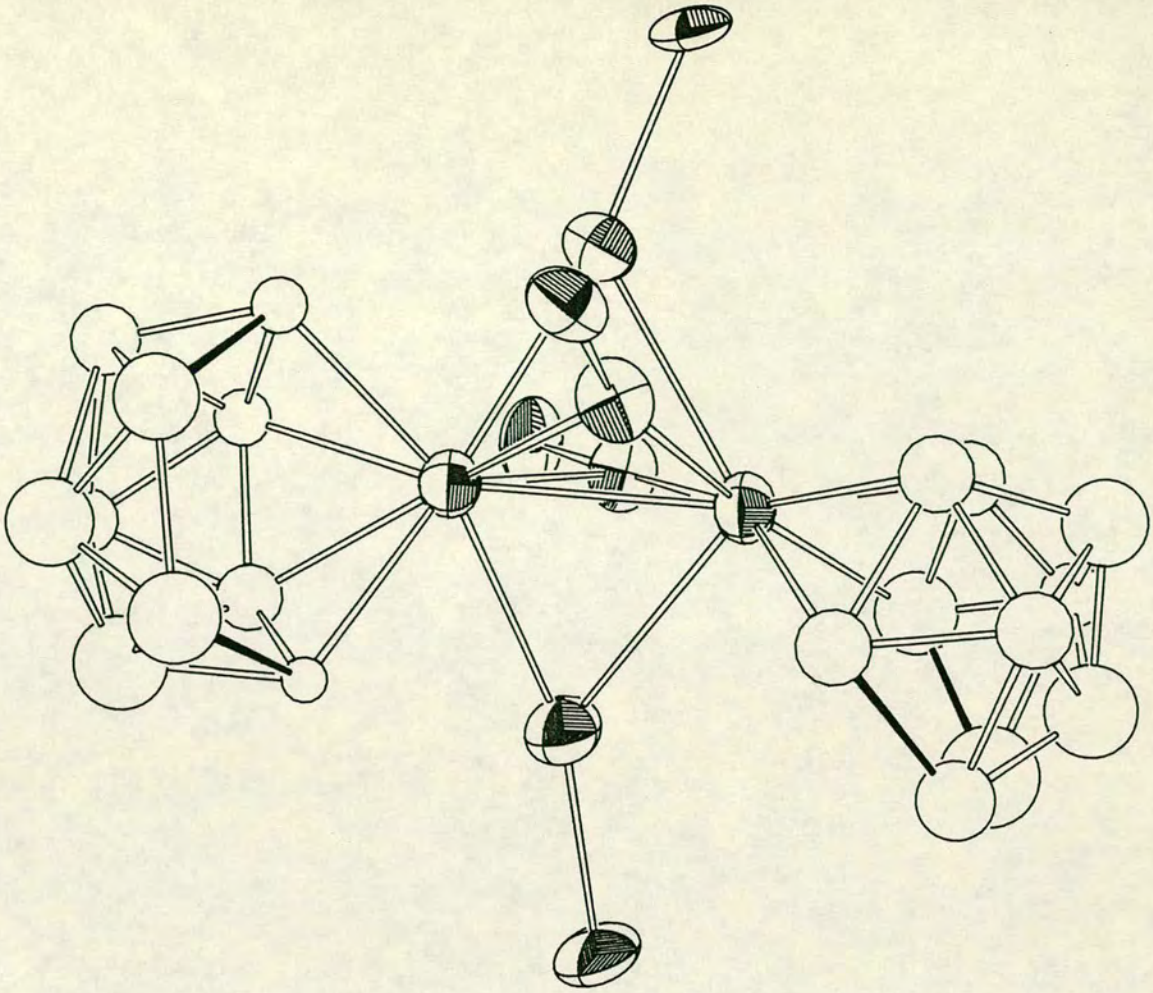

(a)

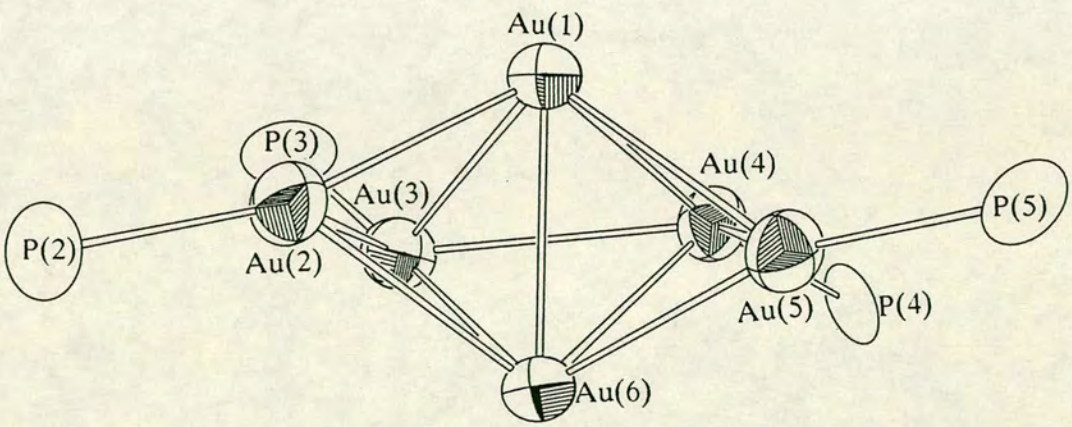

(b)

Figure 5.3. (a) the molecular structure of $(B_{10}H_{12}Au)_2(AuPPh_3)_4$ with the phenyl groups omitted for clarity. (b) the central Au_6 core showing the gold atom numbering scheme.

to that of **(21)**, but it is interesting to note that the molecule chosen for the plot is of the other enantiomer (the right-hand cage is up or down). Since the space groups for both determinations are centrosymmetric, the crystals must be composed of a racemic mixture. Relevant bond lengths and angles are in Table 5.2 on page 169, and the crystallographic details start on page 261.

5.5.1 The Structure of the Two $\{AuB_{10}H_{12}\}$ Fragments.

The structures of the $\{B_{10}\}$ cages were compared against others to try and determine the precise cage architecture. The results are:

Comparison	Cage 1.	Cage 2.
$[B_{10}H_{14}]$	13.1	14.1
$[B_{10}H_{13}]^-$	14.5	13.6
$[B_{10}H_{14}]^{2-}$	14.7	15.6
$[B_{11}H_{13}]^{2-}$	19.2	18.3
$Cy_3PAuB_{10}H_{13}$	14.1	14.6
$[Cy_3PAuB_{10}H_{12}]^-$	13.4 (13.6)†	12.5 (12.2)
$[(B_{10}H_{12})_2Au]^-$	12.2 (12.2)	16.0 (15.4)

† the figure in parentheses includes the gold atom position in the comparison.

These results suggest that the cage geometry is different. There are also anomalously long connectivities such as the B(56)-B(510) 196(11), B(58)-B(59) 202(10), and B(53)-B(58) 196(9)pm which reinforce this view.

Presumably the gold-borane interaction is similar to that in **(21)**, above, but there is no evidence for this.

The ^{11}B-$\{^1H\}$ n.m.r. spectrum, Figure 5.4, page 157, is different from that of **(21)**, both in the chemical shifts of the resonances, and their relative integrals.

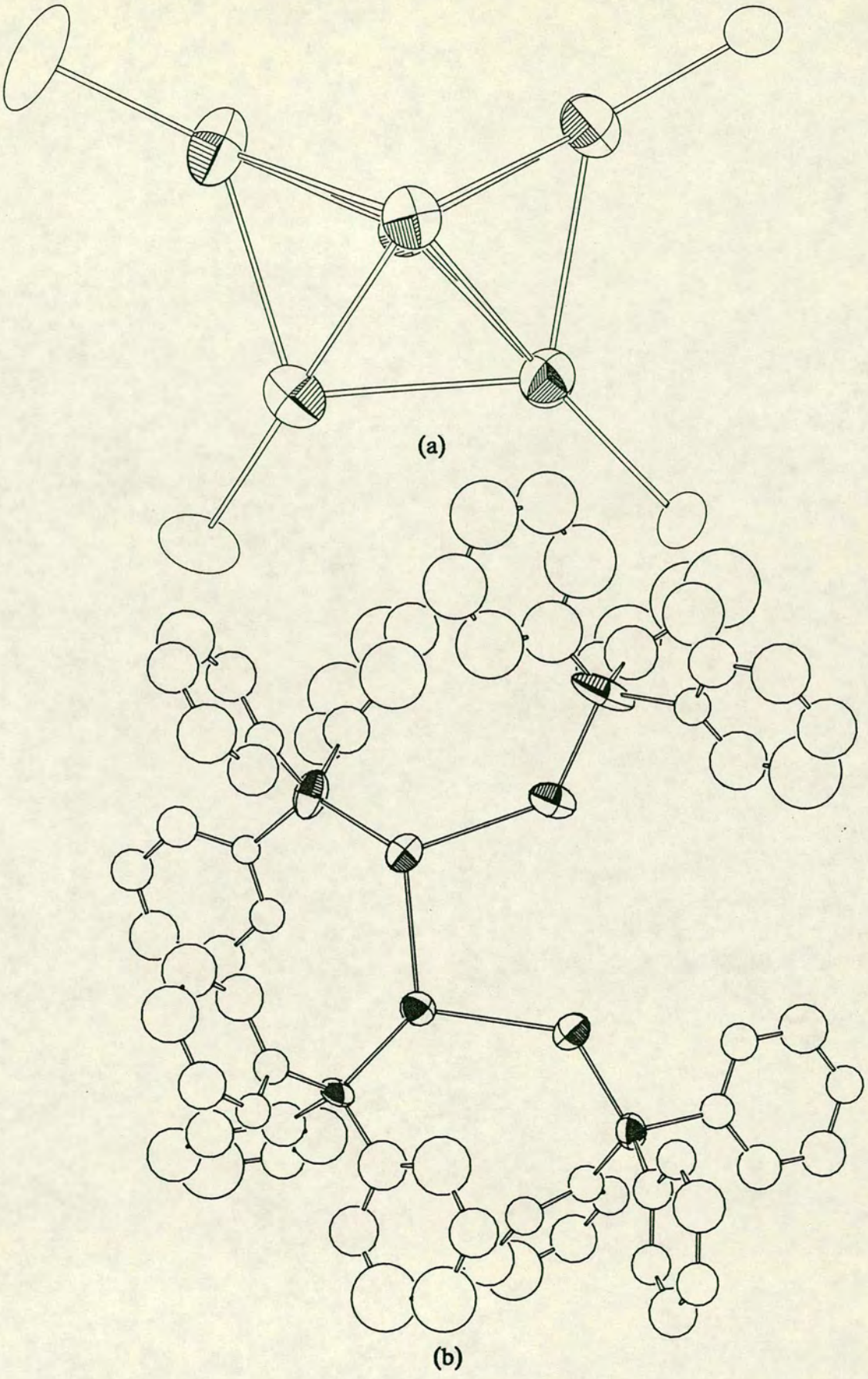

Figure 5.4. Two more views of the Au_6 core of $(B_{10}H_{12}Au)_2(AuPPh_3)_4$. (a) shows the open side of the cluster. (b) shows the Au_4 'belt' with the carbon atoms included.

This contrasts with the two complexes 5,6-μ-(Cy_3PAu)-*nido*-$B_{10}H_{13}$ and 5,6-μ-(*o*-$tolyl_3PAu$)-*nido*-$B_{10}H_{13}$ whose n.m.r. spectra are virtually identical. This difference probably arises from the geometrical effects of the phosphine ligands which have significantly affected the cluster stereochemistry. The ^{1}H-$\{^{11}B\}$ n.m.r. spectrum reveals the presence of ten terminal H atoms and two bridging ones.

5.5.2 The Structure of the Au_6 Core of $(B_{10}H_{12}Au)_2(AuPPh_3)_4$.

Figure 5.3, overleaf, shows several views of the central gold core, and Table 5.3 on page 172 gives some important bond lengths and angles in this part of the molecule. Once again, the bonding at the two gold atoms ligated to the boron cage approximates to square-planar. Au(1) is out of the mid(2,11)-mid(3,8)-Au(2)-Au(4)[‡] plane by 173.2 pm, and Au(6) is out of its plane by 223.9pm, showing that there is greater distortion in **(22)** than **(21)**.

The departure from octahedral geometry is more striking, the Au(2)-Au(5) distance being 433.5(3)pm. However, the other three distances in the 'belt' are actually shorter. Since $\{PPh_3\}$ is a more sterically-demanding ligand than $\{PEt_3\}$, this bond shortening is unexpected. Although this phenomenon has not been fully investigated, one reasonable explanation is that the phenyl rings on adjacent ligands are hydrogen-bonded, and this pulls the $\{PPh_3\}$ groups together, causing the Au-Au bonds to shorten. The distortion from octahedral to three face-fused tetrahedra is more pronounced than in **(21)**,the three tetrahedra having angles which are within 6^{o} of 60^{o} whereas in the fourth 'absent' tetrahedron, they vary from 39.59(6) to 103.23(10)^{o}!

---

‡ where mid(X,Y) is the midpoint of the X-Y connectivity. The boron atoms are those in the cage bonded to the gold atom in question.

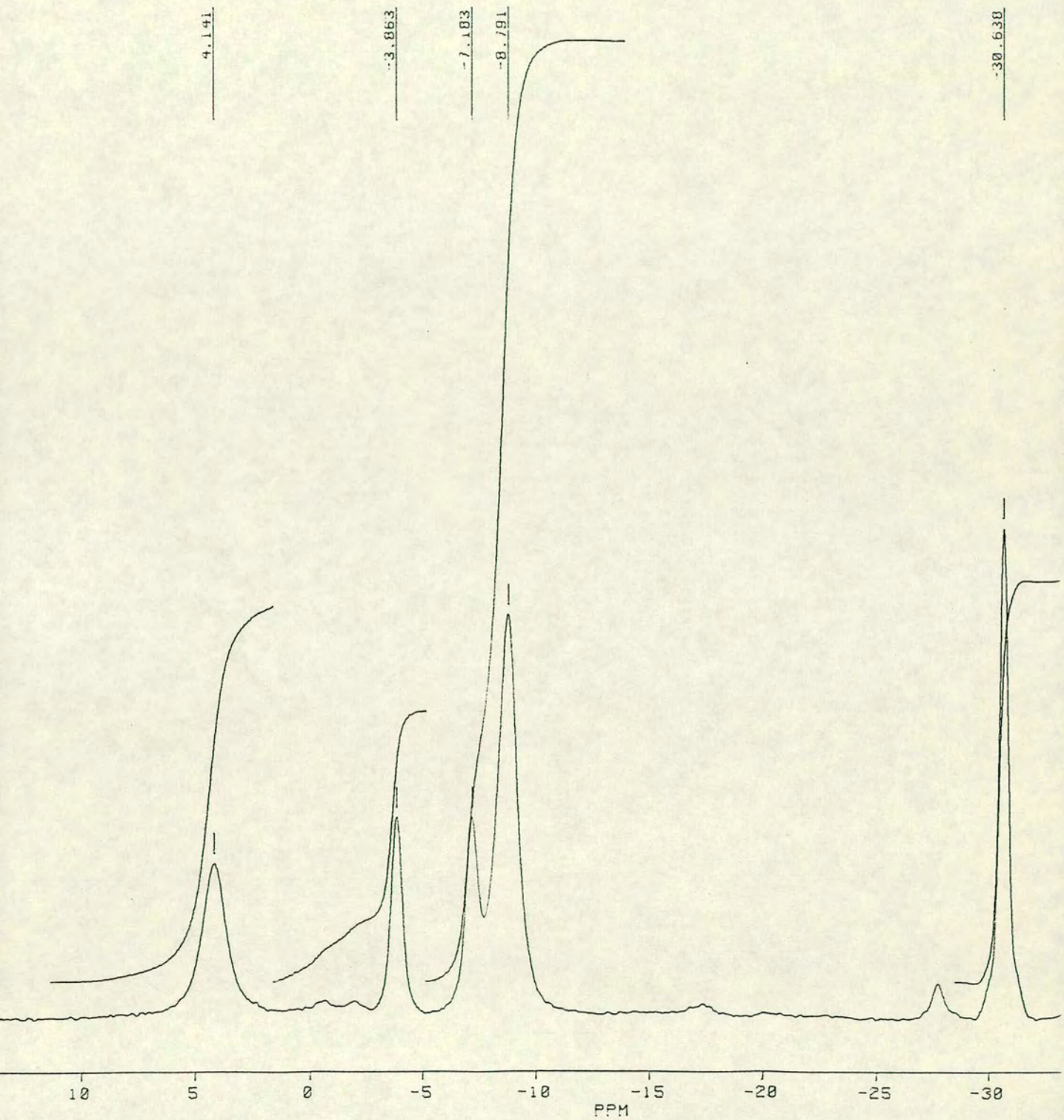

Figure 5.5. The ^{11}B-{^{1}H} n.m.r. spectrum of $(B_{10}H_{12}Au)_2(AuPPh_3)_4$.

5.6 The Structure of $(B_{10}H_{12}Au)_2(AuPCy_3)_4$.

Whilst a data set was collected for $(B_{10}H_{12}Au)_2(AuPCy_3)_4$, **(23)**, it could not be completely solved. This was mostly because the space group could not be unambiguously determined. A further problem was that the volume of the unit cell was consistent with it containing only two molecules, and for tetragonal space groups, a minimum of four molecules per unit cell is required for there to be no crystallographically imposed symmetry. Since **(21)** and **(22)** both have no potential symmetry, this indicated that there was a high probability that the crystal was disordered.

However, it was possible to locate the positions of the six central gold atoms, and their positions and the associated bond lengths are in Table 5.4 on page 173. The rest of the atoms could not be located, and there are no errors on the bonds because the structure was not refined.

The structure is not the same as the previous two, but whether this is because of the symmetry constraints of the space group is not evident. In the central core of **(23)**, the 'belt' is planar and rectangular, with all angles 90^0, and opposite sides of equal lengths (Au(2,a)-Au(2,b) = 389.0, Au(2,a)-Au(2,d) = 327.0pm). The two gold atoms, Au(1,a) and Au(1,b), which are presumably bonded to the boron cages, now bond to the other four equally (Au(1)-Au(2) 283.7pm). This is in marked contrast to the situation in **(21)** and **(22)**. This does suggest that further work is needed on the triple clusters with bulky phosphine ligands.

5.6.1 Spectroscopic Details

The ^{11}B-$\{^1H\}$ n.m.r. spectrum of **(23)** was acquired, and this is shown in Figure 5.6, overleaf. As can be seen, this is not very useful, presumably due to *chemical shift anisotropy.*

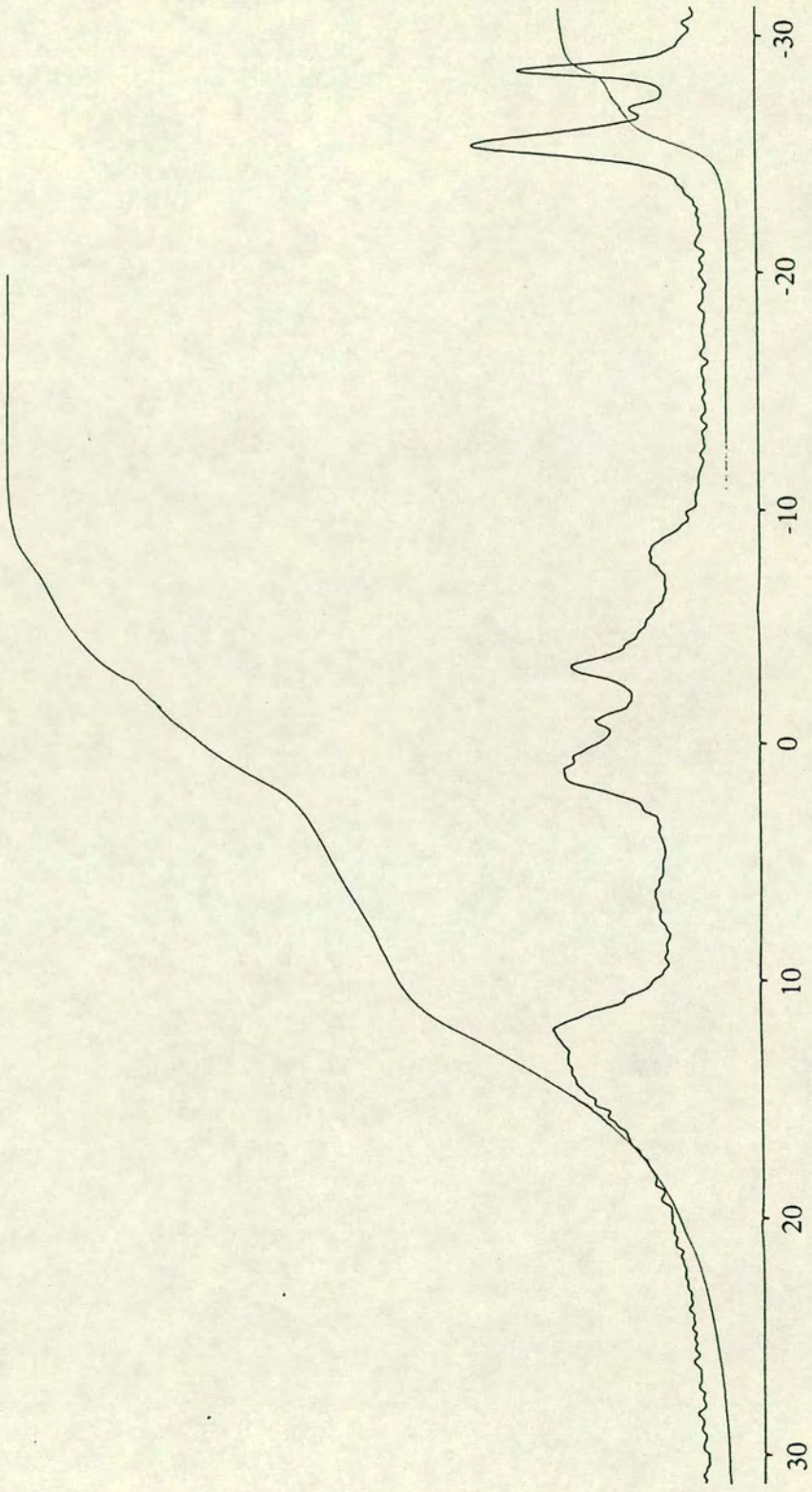

Figure 5.6. The ^{11}B-{^{1}H} n.m.r. spectrum of $(B_{10}H_{12}Au)_2(AuPCy_3)_4$.

Selective ^{11}B decoupling of the ^{1}H n.m.r. spectrum is of course pointless, and so the only evidence for the presence of $\{B_{10}H_{12}\}$ fragments is based on its analogy with the other two compounds above.

5.7 Reactions of the Triple Clusters.

These species proved very difficult to work with, owing to a tendency to decompose to metallic gold. In fact this is suggested as the main chemical interest in these species : as a mild source of $\{AuPR_3\}$.

Conclusive evidence for these species being readily decomposed is the reaction with hydrogen chloride. It was found in Chapter 2 that reacting 5,6-μ-(Cy_3PAu)-*nido*-$B_{10}H_{13}$ with H-Cl cleaved the gold-boron bond to afford $AuCl(PCy_3)$ and $B_{10}H_{14}$. Accordingly this reaction was tried with $(B_{10}H_{12}Au)_2(AuPPh_3)_4$, **(22)** to see if it was possible to synthesise Au_6 clusters by cleavage of the gold-boron bonds in **(22)**. However the only product present in the $^{31}P\text{-}\{^{1}H\}$ n.m.r. spectrum was $AuCl(PPh_3)$ indicating that the Au-Au bonds were prone to cleavage by this reagent.

When the acid was changed to HBF_4 in order to reduce the possibility that the gold would coordinate to the proton's counterion, the reaction produced a black solid which readily decomposed to elemental gold, and which did not absorb in the UV/visible region expected for gold clusters, indicating that degradation of the cluster had happened again.

Refluxing **(22)** in acetonitrile or toluene led to deposition of a gold mirror on the glass, indicating that these species are thermally unstable.

5.8 Synthesis of the Double Cluster.

This was synthesised from $[NHEt_3]^+$ $[Cy_3PAuB_{10}H_{12}]^-$, **(15)**, as a result of the observation that this slowly goes brown if left in air for several weeks. In an attempt to find out why this complex is unstable, $[NHEt_3]^+$ **(15)** was left stirring in dichloromethane solution under a nitrogen atmosphere for five days, and then the reaction products were worked up. Only one species was subsequently identified. This was the gold-boron *double cluster*, $(B_{10}H_{12}Au)(AuPCy_3)_3$, **(24)**, which is illustrated in Figure 5.7, overleaf. Relevant bond lengths and angles are given in Table 5.5, on page 175, and the crystallographic details start on page 270. The structure is analysed in the next Section.

5.9 The Structure of (24).

The overall formula of these crystals is $(B_{10}H_{12}Au)(AuPCy_3)_3.2.5CH_2Cl_2$, and experimental difficulties resulted from solvent loss which meant that, at room temperature, the crystal was no longer diffracting after *ca.* 12 hours. Accordingly, this structural determination was carried out at 185K, which slowed down the rate of solvent loss sufficiently so that a reasonable data set could be collected. However, the intensity control reflections deteriorated by about 13.6% during this collection. Whilst the data were corrected[150] for this, it does introduce a source of error. Moreover, the central Au_4 cluster meant that absorption effects were a serious problem. Despite empirical correction[151] for this, and refining the gold atoms with anisotropic thermal parameters, there are still spurious peaks of 1600 enm^{-3} around the gold atoms in the final ΔF map.

These two factors mean that this determination is not as accurate as was hoped. This is shown in the C-C bond lengths (page 276) which vary from 109(11) to 200(9) pm. However, since the boron atoms are located on a spherical

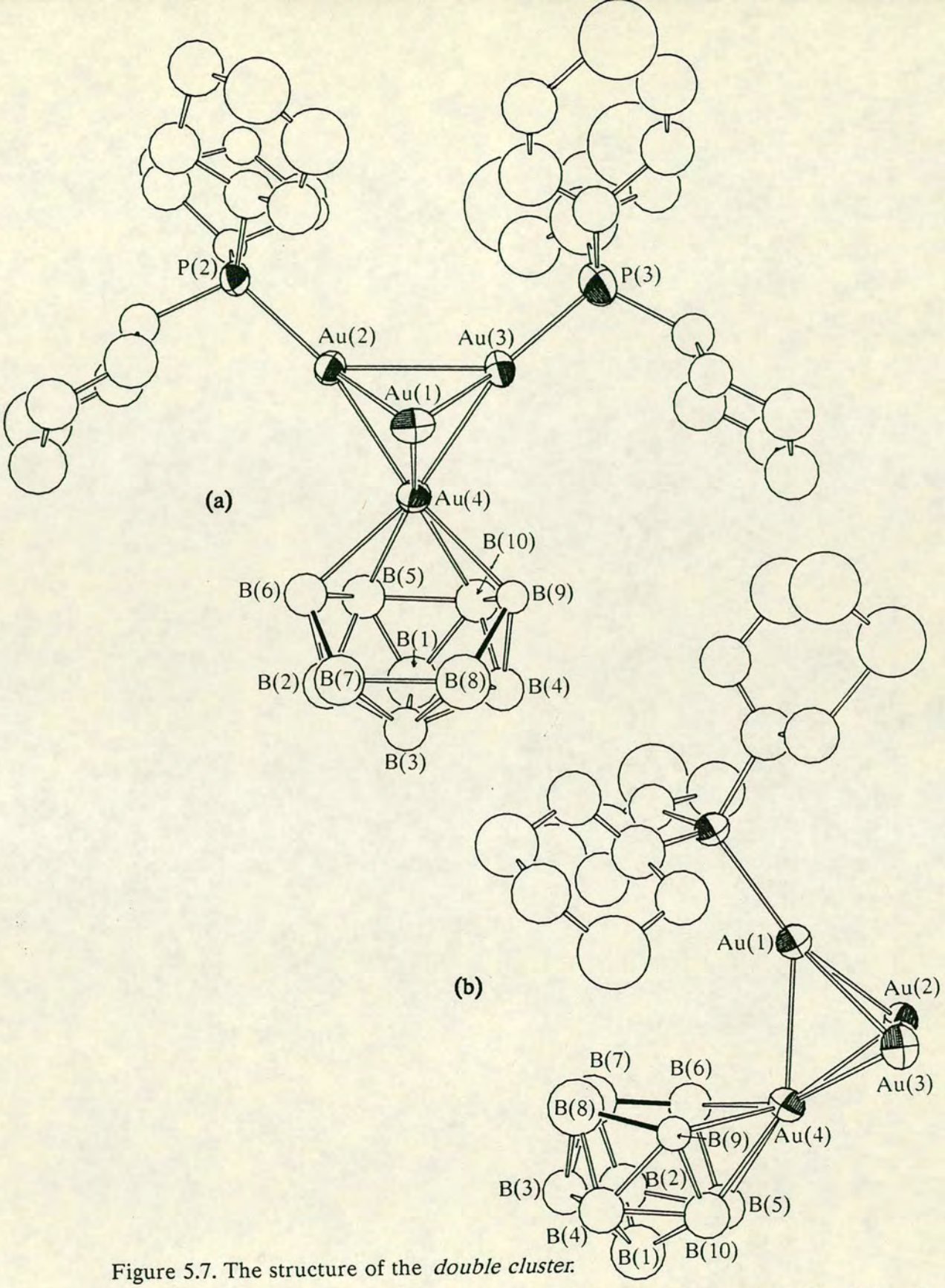

Figure 5.7. The structure of the *double cluster.*

(a) shows the relationship of the B_{10} cage to that of decaborane and has P(1) and the C(1*xx*) (*xx* = 11-36) atoms omitted for clarity.

(b) shows the open face of the $\{AuB_{10}H_{12}\}$ fragment, and also P(1) and its carbon atoms which were omitted in (a). P(2), P(3), and their cyclohexyl rings have been omitted for clarity.

surface, they are more rigidly held than the carbon atoms in a ring, and so their positions are more accurately defined.

In **(24)**, a Au_4 tetrahedron is fused about a common Au vertex (numbered Au(4)) with a $\{AuB_{10}H_{12}\}$ auraborane. The other three gold atoms are ligated by one tricyclohexylphosphine ligand each.

(24) has effective mirror symmetry, the mirror passing through Au(1), Au(4), and the centre of the $\{B_{10}\}$ cage. Hence Au(2) and Au(3) are equivalent, but are both in a different environment to Au(1). This is reflected (pun intended), for example in the Au-P bond lengths: Au(1)-P(1) is 228.5(8) pm; whereas Au(2)-P(2) is 222.4(6) and Au(3)-P(3) is 221.7(10) pm. It is also reflected in the Au-Au, and Au-B interatomic distances listed in Table 5.5.

5.10 Structural Comparisons.

A search of the literature revealed that there were only six structurally characterised Au_4 clusters[152-7]. There are two basic geometries: tetrahedral and planar. Four of these clusters are tetrahedral:-

	Cluster	Reference
(25)	$[Au_4(\mu\text{-}I)_2(PPh_3)_4]$	152
(26)	$[Au_4(I)(\mu_3\text{-}I)(dppm)_3]$	153
(27)	$[Au_4(dppm)_3Au(dppm\text{-}H)]^*$	154
(28)	$[Au_4(PPh_3)_4N]^+ BF_4^-$	155

* (dppm-H) = $[(Ph_2P)_2CH]^-$.

(25) has each gold atom bonded to one $\{PPh_3\}$ ligand, and to one end of a iodine bridge. The Au-Au distances are 264.9(1) pm (bridged) and 274.4(1) pm (unbridged).

In **(26)**, one iodine atom is σ-bonded to Au(4). The other caps the Au(1)-Au(2)-Au(3) face. Au(1), Au(2), and Au(3) are also bonded to two

phosphorus atoms from different dppm ligands which therefore bridge the gold-gold bonds. The Au *(n)*-Au(4) connectivities vary from 272.4(1) to 277.1(1) pm, and the others from 285.8(1) to 294.7(1) pm.

(27) consists of an Au_4 tetrahedron which has two adjacent edges (Au(1)-Au(2) and Au(1)-Au(3)) bridged by dppm ligands. The third dppm ligand bridges the bond between Au(4) which is the final vertex in the tetrahedron, and Au(5) which is *exo*-polyhedral. Au(5) is bonded to the CH group of the (dppm-H) ligand which bonds to Au(3) and Au(4) via the two P atoms. The gold-gold distances were reported as being between 270 and 301 pm.

In **(28)**, there is a Au_4 tetrahedron in which each Au is bonded to a $\{PPh_3\}$ ligand. The N atom is located in the centre of the tetrahedron, and it is the presence of this interstitial atom which causes the very long gold-gold bonds, which vary from 301.2 to 350.4 pm.

The two planar clusters both have each connectivity bridged by one bidentate ligand: either S_2CMe[156] or PhNNNPh[157].

The Au_4 tetrahedron in **(24)** is therefore unique in that it is the first structurally-characterised one which has no bridging or capping ligands whatsoever. The interatomic distances are mostly similar to the unbridged lengths in **(25)**-**(28)**, except for the Au(4) to Au(2) and Au(3) ones which are as short as the bridged connectivities in **(26)**.‡

Finally consider the electron-count for this cluster. In general, the electron count for a *closo* transition metal cluster is given by 14n + 2, which produces a value of 58 for a tetrahedron. However, the values which are found are:

---

‡ **(26)** is an anomaly in that its bridged connectivities are shorter than equivalent unbridged ones.

(25)

4 x Au	= 44
4 x PPh_3	= 8
2 x I	= 2
total	= 54

(28)

4 x Au	= 44
4 x PPh_3	= 8
1 x N^+	= 4
total	= 56

(26)

4 x Au	= 44
2 x I	= 2
3 x dppm	= 12
total	= 58

(24)

4 x Au	= 44
3 x PCy_3	= 6
1 x $[B_{10}H_{12}]$	= 2
total	= 52

In **(25)**, the paper [152] reported that the 'correct' electron-count consisted of 44 electrons from the Au_4 core and 14 from the ligands. This would require that each iodine atom formally donates three electrons to cluster bonding. If the iodine is thought of as being tetrahedral, for it to donate three electrons it would have to utilise one of its three lone-pairs, and thus the gold-iodine-gold angle would be close to tetrahedral i.e. 109^o. However, and this was not mentioned in the communication, it is only 53.4^o. Such a small angle means that it is very unlikely that the iodine does contribute three electrons, and so the anomalous electron-count of 54 is far more probable[140], with the iodine atom acting as a one-electron bridge.

It is generally held that as the number of skeletal electrons increases, the cluster will open up because orbitals which are anti-bonding with respect to metal-metal connectivities are progressively filled. Given that these four clusters are all tetrahedral, this is not evident.

5.11 Structural Analysis of the Auraborane Fragment.

It was assumed that the $\{B_{10}H_{12}\}$ fragment was acting as a 2-electron donor to cluster bonding. This conclusion was reached after analysis of the structure. The structure of the $\{B_{10}\}$ cage was compared against those of $[B_{10}H_{14}]$ and

$[B_{10}H_{14}]^{2-}$, for the reasons outlined above, and also in view of the comments about the accuracy of this structural determination. This yielded misfits of 100 and 133 pm respectively, and these values suggest that the structure is slightly inaccurate. In view of the long B(5)-B(10)† and B(7)-B(8) connectivities of 199(6) and 209(8) pm respectively, this $\{B_{10}\}$ cage is probably best thought of as a $[B_{10}H_{12}]^{2-}$ ligand which is a four-electron donor to cluster bonding. Hence the $[B_{10}H_{12}]^{\cdot\cdot}$ fragment generated by loss of two hydrogen atoms from decaborane will act as a two electron donor, as was assumed above.

Unfortunately, this complex is very insoluble, and a combination of this, plus the fact that only very small amounts were isolated, precluded the acquisition of any spectroscopic data.

5.12 The Relationship Between the Multiple Clusters.

Since **(24)** is one $\{Au_4\}$ tetrahedron bonded to a $\{B_{10}\}$ cage, and **(21)-(23)** can be described as three tetrahedra bonded to two $\{B_{10}\}$ cages, there is a common structural fragment, $\{Au_4B_{10}H_{12}\}$. This does suggest that a triple cluster is built up by first synthesising a double cluster which then further 'aggregates' into the final product. In this respect, the lack of an independent source of $\{AuPR_3\}$ in the synthesis of **(24)** is presumably the reason why it can be isolated, since if three $\{Cy_3PAu\}$ have already lost their ligated $\{B_{10}H_{12}\}$ cages, there is a ready source of $\{B_{10}\}$ in solution.

---

† *nido*-decaborane numbering.

5.13 Conclusions.

It has been shown that the "triple clusters" have structures which are more accurately described as quintuple, with two $\{AuB_{10}H_{12}\}$ cages bonded *via* common gold vertices to a central Au_6 core whose geometry is best described as three face-fused tetrahedra. $(B_{10}H_{12}Au)_2(AuPEt_3)_4$ and $(B_{10}H_{12}Au)_2(AuPPh_3)_4$ were structurally characterised, and the main difference in the two geometries is that the distortion from octahedral is more pronounced in $(B_{10}H_{12}Au)_2(AuPPh_3)_4$, and the two gold atoms bonded to the boron cages retain more square-planar character in $(B_{10}H_{12}Au)_2(AuPEt_3)_4$.

The third member of this series, $(B_{10}H_{12}Au)_2(AuPCy_3)_4$, was less well characterised, because the single crystal X-ray diffraction study could not be fully solved, and because its $^{11}B\text{-}\{^1H\}$ n.m.r. spectrum suffered from chemical shift anisotropy.

The reactivity of these species is very limited : H-Cl gas destroys the complex, regenerating $AuCl(PR_3)$, and HBF_4 decomposes it as well. Finally they are thermally unstable, decomposing in refluxing MeCN or toluene.

The final compound is the $(B_{10}H_{12}Au)(AuPCy_3)_3$ 'double cluster'. The structural determination of this species was of poor accuracy due to experimental difficulties, but it undoubtably consists of a Au_4 tetrahedron with one Au atom η^4-ligated to a $\{B_{10}H_{12}\}$ cage. The shape of this cage is more consistent with that of $B_{10}H_{14}$, rather than $[B_{10}H_{14}]^{2-}$, although the misfits are both quite high. The other three gold atoms are each ligated by $\{PCy_3\}$, and the structure has potential mirror symmetry. The Au_4 tetrahedron is the first to be characterised that has no bridging or capping ligands, and although most of the Au-Au bonds are of the order expected, two are unusually short. This may be related to the unusually low electron-count obtained for this cluster.

Table 5.1. Selected Bond Lengths(pm) and Angles(°) Involving the Au_6 Core in $(B_{10}H_{12}Au)_2(AuPEt_3)_4$.

The Geometry at the Two Golds Ligated to the Borane Cages.

Au(1)-mid(2,11)‡	212(4)	Au(6)-mid(2,11)	219(7)
Au(1)-mid(3,8)	216(4)	Au(6)-mid(3,8)	210(9)

mid(2,11)-Au(1)	-mid(3,8)	77.2(18)	mid(2,11)-Au(6)	-mid(3,8)	77.2(21)
mid(2,11)-Au(1)	-Au(2)	77.0(10)	mid(2,11)-Au(6)	-Au(3)	83.7(15)
mid(2,11)-Au(1)	-Au(4)	162.7(9)	mid(2,11)-Au(6)	-Au(5)	157.1(16)
mid(3,8)-Au(1)	-Au(2)	153.7(9)	mid(3,8)-Au(6)	-Au(3)	159.7(13)
mid(3,8)-Au(1)	-Au(4)	85.8(8)	mid(3,8)-Au(6)	-Au(5)	80.2(14)
Au(2)-Au(1)	-Au(4)	119.63(6)	Au(3)-Au(6)	-Au(5)	119.13(6)
Au(1)-Au(2)	-P(2)	171.8(3)	Au(6)-Au(3)	-P(3)	173.49(21)
Au(1)-Au(4)	-P(4)	164.25(22)	Au(6)-Au(5)	-P(5)	162.7(3)
Au(1)-Au(3)	-P(3)	121.94(21)	Au(6)-Au(2)	-P(2)	123.3(3)
Au(1)-Au(5)	-P(5)	130.6(3)	Au(6)-Au(4)	-P(4)	130.93(22)

Notes
‡ where mid(X,Y) is the midpoint of the X-Y connectivity.

Gold-Gold Distances(pm).

Atom	Au(1)	Au(2)	Au(3)	Au(4)	Au(5)	Au(6)
Au(1)	———	262.4(2)	280.9(2)	263.6(2)	276.1(2)	291.9(2)
Au(2)	262.4(2)	———	305.5(2)	454.7(2)	364.9(2)	281.6(2)
Au(3)	280.9(2)	305.5(2)	———	306.0(2)	455.9(2)	265.0(2)
Au(4)	263.6(2)	454.7(2)	306.0(2)	———	318.8(2)	280.4(2)
Au(5)	276.1(2)	364.9(2)	455.9(2)	318.8(2)	———	263.8(2)
Au(6)	291.9(2)	281.6(2)	265.0(2)	280.4(2)	263.8(2)	———

The Gold-Boron Bond Lengths(pm) and Angles(°).

Au(1)-B(2)	226(3)		Au(6)-B(2)	263(8)	
Au(1)-B(3)	231(4)		Au(6)-B(3)	227(4)	
Au(1)-B(8)	238(4)		Au(6)-B(8)	232(6)	
Au(1)-B(11)	238(4)		Au(6)-B(11)	229(5)	

B(3) -Au(1)	-B(2)	49.9(12)	B(3) -Au(6)	-B(2)	49.8(21)
B(11)-Au(1)	-B(2)	48.16(12)	B(11)-Au(6)	-B(2)	54.4(21)
B(8) -Au(1)	-B(3)	45.7(12)	B(8) -Au(6)	-B(3)	46.8(18)

The Bond Lengths(pm) and Angles(°) for Tetrahedron 1 : Au(1)-Au(2)-Au(3)-Au(6)

Au(1)-Au(2)	262.4(2)		Au(2)-Au(3)	305.5(2)	
Au(1)-Au(3)	280.9(2)		Au(2)-Au(6)	281.6(2)	
Au(1)-Au(6)	291.9(2)		Au(3)-Au(6)	265.0(2)	

Au(2)-Au(1)	-Au(3)	68.34(5)	Au(1)-Au(3)	-Au(2)	52.95(4)
Au(2)-Au(1)	-Au(6)	60.79(4)	Au(1)-Au(3)	-Au(6)	64.57(4)
Au(3)-Au(1)	-Au(6)	55.06(4)	Au(2)-Au(3)	-Au(6)	58.64(4)
Au(1)-Au(2)	-Au(3)	58.71(4)	Au(1)-Au(6)	-Au(2)	54.42(4)
Au(1)-Au(2)	-Au(6)	64.79(5)	Au(1)-Au(6)	-Au(3)	60.36(4)
Au(3)-Au(2)	-Au(6)	53.46(4)	Au(2)-Au(6)	-Au(3)	67.90(5)

The Bond lengths(pm) and Angles(°) for Tetrahedron 2 : Au(1)-Au(3)-Au(4)-Au(6)

Au(1)-Au(3)	280.9(2)	Au(3)-Au(4)	306.0(2)
Au(1)-Au(4)	263.6(2)	Au(3)-Au(6)	265.0(2)
Au(1)-Au(6)	291.9(2)	Au(4)-Au(6)	280.4(2)

Au(3)-Au(1)	-Au(4)	68.30(4)	Au(1)-Au(4)	-Au(3)	58.53(4)
Au(3)-Au(1)	-Au(6)	55.06(4)	Au(1)-Au(4)	-Au(6)	64.81(4)
Au(4)-Au(1)	-Au(6)	60.37(4)	Au(3)-Au(4)	-Au(6)	53.51(4)
Au(1)-Au(3)	-Au(4)	53.17(4)	Au(1)-Au(6)	-Au(3)	60.36(4)
Au(1)-Au(3)	-Au(6)	64.57(4)	Au(1)-Au(6)	-Au(4)	54.81(4)
Au(4)-Au(3)	-Au(6)	60.37(4)	Au(3)-Au(6)	-Au(4)	68.20(4)

The Bond lengths(pm) and Angles(°) for Tetrahedron 3 : Au(1)-Au(4)-Au(5)-Au(6)

Au(1)-Au(4)	263.6(2)	Au(4)-Au(5)	318.8(2)
Au(1)-Au(5)	276.1(2)	Au(4)-Au(6)	280.4(2)
Au(1)-Au(6)	291.9(2)	Au(5)-Au(6)	263.8(2)

Au(4)-Au(1)	-Au(5)	72.38(5)	Au(1)-Au(5)	-Au(4)	52.00(4)
Au(4)-Au(1)	-Au(6)	60.37(4)	Au(1)-Au(5)	-Au(6)	65.41(5)
Au(5)-Au(1)	-Au(6)	55.26(4)	Au(4)-Au(5)	-Au(6)	56.59(4)
Au(1)-Au(4)	-Au(5)	55.62(4)	Au(1)-Au(6)	-Au(4)	54.81(4)
Au(1)-Au(4)	-Au(6)	64.81(4)	Au(1)-Au(6)	-Au(5)	59.33(4)
Au(5)-Au(4)	-Au(6)	51.75(2)	Au(4)-Au(6)	-Au(5)	71.66(2)

The Bond lengths(pm) and Angles(°) for "Tetrahedron" 4 : Au(1)-Au(2)-Au(5)-Au(6)

Au(1)-Au(2)	262.4(2)	Au(2)-Au(5)	364.9(2)
Au(1)-Au(5)	276.1(2)	Au(2)-Au(6)	291.9(2)
Au(1)-Au(6)	291.9(2)	Au(5)-Au(6)	263.8(2)

Au(2)-Au(1)	-Au(5)	85.29(5)	Au(1)-Au(5)	-Au(2)	45.77(4)
Au(2)-Au(1)	-Au(6)	60.79(4)	Au(1)-Au(5)	-Au(6)	65.41(5)
Au(5)-Au(1)	-Au(6)	55.26(4)	Au(2)-Au(5)	-Au(6)	50.11(4)
Au(1)-Au(2)	-Au(5)	48.94(4)	Au(1)-Au(6)	-Au(2)	54.42(4)
Au(1)-Au(2)	-Au(6)	64.79(5)	Au(1)-Au(6)	-Au(5)	59.33(4)
Au(5)-Au(2)	-Au(6)	45.96(4)	Au(2)-Au(6)	-Au(5)	83.94(5)

Table 5.2. Relevant Bond Lengths(pm) and Angles(°) in $(B_{10}H_{12}Au)_2(AuPPh_3)_4$.

Au(1) -Au(2)	291.3(4)	B(53) -B(58)	196(9)
Au(1) -Au(57)	267.3(4)	B(54) -B(55)	187(11)
Au(1) -Au(67)	283.8(4)	B(54) -B(58)	184(9)
Au(2) -Au(3)	295.5(4)	B(54) -B(59)	191(9)
Au(2) -Au(57)	284.0(4)	B(55) -B(56)	181(11)
Au(2) -Au(67)	266.5(4)	B(55) -B(59)	168(11)
Au(3) -Au(4)	298.3(4)	B(55) -B(510)	160(12)

Au(3) -Au(57)	265.1(4)	B(56) -B(510)	196(11)
Au(3) -Au(67)	281.8(4)	B(56) -B(511)	160(9)
Au(4) -Au(57)	285.6(4)	B(58) -B(59)	202(10)
Au(4) -Au(67)	269.1(4)	B(59) -B(510)	192(11)
Au(57)-Au(67)	279.2(4)	B(510)-B(511)	186(11)
Au(1) - P(1)	227.3(15)	B(61) -B(62)	174(8)
Au(2) - P(2)	227.0(14)	B(61) -B(63)	179(8)
Au(3) - P(3)	228.6(16)	B(61) -B(64)	192(9)
Au(4) - P(4)	227.8(21)	B(61) -B(65)	199(10)
Au(57)-B(52)	223(6)	B(61) -B(66)	190(10)
Au(57)-B(53)	224(6)	B(62) -B(63)	176(8)
Au(57)-B(58)	250(7)	B(62) -B(66)	180(10)
Au(57)-B(511)	242(7)	B(62) -B(611)	162(8)
Au(67)-B(62)	224(6)	B(63) -B(64)	181(8)
Au(67)-B(63)	223(5)	B(63) -B(68)	185(7)
Au(67)-B(68)	240(5)	B(64) -B(65)	204(10)
Au(67)-B(611)	241(5)	B(64) -B(68)	168(8)
B(51) -B(52)	171(10)	B(64) -B(69)	177(10)
B(51) -B(53)	182(10)	B(65) -B(66)	160(11)
B(51) -B(54)	184(10)	B(65) -B(69)	165(11)
B(51) -B(55)	180(12)	B(65) -B(610)	162(11)
B(51) -B(56)	179(10)	B(66) -B(610)	156(11)
B(52) -B(53)	193(9)	B(66) -B(611)	172(9)
B(52) -B(56)	162(9)	B(68) -B(69)	186(9)
B(52) -B(511)	171(9)	B(69) -B(610)	205(11)
B(53) -B(54)	176(9)	B(610)-B(611)	182(9)

Au(2) -Au(1) -Au(57)	60.94(8)	B(54) -B(51) -B(55)	62(4)
Au(2) -Au(1) -Au(67)	55.19(7)	B(55) -B(51) -B(56)	61(4)
Au(57)-Au(1) -Au(67)	60.80(8)	Au(57)-B(52) -B(53)	65(3)
Au(1) -Au(2) -Au(3)	102.67(9)	Au(57)-B(52) -B(511)	74(3)
Au(1) -Au(2) -Au(57)	55.36(7)	B(51) -B(52) -B(53)	60(4)
Au(1) -Au(2) -Au(67)	60.98(8)	B(51) -B(52) -B(56)	65(4)
Au(3) -Au(2) -Au(57)	54.42(7)	B(56) -B(52) -B(511)	58(4)
Au(3) -Au(2) -Au(67)	59.93(8)	Au(57)-B(53) -B(52)	64(3)
Au(57)-Au(2) -Au(67)	60.87(8)	Au(57)-B(53) -B(58)	73(3)
Au(2) -Au(3) -Au(4)	102.85(10)	B(51) -B(53) -B(52)	54(4)
Au(2) -Au(3) -Au(57)	60.59(8)	B(51) -B(53) -B(54)	62(4)
Au(2) -Au(3) -Au(67)	54.93(7)	B(54) -B(53) -B(58)	59(4)
Au(4) -Au(3) -Au(57)	60.58(8)	B(51) -B(54) -B(53)	61(4)
Au(4) -Au(3) -Au(67)	55.18(8)	B(51) -B(54) -B(55)	58(4)
Au(57)-Au(3) -Au(67)	61.31(8)	B(53) -B(54) -B(58)	66(4)
Au(3) -Au(4) -Au(57)	53.96(8)	B(55) -B(54) -B(59)	53(4)
Au(3) -Au(4) -Au(67)	59.29(8)	B(58) -B(54) -B(59)	65(4)
Au(57)-Au(4) -Au(67)	60.37(8)	B(51) -B(55) -B(54)	60(4)
Au(1) -Au(57) -Au(2)	63.70(8)	B(51) -B(55) -B(56)	59(4)
Au(1) -Au(57) -Au(3)	118.72(11)	B(54) -B(55) -B(59)	65(4)
Au(1) -Au(57) -Au(4)	103.19(10)	B(56) -B(55) -B(510)	70(5)
Au(1) -Au(57) -Au(67)	62.52(8)	B(59) -B(55) -B(510)	72(5)
Au(2) -Au(57) -Au(3)	64.99(8)	B(51) -B(56) -B(52)	60(4)
Au(2) -Au(57) -Au(4)	109.15(10)	B(51) -B(56) -B(55)	60(4)
Au(2) -Au(57) -Au(67)	56.47(7)	B(52) -B(56) -B(511)	64(4)
Au(3) -Au(57) -Au(4)	65.46(9)	B(55) -B(56) -B(510)	50(4)
Au(3) -Au(57) -Au(67)	62.28(8)	B(510)-B(56) -B(511)	62(4)

Au(4)	-Au(57)	-Au(67)	56.88(8)	Au(57)-B(58)	-B(53)	59(3)
Au(1)	-Au(67)	-Au(2)	63.83(8)	B(53) -B(58)	-B(54)	55(3)
Au(1)	-Au(67)	-Au(3)	108.19(10)	B(54) -B(58)	-B(59)	59(3)
Au(1)	-Au(67)	-Au(4)	103.23(10)	B(54) -B(59)	-B(55)	62(4)
Au(1)	-Au(67)	-Au(57)	56.68(8)	B(54) -B(59)	-B(58)	56(3)
Au(2)	-Au(67)	-Au(3)	65.14(8)	B(55) -B(59)	-B(510)	52(4)
Au(2)	-Au(67)	-Au(4)	120.16(11)	B(55) -B(510)	-B(56)	60(5)
Au(2)	-Au(67)	-Au(57)	62.67(8)	B(55) -B(510)	-B(59)	56(5)
Au(3)	-Au(67)	-Au(4)	65.52(9)	B(56) -B(510)	-B(511)	49(4)
Au(3)	-Au(67)	-Au(57)	56.40(7)	Au(57)-B(511)	-B(52)	63(3)
Au(4)	-Au(67)	-Au(57)	62.75(8)	B(52) -B(511)	-B(56)	58(4)
Au(1)	-Au(57)	-B(52)	124.9(17)	B(56) -B(511)	-B(510)	68(4)
Au(1)	-Au(57)	-B(53)	78.5(17)	B(62) -Au(67)	-B(63)	46.3(21)
Au(1)	-Au(57)	-B(58)	70.8(15)	B(62) -Au(67)	-B(611)	40.7(19)
Au(1)	-Au(57)	-B(511)	161.4(16)	B(63) -Au(67)	-B(68)	46.8(19)
Au(2)	-Au(57)	-B(52)	108.5(17)	B(62) -B(61)	-B(63)	60(3)
Au(2)	-Au(57)	-B(53)	108.8(17)	B(62) -B(61)	-B(66)	59(4)
Au(2)	-Au(57)	-B(58)	132.9(15)	B(63) -B(61)	-B(64)	58(3)
Au(2)	-Au(57)	-B(511)	129.4(16)	B(64) -B(61)	-B(65)	63(3)
Au(3)	-Au(57)	-B(52)	101.3(17)	B(65) -B(61)	-B(66)	49(4)
Au(3)	-Au(57)	-B(53)	150.2(17)	Au(67)-B(62)	-B(63)	67(3)
Au(3)	-Au(57)	-B(58)	156.4(15)	Au(67)-B(62)	-B(611)	75(3)
Au(3)	-Au(57)	-B(511)	79.8(16)	B(61) -B(62)	-B(63)	62(3)
Au(4)	-Au(57)	-B(52)	128.2(17)	B(61) -B(62)	-B(66)	65(4)
Au(4)	-Au(57)	-B(53)	138.1(17)	B(66) -B(62)	-B(611)	60(4)
Au(4)	-Au(57)	-B(58)	91.7(15)	Au(67)-B(63)	-B(62)	67(3)
Au(4)	-Au(57)	-B(511)	85.5(16)	Au(67)-B(63)	-B(68)	71.6(24)
Au(67)	-Au(57)	-B(52)	160.6(17)	B(61) -B(63)	-B(62)	59(3)
Au(67)	-Au(57)	-B(53)	141.0(17)	B(61) -B(63)	-B(64)	64(3)
Au(67)	-Au(57)	-B(58)	111.5(15)	B(64) -B(63)	-B(68)	55(3)
Au(67)	-Au(57)	-B(511)	134.3(16)	B(61) -B(64)	-B(63)	57(3)
Au(1)	-Au(67)	-B(62)	139.3(15)	B(61) -B(64)	-B(65)	60(3)
Au(1)	-Au(67)	-B(63)	132.3(14)	B(63) -B(64)	-B(68)	64(3)
Au(1)	-Au(67)	-B(68)	85.6(13)	B(65) -B(64)	-B(69)	51(4)
Au(1)	-Au(67)	-B(611)	102.6(11)	B(68) -B(64)	-B(69)	65(4)
Au(2)	-Au(67)	-B(62)	147.0(15)	B(61) -B(65)	-B(64)	57(3)
Au(2)	-Au(67)	-B(63)	101.4(14)	B(61) -B(65)	-B(66)	63(4)
Au(2)	-Au(67)	-B(68)	77.9(13)	B(64) -B(65)	-B(69)	56(4)
Au(2)	-Au(67)	-B(611)	164.0(11)	B(66) -B(65)	-B(610)	58(5)
Au(3)	-Au(67)	-B(62)	110.5(15)	B(69) -B(65)	-B(610)	77(5)
Au(3)	-Au(67)	-B(63)	104.2(14)	B(61) -B(66)	-B(62)	56(4
Au(3)	-Au(67)	-B(68)	127.1(13)	B(61) -B(66)	-B(65)	69(4)
Au(3)	-Au(67)	-B(611)	129.9(11)	B(62) -B(66)	-B(611)	55(3)
Au(4)	-Au(67)	-B(62)	82.0(15)	B(65) -B(66)	-B(610)	62(5)
Au(4)	-Au(67)	-B(63)	121.8(14)	B(610)-B(66)	-B(611)	67(5)
Au(4)	-Au(67)	-B(68)	161.9(13)	Au(67)-B(68)	-B(63)	61.8(23)
Au(4)	-Au(67)	-B(611)	69.6(11)	B(63) -B(68)	-B(64)	62(3)
Au(57)	-Au(67)	-B(62)	144.8(15)	B(64) -B(68)	-B(69)	60(4)
Au(57)	-Au(67)	-B(63)	158.1(14)	B(64) -B(69)	-B(65)	73(4)
Au(57)	-Au(67)	-B(68)	133.8(13)	B(64) -B(69)	-B(68)	55(3)
Au(57)	-Au(67)	-B(611)	118.4(11)	B(65) -B(69)	-B(610)	51(4)
B(52)	-Au(57)	-B(53)	51.3(24)	B(65) -B(610)	-B(66)	61(5)
B(52)	-Au(57)	-B(511)	42.9(23)	B(65) -B(610)	-B(69)	52(4)
B(53)	-Au(57)	-B(58)	48.5(23)	B(66) -B(610)	-B(611)	60(4)
B(52)	-B(51)	-B(53)	66(4)	Au(67)-B(611)	-B(62)	64(3)

B(52) -B(51)	-B(56)	55(4)	B(62) -B(611)	-B(66)	65(4)
B(53) -B(51)	-B(54)	58(4)	B(66) -B(611)	-B(610)	52(4)

Table 5.3. The Bond Lengths(pm) and Angles(°) for the $\{Au_6\}$ Core of $(B_{10}H_{12}Au)_2(AuPPh_3)_4$.

The Bond Lengths(pm) and Angles(°) for the Two Golds Ligated to the Boranes.

Au(1)-mid(2,11)	216(9)	Au(6)-mid(2,11)	217(8)
Au(1)-mid(3,8)	216(9)	Au(6)-mid(3,8)	212(7)

mid(2,11)-Au(1)	-mid(3,8)	78.82(24)	mid(2,11)-Au(6)	-mid(3,8)	75.06(22)
mid(2,11)-Au(1)	-Au(2)	72.92(19)	mid(2,11)-Au(6)	-Au(3)	164.18(16)
mid(2,11)-Au(1)	-Au(4)	168.35(21)	mid(2,11)-Au(6)	-Au(5)	74.72(15)
mid(3,8)-Au(1)	-Au(2)	145.58(22)	mid(3,8)-Au(6)	-Au(3)	89.12(17)
mid(3,8)-Au(1)	-Au(4)	90.14(20)	mid(3,8)-Au(6)	-Au(5)	144.46(18)
Au(2)-Au(1)	-Au(4)	118.72(11)	Au(3)-Au(6)	-Au(5)	120.16(11)

The Gold-Gold Distances(pm) in $(B_{10}H_{12}Au)_2(AuPPh_3)_4$.

Atom	Au(1)	Au(2)	Au(3)	Au(4)	Au(5)	Au(6)
Au(1)	———	267.3(3)	284.0(3)	265.1(3)	285.6(3)	279.2(3)
Au(2)	267.3(3)	———	291.3(3)	458.1(3)	433.5(3)	283.8(3)
Au(3)	284.0(3)	291.3(3)	———	295.4(3)	464.2(3)	266.5(3)
Au(4)	265.1(3)	458.1(3)	295.4(3)	———	298.3(3)	281.8(3)
Au(5)	285.6(3)	433.5(3)	464.6(2)	298.3(3)	———	269.1(3)
Au(6)	279.2(3)	283.8(3)	266.5(3)	281.8(3)	269.1(3)	———

The Bond Lengths(pm) and Angles(°) for Tetrahedron 1 : Au(1)-Au(2)-Au(3)-Au(6).

Au(1)-Au(2)	267.3(3)	Au(2)-Au(3)	291.3(3)
Au(1)-Au(3)	284.0(3)	Au(2)-Au(6)	283.8(3)
Au(1)-Au(6)	279.2(3)	Au(3)-Au(6)	266.5(3)

Au(2)-Au(1)	-Au(3)	63.70(8)	Au(1)-Au(3)	-Au(2)	55.36(8)
Au(2)-Au(1)	-Au(6)	62.52(8)	Au(1)-Au(3)	-Au(6)	60.87(8)
Au(3)-Au(1)	-Au(6)	56.47(7)	Au(2)-Au(3)	-Au(6)	60.98(8)
Au(1)-Au(2)	-Au(3)	60.94(8)	Au(1)-Au(6)	-Au(2)	56.68(8)
Au(1)-Au(2)	-Au(6)	60.80(8)	Au(1)-Au(6)	-Au(3)	62.67(8)
Au(3)-Au(2)	-Au(6)	55.19(8)	Au(2)-Au(6)	-Au(6)	63.83(8)

The Bond Lengths(pm) and Angles(°) for Tetrahedron 2 : Au(1)-Au(3)-Au(4)-Au(6).

Au(1)-Au(3)	284.0(3)	Au(3)-Au(4)	295.4(3)
Au(1)-Au(4)	265.1(3)	Au(3)-Au(6)	266.5(3)
Au(1)-Au(6)	279.2(3)	Au(4)-Au(6)	281.8(3)

Au(3)-Au(1)	-Au(4)	64.99(8)	Au(1)-Au(4)	-Au(3)	60.59(8)
Au(3)-Au(1)	-Au(6)	56.47(7)	Au(1)-Au(4)	-Au(6)	61.31(8)
Au(4)-Au(1)	-Au(6)	62.28(8)	Au(3)-Au(4)	-Au(6)	54.93(7)
Au(1)-Au(3)	-Au(4)	54.42(7)	Au(1)-Au(6)	-Au(3)	62.67(8)
Au(1)-Au(3)	-Au(6)	60.87(8)	Au(1)-Au(6)	-Au(4)	56.40(8)
Au(4)-Au(3)	-Au(6)	59.93(8)	Au(3)-Au(6)	-Au(4)	65.14(8)

The Bond Lengths(pm) and Angles(^{o}) for Tetrahedron 3 : Au(1)-Au(4)-Au(5)-Au(6).

Au(1)-Au(4)	265.1(3)	Au(4)-Au(5)	298.3(3)
Au(1)-Au(5)	285.6(3)	Au(4)-Au(6)	283.8(3)
Au(1)-Au(6)	279.2(3)	Au(5)-Au(6)	269.1(3)

Au(4)-Au(1)	-Au(5)	65.46(9)	Au(1)-Au(5)	-Au(4)	53.96(8)
Au(4)-Au(1)	-Au(6)	62.28(8)	Au(1)-Au(5)	-Au(6)	60.37(8)
Au(5)-Au(1)	-Au(6)	56.88(8)	Au(4)-Au(5)	-Au(6)	59.29(8)
Au(1)-Au(4)	-Au(5)	60.58(8)	Au(1)-Au(6)	-Au(4)	56.40(8)
Au(1)-Au(4)	-Au(6)	61.31(8)	Au(1)-Au(6)	-Au(5)	62.75(8)
Au(5)-Au(4)	-Au(6)	55.18(8)	Au(4)-Au(6)	-Au(5)	65.52(9)

Bond Lengths(pm) and Angles(^{o}) for "Tetrahedron" 4 : Au(1)-Au(2)-Au(5)-Au(6).

Au(1)-Au(2)	267.3(3)	Au(2)-Au(5)	433.5(3)
Au(1)-Au(5)	285.6(3)	Au(2)-Au(6)	283.8(3)
Au(1)-Au(6)	279.2(3)	Au(5)-Au(6)	269.1(3)

Au(2)-Au(1)	-Au(5)	103.19(10)	Au(1)-Au(5)	-Au(2)	36.90(6)
Au(2)-Au(1)	-Au(6)	62.52(8)	Au(1)-Au(5)	-Au(6)	60.37(8)
Au(5)-Au(1)	-Au(6)	56.88(8)	Au(2)-Au(5)	-Au(6)	39.59(6)
Au(1)-Au(2)	-Au(5)	39.91(7)	Au(1)-Au(6)	-Au(2)	56.68(8)
Au(1)-Au(2)	-Au(6)	60.80(8)	Au(1)-Au(6)	-Au(5)	62.75(8)
Au(5)-Au(2)	-Au(6)	37.18(6)	Au(2)-Au(6)	-Au(5)	103.23(10)

Table 5.4. Fractional Coordinates, Bond Lengths(pm), and Angles(^{o}) for the Central Au_6 core of $(B_{10}H_{12}Au)_2(AuPCy_3)_4$.

Space group = *P4/nnc* Unit cell dimensions : c = 1.5828(24), a = 1.8828(7)nm.

Au(1,a)	0.2500	0.2500	0.6749
Au(1,b)	0.2500	0.2500	0.8251
Au(2,a)	0.1467	0.1467	0.7500
Au(2,b)	0.1467	0.3533	0.7500
Au(2,c)	0.3533	0.3533	0.7500
Au(2,d)	0.3533	0.1467	0.7500

Notes.

Au(n,x), n is the independent Au atom (1 or 2), and x is the symmetry transformation in order to generate the atom in question. These are : (a) x,y,z (b) x,0.5-y,1.5-z (c) 0.5-x,0.5-y,z (d) 0.5-x,y,1.5-z

	Au(1,a)	Au(1,b)	Au(2,a)	Au(2,b)	Au(2,c)	Au(2,d)
Au(1,a)	——	283.7	291.0	291.0	291.0	291.0
Au(1,b)	283.7	——	291.0	291.0	291.0	291.0
Au(2,a)	291.0	291.0	——	389.0	508.2	327.0
Au(2,b)	291.0	291.0	389.0	——	327.0	508.2
Au(2,c)	291.0	291.0	508.2	327.0	——	389.0
Au(2,d)	291.0	291.0	327.0	508.2	389.0	——

Au(1,b)-Au(1,a)-Au(2,x)	60.83	Au(1,a)-Au(1,b)-Au(2,x)	60.83
Au(2,a)-Au(1,a)-Au(2,b)	83.89	Au(2,a)-Au(1,b)-Au(2,b)	83.89
Au(2,a)-Au(1,a)-Au(2,c)	121.66	Au(2,a)-Au(1,b)-Au(2,c)	121.66
Au(2,a)-Au(1,a)-Au(2,d)	68.37	Au(2,a)-Au(1,b)-Au(2,d)	68.37
Au(2,b)-Au(1,a)-Au(2,c)	68.37	Au(2,b)-Au(1,b)-Au(2,c)	68.37
Au(2,b)-Au(1,a)-Au(2,d)	121.66	Au(2,b)-Au(1,b)-Au(2,d)	121.66
Au(2,c)-Au(1,a)-Au(2,d)	83.89	Au(2,c)-Au(1,b)-Au(2,d)	83.89
Au(1,x)-Au(2,a)-Au(2,b)	48.06	Au(1,x)-Au(2,b)-Au(2,a)	48.06
Au(1,x)-Au(2,a)-Au(2,c)	29.17	Au(1,x)-Au(2,b)-Au(2,c)	29.17
Au(1,x)-Au(2,a)-Au(2,d)	55.81	Au(1,x)-Au(2,b)-Au(2,d)	55.81
Au(2,b)-Au(2,a)-Au(2,c)	40.05	Au(2,a)-Au(2,b)-Au(2,c)	90.00
Au(2,b)-Au(2,a)-Au(2,d)	90.00	Au(2,a)-Au(2,b)-Au(2,d)	40.05
Au(2,c)-Au(2,a)-Au(2,d)	49.95	Au(2,c)-Au(2,b)-Au(2,d)	49.95
Au(1,x)-Au(2,c)-Au(2,a)	29.17	Au(1,x)-Au(2,d)-Au(2,a)	29.17
Au(1,x)-Au(2,c)-Au(2,b)	55.81	Au(1,x)-Au(2,d)-Au(2,b)	55.81
Au(1,x)-Au(2,c)-Au(2,d)	48.06	Au(1,x)-Au(2,d)-Au(2,d)	48.06
Au(2,a)-Au(2,c)-Au(2,b)	49.95	Au(2,a)-Au(2,d)-Au(2,b)	49.95
Au(2,a)-Au(2,c)-Au(2,d)	40.05	Au(2,a)-Au(2,d)-Au(2,c)	90.00
Au(2,b)-Au(2,c)-Au(2,d)	90.00	Au(2,b)-Au(2,d)-Au(2,c)	40.05
Au(1,a)-Au(2,x)-Au(1,b)	58.37		

Table 5.5. Bond Lengths(pm) and Angles(^{o}) for the Au and B Atoms in $(B_{10}H_{12}Au)(AuPCy_3)_3$.

Au(1) -Au(2)	273.96(17)	Au(4)-B(10)	233(4)	B(1) -B(10)	183(7)
Au(1) -Au(3)	270.69(17)	B(2) - B(3)	163(6)	B(5) -B(10)	199(6)
Au(1) -Au(4)	270.35(13)	B(2) - B(5)	181(6)	B(1) - B(2)	168(7)
Au(2) -Au(3)	288.22(16)	B(2) - B(6)	180(6)	B(6) - B(7)	173(6)
Au(2) -Au(4)	262.77(12)	B(2) - B(7)	164(7)	B(1) - B(3)	157(7)
Au(3) -Au(4)	263.75(12)	B(3) - B(4)	180(5)	B(7) - B(8)	209(8)
Au(1) - P(1)	228.5(8)	B(3) - B(7)	177(6)	B(1) - B(4)	192(7)
Au(2) - P(2)	222.4(6)	B(3) - B(8)	188(7)	B(8) - B(9)	186(7)
Au(3) - P(3)	221.7(10)	B(4) - B(8)	176(7)	B(1) - B(5)	171(7)
Au(4) - B(5)	235(4)	B(4) - B(9)	176(5)	B(9) -B(10)	165(5)
Au(4) - B(6)	249(4)	B(4) -B(10)	176(5)		
Au(4) - B(9)	245(3)	B(5) - B(6)	191(5)		

Au(2) -Au(1)	-Au(3)	63.90(4)	B(5) - B(1)	-B(10)	68(3)
Au(2) -Au(1)	-Au(4)	57.73(4)	B(1) - B(2)	- B(3)	57(3)
Au(3) -Au(1)	-Au(4)	58.35(4)	B(1) - B(2)	- B(5)	59(3)
Au(1) -Au(2)	-Au(3)	57.50(4)	B(3) - B(2)	- B(7)	66(3)
Au(1) -Au(2)	-Au(4)	60.45(4)	B(5) - B(2)	- B(6)	63.8(24)
Au(3) -Au(2)	-Au(4)	56.97(3)	B(6) - B(2)	- B(7)	60(3)
Au(1) -Au(3)	-Au(2)	58.60(4)	B(1) - B(3)	- B(2)	63(3)
Au(1) -Au(3)	-Au(4)	60.76(4)	B(1) - B(3)	- B(4)	69(3)
Au(2) -Au(3)	-Au(4)	56.65(3)	B(2) - B(3)	- B(7)	57(3)
Au(1) -Au(4)	-Au(2)	61.83(4)	B(4) - B(3)	- B(8)	57.0(25)
Au(1) -Au(4)	-Au(3)	60.89(4)	B(7) - B(3)	- B(8)	70(3)
Au(2) -Au(4)	-Au(3)	66.38(4)	B(1) - B(4)	- B(3)	49.9(23)
Au(2) -Au(1)	- P(1)	149.20(21)	B(1) - B(4)	-B(10)	59.5(24)
Au(3) -Au(1)	- P(1)	142.10(21)	B(3) - B(4)	- B(8)	64(3)
Au(4) -Au(1)	- P(1)	141.77(20)	B(8) - B(4)	- B(9)	63.8(25)
Au(1) -Au(2)	- P(2)	132.35(17)	B(9) - B(4)	-B(10)	56.1(19)
Au(3) -Au(2)	- P(2)	137.34(17)	Au(4)- B(5)	- B(6)	70.8(17)
Au(4) -Au(2)	- P(2)	162.76(17)	Au(4)- B(5)	-B(10)	64.2(16)
Au(1) -Au(3)	- P(3)	135.2(3)	B(1) - B(5)	- B(2)	57(27)
Au(2) -Au(3)	- P(3)	138.6(3)	B(1) - B(5)	-B(10)	58.5(25)
Au(4) -Au(3)	- P(3)	159.7(3)	B(2) - B(5)	- B(6)	57.8(22)
Au(1) -Au(4)	- B(5)	145.3(10)	Au(4)- B(6)	- B(5)	63.0(16)
Au(2) -Au(4)	- B(5)	118.9(10)	B(2) - B(6)	- B(5)	58.5(22)
Au(3) -Au(4)	- B(5)	153.7(10)	B(2) - B(6)	- B(7)	55.2(25)
Au(1) -Au(4)	- B(6)	99.4(8)	B(2) - B(7)	- B(3)	57(3)
Au(2) -Au(4)	- B(6)	98.1(8)	B(2) - B(7)	- B(6)	64(3)
Au(3) -Au(4)	- B(6)	158.7(8)	B(3) - B(7)	- B(8)	57.6(25)
Au(1) -Au(4)	- B(9)	95.6(6)	B(3) - B(8)	- B(4)	59.1(25)
Au(2) -Au(4)	- B(9)	156.8(6)	B(3) - B(8)	- B(7)	52.5(24)
Au(3) -Au(4)	- B(9)	99.0(6)	B(4) - B(8)	- B(9)	58.0(24)
Au(1) -Au(4)	-B(10)	135.9(10)	Au(4)- B(9)	-B(10)	65.8(16)
Au(2) -Au(4)	-B(10)	161.9(10)	B(4) - B(9)	- B(8)	58.2(24)
Au(3) -Au(4)	-B(10)	116.1(10)	B(4) - B(9)	-B(10)	61.9(21)
B(5) -Au(4)	- B(6)	46.2(13)	Au(4)-B(10)	- B(5)	65.3(16)
B(5) -Au(4)	-B(10)	50.4(14)	Au(4)-B(10)	- B(9)	73.9(17)
B(9) -Au(4)	-B(10)	40.3(11)	B(1) -B(10)	- B(4)	65(3)
B(2) - B(1)	- B(3)	60(3)	B(1) -B(10)	- B(5)	53.1(24)
B(2) - B(1)	- B(5)	64(3)	B(4) -B(10)	- B(9)	62.0(21)
B(3) - B(1)	- B(4)	61(3)	B(5) -B(10)	- B(9)	120(3)
B(4) - B(1)	-B(10)	55.8(23)			

Chapter 6:

Experimental.

6.1 Introduction.

This chapter describes the experimental procedures which led to the results discussed in the previous four chapters. There are two main parts to this work : synthetic methodology and crystallographic procedures.

The synthetic methodology starts with a section on the general procedures including purification of solvents and details of all apparatus used. The next section then details the syntheses of starting materials developed by myself, along with references for literature preparations. The final section consists of the syntheses and reactions of all of the complexes reported herein.

The second part details the general procedure for the crystallographic determinations, and is subdivided into : data collection, data processing, structure solution and refinement, and processing of results.

6.2 General Techniques.

All the experiments were carried out under an atmosphere of dry, oxygen-free nitrogen, using standard Schlenk techniques.

The dichloromethane, tetrahydrofuran, hexane, and toluene used were previously dried and distilled under nitrogen. The ether and pentane were previously dried with sodium wire. All other solvents were used as received.

The infra-red spectra were recorded either as KBr discs or dichloromethane solutions referenced against solvent in calcium fluoride solution cells on a Perkin-Elmer 598 spectrophotometer. N.m.r. spectra were recorded at ambient

temperature (unless otherwise specified) using the following spectrometers

^{31}P-$\{^{1}H\}$: Jeol FX-60Q, and Bruker WP200SY

^{11}B-$\{^{1}H\}$, ^{11}B, ^{11}B(COSY): Bruker WP200SY or Bruker WH360

^{1}H-$\{^{11}B\}$: Bruker WH360

Techniques for recording ^{1}H-$\{^{11}B\}$ and ^{11}B(COSY) n.m.r. experiments have been described previously [95-97]. Chemical shifts are reported relative to external $SiMe_4$ (^{1}H); 85% H_3PO_4 (^{31}P); and BF_3OEt_2 (^{11}B); positive shifts to high frequency.

U.V./visible spectra were recorded as dichloromethane solutions referenced against dichloromethane on a Perkin-Elmer SP8-400 spectrophotometer, and microanalyses were by the departmental service.

6.3 Synthesis of Starting Materials.

6.3.1 Synthesis of Gold-Containing Starting Materials.

Synthesis of $AuCl(PR_3)$ (R = Ph, Cy, *o*-tolyl).

Chlorotrialkylphosphinegold(I) was synthesised according to literature methods [158,159]. $AuCl(PEt_3)$ was synthesised using degassed acetone as solvent, the rest used ethanol.

Synthesis of $AuMe(PR_3)$ (R = Et,Ph,Cy, *o*-tolyl).

The $AuCl(PR_3)$ was then methylated using a method modified from that of Schmidbaur *et al* [160].

$AuCl(PR_3)$ (ca. 1.5 g) was suspended in thf (20 ml) and to it was added, at 0°C, methyllithium (1.5 molar equivalent) dropwise over ca. thirty minutes. Ether (15 ml) was then added to wash in any methyllithium, and to ensure separation in the next step, because thf and water are miscible. Next, distilled water (5 ml) was

slowly added, at 0°C. After about five minutes, the aqueous layer was syringed off, anhydrous magnesium sulphate added and the suspension dried overnight. The solution was then filtered and the magnesium sulphate washed with plenty of ether. The washings were combined with the solution and the solvent removed *in vacuo*.The product was then recrystallised from trichloromethane/hexane.

yield 50-80%

	N.M.R.		Microanalysis				
R	$\delta^{31}P$-{^1H}	calc. for :	%C	%H	Found:	%C	%H
Ph	47.4[b]	$C_{19}H_{18}AuP$:	48.1	3.83		48.2	3.83
Cy	59.95[a]	$C_{19}H_{36}AuP$:	46.3	7.37		45.7	7.27
o-tolyl	37.02[b]	$C_{22}H_{24}AuP$:	51.2	4.68		50.2	4.50

Notes

[a] CD_2Cl_2, [b] $CDCl_3$

6.3.2 Synthesis of Polyhedral Borane Starting Materials.

$[NHEt_3]^+$ $[B_{10}H_{13}]^-$ [22], $[B_{10}H_{12}(MeCN)_2]$ [161], and $B_{10}H_{12}(SMe_2)_2$ [28], were synthesised by literature methods.

Synthesis of $[PhCH_2NMe_3]^+$ $[B_{10}H_{13}]^-$

This was synthesised in a manner similar to that reported for tetraalkylammonium salts in reference 22. $B_{10}H_{14}$ (0.1589g, 1.301mmol) was dissolved in thf(10 ml) and to it was added KOH (0.0922g, 1.646mmol) dissolved in distilled water (10 ml). After fifteen minutes, the solution had gone yellow, and to it was added excess $PhCH_2NMe_3Cl$ dissolved in distilled water (5ml). No precipitation occurred, and so the volume of solvent was reduced *in vacuo* until a yellow precipitate was observed. This was filtered off, and washed with ether. Yellow blocky crystals were grown from diffusion of hexane into a dichloromethane solution.

Yield = 0.2311g, 65.5 %

Synthesis of $B_{10}H_{12}(PPh_3)_2$

This product was reported in the literature[162], but there were no experimental details in the communication. $B_{10}H_{14}$ (1.023 g, 8.373 mmol) and PPh_3 (4.413 g, 16.84 mmol) were stirred in diethylether (20 ml) for two hours at room temperature, during which time gaseous evolution was noted, along with deposition of a white solid. The precipitate was filtered off, washed with ether, and dried *in vacuo*.

Yield 4.513g, 83.7%

6.4 Syntheses and Reactions of Auraboranes.

6.4.1 Synthesis of 5,6-μ-(Cy_3PAu)-*nido*-$B_{10}H_{13}$ and 5,6-μ-(o-tolyl$_3$PAu)-*nido*-$B_{10}H_{13}$ [113].

See also ref. 113 (a copy of which is in Appendix 4) for an alternative route using $[NHEt_3]^+$ $[B_{10}H_{13}]^-$ and $AuCl(PCy_3)$. $AuMe(PCy_3)$ (0.5283g, 1.073 mmol) was dissolved in dichloromethane (20 ml) and to it was added, with stirring, a solution of $B_{10}H_{14}$ (0.1078 g, 0.883 mmol) in dichloromethane (10 ml). The dropping funnel was then washed with a further aliquot of dichloromethane (5 ml) which was added to the reaction.

During this addition, the initially colourless solution slowly went pale yellow with concomitant gaseous evolution and deposition of a white, microcrystalline precipitate. After stirring for a further five minutes, the volume of the solution was reduced *in vacuo* to ca. 5 ml. The white precipitate was filtered off and washed with a little dichloromethane.

Yield = 0.4235 g, 66.1 %.

N.M.R. Parameters/ppm. (^{11}B and ^{1}H in $CDCl_3$, ^{31}P in CD_2Cl_2)

$\delta^{11}B$-{^{1}H} : 16.12(1B), 9.32(1B), 8.41(1B), 2.82(1B), 1.41(1B), -0.57(2B), -1.01(1B), -29.53(1B), and -35.53(1B).

$\delta^{1}H$-{^{11}B} : 5.05, 3.72, 3.50, 3.29, 3.17, 2.90, 2.62, 0.64, 0.60, (all B-H); -0.13, -2.93, and -3.48 (all B-H-B).

$\delta^{31}P$-{^{1}H} : 68.9.

Microanalysis	%C	%H
Calculated for $C_{18}H_{46}AuB_{10}P$:	36.1	7.75
Found:	35.7	7.68

5,6-μ-(*o*-tolyl$_3$PAu)-*nido*-$B_{10}H_{13}$ was synthesised analogously, except that there was no precipitate until a saturated solution was cooled to -30°C. This was filtered off and washed with ether.

N.M.R. Parameters/ppm (in CD_2Cl_2)

$\delta^{11}B$-{^{1}H} : 15.13(1B), 9.41(1B), 8.34(1B), 2.15(1B), 1.40(1B), -1.00(3B), -30.73(1B), and -35.85(1B).

$\delta^{1}H$-{^{11}B} : 5.27, 3.67, 3.66, 3.18, 3.10, 2.85, 2.64, 0.51, and 0.45 (all B-H); -0.10, -2.80, and -3.34 (all B-H-B).

$\delta^{31}P$-{^{1}H} : 26.9.

Microanalysis	%C	%H
Calculated for $C_{21}H_{34}AuB_{10}P$:	40.5	5.51
Found :	40.4	5.49

6.4.2 Reaction of 5,6-μ-(Cy$_3$PAu)-*nido*-$B_{10}H_{13}$ and Hydrogen Chloride.

$Cy_3PAuB_{10}H_{13}$ (0.450 g, 0.752 mmol) was suspended in dichloromethane (20 ml), and cooled to 0°C. Hydrogen chloride gas was bubbled through the suspension for thirty minutes, then the gas flow was stopped, and the reaction allowed to stir for a further eighteen hours. Removal of the solvent *in vacuo* gave a colourless powder. The only species present in the ^{31}P-{^{1}H} and ^{11}B-{^{1}H}

n.m.r. spectra were $AuCl(PCy_3)$ and $B_{10}H_{14}$ respectively.

6.4.3 Synthesis of $[(Cy_3P)_2Au]^+ [(B_{10}H_{12})_2Au]^-$.

See also Section 6.4.8, below, for alternative routes. $Cy_3PAuB_{10}H_{13}$ (0.124 g, 0.208 mmol) was suspended in acetonitrile (20 ml) and the solution refluxed for one hour, during which time the solution slowly went yellow and then red, accompanied by dissolution of the suspended material. The solution was then filtered hot, and the filtrate cooled to 0 °C whereupon a brownish-yellow crystalline precipitate was obtained. This was filtered off and washed with ether. Crystallisation from dichloromethane/hexane yielded bright yellow crystals of $[(Cy_3P)_2Au]^+ [(B_{10}H_{12})_2Au]^-$.

Yield = 0.075 g, 30 % Au incorporated into cage.

N.M.R. parameters/ppm (in CD_2Cl_2)

$\delta^{11}B-\{^1H\}$: 17.16(2B), 16.64(1B) (sh.), 15.13(2B), 4.96(1B), 2.50(2B), and -22.56(2B).

$\delta^1H-\{^{11}B\}$: 3.77, 3.30, 3.17, 2.79, 2.69, and 1.87 (all B-H); and -1.96 (B-H-B).

$\delta^{31}P-\{^1H\}$: 65.04.

Microanalysis	%C	%H
Calculated for $C_{36}H_{90}Au_2B_{20}P_2$:	36.2	7.59
Found :	35.9	7.48

6.4.4 Synthesis of $[NHEt_3]^+ [Cy_3PAuB_{10}H_{12}]^-$.

See also Section 6.4.5 for an alternative method using KOH. $Cy_3PAuB_{10}H_{13}$ (0.4747 g, 0.794 mmol) was suspended in dichloromethane (20 ml) and to it was added, dropwise, triethylamine (0.080 g, 0.791 mmol) in dichloromethane (10 ml).

The initially colourless solution instantly went yellow, and then orange along with dissolution of the colourless suspension. Once the solution was cherry-red,

and all the suspension had dissolved, the solvent was removed *in vacuo* to yield an orange powder. Red crystals were then obtained by diffusion of hexane into a dichloromethane solution.

Yield : quantitative.

N.M.R. Parameters/ppm (in CD_2Cl_2)

$\delta^{11}B$-{^1H} : 3.74(2B), -6.38(1B), -9.69(2B), -10.99(2B), -28.18(1B), -31.07(2B).

$\delta^{1}H$-{^{11}B} : 2.92, 1.79, 1.77, 1.73, 0.63, 0.51 (all B-H), -4.80 (B-H-B).

$\delta^{31}P$-{^1H} : 60.9.

Microanalysis	%C	%H	%N
Calculated for $C_{24}H_{61}AuB_{10}NP$:	40.1	9.07	2.03
Found:	40.3	8.74	1.98

6.4.5 Synthesis of $[PhCH_2NMe_3]^+$ $[Cy_3PAuB_{10}H_{12}]^-$ and $(B_{10}H_{12}Au)(AuPCy_3)_3$ using KOH/MeOH.

See also Sections 6.4.4 and 6.4.13 for alternative syntheses of the $[Cy_3PAuB_{10}H_{12}]^-$ anion and $(B_{10}H_{12}Au)(AuPCy_3)_3$ respectively. $Cy_3PAuB_{10}H_{13}$ (0.300g, 0.500 mmol) was suspended in methanol (20 ml) and to it was added KOH (0.080g, 2.22 mmol). The solution slowly went orange, with concomitant dissolution of the suspension.

The reaction was stirred overnight, and then the solution was filtered. The precipitate was dissolved in the minimum of dichloromethane and hexane layered on top. Red crystals of $(B_{10}H_{12}Au)(AuPCy_3)_3$ slowly grew as the hexane diffused into the solution. These were identified by measuring the unit cell of the crystals, and comparing it against that previously obtained (from the product obtained in Section 6.4.13, below).

The filtrate was added to an aqueous solution of excess benzyltrimethylammonium bromide, and the orange, crystalline precipitate was filtered off. A crystallisation from dichloromethane/hexane yielded red crystals.

Identified as benzyltrimethylammonium $[Cy_3PAuB_{10}H_{12}]^-$ by $^{31}P-\{^1H\}$ and $^{11}B-\{^1H\}$ n.m.r. spectroscopies.

Yield = 0.2695 g (72 %)

6.4.6 Reaction of $[NHEt_3]^+$ $[Cy_3PAuB_{10}H_{12}]^-$ with Trifluoroacetic Acid.

$[NHEt_3]^+$ $[Cy_3PAuB_{10}H_{12}]^-$ (0.323 g, 0.462 mmol) was dissolved in dichloromethane (20 ml) To the stirred solution was added CF_3CO_2H (0.460 mmol as a solution in dichloromethane),. The red solution instantly decolourised to a very pale yellow. Removal of the solvent *in vacuo* afforded a very pale yellow solid. The only species present in the $^{31}P-\{^1H\}$ n.m.r. spectrum was 5,6-μ-(Cy_3PAu)-*nido*-$B_{10}H_{13}$.

6.4.7 Synthesis of $(Cy_3PAu)_2B_8H_{10}$.

To a mixture of $AuMe(PCy_3)$ (0.1313g, 0.267 mmol) and $B_{10}H_{12}(PPh_3)_2$ (0.1834g, 0.285 mmol) was added dichloromethane (20 ml). Over a period of ca. 18 hours, the solution slowly went yellow. The solvent was then removed *in vacuo* to yield a yellow-white powder.

This was dissolved in the minimum of dichloromethane and chromatographed on an alumina column (6 cm) using thf as stationary phase and eluent. The yellow band was collected, and the solvent removed *in vacuo* to yield a yellow solid. Yellow crystals of $(Cy_3PAu)_2B_8H_{10}.H_2O$ were grown from this by diffusion of hexane into a concentrated dichloromethane solution.

Yield = 21.4 mg, 15.3%

N.M.R. Parameters/ppm (in CD_2Cl_2)

$\delta^{11}B-\{^1H\}$: 1.49(4B), -27.56(2B), and -21.86(2B)

$\delta^1H-\{^{11}B\}$: 4.44, 0.65, and 0.18 (all B-H); -2.90 (B-H-B)

$\delta^{31}P-\{^1H\}$: 68.93

6.4.8 Alternative Syntheses of $[(R_3P)_2Au]^+ [(B_{10}H_{12})_2Au]^-$.

There are a number of other routes by which this species can be synthesised, although the route described above in Section 6.4.3 is probably the easiest in terms of yield and ease of work-up. Coworkers[148] have examined the reaction of $AuCl(PPh_3)$ and $[NHEt_3]^+ [B_{10}H_{13}]^-$, and the other main route is as follows.

$Cy_3PAuB_{10}H_{13}$ (0.1028g, 0.172mmol) was suspended in dimethylsulphide (10 ml) and stirred for twenty-four hours during which time the suspension dissolved to yield a bright yellow solution. The solvent was removed *in vacuo* and the yellowy solid redissolved in dichloromethane and hexane layered on top. Crystals of $[(Cy_3P)_2Au]^+ [(B_{10}H_{12})_2Au]^-$ were grown, along with decomposition to an insoluble black residue. The crystals were identified by unit-cell measurements. Yield not measured owing to the mixed products formed.

6.4.9 Synthesis of $[(Cy_3P)_2Au]^+_2 [(B_{10}H_{12})Au(B_{10}H_{13})]^{2-}$.

To methyltricyclohexylphosphinegold(I) (0.7715g, 1.567 mmol) dissolved in dichloromethane was added, dropwise, a solution of decaborane (0.1913g, 1.567 mmol) in dichloromethane (10 ml) and this was washed in with dichloromethane (5 ml).

After stirring for thirty minutes, the solvent was reduced in volume *in vacuo*, and the off-white precipitate filtered off and washed with dichloromethane. The washings and filtrate were combined, and the solvent removed *in vacuo*. To the residue was added dichloromethane (5 ml), and the solution filtered. The solution was then put onto silica tlc plates (silica gel 60 F_{254}, pre-coated, layer thickness 0.25 mm) which had previously been washed with thf, and then the plates were eluted with thf. Band 1 (R_F = 0.90) was then removed from the silica with dichloromethane which was then removed *in vacuo*. Bright yellow

crystals of $[(Cy_3P)_2Au]^+_2$ $[(B_{10}H_{12})Au(B_{10}H_{13})]^{2-}$ were then grown by diffusion of hexane into a dichloromethane solution.

Yield not recorded but < 5%.

N.M.R. Parameters/ppm (in CD_2Cl_2)

$\delta^{11}B$-{^1H} : 16.30, 9.02, 8.07, 2.69, 1.35, -0.67, -9.33, -29.70, -30.51, -38.87.

δ^1H-{^{11}B} : μ-H resonances at : -1.85(1H), -3.75(1H), -4.12(2H), and -4.78(1H).

$\delta^{31}P$-{^1H} : 65.04.

Microanalysis	%C	%H
Calculated for $C_{72}H_{157}Au_3B_{20}P_4$:	44.3	8.10
Found :	45.0	8.64

6.4.10 Synthesis of $(B_{10}H_{12}Au)_2(AuPPh_3)_4$.

The direct reaction between $B_{10}H_{14}$ and $AuMe(PPh_3)$ is less satisfactory than the reaction between $Cy_3PAuB_{10}H_{13}$ and $AuMe(PPh_3)$, due to difficulties in the purification.

$Cy_3PAuB_{10}H_{13}$ (0.1017g, 0.170 mmol) was suspended in dichloromethane, and to it was added $AuMe(PPh_3)$ (0.1670g, 0.352mmol). Over a period of *ca.* twelve hours, the solution slowly went red, and gaseous evolution was noted.

The solvent was then removed *in vacuo*, and the red residue was redissolved in the minimum of dichloromethane, prior to being eluted on an alumina column (1.5 cm diameter, 6 cm long) using thf as stationary phase, and eluent. One red/brown band was collected, and the solvent removed. Dark red/black crystals were grown by diffusion of hexane into a dichloromethane solution.

Yield = 22.4 mg, 32%

N.M.R. Parameters/ppm (in CD_2Cl_2)

$\delta^{11}B$-{^1H} : 4.14(2B), -3.86(1B), -7.18(1B), -8.79(4B), -30.64(2B).

δ^1H-{^{11}B} : 3.04(2H), 2.15(1H), 2.00(1H), 1.80(2H), 0.97(2H), 0.83(2H), -4.38(2H).

$\delta^{31}P$-{^1H} : 48.03.

6.4.11 Synthesis of $(B_{10}H_{12}Au)_2(AuPCy_3)_4$

$B_{10}H_{14}$ (0.166g, 1.359mmol) and $AuMe(PCy_3)$ (0.8024g, 1.629mmol) were dissolved in dichloromethane, and stirred for two hours, during which time the solution went yellowy-orange, and gaseous evolution was noted. After filtering off the precipitated $Cy_3PAuB_{10}H_{13}$, the solvent was removed *in vacuo* to yield an orange-red solid. To this was added *ca.* dichloromethane (*ca.* 5 ml), and then, after filtration, the filtrate was chromatographed on silica t.l.c. plates (silica gel 60 F_{254} pre-coated layer thickness 0.25 mm) which had previously been washed with thf. Elution was with thf. The red/brown band, R_f = 0.60 - 0.65, was collected and removed from the silica with dichloromethane. The dichloromethane was removed *in vacuo* to yield a dark red solid. Red-black crystals of $(B_{10}H_{12}Au)_2(AuPCy_3)_4$ were grown from dichloromethane/hexane.

Yield < 5%

N.M.R. Parameters/ppm (in CD_2Cl_2)

$\delta^{11}B$-$\{^1H\}$, and δ^1H-$\{^{11}B\}$: see text, Chapter 5, page 158.

$\delta^{31}P$-$\{^1H\}$: 43.04.

No microanalysis obtained due to the low yield.

6.4.12 Reaction of $(B_{10}H_{12}Au)_2(AuPPh_3)_4$ with Hydrogen Chloride.

$(B_{10}H_{12}Au)_2(AuPPh_3)_4$ (0.065g, 0.0213mmol) was dissolved in dichloromethane (20 ml), and hydrogen chloride gas bubbled into the solution for fifteen minutes, during which time the red colour of the solution faded. The gas flow was then stopped, and the solvent removed *in vacuo* to yield an off-white solid. The only signal in the ^{31}P-$\{^1H\}$ n.m.r. spectrum was assigned as due to $AuCl(PPh_3)$.

6.4.13 Synthesis of $(B_{10}H_{12}Au)(AuPCy_3)_3$.

See also Section 6.4.5 for an alternative method using KOH. $[NHEt_3]^+[Cy_3PAuB_{10}H_{12}]^-$ (0.407g, 0.583 mmol) was dissolved in dichloromethane (20 ml) and stirred at room temperature for five days. The solvent was then removed *in vacuo* and the red oily residue redissolved in the minimum of dichloromethane.

This was then chromatographed on silica t.l.c. plates (silica gel 60 F_{254}, pre-coated layer thickness 0.25 mm) which had previously been washed with thf. Elution was with thf, and several bands were observed. Band 1, R_f = 1.0 was brown, and removed from the silica with dichloromethane. This was then removed *in vacuo* and red crystals of $(B_{10}H_{12}Au)(AuPCy_3)_3$ grown by diffusion of hexane into a dichloromethane solution.

Yield minimal. Owing to small amount produced, no microanalysis was obtained.
N.M.R. Parameters/ppm (in CD_2Cl_2)
$\delta^{31}P\text{-}\{^1H\}$: -52.86

Note that this spectrum was obtained after pulsing the sample for 17 hours. Due to this, the $^{11}B\text{-}\{^1H\}$ and $^1H\text{-}\{^{11}B\}$ n.m.r. spectra were not obtained.

6.5 Crystallographic Determinations.

This is a brief description of the general procedures used to solve and refine the structures reported herein. The discussion on each structure is in the relevant Chapter, and all the crystallographic tables (fractional coordinates, bond lengths and angles, etc.) are listed in Appendix 2. To aid the reader, Table 6.1,page189, lists the cross-references so that the rest of the work may be put together.

All intensity data were collected on an Enraf-Nonius CAD4 diffractometer equipped for low-temperature operation and using graphite-monochromated Mo-K_α *X* radiation, λ = 71.069 pm. Diffraction-quality crystals of all complexes

were grown by the diffusion of hexane into a dichloromethane solution of the material.

Data Collection and Processing.

ω-2θ scans in 96 steps with ω scan width = 0.8 + 0.35tanθ (except for the structure of the $[B_{10}H_{13}]^-$ anion, where scan width was 0.8 + 0.34tanθ). Variable scan speeds, no. of data measured, and no. of data subsequently used are listed in in the section in Appendix 2 for the individual structure. Crystal movement was not usually observed, and if crystal decay was noted, it was corrected (computer program *CADABS* [150]). The data were corrected for Lorentz and polarisation effects (*CADABS*).

Structure Solution and Refinement.

In general, the structures were solved by locating the gold atom(s) first. Their positions were determined either by the interpretation of a Patterson map (generated by the computer program *SHELX76* [163]), or else automatic direct methods were used to locate the gold(s) directly (*SHELX86* [164]) The remaining atoms were located by subsequent ΔF syntheses (*SHELX76*) and iterative full-matrix least-squares refinement.

Once isotropic convergence was attained the data were empirically corrected for absorption effects (*DIFABS* [151]). Au, P, B, and if the data : variable ratio permitted, C atoms were all allowed anisotropic thermal motion. Phenyl rings were constrained to be planar with equal bond lengths and angles (C-C = 139.5 pm, C-C-C = 120^0). Disorder, if present, was modelled as discussed in the text. Organic H atoms were set in calculated positions (C-H = 108 pm), and refined with one overall group thermal parameter. Cage H atoms were sometimes located and satisfactorily refined, or else were set in calculated positions (CALC [107]) where each atom was positioned 118 pm away from the boron atom to which it

was bonded, along the vector from the cluster centroid to the boron atom in question. Again, these H atoms were refined with one overall group thermal parameter.

The data were weighted using the formula $w^{-1} = [\sigma^2(F) + g(F)^2]$ and g was refined to convergence. Its value is given in Appendix 2 for each structure.

Scattering factors for C, H, O, N, Cl and B are inlaid in *SHELX76*, those for Au were from *International Tables*[165]. Geometrical calculations were carried out by CALC, as discussed in Chapter 1. Tables were formed by *TABLES*[166] or *SCTABLES*[166] and diagrams were produced by *EASYORTEP*[167], a modified version of *ORTEP-II*[168]. Tables of observed and calculated structure factors were modified from those obtained from *SHELX76* by using *LATOPO*[166], and are available from the author.

Table 6.1. Where to Find the Crystallographic Work in this Thesis.

Structure	Figure	Text	Bonds/Angles	Structure Details
5,6-μ-(Cy_3PAu)- *nido*-$B_{10}H_{13}$	37	36	60, 208	204
5,6-μ-(*o*-tolyl$_3$PAu)- *nido*-$B_{10}H_{13}$	47	46	62, 215	211
$[PhCH_2NMe_3]^+$ $[B_{10}H_{13}]^-$	66	65	105, 220	217
$[NHEt_3]^+$ $[Cy_3PAuB_{10}H_{12}]^-$	71	70	106, 227	223
$(Cy_3PAu)_2B_8H_{10}$	84	93	111, 234	230
$[(Cy_3P)_2Au]^+_2$ $[(B_{10}H_{12})Au(B_{10}H_{13})]^{2-}$	115, 117	114	140, 141, 240	235
$[($*o*-tolyl$_3$P$)_2$Au$]^+$ $[(B_{10}H_{12})_2Au]^-$	125	123	142, 247	243
$[(Cy_3P)_2Au]^+$ $[(B_{10}H_{12})_2Au]^-$	128	126	143, 144, 255	250
$(B_{10}H_{12}Au)_2(AuPPh_3)_4$	153, 155	152	169, 172, 266	261
$(B_{10}H_{12}Au)(AuPCy_3)_3$	162	161	175, 276	270

Conclusions.

Most of the synthetic methodology developed for this thesis is summarised in Scheme 4, overleaf. The acid/base chemistry is outlined in Scheme 5, as a catalytic cycle. It has been shown that the gold-methyl/neutral borane route to auraboranes results in a variety of products, and by carefully controlling the reaction conditions, different products can be obtained. It is probably worth extending this synthetic approach to other transition metals.

Structurally, the η^4-$\{B_{10}H_{12}\}$ fragment predominates, although there are examples of η^2 and η^3 bonding modes. Another notable feature of most of these systems is the steric protection given to the open face of the cluster by the substituents on the gold ligated to the cage (whether $\{PCy_3\}$ or $\{AuPPh_3\}$).

The structures show distinct trends, based upon the formal oxidation state of the gold bonded to the cage. If it is Au(I), then the gold does not perturb the cage architecture away from that of the parent borane i.e. it can always be described as a bridge. If it is Au(III), then the gold is formally square-planar, and is a two-orbital source for cage bonding. However, the structure is not fully eleven-vertex because of this.

It has also been shown that the 'idealisation' technique is a valid method of analysing the structures of these complexes, and it is sufficiently sensitive to discover differences in the structures which had previously gone unnoticed (the late transition metal sub-group metallaboranes).

Based on this methodology, it should now be possible to critically re-examine the structures of all of the metallaboranes, and thus to reappraise the role of the 'electron-counting' rules in metallaborane chemistry.

Scheme 4. The Syntheses and Relationships Between the Auraboranes.

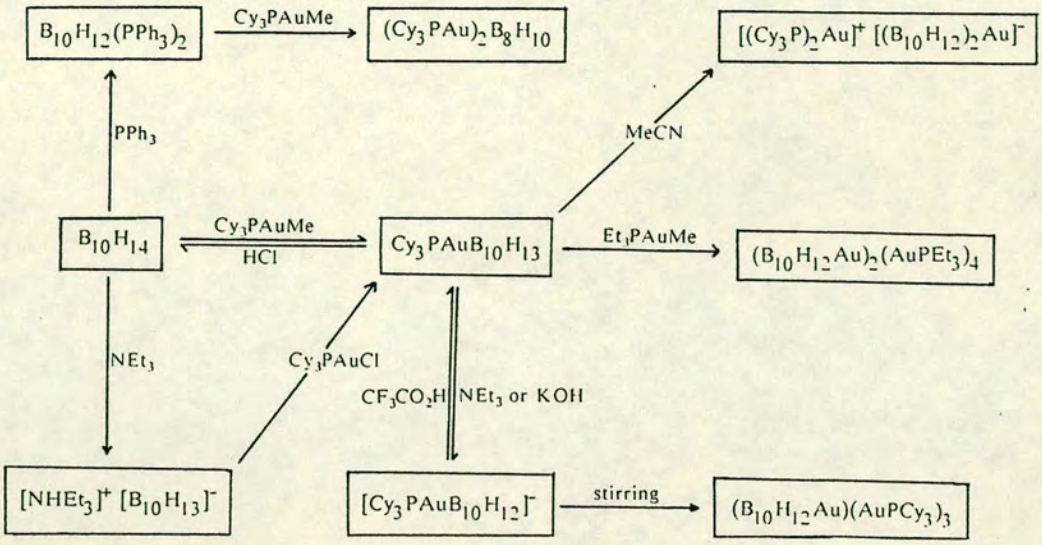

Scheme 5. The Acid/Base Chemistry of 5,6-μ-(Cy_3PAu)-*nido*-$B_{10}H_{13}$ and the $[Cy_3PAuB_{10}H_{12}]^-$ Anion.

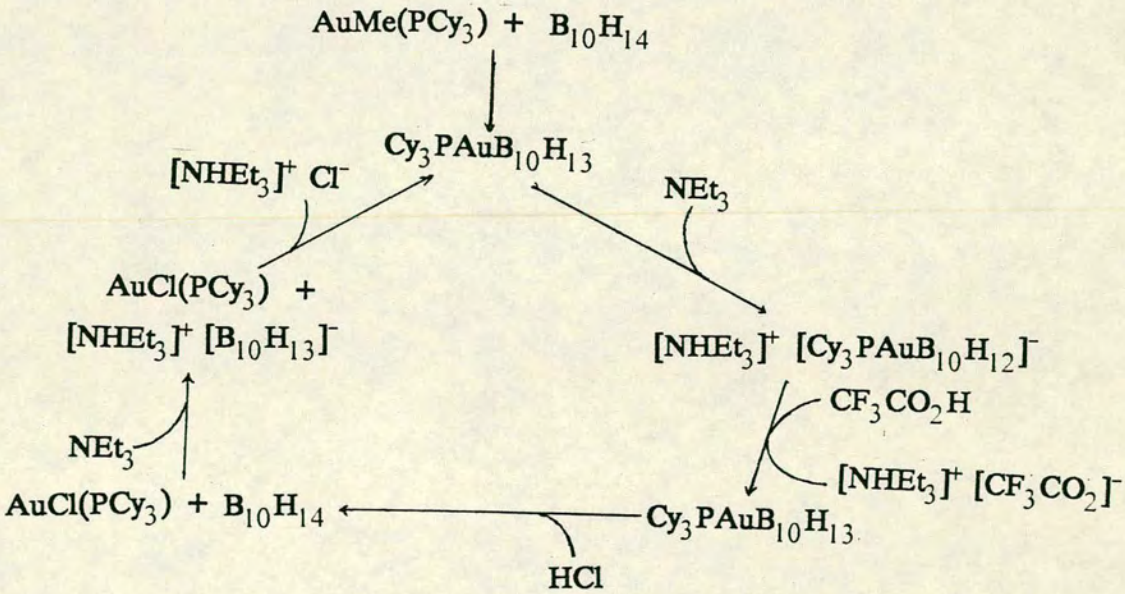

References.

1. N.V.Sidgwick, *The Chemical Elements and their Compounds,* Oxford University Press, 1950, **1**, 338.

2. A.Stock, *The Hydrides of Boron and Silicon,* Cornell University Press, New York, 1933.

3. W.N.Lipscomb, *Boron Hydrides,* Benjamin, New York, 1963.

4. K.Wade, *Adv. Inorg. Chem. Radiochem.,* 1976, **18**, 1.

5. R.W.Rudolph, *Acc. Chem. Res.,* 1976, **9**, 446.

6. R.E.Williams, *Inorg. Chem.,* 1971, **10**, 211.

7. K.Wade, *J. Chem. Soc., Chem. Commun.,* 1971, 792.

8. D.M.P.Mingos, *Acc. Chem. Res.,* 1984, **17**, 311.

9. K.P.Callahan, and M.F.Hawthorne, *Adv. Organomet. Chem.,* 1976, **14**, 145.

10. M.E.O'Neill, and K.Wade, in *Metal Interactions with Boron Clusters,* ed. R.N.Grimes, New York, 1982, chapter 1.

11. C.E.Housecroft, and T.P.Fehlner, *Adv. Organomet. Chem.,* 1981, **21**, 57.

12. G.K.Barker, M.Green, F.G.A.Stone, A.J.Welch, T.P.Onak, and G.Siwapanyoyos, *J. Chem. Soc., Dalton Trans.,* 1979, 1687.

13. M.Green, J.L.Spencer, and F.G.A.Stone, *J. Chem. Soc., Dalton Trans.,* 1979, 1679.

14. D.M.P.Mingos, *J. Chem. Soc., Dalton Trans.,* 1977, 602.

15. S.K.Boocock, N.N.Greenwood, J.D.Kennedy, W.S.M^{c}Donald, and J.Staves, *J. Chem. Soc., Dalton Trans.,* 1981, 2573.

16. J.E.Crook, M.Elrington, N.N.Greenwood, J.D.Kennedy, and J.D.Woollins, *Polyhedron,* 1984, **3**, 901.

17. J.E.Crook, M.Elrington, N.N.Greenwood, J.D.Kennedy, M.Thornton-Pett, and J.D.Woollins, *J. Chem. Soc., Dalton Trans.,* 1985, 2407.

18. H.Fowkes, N.N.Greenwood, J.D.Kennedy, and M.Thornton-Pett, *J. Chem.*

Soc., Dalton Trans., 1986, 517.

19. N.N.Greenwood, in *Comprehensive Inorganic Chemistry*, eds. J.C.Bailar Jnr., N.J.Emelius, R.Nyholm, and A.F.Trotman-Dickenson, Pergamon, New York, 1973, **1**, chapter 11.

20. R.N.Grimes, in *Comprehensive Organometallic Chemistry*, eds. G.Wilkinson, F.G.A.Stone, and E.W.Abel, Pergamon, New York, 1982, **1**, chapter 5.5.

21. N.N.Greenwood, and D.N.Sharrocks, *J. Chem. Soc. (A)*, 1969, 2334.

22. M.F.Hawthorne, A.R.Pitochelli, R.D.Strahm, and J.J.Miller, *J. Am. Chem. Soc.*, 1960, **82**, 1825.

23. M.F.Hawthorne, and A.R.Pitochelli, *J. Am. Chem. Soc.*, 1959, **81**, 5519.

24. R.J.Pace, J.Williams, and R.L.Williams, *J. Chem. Soc.*, 1961, 2196.

25. L.E.Benjamin, S.F.Stafiej, and E.A.Takacs, *J. Am. Chem. Soc.*, 1963, **85**, 2674.

26. V.D.Aftandilian, H.C.Miller, G.W.Parshall, and E.L.Muetterties, *Inorg. Chem.*, 1962, **1**, 734.

27. E.L.Muetterties, *Inorg. Chem.*, 1963, **2**, 647.

28. R.H.Cragg, M.S.Fortuin, and N.N.Greenwood, *J. Chem. Soc. (A)*, 1970, 1817.

29. J.Reddy, and W.N.Lipscomb, *J. Chem. Phys.*, 1959, **31**, 610.

30. A.Baidana, N.V.Podberezskayo, V.V.Volkov, and S.V.Borisov, *Zh. Strukt. Khim.*, 1978, **19**, 550.

31. D.E.Sands, and Z.Zalkin, *Acta Crystallogr.*, 1962, **15**, 410.

32. T.L.Heying, J.W.Ager Jr., S.L.Clark, D.J.Mangold, H.L.Goldstein, M.Hillman, R.J.Polak, and J.W.Szmanski, *Inorg. Chem.*, 1963, **2**, 1089.

33. W.H.Knoth, and E.L.Muetterties, *J. Inorg. Nucl. Chem.*, 1961, **20**, 66.

34. B.Stibr, J.Plesek, and S.Hermanek, *Coll. Czech. Chem. Commun.*, 1969, **34**, 194.

35. J.Plesek, S.Hermanek, and B.Stibr, *Coll. Czech. Chem. Commun.*, 1968, **33**, 691.

36. I.Dunstan, R.L.Williams, and N.J.Blay, *J. Chem. Soc.*, 1960, 5012.

37. M.Hillman, *J. Am. Chem. Soc.*, 1960, **82**, 1096.

38. N.J.Blay, R.J.Pace, and R.L.Williams, *J. Chem. Soc.*, 1962, 3416.

39. H.Schroeder, *Inorg. Chem.*, 1963, **2**, 390.

40. L.J.Todd in ref. 10, chapter 4.

41. A.Arafat, J.Baer, J.C.Huffman, and L.J.Todd, *Inorg. Chem.*, 1986, **25**, 3757.

42. K.Base, J.Plesek, S.Hermanek, J.Huffman, P.Ragatz, and R.Schaeffer, *J. Chem. Soc., Chem. Commun.*, 1975, 934.

43. K.Base, F.Hanousek, J.Plesek, and B.Stibr, *J. Chem. Soc., Chem. Commun.*, 1981, 1162.

44. W.R.Hertler, F.Klanberg, and E.L.Muetterties, *Inorg. Chem.*, 1967, **6**, 1696.

45. A.R.Siedle, G.M.Bodner, A.R.Garber, and L.J.Todd, *Inorg. Chem.*, 1974, **13**, 1756.

46. W.R.Pretzer, and R.W.Rudolph, *J. Am. Chem. Soc.*, 1973, **95**, 931.

47. J.L.Little, S.S.Pao, and K.K.Sugatha, *Inorg. Chem.*, 1974, **13**, 1752.

48. J.D.Kennedy, (a) *Prog. Inorg. Chem.*, 1984, **32**, 519; (b) 1986, **34**, 211 and references therein.

49. N.N.Greenwood, and I.M.Ward, *Chem. Soc. Rev.*, 1974, **3**, 231.

50. N.N.Greenwood, and N.F.Travers, *J. Chem. Soc., Chem. Commun.*, 1967, 216.

51. T.E.Paxson, and M.F.Hawthorne, *Inorg. Chem.*, 1975, **14**, 1604.

52. J.W.Lott, and D.F.Gaines, *J. Am. Chem. Soc.*, 1973, **95**, 3042.

53. S.J.Lippard, and K.M.Melmed, *Inorg. Chem.*, 1969, **8**, 2755.

54. J.T.Gill, and S.J.Lippard, *Inorg. Chem.*, 1975, **14**, 751.

55. R.D.Dobrett, and W.N.Lipscomb, *J. Chem. Phys.*, 1962, **37**, 1779.

56. N.N.Greenwood, J.A.M^{c}Ginnety, and J.D.Owen, *J. Chem. Soc., Dalton Trans.*, 1972, 989.

57. N.N.Greenwood, and N.F.Travers, *J. Chem. Soc. (A)*, 1967, 880.

58. N.N.Greenwood, and N.F.Travers, *J. Chem. Soc. (A)*, 1968, 15.

59. N.N.Greenwood, and J.A.Howard, *J. Chem. Soc., Dalton Trans.*, 1976, 177.

60. C.M.Mitchell, and F.G.A.Stone, *J. Chem. Soc., Chem. Commun.*, 1970, 1263.

61. C.P.Magee, L.G.Sneddon, D.C.Beer, and R.N.Grimes, *J. Organomet. Chem.*, 1975, **86**, 159.

62. G.K.Barker, N.R.Godfrey, M.Green, H.E.Parge, F.G.A.Stone, and A.J.Welch, *J. Chem. Soc., Chem. Commun.*, 1983, 277.

63. S.Bresadola in ref. 10, chapter 5, p.227.

64. L.F.Warren, and M.F.Hawthorne, *J. Am. Chem. Soc.*, 1968, **90**, 4823.

65. (a) H.M.Colquhoun, T.J.Greenhough, and M.G.H.Wallbridge, *J. Chem. Soc., Chem. Commun.*, 1976,1019; (b) H.M.Colquhoun, T.J.Greenhough, and M.G.H.Wallbridge, *J. Chem. Soc., Dalton Trans.*, 1978, 303.

66. H.M.Colquhoun, T.J.Greenhough, and M.G.H.Wallbridge, *J. Chem. Soc., Chem. Commun.*, 1980, 192.

67. H.M.Colquhoun, T.J.Greenhough, and M.G.H.Wallbridge, *Acta Crystallogr. Sect. B*, 1977, **33**, 3604.

68. ref. 10, pp 26-33.

69. E.L.Muetterties, W.G.Peet, P.A.Wagner, and C.W.Alegranti, *Inorg. Chem.*, 1970, **9**, 2447.

70. F.Klanberg, E.L.Muetterties, and L.J.Guggenberger, *Inorg. Chem.*, 1968, **7**, 2272.

71. N.N.Greenwood, and I.Staves, *J. Chem. Soc., Dalton Trans.*, 1978, 1144.

72. *C.R.C. Handbook of Chem. and Physics*, 62nd edition, ed. R.C.Weast, Chemical Rubber Publishing Co., Boca Raton, Florida, 1983 pp.D-133.

73. K.P.Hall, and D.M.P.Mingos, *Prog. Inorg. Chem.*, 1984, **32**, 237.

74. G.Schmid, R.Pfail, R.Boese, F.Bandermann, S.Meyer, G.H.M.Calis, and J.A.W. van der Velden, *Chem. Ber.*, 1981, **11**, 4634.

75. ref. 48(b), p.374.

76. M.A.Beckett, J.E.Crook, N.N.Greenwood, and J.D.Kennedy, *J. Chem. Soc.,*

Dalton Trans., 1984, 1427.

77. R.Hoffmann, *Angew. Chem. Int. Ed. Engl.*, 1982, **21**, 711.

78. C.E.Housecroft, and A.L.Rheingold, *Organometallics*, 1987, **6**, 1332.

79. L.W.Bateman, M.Green, K.A.Mead, R.M.Mills, I.D.Salter, F.G.A.Stone, and P.Woodward, *J. Chem. Soc., Dalton Trans.*, 1983, 2599.

80. C.P.Horowitz, E.M.Holt, C.P.Brock, and D.F.Shriver, *J. Am. Chem. Soc.*, 1985, **107**, 8136, and refs. therein.

81. N.W.Alcock, L.Parkhill, and M.G.H.Wallbridge, *Acta Crystallogr. Sect. C*, 1985, **41**, 716.

82. S.E.Robins, *Honours Project Report*, University of Edinburgh, 1984.

83. A.J.Wynd, S.E.Robins, D.A.Welch, and A.J.Welch, *J. Chem. Soc., Chem. Commun.*, 1985, 819.

84. D.M.P.Mingos, *J. Chem. Soc., Dalton Trans.*, 1976, 1163.

85. P.Bellon, M.Manassero, and M.Sansoni, *J. Chem. Soc., Dalton Trans.*, 1973, 2423.

86. C.E.Briant, K.P.Hall, and D.M.P.Mingos, *J. Organomet. Chem.*, 1983, **254**, C18.

87. J.A.Schuerman, F.R.Fronczak, and J.Selbin, *J. Am. Chem. Soc.*, 1986, **108**, 336.

88. J.W.A. van der Velden, J.J.Bour, J.J.Steggerda, P.T.Beurskens, M.Roseboum, and J.H.Noordik, *Inorg. Chem.*, 1982, **21**, 4321.

89. D.M.P.Mingos, *Gold Bull.*, 1984, **17**, 5.

90. M.Bown, X.L.R.Fontaine, N.N.Greenwood, P.MacKinnon, J.D.Kennedy, and M.Thornton-Pett, *J. Chem. Soc., Chem. Commun.*, 1987, 442.

91. M.Bown, X.L.R.Fontaine, N.N.Greenwood, P.MacKinnon, J.D.Kennedy, and M.Thornton-Pett, *J. Chem. Soc., Dalton Trans.*, 1987, 2781.

92. H.C.Kang, Y.Do, C.B.Knobler, and M.F.Hawthorne, *J. Am. Chem. Soc.*, 1987, **109**, 6530.

93. A.J.Wynd, and A.J.Welch, unpublished work.

94. C.A.Tolman, *Chem. Rev.*, 1977, **77**, 413.

95. J.D.Kennedy, and B.Wrackmeyer, *J. Magn. Reson.*, 1980, **38**, 529.

96. A.Bax, and R.Freeman, *J. Magn. Reson.*, 1981, **42**, 164; 1981, **44**, 542.

97. T.L.Venable, W.C.Hutton, and R.N.Grimes, *J. Am. Chem. Soc.*, 1982, **104**, 4716.

98. T.L.Venable, W.C.Hutton, and R.N.Grimes, *J. Am. Chem. Soc.*, 1984, **106**, 29.

99. R.Benn, and H.Gunther, *Angew. Chem. Int. Ed. Engl.*, 1983, **22**, 350.

100. E.A.V.Ebsworth, D.W.H.Rankin, and S.Craddock, *Structural Methods in Inorg. Chem.*, Blackwell Scientific, London, 1987.

101.The following debate illustrates this: (a) R.T.Baker, *Inorg. Chem.*, 1986, **25**, 109. (b) J.D.Kennedy, *Inorg. Chem.*, 1986, **25**, 111. (c) R.J.Johnson, and D.M.P.Mingos, *Inorg. Chem.*, 1986, **25**, 3321.

102. N.N.Greenwood, and T.C.Gibb, *Mossbauer Spectroscopy*, Chapman and Hall, London, 1971.

103. G.M.Bancroft, *Mossbauer Spectroscopy*, M^{c} Graw-Hill, London, 1973.

104. H.Schmidbaur, C.Hartmann, and F.E.Wagner, *Angew. Chem. Int. Ed. Engl.*, 1987, **26**, 1148.

105. J.Howell, A.Rossi, D.Wallace, K.Haraki, and R.Hoffmann, ICON, Quantum Chemistry Program Exchange, Univ. Indiana, 1977, no. 344.

106. J.H.Ammeter, H-B.Burgi, J.C.Thibeault, and R.Hoffmann, *J. Am. Chem. Soc.*, 1982, **100**, 3686.

107. R.O.Gould, and P.Taylor, University of Edinburgh, 1988.

108. G.F.Mitchell, and A.J.Welch, *J. Chem. Soc.,Dalton Trans.*, 1987, 1017.

109. R.Brill, H.Dietrich, H.Dierks, *Acta Crystallogr. Sect. B*, 1971, **27**, 2003.

110. D.S.Kendall, and W.N.Lipscomb, *Inorg. Chem.*, 1973, **12**, 546.

111. C.J.Fritchie, *Inorg. Chem.*, 1967, **6**, 1199.

112. A.J.Wynd, and A.J.Welch, *Acta Crystallogr. Sect. C*, submitted.

113. A.J.Wynd, A.J.M^{c}Lennan, D.Reed, and A.J.Welch, *J. Chem. Soc., Dalton Trans.*, 1987, 2761.

114. N.N.Greenwood, and A.Earnshaw, *Chemistry of the Elements*, Pergamon Press, Oxford, 1984, p.70.

115. R.A.Schunn, chapter 5 of *Transition Metal Hydrides*, ed. E.L.Muetterties, Marcel Dekker, New York 1971.

116. R.J.Puddephatt, in *Comprehensive Organometallic Chemistry*, eds. G.Wilkinson, F.G.A.Stone, and E.W.Abel, Pergamon, New York, 1982, **2**, chapter 15.

117. J.A.Muir, M.M.Muir, L.B.Pulgar, and G.M.Sheldrick, *Acta Crystallogr. Sect. C*, 1985, **41**, 1174.

118. J.A.Muir, M.M.Muir, and E.Lorca, *Acta Crystallogr. Sect. B*, 1980, **36**, 931.

119. C.E.Briant, R.W.M.Wardle, and D.M.P.Mingos, *J. Organomet. Chem.*, 1984, **267**, C49.

120. D.M.P.Mingos, and R.W.M.Wardle, *J. Chem. Soc., Dalton Trans.*, 1986, 73.

121. D.C.Finster, and R.N.Grimes, *Inorg. Chem*, 1981, **20**, 863.

122. J.L.Wardell in *Comprehensive Organometallic Chemistry*, eds. G.Wilkinson, F.G.A.Stone, and E.W.Abel, Pergamon, New York, 1982, **2**, chapter 17.

123. M.Brookhart, and M.L.H.Green, *J. Organomet. Chem.*, 1983, **250**, 395.

124. J.D.Kennedy, and J.Staves, *Z. Naturforsch., Teil. B*, 1979, **34**, 808.

125. R.L.Pilling, F.N.Tebbe, M.F.Hawthorne, and E.A.Pier, *Proc. Chem. Soc.*, 1964, 402 ; P.C.Keller, D.Maclean, and R.O.Schaeffer, *Chem. Commun.*, 1965, 204.

126. e.g. D.Reed, *J. Chem. Research (S)*, 1984, 198.

127. R.V.Parish, *Hyperfine Interactions*, 1988, **40**, 159.

128. R.O.Gould, and P.Taylor, University of Edinburgh, 1987.

129. A.R.Siedle, G.M.Bodner, and L.J.Todd, *J. Inorg. Nucl. Chem.*, 1971, **33**, 3671.

130. L.G.Sneddon, J.C.Huffman, R.O.Schaeffer, and W.E.Streib, *J. Chem. Soc.*,

Chem. Commun., 1972, 474.

131. ref. 48(b), p.326.

132. G.Shoham, D.Schomburg, and W.N.Lipscomb, *Cryst. Struc. Commun.*, 1980, **9**, 429.

133. Ref 48(b), page 353; J.E.Crook, Ph.D. thesis, University of Leeds, 1982; M.Thornton-Pett, University of Leeds, personal communication.

134. X.L.R.Fontaine, H.Fowkes, N.N.Greenwood, J.D.Kennedy, and M.Thornton-Pett, *J. Chem. Soc.,Chem. Commun*., 1985, 1165.

135. L.J.Guggenberger, *J. Am. Chem. Soc*., 1972, **94**, 114.

136. J.E.Crook, N.N.Greenwood, J.D.Kennedy, W.S.M^{c}Donald, *J. Chem. Soc., Dalton Trans*., 1984, 2487.

137. A.J.Wynd, and A.J.Welch, *J. Chem. Soc., Chem. Commun.*, 1987, 1174.

138. N.N.Greenwood, J.A.M^{c}Ginnety, J.D.Owen, *J. Chem. Soc.(A)*, 1971, 809.

139. I.Fleming, *Frontier Orbitals and Organic Chemical Reactions*, Wiley-Interscience, 1985.

140. D.G.Evans, and D.M.P.Mingos, *J. Organomet. Chem.*, 1982, **232**, 171.

141. T.V.Baukova, Yu.L.Slovokhotov, and Yu.T.Strukhov, *J. Organomet. Chem.*, 1981, **220**, 125.

142. M.I.Forsyth, D.M.P.Mingos, and A.J.Welch, *J. Chem. Soc., Dalton Trans.*, 1978, 1363.

143. M.A.Beckett, J.D.Kennedy, and O.W.Howarth, *J. Chem. Soc., Chem. Commun.*, 1985, 855.

144. X.L.R.Fontaine, H.Fowkes, N.N.Greenwood, J.D.Kennedy, and M.Thornton-Pett, *J. Chem. Soc., Dalton Trans.*, 1987, 2417.

145. R.E.Enrione, F.P.de Boer, and W.N.Lipscomb, *Inorg. Chem.*, 1964, **3**, 1659; *J. Am. Chem. Soc.*, 1964, **86**, 1451.

146. J.B.Casey, W.J.Evans, and W.H.Powell, *Inorg. Chem.*, 1981, **20**, 1333.

147. ref. 48(b), pages 327, 348, 358, and 368.

148. T.D.Getman, J.A.Krause, and S.G.Shore, *Inorg. Chem.*, 1988, **27**(14), 2398.

149. A.J.McLennan, and A.J.Welch, unpublished work.

150. R.O.Gould, and D.E.Smith, University of Edinburgh, 1986.

151. N.G.Walker, and D.Stuart, *Acta Crystallogr., Sect. A*, 1983, **39**, 158.

152. F.Demartin, M.Manassero, L.Naldini, R.Ruggeri, and M.Sansoni, *J. Chem. Soc., Chem. Commun.*, 1981, 222.

153. J.W.A. van der Velden, J.J.Bour, R.Pet, W.P.Bosman, and J.H.Noordik, *Inorg. Chem.*, 1983, **22**, 3112.

154. J.W.A. van der Velden, J.J.Bour, F.A.Vollenbroek, P.T.Beurskens, and J.M.M.Smits, *J. Chem. Soc., Chem. Commun.*, 1979, 1162.

155. Y.L.Slovokhotov, and Y.T.Struchkov, *J. Organomet. Chem.*, 1984, **277**, 143.

156. B.Chiari, O.Piovesana, T.Taranteli, and P.F.Zanazzi, *Inorg. Chem.*, 1985, **24**, 366.

157. J.Beck, and J.Strahle, *Angew. Chemie, Int. Ed. Engl.*, 1986, **25**, 95.

158. B.J.Gregory, and C.K.Ingold, *J. Chem. Soc. (B)*, 1969, 276.

159. A.J.Carty, and A.Efraty, *Inorg. Chem*, 1969, **8**, 543.

160. H.Schmidbaur, Th.Pollock, R.Herr, F.E.Wagner, R.Bau, J.Riede, and G.Muller, *Organomets*, 1986, **5**, 566.

161. R.O.Schaeffer, *J. Am. Chem. Soc.*, 1957, **79**, 1006.

162. M.F.Hawthorne, and A.R.Pitochelli, *J. Am. Chem. Soc*, 1958, **80**, 6685.

163. G.M.Sheldrick, University of Cambridge, 1976.

164. G.M.Sheldrick, University of Gottingen, Federal Republic of Germany, 1986.

165. *International Tables for X-ray Crystallography*, Kynoch Press, Birmingham, 1974, **4**, 99.

166. P.Taylor, and R.O.Gould, University of Edinburgh, 1988.

167. P.R.Mallinson, University of Glasgow, 1982.

168. C.K.Johnson, Report ORNL-5138, Oak Ridge National Laboratory, Tennessee, U.S.A., 1976.

Appendix 1:

The Postgraduate Lecture Courses Attended.

(1) Diffraction Studies of DNA Fragments and an Introduction to the Cambridge Crystallographic Databases by Drs. T. Brown, O. Kennard, F. H. Allen, S. H. Bellard, D.G.Watson.

(2) N.m.r. Spectroscopy by Dr. I.H.Sadler.

(3) Mass Spectrometry by Prof. K.R. Jennings.

(4) X-ray Crystallography by Drs. A.J. Blake and R.O. Gould.

(5) Spectroelectrochemistry by Drs. L. Yellowlees and H.H.J. Girault.

(6) Introduction to Management by Prof. S.Coke, J.Fleck, F.Mitchell, and Dr. B.Schlegelmilch of the Department of Business Studies, University of Edinburgh.

(7) SCRIBE - an introduction to the document processing program by R. J. Hare.

(8) Transition Metal Group Meetings 1986/7.

(9) Inorganic Chemistry (Evening) Seminars 1985/6, 1986/7, 1987/8.

(10) U.S.I.C. Conferences 1986, and 1987.

(11) The Royal Society of Chemistry, Dalton Division, Scottish Meetings in 1986 and 1988.

(12) Intraboron VII and Intraboron VIII : the seventh and eighth national meetings of inorganic boron chemists, at Loch Lomond in 1987, and at the University of Cambridge in 1988, respectively.

(13) The Eleventh European Crystallographic Meeting in Vienna, Austria, from the 28th August to 2nd September 1988.

Additionally, there was the S.E.R.C. School of Crystallography in Jan. 1987 at the University of Aston in Birmingham.

Appendix 2:

Crystallographic Tables.

Introduction.

This appendix contains all of the tables derived from the crystallographic determinations discussed within the body of the thesis. An outline of the procedures used for these determinations can be found in Chapter 6, starting on page 187. This also includes a list of the computer programs used. Tables of observed and calculated structure factors for any structure reported here may be obtained from the author on request.

This appendix is organised in the following manner : each structure occupies one section of this appendix. The initial part of each section gives the experimental details about the structural determination - the unit cell dimensions, structure solution, unusual details about each model, etc. Following on from this are the crystallographic tables. Each Table is numbered in the form A2.n.x, where A2 refers to appendix 2, n is the structure number (see below), and x is the number of the particular table. The tables are all listed in the order (ie x =):-

1. Fractional coordinates of all non-hydrogen atoms.
2. Fractional coordinates of all hydrogen atoms. If these have errors then the H atom was refined, possibly subject to restraint (see the associated text). If no errors are given, then the atom was set in a calculated position.
3. Anisotropic thermal parameters.
4. Bond lengths and angles for all non-hydrogen atoms. If the complex is ionic there is a further division into the cation and anion (tables A2.n.4c and A2.n.4a respectively).
5. Bond lengths and angles involving the cage hydrogen atoms if the hydrogen atoms were included in the refinement.

A2.1 5,6-μ-(Cy_3PAu)-*nido*-$B_{10}H_{13}$.

The Molecular Structure and Associated Numbering Scheme for 5,6-μ-(Cy_3PAu)-*nido*-$B_{10}H_{13}$.

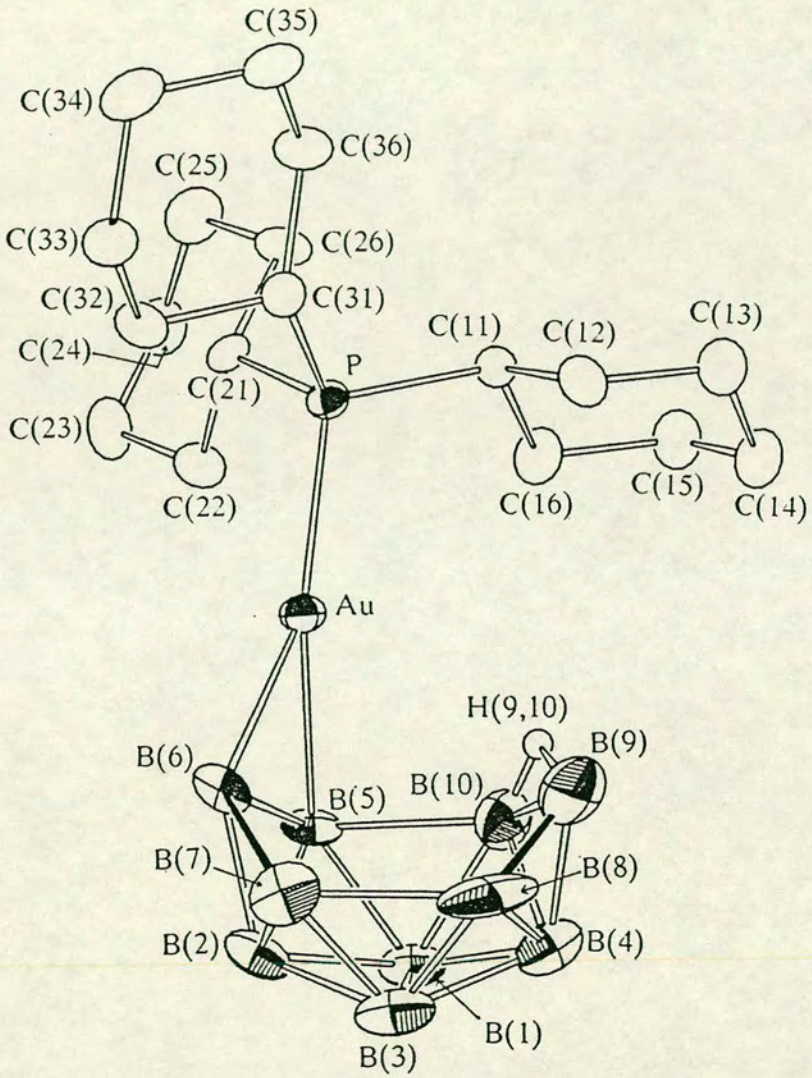

Crystal data. $C_{18}H_{46}AuB_{10}P$, M = 598.6, monoclinic, with a = 1.1598(3), b = 2.2459(4), c = 1.13943(21) nm, and β = 118.00(2)°. U = 2.6206 nm^3, D_x = 1.517 Mgm^{-3}, μ(Mo-K_α) = 5.451mm^{-1}, *F(000)* = 1191.83, Z = 4, and space group = $P2_1/a$

Data collection and processing. Θ_{max} = 28°, and $+h + k \pm l$. 5817 data were measured yielding 5577 unique (R_{merge} = 0.0255) of which 5442 with $F > 2\sigma(F)$ were retained. Variable scan speeds between 0.824 and 2.354 °min^{-1}. Slight crystal decay noted and corrected.

Structure solution and refinement. Starting-point for the refinement was the previously determined model. All Au, P, C, and B atoms allowed anisotropic thermal motion. Cyclohexyl H atoms group thermal parameter = 390(40) pm^2 at convergence. Terminal H atoms set in calculated positions (B-H = 118pm) and structure refined to convergence, then the process was repeated. Bridging H atoms set where found in ΔF synthesis. All refined with one group thermal parameter (760(100) pm^2 at convergence).

Weighting scheme $w^{-1} = [\sigma^2(F) + 0.000311(F)^2]$. R = 0.0458, R_w = 0.0668, S = 1.524. Data : variable = 20 : 1. Maximum residue and minimum trough were 455 enm^{-3} and -621 enm^{-3}. Maximum shift/e.s.d. in final cycle of least-squares refinement was 0.029.

Table A2.1.1. Fractional Coordinates of Refined Atoms in 5,6-μ-(Cy_3PAu)-*nido*-$B_{10}H_{13}$. U_{eq} in $10^4 pm^2$.

	x	y	z	U_{eq}
Au	0.19044(3)	0.231300(10)	0.42280(3)	0.02414(18)
P	0.18283(18)	0.13935(8)	0.32876(18)	0.0220(10)
B(1)	0.2221(9)	0.3343(4)	0.7019(10)	0.036(6)
B(2)	0.2121(9)	0.3774(4)	0.5636(11)	0.038(6)
B(3)	0.3579(12)	0.3808(5)	0.7175(12)	0.053(8)
B(4)	0.3890(9)	0.3148(5)	0.8154(10)	0.041(6)
B(5)	0.1526(8)	0.3019(4)	0.5399(9)	0.032(5)
B(6)	0.2312(9)	0.3305(4)	0.4512(10)	0.032(5)
B(7)	0.3640(10)	0.3735(5)	0.5682(11)	0.043(7)
B(8)	0.4832(10)	0.3334(6)	0.7409(13)	0.063(8)
B(9)	0.4566(13)	0.2628(7)	0.7576(12)	0.062(9)
B(10)	0.2774(10)	0.2605(5)	0.7061(11)	0.041(6)
C(11)	0.2425(7)	0.0815(3)	0.4585(7)	0.021(4)
C(12)	0.1627(8)	0.0834(4)	0.5359(8)	0.034(5)
C(13)	0.2211(8)	0.0400(4)	0.6535(8)	0.038(5)
C(14)	0.3619(8)	0.0512(4)	0.7439(8)	0.036(5)
C(15)	0.4403(8)	0.0479(4)	0.6679(8)	0.033(5)
C(16)	0.3877(7)	0.0903(4)	0.5522(8)	0.030(5)
C(21)	0.0160(7)	0.1195(3)	0.1993(7)	0.022(4)
C(22)	-0.0897(7)	0.1515(3)	0.2229(8)	0.029(4)
C(23)	-0.2268(8)	0.1404(4)	0.1055(8)	0.034(5)
C(24)	-0.2553(8)	0.0750(4)	0.0860(8)	0.036(5)
C(25)	-0.1490(9)	0.0408(4)	0.0688(9)	0.043(6)
C(26)	-0.0127(8)	0.0518(3)	0.1824(8)	0.032(5)
C(31)	0.2910(7)	0.1385(3)	0.2513(7)	0.025(4)
C(32)	0.2573(8)	0.1892(4)	0.1503(8)	0.034(5)
C(33)	0.3610(8)	0.1910(4)	0.1004(8)	0.037(5)
C(34)	0.3705(8)	0.1322(4)	0.0432(8)	0.037(5)
C(35)	0.4015(8)	0.0821(4)	0.1402(8)	0.036(5)
C(36)	0.2970(8)	0.0782(4)	0.1903(8)	0.033(5)

Table A2.1.2. Fractional Coordinates of the Hydrogen Atoms in 5,6-μ-(Cy_3PAu)-*nido*-$B_{10}H_{13}$.

	x	y	z
H(1)	0.1443	0.3402	0.7400
H(2)	0.1380	0.4141	0.4968
H(3)	0.3957	0.4269	0.7707
H(4)	0.4430	0.3059	0.9304
H(5)	0.0470	0.2856	0.4639

H(6)	0.1838	0.3326	0.3346
H(7)	0.3977	0.4052	0.5078
H(8)	0.5975	0.3378	0.7984
H(9)	0.5348	0.2262	0.8152
H(10)	0.2524	0.2157	0.7415
H(6,7)	0.3559	0.3200	0.5205
H(8,9)	0.4769	0.2835	0.6632
H(9,10)	0.3643	0.2339	0.7332
H(11)	0.2298	0.0383	0.4125
H(12a)	0.0628	0.0709	0.4702
H(12b)	0.1651	0.1280	0.5726
H(13a)	0.2104	-0.0048	0.6151
H(13b)	0.1681	0.0443	0.7096
H(14a)	0.3731	0.0950	0.7872
H(14b)	0.3980	0.0182	0.8219
H(15a)	0.4352	0.0031	0.6313
H(15b)	0.5408	0.0591	0.7343
H(16a)	0.4026	0.1353	0.5902
H(16b)	0.4408	0.0838	0.4967
H(21)	0.0120	0.1348	0.1076
H(22a)	-0.0702	0.1988	0.2326
H(22b)	-0.0867	0.1348	0.3131
H(23a)	-0.2311	0.1590	0.0160
H(23b)	-0.2989	0.1618	0.1259
H(24a)	-0.2607	0.0576	0.1717
H(24b)	-0.3480	0.0686	-0.0017
H(25a)	-0.1513	0.0547	-0.0230
H(25b)	-0.1698	-0.0063	0.0641
H(26a)	-0.0065	0.0340	0.2733
H(26b)	0.0582	0.0300	0.1610
H(31)	0.3882	0.1457	0.3317
H(32a)	0.1618	0.1816	0.0673
H(32b)	0.2574	0.2311	0.1970
H(33a)	0.4549	0.2018	0.1828
H(33b)	0.3339	0.2248	0.0247
H(34a)	0.4465	0.1349	0.0141
H(34b)	0.2783	0.1230	-0.0431
H(35a)	0.4024	0.0408	0.0922
H(35b)	0.4965	0.0896	0.2240
H(36a)	0.3240	0.0437	0.2645
H(36b)	0.2027	0.0681	0.1078

Table A2.1.3. Anisotropic Thermal Parameters(10^4 pm^2) for Atoms in 5,6-μ-(Cy_3PAu)-*nido*-$B_{10}H_{13}$.

	U_{11}	U_{22}	U_{33}	U_{23}	U_{13}	U_{12}
Au	0.02186(15)	0.02237(16)	0.02173(15)	-0.00447(12)	0.00972(11)	0.00144(13)
P	0.0214(9)	0.0215(9)	0.0194(8)	-0.0010(7)	0.0127(7)	-0.0003(7)
B(1)	0.030(5)	0.033(5)	0.041(5)	-0.011(4)	0.029(4)	-0.005(4)

B(2)	0.029(5)	0.019(4)	0.056(6)	-0.004(4)	0.026(5)	-0.002(4)
B(3)	0.056(7)	0.036(6)	0.056(7)	-0.022(5)	0.035(6)	-0.015(5)
B(4)	0.030(5)	0.051(6)	0.033(5)	-0.014(5)	0.018(4)	-0.007(5)
B(5)	0.024(4)	0.028(5)	0.039(5)	-0.010(4)	0.022(4)	0.003(4)
B(6)	0.029(4)	0.013(4)	0.051(5)	0.005(3)	0.031(4)	-0.007(3)
B(7)	0.035(5)	0.047(6)	0.044(6)	-0.005(5)	0.031(5)	-0.014(5)
B(8)	0.023(5)	0.088(10)	0.062(7)	-0.051(7)	0.014(5)	0.008(5)
B(9)	0.047(7)	0.070(10)	0.038(6)	-0.012(6)	-0.010(5)	-0.004(6)
B(10)	0.032(5)	0.042(6)	0.037(5)	-0.001(4)	0.012(4)	0.003(4)
C(11)	0.020(3)	0.022(3)	0.020(3)	0.004(3)	0.016(3)	0.001(3)
C(12)	0.024(4)	0.048(5)	0.029(4)	0.008(4)	0.020(3)	0.004(4)
C(13)	0.036(5)	0.039(5)	0.033(4)	0.010(4)	0.022(4)	0.000(4)
C(14)	0.031(4)	0.043(5)	0.027(4)	0.007(4)	0.017(3)	0.001(4)
C(15)	0.023(4)	0.040(5)	0.029(4)	0.005(3)	0.013(3)	0.000(3)
C(16)	0.023(4)	0.026(4)	0.032(4)	0.004(3)	0.015(3)	0.001(3)
C(21)	0.021(3)	0.026(4)	0.016(3)	-0.004(3)	0.011(3)	-0.001(3)
C(22)	0.019(3)	0.026(4)	0.034(4)	-0.002(3)	0.013(3)	0.000(3)
C(23)	0.026(4)	0.032(4)	0.032(4)	0.008(3)	0.007(3)	-0.007(3)
C(24)	0.032(4)	0.030(4)	0.036(4)	-0.001(4)	0.014(4)	-0.015(4)
C(25)	0.042(5)	0.037(5)	0.035(5)	-0.008(4)	0.008(4)	-0.013(4)
C(26)	0.028(4)	0.019(4)	0.041(5)	-0.008(3)	0.019(4)	-0.004(3)
C(31)	0.024(4)	0.024(4)	0.021(3)	-0.000(3)	0.009(3)	0.001(3)
C(32)	0.031(4)	0.029(4)	0.037(4)	0.005(3)	0.027(4)	0.009(3)
C(33)	0.042(4)	0.032(4)	0.037(4)	0.007(3)	0.036(4)	0.005(4)
C(34)	0.029(4)	0.048(5)	0.030(4)	-0.007(4)	0.024(4)	-0.004(4)
C(35)	0.031(4)	0.045(5)	0.028(4)	-0.008(4)	0.018(3)	0.004(4)
C(36)	0.032(4)	0.025(4)	0.035(4)	-0.007(3)	0.021(4)	-0.003(3)

Table A2.1.4. Bond Lengths(pm) and Angles(°) for the Non-Hydrogen Atoms in 5,6-μ-(Cy_3PAu)-*nido*-$B_{10}H_{13}$.

Au - P	230.91(21)	B(9) -B(10)	187.7(19)
Au - B(5)	224.5(10)	P -C(11)	184.2(8)
Au - B(6)	227.0(10)	P -C(21)	185.4(8)
B(1) - B(2)	180.7(15)	P -C(31)	184.2(8)
B(1) - B(3)	182.8(17)	C(11) -C(12)	155.0(12)
B(1) - B(4)	180.6(15)	C(11) -C(16)	152.5(11)
B(1) - B(5)	178.5(14)	C(12) -C(13)	153.4(13)
B(1) -B(10)	177.0(16)	C(13) -C(14)	148.7(13)
B(2) - B(3)	177.7(17)	C(14) -C(15)	152.5(13)
B(2) - B(5)	180.3(14)	C(15) -C(16)	150.5(12)
B(2) - B(6)	175.1(15)	C(21) -C(22)	155.0(11)
B(2) - B(7)	174.0(16)	C(21) -C(26)	155.0(11)
B(3) - B(4)	178.8(17)	C(22) -C(23)	154.3(12)
B(3) - B(7)	174.3(17)	C(23) -C(24)	149.9(13)
B(3) - B(8)	171.7(19)	C(24) -C(25)	154.2(14)
B(4) - B(8)	172.0(18)	C(25) -C(26)	152.1(13)
B(4) - B(9)	170.1(19)	C(31) -C(32)	153.3(12)
B(4) -B(10)	178.9(16)	C(31) -C(36)	153.9(12)
B(5) - B(6)	177.0(14)	C(32) -C(33)	155.4(13)

B(5) -B(10)	199.4(15)	C(33) -C(34)	150.0(13)
B(6) - B(7)	177.6(15)	C(34) -C(35)	149.6(13)
B(7) - B(8)	201.0(18)	C(35) -C(36)	156.6(13)
B(8) - B(9)	164.3(20)		

P - Au - B(5)	158.8(3)	B(4) - B(9) - B(8)	61.9(8)
P - Au - B(6)	154.7(3)	B(4) - B(9) -B(10)	59.8(7)
B(5) - Au - B(6)	46.2(4)	B(1) -B(10) - B(4)	61.0(6)
B(2) - B(1) - B(3)	58.5(6)	B(1) -B(10) - B(5)	56.3(6)
B(2) - B(1) - B(5)	60.2(6)	B(4) -B(10) - B(9)	55.2(7)
B(3) - B(1) - B(4)	58.9(6)	Au - P -C(11)	109.9(3)
B(4) - B(1) -B(10)	60.0(6)	Au - P -C(21)	112.5(3)
B(5) - B(1) -B(10)	68.2(6)	Au - P -C(31)	110.2(3)
B(1) - B(2) - B(3)	61.3(6)	C(11) - P -C(21)	109.1(3)
B(1) - B(2) - B(5)	59.3(6)	C(11) - P -C(31)	107.1(4)
B(3) - B(2) - B(7)	59.4(7)	C(21) - P -C(31)	107.9(4)
B(5) - B(2) - B(6)	59.7(6)	P -C(11) -C(12)	109.7(5)
B(6) - B(2) - B(7)	61.1(6)	P -C(11) -C(16)	110.2(5)
B(1) - B(3) - B(2)	60.2(6)	C(12) -C(11) -C(16)	110.9(6)
B(1) - B(3) - B(4)	59.9(6)	C(11) -C(12) -C(13)	110.0(7)
B(2) - B(3) - B(7)	59.2(7)	C(12) -C(13) -C(14)	112.9(8)
B(4) - B(3) - B(8)	58.7(7)	C(13) -C(14) -C(15)	110.6(7)
B(7) - B(3) - B(8)	71.0(8)	C(14) -C(15) -C(16)	111.2(7)
B(1) - B(4) - B(3)	61.1(6)	C(11) -C(16) -C(15)	113.0(7)
B(1) - B(4) -B(10)	59.0(6)	P -C(21) -C(22)	111.4(5)
B(3) - B(4) - B(8)	58.6(7)	P -C(21) -C(26)	114.7(5)
B(8) - B(4) - B(9)	57.4(8)	C(22) -C(21) -C(26)	109.6(6)
B(9) - B(4) -B(10)	65.0(7)	C(21) -C(22) -C(23)	110.6(7)
Au - B(5) - B(6)	67.7(5)	C(22) -C(23) -C(24)	110.7(7)
B(1) - B(5) - B(2)	60.5(6)	C(23) -C(24) -C(25)	111.9(8)
B(1) - B(5) -B(10)	55.5(5)	C(24) -C(25) -C(26)	112.6(8)
B(2) - B(5) - B(6)	58.7(6)	C(21) -C(26) -C(25)	110.0(7)
Au - B(6) - B(5)	66.2(4)	P -C(31) -C(32)	111.2(6)
B(2) - B(6) - B(5)	61.6(6)	P -C(31) -C(36)	114.3(6)
B(2) - B(6) - B(7)	59.1(6)	C(32) -C(31) -C(36)	111.3(7)
B(2) - B(7) - B(3)	61.3(7)	C(31) -C(32) -C(33)	109.0(7)
B(2) - B(7) - B(6)	59.7(6)	C(32) -C(33) -C(34)	111.3(7)
B(3) - B(7) - B(8)	53.9(7)	C(33) -C(34) -C(35)	112.5(8)
B(3) - B(8) - B(4)	62.7(7)	C(34) -C(35) -C(36)	110.6(7)
B(3) - B(8) - B(7)	55.1(6)	C(31) -C(36) -C(35)	108.8(7)
B(4) - B(8) - B(9)	60.7(8)		

Table A2.1.5. Bond Angles(°) Involving the Cage Hydrogen Atoms in 5,6-μ-(Cy_3PAu)-*nido*-$B_{10}H_{13}$.

B(2) - B(1) - H(1)	120.9	B(4) - B(9) - H(9)	129.8
B(3) - B(1) - H(1)	132.4	B(8) - B(9) - H(9)	127.2
B(4) - B(1) - H(1)	120.8	B(10)- B(9) - H(9)	127.4

B(5)	- B(1)	- H(1)	112.0	B(1)	-B(10)	-H(10)	132.0
B(10)	- B(1)	- H(1)	115.2	B(4)	-B(10)	-H(10)	124.1
B(1)	- B(2)	- H(2)	132.0	B(5)	-B(10)	-H(10)	122.8
B(3)	- B(2)	- H(2)	132.6	B(9)	-B(10)	-H(10)	109.5
B(5)	- B(2)	- H(2)	116.8	B(7)	- B(6)	-H(6,7)	47.0
B(6)	- B(2)	- H(2)	104.7	H(6)	- B(6)	-H(6,7)	119.2
B(7)	- B(2)	- H(2)	118.5	Au	- B(6)	-H(6,7)	90.4
B(1)	- B(3)	- H(3)	130.5	B(2)	- B(6)	-H(6,7)	98.7
B(2)	- B(3)	- H(3)	119.8	B(5)	- B(6)	-H(6,7)	108.1
B(4)	- B(3)	- H(3)	119.5	B(2)	- B(7)	-H(6,7)	99.3
B(7)	- B(3)	- H(3)	114.1	B(3)	- B(7)	-H(6,7)	117.8
B(8)	- B(3)	- H(3)	112.4	B(6)	- B(7)	-H(6,7)	47.1
B(1)	- B(4)	- H(4)	132.1	H(7)	- B(7)	-H(6,7)	106.9
B(3)	- B(4)	- H(4)	133.1	B(3)	- B(8)	-H(8,9)	127.2
B(8)	- B(4)	- H(4)	117.6	B(4)	- B(8)	-H(8,9)	105.0
B(9)	- B(4)	- H(4)	102.4	B(9)	- B(8)	-H(8,9)	49.3
B(10)	- B(4)	- H(4)	119.6	H(8)	- B(8)	-H(8,9)	97.4
Au	- B(5)	- H(5)	76.7	B(4)	- B(9)	-H(8,9)	112.0
B(1)	- B(5)	- H(5)	134.0	B(8)	- B(9)	-H(8,9)	55.9
B(2)	- B(5)	- H(5)	126.5	B(10)	- B(9)	-H(8,9)	111.0
B(6)	- B(5)	- H(5)	109.2	H(9)	- B(9)	-H(8,9)	108.9
B(10)	- B(5)	- H(5)	126.4	B(4)	- B(9)	-H(9,10)	86.3
Au	- B(6)	- H(6)	85.6	B(8)	- B(9)	-H(9,10)	135.2
B(2)	- B(6)	- H(6)	130.5	B(10)	- B(9)	-H(9,10)	32.2
B(5)	- B(6)	- H(6)	124.5	H(9)	- B(9)	-H(9,10)	97.1
B(7)	- B(6)	- H(6)	127.4	(8,9)	- B(9)	-H(9,10)	120.5
B(2)	- B(7)	- H(7)	124.2	B(1)	-B(10)	-H(9,10)	143.1
B(3)	- B(7)	- H(7)	133.7	B(4)	-B(10)	-H(9,10)	84.5
B(6)	- B(7)	- H(7)	107.4	B(5)	-B(10)	-H(9,10)	133.7
B(3)	- B(8)	- H(8)	133.3	B(9)	-B(10)	-H(9,10)	35.1
B(4)	- B(8)	- H(8)	123.8	H(10)	-B(10)	-H(9,10)	77.1
B(9)	- B(8)	- H(8)	103.9				

A2.2 5,6-μ-(*o*-tolyl$_3$PAu)-*nido*-$B_{10}H_{13}$.CH_2Cl_2.

The Molecular Structure and Associated Numbering Scheme for 5,6-μ-(*o*-tolyl$_3$PAu)-*nido*-$B_{10}H_{13}$.

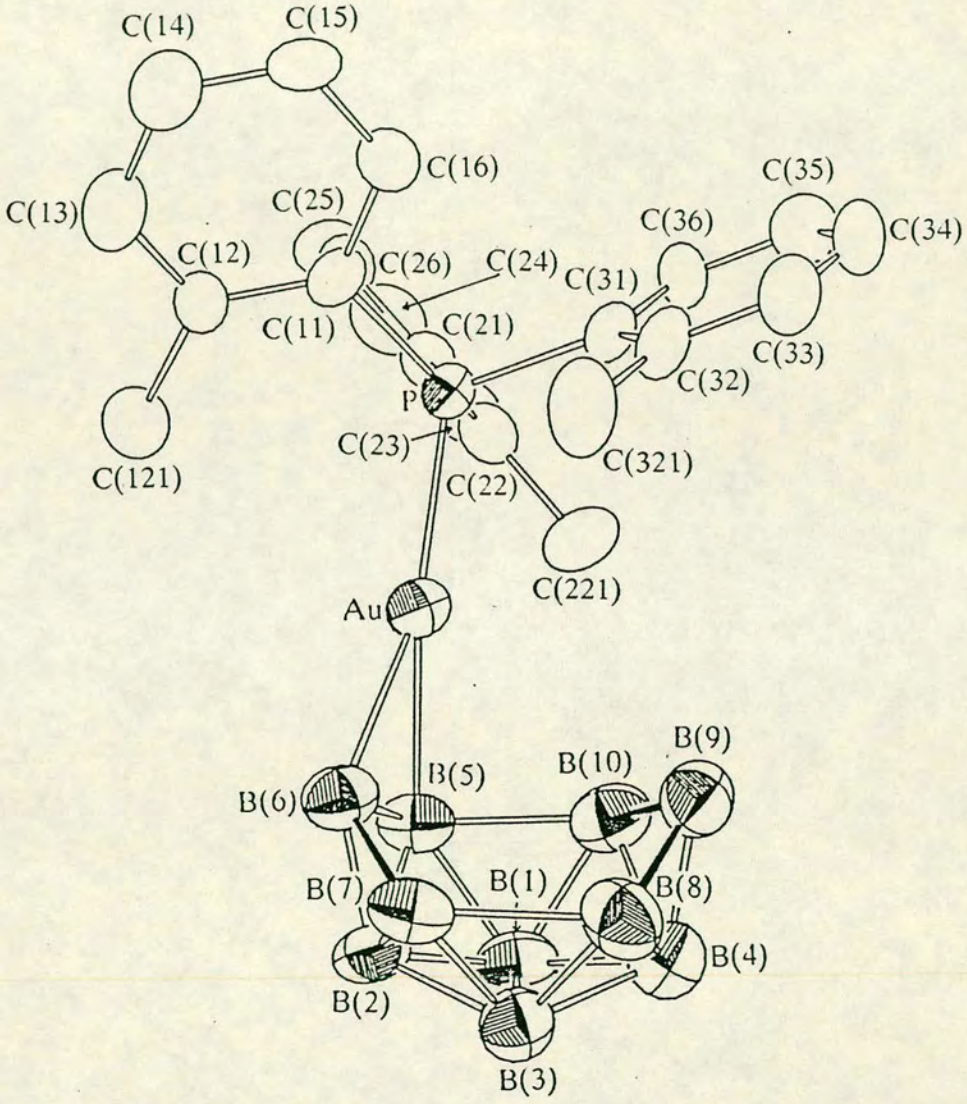

Crystal data. $C_{21}H_3AuB_{10}P.CH_2Cl_2$, M = 707.5, monoclinic with a = 1.0370(3), b = 2.0100(4), c = 1.5283(4) nm, and β = 106.782(23)°. U = 3.050 nm^3 and the space group is $P2_1/c$. Z = 4, D_x = 1.541 Mgm^{-3}, μ(Mo-K_α) = 5.06 mm^{-1}, and $F(000)$ = 1348.

Data collection and processing. Θ_{max} = 22°, and $+h + k \pm l$. 3279 data were measured yielding 3072 unique (R_{merge} = 0.0170), all of which had $F > 2\sigma(F)$ and were retained. Variable scan speeds between 1.03 and 2.35 $^{o}min^{-1}$. Crystal decayed by *ca.* 4% during the experiment and correction was applied.

Structure solution and refinement. Au atom located by automatic direct methods. Au, B, P, C, and Cl atoms allowed anisotropic thermal motion. Phenyl rings constrained to be regular, planar hexagons. Phenyl H atoms group thermal parameter = 440(70)pm^2 at convergence. Methyl group and cage H atoms could not be satisfactorily modelled and remain absent. Weighting scheme g = 0.000117. R = 0.0426, R_w = 0.0492, S = 1.190. Data : variable = 10 : 1, $(\Delta\rho)_{max}$ = 707, $(\Delta\rho)_{min}$ = -550 enm^{-3}, and the Δ/σ in final least-squares cycle was 0.074.

Table A2.2.1. Fractional Coordinates of Refined Atoms in 5,6-μ-(*o*-tolyl$_3$PAu)-*nido*-$B_{10}H_{13}.CH_2Cl_2$. U_{eq} in 10^4pm^2.

	x	y	z	U_{eq}
Au	0.54124(4)	0.55246(2)	0.21155(3)	0.0458(3)
B(1)	0.2588(15)	0.6682(8)	0.0867(10)	0.062(10)
B(2)	0.2404(15)	0.5885(8)	0.0327(10)	0.058(10)
B(3)	0.2679(15)	0.6596(8)	-0.0277(10)	0.060(10)
B(4)	0.3620(16)	0.7244(8)	0.0423(10)	0.062(10)
B(5)	0.3352(14)	0.5960(8)	0.1469(10)	0.057(10)
B(6)	0.3785(15)	0.5412(7)	0.0713(11)	0.059(10)
B(7)	0.3508(14)	0.5821(8)	-0.0325(10)	0.059(10)

B(8)	0.4336(16)	0.6769(8)	-0.0305(11)	0.069(11)
B(9)	0.5311(16)	0.7023(8)	0.0803(12)	0.067(11)
B(10)	0.4257(16)	0.6854(8)	0.1554(11)	0.064(11)
P	0.7363(3)	0.52903(13)	0.32600(18)	0.0350(16)
C(11)	0.8124	0.4484	0.3184	0.035(6)
C(12)	0.7364	0.3903	0.2965	0.035(7)
C(13)	0.8000	0.3296	0.2926	0.053(8)
C(14)	0.9397	0.3272	0.3104	0.058(9)
C(15)	1.0157	0.3853	0.3322	0.052(8)
C(16)	0.9521(5)	0.4459(3)	0.3362(5)	0.042(7)
C(121)	0.5839(12)	0.3878(6)	0.2814(9)	0.059(9)
C(21)	0.7064	0.5294	0.4371	0.035(6)
C(22)	0.6390	0.5818	0.4646	0.043(7)
C(23)	0.6130	0.5795	0.5491	0.055(8)
C(24)	0.6543	0.5246	0.6062	0.063(9)
C(25)	0.7217	0.4721	0.5788	0.052(8)
C(26)	0.7477(7)	0.4745(3)	0.4942(5)	0.042(7)
C(221)	0.5901(13)	0.6448(6)	0.4065(9)	0.060(9)
C(31)	0.8701	0.5889	0.3319	0.038(7)
C(32)	0.9156	0.6018	0.2561	0.048(7)
C(33)	1.0194	0.6474	0.2628	0.059(9)
C(34)	1.0777	0.6801	0.3452	0.065(9)
C(35)	1.0321	0.6673	0.4210	0.059(8)
C(36)	0.9283(7)	0.6217(4)	0.4143(4)	0.043(7)
C(321)	0.8555(15)	0.5659(6)	0.1628(8)	0.066(9)
C(sol)	0.1283(23)	0.3369(12)	0.1163(19)	0.154(23)
Cl(1)	0.2455(7)	0.2975(5)	0.2118(5)	0.194(8)
Cl(2a)	0.1922(21)	0.4070(14)	0.1336(16)	0.261(25)
Cl(2b)	0.1647(10)	0.3027(5)	0.0148(7)	0.142(10)

Table A2.2.2. Fractional Coordinates of H Atoms on the Phenyl Rings in 5,6-μ-(*o*-tolyl$_3$PAu)-*nido*-$B_{10}H_{13}$.CH_2Cl_2.

	x	y	z
H(13)	0.7412	0.2846	0.2756
H(14)	0.9889	0.2802	0.3073
H(15)	1.1238	0.3834	0.3460
H(16)	1.0110	0.4909	0.3531
H(23)	0.5608	0.6201	0.5704
H(24)	0.6342	0.5227	0.6717
H(25)	0.7538	0.4296	0.6230
H(26)	0.7999	0.4339	0.4730
H(33)	1.0547	0.6573	0.2042
H(34)	1.1580	0.7155	0.3504
H(35)	1.0772	0.6927	0.4848
H(36)	0.8930	0.6117	0.4729

Table A2.2.3. Anisotropic Thermal Parameters(10^4 pm^2) in 5,6-μ-(*o*-tolyl$_3$PAu)-*nido*-$B_{10}H_{13}$.

	U_{11}	U_{22}	U_{33}	U_{23}	U_{13}	U_{12}
Au	0.0435(3)	0.0444(3)	0.0450(3)	0.00497(23)	0.01181(21)	0.00577(22)
B(1)	0.051(9)	0.071(10)	0.059(9)	0.005(8)	0.018(7)	0.016(8)
B(2)	0.051(9)	0.061(9)	0.055(9)	0.019(7)	0.005(7)	0.011(7)
B(3)	0.062(9)	0.061(9)	0.053(9)	0.004(7)	0.018(7)	0.001(8)
B(4)	0.070(10)	0.067(10)	0.046(9)	-0.001(7)	0.021(8)	0.000(8)
B(5)	0.046(9)	0.064(10)	0.054(9)	0.002(7)	0.010(7)	0.012(7)
B(6)	0.050(9)	0.060(10)	0.062(10)	0.006(7)	0.017(7)	0.010(7)
B(7)	0.044(9)	0.078(10)	0.050(9)	0.002(8)	0.012(7)	0.008(7)
B(8)	0.066(10)	0.070(11)	0.064(10)	-0.017(8)	0.011(8)	-0.005(8)
B(9)	0.059(10)	0.060(10)	0.078(11)	0.005(8)	0.026(9)	0.001(8)
B(10)	0.065(10)	0.060(10)	0.062(10)	0.001(8)	0.016(8)	0.015(8)
P	0.0369(16)	0.0326(14)	0.0338(15)	0.0019(12)	0.0155(13)	0.0019(12)
C(11)	0.044(7)	0.031(6)	0.031(5)	0.001(5)	0.021(5)	0.008(5)
C(12)	0.039(6)	0.034(6)	0.031(6)	0.000(4)	0.018(5)	-0.005(5)
C(13)	0.069(9)	0.044(7)	0.047(7)	-0.001(5)	0.032(6)	-0.006(6)
C(14)	0.060(9)	0.051(8)	0.065(9)	-0.003(6)	0.038(7)	0.004(6)
C(15)	0.035(7)	0.052(8)	0.062(8)	0.004(6)	0.007(6)	0.015(6)
C(16)	0.039(7)	0.045(7)	0.041(6)	-0.007(5)	0.018(5)	-0.001(5)
C(121)	0.046(7)	0.054(8)	0.073(9)	0.003(6)	0.026(6)	-0.005(6)
C(21)	0.031(6)	0.043(6)	0.032(6)	0.001(5)	0.020(5)	-0.004(5)
C(22)	0.039(6)	0.053(7)	0.037(6)	-0.002(5)	0.016(5)	-0.007(5)
C(23)	0.044(7)	0.068(8)	0.052(8)	-0.009(6)	0.027(6)	-0.002(6)
C(24)	0.051(8)	0.085(9)	0.052(8)	-0.001(7)	0.027(6)	-0.004(7)
C(25)	0.049(7)	0.055(7)	0.048(7)	0.012(6)	0.012(6)	0.008(6)
C(26)	0.043(7)	0.047(6)	0.035(6)	0.002(5)	0.022(5)	-0.007(5)
C(221)	0.064(8)	0.051(8)	0.062(8)	0.005(6)	0.025(7)	0.022(6)
C(31)	0.041(6)	0.028(6)	0.044(7)	0.008(5)	0.018(5)	0.002(5)
C(32)	0.060(8)	0.031(6)	0.052(7)	0.009(5)	0.027(6)	0.000(5)
C(33)	0.063(8)	0.053(8)	0.059(8)	0.014(6)	0.032(7)	-0.009(6)
C(34)	0.051(8)	0.046(7)	0.094(11)	0.020(7)	0.027(7)	-0.013(6)
C(35)	0.056(8)	0.049(7)	0.065(9)	-0.011(6)	0.017(6)	0.004(6)
C(36)	0.041(7)	0.032(6)	0.054(7)	-0.006(5)	0.021(6)	-0.008(5)
C(321)	0.102(11)	0.059(8)	0.034(7)	-0.003(6)	0.034(7)	-0.024(7)
C(sol)	0.113(17)	0.152(22)	0.178(25)	0.011(17)	0.026(17)	0.028(16)
Cl(1)	0.113(5)	0.258(9)	0.193(8)	-0.048(6)	0.024(5)	0.012(5)
Cl(2A)	0.178(19)	0.29(3)	0.27(3)	0.085(22)	-0.009(17)	-0.141(19)
Cl(2B)	0.136(9)	0.142(9)	0.141(9)	0.068(7)	0.064(7)	0.014(6)

Table A2.2.4. Internuclear Distances(pm) and Interbond Angles(°) in 5,6-μ-(*o*-tolyl$_3$PAu)-*nido*-$B_{10}H_{13}.CH_2Cl_2$

Au - P	230.8(3)	B(1) - B(2)	178.6(22)
Au - B(5)	225.6(15)	B(1) - B(3)	178.8(22)
Au - B(6)	232.5(16)	B(1) - B(4)	181.8(22)
P -C(11)	182.2(7)	B(1) - B(5)	177.6(22)
P -C(21)	181.2(7)	B(1) -B(10)	177.9(23)
P -C(31)	181.9(7)	B(2) - B(3)	176.7(22)
C(12) -C(121)	153.2(14)	B(2) - B(5)	174.5(21)
C(22) -C(221)	154.5(14)	B(2) - B(6)	167.7(22)
C(32) -C(321)	155.9(15)	B(2) - B(7)	172.6(22)
B(3) - B(4)	176.5(23)	B(3) - B(7)	179.0(22)
B(4) - B(8)	178.3(23)	B(3) - B(8)	176.5(23)
B(4) -B(10)	183.8(23)	B(4) - B(9)	173.8(23)
B(5) -B(10)	201.3(22)	B(5) - B(6)	174.5(22)
B(8) - B(9)	177.9(24)	B(7) - B(8)	208.6(23)
B(6) - B(7)	173.5(22)	B(9) -B(10)	183.0(23)
C(sol)-Cl(2a)	155(4)	C(sol)-Cl(1)	179(3)
C(sol)-Cl(2b)	183(3)		

P	- Au	- B(5)	157.3(4)	B(1)-	B(3)	- B(4)	61.1(9)
P	- Au	- B(6)	157.3(4)	B(2)-	B(3)	- B(7)	58.0(9)
Au	- P	-C(11)	115.73(24)	B(4)-	B(3)	- B(8)	60.3(9)
Au	- P	-C(21)	111.09(24)	B(7)-	B(3)	- B(8)	71.8(9)
Au	- P	-C(31)	113.03(25)	B(1)-	B(4)	- B(3)	59.5(9)
P	-C(11)	-C(16)	117.6(5)	B(3)-	B(4)	- B(8)	59.3(9)
P	-C(11)	-C(12)	122.3(5)	B(8)-	B(4)	- B(9)	60.7(9)
P	-C(21)	-C(22)	121.4(5)	B(1)-	B(4)	-B(10)	58.2(9)
P	-C(21)	-C(26)	118.6(5)	B(9)-	B(4)	-B(10)	61.5(9)
P	-C(31)	-C(32)	121.2(5)	Au	- B(5)	- B(6)	69.7(7)
P	-C(31)	-C(36)	118.8(5)	B(1)-	B(5)	- B(2)	61.0(9)
C(11)-	P	-C(31)	104.7(3)	B(2)-	B(5)	- B(6)	57.5(9)
C(21)-	P	-C(31)	106.6(3)	B(1)-	B(5)	-B(10)	55.6(8)
C(11)-	P	-C(21)	105.0(3)	Au	- B(5)	-B(10)	87.3(7)
C(11)-	C(12)	-C(121)	123.4(7)	Au	- B(6)	- B(5)	65.5(7)
C(13)-	C(12)	-C(121)	116.5(7)	Au	- B(6)	- B(7)	132.9(10)
C(21)-	C(22)	-C(221)	123.8(7)	B(2)-	B(6)	- B(5)	61.3(9)
C(23)-	C(22)	-C(221)	116.2(7)	B(2)-	B(6)	- B(7)	60.7(9)
C(33)-	C(32)	-C(321)	117.9(7)	B(2)-	B(7)	- B(3)	60.3(9)
C(31)-	C(32)	-C(321)	122.1(7)	B(2)-	B(7)	- B(6)	58.0(9)
B(5)-	Au	- B(6)	44.8(5)	B(3)-	B(7)	- B(8)	53.5(8)
B(2)-	B(1)	- B(3)	59.3(9)	B(3)-	B(8)	- B(4)	60.5(9)
B(2)-	B(1)	- B(5)	58.6(9)	B(3)-	B(8)	- B(7)	54.6(8)
B(3)-	B(1)	- B(4)	59.4(9)	B(4)-	B(8)	- B(9)	58.4(9)
B(4)-	B(1)	-B(10)	61.4(9)	B(4)-	B(9)	- B(8)	60.9(9)
B(5)-	B(1)	-B(10)	69.0(9)	B(4)-	B(9)	-B(10)	62.0(9)
B(1)-	B(2)	- B(3)	60.4(9)	B(5)-	B(10)	- B(1)	55.4(8)
B(1)-	B(2)	- B(5)	60.4(9)	B(1)-	B(10)	- B(4)	60.3(9)
B(3)-	B(2)	- B(7)	61.7(9)	B(4)-	B(10)	- B(9)	56.6(9)
B(5)-	B(2)	- B(6)	61.3(9)	B(6)-	B(7)	- B(8)	117.4(11)
B(6)-	B(2)	- B(7)	61.3(9)	B(7)-	B(8)	- B(9)	113.2(11)

B(1)-	B(3)	- B(2)	60.3(9)	B(8)-	B(9)	-B(10)	105.4(11)
B(5)-	B(10)	- B(9)	118.5(11)	Cl(1)-	C(sol)	-Cl(2a)	96.2(16)
				Cl(1)-	C(sol)	-Cl(2b)	105.5(14)

A2.3 $[PhCH_2NMe_3]^+$ $[B_{10}H_{13}]^-$.

The Molecular Structure and Associated Numbering Scheme for $[PhCH_2NMe_3]^+$ $[B_{10}H_{13}]^-$.

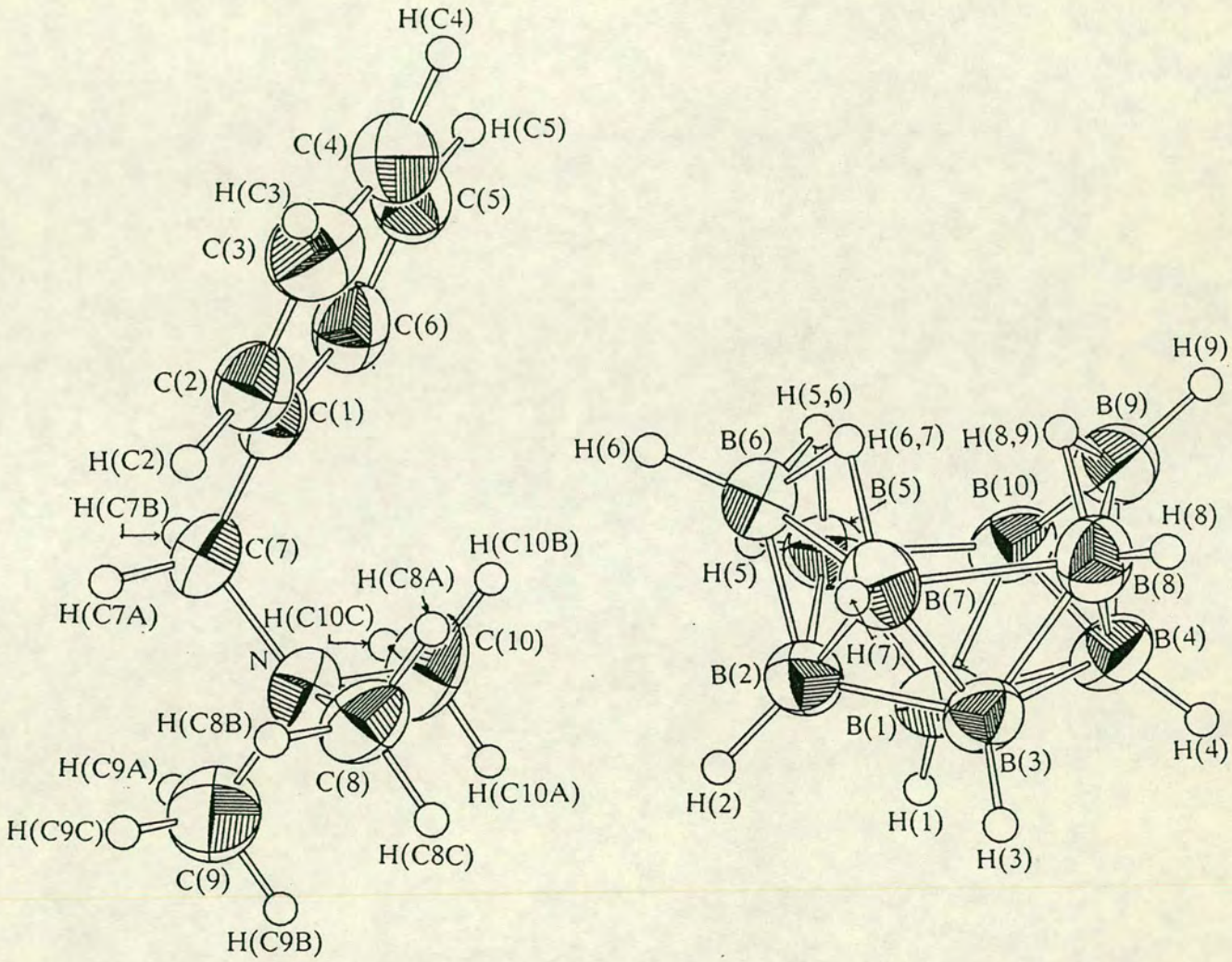

Crystal data. $C_{10}H_{35}B_{10}N$, M = 277.3, monoclinic with a = 0.88759(13), b = 1.8739(3), c = 1.08215(13) nm and β = 96.223(11)°. U = 1.7893 nm^3, D_x = 1.008 Mgm^{-3}, μ(Mo-K_α) = 0.046 mm^{-1}, *F(000)* = 584 and space group = $P2_1/c$.

Data collection and processing. Θ_{max} = 22°, + h + k ± l. 2359 reflections were measured, with scan speeds of 1.268 - 3.296 $^{o}min^{-1}$. These yielded 2194 unique (R_{merge} = 0.0103) data, of which 1581 with $F > 2\sigma(F)$ were retained and used in the refinement. No crystal decay or movement was noted.

Structure solution and refinement. Structure solved by automatic direct methods which revealed the position of most of the atoms, the rest were located by subsequent ΔF syntheses. All non-hydrogen atoms refined anisotropically, and the phenyl ring constrained to be a planar, regular hexagon. Cation H atoms group thermal parameter = 1030(30)pm^2 at convergence. All cage H atoms located and successfully refined with no constraints. Group thermal parameter = 719(24)pm^2 at convergence. Weighting scheme g = 0.002200. R = 0.0524, R_w = 0.0730, S = 1.079, data : variable = 7 : 1. Maximum and minimum residues in final ΔF map were 132 and 161 enm^{-3} respectively. Δ/σ in final cycle was 0.063.

Table A2.3.1. Fractional Coordinates of Non-Hydrogen Atoms in $[PhCH_2NMe_3]^+ [B_{10}H_{13}]^-$. U_{eq} in $10^4 pm^2$.

	x	y	z	U_{eq}
B(1)	0.6211(4)	0.83986(19)	0.2036(3)	0.0584(22)
B(2)	0.6020(4)	0.74532(18)	0.1913(3)	0.0551(21)
B(3)	0.7832(4)	0.78474(18)	0.1965(3)	0.0535(20)
B(4)	0.7783(4)	0.87201(18)	0.1372(3)	0.0578(22)
B(5)	0.4820(4)	0.80292(20)	0.0907(3)	0.0608(23)
B(6)	0.5408(4)	0.71686(21)	0.0446(3)	0.0620(23)
B(7)	0.7370(4)	0.71450(19)	0.0951(3)	0.0582(22)
B(8)	0.8491(4)	0.80227(19)	0.0521(3)	0.0582(22)

B(9)	0.7315(5)	0.87047(21)	-0.0227(4)	0.0681(25)
B(10)	0.5905(4)	0.88447(19)	0.0630(3)	0.0588(22)
N	0.19902(25)	0.59661(12)	0.26319(20)	0.0534(15)
C(1)	0.15660	0.55862	0.03550	0.0474(16)
C(2)	0.24947(22)	0.50316(9)	0.00303(18)	0.0579(19)
C(3)	0.30173	0.50239	-0.11397	0.0754(23)
C(4)	0.26113	0.55709	-0.19851	0.080(3)
C(5)	0.16826	0.61256	-0.16605	0.0760(24)
C(6)	0.11600	0.61332	-0.04904	0.0632(20)
C(7)	0.0989(3)	0.55784(15)	0.1608(3)	0.0552(18)
C(8)	0.3577(3)	0.57068(17)	0.2716(3)	0.0623(20)
C(9)	0.1382(4)	0.58131(21)	0.3841(3)	0.089(3)
C(10)	0.1980(4)	0.67514(16)	0.2394(4)	0.0796(24)

Table A2.3.2. Fractional Coordinates of Hydrogen Atoms.

	x	y	z
H(1)	0.581(3)	0.8610(15)	0.288(3)
H(2)	0.564(3)	0.7171(15)	0.276(3)
H(3)	0.865(3)	0.7689(15)	0.279(3)
H(4)	0.846(3)	0.9143(16)	0.185(3)
H(5)	0.359(4)	0.8095(14)	0.0951(24)
H(6)	0.465(3)	0.6713(15)	0.016(3)
H(7)	0.799(3)	0.6646(16)	0.102(3)
H(8)	0.960(4)	0.7909(15)	0.0334(25)
H(9)	0.762(3)	0.9069(15)	-0.101(3)
H(10)	0.522(3)	0.9359(16)	0.0585(24)
H(5,6)	0.499(3)	0.7691(16)	-0.016(3)
H(6,7)	0.655(3)	0.7123(15)	-0.017(3)
H(8,9)	0.766(3)	0.8039(15)	-0.048(3)
H(C2)	0.28094	0.46080	0.06844
H(C3)	0.37359	0.45951	-0.13918
H(C4)	0.30145	0.55659	-0.28908
H(C5)	0.13667	0.65496	-0.23135
H(C6)	0.04403	0.65625	-0.02372
H(C7A)	-0.0115	0.58274	0.1519
H(C7B)	0.0886	0.50290	0.1889
H(C8A)	0.4038	0.58122	0.1850
H(C8B)	0.3599	0.51396	0.2894
H(C8C)	0.4249	0.59791	0.3464
H(C9A)	0.0226	0.59992	0.3798
H(C9B)	0.2065	0.60847	0.4583
H(C9C)	0.1415	0.52453	0.4013
H(C10A)	0.0830	0.69473	0.2332
H(C10B)	0.2448	0.68571	0.1532
H(C10C)	0.2655	0.70175	0.3148

Table A2.3.3. Anisotropic Thermal Parameters($10^4 pm^2$).

	U_{11}	U_{22}	U_{33}	U_{23}	U_{13}	U_{12}
B(1)	0.0608(23)	0.0633(23)	0.0495(20)	-0.0067(17)	-0.0021(17)	0.0111(18)
B(2)	0.0542(21)	0.0600(22)	0.0501(20)	0.0057(17)	0.0014(16)	0.0007(17)
B(3)	0.0531(20)	0.0534(21)	0.0518(19)	0.0056(16)	-0.0084(16)	0.0009(17)
B(4)	0.0674(23)	0.0427(20)	0.0601(21)	-0.0011(16)	-0.0158(18)	-0.0024(17)
B(5)	0.0572(23)	0.072(3)	0.0517(20)	0.0023(18)	0.0019(17)	0.0046(19)
B(6)	0.0637(24)	0.0627(24)	0.0586(21)	-0.0013(18)	0.0037(18)	-0.0136(20)
B(7)	0.0626(23)	0.0455(20)	0.0659(23)	0.0039(16)	0.0097(18)	0.0042(17)
B(8)	0.0483(21)	0.0596(23)	0.0656(23)	0.0056(18)	0.0025(18)	-0.0022(17)
B(9)	0.084(3)	0.0568(24)	0.0616(23)	0.0116(18)	-0.0068(20)	-0.0080(20)
B(10)	0.0657(23)	0.0481(20)	0.0597(21)	-0.0028(16)	-0.0129(18)	0.0069(18)
N	0.0496(15)	0.0477(14)	0.0622(15)	-0.0073(11)	0.0056(11)	-0.0050(11)
C(1)	0.0371(15)	0.0467(16)	0.0568(17)	-0.0019(14)	-0.0051(13)	-0.0059(13)
C(2)	0.0516(18)	0.0513(17)	0.0696(20)	-0.0015(14)	0.0014(15)	0.0004(16)
C(3)	0.0599(21)	0.0861(24)	0.0796(24)	-0.0123(20)	0.0101(18)	0.0011(18)
C(4)	0.0706(24)	0.103(3)	0.0669(22)	-0.0002(21)	0.0093(18)	-0.0248(22)
C(5)	0.0774(24)	0.0768(24)	0.0714(23)	0.0175(18)	-0.0060(18)	-0.0168(20)
C(6)	0.0509(18)	0.0585(20)	0.0782(22)	0.0088(17)	-0.0059(16)	-0.0028(15)
C(7)	0.0442(17)	0.0535(18)	0.0666(18)	-0.0075(14)	-0.0011(14)	-0.0093(14)
C(8)	0.0470(18)	0.0699(21)	0.0673(19)	-0.0036(15)	-0.0117(14)	0.0022(15)
C(9)	0.103(3)	0.090(3)	0.0758(23)	-0.0268(19)	0.0339(21)	-0.0184(22)
C(10)	0.0734(23)	0.0463(19)	0.116(3)	-0.0134(18)	-0.0036(20)	0.0007(17)

Table A2.3.4c. Bond Lengths(pm) and Angles(^{o}) for the Atoms in the $[PhCH_2NMe_3]^+$ Cation.

N -C(8)	148.3(4)	N - C(7)	152.7(4)
N -C(9)	149.6(4)	C(1) - C(7)	150.1(3)
N -C(10)	149.4(4)		

C(8)- N -C(9)	108.29(23)	C(10)- N - C(7)	110.59(22)
C(8)- N -C(10)	108.74(22)	N - C(7) - C(1)	114.96(21)
C(9)- N -C(10)	110.09(24)	C(2) - C(1) - C(7)	119.29(18)
C(8)- N - C(7)	111.27(21)	C(6) - C(1) - C(7)	120.70(18)
C(9)- N - C(7)	107.83(22)		

Table A2.3.4a. Bond Lengths(pm) and Angles(°) in the $[B_{10}H_{13}]^-$ Anion.

B(1) - B(2)	178.3(5)	B(3) - B(8)	175.8(5)
B(1) - B(3)	178.0(5)	B(4) - B(8)	175.4(5)
B(1) - B(4)	174.5(5)	B(4) - B(9)	173.6(5)
B(1) - B(5)	178.0(5)	B(4) -B(10)	178.6(5)
B(1) -B(10)	173.1(5)	B(5) - B(6)	178.3(5)
B(2) - B(3)	176.5(5)	B(5) -B(10)	184.8(5)
B(2) - B(5)	179.8(5)	B(6) - B(7)	176.8(5)
B(2) - B(6)	170.7(5)	B(7) - B(8)	200.3(5)
B(2) - B(7)	176.7(5)	B(8) - B(9)	178.8(5)
B(3) - B(4)	175.6(5)	B(9) -B(10)	165.7(5)
B(3) - B(7)	173.4(5)		

B(2) - B(1)	- B(3)	59.39(19)	B(8) - B(4)	- B(9)	61.63(21)
B(2) - B(1)	- B(5)	60.61(20)	B(9) - B(4)	-B(10)	56.13(20)
B(3) - B(1)	- B(4)	59.74(19)	B(1) - B(5)	- B(2)	59.78(20)
B(4) - B(1)	-B(10)	61.81(20)	B(1) - B(5)	-B(10)	56.98(19)
B(5) - B(1)	-B(10)	63.48(21)	B(2) - B(5)	- B(6)	56.93(20)
B(1) - B(2)	- B(3)	60.20(19)	B(2) - B(6)	- B(5)	61.99(21)
B(1) - B(2)	- B(5)	59.61(20)	B(2) - B(6)	- B(7)	61.10(21)
B(3) - B(2)	- B(7)	58.80(19)	B(2) - B(7)	- B(3)	60.54(20)
B(5) - B(2)	- B(6)	61.08(21)	B(2) - B(7)	- B(6)	57.74(20)
B(6) - B(2)	- B(7)	61.16(21)	B(3) - B(7)	- B(8)	55.57(19)
B(1) - B(3)	- B(2)	60.41(19)	B(3) - B(8)	- B(4)	59.98(20)
B(1) - B(3)	- B(4)	59.16(19)	B(3) - B(8)	- B(7)	54.43(18)
B(2) - B(3)	- B(7)	60.66(20)	B(4) - B(8)	- B(9)	58.68(21)
B(4) - B(3)	- B(8)	59.89(20)	B(4) - B(9)	- B(8)	59.69(21)
B(7) - B(3)	- B(8)	70.01(21)	B(4) - B(9)	-B(10)	63.46(22)
B(1) - B(4)	- B(3)	61.10(20)	B(1) -B(10)	- B(4)	59.48(20)
B(1) - B(4)	-B(10)	58.71(20)	B(1) -B(10)	- B(5)	59.55(20)
B(3) - B(4)	- B(8)	60.13(20)	B(4) -B(10)	- B(9)	60.40(21)

Table A2.3.5. Bond Lengths(pm) and Angles(°) Involving the Cage Hydrogen Atoms.

B(1) - H(1)	109(3)	B(9) - H(9)	114(3)
B(2) - H(2)	114(3)	B(10)-H(10)	114(3)
B(3) - H(3)	113(3)	B(5) -H(5,6)	134(3)
B(4) - H(4)	109(3)	B(6) -H(5,6)	121(3)
B(5) - H(5)	111(3)	B(6) -H(6,7)	128(3)
B(6) - H(6)	111(3)	B(7) -H(6,7)	135(3)
B(7) - H(7)	108(3)	B(8) -H(8,9)	124(3)
B(8) - H(8)	105(3)	B(9) -H(8,9)	132(3)

B(2) - B(1)	- H(1)	112.8(15)	B(4) - B(9)	- H(9)	132.6(15)
B(3) - B(1)	- H(1)	125.8(15)	B(8) - B(9)	- H(9)	126.0(15)

B(4) - B(1)	- H(1)	124.5(15)	B(10)- B(9)	- H(9)	125.1(15)
B(5) - B(1)	- H(1)	117.0(15)	B(1) -B(10)	-H(10)	118.7(15)
B(10)- B(1)	- H(1)	121.7(15)	B(4) -B(10)	-H(10)	126.6(15)
B(1) - B(2)	- H(2)	115.7(14)	B(5) -B(10)	-H(10)	115.2(15)
B(3) - B(2)	- H(2)	120.9(14)	B(9) -B(10)	-H(10)	122.7(15)
B(5) - B(2)	- H(2)	124.0(14)	B(1) - B(5)	-H(5,6)	129.8(13)
B(6) - B(2)	- H(2)	120.9(15)	B(2) - B(5)	-H(5,6)	97.0(13)
B(7) - B(2)	- H(2)	126.8(15)	B(6) - B(5)	-H(5,6)	42.8(13)
B(1) - B(3)	- H(3)	125.0(15)	B(10)- B(5)	-H(5,6)	98.2(13)
B(2) - B(3)	- H(3)	115.0(15)	H(5) - B(5)	-H(5,6)	107.2(19)
B(4) - B(3)	- H(3)	121.4(15)	B(2) - B(6)	-H(5,6)	107.2(14)
B(7) - B(3)	- H(3)	112.9(15)	B(5) - B(6)	-H(5,6)	48.6(14)
B(8) - B(3)	- H(3)	120.3(15)	B(7) - B(6)	-H(5,6)	114.8(14)
B(1) - B(4)	- H(4)	118.3(16)	H(6) - B(6)	-H(5,6)	109.2(20)
B(3) - B(4)	- H(4)	120.8(16)	B(2) - B(6)	-H(6,7)	108.5(13)
B(8) - B(4)	- H(4)	125.8(16)	B(5) - B(6)	-H(6,7)	118.7(13)
B(9) - B(4)	- H(4)	123.3(16)	B(7) - B(6)	-H(6,7)	49.3(13)
B(10)- B(4)	- H(4)	123.8(16)	H(6) - B(6)	-H(6,7)	107.0(20)
B(1) - B(5)	- H(5)	122.8(15)	H(5,6)- B(6)	-H(6,7)	89.2(19)
B(2) - B(5)	- H(5)	124.3(15)	B(2) - B(7)	-H(6,7)	101.9(12)
B(6) - B(5)	- H(5)	115.7(15)	B(3) - B(7)	-H(6,7)	131.4(12)
B(10)- B(5)	- H(5)	116.7(15)	B(6) - B(7)	-H(6,7)	45.9(12)
B(2) - B(6)	- H(6)	128.6(15)	H(7) - B(7)	-H(6,7)	105.0(20)
B(5) - B(6)	- H(6)	126.0(15)	B(3) - B(8)	-H(8,9)	123.8(13)
B(7) - B(6)	- H(6)	127.9(15)	B(4) - B(8)	-H(8,9)	103.1(13)
B(2) - B(7)	- H(7)	127.6(16)	B(9) - B(8)	-H(8,9)	47.6(13)
B(3) - B(7)	- H(7)	121.8(16)	H(8) - B(8)	-H(8,9)	108.5(21)
B(6) - B(7)	- H(7)	121.2(16)	B(4) - B(9)	-H(8,9)	100.6(13)
B(3) - B(8)	- H(8)	122.9(16)	B(8) - B(9)	-H(8,9)	43.8(12)
B(4) - B(8)	- H(8)	130.5(16)	B(10)- B(9)	-H(8,9)	118.2(13)
B(9) - B(8)	- H(8)	124.9(16)	H(9) - B(9)	-H(8,9)	109.5(19)

A2.4 $[NHEt_3]^+$ $[Cy_3PAuB_{10}H_{12}]^-$.

The Molecular Structure and Associated Numbering Scheme for $[NHEt_3]^+$ $[Cy_3PAuB_{10}H_{12}]^-$.

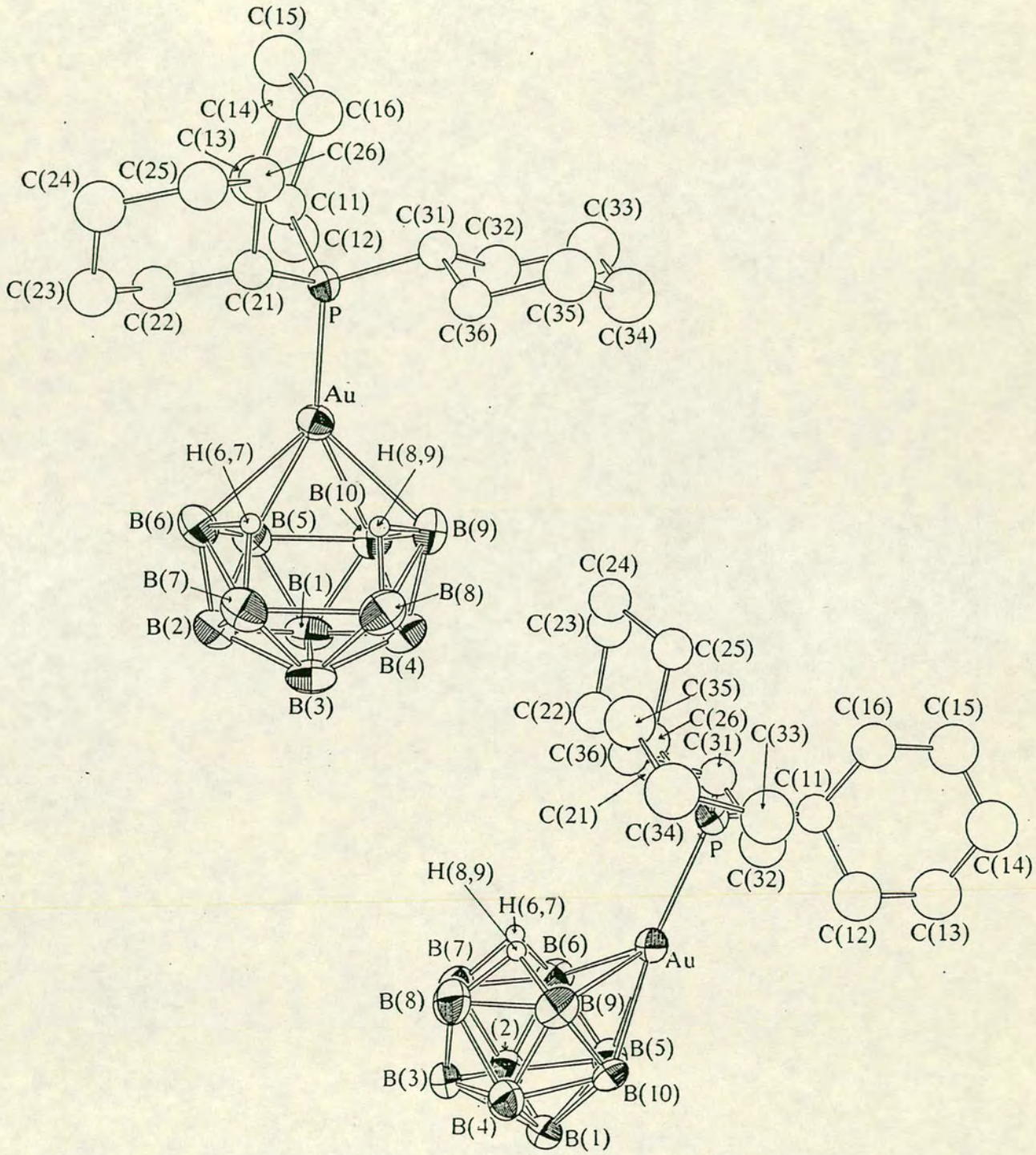

Crystal data. $C_{24}H_{61}AuB_{10}NP$, M = 699.8, monoclinic, with a = 1.75598(23), b = 1.16929(20), c = 1.8533(3) nm, and β = 116.797(11)°. U = 3.3965 nm^{-3}, D_x = 1.368 Mgm^{-3}, μ(Mo-K_α) = 4.384mm^{-1}, $F(000)$ = 1423, space group = $P2_1/a$, and Z = 4.

Data collection and processing. Θ_{max} = 25°, + h + k ± l. 6437 unique data were measured yielding 4617 unique data (R_{merge} = 0.0162) of which 4474 with $F > 2\sigma(F)$ were retained. Variable scan speeds between 0.824 and 2.747 $^{o}min^{-1}$. Very strong C-centring noted. Slight crystal decay noted and corrected.

Structure solution and refinement. Au position determined by inspection of a Patterson map- the near-zero y coordinate was responsible for the pseudo-centring. The Au,P,B and N atoms were refined anisotropically. All the carbon atoms were refined isotropically and freely in the anion. In the cation, however, 5/6 C atoms were equally disordered over pairs of sites, with one common C-N distance (155(1)pm at convergence) and one common C-C distance (141(1)pm at convergence). Cage hydrogen atoms all located and refined with a group thermal parameter (494(70) pm^2 at convergence). Terminal H atoms freely refined, but bridging hydrogens constrained to a common B-H distance (130(1)pm at convergence). Cyclohexyl H atoms set in calculated positions and refined with a group thermal parameter (700(50) pm^2 at convergence).

Weighting scheme $w^{-1} = [\sigma^2(F) + 0.000634(F)^2]$. Maximum peak and minimum trough in final ΔF synthesis 73.3 and -60.7 enm^{-3}, and the maximum shift/e.s.d. in final least squares refinement cycle was 0.398. R = 0.0411, R_w = 0.0531, S = 1.205 and data : variable > 16 : 1.

Table A2.4.1. Fractional Coordinates for the Non-Hydrogen Atoms in $[NHEt_3]^+$ $[Cy_3PAuB_{10}H_{12}]^-$. U_{eq} in $10^4 pm^2$.

	x	y	z	U_{eq}
Au	0.147840(20)	-0.008840(20)	0.261470(20)	0.03687(20)
P	0.21582(12)	0.00406(14)	0.18112(11)	0.0350(11)
B(1)	0.0269(6)	-0.0316(8)	0.3672(6)	0.047(6)
B(2)	0.0248(6)	-0.1749(8)	0.3333(6)	0.046(6)
B(3)	-0.0645(6)	-0.0838(8)	0.2789(6)	0.045(6)
B(4)	-0.0364(6)	0.0621(8)	0.2880(6)	0.045(6)
B(5)	0.1171(6)	-0.0849(8)	0.3594(6)	0.044(6)
B(6)	0.0866(6)	-0.1883(7)	0.2828(6)	0.045(6)
B(7)	-0.0268(7)	-0.1759(8)	0.2281(6)	0.048(7)
B(8)	-0.0708(6)	-0.0103(8)	0.1946(6)	0.051(6)
B(9)	0.0130(6)	0.0967(7)	0.2286(6)	0.045(6)
B(10)	0.0757(6)	0.0662(7)	0.3268(5)	0.039(6)
C(11)	0.3334(5)	0.0059(6)	0.2388(4)	0.0415(17)
C(12)	0.3642(6)	0.0506(9)	0.3241(6)	0.066(3)
C(13)	0.4602(7)	0.0386(9)	0.3744(7)	0.071(3)
C(14)	0.5062(7)	0.0924(9)	0.3304(6)	0.075(3)
C(15)	0.4783(7)	0.0499(9)	0.2513(6)	0.069(3)
C(16)	0.3830(5)	0.0604(8)	0.1982(5)	0.0539(22)
C(21)	0.1884(5)	-0.1205(6)	0.1126(5)	0.0370(18)
C(22)	0.2193(5)	-0.2321(6)	0.1604(5)	0.0433(19)
C(23)	0.1843(6)	-0.3352(7)	0.1063(5)	0.0525(22)
C(24)	0.2045(6)	-0.3319(7)	0.0356(5)	0.0566(23)
C(25)	0.1748(6)	-0.2192(7)	-0.0117(5)	0.0514(22)
C(26)	0.2142(5)	-0.1176(7)	0.0437(5)	0.0477(20)
C(31)	0.1841(5)	0.1328(6)	0.1156(4)	0.0365(17)
C(32)	0.1971(6)	0.2401(7)	0.1672(5)	0.0552(23)
C(33)	0.1677(7)	0.3498(8)	0.1170(6)	0.068(3)
C(34)	0.0744(7)	0.3365(8)	0.0492(6)	0.070(3)
C(35)	0.0640(7)	0.2314(7)	-0.0017(6)	0.062(3)
C(36)	0.0915(5)	0.1241(6)	0.0509(5)	0.0409(18)
N	0.3023(5)	0.5815(6)	0.4584(5)	0.065(6)
C(11a)	0.3158(12)	0.7092(13)	0.4428(15)	0.091(7)
C(11b)	0.3623(17)	0.6516(22)	0.4343(19)	0.116(9)
C(12b)	0.372(3)	0.7697(22)	0.4270(23)	0.157(14)
C(12a)	0.4052(10)	0.7266(14)	0.4744(10)	0.045(4)
C(21a)	0.2084(9)	0.5694(17)	0.4424(10)	0.070(5)
C(21b)	0.2346(12)	0.6595(14)	0.4660(13)	0.080(6)
C(22t)	0.1887(8)	0.6088(9)	0.5041(7)	0.084(3)
C(31a)	0.3194(16)	0.4971(17)	0.4023(13)	0.091(7)
C(31b)	0.2622(16)	0.4718(18)	0.4109(19)	0.131(11)
C(32a)	0.2467(20)	0.470(3)	0.3299(19)	0.150(13)
C(32b)	0.3175(15)	0.3935(18)	0.4014(15)	0.080(6)

Table A2.4.2. Fractional Coordinates of the Hydrogen Atoms in $[NHEt_3]^+$ $[Cy_3PAuB_{10}H_{12}]^-$.

	x	y	z
H(1)	0.036(5)	-0.021(6)	0.430(5)
H(2)	0.016(5)	-0.244(6)	0.379(4)
H(3)	-0.130(5)	-0.118(6)	0.272(5)
H(4)	-0.077(5)	0.123(6)	0.303(5)
H(5)	0.180(5)	-0.106(6)	0.419(5)
H(6)	0.117(5)	-0.281(6)	0.270(4)
H(7)	-0.059(5)	-0.234(6)	0.195(5)
H(8)	-0.127(6)	-0.021(6)	0.149(5)
H(9)	-0.009(5)	0.170(6)	0.190(4)
H(10)	0.109(5)	0.119(6)	0.357(5)
H(6,7)	0.0352(10)	-0.151(6)	0.211(3)
H(8,9)	-0.004(3)	0.006(4)	0.184(4)
H(11)	0.3483	-0.0840	0.2409
H(12a)	0.3476	0.1400	0.3212
H(12b)	0.3328	0.0033	0.3531
H(13a)	0.4765	-0.0510	0.3845
H(13b)	0.4795	0.0810	0.4318
H(14a)	0.5736	0.0752	0.3646
H(14b)	0.4955	0.1836	0.3271
H(15a)	0.5107	0.0968	0.2231
H(15b)	0.4954	-0.0394	0.2552
H(16a)	0.3662	0.1497	0.1873
H(16b)	0.3666	0.0178	0.1414
H(21)	0.1196	-0.1157	0.0815
H(22a)	0.1984	-0.2346	0.2069
H(22b)	0.2882	-0.2347	0.1878
H(23a)	0.1159	-0.3373	0.0838
H(23b)	0.2120	-0.4115	0.1411
H(24a)	0.2726	-0.3400	0.0576
H(24b)	0.1728	-0.4024	-0.0044
H(25a)	0.1061	-0.2136	-0.0374
H(25b)	0.1938	-0.2180	-0.0596
H(26a)	0.2828	-0.1219	0.0686
H(26b)	0.1917	-0.0393	0.0098
H(31)	0.2240	0.1385	0.0853
H(32a)	0.1614	0.2304	0.2014
H(32b)	0.2642	0.2480	0.2082
H(33a)	0.1704	0.4199	0.1560
H(33b)	0.2094	0.3674	0.0897
H(34a)	0.0579	0.4110	0.0107
H(34b)	0.0320	0.3299	0.0768
H(35a)	-0.0022	0.2231	-0.0453
H(35b)	0.1028	0.2405	-0.0329
H(36a)	0.0851	0.0509	0.0130
H(36b)	0.0508	0.1132	0.0801

Table A2.4.3. Anisotropic Thermal Parameters($10^4 pm^2$) for Atoms in $[NHEt_3]^+$ $[Cy_3PAuB_{10}H_{12}]^-$.

	U_{11}	U_{22}	U_{33}	U_{23}	U_{13}	U_{12}
Au	0.03415(17)	0.03443(18)	0.03360(17)	-0.00224(15)	0.01563(13)	-0.00406(15)
P	0.0345(9)	0.0249(9)	0.0369(10)	0.0010(8)	0.0170(8)	-0.0006(8)
B(1)	0.042(5)	0.055(5)	0.039(5)	-0.010(4)	0.024(5)	-0.013(4)
B(2)	0.042(6)	0.043(5)	0.041(6)	0.004(4)	0.018(5)	-0.006(4)
B(3)	0.030(5)	0.060(6)	0.036(5)	-0.008(4)	0.016(5)	-0.011(4)
B(4)	0.031(5)	0.049(5)	0.044(6)	-0.006(4)	0.014(5)	0.003(4)
B(5)	0.038(6)	0.042(5)	0.040(6)	0.006(4)	0.014(5)	-0.004(4)
B(6)	0.050(6)	0.040(5)	0.034(5)	0.004(4)	0.019(5)	-0.004(4)
B(7)	0.047(6)	0.042(5)	0.042(6)	-0.011(4)	0.017(5)	-0.015(4)
B(8)	0.033(5)	0.059(6)	0.045(6)	0.001(5)	0.008(4)	0.004(5)
B(9)	0.048(6)	0.031(4)	0.042(5)	-0.001(4)	0.017(5)	0.006(4)
B(10)	0.042(5)	0.034(5)	0.033(5)	-0.014(4)	0.017(4)	-0.006(4)
N	0.055(5)	0.061(5)	0.067(5)	0.014(4)	0.032(4)	0.011(4)

Table A2.4.4c. The Angles(°) for the Non-Hydrogen Atoms in the $[NHEt_3]^+$ Cation.

C(11a)-	N	-C(21a)	106.8(11)	N	-C(11a)	-C(12a)	107.0(16)
C(11a)-	N	-C(31a)	113.1(13)	N	-C(21a)	-C(22t)	116.4(13)
C(21a)-	N	-C(31a)	108.9(12)	N	-C(31a)	-C(32a)	114.5(22)
C(11b)-	N	-C(21b)	111.2(15)	N	-C(11b)	-C(12b)	132.2(27)
C(11b)-	N	-C(31b)	118.2(16)	N	-C(21b)	-C(22t)	115.4(15)
C(21b)-	N	-C(31b)	111.8(14)	N	-C(31b)	-C(32b)	116.9(22)

Table A2.4.4a. The Bond Lengths(pm) and Angles(°) for the Non-Hydrogen Atoms in the $[Cy_3PAuB_{10}H_{12}]^-$ Anion.

Au - P	229.52(20)	B(8) - B(9)	181.3(15)
Au - B(5)	229.4(10)	B(9) -B(10)	168.7(14)
Au - B(6)	246.9(10)	P -C(11)	184.8(8)
Au - B(9)	249.0(10)	P -C(21)	184.8(8)
Au -B(10)	228.5(10)	P -C(31)	185.5(8)
B(1) - B(2)	178.4(15)	C(11) -C(12)	151.4(14)
B(1) - B(3)	180.4(15)	C(12) -C(13)	152.1(16)
B(1) - B(4)	176.5(15)	C(13) -C(14)	151.8(16)
B(1) - B(5)	176.7(15)	C(14) -C(15)	141.1(16)
B(1) -B(10)	178.3(14)	C(15) -C(16)	151.6(15)

B(2) - B(3)	178.5(15)	C(16) -C(11)	152.4(12)
B(2) - B(5)	180.4(15)	C(21) -C(22)	153.3(12)
B(2) - B(6)	172.9(14)	C(22) -C(23)	151.0(13)
B(2) - B(7)	174.0(15)	C(23) -C(24)	150.4(13)
B(3) - B(4)	176.3(15)	C(24) -C(25)	153.7(13)
B(3) - B(7)	174.6(15)	C(25) -C(26)	151.8(13)
B(3) - B(8)	174.3(15)	C(26) -C(21)	153.5(12)
B(4) - B(8)	177.0(15)	C(31) -C(32)	153.0(13)
B(4) - B(9)	172.9(14)	C(32) -C(33)	153.1(15)
B(4) -B(10)	176.6(14)	C(33) -C(34)	155.9(16)
B(5) - B(6)	175.4(15)	C(34) -C(35)	150.8(15)
B(5) -B(10)	190.3(14)	C(35) -C(36)	152.8(13)
B(6) - B(7)	178.6(15)	C(36) -C(31)	152.8(11)
B(7) - B(8)	207.4(16)		

P - Au - B(5)	156.3(3)	B(4) - B(8) - B(9)	57.7(6)
P - Au - B(6)	123.45(24)	Au - B(9) -B(10)	62.9(5)
P - Au - B(9)	121.60(24)	B(4) - B(9) - B(8)	59.9(6)
P - Au -B(10)	153.3(3)	B(4) - B(9) -B(10)	62.2(6)
B(5) - Au - B(6)	43.0(4)	Au -B(10) - B(5)	65.7(4)
B(5) - Au -B(10)	49.1(4)	Au -B(10) - B(9)	76.0(5)
B(9) - Au -B(10)	41.1(3)	B(1) -B(10) - B(4)	59.7(6)
B(2) - B(1) - B(3)	59.7(6)	B(1) -B(10) - B(5)	57.2(5)
B(2) - B(1) - B(5)	61.1(6)	B(4) -B(10) - B(9)	60.1(6)
B(3) - B(1) - B(4)	59.2(6)	Au - P -C(11)	113.4(3)
B(4) - B(1) -B(10)	59.7(6)	Au - P -C(21)	110.1(3)
B(5) - B(1) -B(10)	64.8(6)	Au - P -C(31)	112.8(3)
B(1) - B(2) - B(3)	60.7(6)	C(11) - P -C(21)	106.5(4)
B(1) - B(2) - B(5)	59.0(6)	C(11) - P -C(31)	107.2(4)
B(3) - B(2) - B(7)	59.4(6)	C(21) - P -C(31)	106.4(4)
B(5) - B(2) - B(6)	59.5(6)	P -C(11) -C(12)	112.8(6)
B(6) - B(2) - B(7)	62.0(6)	P -C(11) -C(16)	117.3(6)
B(1) - B(3) - B(2)	59.6(6)	C(12) -C(11) -C(16)	110.8(7)
B(1) - B(3) - B(4)	59.3(6)	C(11) -C(12) -C(13)	112.6(9)
B(2) - B(3) - B(7)	59.0(6)	C(12) -C(13) -C(14)	110.1(9)
B(4) - B(3) - B(8)	60.7(6)	C(13) -C(14) -C(15)	113.1(10)
B(7) - B(3) - B(8)	72.9(7)	C(14) -C(15) -C(16)	114.2(9)
B(1) - B(4) - B(3)	61.5(6)	C(11) -C(16) -C(15)	110.9(8)
B(1) - B(4) -B(10)	60.7(6)	P -C(21) -C(22)	111.1(6)
B(3) - B(4) - B(8)	59.1(6)	P -C(21) -C(26)	118.1(6)
B(8) - B(4) - B(9)	62.4(6)	C(22) -C(21) -C(26)	109.8(7)
B(9) - B(4) -B(10)	57.7(6)	C(21) -C(22) -C(23)	111.4(7)
Au - B(5) - B(6)	73.8(5)	C(22) -C(23) -C(24)	111.8(8)
Au - B(5) -B(10)	65.2(4)	C(23) -C(24) -C(25)	111.5(8)
B(1) - B(5) - B(2)	59.9(6)	C(24) -C(25) -C(26)	110.5(8)
B(1) - B(5) -B(10)	58.0(6)	C(21) -C(26) -C(25)	109.3(7)
B(2) - B(5) - B(6)	58.1(6)	P -C(31) -C(32)	109.9(6)
Au - B(6) - B(5)	63.2(5)	P -C(31) -C(36)	111.0(5)
B(2) - B(6) - B(5)	62.4(6)	C(32) -C(31) -C(36)	110.6(7)
B(2) - B(6) - B(7)	59.3(6)	C(31) -C(32) -C(33)	113.1(8)
B(2) - B(7) - B(3)	61.6(6)	C(32) -C(33) -C(34)	110.5(9)
B(2) - B(7) - B(6)	58.7(6)	C(33) -C(34) -C(35)	111.9(9)
B(3) - B(7) - B(8)	53.4(6)	C(34) -C(35) -C(36)	110.8(8)
B(3) - B(8) - B(4)	60.2(6)	C(31) -C(36) -C(35)	111.4(7)
B(3) - B(8) - B(7)	53.6(6)		

Table A2.4.5. The Bond Lengths(pm) and Angles(^{o}) Involving the Cage Hydrogen Atoms in the $[Cy_3PAuB_{10}H_{12}]^-$ Anion.

B(1) - H(1)	112(8)	B(8) - H(8)	97(9)
B(2) - H(2)	123(8)	B(9) - H(9)	107(8)
B(3) - H(3)	116(8)	B(10)-H(10)	86(8)
B(4) - H(4)	113(8)	B(6) -H(6,7)	130(5)
B(5) - H(5)	118(8)	B(7) -H(6,7)	130(5)
B(6) - H(6)	128(8)	B(8) -H(8,9)	130(6)
B(7) - H(7)	92(8)	B(9) -H(8,9)	130(6)

B(2) - B(1)	- H(1)	116(4)	B(6) - B(7)	- H(7)	121(5)
B(3) - B(1)	- H(1)	130(4)	B(3) - B(8)	- H(8)	110(5)
B(4) - B(1)	- H(1)	123(4)	B(4) - B(8)	- H(8)	132(5)
B(5) - B(1)	- H(1)	115(4)	B(9) - B(8)	- H(8)	138(5)
B(10)- B(1)	- H(1)	120(4)	Au - B(9)	- H(9)	125(4)
B(1) - B(2)	- H(2)	112(4)	B(4) - B(9)	- H(9)	119(4)
B(3) - B(2)	- H(2)	116(4)	B(8) - B(9)	- H(9)	109(4)
B(5) - B(2)	- H(2)	125(4)	B(10)- B(9)	- H(9)	139(4)
B(6) - B(2)	- H(2)	128(4)	Au -B(10)	-H(10)	104(6)
B(7) - B(2)	- H(2)	127(4)	B(1) -B(10)	-H(10)	120(6)
B(1) - B(3)	- H(3)	131(4)	B(4) -B(10)	-H(10)	126(6)
B(2) - B(3)	- H(3)	116(4)	B(5) -B(10)	-H(10)	114(6)
B(4) - B(3)	- H(3)	124(4)	B(9) -B(10)	-H(10)	118(6)
B(7) - B(3)	- H(3)	109(4)	Au - B(6)	-H(6,7)	72.7(23)
B(8) - B(3)	- H(3)	114(4)	B(2) - B(6)	-H(6,7)	102.1(24)
B(1) - B(4)	- H(4)	115(4)	B(5) - B(6)	-H(6,7)	114.6(24)
B(3) - B(4)	- H(4)	117(4)	B(7) - B(6)	-H(6,7)	46.5(23)
B(8) - B(4)	- H(4)	125(4)	H(6) - B(6)	-H(6,7)	104(4)
B(9) - B(4)	- H(4)	125(4)	B(2) - B(7)	-H(6,7)	101.7(24)
B(10)- B(4)	- H(4)	127(4)	B(3) - B(7)	-H(6,7)	123.9(24)
Au - B(5)	- H(5)	111(4)	B(6) - B(7)	-H(6,7)	46.7(23)
B(1) - B(5)	- H(5)	120(4)	H(7) - B(7)	-H(6,7)	110(6)
B(2) - B(5)	- H(5)	119(4)	B(3) - B(8)	-H(8,9)	121(3)
B(6) - B(5)	- H(5)	115(4)	B(4) - B(8)	-H(8,9)	99(3)
B(10)- B(5)	- H(5)	123(4)	B(9) - B(8)	-H(8,9)	46(3)
Au - B(6)	- H(6)	116(4)	H(8) - B(8)	-H(8,9)	122(6)
B(2) - B(6)	- H(6)	127(4)	Au - B(9)	-H(8,9)	70(3)
B(5) - B(6)	- H(6)	137(4)	B(4) - B(9)	-H(8,9)	101(3)
B(7) - B(6)	- H(6)	114(4)	B(8) - B(9)	-H(8,9)	46(3)
B(2) - B(7)	- H(7)	127(5)	B(10)- B(9)	-H(8,9)	112(3)
B(3) - B(7)	- H(7)	123(5)	H(9) - B(9)	-H(8,9)	109(5)

A2.5 $(Cy_3PAu)_2B_8H_{10}$.

The Molecular Structure and Associated Numbering Scheme for $(Cy_3PAu)_2B_8H_{10}$.

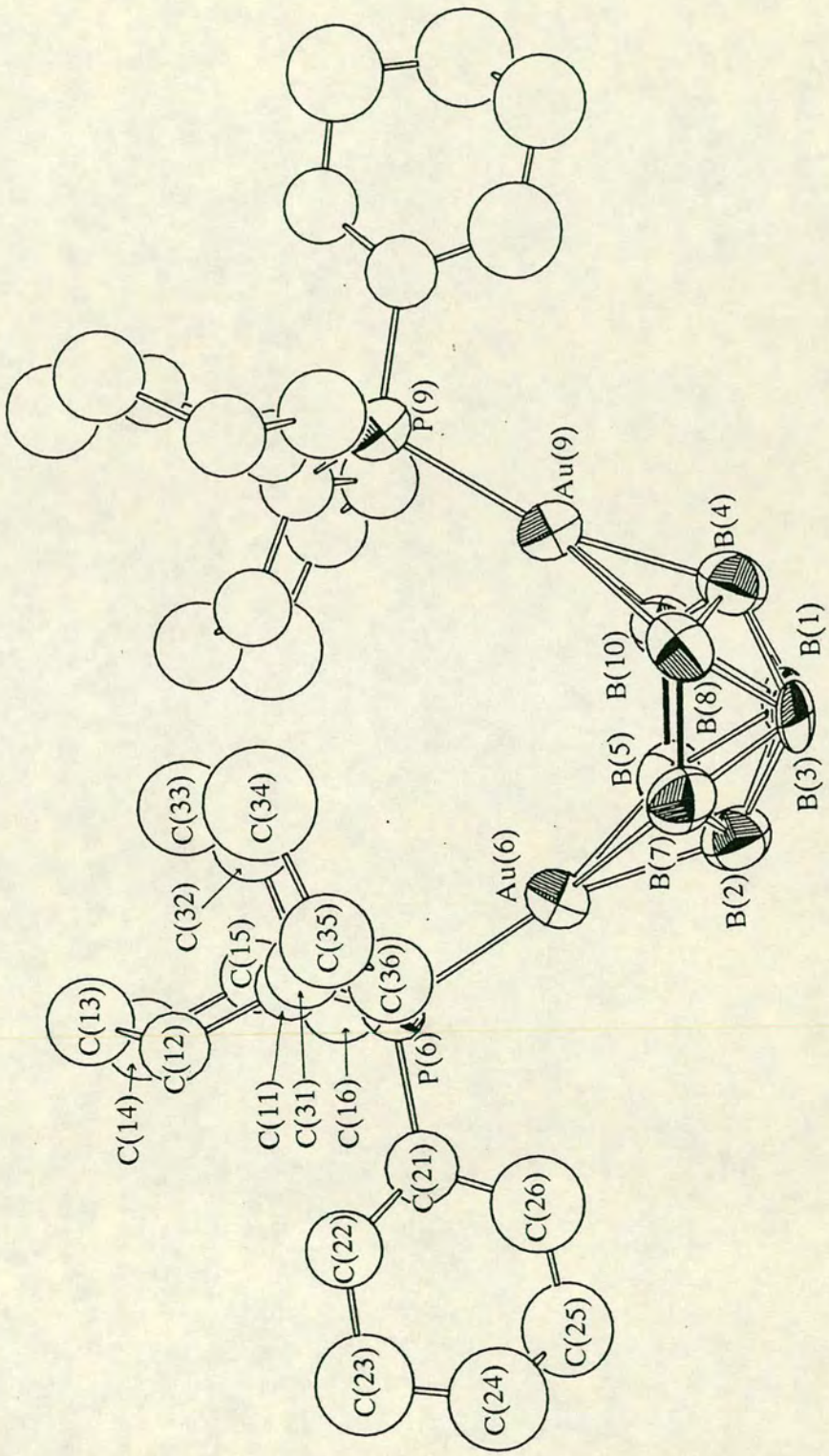

Crystal Data. $C_{36}H_{76}Au_2B_8P_2.2H_2O$, M = 1051.4, Monoclinic with a = 1.7506(7) b = 1.4064(3) c = 2.0179(3) nm, and β = 105.012(22)°. U = 4.7985 nm^3, Z = 4, Space Group $C2/c$ D_c = 1.455 Mgm^{-3}, μ(Mo-K_α) = 6.17 mm^{-1}, and $F(000)$ = 2183.

Data collection and processing. 3052 data were measured yielding 2936 unique data (R_{merge} = 0.0736) of which 2512 with F > 1σ(F) were used. θ_{max} = 22°, + h + k ± l Crystal decayed by *ca.* 10%, and correction was applied.

Structure solution and refinement. Au position located by automatic direct methods. Cage H atoms could not be satisfactorily refined and remain absent. All Au, P, B, C, and O atoms allowed anisotropic thermal motion. The molecule is located on a crystallographic 2-fold axis, and so the asymmetric unit is half of the molecule. Consequently, Au(9) is the image of Au(6), and so was renumbered as Au(6') to show this. This is also true for B(3), B(4), B(8), and B(10) which were numbered as B(1'), B(2'), B(5'), and B(7') respectively. Cyclohexyl-H atoms group thermal parameter = 162(11) pm^2 weighting scheme g = 0.002726 R = 0.0469, R' = 0.0679, S = 1.109. Data : variable ratio = 11 : 1, and maximum and minimum residues were 122.2 and 76.3 enm^{-3} respectively.

Table A2.5.1. Fractional Coordinates of Non-Hydrogen Atoms in $(Cy_3PAu)_2B_8H_{10}$. U_{eq} in $10^4 pm^2$.

	x	y	z	U_{eq}
Au(6)	0.56268(3)	0.02423(3)	0.67346(2)	0.0647(4)
P	0.61615(16)	-0.11439(21)	0.64394(14)	0.0609(17)
B(1)	0.5429(8)	0.2195(8)	0.7811(7)	0.070(9)
B(2)	0.5424(8)	0.1745(9)	0.6990(6)	0.069(8)
B(5)	0.6055(7)	0.1220(10)	0.7764(7)	0.067(8)
B(7)	0.4449(7)	0.1225(9)	0.6619(6)	0.062(8)
C(11)	0.5429(7)	-0.2015(8)	0.5961(6)	0.075(8)
C(12)	0.5752(7)	-0.2966(7)	0.5831(6)	0.076(8)
C(13)	0.5111(9)	-0.3671(11)	0.5485(8)	0.110(12)
C(14)	0.4592(11)	-0.3256(11)	0.4873(8)	0.117(13)
C(15)	0.4223(7)	-0.2304(10)	0.4995(7)	0.091(10)
C(16)	0.4880(8)	-0.1632(10)	0.5329(7)	0.097(10)
C(21)	0.6852(8)	-0.0919(9)	0.5912(6)	0.091(10)
C(22)	0.7500(7)	-0.1598(9)	0.5941(7)	0.090(9)
C(23)	0.8007(10)	-0.1349(12)	0.5448(10)	0.132(15)
C(24)	0.8161(12)	-0.0394(14)	0.5388(13)	0.167(21)
C(25)	0.7513(15)	0.0276(12)	0.5303(11)	0.145(18)
C(26)	0.6991(13)	0.0050(11)	0.5791(13)	0.175(21)
C(31)	0.6704(7)	-0.1773(9)	0.7205(5)	0.075(8)
C(32)	0.6116(8)	-0.2158(10)	0.7600(6)	0.088(9)
C(33)	0.6618(11)	-0.2703(14)	0.8264(8)	0.131(15)
C(34)	0.7178(11)	-0.1981(18)	0.8742(8)	0.154(17)
C(35)	0.7732(8)	-0.1588(15)	0.8337(7)	0.132(14)
C(36)	0.7317(8)	-0.1122(11)	0.7679(6)	0.101(10)
O	0.4262(13)	0.4807(10)	0.2635(14)	0.275(23)

Table A2.5.2. Fractional Coordinates of Hydrogen Atoms.

	x	y	z
H(11)	0.5084	-0.2151	0.6324
H(12a)	0.6147	-0.2864	0.5505
H(12b)	0.6077	-0.3262	0.6316
H(13a)	0.4767	-0.3863	0.5838
H(13b)	0.5386	-0.4300	0.5343
H(14a)	0.4930	-0.3144	0.4502
H(14b)	0.4119	-0.3753	0.4669
H(15a)	0.3837	-0.2410	0.5327
H(15b)	0.3889	-0.2013	0.4511
H(16a)	0.4620	-0.0986	0.5460
H(16b)	0.5218	-0.1472	0.4964
H(21)	0.6492	-0.1145	0.5418
H(22a)	0.7877	-0.1606	0.6458
H(22b)	0.7248	-0.2296	0.5812

H(23a)	0.7703	-0.1608	0.4945
H(23b)	0.8567	-0.1712	0.5623
H(24a)	0.8604	-0.0191	0.5846
H(24b)	0.8400	-0.0317	0.4948
H(25a)	0.7752	0.0984	0.5415
H(25b)	0.7157	0.0247	0.4779
H(26a)	0.6421	0.0373	0.5576
H(26b)	0.7263	0.0374	0.6280
H(31)	0.7017	-0.2357	0.7047
H(32a)	0.5796	-0.1575	0.7750
H(32b)	0.5703	-0.2643	0.7277
H(33a)	0.6965	-0.3257	0.8112
H(33b)	0.6221	-0.3015	0.8535
H(34a)	0.7515	-0.2337	0.9199
H(34b)	0.6837	-0.1412	0.8884
H(35a)	0.8083	-0.2167	0.8223
H(35b)	0.8115	-0.1070	0.8653
H(36a)	0.7017	-0.0497	0.7793
H(36b)	0.7753	-0.0916	0.7412

Table A2.5.3. Anisotropic Thermal Parameters(10^4 pm^2) in $(Cy_3PAu)_2B_8H_{10}$.

	U_{11}	U_{22}	U_{33}	U_{23}	U_{13}	U_{12}
Au(6)	0.0685(4)	0.0626(4)	0.0611(4)	-0.0054(2)	0.0270(2)	0.0031(2)
P	0.0607(16)	0.0616(17)	0.0572(16)	-0.0069(13)	0.0189(12)	0.0025(13)
B(1)	0.10(10)	0.032(6)	0.076(8)	-0.013(6)	0.031(7)	-0.013(6)
B(2)	0.085(8)	0.060(8)	0.059(7)	0.001(6)	0.027(7)	-0.011(7)
B(5)	0.053(7)	0.071(9)	0.075(8)	-0.008(6)	0.024(6)	-0.009(6)
B(7)	0.063(7)	0.060(8)	0.056(7)	-0.004(6)	0.012(5)	0.000(6)
C(11)	0.085(8)	0.068(8)	0.066(7)	-0.014(6)	0.015(6)	-0.005(6)
C(12)	0.080(7)	0.049(7)	0.096(9)	-0.016(6)	0.032(7)	-0.005(6)
C(13)	0.100(10)	0.086(10)	0.130(13)	-0.046(9)	0.013(9)	-0.019(8)
C(14)	0.150(14)	0.089(11)	0.097(11)	-0.009(9)	0.01(10)	-0.04(10)
C(15)	0.078(8)	0.102(11)	0.085(9)	-0.016(8)	0.009(7)	-0.007(8)
C(16)	0.10(10)	0.069(8)	0.10(10)	-0.000(7)	0.002(8)	-0.010(7)
C(21)	0.116(10)	0.074(9)	0.086(8)	0.002(6)	0.065(8)	0.003(7)
C(22)	0.073(8)	0.067(8)	0.132(11)	-0.006(7)	0.056(8)	0.013(6)
C(23)	0.121(13)	0.107(14)	0.172(17)	-0.001(11)	0.090(12)	0.006(10)
C(24)	0.141(16)	0.112(16)	0.26(3)	-0.028(14)	0.138(18)	-0.042(12)
C(25)	0.185(21)	0.094(12)	0.161(18)	0.005(10)	0.108(17)	-0.011(12)
C(26)	0.196(21)	0.072(10)	0.280(3)	0.031(13)	0.189(22)	0.015(11)
C(31)	0.080(8)	0.084(8)	0.057(7)	-0.004(6)	0.022(6)	0.0136(7)
C(32)	0.089(8)	0.107(11)	0.067(7)	0.019(7)	0.035(6)	0.019(8)
C(33)	0.153(15)	0.154(18)	0.082(11)	0.029(10)	0.046(10)	0.046(13)
C(34)	0.134(15)	0.240(24)	0.081(11)	0.025(13)	0.030(11)	0.104(16)
C(35)	0.076(9)	0.212(20)	0.092(11)	-0.013(11)	-0.013(8)	0.062(11)
C(36)	0.079(8)	0.157(14)	0.059(8)	-0.014(8)	0.007(6)	0.004(9)
O	0.279(24)	0.117(12)	0.36(3)	0.125(16)	-0.075(22)	0.035(12)

Table A2.5.4. Bond Lengths(pm) and Angles(°) for $(Cy_3PAu)_2B_8H_{10}$.

Au(6) - P	230.7(3)	C(24) -C(25)	145(3)
Au(6) - B(2)	222.5(13)	C(25) -C(26)	154(3)
Au(6) - B(5)	244.2(13)	C(31) -C(32)	155.3(18)
Au(6) - B(7)	244.3(12)	C(31) -C(36)	154.1(18)
P -C(11)	185.4(12)	C(32) -C(33)	159.6(23)
P -C(21)	183.4(14)	C(33) -C(34)	156(3)
P -C(31)	182.0(12)	C(34) -C(35)	152(3)
C(11) -C(12)	150.1(17)	C(35) -C(36)	149.0(22)
C(11) -C(16)	148.5(18)	B(1) -B(1')	168.9(18)
C(12) -C(13)	152.5(20)	B(1) -B(2')	176.1(19)
C(13) -C(14)	145.2(23)	B(1) -B(7')	176.1(18)
C(14) -C(15)	153.3(22)	B(2) - B(5)	182.0(19)
C(15) -C(16)	150.7(20)	B(2) - B(1)	177.2(19)
C(21) -C(22)	147.2(19)	B(2) - B(7)	182.9(18)
C(21) -C(26)	142(3)	B(5) -B(7')	170.3(18)
C(22) -C(23)	153.6(23)	B(5) - B(1)	177.4(18)
C(23) -C(24)	138(3)		

P -Au(6) - B(2)	164.2(4)	P -C(31) -C(32)	109.6(8)
P -Au(6) - B(5)	129.8(3)	P -C(31) -C(36)	111.4(9)
P -Au(6) - B(7)	147.4(3)	C(32) -C(31) -C(36)	109.7(10)
Au(2) -Au(6) - B(5)	45.6(5)	C(31) -C(32) -C(33)	107.8(11)
Au(2) -Au(6) - B(7)	45.9(4)	C(32) -C(33) -C(34)	109.1(14)
Au(6) - P -C(11)	114.9(4)	C(33) -C(34) -C(35)	106.9(16)
Au(6) - P -C(21)	112.2(4)	C(34) -C(35) -C(36)	114.0(14)
Au(6) - P -C(31)	110.4(4)	C(31) -C(36) -C(35)	113.1(12)
C(11) - P -C(21)	106.4(6)	B(5) - B(1) -B(7')	57.6(7)
C(11) - P -C(31)	105.0(5)	B(7') - B(1) -B(2')	62.6(7)
C(21) - P -C(31)	107.4(6)	B(2') - B(1) -B(1')	61.8(8)
P -C(11) -C(12)	116.0(8)	B(1') - B(1) - B(2)	61.1(8)
P -C(11) -C(16)	114.4(9)	B(1) - B(2) -B(1')	57.1(7)
C(12) -C(11) -C(16)	111.3(10)	B(1') - B(2) - B(7)	58.7(7)
C(11) -C(12) -C(13)	113.2(11)	Au(6) - B(2) - B(5)	73.5(6)
C(12) -C(13) -C(14)	110.6(13)	Au(6) - B(2) - B(7)	73.4(6)
C(13) -C(14) -C(15)	114.3(14)	B(5) - B(2) - B(1)	59.2(7)
C(14) -C(15) -C(16)	108.4(12)	Au(6) - B(5) - B(2)	60.9(6)
C(11) -C(16) -C(15)	113.9(11)	Au(6) - B(5) -B(7')	121.4(8)
P -C(21) -C(22)	118.8(10)	B(1) - B(5) -B(7')	60.8(7)
P -C(21) -C(26)	115.7(12)	B(2) - B(5) - B(1)	59.1(7)
C(22) -C(21) -C(26)	117.8(14)	B(2) - B(1) - B(5)	61.8(7)
C(21) -C(22) -C(23)	113.2(12)	Au(6) - B(7) - B(2)	60.8(5)
C(22) -C(23) -C(24)	115.9(16)	Au(6) - B(7) -B(5')	120.9(8)
C(23) -C(24) -C(25)	118.5(20)	B(2) - B(7) -B(1')	58.7(7)
C(24) -C(25) -C(26)	111.5(18)	B(1') - B(7) -B(5')	61.6(7)
C(21) -C(26) -C(25)	117.7(17)		

A2.6 $[(Cy_3P)_2Au]^+_2$ $[(B_{10}H_{12})Au(B_{10}H_{13})]^{2-}.4CH_2Cl_2$.

The Molecular Structure and Associated Numbering Scheme for $[(Cy_3P)_2Au]^+_2$ $[(B_{10}H_{12})Au(B_{10}H_{13})]^{2-}$.

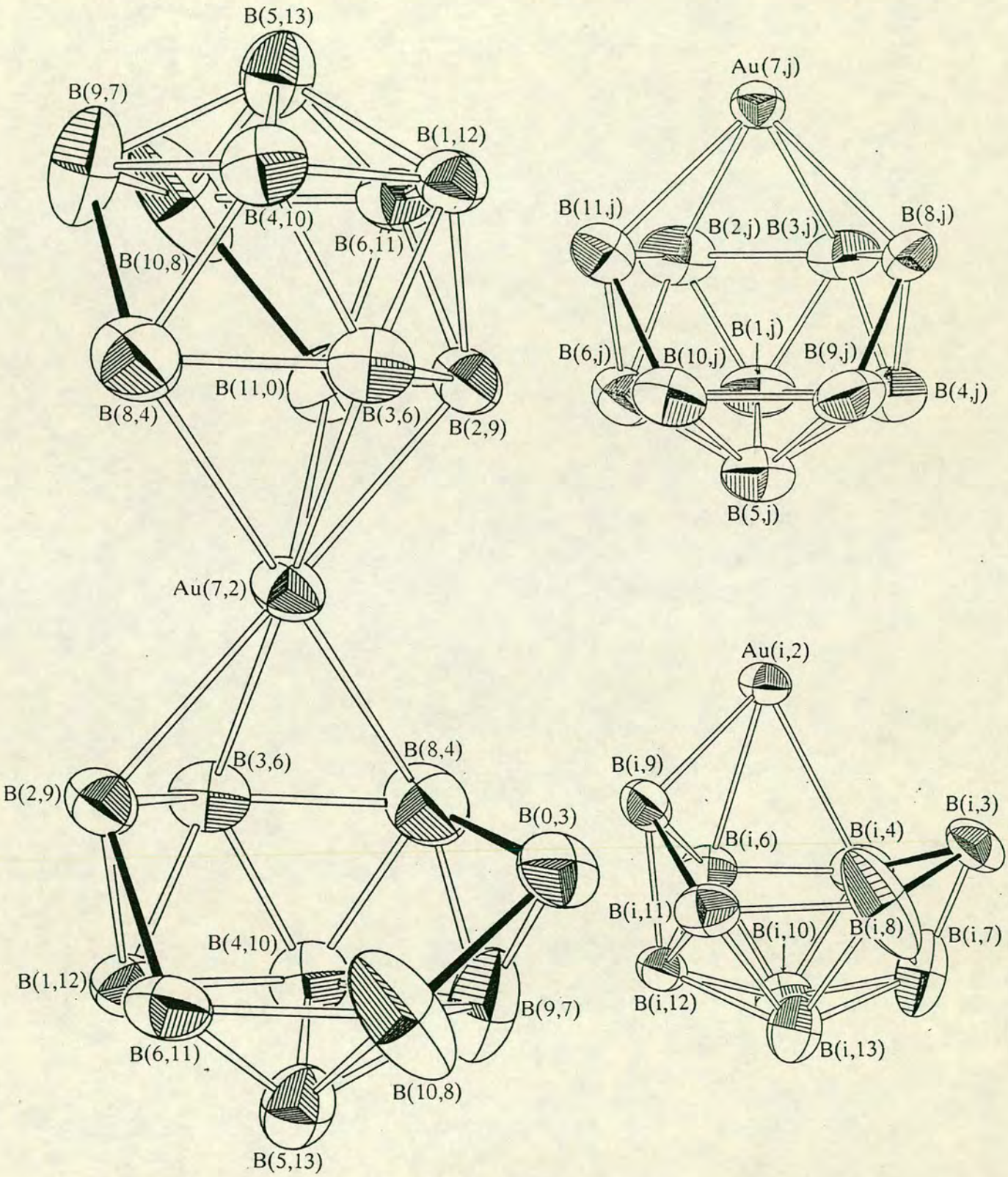

Crystal data. $C_{72}H_{157}Au_3B_{20}P_4.4CH_2Cl_2$, M = 2293.8. Triclinic with *a* = 1.2631(5), *b* = 1.5146(7), *c* = 1.5184(6)nm, α = 76.60(3), β = 69.84(3), γ = 80.84°. *U* = 2.5693nm^3, μ(Mo-K_α) = 4.446 mms^{-1}, D_x = 1.441 Mgm^{-3}, *F(000)* = 1154, *Z* = 1, and space group *P1*.

data collection and processing. 7931 unique data were measured, (θ_{max} = 25°, ± *h* ± *k* + *l*), of which 7874 with $F > 2\sigma(F)$ were retained. Scan speeds 1.030 to 3.296 °min^{-1}. Slight crystal decay was noted but not corrected.

Structure solution and refinement. Au atom positions located by inspection of a Patterson synthesis. Au, P, B, and Cl atoms allowed anisotropic thermal motion. No disorder apart from that of the boron atoms (B(0,3) and B(11,0) have occupancy factors 0.5) discussed in the text (chapter 5,page 117) Cyclohexyl H atoms group thermal parameter was 680(40)pm^2 at convergence. Cage H atoms absent. Weighting scheme g = 0.000622, *R* = 0.048, R_w = 0.066, *S* = 3.123, data : variable > 24 : 1. Maximum and minimum residues were 367 and -962 enm^{-3}. Maximum shift/e.s.d. in final least squares refinement cycle was 0.011.

Table A2.6.1. Fractional Coordinates of Refined Atoms in $[(Cy_3P)_2Au]^+_2[(B_{10}H_{12})Au(B_{10}H_{13})]^{2-}.4H_2Cl_2$. U_{eq} in 10^4pm^2.

	x	y	z	U_{eq}
Au(7,2)	0.00000	0.00000	0.00000	0.0346(3)
B(1,12)	-0.0371(7)	-0.2392(6)	0.1173(6)	0.035(5)
B(2,9)	0.0470(8)	-0.1438(6)	0.0894(7)	0.038(5)
B(3,6)	-0.1044(7)	-0.1234(6)	0.0940(7)	0.038(5)
B(4,10)	-0.1367(7)	-0.2078(6)	0.0534(7)	0.042(6)
B(5,13)	-0.0127(8)	-0.2742(7)	0.0123(7)	0.046(6)
B(6,11)	0.1009(8)	-0.2390(6)	0.0331(7)	0.041(6)
B(8,4)	-0.1252(9)	-0.0909(7)	-0.0251(8)	0.055(7)
B(9,7)	-0.0687(9)	-0.1904(9)	-0.0738(8)	0.066(8)
B(10,8)	0.0926(11)	-0.2056(9)	-0.0905(8)	0.074(9)
B(11,0)	0.1441(16)	-0.1299(14)	-0.0284(15)	0.047(13)

B(0,3)	-0.0015(16)	-0.1059(12)	-0.1443(14)	0.043(11)
Au(2)	0.31831(2)	0.27744(2)	0.21841(2)	0.0266(2)
P(1)	0.42194(15)	0.13654(12)	0.22420(13)	0.0274(10)
P(2)	0.21711(14)	0.41991(11)	0.20892(13)	0.2580(10)
C(101)	0.3342(6)	0.0353(4)	0.3030(5)	0.0277(15)
C(102)	0.2122(7)	0.0573(5)	0.3053(6)	0.0399(18)
C(103)	0.1347(7)	-0.0233(6)	0.3802(7)	0.0469(20)
C(104)	0.1827(7)	-0.1166(6)	0.3587(7)	0.0474(20)
C(105)	0.3036(7)	-0.1376(5)	0.3568(6)	0.0391(18)
C(106)	0.3770(6)	-0.0571(5)	0.2824(6)	0.0336(16)
C(111)	0.4852(6)	0.1267(5)	0.0990(5)	0.0286(15)
C(112)	0.3956(6)	0.1270(5)	0.0542(5)	0.0292(15)
C(113)	0.4457(6)	0.1290(5)	-0.0533(5)	0.0321(15)
C(114)	0.5188(7)	0.2115(5)	-0.1123(6)	0.0414(18)
C(115)	0.6135(8)	0.2067(7)	-0.0699(7)	0.0527(22)
C(116)	0.5619(7)	0.2105(6)	0.0357(6)	0.0435(19)
C(121)	0.5394(6)	0.1304(5)	0.2719(6)	0.0340(16)
C(122)	0.5092(8)	0.1711(7)	0.3543(7)	0.0584(24)
C(123)	0.6092(8)	0.1696(7)	0.3888(8)	0.0605(25)
C(124)	0.6725(9)	0.0801(7)	0.4086(8)	0.067(3)
C(125)	0.7030(8)	0.0381(6)	0.3226(7)	0.0515(22)
C(126)	0.6087(7)	0.0367(6)	0.2883(7)	0.0451(19)
C(201)	0.2312(6)	0.4881(4)	0.0811(5)	0.0262(14)
C(202)	0.2062(6)	0.4262(5)	0.0290(6)	0.0345(16)
C(203)	0.2206(7)	0.4776(6)	-0.0785(6)	0.0425(18)
C(204)	0.3387(7)	0.5135(5)	-0.1319(6)	0.0401(18)
C(205)	0.3658(6)	0.5758(5)	-0.0835(6)	0.0358(16)
C(206)	0.3498(6)	0.5254(5)	0.0252(5)	0.0315(15)
C(211)	0.0642(6)	0.4070(5)	0.2794(5)	0.0288(15)
C(212)	0.0272(7)	0.3093(5)	0.2988(6)	0.0391(18)
C(213)	-0.0975(7)	0.3012(6)	0.3676(7)	0.0479(20)
C(214)	-0.1739(8)	0.3762(6)	0.3252(7)	0.0493(21)
C(215)	-0.1350(7)	0.4732(5)	0.3034(6)	0.0402(18)
C(216)	-0.0140(6)	0.4834(5)	0.2360(5)	0.0327(16)
C(221)	0.2728(6)	0.4875(5)	0.26210(5)	0.0305(15)
C(222)	0.2842(8)	0.4279(6)	0.3622(7)	0.0484(21)
C(223)	0.3309(8)	0.4800(7)	0.4090(8)	0.0591(24)
C(224)	0.2664(9)	0.5726(7)	0.4131(8)	0.0600(25)
C(225)	0.2601(8)	0.6326(6)	0.3142(7)	0.0524(22)
C(226)	0.2052(7)	0.5799(5)	0.2698(6)	0.0385(17)
C(1)	0.6649(10)	0.7181(8)	0.3075(10)	0.081(3)
C(2)	0.9075(10)	0.8054(8)	0.3740(9)	0.072(3)
Cl(11)	0.6195(3)	0.77291(21)	0.3985(3)	0.0922(24)
Cl(12)	0.5826(3)	0.62726(25)	0.3299(3)	0.101(3)
Cl(21)	0.8523(3)	0.84152(23)	0.48005(24)	0.0933(24)
Cl(22)	0.9491(3)	0.6862(3)	0.40651(25)	0.110(3)

Table A2.6.2. The Fractional Coordinates of the Hydrogen Atoms in the $[(Cy_3P)_2Au]^+$ Cation.

	x	y	z
H(101)	0.3405	0.0245	0.3751
H(102a)	0.1826	0.1209	0.3258
H(102b)	0.2074	0.0676	0.2329
H(103a)	0.0507	-0.0082	0.3738
H(103b)	0.1312	-0.0287	0.4539
H(104a)	0.1776	-0.1128	0.2879
H(104b)	0.1326	-0.1726	0.4150
H(105a)	0.3083	-0.1472	0.4291
H(105b)	0.3345	-0.2010	0.3364
H(106a)	0.3770	-0.0513	0.2096
H(106b)	0.4621	-0.0726	0.2861
H(111)	0.5343	0.0611	0.1017
H(112a)	0.3484	0.0647	0.0953
H(112b)	0.3395	0.1883	0.0585
H(113a)	0.3780	0.1343	-0.0833
H(113b)	0.4961	0.0650	-0.0577
H(114a)	0.5548	0.2105	-0.1876
H(114b)	0.4679	0.2756	-0.1097
H(115a)	0.6638	0.1421	-0.0709
H(116a)	0.6287	0.2070	0.0661
H(116b)	0.5121	0.2754	0.0362
H(121)	0.5990	0.1761	0.2106
H(122a)	0.4787	0.2430	0.3301
H(122b)	0.4433	0.1315	0.4151
H(123a)	0.5780	0.1893	0.4558
H(123b)	0.6666	0.2207	0.3327
H(124a)	0.7494	0.0906	0.4190
H(124b)	0.6221	0.0318	0.4747
H(125a)	0.7353	-0.0332	0.3466
H(125b)	0.7679	0.0788	0.2617
H(126a)	0.6420	0.0201	0.2196
H(126b)	0.5533	-0.0170	0.3424
H(201)	0.1716	0.5477	0.0817
H(202a)	0.1203	0.4049	0.0653
H(202b)	0.2635	0.3650	0.0339
H(203a)	0.2066	0.4301	-0.1127
H(203b)	0.1595	0.5362	-0.0837
H(204a)	0.3446	0.5530	-0.2070
H(204b)	0.3992	0.4544	-0.1311
H(205a)	0.4524	0.5951	-0.1200
H(205b)	0.3104	0.6382	-0.0902
H(206a)	0.4112	0.4671	0.0312
H(206b)	0.3634	0.5739	0.0583
H(211)	0.0558	0.4165	0.3490
H(212a)	0.0330	0.2989	0.2302
H(212b)	0.0807	0.2570	0.3338
H(213a)	-0.1009	0.3073	0.4374
H(213b)	-0.1261	0.2336	0.3786

H(214a)	-0.1750	0.3673	0.2579
H(214b)	-0.2580	0.3699	0.3772
H(215a)	-0.1408	0.4846	0.3715
H(215b)	-0.1889	0.5248	0.2680
H(216a)	-0.0097	0.4781	0.1656
H(216b)	0.0130	0.5511	0.2262
H(221)	0.3555	0.5067	0.2110
H(222a)	0.3400	0.3675	0.3525
H(222b)	0.2017	0.4049	0.4110
H(223a)	0.3255	0.4367	0.4830
H(223b)	0.4183	0.4933	0.3667
H(224a)	0.3084	0.6098	0.4403
H(224b)	0.1817	0.5589	0.4627
H(225a)	0.2098	0.6960	0.3216
H(225b)	0.3443	0.6503	0.2656
H(226a)	0.2045	0.6235	0.1974
H(226b)	0.1196	0.5650	0.3166

Table A2.6.3. The Anisotropic Thermal Parameters($10^4 pm^2$) in $[(Cy_3P)_2Au]^+_2$ $[(B_{10}H_{12})Au(B_{10}H_{13})]^{2-}$.

	U_{11}	U_{22}	U_{33}	U_{23}	U_{13}	U_{12}
Au(7,2)	0.0271(2)	0.0264(2)	0.0407(3)	-0.0032(2)	-0.0126(2)	-0.0048(2)
Au(2)	0.0256(2)	0.0242(2)	0.0245(2)	-0.0105(1)	-0.0077(1)	0.0010(1)
P(1)	0.0265(9)	0.0254(8)	0.0247(9)	-0.0106(7)	-0.0090(7)	0.0016(7)
P(2)	0.0261(9)	0.0242(8)	0.0210(9)	-0.0090(7)	-0.0058(7)	0.0009(7)
B(1,12)	0.036(5)	0.028(4)	0.030(4)	-0.006(3)	-0.006(4)	-0.007(3)
B(2,9)	0.045(5)	0.027(4)	0.031(5)	-0.004(4)	-0.010(4)	-0.002(4)
B(3,6)	0.025(4)	0.036(4)	0.042(5)	-0.011(4)	-0.005(4)	-0.004(3)
B(4,10)	0.025(4)	0.042(5)	0.047(6)	-0.014(4)	-0.009(4)	-0.004(4)
B(5,13)	0.039(5)	0.051(6)	0.036(5)	-0.020(4)	-0.009(4)	0.003(4)
B(6,11)	0.037(5)	0.026(4)	0.051(6)	-0.012(4)	-0.017(4)	0.003(3)
B(8,4)	0.049(6)	0.043(5)	0.060(7)	-0.0015(5)	-0.027(5)	-0.013(4)
B(9,7)	0.049(6)	0.092(9)	0.047(6)	-0.033(6)	-0.024(5)	0.012(6)
B(10,8)	0.072(8)	0.074(8)	0.035(6)	0.005(6)	0.014(6)	0.037(7)
B(11,0)	0.032(9)	0.050(11)	0.047(12)	-0.027(9)	-0.004(8)	0.007(8)
B(0,3)	0.045(11)	0.036(9)	0.031(9)	-0.007(8)	0.006(8)	-0.011(8)

Table A2.6.4c. Bond Lengths(pm) and Angles(°) for the $[(Cy_3P)_2Au]^+$ cation.

Au(2) - P(1)	231.05(19)	C(125)-C(126)	146.0(14)
Au(2) - P(2)	231.32(18)	C(201)-C(202)	153.7(11)
P(1) -C(101)	184.9(7)	C(201)-C(206)	153.5(10)
P(1) -C(111)	183.8(8)	C(202)-C(203)	151.6(12)
P(1) -C(121)	184.0(8)	C(203)-C(204)	152.0(12)
P(2) -C(201)	183.1(7)	C(204)-C(205)	151.1(12)
P(2) -C(211)	186.3(8)	C(205)-C(206)	152.6(11)
P(2) -C(221)	183.4(6)	C(211)-C(212)	152.6(11)
C(101)-C(102)	151.4(11)	C(211)-C(216)	152.5(11)
C(101)-C(106)	151.0(11)	C(105)-C(106)	153.0(12)
C(102)-C(103)	155.9(13)	C(212)-C(213)	155.9(13)
C(103)-C(104)	153.9(14)	C(213)-C(214)	149.3(14)
C(104)-C(105)	150.2(13)	C(214)-C(215)	151.7(13)
C(111)-C(112)	150.6(11)	C(215)-C(216)	151.6(11)
C(111)-C(116)	155.3(12)	C(221)-C(222)	153.1(12)
C(112)-C(113)	152.6(11)	C(221)-C(226)	153.6(10)
C(113)-C(114)	150.6(11)	C(222)-C(223)	151.1(15)
C(114)-C(115)	152.4(14)	C(223)-C(224)	151.4(16)
C(115)-C(116)	152.6(14)	C(224)-C(225)	149.7(15)
C(121)-C(122)	148.3(13)	C(225)-C(226)	155.8(13)
C(121)-C(126)	153.7(12)	C(1) -Cl(11)	172.9(14)
C(122)-C(123)	151.9(15)	C(1) -Cl(12)	172.9(14)
C(123)-C(124)	145.5(16)	C(2) -Cl(21)	175.2(13)
C(124)-C(125)	154.4(15)	C(2) -Cl(22)	175.0(13)

P(1) -Au(2) - P(2)	178.68(7)	C(123)-C(124) -C(125)	111.4(9)
Au(2) - P(1) -C(101)	111.93(24)	C(124)-C(125) -C(126)	114.6(9)
Au(2) - P(1) -C(111)	109.3(3)	C(121)-C(126) -C(125)	113.4(8)
Au(2) - P(1) -C(121)	111.2(3)	P(2) -C(201) -C(202)	109.3(5)
C(101)- P(1) -C(111)	109.5(3)	P(2) -C(201) -C(206)	111.9(5)
C(101)- P(1) -C(121)	108.0(3)	C(202)-C(201) -C(206)	109.4(6)
C(111)- P(1) -C(121)	106.7(4)	C(201)-C(202) -C(203)	111.9(7)
Au(2) - P(2) -C(201)	111.26(24)	C(202)-C(203) -C(204)	111.0(7)
Au(2) - P(2) -C(211)	112.81(25)	C(203)-C(204) -C(205)	111.5(7)
Au(2) - P(2) -C(221)	108.77(21)	C(204)-C(205) -C(206)	111.0(7)
C(201)- P(2) -C(211)	108.7(3)	C(201)-C(206) -C(205)	112.6(6)
C(201)- P(2) -C(221)	108.1(3)	P(2) -C(211) -C(212)	111.9(5)
C(211)- P(2) -C(221)	107.0(3)	P(2) -C(211) -C(216)	114.5(5)
P(1) -C(101) -C(102)	111.4(5)	C(212)-C(211) -C(216)	111.5(6)
P(1) -C(101) -C(106)	116.2(5)	C(102)-C(101) -C(106)	110.9(6)
C(101)-C(102) -C(103)	112.0(7)	C(211)-C(212) -C(213)	108.4(7)
C(102)-C(103) -C(104)	109.7(7)	C(212)-C(213) -C(214)	111.8(8)
C(103)-C(104) -C(105)	112.4(8)	C(213)-C(214) -C(215)	111.6(8)
P(1) -C(111) -C(112)	111.2(5)	C(214)-C(215) -C(216)	110.9(7)
P(1) -C(111) -C(116)	108.3(5)	C(211)-C(216) -C(215)	110.9(6)
C(112)-C(111) -C(116)	110.1(6)	P(2) -C(221) -C(222)	111.1(5)
C(111)-C(112) -C(113)	112.2(6)	P(2) -C(221) -C(226)	114.1(5)
C(112)-C(113) -C(114)	110.7(6)	C(222)-C(221) -C(226)	110.5(6)
C(113)-C(114) -C(115)	110.1(7)	C(221)-C(222) -C(223)	113.3(8)
C(114)-C(115) -C(116)	109.0(8)	C(222)-C(223) -C(224)	112.1(9)

C(111)-C(116)	-C(115)	110.1(7)	C(223)-C(224)	-C(225)	112.0(9)
P(1) -C(121)	-C(122)	113.5(6)	C(224)-C(225)	-C(226)	110.7(8)
P(1) -C(121)	-C(126)	116.5(6)	C(221)-C(226)	-C(225)	110.1(7)
C(122)-C(121)	-C(126)	113.8(7)	Cl(11)- C(1)	-Cl(12)	113.4(8)
C(121)-C(122)	-C(123)	112.4(8)	Cl(21)- C(2)	-Cl(22)	109.4(7)
C(122)-C(123)	-C(124)	115.7(9)	C(104)-C(105)	-C(106)	110.8(7)

Table A2.6.4a(1). Bond Lengths(pm) and Angles(^{o}) for the *Nido*-7-$AuB_{10}H_{12}$ Fragment in the $[(B_{10}H_{12})Au(B_{10}H_{13})]^{2-}$ Anion. For clarity, the *arachno* component in the numbering of B(i,j) has been replaced by j.

Au(7,j)-B(2,j)	226.2(10)	B(3,j)-B(8,j)	180.8(15)
Au(7,j)-B(3,j)	223.1(10)	B(4,j)-B(5,j)	175.8(14)
Au(7,j)-B(8,j)	244.7(12)	B(4,j)-B(8,j)	176.8(15)
Au(7,j)-B(11,j)	249.9(21)	B(4,j)-B(9,j)	176.7(16)
B(1,j)-B(2,j)	177.9(13)	B(5,j)-B(6,j)	176.3(14)
B(1,j)-B(3,j)	180.3(13)	B(5,j)-B(9,j)	175.3(17)
B(1,j)-B(4,j)	176.2(14)	B(5,j)-B(10,j)	179.7(17)
B(1,j)-B(5,j)	175.9(14)	B(6,j)-B(10,j)	180.6(17)
B(1,j)-B(6,j)	177.6(13)	B(6,j)-B(11,j)	167.8(23)
B(2,j)-B(3,j)	186.8(13)	B(8,j)-B(9,j)	183.5(17)
B(2,j)-B(6,j)	183.5(14)	B(9,j)-B(10,j)	195.2(19)
B(2,j)-B(11,j)	175.0(23)	B(10,j)-B(11,j)	200.0(25)
B(3,j)-B(4,j)	174.4(14)		

B(2,j)-Au(7,j)	-B(3,j)	49.1(3)	B(1,j) -B(5,j)	-B(4,j)	60.2(6)
B(2,j)-Au(7,j)	-B(11,j)	42.8(5)	B(1,j) -B(5,j)	-B(6,j)	60.6(6)
B(3,j)-Au(7,j)	-B(8,j)	45.2(4)	B(4,j) -B(5,j)	-B(9,j)	60.4(6)
B(2,j)-B(1,j)	-B(3,j)	62.9(5)	B(6,j) -B(5,j)	-B(10,j)	61.0(6)
B(2,j)-B(1,j)	-B(6,j)	62.2(5)	B(9,j) -B(5,j)	-B(10,j)	66.7(7)
B(3,j)-B(1,j)	-B(4,j)	58.6(5)	B(1,j) -B(6,j)	-B(2,j)	59.0(5)
B(4,j)-B(1,j)	-B(5,j)	59.9(6)	B(1,j) -B(6,j)	-B(5,j)	59.6(5)
B(5,j)-B(1,j)	-B(6,j)	59.8(5)	B(2,j) -B(6,j)	-B(11,j)	59.6(9)
Au(7,j)-B(2,j)	-B(3,j)	64.6(4)	B(5,j) -B(6,j)	-B(10,j)	60.4(6)
Au(7,j)-B(2,j)	-B(11,j)	75.8(8)	B(10,j)-B(6,j)	-B(11,j)	70.0(9)
B(1,j)-B(2,j)	-B(3,j)	59.2(5)	Au(7,j)-B(8,j)	-B(3,j)	61.1(4)
B(1,j)-B(2,j)	-B(6,j)	58.8(5)	B(3,j) -B(8,j)	-B(4,j)	58.4(6)
B(6,j)-B(2,j)	-B(11,j)	55.7(8)	B(4,j) -B(8,j)	-B(9,j)	58.7(6)
Au(7,j)-B(3,j)	-B(2,j)	66.3(4)	B(4,j) -B(9,j)	-B(5,j)	59.9(6)
Au(7,j)-B(3,j)	-B(8,j)	73.8(5)	B(4,j) -B(9,j)	-B(8,j)	58.8(6)
B(1,j)-B(3,j)	-B(2,j)	58.0(5)	B(5,j) -B(9,j)	-B(10,j)	57.7(7)
B(1,j)-B(3,j)	-B(4,j)	59.6(5)	B(5,j) -B(10,j)	-B(6,j)	58.6(6)
B(4,j)-B(3,j)	-B(8,j)	59.7(6)	B(5,j) -B(10,j)	-B(9,j)	55.6(6)
B(1,j)-B(4,j)	-B(3,j)	61.9(5)	B(6,j) -B(10,j)	-B(11,j)	52.0(8)
B(1,j)-B(4,j)	-B(5,j)	60.0(6)	Au(7,j)-B(11,j)	-B(2,j)	61.4(7)
B(3,j)-B(4,j)	-B(8,j)	61.9(6)	B(2,j) -B(11,j)	-B(6,j)	64.7(9)
B(5,j)-B(4,j)	-B(9,j)	59.7(6)	B(6,j) -B(11,j)	-B(10,j)	58.0(8)
B(8,j)-B(4,j)	-B(9,j)	62.5(7)			

Table A2.6.4a(2). Bond Lengths(pm) and Angles(°) for the *Arachno*-2-$AuB_{10}H_{13}$ Fragment of the $[(B_{10}H_{12})Au(B_{10}H_{13})]^{2-}$ Anion. For clarity, the *nido* numbering of the Atoms B(i,j) has been replaced by i.

Au(i,2)-B(i,4)	244.7(12)	B(i,7) -B(i,10)	176.7(16)
Au(i,2)-B(i,6)	223.1(10)	B(i,7) -B(i,13)	175.3(17)
Au(i,2)-B(i,9)	226.2(10)	B(i,8) -B(i,11)	180.6(17)
B(i,3)-B(i,7)	152.8(24)	B(i,8) -B(i,13)	179.7(17)
B(i,3)-B(i,8)	191.3(24)	B(i,9) -B(i,11)	183.5(14)
B(i,4)-B(i,6)	180.8(15)	B(i,9) -B(i,12)	177.9(13)
B(i,4)-B(i,7)	183.5(17)	B(i,10)-B(i,12)	176.2(14)
B(i,4)-B(i,10)	176.8(15)	B(i,10)-B(i,13)	175.8(14)
B(i,6)-B(i,9)	186.8(13)	B(i,11)-B(i,12)	177.6(13)
B(i,6)-B(i,10)	174.4(14)	B(i,11)-B(i,13)	176.3(14)
B(i,6)-B(i,12)	180.3(13)	B(i,12)-B(i,13)	175.9(14)
B(i,7)-B(i,8)	195.2(19)		

B(i,4)-Au(i,2)	-B(i,6)	45.2(4)	B(i,6) -B(i,9)	-B(i,12)	59.2(5)
B(i,6)-Au(i,2)	-B(i,9)	49.1(3)	B(i,11)-B(i,9)	-B(i,12)	58.8(5)
B(i,7)-B(i,3)	-B(i,8)	68.1(10)	B(i,4) -B(i,10)	-B(i,6)	61.9(6)
Au(i,2)-B(i,4)	-B(i,6)	61.1(4)	B(i,4) -B(i,10)	-B(i,7)	62.5(7)
B(i,6)-B(i,4)	-B(i,10)	58.4(6)	B(i,6) -B(i,10)	-B(i,12)	61.9(5)
B(i,7)-B(i,4)	-B(i,10)	58.7(6)	B(i,7) -B(i,10)	-B(i,13)	59.7(6)
Au(i,2)-B(i,6)	-B(i,4)	73.8(5)	B(i,12)-B(i,10)	-B(i,13)	60.0(6)
Au(i,2)-B(i,6)	-B(i,9)	66.3(4)	B(i,8) -B(i,11)	-B(i,13)	60.4(6)
B(i,4)-B(i,6)	-B(i,10)	59.7(6)	B(i,9) -B(i,11)	-B(i,12)	59.0(5)
B(i,9)-B(i,6)	-B(i,12)	58.0(5)	B(i,12)-B(i,11)	-B(i,13)	59.6(5)
B(i,10)-B(i,6)	-B(i,12)	59.6(5)	B(i,6) -B(i,12)	-B(i,9)	62.9(5)
B(i,3)-B(i,7)	-B(i,4)	72.5(10)	B(i,6) -B(i,12)	-B(i,10)	58.6(5)
B(i,3)-B(i,7)	-B(i,8)	65.4(10)	B(i,9) -B(i,12)	-B(i,11)	62.2(5)
B(i,4)-B(i,7)	-B(i,10)	58.8(6)	B(i,10)-B(i,12)	-B(i,13)	59.9(6)
B(i,8)-B(i,7)	-B(i,13)	57.7(7)	B(i,11)-B(i,12)	-B(i,13)	59.8(5)
B(i,10)-B(i,7)	-B(i,13)	59.9(6)	B(i,7) -B(i,13)	-B(i,8)	66.7(7)
B(i,3)-B(i,8)	-B(i,7)	46.5(8)	B(i,7) -B(i,13)	-B(i,10)	60.4(6)
B(i,7)-B(i,8)	-B(i,13)	55.6(6)	B(i,8) -B(i,13)	-B(i,11)	61.0(6)
B(i,11)-B(i,8)	-B(i,13)	58.6(6)	B(i,10)-B(i,13)	-B(i,12)	60.2(6)
Au(i,2)-B(i,9)	-B(i,6)	64.6(4)	B(i,11)-B(i,13)	-B(i,12)	60.6(6)

A2.7 $[(o\text{-tolyl}_3P)_2Au]^+ [(B_{10}H_{12})_2Au]^-$.

The Molecular Structure and Associated Numbering Scheme for $[(o\text{-tolyl}_3P)_2Au]^+ [(B_{10}H_{12})_2Au]^-$.

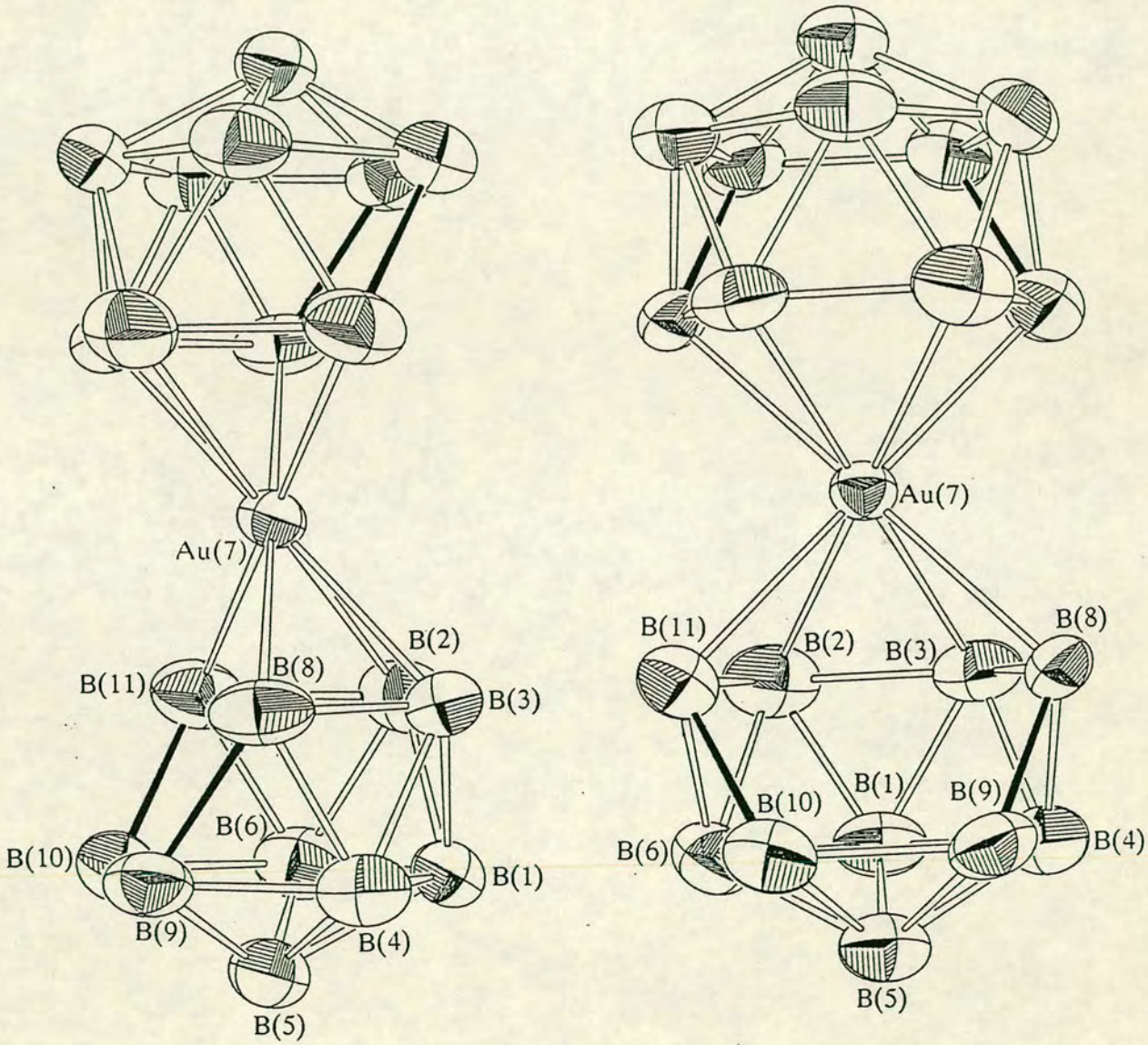

Crystal data. $C_{42}H_{66}Au_2B_{20}P_2$, M = 1243.1, Triclinic, with a = 1.0571(3), b = 1.16648(25), c = 1.1711(3)nm, α = 73.658(20), β = 70.360(25), γ = 86.680(22)°. U = 1.3041 nm^3, Z = 1, D_x = 1.583 gcm^{-3}, μ(Mo-K_α) = 5.699 mm^{-1}, *F(000)* = 606. Space Group $P\bar{1}$.

Data collection and processing. 3164 reflections were measured to θ_{max} = 25° with scan speeds varying from 1.030 to 3.296°min^{-1}. These yielded 2979 unique data (R_{merge} = 0.0141), of which 2973 with $F > 5\sigma(F)$ were retained. Slight crystal decay noted and corrected. Weighting scheme g = 0.000479.

Structure solution and refinement. Au atoms found by inspection of a Patterson synthesis. Au, P, B, and C atoms ultimately allowed anisotropic thermal motion. Phenyl rings constrained to be planar, regular hexagons.

Cage disordered in that the vacant vertex is partially occupied as a result of rotational disorder. Successfully modelled by refining an additional B atom (B(x)) in this position, with an occupancy factor of 0.36, and reducing the occupancy factors of B(8) and B(11) to 0.82. Such disorder is not uncommon in such systems.

Phenyl ring H atoms group thermal parameter = 850(80) pm^2 at convergence, but methyl group H atoms could not be satisfactorily modelled, and are absent. Cage H atoms group thermal parameter = 610(70) pm^2 at convergence. R = 0.0265, R_w = 0.0361, S = 1.132, data variable ratio = 9.65 : 1, with maximum and minimum residues in final ΔF map = 339 and -901 enm^{-3} respectively. Maximum shift / e.s.d. in final least-squares cycle was 0.901.

Table A2.7.1. Fractional Coordinates of Atoms in $[(o\text{-tolyl}_3P)_2Au]^+$ $[(B_{10}H_{12})_2Au]^-$. U_{eq} in $10^4 pm^2$.

	x	y	z	U_{eq}
Au(7)	0.00000	0.00000	0.00000	0.0363(3)
B(1)	0.1463(8)	-0.1982(9)	0.1937(9)	0.054(6)
B(2)	0.0695(9)	-0.1834(8)	0.0743(10)	0.055(6)
B(3)	0.0179(10)	-0.0942(11)	0.1922(9)	0.063(7)
B(4)	0.1689(10)	-0.0554(10)	0.2161(10)	0.061(7)
B(5)	0.3018(9)	-0.1170(9)	0.1144(9)	0.054(6)
B(6)	0.2449(10)	-0.2015(9)	0.0360(10)	0.058(7)
B(8)	0.1001(13)	0.0622(12)	0.1221(14)	0.067(9)
B(9)	0.2822(10)	0.0364(9)	0.0653(10)	0.058(6)
B(10)	0.3296(9)	-0.0576(9)	-0.0472(9)	0.052(6)
B(11)	0.1861(12)	-0.1041(12)	-0.0744(11)	0.052(7)
B(x)	0.220(3)	0.056(3)	-0.068(3)	0.049(6)
Au(1)	0.50000	0.50000	0.50000	0.0350(3)
P(1)	0.61880(18)	0.39467(15)	0.36106(17)	0.0332(10)
C(11)	0.5216	0.2591	0.3924	0.038(4)
C(12)	0.4622	0.1867	0.5152	0.044(4)
C(13)	0.3700	0.0948	0.5388	0.054(5)
C(14)	0.3373	0.0754	0.4397	0.062(6)
C(15)	0.3967	0.1478	0.3169	0.062(6)
C(16)	0.4888(5)	0.2396(4)	0.2933(3)	0.048(5)
C(121)	0.4974(10)	0.1994(7)	0.6291(7)	0.061(6)
C(21)	0.7817	0.3528	0.3747	0.039(4)
C(22)	0.8687	0.4365	0.3778	0.051(5)
C(23)	0.9932	0.4023	0.3899	0.074(7)
C(24)	1.0309	0.2843	0.3989	0.083(8)
C(25)	0.9439	0.2006	0.3958	0.073(7)
C(26)	0.8194(5)	0.2348(4)	0.3837(5)	0.057(5)
C(221)	0.8361(9)	0.5690(8)	0.3651(9)	0.069(7)
C(31)	0.6509	0.4749	0.1969	0.037(4)
C(32)	0.5544	0.5447	0.1561	0.046(5)
C(33)	0.5872	0.6134	0.0307	0.058(6)
C(34)	0.7166	0.6122	-0.0539	0.067(6)
C(35)	0.8131	0.5423	-0.0131	0.070(7)
C(36)	0.7803(4)	0.4736(4)	0.1123(4)	0.052(5)
C(321)	0.4083(9)	0.5457(8)	0.2398(8)	0.058(6)

Table A2.7.2. Fractional Coordinates of Hydrogen Atoms in $[(o\text{-tolyl}_3P)_2Au]^+$ $[(B_{10}H_{12})_2Au]^-$.

	x	y	z
H(1)	0.135(7)	-0.278(6)	0.277(7)
H(2)	-0.023(6)	-0.211(6)	0.057(6)
H(3)	-0.070(6)	-0.094(6)	0.260(6)
H(4)	0.193(6)	-0.060(6)	0.324(6)
H(5)	0.392(7)	-0.136(6)	0.149(6)
H(6)	0.305(7)	-0.281(6)	0.012(6)
H(8)	0.062(8)	0.137(7)	0.144(8)
H(9)	0.366(7)	0.093(6)	0.058(6)
H(10)	0.437(7)	-0.022(6)	-0.093(6)
H(11)	0.204(8)	-0.116(7)	-0.138(8)
H(8,9)	0.199(8)	0.076(7)	0.013(8)
H(10,11)	0.217(8)	-0.029(8)	-0.087(8)
H(13)	0.3240	0.0388	0.6339
H(14)	0.2659	0.0043	0.4580
H(15)	0.3713	0.1327	0.2402
H(16)	0.5348	0.2957	0.1982
H(23)	1.0605	0.4672	0.3922
H(24)	1.1273	0.2579	0.4082
H(25)	0.9731	0.1093	0.4028
H(26)	0.7521	0.1700	0.3813
H(33)	0.5125	0.6676	-0.0008
H(34)	0.7420	0.6655	-0.1509
H(35)	0.9132	0.5414	-0.0785
H(36)	0.8550	0.4195	0.1439

Table A2.7.3. Anisotropic Vibration Parameters(10^4 pm^2) in $[(o\text{-tolyl}_3P)_2Au]^+$ $[(B_{10}H_{12})_2Au]^-$.

	U_{11}	U_{22}	U_{33}	U_{23}	U_{13}	U_{12}
Au(7)	0.0269(2)	0.0408(3)	0.0343(3)	-0.0101(2)	-0.0118(2)	0.0021(2)
B(1)	0.035(5)	0.057(6)	0.054(6)	0.002(5)	-0.018(4)	-0.004(4)
B(2)	0.045(5)	0.041(5)	0.067(6)	-0.004(4)	-0.031(5)	0.005(4)
B(3)	0.036(5)	0.097(8)	0.038(5)	-0.006(5)	-0.006(4)	0.002(5)
B(4)	0.051(6)	0.078(7)	0.045(5)	-0.022(5)	-0.023(5)	0.008(5)
B(5)	0.037(5)	0.063(6)	0.050(5)	-0.006(4)	-0.017(4)	0.001(4)
B(6)	0.047(5)	0.060(6)	0.057(6)	-0.016(5)	-0.026(5)	0.012(5)
B(8)	0.056(7)	0.064(8)	0.077(9)	-0.033(7)	-0.039(7)	0.010(6)
B(9)	0.045(5)	0.059(6)	0.059(6)	-0.012(5)	-0.026(5)	-0.002(4)
B(10)	0.032(4)	0.064(6)	0.047(5)	-0.012(4)	-0.01374)	0.014(4)
B(11)	0.039(6)	0.070(8)	0.041(6)	-0.027(6)	-0.017(5)	0.026(5)
Au(1)	0.0377(3)	0.0275(2)	0.0325(3)	-0.0102(2)	-0.0101(2)	0.0012(2)
P(1)	0.0357(9)	0.0272(8)	0.0297(8)	-0.0066(7)	-0.0114(7)	0.0020(7)
C(11)	0.039(4)	0.026(3)	0.039(4)	-0.009(3)	-0.010(3)	0.004(3)

C(12)	0.049(4)	0.029(3)	0.041(4)	-0.009(3)	-0.010(3)	0.005(3)
C(13)	0.054(5)	0.034(4)	0.057(5)	-0.002(4)	-0.009(4)	-0.007(4)
C(14)	0.061(5)	0.039(4)	0.073(6)	-0.015(4)	-0.021(5)	-0.004(4)
C(15)	0.066(5)	0.039(4)	0.075(6)	-0.024(4)	-0.038(5)	0.004(4)
C(16)	0.051(4)	0.038(4)	0.048(4)	-0.016(3)	-0.019(4)	0.004(3)
C(121)	0.096(7)	0.040(4)	0.036(4)	-0.001(3)	-0.027(4)	-0.005(5)
C(21)	0.033(4)	0.042(4)	0.032(4)	-0.003(3)	-0.011(3)	0.005(3)
C(22)	0.038(4)	0.069(5)	0.036(4)	-0.014(4)	-0.009(3)	0.004(4)
C(23)	0.037(5)	0.119(9)	0.054(5)	-0.020(5)	-0.020(4)	0.001(5)
C(24)	0.046(5)	0.116(9)	0.067(6)	-0.006(6)	-0.025(5)	0.024(6)
C(25)	0.067(6)	0.073(6)	0.059(6)	-0.016(5)	-0.015(5)	0.039(5)
C(26)	0.054(5)	0.051(5)	0.049(5)	-0.002(4)	-0.014(4)	0.015(4)
C(221)	0.059(6)	0.056(5)	0.078(6)	-0.015(5)	-0.019(5)	-0.024(4)
C(31)	0.043(4)	0.032(3)	0.030(3)	-0.001(3)	-0.015(3)	-0.006(3)
C(32)	0.051(4)	0.036(4)	0.044(4)	-0.007(3)	-0.024(4)	0.003(3)
C(33)	0.065(5)	0.053(5)	0.042(4)	0.003(4)	-0.024(4)	0.004(4)
C(34)	0.066(6)	0.077(6)	0.042(5)	0.004(4)	-0.022(4)	-0.012(5)
C(35)	0.053(5)	0.103(8)	0.032(4)	-0.003(5)	-0.001(4)	-0.023(5)
C(36)	0.047(4)	0.055(5)	0.040(4)	-0.005(4)	-0.014(4)	-0.001(4)
C(321)	0.050(5)	0.060(5)	0.055(5)	-0.016(4)	-0.024(4)	0.018(4)

Table A2.7.4c. Bond Lengths(pm) and Angles(^{0}) for the $[(o\text{-tolyl}_3P)_2Au]^+$ Cation.

Au(1) - P(1)	230.37(19)	C(12) -C(121)	154.7(10)
P(1) -C(11)	181.7(5)	C(22) -C(221)	154.0(11)
P(1) -C(21)	181.0(6)	C(32) -C(321)	152.8(10)
P(1) -C(31)	180.9(5)		

Au(1) - P(1)	-C(11)	108.50(17)		P(1) -C(11)	-C(12)	121.3(3)
Au(1) - P(1)	-C(21)	113.15(19)		C(23) -C(22)	-C(221)	116.8(6)
Au(1) - P(1)	-C(31)	113.89(18)		C(21) -C(22)	-C(221)	123.2(6)
C(11) - P(1)	-C(21)	108.31(24)		P(1) -C(21)	-C(26)	119.2(4)
C(11) - P(1)	-C(31)	107.03(23)		P(1) -C(21)	-C(22)	120.8(4)
C(21) - P(1)	-C(31)	105.67(25)		C(33) -C(32)	-C(321)	116.3(5)
C(13) -C(12)	-C(121)	116.9(5)		C(31) -C(32)	-C(321)	123.6(5)
C(11) -C(12)	-C(121)	123.1(5)		P(1) -C(31)	-C(36)	117.9(4)
P(1) -C(11)	-C(16)	117.9(3)		P(1) -C(31)	-C(32)	121.9(4)

Table A2.7.4a. Bond Lengths(pm) and Angles(^{0}) in the $[(B_{10}H_{12})_2Au]^-$ Anion.

Au(7)- B(2)	225.3(10)	B(4) - B(5)	177.5(15)
Au(7)- B(3)	227.5(11)	B(4) - B(8)	178.7(19)
Au(7)- B(8)	231.9(15)	B(4) - B(9)	183.3(16)
Au(7)-B(11)	229.6(14)	B(5) - B(6)	176.8(15)
Au(7)- B(x)	226(3)	B(5) - B(9)	174.2(15)
B(1) - B(2)	180.4(14)	B(5) -B(10)	174.9(14)
B(1) - B(3)	176.9(15)	B(6) -B(10)	179.9(15)

B(1) - B(4)	179.8(15)	B(6) -B(11)	172.6(17)
B(1) - B(5)	176.7(14)	B(8) - B(9)	185.0(18)
B(1) - B(6)	180.0(15)	B(9) -B(10)	187.0(15)
B(2) - B(3)	187.6(15)	B(10)-B(11)	179.3(17)
B(2) - B(6)	176.9(15)	B(8) - B(x)	218(3)
B(2) -B(11)	178.6(17)	B(9) - B(x)	184(3)
B(3) - B(4)	181.3(16)	B(10)- B(x)	172(3)
B(3) - B(8)	190.2(19)	B(11)- B(x)	195(3)

B(2) -Au(7)	- B(3)	49.0(4)	B(2) - B(6)	-B(11)	61.4(7)
B(2) -Au(7)	-B(11)	46.2(4)	B(5) - B(6)	-B(10)	58.7(6)
B(3) -Au(7)	- B(8)	48.9(5)	B(10)- B(6)	-B(11)	61.1(7)
B(2) - B(1)	- B(3)	63.4(6)	Au(7)- B(8)	- B(3)	64.3(6)
B(2) - B(1)	- B(6)	58.8(6)	B(3) - B(8)	- B(4)	58.8(7)
B(3) - B(1)	- B(4)	61.1(6)	B(4) - B(8)	- B(9)	60.5(7)
B(4) - B(1)	- B(5)	59.7(6)	B(4) - B(9)	- B(5)	59.5(6)
B(5) - B(1)	- B(6)	59.4(6)	B(4) - B(9)	- B(8)	58.0(7)
Au(7)- B(2)	- B(3)	66.2(5)	B(5) - B(9)	-B(10)	57.8(6)
Au(7)- B(2)	-B(11)	68.2(5)	B(5) -B(10)	- B(6)	59.7(6)
B(1) - B(2)	- B(3)	57.4(6)	B(5) -B(10)	- B(9)	57.4(6)
B(1) - B(2)	- B(6)	60.5(6)	B(6) -B(10)	-B(11)	57.4(6)
B(6) - B(2)	-B(11)	58.1(6)	Au(7)-B(11)	- B(2)	65.6(5)
Au(7)- B(3)	- B(2)	64.9(5)	B(2) -B(11)	- B(6)	60.5(7)
Au(7)- B(3)	- B(8)	66.7(6)	B(6) -B(11)	-B(10)	61.5(7)
B(1) - B(3)	- B(2)	59.2(6)	Au(7)- B(x)	- B(8)	62.9(9)
B(1) - B(3)	- B(4)	60.3(6)	B(8) -Au(7)	- B(x)	56.8(8)
B(4) - B(3)	- B(8)	57.5(7)	B(11)-Au(7)	- B(x)	50.6(8)
B(1) - B(4)	- B(3)	58.6(6)	Au(7)- B(8)	- B(x)	60.3(9)
B(1) - B(4)	- B(5)	59.3(6)	B(9) - B(8)	- B(x)	53.5(9)
B(3) - B(4)	- B(8)	63.8(7)	B(8) - B(9)	- B(x)	72.4(11)
B(5) - B(4)	- B(9)	57.7(6)	B(10)- B(9)	- B(x)	55.4(10)
B(8) - B(4)	- B(9)	61.4(7)	B(9) -B(10)	- B(x)	61.4(11)
B(1) - B(5)	- B(4)	61.0(6)	B(11)-B(10)	- B(x)	67.2(12)
B(1) - B(5)	- B(6)	61.2(6)	Au(7)-B(11)	- B(x)	63.8(10)
B(4) - B(5)	- B(9)	62.8(6)	B(10)-B(11)	- B(x)	54.7(10)
B(6) - B(5)	-B(10)	61.5(6)	Au(7)- B(x)	-B(11)	65.6(10)
B(9) - B(5)	-B(10)	64.8(6)	B(8) - B(x)	- B(9)	54.1(9)
B(1) - B(6)	- B(2)	60.7(6)	B(9) - B(x)	-B(10)	63.2(11)
B(1) - B(6)	- B(5)	59.4(6)	B(10)- B(x)	-B(11)	58.1(11)

Table A2.7.5. Bond Lengths(pm) and Angles(^{o}) Involving the Hydrogen Atoms in the $[(B_{10}H_{12})_2Au]^-$ anion.

B(1) - H(1)	112(7)	B(9) - H(9)	109(7)
B(2) - H(2)	115(7)	B(10) -H(10)	113(7)
B(3) - H(3)	100(7)	B(11) -H(11)	75(9)
B(4) - H(4)	135(7)	B(8) -H(8,9)	132(9)
B(5) - H(5)	115(7)	B(9) -H(8,9)	123(9)

B(6) - H(6)	114(7)	B(10) -H(10,11)	141(9)
B(8) - H(8)	100(9)	B(11) -H(10,11)	90(9)

B(2) - B(1)	- H(1)	126(4)	B(9) - B(8)	- H(8)	124(5)
B(3) - B(1)	- H(1)	121(4)	B(4) - B(9)	- H(9)	124(4)
B(4) - B(1)	- H(1)	116(4)	B(5) - B(9)	- H(9)	115(4)
B(5) - B(1)	- H(1)	120(4)	B(8) - B(9)	- H(9)	128(4)
B(6) - B(1)	- H(1)	122(4)	B(10)- B(9)	- H(9)	114(4)
Au(7)- B(2)	- H(2)	81(4)	B(5) -B(10)	-H(10)	107(4)
B(1) - B(2)	- H(2)	143(4)	B(6) -B(10)	-H(10)	136(4)
B(3) - B(2)	- H(2)	110(4)	B(9) -B(10)	-H(10)	95(4)
B(6) - B(2)	- H(2)	142(4)	B(11)-B(10)	-H(10)	145(4)
B(11)- B(2)	- H(2)	108(4)	Au(7)-B(11)	-H(11)	122(7)
Au(7)- B(3)	- H(3)	110(4)	B(2) -B(11)	-H(11)	130(7)
B(1) - B(3)	- H(3)	129(4)	B(6) -B(11)	-H(11)	117(7)
B(2) - B(3)	- H(3)	130(4)	B(10)-B(11)	-H(11)	112(7)
B(4) - B(3)	- H(3)	118(4)	Au(7)- B(8)	-H(8,9)	77(4)
B(8) - B(3)	- H(3)	110(4)	B(3) - B(8)	-H(8,9)	114(4)
B(1) - B(4)	- H(4)	115(3)	B(4) - B(8)	-H(8,9)	98(4)
B(3) - B(4)	- H(4)	131(3)	B(9) - B(8)	-H(8,9)	42(4)
B(5) - B(4)	- H(4)	111(3)	H(8) - B(8)	-H(8,9)	117(6)
B(8) - B(4)	- H(4)	129(3)	B(4) - B(9)	-H(8,9)	99(4)
B(9) - B(4)	- H(4)	119(3)	B(5) - B(9)	-H(8,9)	121(4)
B(1) - B(5)	- H(5)	123(4)	B(8) - B(9)	-H(8,9)	45(4)
B(4) - B(5)	- H(5)	112(4)	B(10)- B(9)	-H(8,9)	84(4)
B(6) - B(5)	- H(5)	127(4)	H(9) - B(9)	-H(8,9)	122(6)
B(9) - B(5)	- H(5)	110(4)	B(5) -B(10)	-H(10,11)	118(4)
B(10)- B(5)	- H(5)	119(4)	B(6) -B(10)	-H(10,11)	85(4)
B(1) - B(6)	- H(6)	124(4)	B(9) -B(10)	-H(10,11)	95(4)
B(2) - B(6)	- H(6)	129(4)	B(11)-B(10)	-H(10,11)	30(4)
B(5) - B(6)	- H(6)	118(4)	H(10)-B(10)	-H(10,11)	131(5)
B(10)- B(6)	- H(6)	115(4)	B(10)-B(11)	-H(10,11)	51(6)
B(11)- B(6)	- H(6)	120(4)	Au(7)-B(11)	-H(10,11)	74(6)
Au(7)- B(8)	- H(8)	113(5)	B(2) -B(11)	-H(10,11)	121(6)
B(3) - B(8)	- H(8)	127(5)	B(6) -B(11)	-H(10,11)	108(6)
B(4) - B(8)	- H(8)	126(5)	H(11)-B(11)	-H(10,11)	108(9)

A2.8 $[(Cy_3P)_2Au]^+$ $[(B_{10}H_{12})_2Au]^-$

The Molecular Structure and Associated Numbering Scheme for $[(Cy_3P)_2Au]^+$ $[(B_{10}H_{12})_2Au]^-$.

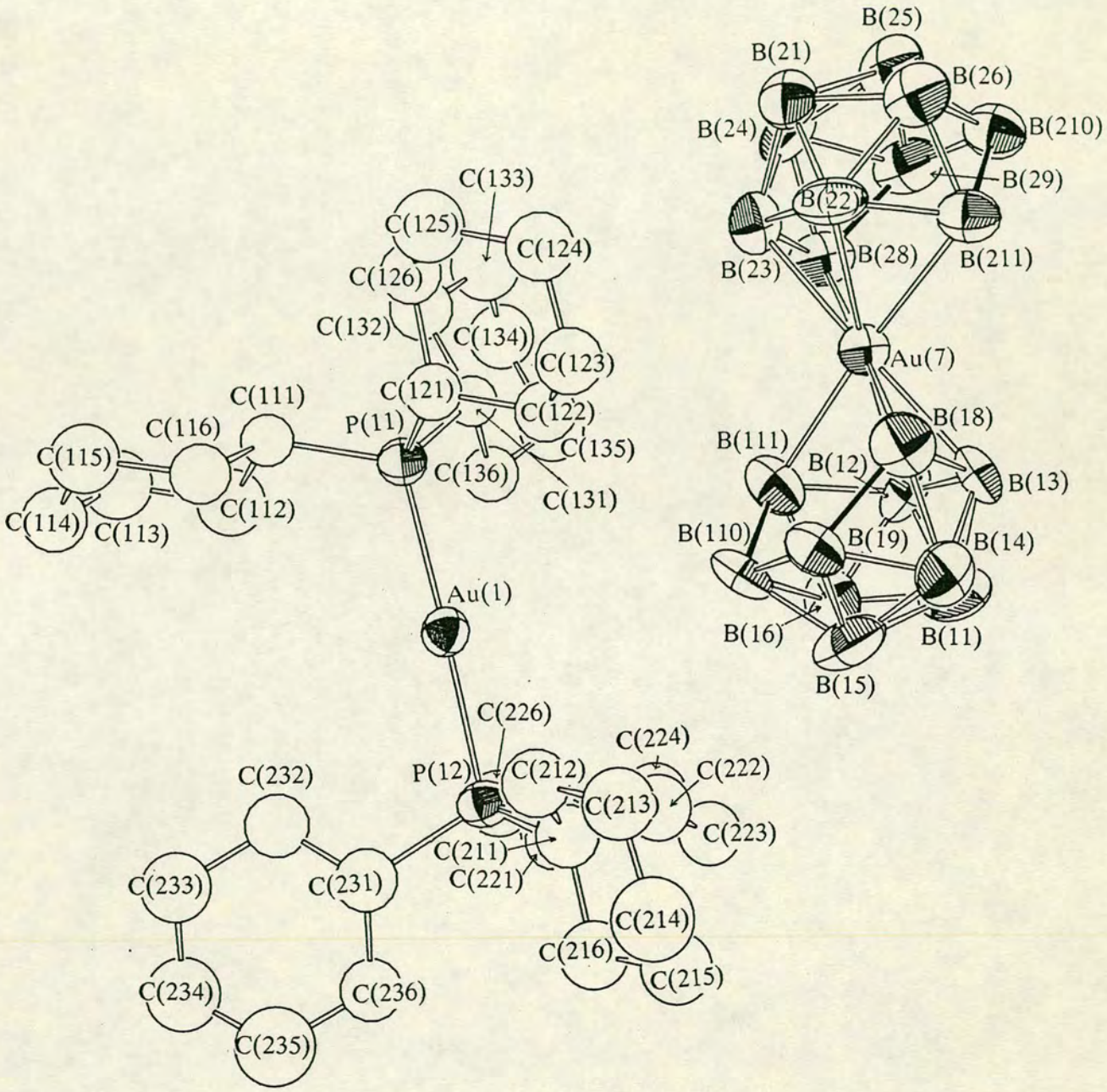

Crystal data. $C_{36}H_{90}Au_2B_{20}P_2$, M = 1195.2, monoclinic with a = 2.14457(23), b = 1.16077(13), c = 2.26292(18) nm, and β = 105.334(7) °. U = 5.433 nm^3, D_x = 1.461 Mgm^{-3}, μ-(Mo-K_α) = 5.469 mm^{-1} and $F(000)$ = 2376. Z = 4, and the space group is *Cc.*

Data collection and processing. 4667 unique reflections ($+h +k \pm l$) were measured to θ_{max} = 25°, of which 4040 with $F > 2\sigma(F)$ were retained. Variable scan speeds between 0.589 and 2.354° min^{-1}. Crystal decayed by *ca.* 7% and correction was applied.

Structure solution and refinement. Au atom positions located by automatic direct methods. Au, P, and B atoms allowed anisotropic thermal motion. Cyclohexyl H atoms group thermal parameter 900(90) pm^2 at convergence. Cage H atoms set in calculated positions and their group thermal parameter was 860(150) pm^2 at convergence. Cage μ-H atoms refined with constraints : μ-H-B = 130, μ-H-Au = 230, and μ-H-B(*) = 380pm, where B(*) is B(2) or B(3) on the other cage, whichever is 'trans' to the H atom, eg. for H(18,19), B(*) is B(23). These parameters are as found in the $[(o\text{-tolyl}_3P)_2Au]^+ [(B_{10}H_{12})_2Au]^-$ structure.

Unit weights. R = 0.0449, R_w = 0.0477, S = 6.880, and data : variable = 9 : 1. Maximum residue and minimum trough in final ΔF map 667 and -615 enm^{-3} respectively, and maximum shift/e.s.d. in final least-squares cycle was 0.745.

Table A2.8.1. Fractional Coordinates of Refined Atoms in $[(Cy_3P)_2Au]^+$ $[(B_{10}H_{12})_2Au]^-$. U_{eq} in $10^4 pm^2$.

	x	y	z	U_{eq}
Au(1)	0.50000	0.30735(8)	0.75000	0.0455(7)
P(11)	0.47588(24)	0.2344(4)	0.65100(22)	0.045(3)
P(12)	0.52177(25)	0.3844(4)	0.84814(22)	0.047(3)
Au(7)	0.65738(4)	-0.19069(9)	0.75128(4)	0.0489(7)
B(11)	0.6918(18)	-0.122(3)	0.9042(13)	0.087(22)
B(12)	0.6336(13)	-0.1897(23)	0.8423(10)	0.060(15)
B(13)	0.7233(11)	-0.1798(18)	0.8484(11)	0.054(14)
B(14)	0.7497(12)	-0.0481(24)	0.8789(13)	0.067(17)
B(15)	0.6840(17)	0.029(3)	0.8870(11)	0.082(20)
B(16)	0.6127(16)	-0.0588(24)	0.8722(12)	0.084(21)
B(18)	0.7467(13)	-0.0732(22)	0.8019(14)	0.070(17)
B(19)	0.7158(11)	0.0559(19)	0.8231(11)	0.055(14)
B(110)	0.6216(14)	0.0498(22)	0.8201(13)	0.072(18)
B(111)	0.5846(14)	-0.0865(21)	0.7939(13)	0.068(17)
B(21)	0.6315(14)	-0.268(3)	0.6002(13)	0.065(17)
B(22)	0.6855(13)	-0.1962(23)	0.6619(11)	0.066(16)
B(23)	0.5978(11)	-0.1991(21)	0.6520(11)	0.057(14)
B(24)	0.5669(13)	-0.3319(25)	0.6216(11)	0.066(17)
B(25)	0.6354(16)	-0.4182(23)	0.6218(12)	0.077(19)
B(26)	0.7103(14)	-0.3352(22)	0.6392(13)	0.072(18)
B(28)	0.5678(12)	-0.301(3)	0.6987(12)	0.068(17)
B(29)	0.5973(16)	-0.4344(24)	0.6816(12)	0.074(19)
B(210)	0.6915(13)	-0.4401(22)	0.6879(12)	0.067(17)
B(211)	0.7322(12)	-0.3027(21)	0.7158(11)	0.060(15)
C(111)	0.4162(9)	0.3189(17)	0.5950(9)	0.051(4)
C(112)	0.3552(12)	0.3381(24)	0.6177(12)	0.086(7)
C(113)	0.3052(13)	0.4122(23)	0.5692(12)	0.090(8)
C(114)	0.3337(12)	0.5276(21)	0.5631(12)	0.078(7)
C(115)	0.3940(12)	0.5128(23)	0.5410(11)	0.083(7)
C(116)	0.4456(11)	0.4403(20)	0.5869(11)	0.063(6)
C(121)	0.5486(11)	0.2324(18)	0.6230(10)	0.059(5)
C(122)	0.6063(10)	0.1765(19)	0.6672(10)	0.065(6)
C(123)	0.6685(11)	0.1884(22)	0.6463(10)	0.074(6)
C(124)	0.6600(12)	0.1503(22)	0.5825(11)	0.079(7)
C(125)	0.6019(12)	0.202(3)	0.5380(12)	0.090(8)
C(126)	0.5387(11)	0.1817(21)	0.5573(10)	0.069(6)
C(131)	0.4452(9)	0.0839(16)	0.6487(8)	0.049(4)
C(132)	0.4024(13)	0.0448(22)	0.5850(11)	0.078(7)
C(133)	0.3834(14)	-0.0815(24)	0.5881(13)	0.091(8)
C(134)	0.3454(13)	-0.0985(23)	0.6335(11)	0.085(7)
C(135)	0.3886(12)	-0.0602(21)	0.6986(11)	0.081(7)
C(136)	0.4073(11)	0.0643(18)	0.6964(10)	0.062(5)
C(211)	0.6085(11)	0.3933(22)	0.8821(11)	0.071(7)
C(212)	0.6458(11)	0.4365(23)	0.8381(11)	0.080(7)
C(213)	0.7186(12)	0.4309(23)	0.8666(11)	0.085(7)
C(214)	0.7410(17)	0.480(3)	0.9298(14)	0.115(11)
C(215)	0.7041(12)	0.4405(24)	0.9704(12)	0.089(8)
C(216)	0.6307(12)	0.4524(22)	0.9463(11)	0.081(7)

C(221)	0.4894(10)	0.2930(18)	0.9000(10)	0.060(5)
C(222)	0.5267(15)	0.1863(24)	0.9190(14)	0.082(9)
C(223)	0.4994(12)	-0.1080(22)	0.9601(11)	0.081(7)
C(224)	0.4291(12)	0.0794(23)	0.9294(12)	0.087(7)
C(225)	0.3919(15)	0.185(3)	0.9140(14)	0.108(10)
C(226)	0.4190(13)	0.2661(24)	0.8698(12)	0.086(7)
C(231)	0.4874(12)	0.5303(21)	0.8444(10)	0.073(6)
C(232)	0.4350(11)	0.5512(20)	0.7906(11)	0.072(6)
C(233)	0.4074(13)	0.6736(23)	0.7859(12)	0.090(8)
C(234)	0.3961(14)	0.718(3)	0.8442(12)	0.097(8)
C(235)	0.4466(17)	0.692(3)	0.8983(15)	0.117(10)
C(236)	0.4745(12)	0.5770(21)	0.9041(11)	0.073(6)

Table A2.8.2. Fractional Coordinates of the Hydrogen Atoms in $[(Cy_3P)_2Au]^+$ $[(B_{10}H_{12})_2Au]^-$.

	x	y	z
H(111)	0.4036	0.2722	0.5522
H(112a)	0.3339	0.2560	0.6234
H(112b)	0.3682	0.3830	0.6610
H(113a)	0.2617	0.4229	0.5841
H(113b)	0.2937	0.3687	0.5254
H(114a)	0.2988	0.5788	0.5304
H(114b)	0.3461	0.5704	0.6070
H(115a)	0.3813	0.4697	0.4972
H(115b)	0.4140	0.5966	0.5361
H(116a)	0.4875	0.4294	0.5695
H(116b)	0.4595	0.4839	0.6306
H(121)	0.5577	0.3233	0.6193
H(122a)	0.5965	0.0860	0.6712
H(122b)	0.6137	0.2174	0.7114
H(123a)	0.7059	0.1368	0.6760
H(123b)	0.6830	0.2777	0.6499
H(124a)	0.7027	0.1743	0.5685
H(124b)	0.6549	0.0577	0.5809
H(125a)	0.6094	0.2935	0.5354
H(125b)	0.5970	0.1636	0.4935
H(126a)	0.4989	0.2242	0.5254
H(126b)	0.5290	0.0904	0.5576
H(131)	0.4885	0.0319	0.6591
H(132a)	0.4292	0.0549	0.5511
H(132b)	0.3593	0.0973	0.5725
H(133a)	0.4267	-0.1333	0.6010
H(133b)	0.3546	-0.1080	0.5434
H(134a)	0.3019	-0.0471	0.6211
H(134b)	0.3326	-0.1883	0.6348
H(135a)	0.4317	-0.1126	0.7112
H(135b)	0.3615	-0.0709	0.7322
H(136a)	0.3640	0.1163	0.6846

H(136b)	0.4369	0.0896	0.7409
H(211)	0.6213	0.3040	0.8916
H(212a)	0.6338	0.3840	0.7973
H(212b)	0.6322	0.5248	0.8261
H(213a)	0.7420	0.4781	0.8373
H(213b)	0.7332	0.3416	0.8684
H(214a)	0.7374	0.5724	0.9266
H(214b)	0.7909	0.4554	0.9489
H(215a)	0.7151	0.3505	0.9799
H(215b)	0.7193	0.4894	1.0123
H(216a)	0.6075	0.4114	0.9777
H(216b)	0.6177	0.5425	0.9420
H(221)	0.4939	0.3413	0.9416
H(222a)	0.5278	0.1387	0.8783
H(222b)	0.5753	0.2100	0.9436
H(223a)	0.5026	0.1511	1.0031
H(223b)	0.5272	0.0293	0.9684
H(224a)	0.4095	0.0292	0.9604
H(224b)	0.4261	0.0305	0.8882
H(225a)	0.3424	0.1635	0.8914
H(225b)	0.3935	0.2319	0.9557
H(226a)	0.3916	0.3452	0.8619
H(226b)	0.4148	0.2229	0.8266
H(231)	0.5271	0.5839	0.8400
H(232a)	0.4529	0.5360	0.7509
H(232b)	0.3966	0.4911	0.7906
H(233a)	0.3618	0.6740	0.7512
H(233b)	0.4409	0.7309	0.7723
H(234a)	0.3517	0.6810	0.8494
H(234b)	0.3913	0.8106	0.8407
H(235a)	0.4855	0.7517	0.9002
H(235b)	0.4273	0.7050	0.9372
H(236a)	0.5197	0.5790	0.9393
H(236b)	0.4414	0.5189	0.9176
H(11B)	0.7104	-0.1395	0.9568
H(12B)	0.6316	-0.2736	0.8698
H(13B)	0.7527	-0.2654	0.8543
H(14B)	0.8037	-0.0748	0.9012
H(15B)	0.6837	0.1010	0.9243
H(16B)	0.5818	-0.0761	0.9064
H(18B)	0.7874	-0.0982	0.7768
H(19B)	0.7291	0.1506	0.8105
H(110B)	0.5918	0.1362	0.8182
H(111B)	0.5432	-0.1206	0.7530
H(18,9)	0.6980	-0.0049	0.7737
H(110,11)	0.6190	-0.0144	0.7721
H(21B)	0.6335	-0.2284	0.5532
H(22B)	0.7143	-0.1087	0.6677
H(23B)	0.5527	-0.1334	0.6420
H(24B)	0.5531	-0.3666	0.5695
H(25B)	0.6254	-0.4943	0.5863
H(26B)	0.7572	-0.3446	0.6205
H(28B)	0.5193	-0.2725	0.7095
H(29B)	0.5742	-0.5213	0.6909
H(210B)	0.7220	-0.5182	0.7139

H(211B)	0.7842	-0.2726	0.7438
H(28,9)	0.6082	-0.3728	0.7321
H(210,11)	0.6948	-0.3734	0.7360

Table A2.8.3. Anisotropic Thermal Parameters($10^4 pm^2$) for Atoms in $[(Cy_3P)_2Au]^+ [(B_{10}H_{12})_2Au]^-$.

	U_{11}	U_{22}	U_{33}	U_{23}	U_{13}	U_{12}
Au(1)	0.0471(5)	0.0432(7)	0.0427(7)	0.0029(5)	0.0111(5)	-0.0004(5)
P(11)	0.0432(24)	0.0441(25)	0.044(3)	-0.0016(20)	0.0109(21)	-0.0023(21)
P(12)	0.051(3)	0.043(3)	0.043(3)	-0.0039(20)	0.0126(22)	-0.0100(22)
Au(7)	0.0445(5)	0.0501(8)	0.0489(8)	-0.0013(5)	0.0134(5)	-0.0021(5)
B(11)	0.13(3)	0.083(20)	0.047(16)	0.008(14)	0.045(18)	-0.004(20)
B(12)	0.069(16)	0.068(15)	0.036(12)	0.018(12)	-0.002(11)	0.003(14)
B(13)	0.049(12)	0.035(11)	0.076(16)	0.004(10)	0.030(12)	0.011(10)
B(14)	0.044(13)	0.068(16)	0.081(19)	-0.005(14)	0.003(12)	-0.005(12)
B(15)	0.13(3)	0.072(18)	0.038(14)	-0.002(12)	0.013(15)	-0.023(18)
B(16)	0.120(25)	0.073(17)	0.063(17)	0.034(14)	0.060(18)	0.029(17)
B(18)	0.056(14)	0.050(14)	0.093(21)	-0.008(14)	-0.006(14)	-0.009(12)
B(19)	0.057(13)	0.047(12)	0.059(15)	-0.009(11)	0.022(11)	0.000(11)
B(110)	0.080(18)	0.051(14)	0.083(19)	-0.022(13)	0.039(16)	0.015(13)
B(111)	0.073(17)	0.047(13)	0.081(19)	-0.004(12)	0.034(15)	-0.001(13)
B(21)	0.062(16)	0.072(17)	0.061(17)	0.014(14)	0.028(13)	0.008(14)
B(22)	0.080(18)	0.069(16)	0.049(13)	-0.012(13)	0.034(13)	-0.025(15)
B(23)	0.036(11)	0.057(14)	0.072(16)	-0.005(12)	0.005(11)	-0.011(11)
B(24)	0.067(16)	0.085(19)	0.042(14)	0.006(12)	0.012(12)	-0.004(14)
B(25)	0.115(23)	0.054(15)	0.056(16)	0.015(12)	0.026(16)	-0.019(16)
B(26)	0.080(18)	0.059(15)	0.071(18)	0.001(13)	0.022(15)	-0.017(14)
B(28)	0.051(13)	0.089(19)	0.063(16)	-0.010(15)	0.020(12)	-0.011(14)
B(29)	0.109(23)	0.051(15)	0.056(16)	-0.004(12)	0.022(16)	-0.028(15)
B(210)	0.070(16)	0.057(15)	0.068(17)	-0.010(12)	0.019(14)	-0.006(13)
B(211)	0.068(15)	0.051(13)	0.059(14)	-0.009(11)	0.024(12)	-0.012(12)

Table A2.8.4c. Bond lengths(pm) and Angles(°) for the $[(Cy_3P)_2Au]^+$ Cation.

Au(1) -P(11)	232.2(5)	C(135)-C(136)	150(3)
Au(1) -P(12)	232.4(5)	P(12) -C(211)	182(3)
P(11) -C(111)	183.0(20)	P(12) -C(221)	184.7(22)
P(11) -C(121)	183.3(23)	P(12) -C(231)	184.1(25)
P(11) -C(131)	186.2(20)	C(211)-C(212)	152(4)
C(111)-C(112)	154(3)	C(211)-C(216)	156(4)
C(111)-C(116)	157(3)	C(212)-C(213)	152(4)
C(112)-C(113)	157(4)	C(213)-C(214)	149(4)
C(113)-C(114)	149(4)	C(214)-C(215)	144(4)
C(114)-C(115)	151(4)	C(215)-C(216)	153(4)

C(115)-C(116)	155(4)	C(221)-C(222)	147(4)
C(121)-C(122)	152(3)	C(221)-C(226)	152(3)
C(121)-C(126)	156(3)	C(222)-C(223)	152(4)
C(122)-C(123)	153(3)	C(223)-C(224)	152(4)
C(123)-C(124)	148(4)	C(224)-C(225)	146(4)
C(124)-C(125)	150(4)	C(225)-C(226)	159(4)
C(125)-C(126)	155(4)	C(231)-C(232)	144(3)
C(131)-C(132)	156(3)	C(231)-C(236)	155(3)
C(131)-C(136)	153(3)	C(232)-C(233)	153(4)
C(132)-C(133)	153(4)	C(233)-C(234)	150(4)
C(133)-C(134)	149(4)	C(234)-C(235)	144(5)
C(134)-C(135)	158(4)	C(235)-C(236)	145(4)

P(11)	-Au(1)	-P(12)	178.32(18)	Au(1) -P(12)	-C(211) 110.5(8)
Au(1)	-P(11)	-C(111)	114.2(7)	Au(1) -P(12)	-C(221) 111.8(7)
Au(1)	-P(11)	-C(121)	110.2(7)	Au(1) -P(12)	-C(231) 109.5(8)
Au(1)	-P(11)	-C(131)	110.8(6)	C(211)-P(12)	-C(221) 106.2(11)
C(111)	-P(11)	-C(121)	105.7(10)	C(211)-P(12)	-C(231) 108.6(11)
C(111)	-P(11)	-C(131)	107.8(9)	C(221)-P(12)	-C(231) 110.2(10)
C(121)	-P(11)	-C(131)	107.8(10)	P(12) -C(211)	-C(212) 113.5(17)
P(11)	-C(111)	-C(112)	110.3(15)	P(12) -C(211)	-C(216) 116.4(17)
P(11)	-C(111)	-C(116)	109.3(14)	C(212)-C(211)	-C(216) 112.4(21)
C(112)	-C(111)	-C(116)	108.1(18)	C(211)-C(212)	-C(213) 111.5(21)
C(111)	-C(112)	-C(113)	109.2(20)	C(212)-C(213)	-C(214) 115.0(24)
C(112)	-C(113)	-C(114)	109.6(22)	C(213)-C(214)	-C(215) 114(3)
C(113)	-C(114)	-C(115)	109.6(22)	C(214)-C(215)	-C(216) 115.7(25)
C(114)	-C(115)	-C(116)	111.2(21)	C(211)-C(216)	-C(215) 108.9(21)
C(111)	-C(116)	-C(115)	109.1(19)	P(12) -C(221)	-C(222) 113.7(17)
P(11)	-C(121)	-C(122)	113.4(16)	P(12) -C(221)	-C(226) 109.2(16)
P(11)	-C(121)	-C(126)	114.9(16)	C(222)-C(221)	-C(226) 110.9(21)
C(122)	-C(121)	-C(126)	110.4(18)	C(221)-C(222)	-C(223) 114.4(23)
C(121)	-C(122)	-C(123)	112.5(19)	C(222)-C(223)	-C(224) 110.2(22)
C(122)	-C(123)	-C(124)	112.5(20)	C(223)-C(224)	-C(225) 109.8(23)
C(123)	-C(124)	-C(125)	113.7(22)	C(224)-C(225)	-C(226) 112.3(25)
C(124)	-C(125)	-C(126)	112.6(21)	C(221)-C(226)	-C(225) 108.9(22)
C(121)	-C(126)	-C(125)	107.7(19)	P(12) -C(231)	-C(232) 113.9(17)
P(11)	-C(131)	-C(132)	114.6(15)	P(12) -C(231)	-C(236) 116.4(17)
P(11)	-C(131)	-C(136)	111.7(14)	C(232)-C(231)	-C(236) 113.6(20)
C(132)	-C(131)	-C(136)	108.4(17)	C(231)-C(232)	-C(233) 114.5(21)
C(131)	-C(132)	-C(133)	109.7(20)	C(232)-C(233)	-C(234) 114.1(23)
C(132)	-C(133)	-C(134)	111.1(23)	C(233)-C(234)	-C(235) 115(3)
C(133)	-C(134)	-C(135)	108.3(22)	C(234)-C(235)	-C(236) 118(3)
C(134)	-C(135)	-C(136)	109.5(20)	C(231)-C(236)	-C(235) 114.0(23)
C(131)	-C(136)	-C(135)	111.3(18)		

Table A2.8.4a(1). Bond Lengths(pm) and Angles(°) for Cage 1 in the $[(B_{10}H_{12})_2Au]^-$ Anion.

Au(7) -B(12)	225(3)	B(13) -B(18)	178(4)
Au(7) -B(13)	228.0(23)	B(14) -B(15)	172(4)
Au(7) -B(18)	238(3)	B(14) -B(18)	175(4)
Au(7) -B(111)	237(3)	B(14) -B(19)	176(4)
B(11) -B(12)	179(4)	B(15) -B(16)	179(4)
B(11) -B(13)	172(4)	B(15) -B(19)	178(4)
B(11) -B(14)	173(4)	B(15) -B(110)	175(4)
B(11) -B(15)	180(5)	B(16) -B(110)	177(4)
B(11) -B(16)	182(5)	B(16) -B(111)	174(4)
B(12) -B(13)	190(3)	B(18) -B(19)	175(4)
B(12) -B(16)	177(4)	B(19) -B(110)	201(4)
B(12) -B(111)	177(4)	B(110)-B(111)	180(4)
B(13) -B(14)	171(4)		

B(12)	-Au(7)	-B(13)	49.5(9)	B(11)	-B(15)	-B(14)	58.8(17)
B(12)	-Au(7)	-B(111)	44.9(9)	B(11)	-B(15)	-B(16)	60.8(18)
B(13)	-Au(7)	-B(18)	44.8(9)	B(14)	-B(15)	-B(19)	60.3(16)
B(12)	-B(11)	-B(13)	65.4(16)	B(16)	-B(15)	-B(110)	59.9(17)
B(12)	-B(11)	-B(16)	58.7(16)	B(19)	-B(15)	-B(110)	69.1(17)
B(13)	-B(11)	-B(14)	59.5(16)	B(11)	-B(16)	-B(12)	59.9(17)
B(14)	-B(11)	-B(15)	58.3(17)	B(11)	-B(16)	-B(15)	59.7(18)
B(15)	-B(11)	-B(16)	59.5(18)	B(12)	-B(16)	-B(111)	60.5(16)
Au(7)	-B(12)	-B(13)	66.1(11)	B(15)	-B(16)	-B(110)	59.0(17)
Au(7)	-B(12)	-B(111)	71.2(13)	B(110)	-B(16)	-B(111)	61.6(17)
B(11)	-B(12)	-B(13)	55.4(15)	Au(7)	-B(18)	-B(13)	64.5(11)
B(11)	-B(12)	-B(16)	61.4(17)	B(13)	-B(18)	-B(14)	58.0(15)
B(16)	-B(12)	-B(111)	59.0(16)	B(14)	-B(18)	-B(19)	60.3(15)
Au(7)	-B(13)	-B(12)	64.4(10)	B(14)	-B(19)	-B(15)	58.0(15)
Au(7)	-B(13)	-B(18)	70.7(12)	B(14)	-B(19)	-B(18)	59.8(15)
B(11)	-B(13)	-B(12)	59.2(16)	B(15)	-B(19)	-B(110)	54.7(15)
B(11)	-B(13)	-B(14)	60.6(17)	B(15)	-B(110)	-B(16)	61.1(17)
B(14)	-B(13)	-B(18)	60.2(15)	B(15)	-B(110)	-B(19)	56.2(15)
B(11)	-B(14)	-B(13)	59.9(16)	B(16)	-B(110)	-B(111)	58.4(16)
B(11)	-B(14)	-B(15)	62.8(18)	Au(7)	-B(111)	-B(12)	63.9(12)
B(13)	-B(14)	-B(18)	61.9(15)	B(12)	-B(111)	-B(16)	60.4(16)
B(15)	-B(14)	-B(19)	61.7(16)	B(16)	-B(111)	-B(110)	60.0(16)
B(18)	-B(14)	-B(19)	60.0(15)				

Table A2.8.4a(2). Bond Lengths(pm) and Angles(°) for Cage 2 of the $[(B_{10}H_{12})_2Au]^-$ Anion.

Au(7) -B(22)	226(3)	B(23) -B(28)	182(4)
Au(7) -B(23)	227.5(24)	B(24) -B(25)	178(4)
Au(7) -B(28)	236(3)	B(24) -B(28)	178(4)
Au(7) -B(211)	237(3)	B(24) -B(29)	179(4)
B(21) -B(22)	177(4)	B(25) -B(26)	182(4)
B(21) -B(23)	173(4)	B(25) -B(29)	177(4)
B(21) -B(24)	175(4)	B(25) -B(210)	167(4)
B(21) -B(25)	180(4)	B(26) -B(210)	176(4)
B(21) -B(26)	186(4)	B(26) -B(211)	171(4)
B(22) -B(23)	183(4)	B(28) -B(29)	175(4)
B(22) -B(26)	182(4)	B(29) -B(210)	199(4)
B(22) -B(211)	184(4)	B(210)-B(211)	185(4)
B(23) -B(24)	175(4)		

B(22) -Au(7)	-B(23)	47.7(9)	B(21) -B(25)	-B(24)	58.4(16)
B(22) -Au(7)	-B(211)	46.7(9)	B(21) -B(25)	-B(26)	61.6(16)
B(23) -Au(7)	-B(28)	46.2(9)	B(24) -B(25)	-B(29)	60.8(16)
B(22) -B(21)	-B(23)	63.2(16)	B(26) -B(25)	-B(210)	60.3(16)
B(22) -B(21)	-B(26)	60.0(15)	B(29) -B(25)	-B(210)	70.6(18)
B(23) -B(21)	-B(24)	60.3(16)	B(21) -B(26)	-B(22)	57.6(15)
B(24) -B(21)	-B(25)	60.1(16)	B(21) -B(26)	-B(25)	58.6(16)
B(25) -B(21)	-B(26)	59.8(16)	B(22) -B(26)	-B(211)	62.7(15)
Au(7) -B(22)	-B(23)	66.6(11)	B(25) -B(26)	-B(210)	55.6(16)
Au(7) -B(22)	-B(211)	69.7(12)	B(210)-B(26)	-B(211)	64.2(16)
B(21) -B(22)	-B(23)	57.3(15)	Au(7) -B(28)	-B(23)	64.5(12)
B(21) -B(22)	-B(26)	62.4(16)	B(23) -B(28)	-B(24)	58.1(15)
B(26) -B(22)	-B(211)	55.9(14)	B(24) -B(28)	-B(29)	61.1(16)
Au(7) -B(23)	-B(22)	65.7(11)	B(24) -B(29)	-B(25)	59.9(16)
Au(7) -B(23)	-B(28)	69.3(12)	B(24) -B(29)	-B(28)	60.2(16)
B(21) -B(23)	-B(22)	59.5(15)	B(25) -B(29)	-B(210)	52.5(15)
B(21) -B(23)	-B(24)	60.3(16)	B(25) -B(210)	-B(26)	64.2(17)
B(24) -B(23)	-B(28)	59.7(15)	B(25) -B(210)	-B(29)	56.9(16)
B(21) -B(24)	-B(23)	59.3(15)	B(26) -B(210)	-B(211)	56.7(15)
B(21) -B(24)	-B(25)	61.5(16)	Au(7) -B(211)	-B(22)	63.6(11)
B(23) -B(24)	-B(28)	62.2(15)	B(22) -B(211)	-B(26)	61.4(15)
B(25) -B(24)	-B(29)	59.3(16)	B(26) -B(211)	-B(210)	59.1(15)
B(28) -B(24)	-B(29)	58.7(16)			

Table A2.8.5. Bond Lengths(pm) and Angles(^{o}) Involving the Cage H Atoms in the $[(B_{10}H_{12})_2Au]^-$ Anion.

B(11) -H(11B)	117
B(12) -H(12B)	116
B(13) -H(13B)	117
B(14) -H(14B)	118
B(15) -H(15B)	119
B(16) -H(16B)	116
B(18) -H(18B)	120
B(19) -H(19B)	119
B(110)-H(110B)	118
B(111)-H(111B)	117
B(18) -H(18,9)	133
B(19) -H(18,9)	129
B(110)-H(110,11)	131
B(111)-H(110,11)	130

B(21) -H(21B)	117
B(22) -H(22B)	118
B(23) -H(23B)	120
B(24) -H(24B)	120
B(25) -H(25B)	118
B(26) -H(26B)	119
B(28) -H(28B)	118
B(29) -H(29B)	117
B(210)-H(210B)	118
B(211)-H(211B)	118
B(28) -H(28,9)	129
B(29) -H(28,9)	132
B(210)-H(210,11)	132
B(211)-H(210,11)	131

B(12) -B(11)	-H(11B)	134.7
B(13) -B(11)	-H(11B)	126.1
B(14) -B(11)	-H(11B)	109.9
B(15) -B(11)	-H(11B)	111.9
B(16) -B(11)	-H(11B)	120.5
Au(7) -B(12)	-H(12B)	122.3
B(11) -B(12)	-H(12B)	93.7
B(13) -B(12)	-H(12B)	101.1
B(16) -B(12)	-H(12B)	117.8
B(111)-B(12)	-H(12B)	142.9
Au(7) -B(13)	-H(13B)	104.0
B(11) -B(13)	-H(13B)	123.6
B(12) -B(13)	-H(13B)	117.7
B(14) -B(13)	-H(13B)	127.2
B(18) -B(13)	-H(13B)	115.6
B(11) -B(14)	-H(14B)	116.1
B(13) -B(14)	-H(14B)	96.9
B(15) -B(14)	-H(14B)	146.5
B(18) -B(14)	-H(14B)	98.9
B(19) -B(14)	-H(14B)	131.3
B(11) -B(15)	-H(15B)	123.6
B(14) -B(15)	-H(15B)	126.9
B(16) -B(15)	-H(15B)	111.7
B(19) -B(15)	-H(15B)	121.7
B(110)-B(15)	-H(15B)	111.7
B(11) -B(16)	-H(16B)	107.5
B(12) -B(16)	-H(16B)	110.6
B(15) -B(16)	-H(16B)	125.5
B(110)-B(16)	-H(16B)	138.4
B(111)-B(16)	-H(16B)	122.7
Au(7) -B(18)	-H(18B)	103.1
B(13) -B(18)	-H(18B)	117.9
B(14) -B(18)	-H(18B)	132.4
B(19) -B(18)	-H(18B)	135.3
B(14) -B(19)	-H(19B)	136.6

B(23) -B(21)	-H(21B)	123.6
B(24) -B(21)	-H(21B)	129.9
B(25) -B(21)	-H(21B)	128.2
B(26) -B(21)	-H(21B)	110.4
Au(7) -B(22)	-H(22B)	97.6
B(21) -B(22)	-H(22B)	135.4
B(23) -B(22)	-H(22B)	121.4
B(26) -B(22)	-H(22B)	127.8
B(211)-B(22)	-H(22B)	109.1
Au(7) -B(23)	-H(23B)	111.8
B(21) -B(23)	-H(23B)	128.7
B(22) -B(23)	-H(23B)	139.2
B(24) -B(23)	-H(23B)	106.5
B(28) -B(23)	-H(23B)	97.7
B(21) -B(24)	-H(24B)	83.0
B(23) -B(24)	-H(24B)	130.5
B(25) -B(24)	-H(24B)	78.7
B(28) -B(24)	-H(24B)	164.3
B(29) -B(24)	-H(24B)	117.7
B(21) -B(25)	-H(25B)	123.6
B(24) -B(25)	-H(25B)	114.8
B(26) -B(25)	-H(25B)	122.4
B(29) -B(25)	-H(25B)	113.9
B(210)-B(25)	-H(25B)	117.1
B(21) -B(26)	-H(26B)	128.1
B(22) -B(26)	-H(26B)	121.3
B(25) -B(26)	-H(26B)	130.6
B(210)-B(26)	-H(26B)	120.8
B(211)-B(26)	-H(26B)	110.3
Au(7) -B(28)	-H(28B)	112.7
B(23) -B(28)	-H(28B)	113.7
B(24) -B(28)	-H(28B)	118.7
B(29) -B(28)	-H(28B)	133.5
B(24) -B(29)	-H(29B)	128.6
B(25) -B(29)	-H(29B)	122.3

B(15)	-B(19)	-H(19B)	121.6
B(18)	-B(19)	-H(19B)	126.4
B(15)	-B(110)	-H(110B)	115.5
B(16)	-B(110)	-H(110B)	118.4
B(111)	-B(110)	-H(110B)	123.1
Au(7)	-B(111)	-H(111B)	87.1
B(12)	-B(111)	-H(111B)	117.6
B(16)	-B(111)	-H(111B)	148.6
B(110)	-B(111)	-H(111B)	137.3
Au(7)	-B(18)	-H(18,9)	71.4
B(13)	-B(18)	-H(18,9)	112.9
B(14)	-B(18)	-H(18,9)	101.3
B(19)	-B(18)	-H(18,9)	47.0
H(18B)	-B(18)	-H(18,9)	119.6
B(14)	-B(19)	-H(18,9)	102.6
B(15)	-B(19)	-H(18,9)	121.1
B(18)	-B(19)	-H(18,9)	49.1
H(19B)	-B(19)	-H(18,9)	109.5
B(18)	-H(18,9)	-B(19)	83.9
B(15)	-B(110)	-H(110,11)	119.6
B(16)	-B(110)	-H(110,11)	99.1
B(111)	-B(110)	-H(110,11)	46.1
H(10B)	-B(110)	-H(110,11)	123.4
Au(7)	-B(111)	-H(110,11)	70.9
B(12)	-B(111)	-H(110,11)	111.6
B(16)	-B(111)	-H(110,11)	100.9
B(110)	-B(111)	-H(110,11)	46.5
H(11B)	-B(111)	-H(110,11)	107.8
B(211)	-B(210)	-H(210B)	110.2
H(21B)	-B(211)	-H(210,11)	125.1
B(110)	-H(110,11)	-B(111)	87.4
B(28)	-B(29)	-H(29B)	121.8
B(210)	-B(29)	-H(29B)	115.4
B(25)	-B(210)	-H(210B)	137.3
B(26)	-B(210)	-H(210B)	131.0
B(29)	-B(210)	-H(210B)	118.7
B(22)	-B(211)	-H(211B)	115.4
B(26)	-B(211)	-H(211B)	125.2
B(210)	-B(211)	-H(211B)	137.1
Au(7)	-B(28)	-H(28,9)	73.9
B(23)	-B(28)	-H(28,9)	118.3
B(24)	-B(28)	-H(28,9)	106.2
B(29)	-B(28)	-H(28,9)	48.5
H(28B)	-B(28)	-H(28,9)	123.8
B(24)	-B(29)	-H(28,9)	104.1
B(25)	-B(29)	-H(28,9)	126.6
B(28)	-B(29)	-H(28,9)	47.2
B(210)	-B(29)	-H(28,9)	90.7
H(29B)	-B(29)	-H(28,9)	107.3
B(28)	-H(28,9)	-B(29)	84.4
B(25)	-B(210)	-H(210,11)	121.0
B(26)	-B(210)	-H(210,11)	98.0
B(29)	-B(210)	-H(210,11)	82.6
B(211)	-B(210)	-H(210,11)	45.2
H(20B)	-B(210)	-H(210,11)	98.0
Au(7)	-B(211)	-H(210,11)	72.1
B(22)	-B(211)	-H(210,11)	112.1
B(26)	-B(211)	-H(210,11)	100.7
B(210)	-B(211)	-H(210,11)	45.7
Au(7)	-B(211)	-H(211B)	106.5
B(22)	-B(21)	-H(21B)	110.7
B(210)	-H(210,11)	-B(211)	89.1

A2.9 $(B_{10}H_{12}Au)_2(AuPPh_3)_4$.

The Molecular Structure and Numbering Scheme for $(B_{10}H_{12}Au)_2(AuPPh_3)_4$.

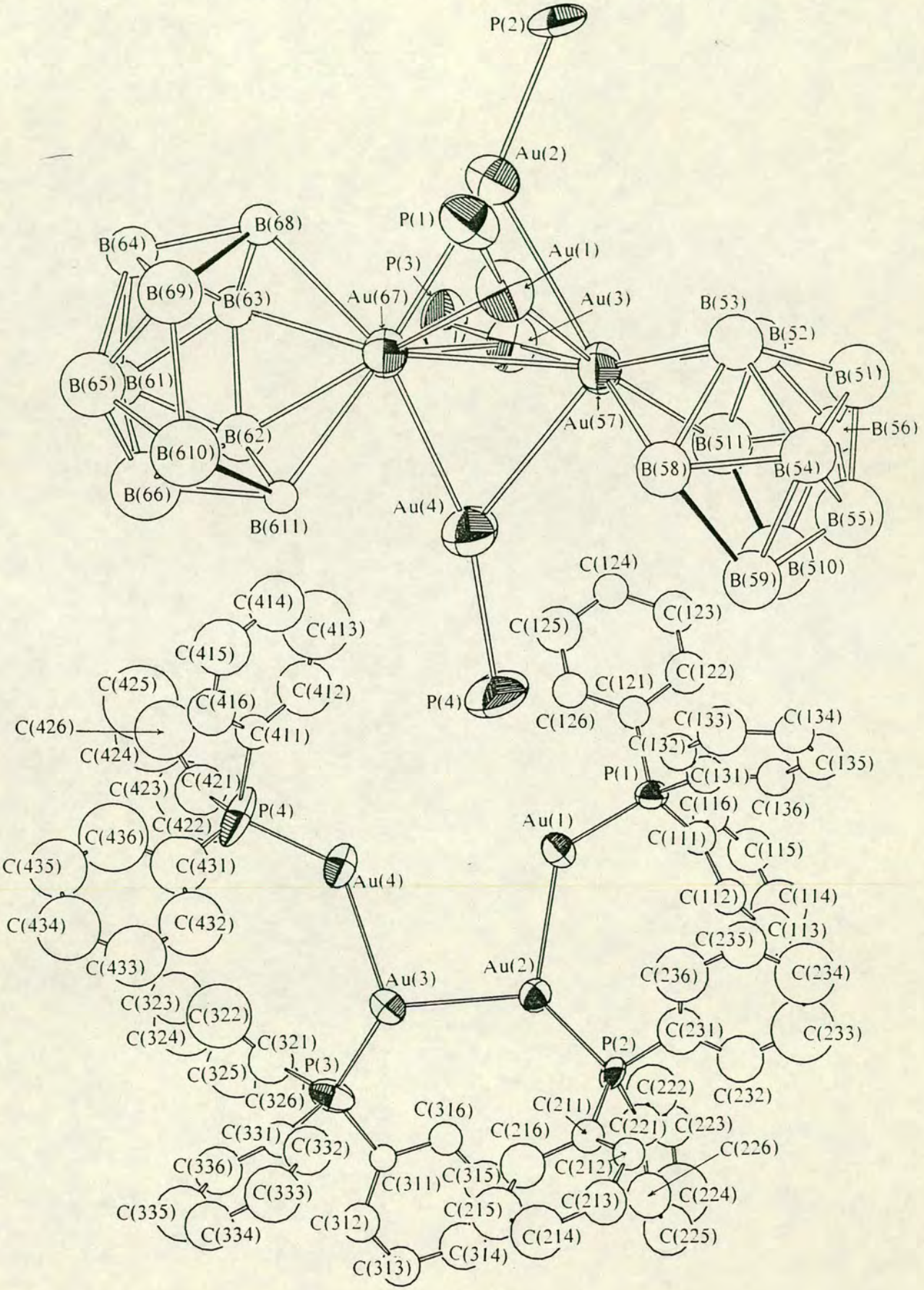

Crystal data. $C_{72}H_{84}Au_6B_{20}P_4$. M = 2471.4, monoclinic with a = 1.4444(10), b = 3.0787(23), c = 2.0946(13) nm, and β = 108.62(5)°. U = 8.8272 nm^3, D_x = 1.859 Mgm^{-3}, μ(Mo-K_α) = 10.027 mm^{-1}, *F(000)* = 4600, Z = 4, and space group $P2_1/n$.

Data collection and processing. Θ_{max} = 20° and $+h +k \pm l$. 6606 data were measured yielding 6270 unique (R_{merge} = 0.0565), all of which have $F > 2\sigma(F)$ and were retained. Variable scans speeds between 1.030 and 3.296 $^{o}min^{-1}$. Crystal decayed by *ca.* 40% (non-linearly) and correction was applied.

Structure solution and refinement. Au atom positions found by automatic direct methods. Only Au and P atoms allowed anisotropic thermal motion. Phenyl rings constrained to be regular, planar hexagons, and their H atoms were set in calculated positions with a fixed group thermal parameter of 1000 pm^2. Weighting scheme g = 0.001502, R = 0.1070, R_w = 0.1587, S = 1.549, data : variable = 19 : 1. $(\Delta\rho)_{max}$ = 2115 and $(\Delta\rho)_{min}$ = -2859 enm^{-3}. Δ/σ in final least-squares cycle was 0.632.

Table A2.9.1. Fractional Coordinates of Refined Atoms in $(B_{10}H_{12}Au)_2(AuPPh_3)_4$. U_{eq} in $10^4 pm^2$.

	x	y	z	U_{eq}
Au(1)	0.80288(16)	0.04244(8)	0.73890(11)	0.0550(16)
Au(2)	0.75912(15)	0.12961(8)	0.77515(10)	0.0511(16)
Au(3)	0.87316(15)	0.18513(8)	0.71261(11)	0.0535(16)
Au(4)	0.91925(16)	0.12504(9)	0.61518(12)	0.0675(19)
Au(57)	0.93508(14)	0.10536(7)	0.75152(10)	0.0456(15)
Au(67)	0.75626(14)	0.11425(7)	0.64933(10)	0.0434(14)
P(1)	0.7283(10)	-0.0204(5)	0.7518(7)	0.051(10)
P(2)	0.7342(9)	0.1449(5)	0.8744(7)	0.050(10)
P(3)	0.8224(11)	0.2546(5)	0.6816(8)	0.061(11)
P(4)	1.0283(12)	0.1324(8)	0.5577(9)	0.100(16)
B(51)	1.139(5)	0.078(3)	0.880(4)	0.072(22)

B(52)	1.060(4)	0.1187(22)	0.845(3)	0.050(17)
B(53)	1.017(4)	0.0589(22)	0.832(3)	0.053(17)
B(54)	1.118(4)	0.0308(22)	0.823(3)	0.053(17)
B(55)	1.204(6)	0.076(3)	0.819(4)	0.090(25)
B(56)	1.172(4)	0.1272(21)	0.848(3)	0.048(16)
B(58)	1.012(4)	0.0336(22)	0.745(3)	0.059(18)
B(59)	1.147(5)	0.0514(23)	0.745(3)	0.059(19)
B(510)	1.186(6)	0.111(3)	0.761(4)	0.09(3)
B(511)	1.089(5)	0.1433(23)	0.780(3)	0.057(18)
B(61)	0.559(4)	0.1340(20)	0.502(3)	0.040(15)
B(62)	0.685(4)	0.1278(20)	0.540(3)	0.042(15)
B(63)	0.614(3)	0.1444(18)	0.590(3)	0.030(13)
B(64)	0.505(4)	0.1111(21)	0.568(3)	0.047(16)
B(65)	0.533(5)	0.070(3)	0.499(4)	0.071(21)
B(66)	0.626(5)	0.086(3)	0.480(4)	0.075(22)
B(68)	0.590(3)	0.1004(18)	0.642(3)	0.029(13)
B(69)	0.548(5)	0.0568(24)	0.578(3)	0.062(19)
B(610)	0.635(5)	0.043(3)	0.520(4)	0.077(22)
B(611)	0.737(3)	0.0809(16)	0.5418(23)	0.020(12)
C(111)	0.6092	-0.0136	0.7556	0.050(14)
C(112)	0.6012(24)	0.0093(12)	0.8111(16)	0.055(15)
C(113)	0.5099	0.0149	0.8194	0.104(24)
C(114)	0.4266	-0.0024	0.7723	0.15(3)
C(115)	0.4346	-0.0253	0.7169	0.093(21)
C(116)	0.5259	-0.0309	0.7085	0.060(16)
C(121)	0.7261	-0.0605	0.6874	0.049(14)
C(122)	0.685(3)	-0.1011(12)	0.6904(16)	0.074(18)
C(123)	0.6761	-0.1315	0.6395	0.081(19)
C(124)	0.7091	-0.1214	0.5855	0.054(15)
C(125)	0.7505	-0.0808	0.5825	0.090(21)
C(126)	0.7590	-0.0504	0.6334	0.054(15)
C(131)	0.8005	-0.0491	0.8288	0.060(15)
C(132)	0.9022(24)	-0.0509(12)	0.8474(18)	0.055(15)
C(133)	0.9551	-0.0749	0.9037	0.097(22)
C(134)	0.9063	-0.0972	0.9414	0.064(17)
C(135)	0.8046	-0.0955	0.9227	0.089(21)
C(136)	0.7517	-0.0714	0.8665	0.059(15)
C(211)	0.8188	0.1842	0.9314	0.043(13)
C(212)	0.8647(24)	0.1775(10)	1.0001(16)	0.043(13)
C(213)	0.9305	0.2082	1.0380	0.074(18)
C(214)	0.9505	0.2456	1.0071	0.109(25)
C(215)	0.9046	0.2523	0.9383	0.106(24)
C(216)	0.8387	0.2216	0.9005	0.082(19)
C(221)	0.6144	0.1651	0.8655	0.076(18)
C(222)	0.537(3)	0.1447(13)	0.8171(23)	0.13(3)
C(223)	0.4417	0.1591	0.8055	0.078(19)
C(224)	0.4233	0.1939	0.8422	0.18(4)
C(225)	0.5005	0.2144	0.8906	0.12(3)
C(226)	0.5961	0.2000	0.9022	0.087(20)
C(231)	0.7540	0.0975	0.9219	0.085(20)
C(232)	0.683(3)	0.0924(16)	0.9535(25)	0.088(21)
C(233)	0.6842	0.0557	0.9930	0.18(4)
C(234)	0.7565	0.0242	1.0009	0.16(3)
C(235)	0.8275	0.0294	0.9694	0.084(20)
C(236)	0.8263	0.0660	0.9299	0.12(3)

C(311)	0.7169	0.2735	0.7048	0.032(12)
C(312)	0.6961(23)	0.3174(9)	0.7088(18)	0.065(16)
C(313)	0.6141	0.3300	0.7258	0.071(17)
C(314)	0.5530	0.2985	0.7388	0.095(22)
C(315)	0.5738	0.2545	0.7349	0.081(19)
C(316)	0.6557	0.2420	0.7179	0.046(13)
C(321)	0.7930	0.2600	0.5886	0.091(21)
C(322)	0.857(3)	0.2523(18)	0.552(3)	0.19(4)
C(323)	0.8252	0.2589	0.4822	0.12(3)
C(324)	0.7302	0.2732	0.4495	0.17(4)
C(325)	0.6666	0.2810	0.4863	0.17(4)
C(326)	0.6980	0.2744	0.5558	0.106(25)
C(331)	0.9226	0.2917	0.7169	0.053(14)
C(332)	0.983(3)	0.2844(13)	0.7827(21)	0.093(22)
C(333)	1.0531	0.3153	0.8152	0.12(3)
C(334)	1.0623	0.3535	0.7819	0.090(21)
C(335)	1.0017	0.3608	0.7161	0.12(3)
C(336)	0.9319	0.3299	0.6836	0.088(21)
C(411)	1.1038	0.0801	0.5698	0.050(14)
C(412)	1.0572(25)	0.0399(17)	0.5639(23)	0.12(3)
C(413)	1.1116	0.0017	0.5720	0.18(4)
C(414)	1.2126	0.0037	0.5859	0.12(3)
C(415)	1.2592	0.0439	0.5918	0.12(3)
C(416)	1.2048	0.0821	0.5838	0.084(20)
C(421)	0.9629	0.1302	0.4659	0.13(3)
C(422)	0.870(4)	0.1470(17)	0.434(3)	0.092(21)
C(423)	0.8235	0.1392	0.3657	0.19(4)
C(424)	0.8701	0.1145	0.3291	0.29(7)
C(425)	0.9631	0.0977	0.3609	0.31(7)
C(426)	1.0095	0.1055	0.4293	0.16(4)
C(431)	1.0907	0.1755	0.5714	0.13(3)
C(432)	1.111(4)	0.2021(23)	0.628(3)	0.16(4)
C(433)	1.1789	0.2358	0.6370	0.15(3)
C(434)	1.2258	0.2429	0.5891	0.17(4)
C(435)	1.2052	0.2163	0.5324	0.14(3)
C(436)	1.1377	0.1826	0.5235	0.18(4)

Table A2.9.2. Fractional Coordinates of Hydrogen Atoms in $(B_{10}H_{12}Au)_2(AuPPh_3)_4$.

	x	y	z
H(112)	0.6657	0.0228	0.8474
H(113)	0.5039	0.0324	0.8626
H(114)	0.3561	0.0015	0.7793
H(115)	0.3702	-0.0390	0.6808
H(116)	0.5319	-0.0487	0.6656
H(122)	0.6592	-0.1090	0.7323
H(123)	0.6441	-0.1629	0.6419
H(124)	0.7024	-0.1449	0.5461

H(125)	0.7757	-0.0729	0.5405
H(126)	0.7907	-0.0189	0.6309
H(132)	0.9401	-0.0334	0.8185
H(133)	1.0336	-0.0770	0.9173
H(134)	0.9469	-0.1170	0.9836
H(135)	0.7666	-0.1134	0.9511
H(136)	0.6730	-0.0698	0.8523
H(212)	0.8497	0.1485	1.0240
H(213)	0.9659	0.2032	1.0912
H(214)	1.0003	0.2697	1.0365
H(215)	0.9184	0.2816	0.9145
H(216)	0.8022	0.2269	0.8474
H(222)	0.5518	0.1173	0.7894
H(223)	0.3821	0.1431	0.7673
H(224)	0.3487	0.2057	0.8307
H(225)	0.4850	0.2426	0.9163
H(226)	0.6547	0.2168	0.9384
H(232)	0.6269	0.1166	0.9473
H(233)	0.6298	0.0517	1.0176
H(234)	0.7585	-0.0040	1.0317
H(235)	0.8842	0.0053	0.9756
H(236)	0.8813	0.0703	0.9053
H(312)	0.7437	0.3418	0.6989
H(313)	0.5979	0.3640	0.7286
H(314)	0.4889	0.3083	0.7513
H(315)	0.5257	0.2303	0.7442
H(316)	0.6714	0.2080	0.7145
H(322)	0.9297	0.2406	0.5769
H(323)	0.8745	0.2532	0.4538
H(324)	0.7070	0.2800	0.3961
H(325)	0.5946	0.2941	0.4616
H(326)	0.6498	0.2815	0.5847
H(332)	0.9763	0.2548	0.8085
H(333)	1.1002	0.3096	0.8660
H(334)	1.1162	0.3774	0.8069
H(335)	1.0083	0.3904	0.6902
H(336)	0.8844	0.3356	0.6327
H(412)	0.9790	0.0382	0.5531
H(413)	1.0766	-0.0294	0.5681
H(414)	1.2558	-0.0253	0.5929
H(415)	1.3374	0.0462	0.6027
H(416)	1.2397	0.1137	0.5877
H(422)	0.8316	0.1633	0.4639
H(423)	0.7510	0.1529	0.3415
H(424)	0.8387	0.1156	0.2732
H(425)	1.0070	0.0886	0.3274
H(426)	1.0877	0.0990	0.4498
H(432)	1.0744	0.1966	0.6648
H(433)	1.1954	0.2560	0.6818
H(434)	1.2800	0.2686	0.5976
H(435)	1.2436	0.2218	0.4965
H(436)	1.1226	0.1625	0.4795

Table A2.9.3. Anisotropic Thermal Parameters($10^4 pm^2$) for Atoms in $(B_{10}H_{12}Au)_2(AuPPh_3)_4$.

	U_{11}	U_{22}	U_{33}	U_{23}	U_{13}	U_{12}
Au(1)	0.0615(14)	0.0436(16)	0.0520(15)	0.0026(12)	0.0138(13)	-0.0042(11)
Au(2)	0.0553(14)	0.0509(17)	0.0426(14)	-0.0019(12)	0.0187(12)	-0.0036(11)
Au(3)	0.0495(13)	0.0440(16)	0.0588(16)	0.0029(12)	0.0115(12)	-0.0009(11)
Au(4)	0.0517(14)	0.0897(22)	0.0578(16)	0.0200(15)	0.0255(13)	0.0123(13)
Au(57)	0.0401(12)	0.0478(16)	0.0422(14)	0.0044(11)	0.0074(11)	0.0014(10)
Au(67)	0.0393(12)	0.0453(15)	0.0399(13)	-0.0013(11)	0.0092(11)	0.0022(10)
P(1)	0.066(9)	0.040(10)	0.040(9)	0.003(7)	0.018(8)	0.016(7)
P(2)	0.041(7)	0.051(10)	0.059(9)	-0.008(8)	0.038(8)	0.012(7)
P(3)	0.058(9)	0.043(11)	0.068(11)	0.004(9)	-0.001(9)	0.015(8)
P(4)	0.053(10)	0.177(23)	0.071(12)	0.037(14)	0.044(10)	0.025(11)

Table A2.9.4. Bond Lengths(pm) and Angles(°) for the Refined Atoms in $(B_{10}H_{12}Au)_2(AuPPh_3)_4$.

Au(1) -Au(2)	291.3(4)	B(55) -B(510)	160(12)
Au(1) -Au(57)	267.3(4)	B(56) -B(510)	196(11)
Au(1) -Au(67)	283.8(4)	B(56) -B(511)	160(9)
Au(2) -Au(3)	295.5(4)	B(58) -B(59)	202(10)
Au(2) -Au(57)	284.0(4)	B(59) -B(510)	192(11)
Au(2) -Au(67)	266.5(4)	B(510)-B(511)	186(11)
Au(3) -Au(4)	298.3(4)	B(61) -B(62)	174(8)
Au(3) -Au(57)	265.1(4)	B(61) -B(63)	179(8)
Au(3) -Au(67)	281.8(4)	B(61) -B(64)	192(9)
Au(4) -Au(57)	285.6(4)	B(61) -B(65)	199(10)
Au(4) -Au(67)	269.1(4)	B(61) -B(66)	190(10)
Au(57)-Au(67)	279.2(4)	B(62) -B(63)	176(8)
Au(1) - P(1)	227.3(15)	B(62)-B(66)	180(10)
Au(2) - P(2)	227.0(14)	B(62)-B(611)	162(8)
Au(3) - P(3)	228.6(16)	B(63)-B(64)	181(8)
Au(4) - P(4)	227.8(21)	B(63)-B(68)	185(7)
Au(57)-B(52)	223(6)	B(64) -B(65)	204(10)
Au(57)-B(53)	224(6)	B(64) -B(68)	168(8)
Au(57)-B(58)	250(7)	B(64) -B(69)	177(10)
Au(57)-B(511)	242(7)	B(65) -B(66)	160(11)
Au(67)-B(62)	224(6)	B(65) -B(69)	165(11)
Au(67)-B(63)	223(5)	B(65) -B(610)	162(11)
Au(67)-B(68)	240(5)	B(66) -B(610)	156(11)
Au(67)-B(611)	241(5)	B(66) -B(611)	172(9)
B(51) -B(52)	171(10)	B(68) -B(69)	186(9)
B(51) -B(53)	182(10)	B(69) -B(610)	205(11)
B(51) -B(54)	184(10)	B(610)-B(611)	182(9)
B(51) -B(55)	180(12)	P(1) -C(111)	176(4)
B(51) -B(56)	179(10)	P(1) -C(121)	182(4)

B(52) -B(53)	193(9)
B(52) -B(56)	162(9)
B(52) -B(511)	171(9)
B(53) -B(54)	176(9)
B(53) -B(58)	196(9)
B(54) -B(55)	187(11)
B(54) -B(58)	184(9)
B(54) -B(59)	191(9)
B(55) -B(56)	181(11)
B(55) -B(59)	168(11)

P(1) -C(131)	184(4)
P(2) -C(211)	186(4)
P(2) -C(221)	179(5)
P(2) -C(231)	174(5)
P(3) -C(311)	184(4)
P(3) -C(321)	187(6)
P(3) -C(331)	181(5)
P(4) -C(411)	191(5)
P(4) -C(421)	185(6)
P(4) -C(431)	158(7)

Au(2) -Au(1)	-Au(57)	60.94(8)
Au(2) -Au(1)	-Au(67)	55.19(7)
Au(57)-Au(1)	-Au(67)	60.80(8)
Au(1) -Au(2)	-Au(3)	102.67(9)
Au(1) -Au(2)	-Au(57)	55.36(7)
Au(1) -Au(2)	-Au(67)	60.98(8)
Au(3) -Au(2)	-Au(57)	54.42(7)
Au(3) -Au(2)	-Au(67)	59.93(8)
Au(57)-Au(2)	-Au(67)	60.87(8)
Au(2) -Au(3)	-Au(4)	102.85(10)
Au(2) -Au(3)	-Au(57)	60.59(8)
Au(2) -Au(3)	-Au(67)	54.93(7)
Au(4) -Au(3)	-Au(57)	60.58(8)
Au(4) -Au(3)	-Au(67)	55.18(8)
Au(57)-Au(3)	-Au(67)	61.31(8)
Au(3) -Au(4)	-Au(57)	53.96(8)
Au(3) -Au(4)	-Au(67)	59.29(8)
Au(57)-Au(4)	-Au(67)	60.37(8)
Au(1) -Au(57)	-Au(2)	63.70(8)
Au(1) -Au(57)	-Au(3)	118.72(11)
Au(1) -Au(57)	-Au(4)	103.19(10)
Au(1) -Au(57)	-Au(67)	62.52(8)
Au(2) -Au(57)	-Au(3)	64.99(8)
Au(2) -Au(57)	-Au(4)	109.15(10)
Au(2) -Au(57)	-Au(67)	56.47(7)
Au(3) -Au(57)	-Au(4)	65.46(9)
Au(3) -Au(57)	-Au(67)	62.28(8)
Au(4) -Au(57)	-Au(67)	56.88(8)
Au(1) -Au(67)	-Au(2)	63.83(8)
Au(1) -Au(67)	-Au(3)	108.19(10)
Au(1) -Au(67)	-Au(4)	103.23(10)
Au(1) -Au(67)	-Au(57)	56.68(8)
Au(2) -Au(67)	-Au(3)	65.14(8)
Au(2) -Au(67)	-Au(4)	120.16(11)
Au(2) -Au(67)	-Au(57)	62.67(8)
Au(3) -Au(67)	-Au(4)	65.52(9)
Au(3) -Au(67)	-Au(57)	56.40(7)
Au(4) -Au(67)	-Au(57)	62.75(8)
Au(2) -Au(1)	- P(1)	127.1(4)
Au(57)-Au(1)	- P(1)	162.9(4)
Au(67)-Au(1)	- P(1)	136.1(4)
Au(1) -Au(2)	- P(2)	122.7(4)
Au(3) -Au(2)	- P(2)	124.1(4)

B(51) -B(55)	-B(54)	60(4)
B(51) -B(55)	-B(56)	59(4)
B(54) -B(55)	-B(59)	65(4)
B(56) -B(55)	-B(510)	70(5)
B(59) -B(55)	-B(510)	72(5)
B(51) -B(56)	-B(52)	60(4)
B(51) -B(56)	-B(55)	60(4)
B(52) -B(56)	-B(511)	64(4)
B(55) -B(56)	-B(510)	50(4)
B(510)-B(56)	-B(511)	62(4)
Au(57)-B(58)	-B(53)	59(3)
B(53) -B(58)	-B(54)	55(3)
B(54) -B(58)	-B(59)	59(3)
B(54) -B(59)	-B(55)	62(4)
B(54) -B(59)	-B(58)	56(3)
B(55) -B(59)	-B(510)	52(4)
B(55) -B(510)	-B(56)	60(5)
B(55) -B(510)	-B(59)	56(5)
B(56) -B(510)	-B(511)	50(4)
Au(57)-B(511)	-B(52)	63(3)
B(52) -B(511)	-B(56)	58(4)
B(56) -B(511)	-B(510)	68(4)
B(62) -Au(67)	-B(63)	46.3(21)
B(62) -Au(67)	-B(611)	40.7(19)
B(63) -Au(67)	-B(68)	46.8(19)
B(62) -B(61)	-B(63)	60(3)
B(62) -B(61)	-B(66)	59(4)
B(63) -B(61)	-B(64)	58(3)
B(64) -B(61)	-B(65)	63(3)
B(65) -B(61)	-B(66)	49(4)
Au(67)-B(62)	-B(63)	67(3)
Au(67)-B(62)	-B(611)	75(3)
B(61) -B(62)	-B(63)	62(3)
B(61) -B(62)	-B(66)	65(4)
B(66) -B(62)	-B(611)	60(4)
Au(67)-B(63)	-B(62)	67(3)
Au(67)-B(63)	-B(68)	71.6(24)
B(61) -B(63)	-B(62)	59(3)
B(61) -B(63)	-B(64)	64(3)
B(64) -B(63)	-B(68)	55(3)
B(61) -B(64)	-B(63)	57(3)
B(61) -B(64)	-B(65)	60(3)
B(63) -B(64)	-B(68)	64(3)

Au(57)-Au(2)	- P(2)	128.8(4)	B(65) -B(64)	-B(69)	51(4)
Au(67)-Au(2)	- P(2)	170.3(4)	B(68) -B(64)	-B(69)	65(4)
Au(2) -Au(3)	- P(3)	119.5(4)	B(61) -B(65)	-B(64)	57(3)
Au(4) -Au(3)	- P(3)	120.5(4)	B(61) -B(65)	-B(66)	63(4)
Au(57)-Au(3)	- P(3)	178.5(4)	B(64) -B(65)	-B(69)	56(4)
Au(67)-Au(3)	- P(3)	120.0(4)	B(66) -B(65)	-B(610)	58(5)
Au(3) -Au(4)	- P(4)	130.0(5)	B(69) -B(65)	-B(610)	77(5)
Au(57)-Au(4)	- P(4)	134.5(5)	B(61) -B(66)	-B(62)	56(4)
Au(67)-Au(4)	- P(4)	164.5(5)	B(61) -B(66)	-B(65)	69(4)
Au(1) -Au(57)	-B(52)	124.9(17)	B(62) -B(66)	-B(611)	55(3)
Au(1) -Au(57)	-B(53)	78.5(17)	B(65) -B(66)	-B(610)	62(5)
Au(1) -Au(57)	-B(58)	70.8(15)	B(610)-B(66)	-B(611)	68(5)
Au(1) -Au(57)	-B(511)	161.4(16)	Au(67)-B(68)	-B(63)	60.6(22)
Au(2) -Au(57)	-B(52)	108.5(17)	B(63) -B(68)	-B(64)	62(3)
Au(2) -Au(57)	-B(53)	108.8(17)	B(64) -B(68)	-B(69)	60(4)
Au(2) -Au(57)	-B(58)	132.9(15)	B(64) -B(69)	-B(65)	73(4)
Au(2) -Au(57)	-B(511)	129.4(16)	B(64) -B(69)	-B(68)	55(3)
Au(3) -Au(57)	-B(52)	101.3(17)	B(65) -B(69)	-B(610)	51(4)
Au(3) -Au(57)	-B(53)	150.2(17)	B(65) -B(610)	-B(66)	61(5)
Au(3) -Au(57)	-B(58)	156.4(15)	B(65) -B(610)	-B(69)	52(4)
Au(3) -Au(57)	-B(511)	79.8(16)	B(66) -B(610)	-B(611)	60(4)
Au(4) -Au(57)	-B(52)	128.2(17)	Au(67)-B(611)	-B(62)	64(3)
Au(4) -Au(57)	-B(53)	138.1(17)	B(62) -B(611)	-B(66)	65(4)
Au(4) -Au(57)	-B(58)	91.7(15)	B(66) -B(611)	-B(610)	52(4)
Au(4) -Au(57)	-B(511)	85.5(16)	Au(1) - P(1)	-C(111)	114.3(14)
Au(67)-Au(57)	-B(52)	160.6(17)	Au(1) - P(1)	-C(121)	112.7(13)
Au(67)-Au(57)	-B(53)	141.0(17)	Au(1) - P(1)	-C(131)	110.8(13)
Au(67)-Au(57)	-B(58)	111.5(15)	C(111)- P(1)	-C(121)	109.1(18)
Au(67)-Au(57)	-B(511)	134.3(16)	C(111)- P(1)	-C(131)	107.8(18)
Au(1) -Au(67)	-B(62)	139.3(15)	C(121)- P(1)	-C(131)	101.2(17)
Au(1) -Au(67)	-B(63)	132.3(14)	Au(2) - P(2)	-C(211)	117.3(12)
Au(1) -Au(67)	-B(68)	85.6(13)	Au(2) - P(2)	-C(221)	114.0(16)
Au(1) -Au(67)	-B(611)	102.6(11)	Au(2) - P(2)	-C(231)	107.8(17)
Au(2) -Au(67)	-B(62)	147.0(15)	C(211)- P(2)	-C(221)	104.8(19)
Au(2) -Au(67)	-B(63)	101.4(14)	C(211)- P(2)	-C(231)	103.0(20)
Au(2) -Au(67)	-B(68)	77.9(13)	C(221)- P(2)	-C(231)	109.2(23)
Au(2) -Au(67)	-B(611)	164.0(11)	Au(3) - P(3)	-C(311)	116.1(13)
Au(3) -Au(67)	-B(62)	110.5(15)	Au(3) - P(3)	-C(321)	109.0(19)
Au(3) -Au(67)	-B(63)	104.2(14)	Au(3) - P(3)	-C(331)	109.4(16)
Au(3) -Au(67)	-B(68)	127.1(13)	C(311)- P(3)	-C(321)	108.5(22)
Au(3) -Au(67)	-B(611)	129.9(11)	C(311)- P(3)	-C(331)	108.4(19)
Au(4) -Au(67)	-B(62)	82.0(15)	C(321)- P(3)	-C(331)	104.8(23)
Au(4) -Au(67)	-B(63)	121.8(14)	Au(4) - P(4)	-C(411)	107.9(16)
Au(4) -Au(67)	-B(68)	161.9(13)	Au(4) - P(4)	-C(421)	109.6(20)
Au(4) -Au(67)	-B(611)	69.6(11)	Au(4) - P(4)	-C(431)	116(3)
Au(57)-Au(67)	-B(62)	144.8(15)	C(411)- P(4)	-C(421)	100.8(25)
Au(57)-Au(67)	-B(63)	158.1(14)	C(411)- P(4)	-C(431)	115(3)
Au(57)-Au(67)	-B(68)	133.8(13)	C(421)- P(4)	-C(431)	107(3)
Au(57)-Au(67)	-B(611)	118.4(11)	P(1) -C(111)	-C(112)	116(3)
B(52) -Au(57)	-B(53)	51.3(24)	P(1) -C(111)	-C(116)	124(3)
B(52) -Au(57)	-B(511)	42.9(23)	P(1) -C(121)	-C(122)	119(3)
B(53) -Au(57)	-B(58)	48.5(23)	P(1) -C(121)	-C(126)	121(3)
B(52) -B(51)	-B(53)	66(4)	P(1) -C(131)	-C(132)	121(3)
B(52) -B(51)	-B(56)	55(4)	P(1) -C(131)	-C(136)	119(3)
B(53) -B(51)	-B(54)	58(4)	P(2) -C(211)	-C(212)	124(3)

B(54)	-B(51)	-B(55)	62(4)	P(2) -C(211) -C(216)	116(3)
B(55)	-B(51)	-B(56)	61(4)	P(2) -C(221) -C(222)	116(3)
Au(57)	-B(52)	-B(53)	65(3)	P(2) -C(221) -C(226)	124(4)
Au(57)	-B(52)	-B(511)	74(3)	P(2) -C(231) -C(232)	111(4)
B(51)	-B(52)	-B(53)	60(4)	P(2) -C(231) -C(236)	129(4)
B(51)	-B(52)	-B(56)	65(4)	P(3) -C(311) -C(312)	122(3)
B(56)	-B(52)	-B(511)	57(4)	P(3) -C(311) -C(316)	118(3)
Au(57)	-B(53)	-B(52)	64(3)	P(3) -C(321) -C(322)	126(4)
Au(57)	-B(53)	-B(58)	73(3)	P(3) -C(321) -C(326)	114(4)
B(51)	-B(53)	-B(52)	54(4)	P(3) -C(331) -C(332)	118(3)
B(51)	-B(53)	-B(54)	62(4)	P(3) -C(331) -C(336)	121(3)
B(54)	-B(53)	-B(58)	59(4)	P(4) -C(411) -C(412)	120(3)
B(51)	-B(54)	-B(53)	61(4)	P(4) -C(411) -C(416)	120(4)
B(51)	-B(54)	-B(55)	58(4)	P(4) -C(421) -C(422)	125(5)
B(53)	-B(54)	-B(58)	66(4)	P(4) -C(421) -C(426)	114(4)
B(55)	-B(54)	-B(59)	53(4)	P(4) -C(431) -C(432)	127(5)
B(58)	-B(54)	-B(59)	65(4)	P(4) -C(431) -C(436)	112(5)

A2.10 $(B_{10}H_{12}Au)(AuPCy_3)_3.2.5CH_2Cl_2$.

The Molecular Structure and Numbering Scheme for $(B_{10}H_{12}Au)(AuPCy_3)_3$.

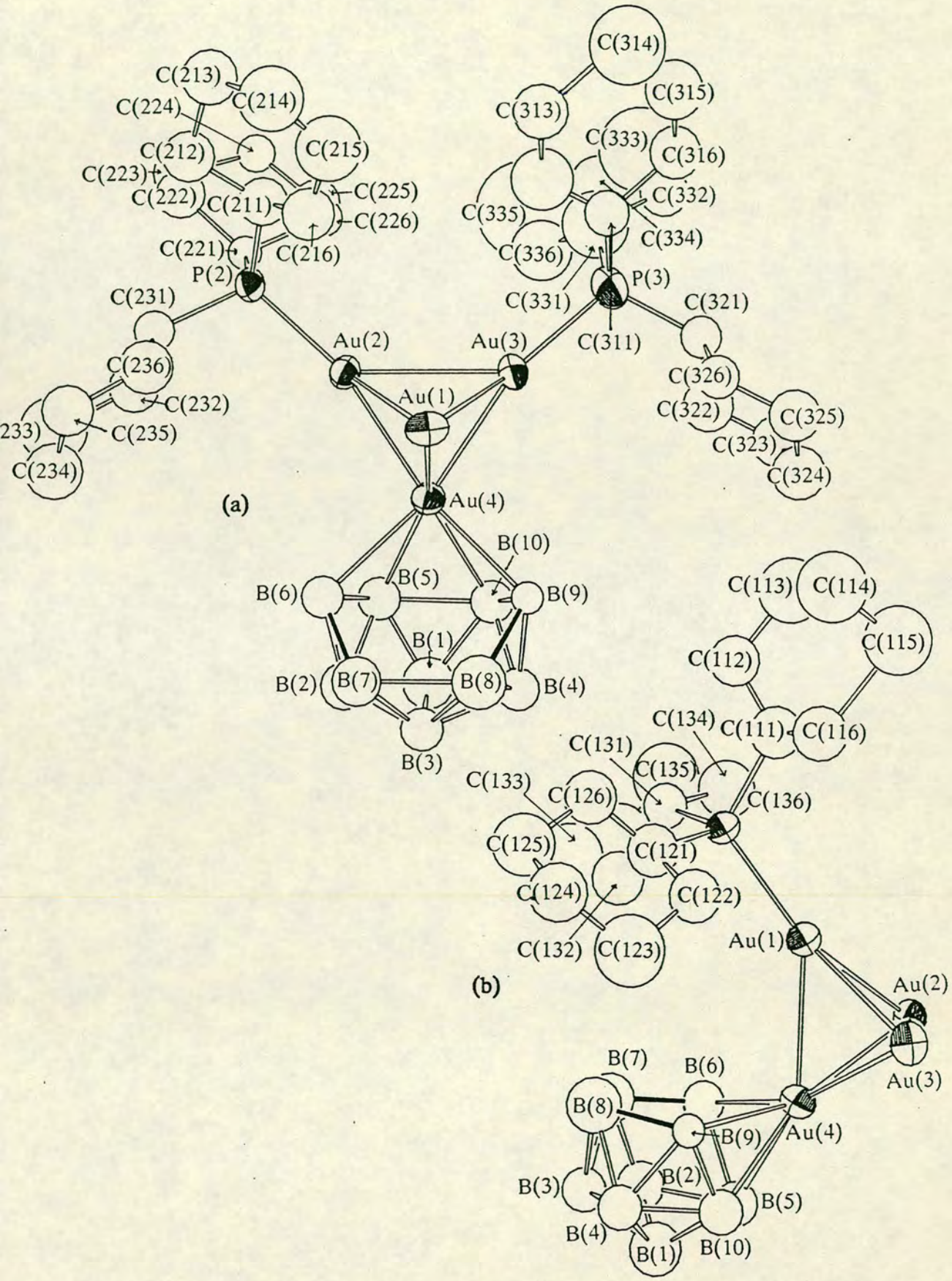

Crystal data. $C_{56.5}H_{116}Au_4B_{10}Cl_5P_3$, M = 1961.7, monoclinic, with a = 1.5658(6), b = 2.6486(18), c = 1.8136(9) nm, and β = 93.59(4) °. U = 7.5066 nm^3, Z = 4, D_x = 1.735 Mgm^{-3}, μ(Mo-K_α) = 8.054 mm^{-1}, *F(000)* = 3804, and space group = *Cc.*

Data collection and processing. Scan speed = 1.030 - 3.296 $^{o}min^{-1}$. 5749 unique data measured, ($1 < \Theta < 25$, $+h + k \pm l$) of which 5695 with $F > 2\sigma(F)$ were used in the refinement. Crystal decayed by ca. 14%, and correction was applied.

Structure solution and refinement. The position of the gold atoms were located by direct methods. Au and P atoms allowed anisotropic thermal motion. The cyclohexyl group numbered *C331* - *C336* could not be satisfactorily refined, and the positions of these atoms were included in the model, but were not refined. Cyclohexyl H atoms group thermal parameter was 410(90) pm^2 at convergence, and the cage H atoms are absent.

Solvent molecules : Molecule 1 has one chlorine atom equally disordered over two sites (Cl12a and Cl12b), refined with occupancy factors of 0.5. Molecule 2 could not be satisfactorily modelled with unit occupancy, but was modelled with the three atoms having fixed thermal parameters (= 1000pm^2), and allowing the group occupancy factor to refine (0.466(18) at convergence). Molecule 3 has an ordered structure.

Weighting scheme g = 0.02248, R = 0.0671, R_w = 0.1100, S = 0.573 data : variable > 28 : 1. Maximum shift/e.s.d. in the final least squares refinement cycle was 0.156, and maximum and minimum residues in the final ΔF map were 2671 and -1700 enm^{-3}.

Table A2.10.1. The Fractional Coordinates of the Non-hydrogen Atoms in $(B_{10}H_{12}Au)(AuPCy_3)_3$. U_{eq} in $10^4 pm^2$.

	x	y	z	U_{iso}
Au(1)	0.90154(8)	0.22707(4)	0.83236(7)	0.0416(5)
Au(2)	0.73969(8)	0.19105(3)	0.79896(7)	0.0351(4)
Au(3)	0.77752(8)	0.29777(3)	0.80939(7)	0.0408(5)
Au(4)	0.82020(8)	0.24053(3)	0.69810(7)	0.0356(5)
P(1)	1.0349(4)	0.2153(4)	0.8881(4)	0.051(4)
P(2)	0.6585(4)	0.13548(21)	0.8549(4)	0.036(3)
P(3)	0.7349(6)	0.3651(3)	0.8704(6)	0.070(5)
B(1)	0.872(4)	0.2402(20)	0.514(3)	0.086(13)
B(2)	0.898(3)	0.1804(18)	0.538(3)	0.073(10)
B(3)	0.9687(25)	0.2249(14)	0.5296(22)	0.057(8)
B(4)	0.951(3)	0.2898(14)	0.5552(22)	0.057(8)
B(5)	0.807(3)	0.2121(15)	0.5751(22)	0.060(8)
B(6)	0.8774(24)	0.1660(13)	0.6323(21)	0.055(7)
B(7)	0.978(3)	0.1791(17)	0.601(3)	0.075(10)
B(8)	1.018(4)	0.2541(19)	0.617(4)	0.088(13)
B(9)	0.9306(16)	0.2949(9)	0.6492(15)	0.032(5)
B(10)	0.849(3)	0.2830(14)	0.5897(22)	0.058(8)
C(111)	1.039(3)	0.2170(16)	0.9880(23)	0.076(10)
C(112)	1.017(3)	0.2660(16)	1.016(3)	0.081(11)
C(113)	0.988(5)	0.2422(25)	1.116(4)	0.131(21)
C(114)	1.083(5)	0.2604(25)	1.135(5)	0.134(23)
C(115)	1.099(4)	0.2053(21)	1.106(3)	0.116(17)
C(116)	1.112(3)	0.2048(14)	1.0265(22)	0.071(9)
C(121)	1.106(3)	0.2657(15)	0.854(3)	0.077(10)
C(122)	1.062(3)	0.3197(15)	0.8500(23)	0.076(9)
C(123)	1.104(5)	0.351(3)	0.791(4)	0.134(21)
C(124)	1.200(3)	0.3553(17)	0.811(3)	0.089(12)
C(125)	1.238(4)	0.3027(18)	0.819(3)	0.102(15)
C(126)	1.194(3)	0.2723(15)	0.8735(25)	0.077(10)
C(131)	1.0802(22)	0.1547(12)	0.8654(18)	0.061(7)
C(132)	1.084(3)	0.1501(16)	0.7827(25)	0.085(11)
C(133)	1.123(5)	0.0900(23)	0.763(4)	0.137(21)
C(134)	1.077(5)	0.061(3)	0.794(4)	0.131(20)
C(135)	1.063(5)	0.060(3)	0.865(4)	0.150(25)
C(136)	1.017(3)	0.1176(19)	0.896(3)	0.099(13)
C(211)	0.666(3)	0.1418(15)	0.9515(20)	0.071(9)
C(212)	0.653(3)	0.0950(15)	0.9991(21)	0.078(10)
C(213)	0.659(3)	0.1070(18)	1.0851(24)	0.087(11)
C(214)	0.742(4)	0.1380(24)	1.104(3)	0.121(18)
C(215)	0.759(5)	0.173(3)	1.057(3)	0.124(18)
C(216)	0.754(3)	0.1623(16)	0.9854(23)	0.081(10)
C(221)	0.5439(15)	0.1425(9)	0.8226(14)	0.037(5)
C(222)	0.481(3)	0.1046(15)	0.8577(23)	0.078(10)
C(223)	0.395(3)	0.1093(15)	0.8328(24)	0.078(10)
C(224)	0.3642(19)	0.1659(10)	0.8324(16)	0.050(6)
C(225)	0.424(3)	0.2025(15)	0.8037(23)	0.076(10)
C(226)	0.5143(17)	0.1983(9)	0.8388(16)	0.044(6)
C(231)	0.6896(18)	0.0711(10)	0.8307(16)	0.049(6)
C(232)	0.660(3)	0.0603(15)	0.7488(23)	0.078(10)

C(233)	0.694(4)	0.006(3)	0.729(4)	0.136(21)
C(234)	0.790(3)	-0.0001(19)	0.743(3)	0.097(13)
C(235)	0.805(3)	0.0078(14)	0.8203(22)	0.076(9)
C(236)	0.776(3)	0.0591(16)	0.844(3)	0.085(11)
C(311)	0.7721(23)	0.3539(13)	0.9761(19)	0.063(8)
C(312)	0.746(4)	0.3134(22)	1.002(3)	0.114(17)
C(313)	0.774(3)	0.3057(16)	1.0903(24)	0.087(12)
C(314)	0.753(7)	0.362(3)	1.143(5)	0.18(3)
C(315)	0.784(4)	0.3911(21)	1.111(3)	0.104(14)
C(316)	0.749(3)	0.4010(17)	1.0243(23)	0.085(11)
C(321)	0.7886(19)	0.4231(12)	0.8411(18)	0.055(7)
C(322)	0.775(3)	0.4348(17)	0.7519(24)	0.088(11)
C(323)	0.816(3)	0.4783(17)	0.731(3)	0.087(11)
C(324)	0.916(3)	0.4753(18)	0.7598(24)	0.089(12)
C(325)	0.931(3)	0.4656(15)	0.8360(23)	0.079(10)
C(326)	0.8883(19)	0.4197(12)	0.8579(18)	0.056(7)
C(331)	0.6349	0.3679	0.8824	0.145(23)
C(332)	0.5855	0.4226	0.8860	0.084(11)
C(333)	0.4848	0.4191	0.8772	0.24(5)
C(334)	0.4429	0.3975	0.8155	0.112(16)
C(335)	0.4791	0.3417	0.8119	0.33(8)
C(336)	0.5778	0.3405	0.8221	0.120(18)
C(1)	0.3542(12)	0.0805(9)	0.0462(23)	0.089(11)
Cl(11)	0.4233(9)	0.0317(5)	0.0344(8)	0.109(4)
Cl(12a)	0.2573(16)	0.0686(13)	0.0032(18)	0.120(9)
Cl(12b)	0.2486(16)	0.0649(16)	0.0490(25)	0.146(12)
C(2)	0.4669(20)	0.4771(20)	0.077(5)	0.1000
Cl(21)	0.5711(18)	0.4953(10)	0.0879(16)	0.1000
Cl(22)	0.3920(19)	0.5171(10)	0.0380(16)	0.1000
C(3)	0.171(4)	0.4025(20)	0.054(3)	0.115(17)
Cl(31)	0.062(4)	0.406(4)	0.050(4)	0.58(6)
Cl(32)	0.198(4)	0.4548(22)	0.006(3)	0.41(3)

Table A2.10.2. The Fractional Coordinates of the Hydrogen Atoms in $(B_{10}H_{12}Au)(AuPCy_3)_3$.

	x	y	z
H(111)	0.9934	0.1872	0.9968
H(112a)	1.0689	0.2928	1.0177
H(112b)	0.9621	0.2823	0.9848
H(113a)	0.9766	0.2020	1.1210
H(113b)	0.9374	0.2627	1.1415
H(114a)	1.0994	0.2673	1.1929
H(114b)	1.1060	0.2913	1.1026
H(115a)	1.0449	0.1816	1.1170
H(115b)	1.1558	0.1905	1.1352
H(116a)	1.1309	0.1672	1.0107
H(116b)	1.1610	0.2316	1.0145
H(121)	1.1121	0.2459	0.8022

H(122a)	1.0716	0.3385	0.9028
H(122b)	0.9948	0.3156	0.8358
H(123a)	1.0953	0.3321	0.7381
H(123b)	1.0751	0.3882	0.7870
H(124a)	1.2302	0.3745	0.7667
H(124b)	1.2090	0.3769	0.8611
H(125a)	1.3038	0.3065	0.8388
H(125b)	1.2344	0.2836	0.7663
H(126a)	1.2004	0.2903	0.9270
H(126b)	1.2241	0.2354	0.8767
H(131)	1.1447	0.1473	0.8871
H(132a)	1.0211	0.1553	0.7559
H(132b)	1.1269	0.1786	0.7634
H(133a)	1.1865	0.0851	0.7875
H(133b)	1.1229	0.0840	0.7039
H(134a)	1.0145	0.0691	0.7683
H(134b)	1.0968	0.0236	0.7788
H(135a)	1.0212	0.0288	0.8766
H(135b)	1.1246	0.0542	0.8939
H(136a)	1.0177	0.1195	0.9560
H(136b)	0.9526	0.1236	0.8734
H(211)	0.6141	0.1685	0.9549
H(212a)	0.5905	0.0798	0.9845
H(212b)	0.7013	0.0671	0.9874
H(213a)	0.6598	0.0720	1.1159
H(213b)	0.6040	0.1292	1.0990
H(214a)	0.7949	0.1118	1.1079
H(214b)	0.7356	0.1556	1.1577
H(215a)	0.8231	0.1866	1.0716
H(215b)	0.7141	0.2038	1.0645
H(216a)	0.7707	0.1958	0.9552
H(216b)	0.8004	0.1329	0.9776
H(221)	0.5411	0.1337	0.7643
H(222a)	0.4837	0.1108	0.9167
H(222b)	0.5016	0.0665	0.8464
H(223a)	0.3886	0.0950	0.7770
H(223b)	0.3557	0.0872	0.8677
H(224a)	0.3540	0.1763	0.8888
H(224b)	0.3043	0.1684	0.7997
H(225a)	0.4264	0.1959	0.7451
H(225b)	0.3995	0.2401	0.8129
H(226a)	0.5556	0.2254	0.8139
H(226b)	0.5145	0.2052	0.8975
H(231)	0.6581	0.0466	0.8684
H(232a)	0.5910	0.0606	0.7429
H(232b)	0.6852	0.0886	0.7128
H(233a)	0.6793	-0.0005	0.6708
H(233b)	0.6616	-0.0220	0.7607
H(234a)	0.8249	0.0271	0.7122
H(234b)	0.8098	-0.0380	0.7293
H(235a)	0.7709	-0.0207	0.8499
H(235b)	0.8726	0.0047	0.8345
H(236a)	0.8120	0.0868	0.8149
H(236b)	0.7906	0.0626	0.9026
H(311)	0.8409	0.3502	0.9783

H(312a)	0.6771	0.3114	0.9934
H(312b)	0.7747	0.2830	0.9722
H(313a)	0.7359	0.2749	1.1102
H(313b)	0.8409	0.2964	1.0982
H(314a)	0.7801	0.3600	1.1994
H(314b)	0.6846	0.3690	1.1444
H(315a)	0.7747	0.4262	1.1405
H(315b)	0.8514	0.3824	1.1121
H(316a)	0.7804	0.4342	1.0035
H(316b)	0.6809	0.4066	1.0209
H(321)	0.7592	0.4530	0.8713
H(322a)	0.7071	0.4382	0.7373
H(322b)	0.8008	0.4035	0.7221
H(323a)	0.8095	0.4825	0.6719
H(323b)	0.7868	0.5105	0.7569
H(324a)	0.9461	0.5108	0.7470
H(324b)	0.9448	0.4451	0.7293
H(325a)	0.9995	0.4609	0.8472
H(325b)	0.9093	0.4974	0.8671
H(326a)	0.9129	0.3876	0.8289
H(326b)	0.9006	0.4146	0.9167
H(331)	0.6401	0.3509	0.9367
H(332a)	0.6070	0.4463	0.8422
H(332b)	0.6029	0.4399	0.9388
H(333a)	0.4614	0.4575	0.8802
H(333b)	0.4651	0.3979	0.9242
H(334a)	0.3746	0.3970	0.8213
H(334b)	0.4566	0.4183	0.7663
H(335a)	0.4599	0.3255	0.7588
H(335b)	0.4527	0.3195	0.8551
H(336a)	0.5938	0.3009	0.8285
H(336b)	0.5998	0.3542	0.7704

Table A2.10.3. The Anisotropic Vibration Parameters($10^4 pm^2$) in $(B_{10}H_{12}Au)(AuPCy_3)_3$.

	U_{11}	U_{22}	U_{33}	U_{23}	U_{13}	U_{12}
Au(1)	0.0323(4)	0.0582(6)	0.0342(6)	0.0013(4)	0.0002(4)	0.0003(4)
Au(2)	0.0344(4)	0.0314(4)	0.0394(5)	0.0017(4)	0.0042(4)	-0.0030(3)
Au(3)	0.0449(5)	0.0299(4)	0.0479(6)	-0.0073(4)	0.0082(5)	-0.0036(4)
Au(4)	0.0396(5)	0.0373(5)	0.0298(5)	-0.0001(4)	0.0020(4)	-0.0018(4)
P(1)	0.028(3)	0.089(5)	0.034(4)	0.004(4)	-0.003(3)	0.000(3)
P(2)	0.048(3)	0.029(3)	0.031(3)	-0.0033(23)	0.002(3)	-0.0062(23)
P(3)	0.073(5)	0.046(4)	0.092(7)	-0.017(4)	0.033(5)	-0.002(4)

Table A2.10.4. The Bond Lengths(pm) and Angles(°) Between the Non-hydrogen Atoms in $(B_{10}H_{12}Au)(AuPCy_3)_3$.

Au(1) -Au(2)	273.96(17)	C(124)-C(125)	151(7)
Au(1) -Au(3)	270.69(17)	C(125)-C(126)	147(7)
Au(1) -Au(4)	270.35(13)	C(121)-C(126)	142(6)
Au(2) -Au(3)	288.22(16)	C(131)-C(132)	151(6)
Au(2) -Au(4)	262.77(12)	C(132)-C(133)	174(8)
Au(3) -Au(4)	263.75(12)	C(133)-C(134)	120(10)
Au(1) - P(1)	228.5(8)	C(134)-C(135)	131(10)
Au(2) - P(2)	222.4(6)	C(135)-C(136)	179(9)
Au(3) - P(3)	221.7(10)	C(131)-C(136)	152(6)
Au(4) - B(5)	235(4)	C(211)-C(212)	152(6)
Au(4) - B(6)	249(4)	C(212)-C(213)	159(6)
Au(4) - B(9)	245(3)	C(213)-C(214)	157(8)
Au(4) -B(10)	233(4)	C(214)-C(215)	130(9)
B(1) - B(2)	168(7)	C(215)-C(216)	134(8)
B(1) - B(3)	157(7)	C(211)-C(216)	157(6)
B(1) - B(4)	192(7)	C(221)-C(222)	157(5)
B(1) - B(5)	171(7)	C(222)-C(223)	139(6)
B(1) -B(10)	183(7)	C(223)-C(224)	157(5)
B(2) - B(3)	163(6)	C(224)-C(225)	146(5)
B(2) - B(5)	181(6)	C(225)-C(226)	152(5)
B(2) - B(6)	180(6)	C(221)-C(226)	158(4)
B(2) - B(7)	164(7)	C(231)-C(232)	155(5)
B(3) - B(4)	180(5)	C(232)-C(233)	158(8)
B(3) - B(7)	177(6)	C(233)-C(234)	152(9)
B(3) - B(8)	188(7)	C(234)-C(235)	142(6)
B(4) - B(8)	176(7)	C(235)-C(236)	150(6)
B(4) - B(9)	176(5)	C(231)-C(236)	139(5)
B(4) -B(10)	176(5)	C(311)-C(312)	125(7)
B(5) - B(6)	191(5)	C(312)-C(313)	165(7)
B(5) -B(10)	199(6)	C(313)-C(314)	182(10)
B(6) - B(7)	173(6)	C(314)-C(315)	109(11)
B(7) - B(8)	209(8)	C(315)-C(316)	166(7)
B(8) - B(9)	186(7)	C(311)-C(316)	157(6)
B(9) -B(10)	165(5)	C(321)-C(322)	165(6)
P(1) -C(111)	181(4)	C(322)-C(323)	138(6)
P(1) -C(121)	186(4)	C(323)-C(324)	163(6)
P(1) -C(131)	181(3)	C(324)-C(325)	141(6)
P(2) -C(211)	176(4)	C(325)-C(326)	145(5)
P(2) -C(221)	186.2(25)	C(321)-C(326)	157(4)
P(2) -C(231)	183(3)	C(331)-C(332)	164.1
P(3) -C(311)	199(4)	C(332)-C(333)	157.7
P(3) -C(321)	184(3)	C(333)-C(334)	138.6
P(3) -C(331)	159.4(10)	C(334)-C(335)	158.1
C(111)-C(112)	144(6)	C(335)-C(336)	154.5
C(112)-C(113)	200(9)	C(331)-C(336)	155.0
C(113)-C(114)	159(11)	C(1) -Cl(11)	170(3)
C(114)-C(115)	157(10)	C(1) -Cl(12a)	169(4)
C(115)-C(116)	147(7)	C(1) -Cl(12b)	171(5)
C(111)-C(116)	134(6)	C(2) -Cl(21)	170(7)
C(121)-C(122)	158(6)	C(2) -Cl(22)	170(7)
C(122)-C(123)	154(8)	C(3) -Cl(31)	170(10)

C(123)-C(124) 151(9)

C(3) -Cl(32) 170(8)

Au(2)	-Au(1)	-Au(3)	63.90(4)	Au(2)	- P(2)	-C(231)	109.7(9)
Au(2)	-Au(1)	-Au(4)	57.73(4)	C(211)	- P(2)	-C(221)	108.2(15)
Au(3)	-Au(1)	-Au(4)	58.35(4)	C(211)	- P(2)	-C(231)	108.9(16)
Au(1)	-Au(2)	-Au(3)	57.50(4)	C(221)	- P(2)	-C(231)	106.3(12)
Au(1)	-Au(2)	-Au(4)	60.45(4)	Au(3)	- P(3)	-C(311)	106.3(11)
Au(3)	-Au(2)	-Au(4)	56.97(3)	Au(3)	- P(3)	-C(321)	111.5(11)
Au(1)	-Au(3)	-Au(2)	58.60(4)	Au(3)	- P(3)	-C(331)	115.6(5)
Au(1)	-Au(3)	-Au(4)	60.76(4)	C(311)	- P(3)	-C(321)	106.8(15)
Au(2)	-Au(3)	-Au(4)	56.65(3)	C(311)	- P(3)	-C(331)	96.3(11)
Au(1)	-Au(4)	-Au(2)	61.83(4)	C(321)	- P(3)	-C(331)	118.0(11)
Au(1)	-Au(4)	-Au(3)	60.89(4)	P(1)	-C(111)	-C(112)	112(3)
Au(2)	-Au(4)	-Au(3)	66.38(4)	P(1)	-C(111)	-C(116)	120(3)
Au(2)	-Au(1)	- P(1)	149.20(21)	C(112)	-C(111)	-C(116)	105(4)
Au(3)	-Au(1)	- P(1)	142.10(21)	C(111)	-C(112)	-C(113)	96(4)
Au(4)	-Au(1)	- P(1)	141.77(20)	C(112)	-C(113)	-C(114)	81(4)
Au(1)	-Au(2)	- P(2)	132.35(17)	C(113)	-C(114)	-C(115)	79(5)
Au(3)	-Au(2)	- P(2)	137.34(17)	C(114)	-C(115)	-C(116)	112(5)
Au(4)	-Au(2)	- P(2)	162.76(17)	C(111)	-C(116)	-C(115)	111(4)
Au(1)	-Au(3)	- P(3)	135.2(3)	P(1)	-C(121)	-C(122)	113(3)
Au(2)	-Au(3)	- P(3)	138.6(3)	P(1)	-C(121)	-C(126)	127(3)
Au(4)	-Au(3)	- P(3)	159.7(3)	C(122)	-C(121)	-C(126)	108(4)
Au(1)	-Au(4)	- B(5)	145.3(10)	C(121)	-C(122)	-C(123)	108(4)
Au(2)	-Au(4)	- B(5)	118.9(10)	C(122)	-C(123)	-C(124)	109(5)
Au(3)	-Au(4)	- B(5)	153.7(10)	C(123)	-C(124)	-C(125)	110(5)
Au(1)	-Au(4)	- B(6)	99.4(8)	C(124)	-C(125)	-C(126)	112(4)
Au(2)	-Au(4)	- B(6)	98.1(8)	C(121)	-C(126)	-C(125)	112(4)
Au(3)	-Au(4)	- B(6)	158.7(8)	P(1)	-C(131)	-C(132)	110(3)
Au(1)	-Au(4)	- B(9)	95.6(6)	P(1)	-C(131)	-C(136)	102(3)
Au(2)	-Au(4)	- B(9)	156.8(6)	C(132)	-C(131)	-C(136)	112(3)
Au(3)	-Au(4)	- B(9)	99.0(6)	C(131)	-C(132)	-C(133)	108(4)
Au(1)	-Au(4)	-B(10)	135.9(10)	C(132)	-C(133)	-C(134)	105(6)
Au(2)	-Au(4)	-B(10)	161.9(10)	C(133)	-C(134)	-C(135)	129(7)
Au(3)	-Au(4)	-B(10)	116.1(10)	C(134)	-C(135)	-C(136)	113(6)
B(5)	-Au(4)	- B(6)	46.2(13)	C(135)	-C(136)	-C(131)	99(4)
B(5)	-Au(4)	-B(10)	50.4(14)	P(2)	-C(211)	-C(212)	119(3)
B(9)	-Au(4)	-B(10)	40.3(11)	P(2)	-C(211)	-C(216)	116(3)
B(2)	- B(1)	- B(3)	60(3)	C(212)	-C(211)	-C(216)	101(3)
B(2)	- B(1)	- B(5)	64(3)	C(211)	-C(212)	-C(213)	113(3)
B(3)	- B(1)	- B(4)	61(3)	C(212)	-C(213)	-C(214)	109(4)
B(4)	- B(1)	-B(10)	56.8(23)	C(213)	-C(214)	-C(215)	116(6)
B(5)	- B(1)	-B(10)	68(3)	C(214)	-C(215)	-C(216)	118(6)
B(1)	- B(2)	- B(3)	57(3)	C(211)	-C(216)	-C(215)	118(4)
B(1)	- B(2)	- B(5)	59(3)	P(2)	-C(221)	-C(222)	115.5(20)
B(3)	- B(2)	- B(7)	66(3)	P(2)	-C(221)	-C(226)	108.8(16)
B(5)	- B(2)	- B(6)	63.8(24)	C(222)	-C(221)	-C(226)	108.7(23)
B(6)	- B(2)	- B(7)	60(3)	C(221)	-C(222)	-C(223)	116(3)
B(1)	- B(3)	- B(2)	63(3)	C(222)	-C(223)	-C(224)	112(3)
B(1)	- B(3)	- B(4)	69(3)	C(223)	-C(224)	-C(225)	115(3)
B(2)	- B(3)	- B(7)	57(3)	C(224)	-C(225)	-C(226)	114(3)
B(4)	- B(3)	- B(8)	57.0(25)	C(221)	-C(226)	-C(225)	105.5(24)
B(7)	- B(3)	- B(8)	70(3)	P(2)	-C(231)	-C(232)	109.3(22)
B(1)	- B(4)	- B(3)	49.9(23)	P(2)	-C(231)	-C(236)	116(3)
B(1)	- B(4)	-B(10)	59.5(24)	C(232)	-C(231)	-C(236)	111(3)

B(3) - B(4)	- B(8)	64(3)	C(231)-C(232)	-C(233)	108(4)
B(8) - B(4)	- B(9)	63.8(25)	C(232)-C(233)	-C(234)	114(5)
B(9) - B(4)	-B(10)	56.1(19)	C(233)-C(234)	-C(235)	105(4)
Au(4) - B(5)	- B(6)	70.8(17)	C(234)-C(235)	-C(236)	112(4)
Au(4) - B(5)	-B(10)	64.2(16)	C(231)-C(236)	-C(235)	118(4)
B(1) - B(5)	- B(2)	57(3)	P(3)	-C(311) -C(312)	114(4)
B(1) - B(5)	-B(10)	58.5(25)	P(3)	-C(311) -C(316)	110.7(25)
B(2) - B(5)	- B(6)	57.8(22)	C(312)-C(311)	-C(316)	112(4)
Au(4) - B(6)	- B(5)	63.0(16)	C(311)-C(312)	-C(313)	113(5)
B(2) - B(6)	- B(5)	58.5(22)	C(312)-C(313)	-C(314)	111(4)
B(2) - B(6)	- B(7)	55.2(25)	C(313)-C(314)	-C(315)	101(7)
B(2) - B(7)	- B(3)	57(3)	C(314)-C(315)	-C(316)	119(7)
B(2) - B(7)	- B(6)	64(3)	C(315)-C(316)	-C(311)	110(3)
B(3) - B(7)	- B(8)	57.6(25)	P(3)	-C(321) -C(322)	114.8(24)
B(3) - B(8)	- B(4)	59.1(25)	P(3)	-C(321) -C(326)	111.1(21)
B(3) - B(8)	- B(7)	52.5(24)	C(322)-C(321)	-C(326)	106(3)
B(4) - B(8)	- B(9)	58.0(24)	C(321)-C(322)	-C(323)	113(4)
Au(4) - B(9)	-B(10)	65.8(16)	C(322)-C(323)	-C(324)	109(4)
B(4) - B(9)	- B(8)	58.2(24)	C(323)-C(324)	-C(325)	115(4)
B(4) - B(9)	-B(10)	61.9(21)	C(324)-C(325)	-C(326)	111(4)
Au(4) -B(10)	- B(5)	65.3(16)	C(321)-C(326)	-C(325)	112(3)
Au(4) -B(10)	- B(9)	73.9(17)	P(3)	-C(331) -C(332)	121.0
B(1) -B(10)	- B(4)	65(3)	P(3)	-C(331) -C(336)	114.4
B(1) -B(10)	- B(5)	53.1(24)	C(332)-C(331)	-C(336)	100.7
B(4) -B(10)	- B(9)	62.0(21)	C(331)-C(332)	-C(333)	114.5
B(5) -B(10)	- B(9)	120(3)	C(332)-C(333)	-C(334)	121.9
Au(1) - P(1)	-C(111)	114.7(14)	C(333)-C(334)	-C(335)	105.2
Au(1) - P(1)	-C(121)	107.7(14)	C(334)-C(335)	-C(336)	111.9
Au(1) - P(1)	-C(131)	112.3(11)	C(331)-C(336)	-C(335)	127.3
C(111)- P(1)	-C(121)	109.2(19)	Cl(11)- C(1)	-Cl(12a)	111.10(20)
C(111)- P(1)	-C(131)	104.9(18)	Cl(11)- C(1)	-Cl(12b)	116.40(22)
C(121)- P(1)	-C(131)	107.8(18)	Cl(21)- C(2)	-Cl(22)	120(4)
Au(2) - P(2)	-C(211)	112.6(13)	Cl(31)- C(3)	-Cl(32)	103(5)
Au(2) - P(2)	-C(221)	110.9(8)			

Appendix 3

Experimental Details from the E.H.M.O. Calculations.

Introduction.

This Appendix lists the fractional coordinates for all of the models used in the Extended Huckel Molecular Orbital calculations discussed in the rest of this Thesis. The coordinates are in orthogonalised angstrom space (i.e. for a unit cell of sides all 100pm in length, and all angles 90^{o}.

Model (8c): $H_3PAuB_{10}H_{13}$

	x	y	z
H(P1)	-0.8452	1.8140	6.6602
H(P2)	-1.4075	3.8498	5.7029
H(P3)	0.7981	3.1340	5.6935
P	-0.5565	2.7174	5.6034
Au	-0.9056	1.6682	3.5770
B(1)	0.0000	0.8896	0.0000
B(2)	-1.5025	0.0037	0.3721
B(3)	0.0000	-0.8896	0.0000
B(4)	1.5025	-0.0037	0.3721
B(5)	-0.9962	1.4185	1.3387
B(6)	-1.7948	0.0077	2.0778
B(7)	-0.9918	-1.4131	1.3427
B(8)	0.9962	-1.4185	1.3387
B(9)	1.7949	-0.0077	2.0778
B(10)	0.9918	1.4131	1.3427
H(1)	0.0038	1.6183	-0.9419
H(2)	-2.4100	0.0067	-0.3917
H(3)	-0.0038	-1.6183	-0.9419
H(4)	2.4100	-0.0067	-0.3917
H(5)	-1.5321	2.4801	1.3719
H(6)	-2.8098	0.0112	2.6740
H(7)	-1.5214	-2.4730	1.3792
H(8)	1.5321	-2.4801	1.3719
H(9)	2.8098	-0.0112	2.6740

H(10)	1.5214	2.4731	1.3792
H(6,7)	-1.0036	-0.9632	2.5914
H(8,9)	1.0209	-0.9812	2.5881
H(9,10)	1.0036	0.9632	2.5914

Model (14): $[H_3PAuB_{10}H_{12}]^-$

	x	y	z
H(P1)	-0.8452	1.8140	6.6602
H(P2)	-1.4075	3.8498	5.7029
H(P3)	0.7981	3.1340	5.6935
P	-0.5565	2.7174	5.6034
Au	-0.9056	1.6682	3.5770
B(1)	0.0000	0.8896	0.0000
B(2)	-1.5025	0.0037	0.3721
B(3)	0.0000	-0.8896	0.0000
B(4)	1.5025	-0.0037	0.3721
B(5)	-0.9962	1.4185	1.3387
B(6)	-1.7948	0.0077	2.0778
B(7)	-0.9918	-1.4131	1.3427
B(8)	0.9962	-1.4185	1.3387
B(9)	1.7949	-0.0077	2.0778
B(10)	0.9918	1.4131	1.3427
H(1)	0.0038	1.6183	-0.9419
H(2)	-2.4100	0.0067	-0.3917
H(3)	-0.0038	-1.6183	-0.9419
H(4)	2.4100	-0.0067	-0.3917
H(5)	-1.5321	2.4801	1.3719
H(6)	-2.8098	0.0112	2.6740
H(7)	-1.5214	-2.4730	1.3792
H(8)	1.5321	-2.4801	1.3719
H(9)	2.8098	-0.0112	2.6740
H(10)	1.5214	2.4731	1.3792
H(6,7)	-1.0036	-0.9632	2.5914
H(8,9)	1.0209	-0.9812	2.5881

Model (9b): $[B_{10}H_{13}]^-$

	x	y	z
B(1)	0.0000	0.8896	0.0000
B(2)	1.5025	-0.0039	0.3721
B(3)	0.0000	-0.8896	0.0000
B(4)	-1.5025	0.0037	0.3721
B(5)	0.9918	1.4131	1.3427
B(6)	1.7949	-0.0077	2.0778
B(7)	0.9962	-1.4185	1.3387
B(8)	-0.9918	-1.4131	1.3427
B(9)	-1.7948	0.0077	2.0778
B(10)	-0.9962	1.4185	1.3387
H(1)	0.0038	1.6183	-0.9419
H(2)	2.4100	-0.0067	-0.3917
H(3)	-0.0038	-1.6183	-0.9419
H(4)	-2.4100	0.0067	-0.3917
H(5)	1.5214	2.4731	1.3792
H(6)	2.8098	-0.0112	2.6740
H(7)	1.5321	-2.4801	1.3719
H(8)	-1.5214	-2.4730	1.3792
H(9)	-2.8098	0.0112	2.6740
H(10)	-1.5321	2.4801	1.3719
H(5,6)	1.0036	0.9632	2.5914
H(6,7)	1.0209	-0.9812	2.5881
H(8,9)	-1.0036	-0.9632	2.5914

Model (16): $[B_{10}H_{12}]^{2-}$

	x	y	z
B(1)	0.0000	0.8896	0.0000
B(2)	-1.5025	0.0037	0.3721
B(3)	0.0000	-0.8896	0.0000
B(4)	1.5025	-0.0037	0.3721
B(5)	-0.9962	1.4185	1.3387
B(6)	-1.7948	0.0077	2.0778
B(7)	-0.9918	-1.4131	1.3427
B(8)	0.9962	-1.4185	1.3387
B(9)	1.7949	-0.0077	2.0778
B(10)	0.9918	1.4131	1.3427
H(1)	0.0038	1.6183	-0.9419

H(2)	-2.4100	0.0067	-0.3917
H(3)	-0.0038	-1.6183	-0.9419
H(4)	2.4100	-0.0067	-0.3917
H(5)	-1.5321	2.4801	1.3719
H(6)	-2.8098	0.0112	2.6740
H(7)	-1.5214	-2.4730	1.3792
H(8)	1.5321	-2.4801	1.3719
H(9)	2.8098	-0.0112	2.6740
H(10)	1.5214	2.4731	1.3792
H(6,7)	-1.0036	-0.9632	2.5914
H(8,9)	1.0209	-0.9812	2.5881

Model (17a/17b): $[AuPH_3]^+$

	x	y	z
Au	0.0000	0.5000	1.7000
P	0.0000	0.5000	4.0000
H(P1)	0.0000	-0.8388	4.4733
H(P2)	-1.1594	1.1694	4.4733
H(P3)	1.1594	1.1694	4.4733

Model (15b): $[H_3PAuB_{10}H_{12}]^-$

	x	y	z
H(P1)	0.0000	-0.8388	4.4733
H(P2)	-1.1594	1.1694	4.4733
H(P3)	1.1594	1.1694	4.4733
P	0.0000	0.5000	4.0000
Au	0.0000	0.5000	1.7000
B(1)	0.0000	-0.9505	-1.4322
B(2)	-1.5025	0.0104	-1.5129
B(3)	0.0000	0.6277	-2.2538
B(4)	1.5025	0.0104	-1.5129
B(5)	-0.9940	-0.7981	0.0000
B(6)	-1.7949	0.7981	0.0000
B(7)	-0.9940	1.7135	-1.3076
B(8)	0.9940	1.7135	-1.3076
B(9)	1.7949	0.7981	0.0000
B(10)	0.9940	-0.7981	0.0000

H(1)	0.0000	-2.0318	-1.9311
H(2)	-2.4100	-0.3423	-2.1904
H(3)	0.0000	0.8390	-3.4258
H(4)	2.4100	-0.3423	-2.1904
H(5)	-1.5267	-1.7229	0.5208
H(6)	-2.8098	1.0734	0.5288
H(7)	-1.5267	2.6705	-1.7666
H(8)	1.5267	2.6705	-1.7666
H(9)	2.8098	1.0734	0.5288
H(10)	1.5267	-1.7229	0.5208
H(6,7)	-1.0126	1.8968	0.0051
H(8,9)	1.0126	1.8968	0.0051

Model (15c): $[H_3PAuB_{10}H_{12}]^-$

	x	y	z
H(P1)	0.0000	0.5124	4.7795
H(P2)	-1.1594	2.3174	3.8992
H(P3)	1.1594	2.3174	3.8982
P	0.0000	1.5082	3.7672
Au	0.0000	0.5000	1.7000
B(1)	0.0000	-0.9505	-1.4322
B(2)	-1.5025	0.0104	-1.5129
B(3)	0.0000	0.6277	-2.2538
B(4)	1.5025	0.0104	-1.5129
B(5)	-0.9940	-0.7981	0.0000
B(6)	-1.7949	0.7981	0.0000
B(7)	-0.9940	1.7135	-1.3076
B(8)	0.9940	1.7135	-1.3076
B(9)	1.7949	0.7981	0.0000
B(10)	0.9940	-0.7981	0.0000
H(1)	0.0000	-2.0318	-1.9311
H(2)	-2.4100	-0.3423	-2.1904
H(3)	0.0000	0.8390	-3.4258
H(4)	2.4100	-0.3423	-2.1904
H(5)	-1.5267	-1.7229	0.5208
H(6)	-2.8098	1.0734	0.5288
H(7)	-1.5267	2.6705	-1.7666
H(8)	1.5267	2.6705	-1.7666
H(9)	2.8098	1.0734	0.5288
H(10)	1.5267	-1.7229	0.5208
H(6,7)	-1.0126	1.8968	0.0051
H(8,9)	1.0126	1.8968	0.0051

Model (18d): $(H_3PAu)_2B_8H_{10}$

	x	y	z
Au(6)	0.0006	-0.6088	-1.8553
P(6)	0.3611	-1.4087	-3.9886
H(61)	-0.3272	-2.6395	-4.1552
H(62)	1.7520	-1.6133	-4.1886
H(63)	-0.1195	-0.4656	-4.9352
Au(9)	-0.0079	-3.2297	1.4613
P(9)	-0.3760	-5.4890	1.1770
H(91)	0.3041	-5.9367	0.0137
H(92)	-1.7683	-5.7272	1.0325
H(93)	0.1097	-6.1939	2.3100
B(1)	0.9269	0.2302	1.5050
B(2)	0.0117	0.6163	0.0000
B(3)	-0.9031	0.2218	1.4863
B(4)	-0.0103	-1.1471	2.2257
B(5)	1.5548	-0.3116	0.0000
B(7)	-1.5664	-0.3047	0.0000
B(8)	-1.5708	-1.3436	1.3128
B(10)	1.5576	-1.3642	1.3385
H(1)	1.4427	0.9866	2.1190
H(2)	0.0354	1.5865	-0.5464
H(3)	-1.3700	1.0390	2.1266
H(4)	0.0525	-1.4478	3.3105
H(5)	2.4007	-0.0213	-0.6157
H(7)	-2.3663	0.0043	-0.6806
H(8)	-2.3931	-1.9524	1.7913
H(10)	2.3951	-1.8285	1.7716
H(7,8)	-1.3978	-1.6283	0.0367
H(5,10)	1.5067	-1.6139	0.1094

Model (18c): $[H_3PAuB_8H_{10}]^-$

	x	y	z
Au(9)	-0.0079	-3.2297	1.4613
P(9)	-0.3760	-5.4890	1.1770
H(91)	0.3041	-5.9367	0.0137
H(92)	-1.7683	-5.7272	1.0325

H(93)	0.1097	-6.1939	2.3100
B(1)	0.9269	0.2302	1.5050
B(2)	0.0117	0.6163	0.0000
B(3)	-0.9031	0.2218	1.4863
B(4)	-0.0103	-1.1471	2.2257
B(5)	1.5548	-0.3116	0.0000
B(7)	-1.5664	-0.3047	0.0000
B(8)	-1.5708	-1.3436	1.3128
B(10)	1.5576	-1.3642	1.3385
H(1)	1.4427	0.9866	2.1190
H(2)	0.0354	1.5865	-0.5464
H(3)	-1.3700	1.0390	2.1266
H(4)	0.0525	-1.4478	3.3105
H(5)	2.4007	-0.0213	-0.6157
H(7)	-2.3663	0.0043	-0.6806
H(8)	-2.3931	-1.9524	1.7913
H(10)	2.3951	-1.8285	1.7716
H(7,8)	-1.3978	-1.6283	0.0367
H(5,10)	1.5067	-1.6139	0.1094

Model (20b): $(H_3P)_2PtB_{10}H_{12}$

	x	y	z
H(P11)	-1.7506	-1.4958	3.9084
H(P12)	-2.9023	-0.0065	2.5546
H(P13)	-1.3386	0.7800	4.0755
H(P21)	0.8695	-2.3663	3.8793
H(P22)	2.2562	-0.5150	3.7165
H(P23)	2.4605	-2.2538	2.1961
P(1)	-1.6587	-0.2779	3.1840
P(2)	1.5472	-1.5008	2.9804
Pt(7)	-0.0079	-0.4591	1.5803
B(1)	-0.0263	1.0517	-1.4837
B(2)	0.8976	0.7983	-0.0011
B(3)	-0.9207	0.8145	0.0010
B(4)	-1.4461	0.0587	-1.4998
B(5)	0.0110	-0.4810	-2.3417
B(6)	1.4562	0.0763	-1.5094
B(8)	-1.6081	-0.8225	-0.0006
B(9)	-0.9692	-1.6534	-1.4757
B(10)	1.0064	-1.6360	-1.5106
B(11)	1.6313	-0.7903	0.0006

H(1)	-0.0692	1.9859	-1.9710
H(2)	1.4339	1.6887	0.5526
H(3)	-1.5844	1.6243	0.3551
H(4)	-2.3868	0.2775	-2.0609
H(5)	-0.0356	-0.6976	-3.3524
H(6)	2.3500	0.4476	-2.1281
H(8)	-2.4390	-1.1359	0.3422
H(9)	-1.4448	-2.5160	-1.9635
H(10)	1.5412	-2.4550	-2.0476
H(11)	2.5184	-0.9893	0.3290
H(8,9)	-0.9862	-1.8737	-0.2848
H(10,11)	1.0003	-1.8100	-0.2304

Model (20c): $[(B_{10}H_{12})_2Au]^-$

	x	y	z
Au(7)	0.0000	0.0000	0.0000
B(1)	1.4553	-2.2778	2.1376
B(2)	0.1777	-1.0620	2.0045
B(3)	0.6919	-2.0810	0.5154
B(4)	2.4361	-2.3545	0.6303
B(5)	3.0023	-1.4316	2.0275
B(6)	1.6799	-0.6887	2.9488
B(8)	1.8514	-1.2409	-0.5519
B(9)	3.2789	-0.7778	0.4293
B(10)	2.8072	0.2934	1.8874
B(11)	0.9954	0.6554	1.9896
H(1)	1.1375	-3.2599	2.7494
H(2)	-0.9501	-1.0385	2.4140
H(3)	-0.0931	-2.7555	-0.0919
H(4)	2.8872	-3.3024	0.0489
H(5)	4.0270	-1.7265	2.5780
H(6)	1.5621	-0.3842	4.1035
H(8)	1.8598	-1.3293	-1.7486
H(9)	4.2573	-0.5614	-0.2309
H(10)	3.4672	1.2395	2.2179
H(11)	0.4978	1.6906	2.3369
H(8,9)	1.9797	0.7703	1.1088
H(10,11)	2.1588	-0.4123	-0.3430
B(1)	-1.4553	2.2778	-2.1376
B(2)	-0.1777	1.0620	-2.0045
B(3)	-0.6919	2.0810	-0.5154
B(4)	-2.4361	2.3545	-0.6303

B(5)	-3.0023	1.4316	-2.0275
B(6)	-1.6799	0.6887	-2.9488
B(8)	-1.8514	1.2409	0.5519
B(9)	-3.2789	0.7778	-0.4293
B(10)	-2.8072	-0.2934	-1.8874
B(11)	-0.9954	-0.6554	-1.9896
H(1)	-1.1375	3.2599	-2.7494
H(2)	0.9501	1.0385	-2.4140
H(3)	0.0931	2.7555	0.0919
H(4)	-2.8872	3.3024	-0.0489
H(5)	-4.0270	1.7265	-2.5780
H(6)	-1.5621	0.3842	-4.1035
H(8)	-1.8598	1.3293	1.7486
H(9)	-4.2573	0.5614	0.2309
H(10)	-3.4672	-1.2395	-2.2179
H(11)	-0.4978	-1.6906	-2.3369
H(8,9)	-1.9797	-0.7703	-1.1088
H(10,11)	-2.1588	0.4123	0.3430

Appendix 4:

Published Work

This appendix covers the publication of the results from this thesis. The first section is a list of all the conferences at which parts of this work was presented. The second section consists of reprints of all published work and copies of all papers submitted for publication.

Conferences at which Work Was Presented.

British Crystallographic Association's Spring Meeting at Heriot-Watt University, Edinburgh on the 8th April 1987

University of Strathclyde Inorganic Chemistry Department's 22nd U. S. I. C. Conference at Ross Priory, Loch Lomond on the 22nd June 1987.

Intraboron VII : the seventh national meeting of inorganic boron chemists at Ross Priory, Loch Lomond on the 16th - 18th September 1987.

Intraboron VIII : the eighth national meeting of inorganic boron chemists at the University of Cambridge, 13th - 15th September 1988.

The 11th European Crystallographic Conference, Vienna, Austria, on the 30th August 1988.

Published Work

The following papers are in the rest of this appendix :

A.J.Wynd, S.E.Robins, D.A.Welch, and A.J.Welch, *J. Chem. Soc., Chem. Commun.,* 1985, 819.

A.J.Wynd, and A.J.Welch, *J. Chem. Soc., Chem. Commun.,* 1987, 1174.

A.J.Wynd, A.J.McLennan, D.Reed, and A.J.Welch, *J. Chem. Soc., Dalton Trans.,* 1987, 2761.

A.J.Wynd, and A.J.Welch, *Zeitschrift fur Kristallographie,* 1988, **185**, 380.

A.J.Wynd, and A.J.Welch, *Acta Crystallogr. Sect. C,* submitted.

Proofs to:- Dr. A. J. Welch,
Department of Chemistry,
University of Edinburgh,
West Mains Road,
Edinburgh EH9 3JJ,
Scotland.

Submitted to *Acta Crystallographica, Section C.*

The Structure of $[PhCH_2NMe_3]^+ [B_{10}H_{13}]^-$.

by Andrew J. Wynd, and Alan J. Welch*,

Department of Chemistry, University of Edinburgh, Edinburgh EH9 3JJ, Scotland.

Abstract. $[PhCH_2NMe_3]^+ [B_{10}H_{13}]^-$, M = 271.5, monoclinic, a = 8.8759(13), b = 18.739(3), c = 10.8215(13) Å, β = 96.223(11)°, V = 1789.3 Å^3, Z = 4, D_x = 1.008 Mgm^{-3}, space group = $P2_1/c$, Mo K_α, λ = 0.71069Å, μ = 0.046 mm^{-1}, *F(000)* = 584, room temperature, R = 0.0524, based on 1581 unique observed reflections. The structural effects of deprotonation are shortenings of the B(9)-B(10) and B(5)-B(10) connectivities, and these changes are rationalised by the results of a molecular orbital calculation.

* to whom correspondence should be addressed.

Introduction. We are currently investigating (Wynd, McLennan, Reed, & Welch, 1987; Wynd, Parish, & Welch, 1988) how the introduction of $\{AuPR_3\}$ (R=alkyl) fragments into $\{B_{10}\}$ cages affects the electronic and consequent geometric structure of the cage. The analysis of the metallaborane cage architecture relies mainly on comparison with the structures of analogous boranes. Whilst the literature contains a communication (Sneddon, Huffman, Schaeffer, & Streib, 1972) reporting the structure of the $[B_{10}H_{13}]^-$ anion, (1), as its $[NHEt_3]^+$ salt, no fractional coordinates were published or deposited, nor are any available from the authors. The structure of the isoelectronic, isovertex species, $B_{10}H_{14}$, is known to a high degree of accuracy (Brill, Dietrich, & Dierks, 1971).

However since the effects of deprotonation can substantially modify the internuclear distances in such species (Mitchell & Welch, 1987), we have determined the structure of $[PhCH_2NMe_3]^+$ (1). This will enable useful comparisons to be drawn against the structures of other boranes and metallaborane derivatives (this paper; Wynd, Parish, & Welch, 1988). $[PhCH_2NMe_3]^+$ (1) was synthesised using a method based on literature preparations (Hawthorne, Pitochelli, Strahm, & Miller, 1960).

Experimental. Yellow blocks were grown by the diffusion of hexane into a CH_2Cl_2 solution; CAD-4 diffractometer, 25 centred reflections ($13 < \theta < 13.5^{\circ}$), graphite-monochromated Mo-K_α; for data collection : $\theta_{max} = 22^{\circ}$, ω-2θ scans in 96 steps, ω-scan width $0.8 + 0.34\tan\theta$, The data (h 0 to 9; k 0 to 19; l -11 to 11) were measured over a period of 46 hours with no detectable crystal movement or decay. 2359 reflections were measured (scan speeds 1.268 - 3.296 $^{\circ}min^{-1}$), yielding 2194 unique ($R_{merge} = 0.0103$) of which 1581 with $F > 2\sigma(F)$ were retained. Space group $P2_1/c$ from systematic absences ($h0l$: $l = 2n$; $0k0$: $k = 2n$).

Atoms located by automatic direct-methods (SHELX86, Sheldrick, 1986) followed by difference-Fourier syntheses with full-matrix, least-squares refinement on F (SHELX76,

Sheldrick, 1976), $w = [\sigma^2 (F) + 0.002200 (F)^2]^{-1}$, anisotropic thermal parameters for all non-H atoms. Phenyl ring constrained to be a regular planar hexagon (C-C = 1.395Å). All organic H atoms set in calculated positions (C-H = 1.08Å) and refined with a group thermal parameter (0.103(3) $Å^2$ at convergence). Cage H atoms freely refined with a group thermal parameter (0.00719(24)$Å^2$ at convergence). R = 0.0524, R_w = 0.0730, S = 1.079, data : variable = 7 : 1, $(\Delta\rho)_{max}$ = 0.132, $(\Delta\rho)_{min}$ = -0.161 $eÅ^{-3}$ respectively. Δ/σ in final cycle was 0.063.

Scattering factors for C, H, B, and N inlaid in SHELX76. Other computer programs used were CADABS (Gould & Smith, 1986), CALC (Gould & Taylor, 1988), and EASYORTEP (Mallinson, 1984, see also Johnson, 1976)

Discussion. Table 1 lists the fractional coordinates of the refined atoms, and figure 1 is a perspective view of one ion-pair, showing the atomic numbering scheme. There are no significant intermolecular contacts, and the bond lengths and angles in the cation are unexceptional.

Table 2 lists the boron-boron internuclear distances and interatomic angles. The B-H and B-(μ-H) distances lie in the range expected. Deprotonation of $B_{10}H_{14}$ removes one μ-H atom (nominally H(9,10)) and there is no structural rearrangement accompanying this loss. Moreover, in the present crystallographic analysis, there is no evidence for disorder of the deprotonated connectivity. As previously reported (Sneddon, Huffman, Schaeffer, & Streib, 1972) there are, however, several significant bond length variations as a consequence of deprotonation.

The B(9)-B(10) connectivity is shortened from 1.788(4) Å (average) in $B_{10}H_{14}$ (Brill, Dietrich, & Dierks, 1971) to 1.657(5) Å in (1); the B(5)-B(10) connectivity is similarly shortened, but the change is less dramatic, 1.987(3) to 1.848(5) Å. Using Edinburgh

software (Gould & Taylor, 1988) we can compare two crystallographically-determined fragments, and calculate their *r.m.s. misfit.* For $[B_{10}H_{14}]$ / (1) this is 0.077Å, with the largest differences involving the atomic positions of B(5) (0.147Å) and B(9) (0.158Å). This is presumably due to the two bond length changes discussed above.

The reason for the shorter B(5)-B(6) and B(5)-B(10) distances in (1) compared to $B_{10}H_{14}$ may be readily understood *via* an extended Huckel molecular orbital calculation (Howell *et al* 1977) on a model of $[B_{10}H_{13}]^-$ derived from the structure of $B_{10}H_{14}$ by μ-H(9,10) deprotonation. The highest occupied molecular orbital of this model is localised on, and bonding between, B(5) and B(6). A minor contribution on B(10) is in phase with that on B(5). Protonation causes partial deoccupation of this orbital (Mitchell and Welch, 1987) thereby lengthening both B(5)-B(6) and B(5)-B(10), but the former more dramatically.

We thank the S.E.R.C. for support.

References

Brill,R., Dietrich,H., & Dierks,H., (1971), *Acta Crystallog. Sect. B,* **27**, 2003-2018.

Gould,R.O., and Taylor,P., (1988), *CALC.* A program for molecular geometry calculations, Univ. of Edinburgh, Scotland.

Gould,R.O., and Smith,D.E., (1985), *CADABS.* A program for data reduction and analysis, Univ. of Edinburgh, Scotland.

Howell,J., Rossi,A., Wallace,D., Haraki,K., and Hoffmann,R., (1977). *ICON,* Quantum Chemistry Program Exchange, Univ. of Indiana no. 344.

Hawthorne,M.F., Pitochelli,A.R., Strahm,R.D., & Miller,J.J., (1960), *J. Am. Chem. Soc.,* **82**, 1825-1829.

Johnson,C.K., (1976), *Report ORNL-5138,* Oak Ridge National Laboratory, Tennessee, U.S.A.

Mallinson,P.R., (1982), *EASYORTEP.* University of Glasgow, U.K.

Mitchell,G.F., & Welch,A.J., (1987), *J. Chem. Soc., Dalton Trans.*, 1017-1025.

Sheldrick,G.M., (1976), *SHELX76.* A program for structure determination. Univ. of Cambridge, U.K.

Sheldrick,G.M., (1986), *SHELX86.* A program for structure solution, Univ. of Gottingen, Federal Republic of Germany.

Sneddon,L.G., Huffman,J.C., Schaeffer,R.O., & Streib,W.E., (1972), *Chem. Commun.*, 474-475.

Wynd,A.J., McLennan,A.J., Reed,D., & Welch,A.J., (1987), *J. Chem. Soc., Dalton Trans.*, 2761-2768.

Wynd,A.J., Parish,R.V., & Welch,A.J., (1988), *paper in preparation.*

Legend to Figure.

Figure 1. A Perspective View of one Ion-Pair. All atoms are drawn at the 50% probability level, except for H atoms, which have been given artificial radii of 0.1Å, for clarity.

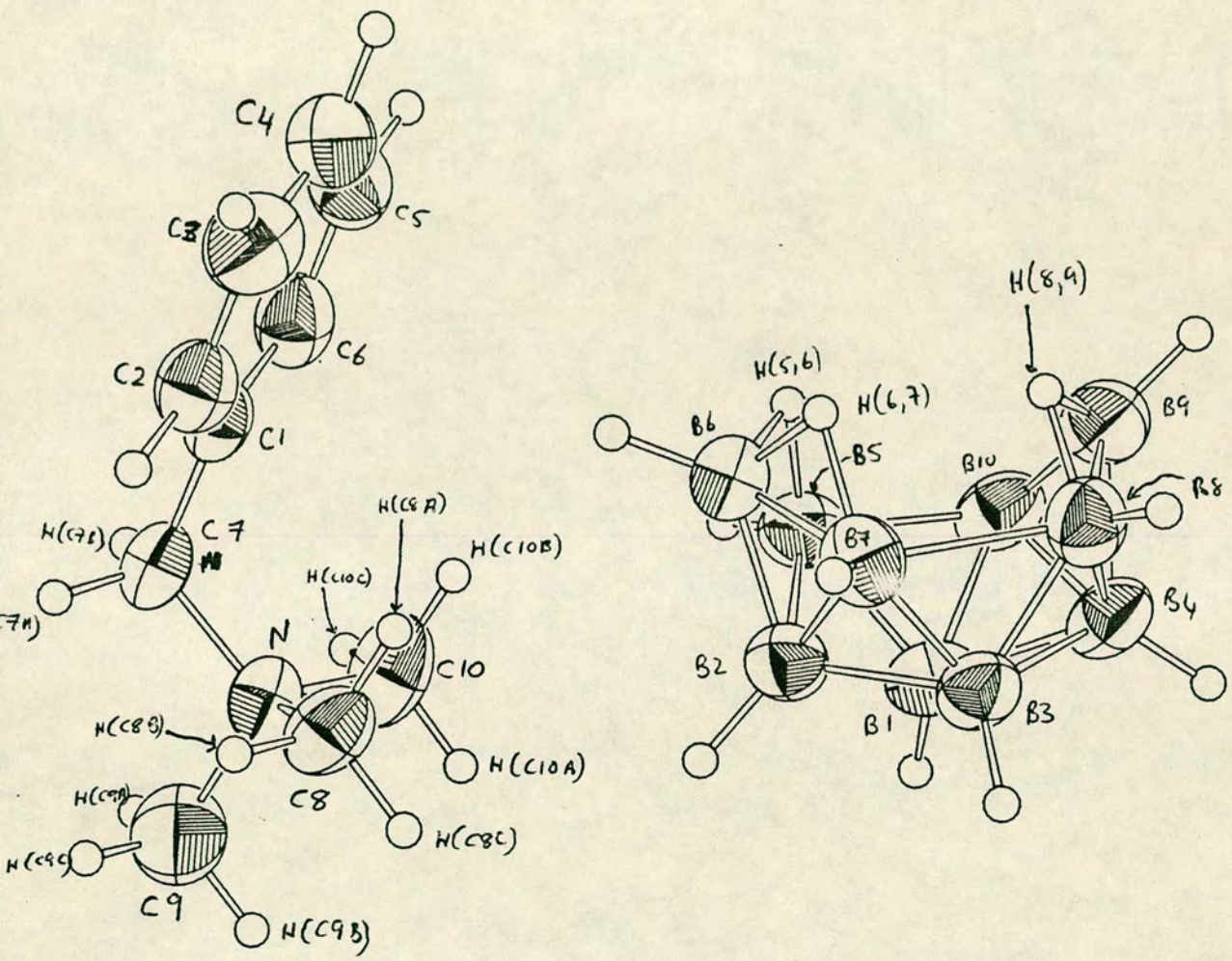
C4
C5
C3
C6
C2
C1
C7
H(C7B)
H(C8A)
H(C10B)
H(C10C)
N
C10
H(C8B)
H(C10A)
C8
H(C8C)
C9
H(C9B)
H(8,9)
H(5,6)
H(6,7)
B6
B5
B9
B10
B8
B7
B4
B2
B1
B3

Table 1. Fractional Coordinates of Refined Atoms in $[PhCH_2NMe_3]^+ [B_{10}H_{13}]^-$.

	x	y	z	U_{iso}
N	0.19902(25)	0.59661(12)	0.26319(20)	0.0534(15)
C(1)	0.15660	0.55862	0.03550	0.0474(16)
C(2)	0.24947(22)	0.50316(9)	0.00303(18)	0.0579(19)
C(3)	0.30173	0.50239	-0.11397	0.0754(23)
C(4)	0.26113	0.55709	-0.19851	0.080(3)
C(5)	0.16826	0.61256	-0.16605	0.0760(24)
C(6)	0.11600	0.61332	-0.04904	0.0632(20)
C(7)	0.0989(3)	0.55784(15)	0.1608(3)	0.0552(18)
C(8)	0.3577(3)	0.57068(17)	0.2716(3)	0.0623(20)
C(9)	0.1382(4)	0.58131(21)	0.3841(3)	0.089(3)
C(10)	0.1980(4)	0.67514(16)	0.2394(4)	0.0796(24)
B(1)	0.6211(4)	0.83986(19)	0.2036(3)	0.0584(22)
B(2)	0.6020(4)	0.74532(18)	0.1913(3)	0.0551(21)
B(3)	0.7832(4)	0.78474(18)	0.1965(3)	0.0535(20)
B(4)	0.7783(4)	0.87201(18)	0.1372(3)	0.0578(22)
B(5)	0.4820(4)	0.80292(20)	0.0907(3)	0.0608(23)
B(6)	0.5408(4)	0.71686(21)	0.0446(3)	0.0620(23)
B(7)	0.7370(4)	0.71450(19)	0.0951(3)	0.0582(22)
B(8)	0.8491(4)	0.80227(19)	0.0521(3)	0.0582(22)
B(9)	0.7315(5)	0.87047(21)	-0.0227(4)	0.0681(25)
B(10)	0.5905(4)	0.88447(19)	0.0630(3)	0.0588(22)
H(1)	0.581(3)	0.8610(15)	0.288(3)	0.0719(24)
H(2)	0.564(3)	0.7171(15)	0.276(3)	
H(3)	0.865(3)	0.7689(15)	0.279(3)	
H(4)	0.846(3)	0.9143(16)	0.185(3)	
H(5)	0.359(4)	0.8095(14)	0.0951(24)	
H(6)	0.465(3)	0.6713(15)	0.016(3)	
H(7)	0.799(3)	0.6646(16)	0.102(3)	
H(8)	0.960(4)	0.7909(15)	0.0334(25)	
H(9)	0.762(3)	0.9069(15)	-0.101(3)	
H(10)	0.522(3)	0.9359(16)	0.0585(24)	
H(5,6)	0.499(3)	0.7691(16)	-0.016(3)	
H(6,7)	0.655(3)	0.7123(15)	-0.017(3)	
H(8,9)	0.766(3)	0.8039(15)	-0.048(3)	

Table 2. Bond Lengths(Å) and Angles(°) in the $[B_{10}H_{13}]^-$ Anion.

B(1) - B(2)	1.783(5)	B(3) - B(8)	1.758(5)
B(1) - B(3)	1.780(5)	B(4) - B(8)	1.754(5)
B(1) - B(4)	1.745(5)	B(4) - B(9)	1.736(5)
B(1) - B(5)	1.780(5)	B(4) -B(10)	1.786(5)
B(1) -B(10)	1.731(5)	B(5) - B(6)	1.783(5)
B(2) - B(3)	1.765(5)	B(5) -B(10)	1.848(5)
B(2) - B(5)	1.798(5)	B(6) - B(7)	1.768(5)
B(2) - B(6)	1.707(5)	B(7) - B(8)	2.003(5)
B(2) - B(7)	1.767(5)	B(8) - B(9)	1.788(5)
B(3) - B(4)	1.756(5)	B(9) -B(10)	1.657(5)
B(3) - B(7)	1.734(5)		

B(2) - B(1)	- B(3)	59.39(19)	B(8) - B(4)	- B(9)	61.63(21)
B(2) - B(1)	- B(5)	60.61(20)	B(9) - B(4)	-B(10)	56.13(20)
B(3) - B(1)	- B(4)	59.74(19)	B(1) - B(5)	- B(2)	59.78(20)
B(4) - B(1)	-B(10)	61.81(20)	B(1) - B(5)	-B(10)	56.98(19)
B(5) - B(1)	-B(10)	63.48(21)	B(2) - B(5)	- B(6)	56.93(20)
B(1) - B(2)	- B(3)	60.20(19)	B(2) - B(6)	- B(5)	61.99(21)
B(1) - B(2)	- B(5)	59.61(20)	B(2) - B(6)	- B(7)	61.10(21)
B(3) - B(2)	- B(7)	58.80(19)	B(2) - B(7)	- B(3)	60.54(20)
B(5) - B(2)	- B(6)	61.08(21)	B(2) - B(7)	- B(6)	57.74(20)
B(6) - B(2)	- B(7)	61.16(21)	B(3) - B(7)	- B(8)	55.57(19)
B(1) - B(3)	- B(2)	60.41(19)	B(3) - B(8)	- B(4)	59.98(20)
B(1) - B(3)	- B(4)	59.16(19)	B(3) - B(8)	- B(7)	54.43(18)
B(2) - B(3)	- B(7)	60.66(20)	B(4) - B(8)	- B(9)	58.68(21)
B(4) - B(3)	- B(8)	59.89(20)	B(4) - B(9)	- B(8)	59.69(21)
B(7) - B(3)	- B(8)	70.01(21)	B(4) - B(9)	-B(10)	63.46(22)
B(1) - B(4)	- B(3)	61.10(20)	B(1) -B(10)	- B(4)	59.48(20)
B(1) - B(4)	-B(10)	58.71(20)	B(1) -B(10)	- B(5)	59.55(20)
B(3) - B(4)	- B(8)	60.13(20)	B(4) -B(10)	- B(9)	60.40(21)

Supplementary Material

for $[PhCH_2NMe_3]^+ [B_{10}H_{13}]^-$

Table S1. Fractional Coordinates of Hydrogen Atoms in the $[PhCH_2NMe_3]^+$ Cation.

	x	y	z
H(C2)	0.28094	0.46080	0.06844
H(C3)	0.37359	0.45951	-0.13918
H(C4)	0.30145	0.55659	-0.28908
H(C5)	0.13667	0.65496	-0.23135
H(C6)	0.04403	0.65625	-0.02372
H(C7A)	-0.0115	0.58274	0.1519
H(C7B)	0.0886	0.50290	0.1889
H(C8A)	0.4038	0.58122	0.1850
H(C8B)	0.3599	0.51396	0.2894
H(C8C)	0.4249	0.59791	0.3464
H(C9A)	0.0226	0.59992	0.3798
H(C9B)	0.2065	0.60847	0.4583
H(C9C)	0.1415	0.52453	0.4013
H(C10A)	0.0830	0.69473	0.2332
H(C10B)	0.2448	0.68571	0.1532
H(C10C)	0.2655	0.70175	0.3148

Table S2. Anisotropic Thermal Parameters (in $Å^2$).

	U_{11}	U_{22}	U_{33}	U_{23}	U_{13}	U_{12}
B(1)	0.0608(23)	0.0633(23)	0.0495(20)	-0.0067(17)	-0.0021(17)	0.0111(18)
B(2)	0.0542(21)	0.0600(22)	0.0501(20)	0.0057(17)	0.0014(16)	0.0007(17)
B(3)	0.0531(20)	0.0534(21)	0.0518(19)	0.0056(16)	-0.0084(16)	0.0009(17)
B(4)	0.0674(23)	0.0427(20)	0.0601(21)	-0.0011(16)	-0.0158(18)	-0.0024(17)
B(5)	0.0572(23)	0.072(3)	0.0517(20)	0.0023(18)	0.0019(17)	0.0046(19)
B(6)	0.0637(24)	0.0627(24)	0.0586(21)	-0.0013(18)	0.0037(18)	-0.0136(20)
B(7)	0.0626(23)	0.0455(20)	0.0659(23)	0.0039(16)	0.0097(18)	0.0042(17)
B(8)	0.0483(21)	0.0596(23)	0.0656(23)	0.0056(18)	0.0025(18)	-0.0022(17)
B(9)	0.084(3)	0.0568(24)	0.0616(23)	0.0116(18)	-0.0068(20)	-0.0080(20)
B(10)	0.0657(23)	0.0481(20)	0.0597(21)	-0.0028(16)	-0.0129(18)	0.0069(18)
N	0.0496(15)	0.0477(14)	0.0622(15)	-0.0073(11)	0.0056(11)	-0.0050(11)
C(1)	0.0371(15)	0.0467(16)	0.0568(17)	-0.0019(14)	-0.0051(13)	-0.0059(13)
C(2)	0.0516(18)	0.0513(17)	0.0696(20)	-0.0015(14)	0.0014(15)	0.0004(16)
C(3)	0.0599(21)	0.0861(24)	0.0796(24)	-0.0123(20)	0.0101(18)	0.0011(18)
C(4)	0.0706(24)	0.103(3)	0.0669(22)	-0.0002(21)	0.0093(18)	-0.0248(22)
C(5)	0.0774(24)	0.0768(24)	0.0714(23)	0.0175(18)	-0.0060(18)	-0.0168(20)
C(6)	0.0509(18)	0.0585(20)	0.0782(22)	0.0088(17)	-0.0059(16)	-0.0028(15)
C(7)	0.0442(17)	0.0535(18)	0.0666(18)	-0.0075(14)	-0.0011(14)	-0.0093(14)
C(8)	0.0470(18)	0.0699(21)	0.0673(19)	-0.0036(15)	-0.0117(14)	0.0022(15)
C(9)	0.103(3)	0.090(3)	0.0758(23)	-0.0268(19)	0.0339(21)	-0.0184(22)
C(10)	0.0734(23)	0.0463(19)	0.116(3)	-0.0134(18)	-0.0036(20)	0.0007(17)

Table S3. Bond Lengths(Å) and Angles(^{o}) for the Atoms in the $[PhCh_2NMe_3]^+$ Cation.

N -C(8)	1.483(4)	N - C(7)	1.527(4)
N -C(9)	1.496(4)	C(1) - C(7)	1.501(3)
N -C(10)	1.494(4)		

C(8)-	N	-C(9)	108.29(23)	C(10)- N	- C(7) 110.59(22)
C(8)-	N	-C(10)	108.74(22)	N	- C(7) - C(1) 114.96(21)
C(9)-	N	-C(10)	110.09(24)	C(2)	- C(1) - C(7) 119.29(18)
C(8)-	N	- C(7)	111.27(21)	C(6)	- C(1) - C(7) 120.70(18)
C(9)-	N	- C(7)	107.83(22)		

Table S4. Bond Lengths(Å) and Angles(°) Involving the Cage Hydrogen Atoms.

B(1) - H(1)	1.09(3)	B(9) - H(9)	1.14(3)
B(2) - H(2)	1.14(3)	B(10)-H(10)	1.14(3)
B(3) - H(3)	1.13(3)	B(5) -H(5,6)	1.34(3)
B(4) - H(4)	1.09(3)	B(6) -H(5,6)	1.21(3)
B(5) - H(5)	1.11(3)	B(6) -H(6,7)	1.28(3)
B(6) - H(6)	1.11(3)	B(7) -H(6,7)	1.35(3)
B(7) - H(7)	1.08(3)	B(8) -H(8,9)	1.24(3)
B(8) - H(8)	1.05(3)	B(9) -H(8,9)	1.32(3)

B(2) - B(1)	- H(1)	112.8(15)	B(4) - B(9)	- H(9)	132.6(15)
B(3) - B(1)	- H(1)	125.8(15)	B(8) - B(9)	- H(9)	126.0(15)
B(4) - B(1)	- H(1)	124.5(15)	B(10)- B(9)	- H(9)	125.1(15)
B(5) - B(1)	- H(1)	117.0(15)	B(1) -B(10)	-H(10)	118.7(15)
B(10)- B(1)	- H(1)	121.7(15)	B(4) -B(10)	-H(10)	126.6(15)
B(1) - B(2)	- H(2)	115.7(14)	B(5) -B(10)	-H(10)	115.2(15)
B(3) - B(2)	- H(2)	120.9(14)	B(9) -B(10)	-H(10)	122.7(15)
B(5) - B(2)	- H(2)	124.0(14)	B(1) - B(5)	-H(5,6)	129.8(13)
B(6) - B(2)	- H(2)	120.9(15)	B(2) - B(5)	-H(5,6)	97.0(13)
B(7) - B(2)	- H(2)	126.8(15)	B(6) - B(5)	-H(5,6)	42.8(13)
B(1) - B(3)	- H(3)	125.0(15)	B(10)- B(5)	-H(5,6)	98.2(13)
B(2) - B(3)	- H(3)	115.0(15)	H(5) - B(5)	-H(5,6)	107.2(19)
B(4) - B(3)	- H(3)	121.4(15)	B(2) - B(6)	-H(5,6)	107.2(14)
B(7) - B(3)	- H(3)	112.9(15)	B(5) - B(6)	-H(5,6)	48.6(14)
B(8) - B(3)	- H(3)	120.3(15)	B(7) - B(6)	-H(5,6)	114.8(14)
B(1) - B(4)	- H(4)	118.3(16)	H(6) - B(6)	-H(5,6)	109.2(20)
B(3) - B(4)	- H(4)	120.8(16)	B(2) - B(6)	-H(6,7)	108.5(13)
B(8) - B(4)	- H(4)	125.8(16)	B(5) - B(6)	-H(6,7)	118.7(13)
B(9) - B(4)	- H(4)	123.3(16)	B(7) - B(6)	-H(6,7)	49.3(13)
B(10)- B(4)	- H(4)	123.8(16)	H(6) - B(6)	-H(6,7)	107.0(20)
B(1) - B(5)	- H(5)	122.8(15)	H(5,6)-B(6)	-H(6,7)	89.2(19)
B(2) - B(5)	- H(5)	124.3(15)	B(2) - B(7)	-H(6,7)	101.9(12)
B(6) - B(5)	- H(5)	115.7(15)	B(3) - B(7)	-H(6,7)	131.4(12)
B(10)- B(5)	- H(5)	116.7(15)	B(6) - B(7)	-H(6,7)	45.9(12)
B(2) - B(6)	- H(6)	128.6(15)	H(7) - B(7)	-H(6,7)	105.0(20)
B(5) - B(6)	- H(6)	126.0(15)	B(3) - B(8)	-H(8,9)	123.8(13)
B(7) - B(6)	- H(6)	127.9(15)	B(4) - B(8)	-H(8,9)	103.1(13)
B(2) - B(7)	- H(7)	127.6(16)	B(9) - B(8)	-H(8,9)	47.6(13)
B(3) - B(7)	- H(7)	121.8(16)	H(8) - B(8)	-H(8,9)	108.5(21)
B(6) - B(7)	- H(7)	121.2(16)	B(4) - B(9)	-H(8,9)	100.6(13)
B(3) - B(8)	- H(8)	122.9(16)	B(8) - B(9)	-H(8,9)	43.8(12)
B(4) - B(8)	- H(8)	130.5(16)	B(10)- B(9)	-H(8,9)	118.2(13)
B(9) - B(8)	- H(8)	124.9(16)	H(9) - B(9)	-H(8,9)	109.5(19)

Synthesis and Characterisation of a Triple Cluster of Gold and Boron

Andrew J. Wynd, Suzanne E. Robins, Dorothy A. Welch, and Alan J. Welch*

Department of Chemistry, University of Edinburgh, Edinburgh, EH9 3JJ, U.K.

Reaction of $B_{10}H_{14}$ with Et_3PAuMe affords the triple cluster $[(H_{12}B_{10}Au)(AuPEt_3)_4(AuB_{10}H_{12})]$, and with Cy_3PAuMe (CY = cyclohexyl) the substituted complex $[Cy_3PAu(B_{10}H_{13})]$ is isolated; a mechanism for the formation of the triple cluster is proposed.

Reprinted from the Journal of The Chemical Society

Chemical Communications 1985

Synthesis and Characterisation of a Triple Cluster of Gold and Boron

Andrew J. Wynd, Suzanne E. Robins, Dorothy A. Welch, and Alan J. Welch*

Department of Chemistry, University of Edinburgh, Edinburgh, EH9 3JJ, U.K.

Reaction of $B_{10}H_{14}$ with Et_3PAuMe affords the triple cluster $[(H_{12}B_{10}Au)(AuPEt_3)_4(AuB_{10}H_{12})]$, and with Cy_3PAuMe (CY = cyclohexyl) the substituted complex $[Cy_3PAu(B_{10}H_{13})]$ is isolated; a mechanism for the formation of the triple cluster is proposed.

The replacement of μ-H atoms in transition-metal cluster complexes by isolobal $\{AuPR_3\}$ fragments frequently leads to derivatives which are more stable and more easily characterised,[1] and close analogies between clusters of boron and clusters of metals have been recognised for several years.[2] Since the readily available borane $B_{10}H_{14}$ has an open face containing four μ-H atoms we became interested in the possible replacement of one or more of these by $\{AuPR_3\}$ fragments, with the potential formation of products with gold–gold bonds.

The addition of R_3PAuMe (R = Et or Ph) to an equimolar amount of $B_{10}H_{14}$ in CH_2Cl_2 at room temperature affords a yellow solution which rapidly becomes dark red. For R = Et the final product has been characterised by microanalysis and multinuclear n.m.r. spectroscopy† as $[(H_{12}B_{10}Au)(\mu\text{-}AuPEt_3)_4(AuB_{10}H_{12})]$ (**1a**). An *X*-ray diffraction study of (**1a**) as its 2MeCN solvate‡ revealed the structure shown in Figure 1.

In (**1a**) two *nido*-icosahedral 7-$AuB_{10}H_{12}$ polyhedra are directly linked by an Au(7)–Au(7′) bond, 2.9188(16) Å. Although not located in the crystallographic study, two bridging hydrogen atoms per cage have been detected by $^1H\{^{11}B\}$ n.m.r., and these are assigned to B(8)–B(9) and B(10)–B(11) (and equivalent primed) connectivities. The two auraborane clusters are twisted with respect to each other by *ca.* 90° about the Au(7)–Au(7′) bond, which is bridged by four $\{Et_3PAu\}$ units in an asymmetric, but regular, manner; the open face of each cage lies below a phosphine ligand whose bound gold atom is somewhat closer to the polyhedral gold atom of the other cage. The arrangement of six gold atoms in (**1a**) is that of a radially compressed octahedron, and thus the species may be regarded overall as a 'triple cluster' with the inner Au_6 part fused to the outer AuB_{10} parts by common gold vertices. Such a system is without precedent.

In an attempt to understand the mechanism by which (**1a**) is formed, the reaction of $B_{10}H_{14}$ with the sterically demanding reagent Cy_3PAuMe (Cy = cyclohexyl) has been studied in the hope of isolating relatively stable reaction intermediates.

In CH_2Cl_2 at room temperature $B_{10}H_{14}$ and Cy_3PAuMe give initially a yellow solution from which a colourless product (**2c**), characterised spectroscopically† and crystallographically‡ as [*nido*-μ-5,6-$(AuPCy_3)$-$B_{10}H_{13}$], is deposited. As shown (Figure 2) the structure of (**2c**) is simply that of $B_{10}H_{14}$ with one μ-H replaced by μ-$AuPCy_3$. Addition of Et_3PAuMe to (**2c**) in CH_2Cl_2 results in the successive production of yellow then red colourations. Free PCy_3 has been detected (as $OPCy_3$, by ^{31}P n.m.r.) in the final mixture.

In light of these results we suggest the mechanism outlined in Scheme 1 for formation of the triple cluster (**1**). Initial

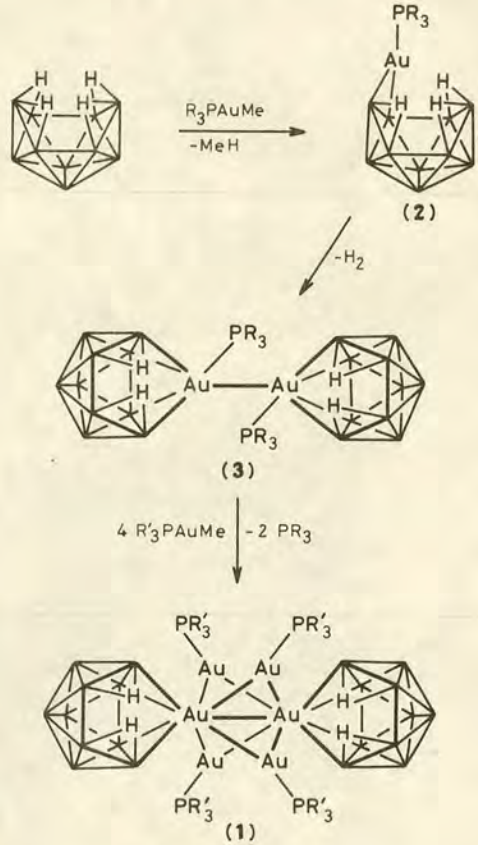

a; R = Et, R′ = Et
b; R = Ph, R′ = Ph
c; R = Cy

Scheme 1

† (**1a**) ($CDCl_3$, 298 K) $^{11}B\{^1H\}$: δ 11.93 (br., 4B), 0.70 (2B), −4.93 (2B), and −24.48 (2B) p.p.m. $^1H\{^{11}B\}$ includes: δ 4.12, 3.41, 2.60, 2.44, 2.39, 1.35 (all B–*H*), and −3.40 (B–*H*–B) p.p.m. (**2c**) ($CDCl_3$, 303 K) $^1B\{^1H\}$: δ 16.12 (1B), 9.32 (1B), 8.41 (1B), 2.82 (1B), 1.41 (1B), −0.57 (2B), −1.01 (1B), −29.53 (1B), and −35.63 (1B) p.p.m. $^1H\{^{11}B\}$ includes: δ 5.05, 3.72, 3.50, 3.29, 3.17, 2.94, 2.90, 2.62, 0.64, 0.60 (all B–*H*), and −0.13, −2.93, and −3.48 (all B–*H*–B) p.p.m.

‡ *Crystal Data:* (**1a**) $C_{24}H_{84}Au_6B_{20}P_4 \cdot 2C_2H_3N$, M = 2061.0, a = 16.817(10), b = 16.067(5), c = 21.798(12) Å, β = 92.02(4)°, U = 5886 Å^3, space group $P2_1/c$, D_c = 2.325 g cm^{-3}, Z = 4, $F(000)$ = 3742, μ(Mo-K_α) = 155.2 cm^{-1}. Using 4855 [$F \geq 5.0\sigma(F)$] out of 10325 symmetry-independent data measured (185 K) to $\theta_{max.}$ 25° on an Enraf-Nonius CAD4, and corrected for *X*-ray absorption, the structure has been refined to a current R index of 0.0620. (**2c**) $C_{18}H_{46}AuB_{10}P$, M = 598.6, a = 11.6583(20), b = 22.663(6), c = 11.418(3) Å, β = 118.061(16)°, U = 2662 Å^3, space group $P2_1/a$, D_c = 1.493, Z = 4, $F(000)$ = 1192, μ(Mo-K_α) = 57.7 cm^{-1}. Of 2473 symmetry-independent data measured at 291K to $\theta_{max.}$ 20°, 1830 [$F \geq 5.0\sigma(F)$] have been used to refine the structure to a current R value of 0.0556. The atomic co-ordinates for this work are available on request from the Director of the Cambridge Crystallographic Data Centre, University Chemical Laboratory, Lensfield Rd., Cambridge CB2 1EW. Any request should be accompanied by the full literature citation for this communication.

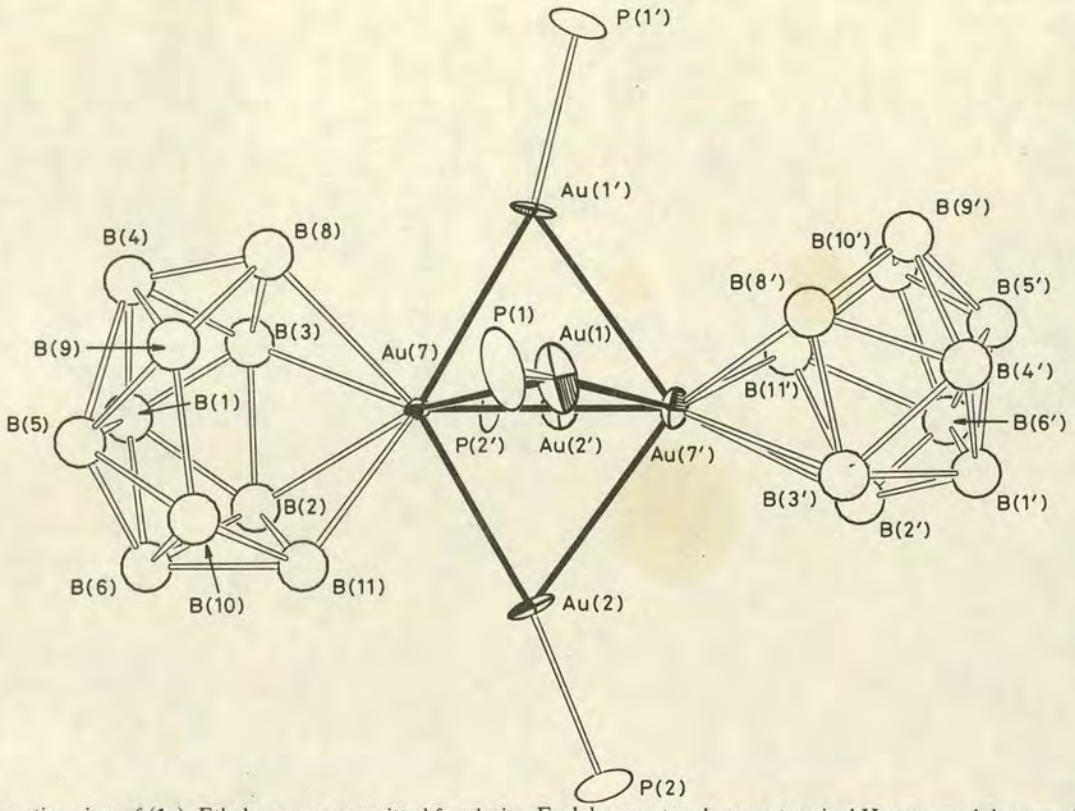

Figure 1. Perspective view of (**1a**). Ethyl groups are omitted for clarity. Each boron atom has one terminal H atom, and there are bridging H's on B(8)–B(9), B(10)–B(11), B(8')–B(9'), and B(10')–B(11') connectivities.

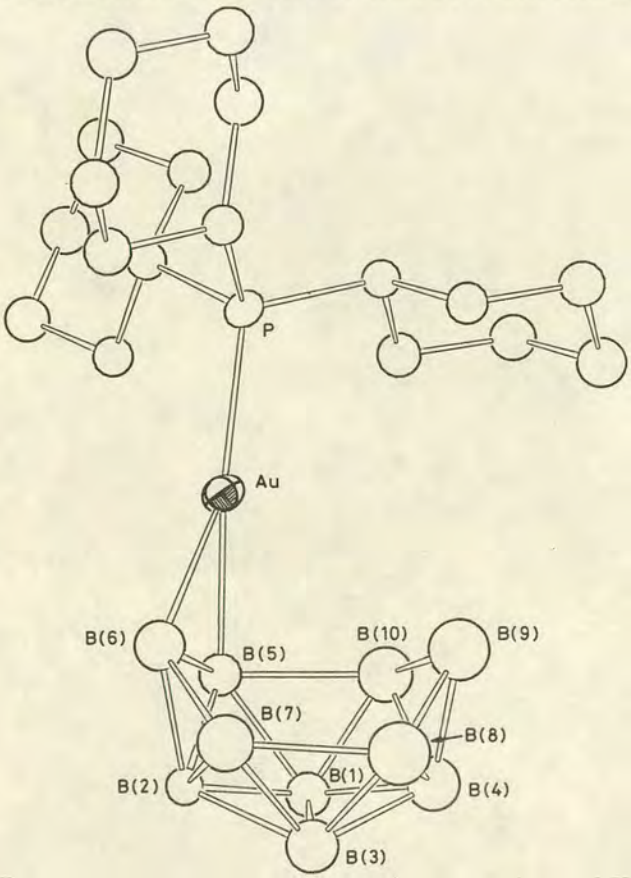

Figure 2. The non-hydrogen skeleton of (**2c**). In addition to 10 H atoms terminal to boron there are μ-H's on the B(6)–B(7), B(8)–B(9), and B(9)–B(10) connectivities.

formation of the colourless Au^{I} complex (**2**) is followed by collapse of the Au atom from an η^2- to η^4-bonded cluster site, with concomitant dimerisation and hydrogen elimination, yielding the yellow Au^{III} species (**3**), for which the structure illustrated is proposed. It may be of relevance that species with Au atoms η^3-bonded to boranes and heteroboranes are known.[3,4] Detailed n.m.r. experiments show no evidence for the presence of a terminal or bridging hydride in (**3**). In the presence of unreacted R_3PAuMe (R = Et or Ph) (**3**) undergoes phosphine loss and is quadruply bridged by $\{AuPR_3\}$ units. We suggest that with Cy_3PAuMe alone the combination of the insolubility of (**2c**) and the large cone angle of the phosphine prevent ultimate formation of a triple cluster.

We thank the Chemistry Department of the University of Edinburgh for a vacation studentship (A. J. Wynd), and Dr. D. Reed for the $^{11}B\{^1H\}$ and $^1H\{^{11}B\}$ n.m.r. spectra.

Received, 28th February 1985; Com. 272

References

1 For example, L. W. Bateman, M. Green, K. A. Mead, R. M. Mills, I. D. Salter, F. G. A. Stone, and P. Woodward, *J. Chem. Soc., Dalton Trans.*, 1983, 2599.
2 K. Wade, *J. Chem. Soc., Chem. Commun.*, 1971, 792.
3 H. M. Colquhoun, T. J. Greenhough, and M. G. H. Wallbridge, *J. Chem. Soc., Chem. Commun.*, 1980, 192.
4 M. A. Beckett, J. E. Crook, N. N. Greenwood, and J. D. Kennedy, *J. Chem. Soc., Dalton Trans.*, 1984, 1427.

Bridge-to-vertex Oxidative Slipping in an Auraborane: Synthesis and Characterisation of $[(B_{10}H_{12})Au(B_{10}H_{13})]^{2-}$ and $[(B_{10}H_{12})Au(B_{10}H_{12})]^{-}$

Andrew J. Wynd and Alan J. Welch*

Department of Chemistry, University of Edinburgh, Edinburgh EH9 3JJ, U.K.

The new auraboranes $[(B_{10}H_{12})Au(B_{10}H_{13})]^{2-}$ and $[(B_{10}H_{12})Au(B_{10}H_{12})]^{-}$ have been synthesised by the addition of $B_{10}H_{14}$ to a solution of R_3PAuMe (R = cyclo-C_6H_{11} or C_6H_4Me-2), a crystallographic study showing that the geometry of the $\{AuB_{10}H_{13}\}$ fragment of the former is that of an *arachno* fragment of a 13-vertex docosahedron; a mechanism is proposed which involves formal oxidative slipping of a gold atom from a B–Au–B bridge to a polyhedral vertex.

Reprinted from the Journal of The Chemical Society
Chemical Communications 1987

Bridge-to-vertex Oxidative Slipping in an Auraborane: Synthesis and Characterisation of $[(B_{10}H_{12})Au(B_{10}H_{13})]^{2-}$ and $[(B_{10}H_{12})Au(B_{10}H_{12})]^{-}$

Andrew J. Wynd and Alan J. Welch*

Department of Chemistry, University of Edinburgh, Edinburgh EH9 3JJ, U.K.

The new auraboranes $[(B_{10}H_{12})Au(B_{10}H_{13})]^{2-}$ and $[(B_{10}H_{12})Au(B_{10}H_{12})]^{-}$ have been synthesised by the addition of $B_{10}H_{14}$ to a solution of R_3PAuMe (R = cyclo-C_6H_{11} or C_6H_4Me-2), a crystallographic study showing that the geometry of the $\{AuB_{10}H_{13}\}$ fragment of the former is that of an *arachno* fragment of a 13-vertex docosahedron; a mechanism is proposed which involves formal oxidative slipping of a gold atom from a B–Au–B bridge to a polyhedral vertex.

We have previously shown[1] that addition of CH_2Cl_2 to a mixture of Cy_3PAuMe (Cy = cyclo-C_6H_{11}) and $B_{10}H_{14}$, the latter in slight excess, produces the colourless $Cy_3PAuB_{10}H_{13}$ (**1**), in which the $\{Cy_3PAu\}$ fragment simply replaces a μ-H atom in the decaborane framework. We now report that dropwise addition of a CH_2Cl_2 solution of $B_{10}H_{14}$ to a slight excess of R_3PAuMe [**a**; R = Cy, **b**; R = *o*-tol (C_6H_4Me-2),] affords, in addition to (**1**) or its *o*-tol analogue[2] as the major product, small amounts of the bright yellow anions $[(B_{10}H_{12})Au(B_{10}H_{13})]^{2-}$ (**2**) and $[(B_{10}H_{12})Au(B_{10}H_{12})]^{-}$ (**3**), as their $[(R_3P)_2Au]^+$ salts. Compounds (**2a**)·$4CH_2Cl_2$ and (**3b**) have been characterised by *X*-ray diffraction studies at 185 and 273 K respectively.†

The structure of (**3**) is shown in Figure 1. Compound (**3**) is isostructural with the known,[3,4] species $[(B_{10}H_{12})M(B_{10}H_{12})]^{2-}$ (M = Ni, Pd, Pt), having a pseudo-square-planar metal co-ordination geometry [in (**3**) the metal is located on a crystallographic inversion centre]. Although H atoms are not shown in Figure 1, all [including the B(8)–H–B(9) and B(10)–H–B(11) bridge H atoms] have been located and successfully refined. $[(B_{10}H_{12})Au(B_{10}H_{12})]^{-}$ has 96

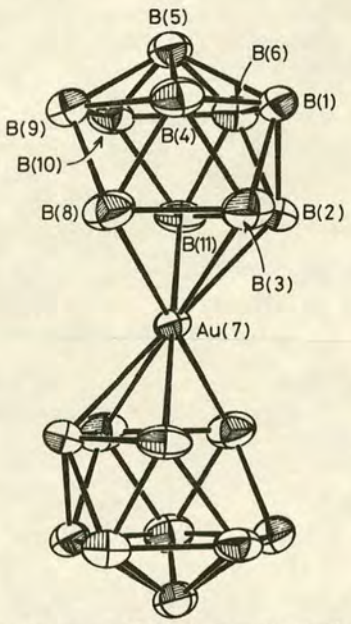

Figure 1. Perspective view of $[(B_{10}H_{12})Au(B_{10}H_{12})]^{-}$ (**3**). Important interatomic distances: Au(7)–B(2) 2.253(9), Au(7)–B(3) 2.275(10), Au(7)–B(8) 2.319(12), and Au(7)–B(11) 2.296(11) Å.

† *Crystal data:* (**2a**)·$4CH_2Cl_2$, $2[C_{36}H_{66}AuP_2][H_{25}AuB_{20}]\cdot 4CH_2Cl_2$, M = 2293.8, triclinic, space group $P\bar{1}$, a = 12.628(6), b = 15.141(7), c = 15.182(6) Å, α = 70.60(4), β = 69.86(3), γ = 80.86(4)°, U = 2567.3 Å^3, Z = 1, D_c = 1.483 g cm^{-3}, μ(Mo-K_α) = 45.8 cm^{-1}. R = 0.0480 for 7874 data measured to $\theta_{max.}$ = 25° on an Enraf-Nonius CAD4 diffractometer. (**3b**) $[C_{44}H_{42}AuP_2][H_{24}AuB_{20}]$, M = 1243.1, triclinic, space group $P\bar{1}$, a = 10.572(3), b = 11.665(3), c = 11.711(3) Å, α = 73.658(20), β = 70.360(24), γ = 86.680(22)°, U = 1304.1 Å^3, Z = 1, D_c = 1.583 g cm^{-3}, μ(Mo-K_α) = 57.0 cm^{-1}. R = 0.0265 for 2973 data to $\theta_{max.}$ = 25°. Atomic co-ordinates, bond lengths and angles, and thermal parameters have been deposited at the Cambridge Crystallographic Data Centre. See Notice to Authors, Issue No. 1.

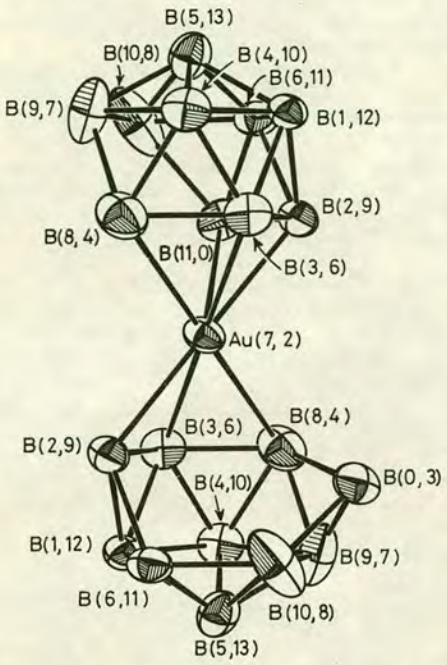

Figure 2. The anion $[(B_{10}H_{12})Au(B_{10}H_{13})]^{2-}$ (**2**). Au(7,2)–B(3,6) 2.231(10), Au(7,2)–B(8,4) 2.447(12), Au(7,2)–B(11,0) 2.499(21), and Au(7,2)–B(2,9) 2.262(10) Å.

valence electrons. This is the correct[5] number for two $\{MB_{10}H_{12}\}$ fragments fused about a common 16 valence electron vertex {compare, for example, $(Me_2PhP)_2Pt(B_{10}H_{12})$ (ref. 6) and $[(B_{10}H_{12})Pt(B_{10}H_{12})]^{2-}$ (refs. 3,4)}, thus implying an effective Au oxidation state in (**3**) of +3.

The structure of the anion of (**2**) (Figure 2) is unprecedented in a metallaborane. It too, is located on a crystallographic inversion centre [at Au(7,2)],‡ a consequence of which is that although the two halves of one ion are chemically different they appear superimposed in the crystallographic study. The mapping of nine B atoms onto their inversion-related equivalents is acceptably good, as evidenced by the refined anisotropic thermal parameters. B(11,0) and B(0,3), however, refine successfully with occupancy factors of 0.5, and their different locations distinguish the two polyhedra present in the ion.

Thus (**2**) consists of $\{AuB_{10}H_{12}\}$ and $\{AuB_{10}H_{13}\}$ fragments fused about a common Au vertex. The former (upper half of Figure 2) has a *nido*-icosahedral geometry with an AuB_4 open face. This sub-unit has previously been found in the 'triple cluster' $(B_{10}H_{12}Au)(AuPEt_3)_4(AuB_{10}H_{12})$[1] and in (**3**), and appears to be a thermodynamically stable entity. The $\{AuB_{10}H_{13}\}$ fragment in (**2**) is, in contrast, structurally based on (and is numbered in accordance with) an *arachno*-fragment derived from a closed 13-vertex C_{2v} polyhedron[7] by removal of vertices 1 and 5. This is the first time such a metallaborane fragment has been structurally characterised, although the geometry of the cage in $(Ph_3P)Ag(C_2B_8H_{11})$ has previously been interpreted in this way.[8] Evidence for the three μ-H atoms associated with the lower cage of (**2**) derives from (i) the fact that the lower cages of (**2**) and (**3**) differ by two skeletal electrons, only one of which is attributable to the change in anionic charge, (ii) the $^1H\{^{11}B\}$ n.m.r. spectrum of (**2**) (CD_2Cl_2, 298 K) which includes resonances at −1.85 (1H), −3.75 (1H), −4.12 (2H), and −4.78 (1H) p.p.m., and (iii) the proposed formulation of (**2**) arises straightforwardly from the mechanism outlined below.

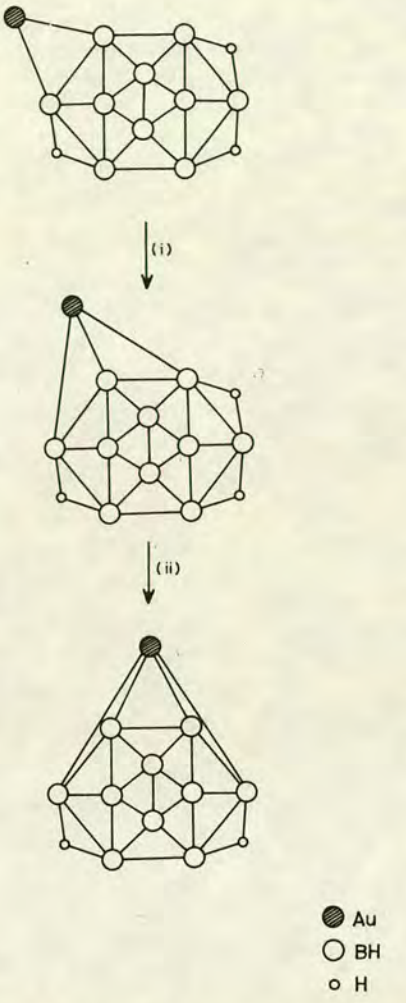

Scheme 1. Schlegel diagrams of the proposed mechanism by which (i) the *nido*-octadecahedral $\{AuB_{10}H_{13}\}$ fragment transforms into the *arachno*-docosahedral $\{AuB_{10}H_{13}\}$ fragment, and (ii) the *arachno*-docosahedral $\{AuB_{10}H_{13}\}$ fragment transforms into the *nido*-icosahedral $\{AuB_{10}H_{12}\}$ fragment.

Compounds (**2**) and (**3**) are nominally related by the loss/addition of a hydride ion, and, since the starting borane in their syntheses is $B_{10}H_{14}$, it is reasonable to suggest that (**3**) is formed from (**2**). The known structure of (**1**) demonstrates the existence of the fragment $\{AuB_{10}H_{13}\}$ in which the metal is simply a one-electron donor bridge. We suggest that this fragment yields the structurally different $\{AuB_{10}H_{13}\}$ fragment in (**2**) by oxidative slippage of the metal from bridge to vertex [this implies that in (**2**) the B(2,9)–B(6,11), B(10,8)–B(0,3), and B(8,4)–B(0,3) connectivities are H-bridged]. Continuation of this lateral movement of the gold atom, with concomitant hydride ion loss, transforms (**2**) into (**3**). This overall sequence is sketched in Schlegel form in Scheme 1.

‡ A consequence of the crystallographic superimposition of the two different polyhedra is that it is necessary to number the atoms (*i*,*j*) where *i* refers to the *nido*-icosahedron and *j* to the *arachno*-docosahedron.

We thank the S.E.R.C. for a maintenance grant (A. J. Wynd), the International Gold Corporation Ltd. for a generous loan of gold salts, and Dr. D. Reed for the $^{1}H\{^{11}B\}$ spectrum of (**2**).

Received, 31st October 1986;§ Com. 1557

References

1 A. J. Wynd, S. E. Robins, A. J. Welch, and D. A. Welch, *J. Chem. Soc., Chem. Commun.*, 1985, 819.

2 A. J. Wynd, A. J. McLennan, D. Reed, and A. J. Welch, *J. Chem. Soc., Dalton Trans.*, in the press.

3 F. Klanberg, P. A. Wegner, G. W. Parshall, and E. L. Muetterties, *Inorg. Chem.*, 1968, **7**, 2072.

4 L. J. Guggenberger, *J. Am. Chem. Soc.*, 1972, **94**, 114.

5 D. M. P. Mingos, *J. Chem. Soc., Chem. Commun.*, 1983, 706.

6 S. K. Boocock, N. N. Greenwood, J. D. Kennedy, W. S. McDonald, and J. Staves, *J. Chem. Soc., Dalton Trans.*, 1981, 2573.

7 J. B. Casey, W. J. Evans, and W. H. Powell, *Inorg. Chem.*, 1981, **20**, 1333.

8 H. M. Colquhoun, T. J. Greenhough, and M. G. H. Wallbridge, *J. Chem. Soc., Chem. Commun.*, 1980, 192.

§ Received in revised form, 13th April 1987.

In memory of T. A. Stephenson

Gold–Boron Chemistry. Part 1. Synthetic, Structural, and Spectroscopic Studies on the Compounds [5,6-μ-(AuPR$_3$)-*nido*-B$_{10}$H$_{13}$] (R = cyclo-C$_6$H$_{11}$ or C$_6$H$_4$Me-2)†

Andrew J. Wynd, Alistair J. McLennan, David Reed, and Alan J. Welch*
Department of Chemistry, University of Edinburgh, Edinburgh EH9 3JJ

The new Class 2 gold–boron compounds [5,6-μ-(AuPR$_3$)-*nido*-B$_{10}$H$_{13}$] (**1a**; R = cyclo-C$_6$H$_{11}$; **1b**, R = C$_6$H$_4$Me-2) have been prepared by the reaction between [AuMe(PR$_3$)] and B$_{10}$H$_{14}$ in CH$_2$Cl$_2$. Compound (**1a**) is also afforded by reaction between [AuCl{P(C$_6$H$_{11}$)$_3$}] and [B$_{10}$H$_{13}$]$^-$. The exact mechanism of the first reaction is unclear, but probably proceeds *via* sequential oxidative addition and reductive elimination. Crystallographic analyses of compounds (**1**) show the expected decaborane-like geometry. There is some evidence of an intramolecular interaction between Au and the B(9)–H–B(10) bridge system. A thorough n.m.r. study of (**1b**) was undertaken, including an ^{11}B(COSY) experiment which allowed almost complete assignment of the ten inequivalent B atoms in the molecule.

There is continuing interest in the synthesis and characterisation of new metallaboranes and carbametallaboranes,[1–6] and important accompaniments to these experimental studies have been the recognition of simple structural patterns and statements of the associated electron-counting principles which serve to underpin the subject.[7]

Transition-metal derivatives of boranes and carbaboranes are now known for an impressive range of metals, but there are relatively few examples involving the Group 1B elements Cu, Ag, and Au. We find it convenient to divide the Group 1B derivatives according to structure type. Class 1 refers to those species in which the Group 1B element resides in a polyhedral vertex[6,8–14] whilst Class 2 refers to those in which the metal atom bridges a polyhedral edge.[15–20] A final group, Class 3, is that in which the polyhedron and Group 1B element are simply connected *via* a single two-centre two-electron bond.[21]

We recognise that some examples of Class 1 Group 1B metallaboranes may be contentious. Thus, for example, for [(Ph$_3$P)$_2$CuB$_3$H$_8$][9,10] it is a moot point whether or not one regards the Cu atom to be an integral part of the polyhedron. Doing so, one recognises that this species is simply a metallaborane derived from B$_4$H$_{10}$. Alternatively one might argue that the relationship between [(Ph$_3$P)$_2$CuB$_3$H$_8$] and [B$_3$H$_8$]$^-$ [22,23] is no more than that between [Cu$_2$B$_{10}$H$_{10}$][24] and [B$_{10}$H$_{10}$]$^{2-}$, *i.e.* covalent bonding between an *exo*-polyhedral B–H electron pair and the metal atom, in much the same way as one regards agostic M/C–H bonding in organometallic complexes.[25] For the present purposes we will regard molecules such as [(Ph$_3$P)$_2$-CuB$_3$H$_8$] as Class 1 metallaboranes.

One of the many successes of the isolobal analogy developed by Hoffmann[26] is the popularity of the replacement of μ-H atoms in transition-metal cluster compounds by the (isolobal) {μ-AuPR$_3$} fragment, affording species that are frequently more stable and generally more readily analysed by *X*-ray crystallography.[27] Given that well known analogies exist between the electronic and consequent geometric structures of polyhedral boron hydrides and low-valent transition-metal clusters,[28] and that the *nido*, *arachno*, and *hypho* families of the former frequently contain several μ-H functions,[29] we became interested in the potential multiple replacement of H bridges in boranes by {AuPR$_3$} fragments, with the additional possibility of products containing gold–gold bonds.

This first paper in this series is concerned with species of the type [5,6-μ-(AuPR$_3$)-*nido*-B$_{10}$H$_{13}$] (**1**), in which a single μ-H atom of B$_{10}$H$_{14}$ is isolobally substituted. Some aspects of this work have been communicated previously.[30]

Experimental

Syntheses.—Standard Schlenk-tube techniques were used throughout, with all solvents thoroughly dried and distilled under N$_2$ before use. N.m.r. spectra were recorded at room temperature on JEOL FX 60 Q (^{31}P) and Brucker WP 200 SY (^{1}H) and WH 360 (^{1}H, ^{11}B) spectrometers, the last fitted with an Aspect 3000 computer. Chemical shifts are relative to external SiMe$_4$ (^{1}H), 85% H$_3$PO$_4$ (^{31}P), and BF$_3$·OEt$_2$ (^{11}B), positive values to high frequency. Techniques for recording ^{1}H-{^{11}B} and ^{11}B(COSY) spectra have been described previously.[31] I.r. spectra were recorded as KBr discs or as CH$_2$Cl$_2$ solutions on a Perkin-Elmer 598 spectrophotometer. Microanalyses were by the departmental service.

[AuX(PR$_3$)] (X = Cl *or* Me; R = *cyclo*-C$_6$H$_{11}$ *or* C$_6$H$_4$-Me-2). The known[32] species [AuCl{P(C$_6$H$_{11}$)$_3$}] was prepared by direct reaction[33] between HAuCl$_4$ and P(C$_6$H$_{11}$)$_3$ in absolute ethanol[34] and its purity checked by C and H microanalysis and by n.m.r. spectroscopy [^{31}P-{^{1}H} (CD_2Cl_2), δ 53.9 (s) p.p.m.]. The compound [AuCl{P(C$_6$H$_4$Me-2)$_3$}] was synthesised analogously as colourless *crystals* in 91% yield (Found: C, 46.9; H, 3.90. C$_{21}$H$_{21}$AuClP requires C, 46.9; H, 3.90%); ^{31}P-{^{1}H} ($CDCl_3$), δ 8.2 (s) p.p.m. Methylation of the phosphine gold chlorides using LiMe in Et$_2$O[35] afforded white *crystals* of [AuMe{P(C$_6$H$_{11}$)$_3$}] [91% (Found: C, 45.7; H, 7.25. C$_{19}$H$_{36}$AuP requires C, 46.3; H, 7.35%); ^{31}P-{^{1}H} (CD_2Cl_2), δ 59.9 (s) p.p.m.] and [AuMe{P(C$_6$H$_4$Me-2)$_3$}] [68% (Found: C, 50.2; H, 4.50. C$_{22}$H$_{24}$AuP requires C, 51.2; H, 4.70%); ^{31}P-{^{1}H} (CD_2Cl_2), δ 37.0 (s) p.p.m.].

† 5,6-μ-[Tri(cyclohexyl)phosphine]aurio- and 5,6-μ-[tri(*o*-tolyl)-phosphine]aurio-*nido*-decaborane, respectively.

Supplementary data available: see Instructions for Authors, *J. Chem. Soc., Dalton Trans.*, 1987, Issue 1, pp. xvii—xx.

[5,6-μ-Au{P(C_6H_{11})$_3$}-*nido*-$B_{10}H_{13}$] (**1a**). To a stirred solution of [AuMe{P(C_6H_{11})$_3$}] (0.7715 g, 1.567 mmol) in CH_2Cl_2 (10 cm^3) was added, dropwise, a solution of $B_{10}H_{14}$ (0.1913 g, 1.567 mmol) in CH_2Cl_2 (10 cm^3 and 15 cm^3 washings). A bright yellow solution was quickly formed, followed by gas evolution and the deposition of a white precipitate. The solid product was filtered off and washed with 2 × 5 cm^3 aliquots of ice-cold CH_2Cl_2. The volume of the combined filtrate and washings was reduced *in vacuo* and cooled to −30 °C to afford a second crop of crystalline solid, subsequently recovered. The combined solid product was purified by recrystallisation from CH_2Cl_2, affording colourless *crystals* (0.703 g, 75%) (Found: C, 35.7; H, 7.70. $C_{18}H_{46}AuB_{10}P$ requires C, 36.1; H, 7.75%); $\nu_{max.}$(KBr) at 2 900, 2 844 (both C–H), 2 530br (B–H), 1 920—1 850vw (B–H–B), 1 440 (C–H), 1 000 (P–C), 510 (Au–P), 470w, and 385w (both Au–B) cm^{-1}. N.m.r.: ^{31}P-{^{1}H} (CD_2Cl_2), δ 68.9 (br); ^{1}H, δ 1.84 (br), 1.63 and 1.27 (br); ^{11}B-{^{1}H} ($CDCl_3$), δ 16.12 (1 B), 9.32 (1 B), 8.41 (1 B), 2.82 (1 B), 1.41 (1 B), −0.57 (2 B), −1.01 (1 B), −29.53 (1 B), and −35.63 (1 B); ^{1}H-{^{11}B} ($CDCl_3$), δ 5.05, 3.72, 3.50, 3.29, 3.17, 2.94, 2.90, 2.62, 0.64, 0.60 (all B–H), −0.13, −2.93, and −3.84 (all B–H–B) p.p.m.

Alternatively, to a freshly prepared,[36] stirred solution of [NEt_3H][$B_{10}H_{13}$] (0.195 mmol) in CH_2Cl_2 (15 cm^3) was added, dropwise, [AuCl{P(C_6H_{11})$_3$}] (0.100 g, 0.195 mmol) in the same solvent (25 cm^3). The resultant bright yellow solution was stirred for *ca.* 4 h at ambient temperature. After removal of solvent *in vacuo*, addition of CH_2Cl_2 afforded a yellow solution and a white precipitate. The latter was identified as compound (**1a**) by ^{31}P-{^{1}H} n.m.r. and microanalysis. Yield 0.060 g, 51%.

[5,6-μ-Au{P(C_6H_4Me-2)$_3$}-*nido*-$B_{10}H_{13}$] (**1b**). This was entirely analogous to the first preparation for compound (**1a**) except that the product was not deposited from CH_2Cl_2 until a concentrated solution was cooled (−30 °C). The product was washed with ice-cold hexane (2 × 5 cm^3) to afford very pale yellow *crystals* in 65% yield. Microanalytical results on a crystalline sample are consistent with the 1:1 solvate [{(C_6H_4-Me-2)$_3$P}$AuB_{10}H_{13}$]· CH_2Cl_2 (Found: C, 37.0; H, 5.10. $C_{21}H_{34}AuB_{10}P{\cdot}CH_2Cl_2$ requires C, 37.4; H, 5.15%); $\nu_{max.}$(CH_2Cl_2) at 2 905, 2 940 (both C–H), 2 550 (B–H), 1 590 (C–C), 1 450 (C–H), 1 010 (P–C), and 555 (Au–P) cm^{-1}. N.m.r. (CD_2Cl_2): ^{31}P-{^{1}H}, δ 26.9 (br) p.p.m.; ^{11}B-{^{1}H} and ^{1}H-{^{11}B} chemical shifts are reported and assignments discussed in the Results and Discussion section.

Crystallographic Studies.—Diffraction-quality single crystals of compounds (**1a**) and (**1b**) were grown by solvent diffusion (CH_2Cl_2–n-hexane, 1:4) at −30 °C, and were studied at 291 and 273 K respectively on an Enraf-Nonius CAD4 diffractometer using graphite-monochromated Mo-K_α *X*-radiation, $\bar{\lambda}$ = 0.710 69 Å.

Crystal data. (**1a**), $C_{18}H_{46}AuB_{10}P$, M = 598.6, monoclinic, a = 11.658 3(20), b = 22.663(6), c = 11.418(3) Å, β = 118.061(16)°, U = 2 662 Å^3, by the least-squares refinement of 25 centred reflections, 12 < θ < 14°, space group $P2_1/a$, Z = 4, D_c = 1.493 g cm^{-3}, μ(Mo-K_α) = 55.8 cm^{-1}, F(000) = 1 192.

(**1b**), $C_{21}H_{34}AuB_{10}P{\cdot}CH_2Cl_2$, M = 707.5, monoclinic, a = 10.370(3), b = 20.100(4), c = 15.283(4) Å, β = 106.782(23)°, U = 3 050 Å^3, derived as above, 13 < θ < 15°, space group $P2_1/c$, Z = 4, D_c = 1.541 g cm^{-3}, μ(Mo-K_α) = 50.6 cm^{-1}, F(000) = 1 348.

Data collection and processing. (**1a**). ω—2θ Scans in 96 steps with ω scan-width 0.8 + 0.35tanθ. Variable scan speeds between 1.27 and 5.49° min^{-1}. 2 473 Unique data were measured (1 < θ < 20°, $+h$ $+k$ $+l$ and $+h$ $+k$ $-l$) yielding 1 821 with $F > 5.0\sigma(F)$. No measurable crystal decay or detectable movement.

(**1b**). As above except scan speeds between 1.03 and 2.35° min^{-1}; 3 976 data ($\theta_{max.}$ 22°) of which 3 072 had $F > 2.0\sigma(F)$; crystal decayed by *ca.* 4% during experiment and correction applied.

Structure solution and refinement. (**1a**). Patterson synthesis for Au atom, and iterative full-matrix least-squares refinement and ΔF syntheses for P, B, and C atoms. Empirical absorption correction[37] applied after isotropic convergence. Ultimately Au, P, and B atoms allowed anisotropic thermal motion. Cyclohexyl hydrogen atoms set in idealised positions (C–H 1.08 Å) with an overall isotropic thermal parameter [0.044(7) Å^2 at convergence]. Weighting scheme w^{-1} = [$\sigma^2(F)$ + 0.000 117(F)^2], R = 0.0426, R' = 0.0492, S = 1.190. Data: variables, 10:1. Maximum and minimum electron-density residues 0.707 and −0.550 e Å^{-3}. Scattering factors for Au from ref. 38, those for P, B, C, and H being inlaid in SHELX 76.[39] Computer programs CADABS,[40] SHELX 76, DIFABS, CALC,[41] and ORTEP II.[42] Co-ordinates of refined atoms are given in Table 1.

(**1b**). Gold atom located by automatic direct methods[43] and P, B, C, and Cl atoms by subsequent iterative full-matrix least-squares refinement and ΔF syntheses. Empirical absorption correction applied after isotropic convergence. Ultimately Au, P, B, C, and Cl atoms allowed anisotropic thermal motion. Phenyl rings were constrained as rigid planar hexagons with fixed bond length (C–C 1.395 Å). Hydrogen atoms of the phenyl rings were set in idealised positions (C–H 1.08 Å) and refined with one overall thermal parameter, 0.062(10) Å^2 at convergence. Hydrogen atoms of the methyl groups and of the B_{10} cage could not be either satisfactorily located or modelled and remain absent. The dichloromethane solvate molecule involves one chlorine atom [Cl(2)] disordered over two positions (a and b) with occupancy factors of 0.430(13) and 0.570 at convergence. Weighting scheme w^{-1} = [$\sigma^2(F)$ + 0.000 773(F)^2], R = 0.0519, R' = 0.0676, S = 1.191. Data: variables = 10:1, with

Table 1. Fractional co-ordinates of refined atoms in compound (**1a**)

Atom	x	y	z
Au	0.192 61(6)	0.229 78(3)	0.422 62(6)
P	0.184 4(4)	0.138 77(18)	0.327 9(4)
C(11)	0.243 9(13)	0.081 1(7)	0.457 9(13)
C(12)	0.163 2(15)	0.082 9(7)	0.532 5(15)
C(13)	0.225 0(15)	0.038 7(8)	0.649 5(15)
C(14)	0.365 1(14)	0.050 2(8)	0.741 5(15)
C(15)	0.444 4(15)	0.048 3(7)	0.664 7(14)
C(16)	0.391 0(13)	0.089 6(7)	0.551 2(13)
C(21)	0.023 6(13)	0.118 9(6)	0.198 2(13)
C(22)	−0.087 8(13)	0.150 0(7)	0.221 3(14)
C(23)	−0.221 7(14)	0.139 6(7)	0.102 5(15)
C(24)	−0.246 7(16)	0.075 3(8)	0.080 6(16)
C(25)	−0.145 2(14)	0.042 3(7)	0.067 7(15)
C(26)	−0.006 0(14)	0.051 3(7)	0.181 9(14)
C(31)	0.291 7(13)	0.138 6(6)	0.249 6(13)
C(32)	0.259 6(13)	0.189 1(7)	0.155 7(14)
C(33)	0.361 5(14)	0.192 9(7)	0.101 0(14)
C(34)	0.372 4(16)	0.133 9(7)	0.041 9(15)
C(35)	0.400 4(15)	0.084 3(7)	0.138 6(15)
C(36)	0.298 9(14)	0.079 9(7)	0.189 9(15)
B(2)	0.209 8(17)	0.375 4(8)	0.557 6(18)
B(5)	0.155 0(18)	0.300 7(8)	0.536 1(17)
B(1)	0.225 4(17)	0.333 2(8)	0.701 8(17)
B(3)	0.359 9(22)	0.378 6(10)	0.717 2(23)
B(10)	0.280 6(21)	0.260 3(11)	0.709 3(19)
B(4)	0.391 2(19)	0.313 8(12)	0.812 6(21)
B(7)	0.363 5(20)	0.371 3(10)	0.564 2(22)
B(6)	0.237 7(20)	0.330 1(9)	0.450 0(21)
B(9)	0.462 3(20)	0.264 4(14)	0.751 2(22)
B(8)	0.486(3)	0.335 0(11)	0.741(3)

Table 2. Fractional co-ordinates of refined atoms in compound (**1b**)

Atom	*x*	*y*	*z*
Au	0.541 24(4)	0.552 46(2)	0.211 55(3)
P	0.736 3(3)	0.529 03(13)	0.326 00(18)
C(16)	0.952 1(5)	0.445 9(3)	0.336 2(5)
C(15)	1.0157	0.3853	0.3322
C(14)	0.9397	0.3272	0.3104
C(13)	0.8000	0.3296	0.2926
C(12)	0.7364	0.3903	0.2965
C(11)	0.8124	0.4484	0.3184
C(121)	0.583 9(12)	0.387 8(6)	0.281 4(9)
C(26)	0.747 7(7)	0.474 5(3)	0.494 2(5)
C(25)	0.7217	0.4721	0.5788
C(24)	0.6543	0.5246	0.6062
C(23)	0.6130	0.5795	0.5491
C(22)	0.6390	0.5818	0.4646
C(21)	0.7064	0.5294	0.4371
C(221)	0.590 1(13)	0.644 8(6)	0.406 5(9)
C(36)	0.928 3(7)	0.621 7(4)	0.414 3(4)
C(35)	1.0321	0.6673	0.4210
C(34)	1.0777	0.6801	0.3452
C(33)	1.0194	0.6474	0.2628
C(32)	0.9156	0.6018	0.2561
C(31)	0.8701	0.5889	0.3319
C(321)	0.855 5(15)	0.565 9(6)	0.162 8(8)
B(1)	0.258 8(15)	0.668 2(8)	0.086 7(10)
B(2)	0.240 4(15)	0.588 5(8)	0.032 7(10)
B(3)	0.267 9(15)	0.659 6(8)	−0.027 7(10)
B(4)	0.362 0(16)	0.724 4(8)	0.042 3(10)
B(5)	0.335 2(14)	0.596 0(8)	0.146 9(10)
B(6)	0.378 5(15)	0.541 2(7)	0.071 3(11)
B(7)	0.350 8(14)	0.582 1(8)	−0.032 5(10)
B(8)	0.433 6(16)	0.676 9(8)	−0.030 5(11)
B(9)	0.531 1(16)	0.702 3(8)	0.080 3(12)
B(10)	0.425 7(16)	0.685 4(8)	0.155 4(11)
C(sol)	0.128 3(23)	0.336 9(12)	0.116 3(19)
Cl(1)	0.245 5(7)	0.297 5(5)	0.211 8(5)
Cl(2a)	0.192 2(21)	0.407 0(14)	0.133 6(16)
Cl(2b)	0.164 7(10)	0.302 7(5)	0.014 8(7)

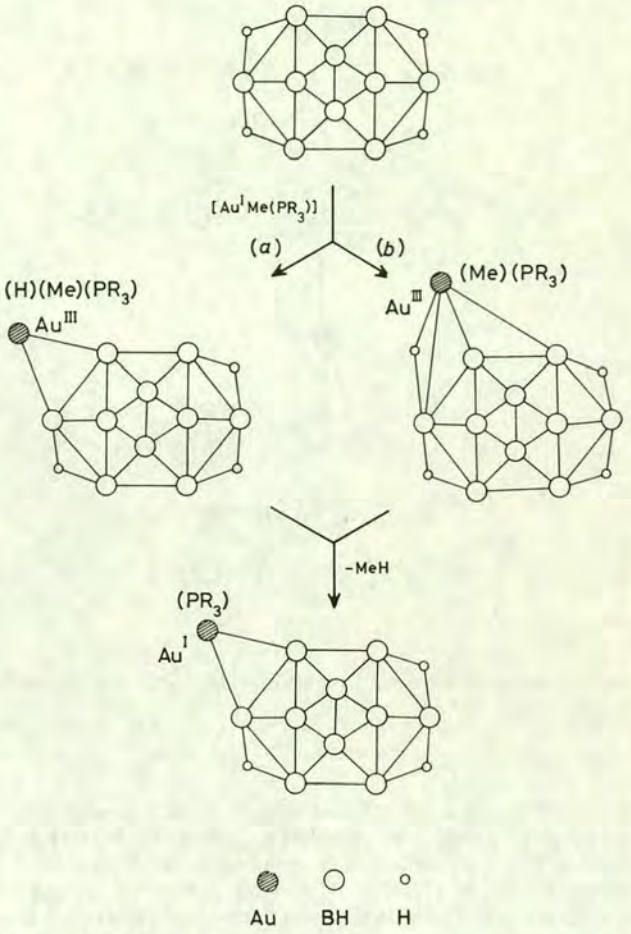

Scheme. Possible routes to compounds (**1**) from $B_{10}H_{14}$ and [AuMe(PR_3)] *via* (*a*) a terminal gold hydride intermediate, and (*b*) a bridging gold hydride intermediate

maximum and minimum electron-density residues of 2.817 and −1.487 e Å^{-3} respectively. Co-ordinates of refined atoms are given in Table 2.

Results and Discussion

Syntheses and Mechanism.—Dropwise addition of a solution of [AuMe(PR_3)] to $B_{10}H_{14}$ affords the air-stable colourless or pale yellow Class 2 crystalline compounds [5,6-μ-(AuPR_3)-*nido*-$B_{10}H_{13}$] (**1a**, R = cyclo-C_6H_{11}; **1b**, R = C_6H_4Me-2) in reasonable yields. If the reaction is performed as above (**1a**) or (**1b**) is the only isolable product. If, however, $B_{10}H_{14}$ is added dropwise to 1 equivalent of [AuMe{$P(C_6H_{11})_3$}] at least two other species may be isolated,[44] although (**1a**) is still the major product. As the following crystallographic and spectroscopic studies show, compounds (**1**) are the first proven examples[6] of the $[B_{10}H_{13}]^-$ unit acting as an η^2-ligand to a metal centre, although in [{$Cd(B_{10}H_{12})(OEt_2)_2$}$_2$][45] the cage functions as a bis η^2-ligand.

Alternatively, (**1a**) may be synthesised directly from [AuCl{$P(C_6H_{11})_3$}] by its reaction with [NEt_3H][$B_{10}H_{13}$]. In this preparation other species are also produced even if the chloride is added slowly to 1 equivalent of the ion. Amongst these additional products [NEt_3H]Cl has been identified. Similar reactions using [AuCl(PPh_3)] and [AuCl(PEt_3)] did not afford analogues of (**1**) in detectable amounts, but instead produced orange-yellow compounds which are currently being studied.[44]

The isolation of compounds (**1a**) and (**1b**) from $B_{10}H_{14}$ and [AuMe(PR_3)] appears to depend upon the large Tolman cone angles[46] of the phosphines [$P(C_6H_{11})_3$, 170°; $P(C_6H_4Me\text{-}2)_3$, 194°]. We have shown[30] that analogous reactions using [AuMe(PPh_3)] or [AuMe(PEt_3)] (phosphine cone angles 145 and 132° respectively) afford the unique 'triple clusters' [$(B_{10}H_{12}Au)(AuPR_3)_4(AuB_{10}H_{12})$] as the only isolable gold–boron species, although it is probable that these arise *via* the initial formation of compounds analogous to (**1a**) and (**1b**). We are actively pursuing alternative routes to these analogues that do not allow their further reaction.

When [AuMe(PR_3)] (R = C_6H_{11} or C_6H_4Me-2) is added to $B_{10}H_{14}$ a bright yellow solution is first formed, suggesting initial oxidation of the gold atom. As this solution then decolourises, gas evolution is noted. To obtain further information on the possible mechanism(s) by which (**1a**) and (**1b**) are produced we have followed the reaction between [AuMe{$P(C_6H_{11})_3$}] and $B_{10}H_{14}$ in CD_2Cl_2 by variable-temperature ^{1}H and ^{31}P-{^{1}H} n.m.r. spectroscopy, and between [AuMe{$P(C_6H_4Me\text{-}2)_3$}] and $B_{10}H_{14}$ in CD_2Cl_2 by variable-temperature ^{1}H, ^{1}H-{^{11}B}, and ^{11}B n.m.r. spectroscopy. In no case could any signals assignable to species other than the appropriate precursors or product be observed.

We cannot, therefore, authoritatively comment on the precise mechanistic details of the formation of compounds (**1**) from the methyl(phosphine)gold compounds at this stage. The bench observations are consistent with initial oxidative addition followed by reductive elimination, the simplest equation for the reactions suggesting elimination of methane. Two possible re-

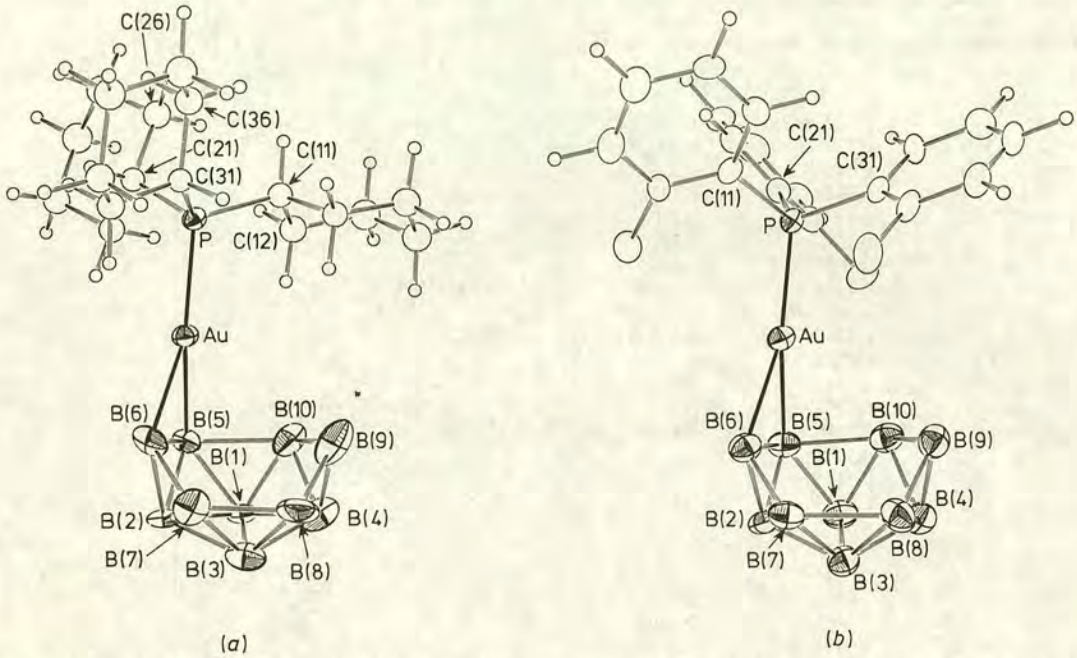

Figure 1. Perspective views of (*a*) compound (**1a**) and (*b*) (**1b**). Non-hydrogen atoms represented by 30% probability ellipsoids, and H atoms given an artificial radius of 0.1 Å

action mechanisms are outlined in the Scheme. One possibility, (*a*) involves insertion of [AuMe(PR_3)] into the B(5)–H–B(6) bond of $B_{10}H_{14}$ to afford the transient species [5,6-μ-(H)Au^{III}-(Me)(PR_3)-$B_{10}H_{13}$]. This compound would be unique in having a terminal Au–H function. Irreversible intramolecular reductive elimination of MeH would then give (**1a**) or (**1b**) as appropriate. Presumably the H and Me ligands of the intermediate would be mutually *cis*, *i.e.* H or Me *trans* to B–B. It should be noted that the oxidative insertion of a $\{Pt^0(PEt_3)_2\}$ fragment into B–H–B bonds of 2,3-$C_2B_4H_8$, 2,3-Me_2-2,3-$C_2B_4H_6$, and 2-CB_5H_9 produces species in which the terminal hydride ligand is *trans* to the metal-bonded B–B edge.[47] An alternative intermediate species, route (*b*), might involve the Au^{III} atom as a vertex in an expanded polyhedron and have an Au–H–B bridge. The precise cage geometry of such an intermediate would depend upon the skeletal electron contribution of the metal vertex, and by analogy with recent studies[44] we suggest an *arachno* 11-vertex architecture for this species. The intermediate would afford (**1**) by eliminating methane and undergoing vertex-to-bridge slipping of the metal fragment in a manner essentially the reverse of that which we have suggested could occur in the formation of bis(cage)gold products.[44] The attraction of this second route is that although gold–hydride species are still rare, all proven examples to date have involved heteronuclear Au–H–X fragments.[48,49]

The proposed oxidative-addition step in the reaction between [AuMe(PR_3)] and $B_{10}H_{14}$ outlined in the above mechanisms may be contrasted with the report[50] that B_2H_6 *reduces* [AuCl(PPh_3)] to [$Au_{55}(PPh_3)_{12}Cl_6$] in benzene solution.

Structural Studies.—Figure 1(*a*) and (*b*) present common views of compounds (**1a**) and (**1b**) respectively, and Tables 3 and 4 list the derived internuclear distance and interbond angle information for each. Both species crystallise as monomers separated by nothing more than normal van der Waals contacts. In the crystal of (**1b**) there is additionally a (partially disordered) molecule of CH_2Cl_2, but this makes no close approach either to (**1b**) or to other solvate molecules.

Compounds (**1**) have decaborane-like cage structures in which the μ-$AuPR_3$ unit simply replaces the 5,6-μ-H atom of $B_{10}H_{14}$. The effect of this isolobal replacement on the geometry of the borane cage appears to be minimal. With Edinburgh software[41] we can quantify the extent to which two similar groups of atoms, located crystallographically, may be best fitted to each other. The refined root mean square (r.m.s.) misfit of the B_{10} cage of (**1a**) to that determined, very accurately,[51] for $B_{10}H_{14}$ (average of two crystallographically independent molecules) is only 0.080 Å. For (**1b**) the value is 0.049 Å. Equally, the optimised r.m.s. misfit between the B_{10} cages of (**1a**) and (**1b**) is 0.067 Å, and only 0.068 Å if Au and P atoms are also included.

Although the overall fit of the B_{10} polyhedra of compounds (**1**) with that of $B_{10}H_{14}$ is very good, a comparison of individual molecular parameters reveals some subtle differences. Thus, we note that the Au atoms of (**1a**) and (**1b**) bridge the B(5)–B(6) connectivity more asymmetrically than do the μ-H atoms of $B_{10}H_{14}$, although the direction of the asymmetry is the same [away from the low-connected atom, B(6)]. In (**1**) the average B(6)–Au bond length is 2.323 Å, whilst the average for B(5)–Au is 2.245 Å [in $B_{10}H_{14}$ average bond lengths are B(6,9)–(μ-H) 1.3485 and B(5,7,8,10)–(μ-H) 1.3250 Å]. This increased asymmetry is accompanied by unequal P–Au–B angles in (**1a**), the wider being to B(5) [this feature is not apparent in (**1b**)], and longer H-bridged B–B distances between B(9) and B(10) than between B(6)–B(7) or B(8)–B(9). Individually these features may be of little statistical significance, but taken together they are not inconsistent with some sort of weak interaction between the Au atom annd the B(9)–H–B(10) bridge system. Unfortunately the relative inaccuracies of the present structural studies of (**1a**) and (**1b**) preclude a more detailed discussion at this time. However, we plan to address this potentially interesting problem by a combined theoretical and highly accurate crystallographic study in the near future.

N.M.R. Studies on (**1b**).—The ^{11}B-{^1H} spectrum of (**1b**) (Figure 2) comprises eight signals with relative areas 1:1:1:1:1:3:1:1, and the ^{11}B spectrum (Figure 3) confirms

Table 3. Internuclear distances (Å) and interbond angles (°) in compound (**1a**)

Au–P	2.310(4)	C(21)–C(22)	1.606(22)	C(35)–C(36)	1.550(23)	B(1)–B(4)	1.80(3)
Au–B(5)	2.233(20)	C(21)–C(26)	1.562(22)	B(2)–B(5)	1.79(3)	B(3)–B(4)	1.76(3)
Au–B(6)	2.321(22)	C(22)–C(23)	1.530(23)	B(2)–B(1)	1.84(3)	B(3)–B(7)	1.77(3)
P–C(11)	1.850(16)	C(23)–C(24)	1.485(24)	B(2)–B(3)	1.84(3)	B(3)–B(8)	1.69(4)
P–C(21)	1.816(15)	C(24)–C(25)	1.463(25)	B(2)–B(7)	1.76(3)	B(10)–B(4)	1.76(3)
P–C(31)	1.848(15)	C(25)–C(26)	1.544(23)	B(2)–B(6)	1.75(3)	B(10)–B(9)	1.94(4)
C(11)–C(12)	1.539(22)	C(31)–C(32)	1.490(21)	B(5)–B(1)	1.83(3)	B(4)–B(9)	1.72(4)
C(11)–C(16)	1.547(21)	C(31)–C(36)	1.515(22)	B(5)–B(6)	1.80(3)	B(4)–B(8)	1.73(4)
C(12)–C(13)	1.550(24)	C(32)–C(33)	1.583(23)	B(5)–B(10)	2.04(3)	B(7)–B(6)	1.71(3)
C(13)–C(14)	1.492(24)	C(33)–C(34)	1.529(23)	B(1)–B(3)	1.81(3)	B(7)–B(8)	2.02(4)
C(14)–C(15)	1.546(23)	C(34)–C(35)	1.500(24)	B(1)–B(10)	1.76(3)	B(9)–B(8)	1.64(4)
C(15)–C(16)	1.478(22)						
P–Au–B(5)	159.7(5)	C(22)–C(21)–C(26)	107.4(12)	Au–B(5)–B(10)	89.6(10)	B(1)–B(4)–B(3)	61.3(13)
P–Au–B(6)	153.4(6)	C(21)–C(22)–C(23)	110.7(12)	B(1)–B(5)–B(10)	53.8(10)	B(1)–B(4)–B(10)	59.3(13)
B(5)–Au–B(6)	46.4(7)	C(22)–C(23)–C(24)	109.7(14)	B(2)–B(5)–B(1)	61.2(11)	B(3)–B(4)–B(8)	57.8(15)
Au–P–C(11)	109.7(5)	C(23)–C(24)–C(25)	114.5(15)	B(2)–B(5)–B(6)	58.3(11)	B(10)–B(4)–B(9)	67.8(15)
Au–P–C(21)	113.8(5)	C(24)–C(25)–C(26)	115.2(14)	B(10)–B(5)–B(6)	111.8(14)	B(9)–B(4)–B(8)	56.6(15)
Au–P–C(31)	109.9(5)	C(21)–C(26)–C(25)	108.3(13)	B(2)–B(1)–B(5)	58.3(10)	B(2)–B(7)–B(3)	62.8(13)
C(11)–P–C(21)	109.4(7)	P–C(31)–C(32)	110.4(10)	B(2)–B(1)–B(3)	60.5(12)	B(2)–B(7)–B(6)	60.4(13)
C(11)–P–C(31)	107.7(7)	P–C(31)–C(36)	114.4(11)	B(5)–B(1)–B(10)	69.4(12)	B(3)–B(7)–B(8)	52.5(13)
C(21)–P–C(31)	106.2(7)	C(32)–C(31)–C(36)	113.5(13)	B(3)–B(1)–B(4)	58.4(13)	B(6)–B(7)–B(8)	119.3(17)
P–C(11)–C(12)	109.2(10)	C(31)–C(32)–C(33)	110.2(13)	B(10)–B(1)–B(4)	59.2(13)	Au–B(6)–B(5)	64.2(9)
P–C(11)–C(16)	109.9(10)	C(32)–C(33)–C(34)	111.1(13)	B(2)–B(3)–B(1)	60.4(12)	Au–B(6)–B(7)	134.2(14)
C(12)–C(11)–C(16)	112.5(12)	C(33)–C(34)–C(35)	111.4(14)	B(2)–B(3)–B(7)	58.2(12)	B(2)–B(6)–B(5)	60.5(12)
C(11)–C(12)–C(13)	107.6(13)	C(34)–C(35)–C(36)	112.7(14)	B(1)–B(3)–B(4)	60.3(13)	B(2)–B(6)–B(7)	61.2(13)
C(12)–C(13)–C(14)	113.9(14)	C(31)–C(36)–C(35)	109.1(13)	B(4)–B(3)–B(8)	60.2(15)	B(5)–B(6)–B(7)	105.9(15)
C(13)–C(14)–C(15)	110.1(14)	B(5)–B(2)–B(1)	60.5(11)	B(7)–B(3)–B(8)	71.2(16)	B(10)–B(9)–B(4)	56.9(14)
C(14)–C(15)–C(16)	111.2(13)	B(5)–B(2)–B(6)	61.2(12)	B(1)–B(10)–B(5)	56.9(11)	B(4)–B(9)–B(8)	62.0(16)
C(11)–C(16)–C(15)	113.5(13)	B(1)–B(2)–B(3)	59.1(11)	B(1)–B(10)–B(4)	61.5(13)	B(8)–B(9)–B(10)	103.5(19)
P–C(21)–C(22)	111.2(10)	B(3)–B(2)–B(7)	59.0(12)	B(4)–B(10)–B(9)	55.3(13)	B(3)–B(8)–B(4)	62.0(15)
P–C(21)–C(26)	115.2(10)	B(7)–B(2)–B(6)	58.4(12)	B(9)–B(10)–B(5)	114.8(16)	B(4)–B(8)–B(9)	61.5(16)
		Au–B(5)–B(6)	69.4(10)			B(7)–B(8)–B(9)	114.0(19)

Table 4. Internuclear distances (Å) and interbond angles (°) in compound (**1b**)

Au–P	2.308(3)	B(3)–B(4)	1.765(23)	B(1)–B(2)	1.786(22)	B(2)–B(7)	1.726(22)
Au–B(5)	2.256(15)	B(4)–B(8)	1.783(23)	B(1)–B(3)	1.788(22)	B(3)–B(7)	1.790(22)
Au–B(6)	2.325(16)	B(4)–B(10)	1.838(23)	B(1)–B(4)	1.818(22)	B(3)–B(8)	1.765(23)
P–C(11)	1.822(7)	B(5)–B(10)	2.013(22)	B(1)–B(5)	1.776(22)	B(4)–B(9)	1.738(23)
P–C(21)	1.812(7)	B(8)–B(9)	1.779(24)	B(1)–B(10)	1.779(23)	B(5)–B(6)	1.745(22)
P–C(31)	1.819(7)	B(6)–B(7)	1.735(22)	B(2)–B(3)	1.767(22)	B(7)–B(8)	2.086(23)
C(12)–C(121)	1.532(14)	C(sol)–Cl(2a)	1.55(4)	B(2)–B(5)	1.745(21)	B(9)–B(10)	1.830(23)
C(22)–C(221)	1.545(14)	C(sol)–Cl(2b)	1.83(3)	B(2)–B(6)	1.677(22)	C(sol)–Cl(1)	1.79(3)
C(32)–C(321)	1.559(15)						
P–Au–B(5)	157.3(4)	C(23)–C(22)–C(221)	116.2(7)	B(1)–B(3)–B(4)	61.1(9)	B(2)–B(6)–B(7)	60.7(9)
P–Au–B(6)	157.3(4)	C(33)–C(32)–C(321)	117.9(7)	B(2)–B(3)–B(7)	58.0(9)	B(2)–B(7)–B(3)	60.3(9)
Au–P–C(11)	115.73(24)	C(31)–C(32)–C(321)	122.1(7)	B(4)–B(3)–B(8)	60.3(9)	B(2)–B(7)–B(6)	58.0(9)
Au–P–C(21)	111.09(24)	B(5)–Au–B(6)	44.8(5)	B(7)–B(3)–B(8)	71.8(9)	B(3)–B(7)–B(8)	53.53(79)
Au–P–C(31)	113.03(25)	B(2)–B(1)–B(3)	59.3(9)	B(1)–B(4)–B(3)	59.5(9)	B(3)–B(8)–B(4)	60.5(9)
P–C(11)–C(16)	117.6(5)	B(2)–B(1)–B(5)	58.6(9)	B(3)–B(4)–B(8)	59.3(9)	B(3)–B(8)–B(7)	54.64(81)
P–C(11)–C(12)	122.3(5)	B(3)–B(1)–B(4)	59.4(9)	B(8)–B(4)–B(9)	60.7(9)	B(4)–B(8)–B(9)	58.4(9)
P–C(21)–C(22)	121.4(5)	B(4)–B(1)–B(10)	61.4(9)	B(1)–B(4)–B(10)	58.2(9)	B(4)–B(9)–B(8)	60.9(9)
P–C(21)–C(26)	118.6(5)	B(5)–B(1)–B(10)	69.0(9)	B(9)–B(4)–B(10)	61.5(9)	B(4)–B(9)–B(10)	62.0(9)
P–C(31)–C(32)	121.2(5)	B(1)–B(2)–B(3)	60.4(9)	Au–B(5)–B(6)	69.7(7)	B(5)–B(10)–B(1)	55.45(81)
P–C(31)–C(36)	118.8(5)	B(1)–B(2)–B(5)	60.4(9)	B(1)–B(5)–B(2)	61.0(9)	B(1)–B(10)–B(4)	60.3(9)
C(11)–P–C(31)	104.7(3)	B(3)–B(2)–B(7)	61.7(9)	B(2)–B(5)–B(6)	57.5(9)	B(4)–B(10)–B(9)	56.6(9)
C(21)–P–C(31)	106.6(3)	B(5)–B(2)–B(6)	61.3(9)	B(1)–B(5)–B(10)	55.58(81)	B(6)–B(7)–B(8)	117.4(11)
C(11)–P–C(21)	105.0(3)	B(6)–B(2)–B(7)	61.3(9)	Au–B(5)–B(10)	87.33(72)	B(7)–B(8)–B(9)	113.2(11)
C(11)–C(12)–C(121)	123.4(7)	B(1)–B(3)–B(2)	60.3(9)	Au–B(6)–B(5)	65.5(7)	B(8)–B(9)–B(10)	105.4(11)
C(13)–C(12)–C(121)	116.5(7)	B(5)–B(10)–B(9)	118.5(11)	Au–B(6)–B(7)	132.9(10)	Cl(1)–C(sol)–Cl(2a)	96.2(16)
C(21)–C(22)–C(221)	123.8(7)			B(2)–B(6)–B(5)	61.3(9)	Cl(1)–C(sol)–Cl(2b)	105.5(14)

that each boron carries one terminal proton (all signals being doublets). A series of ^{1}H spectra with selective ^{11}B decoupling additionally showed which B resonances do not display coupling to bridge protons, namely those signals at $\delta(^{11}B)$ 8.34, 2.15, −30.7, and −35.8 p.p.m. Clearly, given the established decaborane-like structure of (**1b**) the only boron atoms with no direct connection to μ-H atoms are B(1), B(2), B(3), B(4), and B(5). Using the decaborane analogy further, it is reasonable to assume, on chemical shift grounds, that the two low-frequency signals in the boron spectrum derive from B(2) and B(4).

Table 5. Proposed boron assignments for compound (**1b**)

Assignment	$\delta(^{11}B)^a$	$\delta(^{1}H)^b$
6	15.13	5.27 (−3.3)
9	9.41	3.18 (−0.1, −2.8, −3.3)
3	8.34	3.66
1	2.15	3.10
7	1.40	3.67 (−0.1, −2.8, −3.3)
8,10	−1.00[c]	2.64, 2.85 (−0.1, −2.8, −3.3)
5	−1.00[c]	2.85 (−0.1, −2.8, −3.3)
2	−30.73	0.45
4	−35.85	0.51

[a] Relative to $BF_3{\cdot}OEt_2$ (external). [b] Relative to $SiMe_4$ from selective ^1H-{^{11}B} experiments. Chemical shifts of bridge protons enhanced by irradiation at ^{11}B frequencies shown in parentheses. [c] High- and low-frequency components of asymmetric singlet.

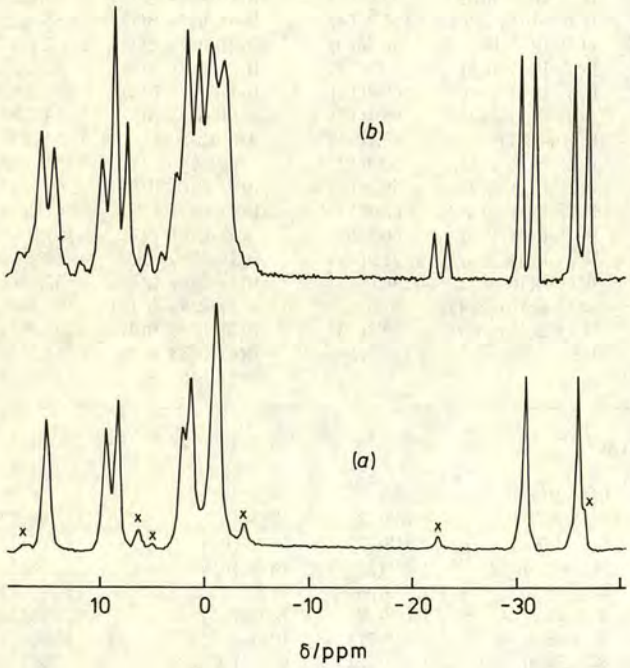

Figure 2. (*a*) ^{11}B-{^1H} and (*b*) ^{11}B n.m.r. spectra of compound (**1b**) obtained as a saturated solution in CD_2Cl_2 at 298 K. Peaks marked with a cross are due to a minor, unidentified impurity

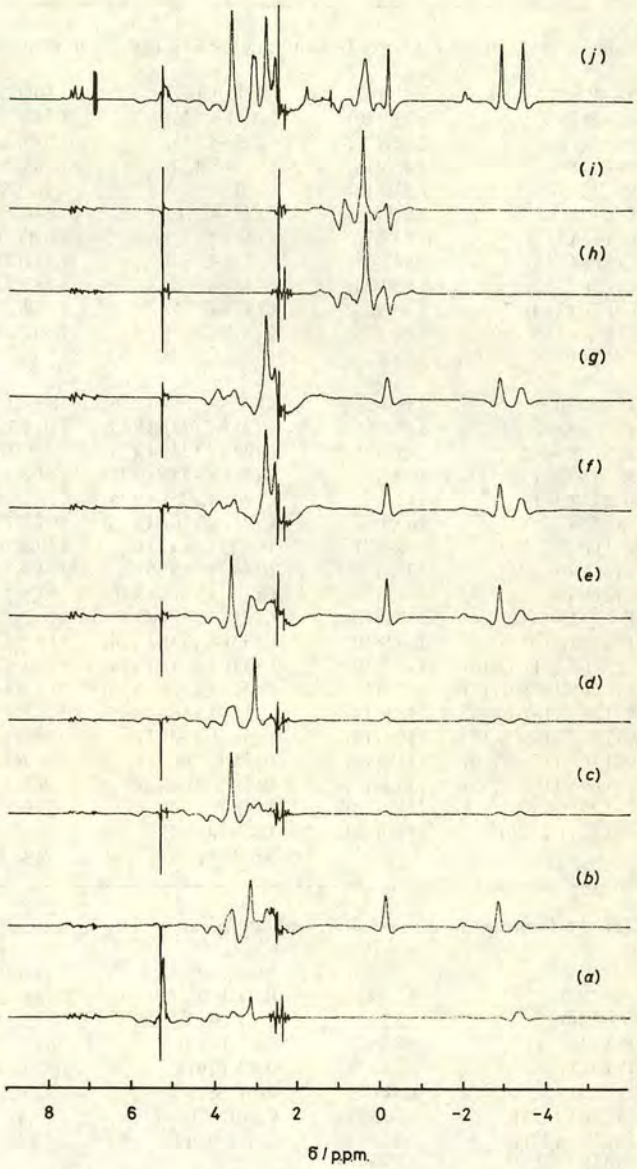

Figure 3. Traces (*a*)—(*i*) represent ^1H-{^{11}B(selective)} n.m.r. results for compound (**1b**) presented as difference spectra by subtraction of an off-resonance decoupled spectrum from each of the ^1H-{^{11}B(selective)} spectra. $\nu(^{11}B)$ correspond to $\delta(^{11}B)$ values of (*a*) 15.13, (*b*) 9.41, (*c*) 8.34, (*d*) 2.15, (*e*) 1.40, (*f*) −1.00 (high ν component), (*g*) −1.00 (low ν component), (*h*) −30.73, and (*i*) −35.85. Trace (*j*) represents a ^1H-{^{11}B(broad band)} n.m.r. result, again presented as a difference spectrum

Equally, on the basis of chemical shift together with the fact that it couples to only one bridging proton, the high-frequency signal at $\delta(^{11}B)$ 15.13 p.p.m. may be ascribed to B(6).

In order to derive more positive assignments for the ^{11}B (and hence the ^1H) signals, the ^{11}B(COSY) spectrum of (**1b**) was obtained (Figure 4). To summarise, the signal at $\delta(^{11}B)$ 15.13 p.p.m. displays coupling to those at 1.40 and −30.7 p.p.m. If our earlier assumptions are correct, then the signal at −30.7 p.p.m. is due to B(2), and by elimination that at −35.8 p.p.m. must arise from B(4). The signal at $\delta(^{11}B)$ 1.40 p.p.m., which shows coupling to that of B(6), also couples to that of B(2). Furthermore, it also shows bridge-H coupling, so it is probably due to B(7). This signal is also coupled to that at 8.34 p.p.m., and since the latter does not display coupling to a bridge proton, it must arise from B(3). The boron atom which resonates at δ 2.15 p.p.m. also has no μ-H attached, and since its signal couples to that of B(2) it must be due to B(1).

This leaves four boron atoms, 5, 8, 9, and 10, unaccounted for. Again, chemical shift arguments would suggest that B(9) gives rise to the signal at $\delta(^{11}B)$ 9.41, leaving the remaining three borons at −1.0 p.p.m. Even here some degree of resolution is possible, since close inspection of the COSY plot shows that the signal from B(4) has coupling to the higher-frequency component of the peak at −1.0 p.p.m. whilst the signal from B(2) couples to the lower-frequency part. This means that B(8) and B(10) resonate at slightly higher frequency than B(5). Unfortunately the coincidence between the former pair could not be resolved, although it may be noted that the selective ^1H-{^{11}B} spectra show that the protons terminal to B(8) and B(10) resonate at slightly different frequencies, specifically 2.85 and 2.64 p.p.m. Table 5 summarises the proposed boron assignments.

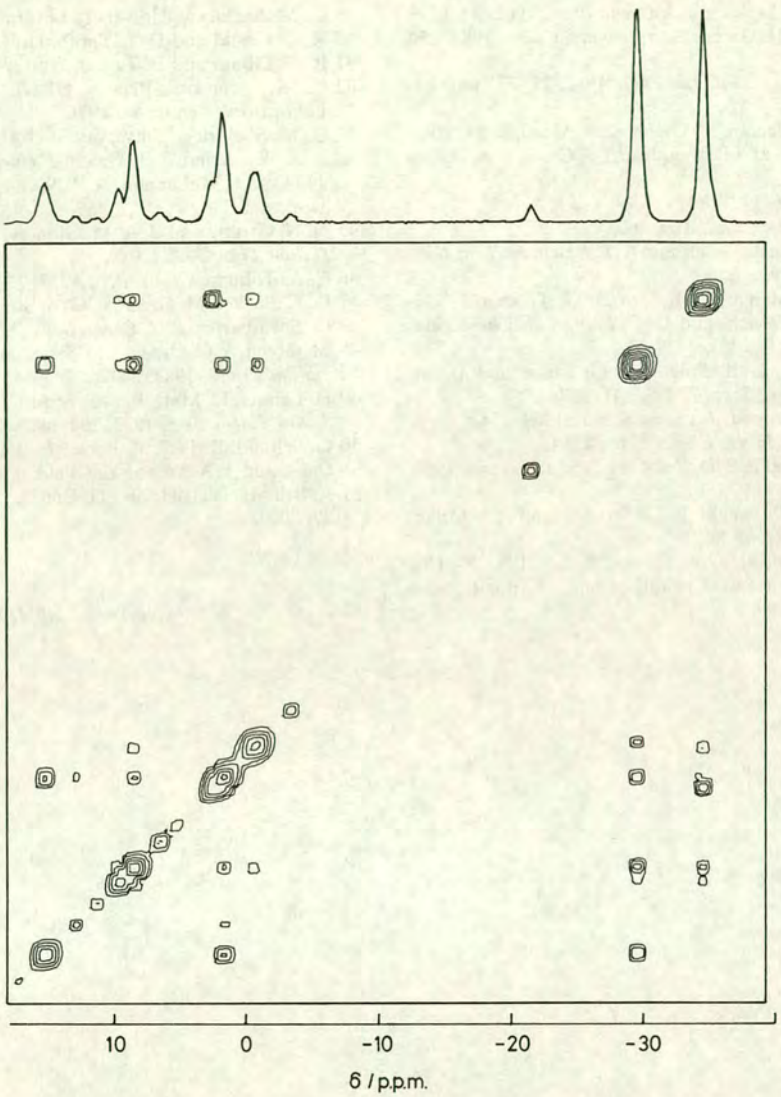

Figure 4. ^{11}B(COSY) plot for compound (**1b**) acquired overnight as a saturated solution in CD_2Cl_2, and transformed using a sine-bell squared function applied in both dimensions. The boron 90° pulse was 19 μs, and broad-band proton decoupling was applied throughout

Acknowledgements

We thank the S.E.R.C. for support, Dr. S. G. D. Henderson for some spectra, and the International Gold Corporation Ltd. for a generous loan of gold salts.

References

1 N. N. Greenwood and I. M. Ward, *Chem. Soc. Rev.*, 1974, **3**, 231.
2 N. N. Greenwood, *Pure Appl. Chem.*, 1977, **49**, 79; 1983, **55**, 77.
3 R. N. Grimes, in 'Comprehensive Organometallic Chemistry,' eds. G. Wilkinson, F. G. A. Stone, and E. W. Abel, Pergamon, Elmsford, 1982.
4 'Metal Interactions with Boron Clusters,' ed. R. N. Grimes, Plenum, New York, 1982, chs. 1—4, 6, and 7.
5 R. N. Grimes, *Acc. Chem. Res.*, 1983, **16**, 22.
6 J. D. Kennedy, *Prog. Inorg. Chem.*, 1984, **32**, 519; 1986, **34**, 211 and refs. therein.
7 N. N. Greenwood, *Chem. Soc. Rev.*, 1984, **13**, 353 and refs. therein.
8 L. F. Warren, jun., and M. F. Hawthorne, *J. Am. Chem. Soc.*, 1968, **90**, 4823.
9 S. J. Lippard and D. A. Ucko, *Inorg. Chem.*, 1968, **7**, 1051.
10 S. J. Lippard and K. M. Melmed, *Inorg. Chem.*, 1969, **8**, 2755.
11 E. L. Muetterties, W. G. Peet, P. A. Wegner, and C. W. Alegranti, *Inorg. Chem.*, 1970, **9**, 2447.
12 J. T. Gill and S. J. Lippard, *Inorg. Chem.*, 1975, **14**, 751.
13 H. M. Colquhoun, T. J. Greenhough, and M. G. H. Wallbridge, *J. Chem. Soc., Chem. Commun.*, 1976, 1019; *J. Chem. Soc., Dalton Trans.*, 1978, 303; *Acta Crystallogr., Sect. B*, 1977, **33**, 3604; *J. Chem. Soc., Chem. Commun.*, 1980, 192.
14 M. A. Beckett, J. E. Crook, N. N. Greenwood, and J. D. Kennedy, *J. Chem. Soc., Dalton Trans.*, 1984, 1427.
15 V. T. Brice and S. G. Shore, *J. Chem. Soc., Dalton Trans.*, 1975, 334.
16 C. G. Outterson, V. T. Brice, and S. G. Shore, *Inorg. Chem.*, 1976, **15**, 1456.
17 N. N. Greenwood, J. A. Howard, and W. S. McDonald, *J. Chem. Soc., Dalton Trans.*, 1977, 37.
18 N. N. Greenwood and J. T. Staves, *J. Chem. Soc., Dalton Trans.*, 1978, 1144.
19 G. K. Barker, N. R. Godfrey, M. Green, H. E. Parge, F. G. A. Stone, and A. J. Welch, *J. Chem. Soc., Chem. Commun.*, 1983, 277.
20 N. W. Alcock, L. Parkhill, and M. G. H. Wallbridge, *Acta Crystallogr., Sect. C*, 1985, **41**, 716.
21 Ref. 4, ch. 5.
22 C. R. Peters and C. E. Nordman, *J. Am. Chem. Soc.*, 1960, **82**, 5758.
23 G. F. Mitchell and A. J. Welch, *J. Chem. Soc., Dalton Trans.*, 1987, 1017.

24 R. D. Dobrott and W. N. Lipscomb, *J. Chem. Phys.*, 1962, **37**, 1779.
25 M. Brookhart and M. L. H. Green, *J. Organomet. Chem.*, 1983, **250**, 395.
26 R. Hoffmann, *Angew. Chem., Int. Ed. Engl.*, 1982, **21**, 771 and refs therein.
27 See, for example, L. W. Bateman, M. Green, K. A. Mead, R. M. Mills, I. D. Salter, F. G. A. Stone, and P. Woodward, *J. Chem. Soc., Dalton Trans.*, 1983, 2599.
28 K. Wade, *Chem. Commun.*, 1971, 792.
29 L. Barton, *Top. Curr. Chem.*, 1982, **100**, 169.
30 A. J. Wynd, S. E. Robins, D. A. Welch, and A. J. Welch, *J. Chem. Soc., Chem. Commun.*, 1985, 819.
31 G. B. Jacobsen, D. G. Meina, J. H. Morris, C. Thomson, S. J. Andrews, D. Reed, A. J. Welch, and D. F. Gaines, *J. Chem. Soc., Dalton Trans.*, 1985, 1645.
32 J. A. Muir, M. M. Muir, L. B. Pulgar, P. G. Jones, and G. M. Sheldrick, *Acta Crystallogr., Sect. C*, 1985, **41**, 1174.
33 B. J. Gregory and C. K. Ingold, *J. Chem. Soc. B*, 1969, 276.
34 A. J. Carty and A. Efraty, *Inorg. Chem.*, 1969, **8**, 543.
35 G. Calvin, G. E. Coates, and P. S. Dixon, *Chem. Ind. (London.)*, 1959, 1628.
36 M. F. Hawthorne, A. R. Pitochelli, R. D. Strahm, and J. J. Miller, *J. Am. Chem. Soc.*, 1960, **82**, 1825.
37 N. G. Walker and D. Stuart, *Acta Crystallogr., Sect. A*, 1983, **39**, 158.
38 International Tables for *X*-Ray Crystallography, Kynoch Press, Birmingham, 1974, vol. 4, 99.
39 G. M. Sheldrick, University of Cambridge, 1976.
40 R. O. Gould and D. E. Smith, University of Edinburgh, 1986.
41 R. O. Gould and P. Taylor, University of Edinburgh, 1986.
42 C. K. Johnson, Report ORNL 5138, Oak Ridge National Laboratory, Tennessee, 1976.
43 G. M. Sheldrick, University of Göttingen, 1986.
44 A. J. Wynd and A. J. Welch, *J. Chem. Soc., Chem. Commun.*, 1987, 1174; A. J. McLennan, A. J. Wynd, and A. J. Welch, unpublished work.
45 N. N. Greenwood, J. A. McGinnety, and J. D. Owen, *J. Chem. Soc., Dalton Trans.*, 1972, 989.
46 C. A. Tolman, *Chem. Rev.*, 1977, **77**, 413.
47 G. K. Barker, M. Green, F. G. A. Stone, A. J. Welch, T. P. Onak, and G. Siwapanyoyos, *J. Chem. Soc., Dalton Trans.*, 1979, 1687.
48 M. Green, A. G. Orpen, I. D. Salter, and F. G. A. Stone, *J. Chem. Soc., Dalton Trans.*, 1984, 2497.
49 H. Lehner, D. Matt, P. S. Pregosin, L. M. Venanzi, and A. Albinati, *J. Am. Chem. Soc.*, 1982, **104**, 6825.
50 G. Schmid, R. Pfeil, R. Boese, F. Bandermann, S. Meyer, G. H. M. Calis, and J. A. W. van der Velden, *Chem. Ber.*, 1981, **11**, 4634.
51 R. Brill, H. Dietrich, and H. Dierks, *Acta Crystallogr., Sect. B*, 1971, **27**, 2003.

Received 12*th December* 1986; *Paper* 6/2395

Zeitschrift für Kristallographie 185, 380 (1988) – P65 3.3.TU

Structural analysis in auraborane chemistry

Andrew J. Wynd and Alan J. Welch,
Department of Chemistry, University of Edinburgh, Edinburgh EH9 3JJ.

The reaction of decaborane ($B_{10}H_{14}$) with methyltricyclohexylphosphinegold (I) yields the complex 5,6-μ-($AuPCy_3$)-*nido*-$B_{10}H_{13}$ **(1)**. The structure of this has been determined by a low-temperature single crystal X-ray diffraction study, and a very unusual interaction between the gold atom and a neighbouring μ-H has been used to account for the observed distortions in the cage architecture.

This complex is readily deprotonated to yield the $[Cy_3PAuB_{10}H_{12}]^-$ anion **(2)**. This has the well-known *nido*-7-metallaundecaborane geometry. However analysis of this structure, and comparison with the other compounds with this cage shows that there are subtle differences, and that there are at least two general types.

(2) rearranges to yield the *double cluster* $(B_{10}H_{12}Au)(AuPCy_3)_3$ **(3)**. This is the first example of a tetrahedral Au_4 cluster which is not edge-bridged.

Finally, reaction of methyltricyclohexylphosphinegold(1) with $B_{10}H_{12}(PPh_3)_2$ yielded the product $(Cy_3PAu)_2B_8H_{10}$ **(4)**. This is very similar to the known species $(dtcAu)_2B_8H_{10}$ (dtc = diethyldithiocarbamate) and the opportunity was taken to compare the two observed geometries, especially when the compounds differ by one skeletal electron pair.

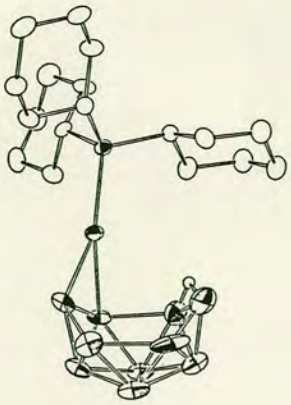

(1)

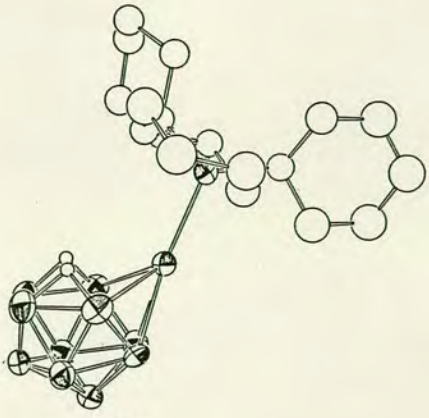

(2)